Design and Synthesis of Application-Oriented Polyethers via Introduction of Nitrogen, Fluorine or Boron

Dissertation

Zur Erlangung des Grades

“Doktor der Naturwissenschaften“

im Promotionsfach Chemie

Am Fachbereich Chemie, Pharmazie und Geowissenschaften

der Johannes Gutenberg-Universität

in Mainz

Larissa Limmer

Geb. in Mainz

Mainz, 2023

Dekanin: Prof. Dr. Eva Rentschler

1. Berichterstatter: Prof. Dr. Holger Frey
2. Berichterstatter: Prof. Dr. [redacted]

Tag der mündlichen Prüfung: 24.05.2023

Die als Dissertation vorgelegte Arbeit wurde in der Zeit von Juli 2019 bis April 2023 am Institut für Organische Chemie bzw. Department Chemie der Johannes Gutenberg-Universität im Arbeitskreis von Herrn Univ.-Prof. Dr. Holger Frey angefertigt.

Hiermit versichere ich gemäß § 10 Abs. 3d der Promotionsordnung vom 24.07.2007:
a) Ich habe die jetzt als Dissertation vorgelegte Arbeit selbst angefertigt und alle benutzten Hilfsmittel (Literatur, Apparaturen, Material) in der Arbeit angegeben.
b) Ich habe oder hatte die jetzt als Dissertation vorgelegte Arbeit nicht als Prüfungsarbeit für eine staatliche oder andere wissenschaftliche Prüfung eingereicht.
c) Ich hatte weder die jetzt als Dissertation eingereichte Arbeit noch Teile davon bei einer anderen Fakultät bzw. einem anderen Fachbereich als Dissertation eingereicht.

_____

Larissa Limmer

Für meine Familie

We all make choices, but in the end our choices make us.

Andrew Ryan, BioShock

Table of Contents

Danksagung

Viele Menschen haben mich auf meinem Weg begleitet oder ihn gekreuzt. Eine besondere Auswahl möchte ich hier festhalten und mich herzlichst bei ihnen bedanken.

An dieser Stelle allen vorangestellt möchte ich mich meinem Doktorvater **Prof. Dr.** [redacted] für das Ermöglichen dieser Arbeit in seinem hervorragenden Arbeitskreis bedanken. Vielen Dank für das Eröffnen dieser spannenden Thematik, den Freiraum sich selbst und die eigenen Ideen zu entwickeln, das Zusammenbringen von Kooperationen und hierbei auch vor allem die Unterstützung meines Forschungsaufenthaltes an der Indiana University in Bloomington, USA.

Vielen Dank und Wertschätzung an **Prof.** [redacted] für die herzliche Aufnahme in seinem Arbeitskreis in Bloomington und die vorangegangene Zusammenarbeit in Mainz. Das gemeinsame Erarbeiten des Projektes und der Blickwechsel in die organisch-katalytische Chemie hat mir viel Spaß gemacht. Ich möchte mich auch bei dem gesamten Arbeitskreis Brown für die großartige Zeit und wertvollen Erlebnisse und Erinnerungen in und außerhalb des Labors bedanken. Insbesondere möchte ich hier [redacted], [redacted] und [redacted] hervorheben.

Bei **Dr.** [redacted] bedanke ich mich für die Eröffnung des Gebietes der Fluorchemie und die erfolgreiche Zusammenarbeit an diesem Thema. Auch möchte ich der **Merck KGaA** für die Bereitstellung der Mittel und **Dr.** [redacted] für das gemeinsame Verfassen des Patentes danken.

Prof. [redacted] und [redacted] danke ich für langanhaltende und fruchtbare Zusammenarbeit im Bereich der KHI-Entwicklung.

Bedanken möchte ich mich auch bei **Dr.** [redacted] für die interessante Kooperation hinsichtlich des biomedizinischen Potentials der Polymere.

Auch intern kamen viele Kooperationen zustande und mein Dank gilt meinen Freunden und Kollegen. Vielen Dank an **Dr.** [redacted] und an [redacted], ohne deren Zutun die Kinetikmessungen nicht zustande gekommen wären. Vielen Dank an **Dr.** [redacted], [redacted] und an [redacted] für die gemeinsame Arbeit und produktives *brain-stormen*. Danke an

[redacted] und [redacted] für das Korrekturlesen Teilen dieser Arbeit. Auch möchte ich mich an dieser Stelle für die großartige Zusammenarbeit mit meinen Bachelor- und Masterstudenten [redacted], [redacted] und [redacted] bedanken.

Besonders herzlich möchte ich mich bei den Festangestellten des Arbeitskreises bedanken, ohne die der Arbeitskreis auseinanderfallen würde. Vielen Dank an [redacted], ohne die alles stillstehen würde. Danke an [redacted], auf deren Organisation Verlass ist. Danke an [redacted] und **Dr.** [redacted] - unsere Expertinnen für analytische Messungen. Danke an [redacted] für ihre tatkräftige Unterstützung im Labor.

Ich möchte mich beim **gesamten Arbeitskreis** und den **Alumni** für die wundervolle Atmosphäre auf der Arbeit aber auch bei Veranstaltungen und Ausflügen bedanken. Ich hatte eine großartige Zeit, an die ich immer gerne zurückdenken werde.

Ein ganz besonderer Dank ist meiner Familie gewidmet. Vielen Dank an meine Mutter [redacted] und meinen Vater [redacted] für all die Jahre Unterstützung – praktisch und moralisch. Auch danke ich meinem Bruder [redacted], der mein Interesse an der Chemie geweckt hat.

Zu guter Letzt danke ich meinen Freunden, die mich zum Teil seit dem Kindergarten begleiten. Unsere Freundschaft ist mir wirklich viel wert und ich blicke voller Freude auf die nächsten Jahrzehnte. Vor allem möchte ich hier [redacted] und [redacted] für die Unterstützung danken.

Collaborations

Some of the chapters of this work were supplemented by contributions of other researchers.

Prof. Dr. H. Frey was involved in the design and editing of **chapters 2.1 to 4**.

Dr. Matthias Bros performed the biomedical assays of chapter **2.1** and was involved in conceptualisation and writing of the chapter. Larissa Limmer conceptualised the studies, performed the synthesis and characterisation of the monomers and polymers and wrote the chapter.

Dr. Jan Blankenburg was involved in the polymer synthesis of **chapter 2.2**. Prof. Malcolm A. Kelland was involved in the conceptualisation of **chapters 2.2 and 2.3**. Qian Zhang performed cloud point and KHI activity measurements. Qian Zhang and Larissa Limmer wrote the chapters and were involved in the conceptualisation. Larissa Limmer furthermore performed the synthesis and characterisation of the monomers and polymers.

Tom Reimers was involved in the monomer and polymer synthesis of **chapter 3** as part of his master thesis. Gregor Linden, Dr. Johannes Liermann, Tom Reimers and Larissa Limmer performed *in situ* ^{1}H NMR measurements. Gregor Linden furthermore interpreted the *in situ* ^{1}H NMR measurements. Dr. Reiner Friedrich was involved in the polymer design and performed surface tension measurements as well as degradation studies. Dr. Elena Berger-Nicoletti performed MALDI-TOF measurements. Larissa Limmer conceptualised the studies, performed the synthesis and characterisation of the monomers and polymers, performed the hydrophobicity/oleophobicity studies and wrote the chapter.

Sandra Schüttner and Philipp Holzmüller were involved in the polymer synthesis of **chapter 4**. Philipp Holzmüller was additionally involved in writing of the chapter. Prof. M. Kevin Brown was involved in the design of the polymer functionalisation. Dr. Elena Berger-Nicoletti performed MALDI-TOF measurements. Larissa Limmer conceptualised the studies, performed the synthesis and characterisation and wrote the chapter.

[redacted] wrote the patent text presented in **chapter A1** with support by Larissa Limmer and Prof. Dr. Holger Frey. Dr. Reiner Friedrich performed the surface

tension measurements. Larissa Limmer conceptualised the studies and performed the synthesis, characterisation, and hydrophobicity studies. Tom Reimers was involved in synthesis and characterisation.

Abbreviations

9-BBN	9-borabicyclo[3.3.1]nonane
AA	anti-agglomerant
AATCC	*American Association of Textile Chemists & Colorists*
AROP	anionic ring-opening polymerisation
AzGA	azepane glycidyl amine
BCy_2	dicyclohexylborane
BMEGA	*N*,*N*-bis(2-methoxyethyl) glycidyl amine
BMGA	*N*-benzyl-*N*-methyl glycidyl amine
BNCT	boron neutron capture therapy
Bora	borinane
BPin	4,4,5,5-tetramethyl-1,2,2-dioxoboryl / pinacol borane
cmc	critical micelle concentration
DAGA	*N*,*N*-diallyl glycidyl amine
DBAG	*N*,*N*-dibenzyl amino glycidol
DButGA	*N*,*N*-di(*n*-butyl) glycidyl amine
DEGA	*N*,*N*-diethyl glycidyl amine
DHexGA	*N*,*N*-di(*n*-hexyl) glycidyl amine
DOctGA	*N*,*N*-di(*n*-octyl) glycidyl amine
ECHA	*European Chemicals Agency*
EO	ethylene oxide
EPA	Environmental Protection Agency (US)
GA	glycidyl amine
GE	glycidyl ether
GLY	glycidyl
GM	*N*-glycidyl morpholine
HPEI-R-AO	hyperbranched polyethyleneimine-alkyl-amine *N*-oxides
ISO	International Organisation for Standardization
KHI	kinetic hydrate inhibitor
LCST	lower critical solution temperature
LDHI	low-dosage hydrate inhibitors
MAROP	monomer-activated anionic ring-opening polymerisation
M_n	number average molar mass
M_w	weight average molar mass
PEG	poly(ethylene glycol) / poly(ethylene oxide)
PEI	polyethylenimine
PFAS	per- and polyfluoroalkyl substances
PFCA	perfluoroalkyl carboxylic acid
PFECA	polyfluorinated ether carbonic acid
PFESA	polyfluorinated ether sulfonate
PFOA	perfluorooctanoic acid
PFOS	perfluorooctanesulfonic acid
PFPrA	perfluorpropionic acid

PGA	poly(glycidyl amine)
PGAO	poly(glycidyl amine-*N*-oxide)
PiGA	piperidine glycidyl amine
PMVE	perfluoromethyl vinyl ether
P_n	degree of polymerisation
PolyNPyMA	poly(*N*-acryloyl-2-pyrrolidone)
POM	polyoxymethylene
POP	persistent organic pollutants
PPO	polypropylene glycol / polypropylene oxide
PPVE	perfluoropropyl vinyl ether
PTFE	polytetrafluoroethylene
PVCap	poly(N-vinylcaprolactam)
PVP	polyvinylpyrrolidone
PyGA	isopropyl-hexahydro-pyrimidine glycidyl amine
PyrGA	pyrrolidinyl glycidyl amine
REACH	*Registration, Evaluation, Authorisation and Restriction of Chemicals*
SEC	size-exclusion chromatography
T_a	rapid hydrate formation temperature
TBAO	tributylamine *N*-oxide
T_{cl}	cloud point
TEB	triethylborane
T_{eq}	hydrate equilibrium temperature
T_g	glass transition temperature
T_m	melting point
T_o	onset temperature
TOP assay	total oxidisable pressures assay
T_{sub}	subcooling

Motivation and Objectives

Polyethers are used all over the world in a multitude of applications. However, to target all those areas various specific properties are required. These polymer properties are highly dependent on the side chains, which are incorporated through substituted epoxide monomers. Poly(ethylene glycol) (PEG) is one of the most prominent polyethers and simultaneously the structurally simplest polyether, bearing no side chains at all. Due to its excellent solubility in water PEG is used, for example, as hydrophilic parts in surfactants, while in consequence of its biocompatible properties it is used in biomedical applications such as PEGylation.[1,2] Nonetheless, PEG exhibits a low functionality with only up to two possible functional groups. A strategy to overcome this problematic is the use of substituted epoxides. Consequently, this thesis studies substituted polyethers and the different sections of this work present their synthesis via anionic ring-opening polymerisation techniques to achieve application-oriented materials.

Section 2 is dealing with polyethers bearing nitrogen atoms in their side chains. Amino-functionalities enable pH-responsive behaviour and may incorporate the ability to bind nucleic acids through electrostatic interactions as shown by polyethyleneimine (PEI). PEI is the gold standard for transfection via non-viral vectors,[3,4] but also bears cytotoxicity.[5] In consequence, research is conducted to balance the transfection activity and the cytotoxicity of polyamines.[6,7] Chapter 2.1 explores amino-functionalities in copolymers with ethylene oxide (EO) in search of a combination of the transfection ability of amines and the biocompatibility of PEG. Due to the toxicity of polyamines depending on the charge density,[8] a reduced toxicity by diluting the amine density with EO units was expected. Furthermore, the immunogenicity of PEG is shown to be introduced by a epitope of at least 4 to 5 repeating units of EO.[9] Interrupting these potential epitopes with the comonomer was expected to prevent immunogenicity. Copolymer series of glycidyl amines and EO with different comonomer ratios as well as different amino-functional monomers were synthesised and investigated for their toxicity as well as their interactions with nucleic acids and cells. Chapters 2.2 and 2.3 focusses on amine-*N*-oxide functionalities and their application as kinetic gas hydrate inhibitors (KHI). Oil production and flow lines in offshore or cold climate regions have to deal with clogging of the equipment by gas clathrate hydrates. Additives are used to assure the fluids flow and prevent damages of the system. For this purpose, most efficient and cost-effective are KHIs, which delay the hydrate formation even in small concentrations.[10] Typically used are water

soluble polymers bearing pendant amide functionalities such as poly(*N*-vinylcaprolactam) (PVCap).[11] Though amine-*N*-oxides were also found to inhibit hydrate nucleation, it is only a little explored class of KHIs.[12,13] The monomers and polymers introduced in chapter 2.1 bear the ability for post-polymerisation oxidation yielding amine-*N*-oxides. The substitution of the hydrocarbon backbone of established KHIs with a polyether backbone grants a typical biocompatible backbone[14] with better degradation properties.[15,16] Furthermore, the established polymers often show low solubility compatibility with the injection conditions of the applications.[17,18] It was expected that the *N*-oxide functionality and the polyether backbone will lead to better solubility properties and therefore an increased compatibility. Chapter 2.2 introduces the concept of poly(glycidyl amine-*N*-oxides)s as KHIs. Chapter 2.3 further explores the effect of different pendant groups located at the nitrogen atom.

Section 3 deals with polyethers bearing polyfluorinated side chains. Organo fluor compounds exhibit special properties originating from the highly stable and poorly polarizable fluor-carbon bond.[19,20] These render poly- and perfluorinated substances (PFAS) to be excellent surface-active substances in aqueous as well as in organic media.[21] In consequence, PFAS in combination with a polar headgroup are efficient surfactants,[21] while PFAS side groups in polymers enable anti-stick coatings for textiles,[22] optical elements[23] and more.[23–25] Nevertheless, the major drawbacks of persistence,[26] bioaccumulation[27] and toxicity[28] of PFAS or their degradation products led to concerns and subsequent governmental restrictions.[29–31] These drawbacks are increasing with the fluorinated chain-length.[32,33] Because PFAS cannot easily be substituted by non-fluorinated compounds, fluorinated alternatives are required[21,34] and currently in development.[35–37] Chapter 3 presents polymers derived from epoxides with degradable polyfluorinated side chains[38] for application as surfactants and surface coatings. The use of multiple polyfluorinated chains in the polymer was expected to allow a short polyfluorinated chain-length while maintaining the surface activity of small-molecule long-chain PFAS. A surfactant series of copolymers consisting of the degradable, short-chain monomer in combination with hydrophilic comonomers was synthesised and studied for their ability to reduce the surface energy of water. Furthermore, these fluorinated monomers were combined with hydrophobic comonomers to yield omniphobic polymers. Subsequently, the polymers were used to coat cellulose and glass surfaces and the resulting water- and oil-

repellencies were explored. In contrast to the other chapters, all polymers of this chapter were synthesised via monomer-activated anionic ring-opening polymerisation (MAROP), due to the monomers being unreactive or unstable under the conditions of the anionic ring-opening polymerisation (AROP).

Section 4 investigates polyethers with pendant borane groups. Organo boranes are a versatile functional group and are available for post-polymerisation modifications like the prominent oxidation to anti-Markovnikov alcohols[39]. The use of pinacolboranes enables boronic acid synthesis,[40] which are known for biomedical applications,[41] or for formation of hydrogels[42] and thermosets[43] by boronic ester or boroxine formation, respectively. Additionally, organo boranes themselves are utilised as catalyst in the polymerisation of epoxides (MAROP), carbon dioxide and cyclic anhydrides.[44,45] These polymerisations typically use excess of small molecule aluminium or borane compounds, which can be hard to remove[46,47] as seen in section 3. If the catalyst is covalently linked to a polymer, an easy purification via precipitation of either the catalyst or the polymerisation product was expected. This would allow furthermore the recycling of the catalyst, which is a valuable ability due to the use ion excess. This chapter describes the synthesis of polymeric organo boranes via poly(allyl glycidyl ether), the derivatisation to polymeric boronic acids, and the utilisation of organo boranes as a recyclable catalyst in the polymerisation of epoxides as well as copolymerisation of epoxides and carbon dioxide.

References

(1) Herzberger, J.; Niederer, K.; Pohlit, H.; Seiwert, J.; Worm, M.; Wurm, F. R.; Frey, H. Polymerization of Ethylene Oxide, Propylene Oxide, and Other Alkylene Oxides: Synthesis, Novel Polymer Architectures, and Bioconjugation. *Chemical reviews* **2016**, *116* (4), 2170–2243. DOI: 10.1021/acs.chemrev.5b00441.

(2) Dingels, C.; Schömer, M.; Frey, H. Die vielen Gesichter des Poly(ethylenglykol)s. *Chemie in unserer Zeit* **2011**, *45* (5), 338–349. DOI: 10.1002/ciuz.201100551.

(3) Patil, S. D.; Rhodes, D. G.; Burgess, D. J. DNA-based therapeutics and DNA delivery systems: a comprehensive review. *The AAPS journal* **2005**, *7* (1), E61-77. DOI: 10.1208/aapsj070109.

(4) Luo, D.; Saltzman, W. M. Synthetic DNA delivery systems. *Nat Biotechnol* **2000**, *18* (1), 33–37. DOI: 10.1038/71889.

(5) Florea, B. I.; Meaney, C.; Junginger, H. E.; Borchard, G. Transfection efficiency and toxicity of polyethylenimine in differentiated Calu-3 and nondifferentiated COS-1 cell cultures. *AAPS J* **2002**, *4* (3), E12. DOI: 10.1208/ps040312.

(6) Leclercq, F.; Dubertret, C.; Pitard, B.; Scherman, D.; Herscovici, J. Synthesis of glycosylated polyethylenimine with reduced toxicity and high transfecting efficiency. *Bioorganic & medicinal chemistry letters* **2000**, *10* (11), 1233–1235. DOI: 10.1016/s0960-894x(00)00195-5.

(7) Petersen, H.; Fechner, P. M.; Fischer, D.; Kissel, T. Synthesis, Characterization, and Biocompatibility of Polyethylenimine- graft -poly(ethylene glycol) Block Copolymers. *Macromolecules* **2002**, *35* (18), 6867–6874. DOI: 10.1021/ma012060a.

(8) Hsiue, G.-H.; Chiang, H.-Z.; Wang, C.-H.; Juang, T.-M. Nonviral gene carriers based on diblock copolymers of poly(2-ethyl-2-oxazoline) and linear polyethylenimine. *Bioconjugate chemistry* **2006**, *17* (3), 781–786. DOI: 10.1021/bc050317u.

(9) Armstrong, J. K. The occurrence, induction, specificity and potential effect of antibodies against poly(ethylene glycol). In *PEGylated Protein Drugs: Basic Science and Clinical Applications*; Birkhäuser Basel, 2009; pp 147–168. DOI: 10.1007/978-3-7643-8679-5_9.

(10) Kelland, M.; Svartaas, T. M.; Dybvik, L. A. Control of Hydrate Formation by Surfactants and Polymers. In *SPE Annual Technical Conference and Exhibition*; Society of Petroleum Engineers, 1994. DOI: 10.2118/28506-MS.

(11) Kelland, M. A. History of the Development of Low Dosage Hydrate Inhibitors. *Energy Fuels* **2006**, *20* (3), 825–847. DOI: 10.1021/ef050427x.

(12) Kelland, M. A.; Magnusson, C.; Lin, H.; Abrahamsen, E.; Mady, M. F. Acylamide and Amine Oxide Derivatives of Linear and Hyperbranched Polyethylenimine. Part 2: Comparison of Gas Kinetic Hydrate Inhibition Performance. *Energy Fuels* **2016**, *30* (7), 5665–5671. DOI: 10.1021/acs.energyfuels.6b01519.

(13) Magnusson, C. D.; Kelland, M. A. Nonpolymeric Kinetic Hydrate Inhibitors: Alkylated Ethyleneamine Oxides. *Energy Fuels* **2015**, *29* (10), 6347–6354. DOI: 10.1021/acs.energyfuels.5b01592.

(14) Knop, K.; Hoogenboom, R.; Fischer, D.; Schubert, U. S. Poly(ethylene glycol) in drug delivery: pros and cons as well as potential alternatives. *Angewandte Chemie (International ed. in English)* **2010**, *49* (36), 6288–6308. DOI: 10.1002/anie.200902672.

(15) McGary, C. W. Degradation of poly(ethylene Oxide). *Journal of Polymer Science* **1960**, *46*, 51–57.

(16) Albertsson, A.; Karlsson, S. The influence of biotic and abiotic environments on the degradation of polyethylene. *Progress in Polymer Science* **1990**, *15* (2), 177–192. DOI: 10.1016/0079-6700(90)90027-X.

(17) Kelland, M. A.; Mønig, K.; Iversen, J. E.; Lekvam, K. Feasibility Study for the Use of Kinetic Hydrate Inhibitors in Deep-Water Drilling Fluids. *Energy Fuels* **2008**, *22* (4), 2405–2410. DOI: 10.1021/ef800109e.

(18) Kelland, M. A.; Iversen, J. E. Kinetic Hydrate Inhibition at Pressures up to 760 Bar in Deep Water Drilling Fluids. *Energy Fuels* **2010**, *24* (5), 3003–3013. DOI: 10.1021/ef9016152.

(19) O'Hagan, D. Understanding organofluorine chemistry. An introduction to the C-F bond. *Chemical Society reviews* **2008**, *37* (2), 308–319. DOI: 10.1039/b711844a. Published Online: Oct. 17, 2007.

(20) Lemal, D. M. Perspective on fluorocarbon chemistry. *The Journal of organic chemistry* **2004**, *69* (1), 1–11. DOI: 10.1021/jo0302556.

(21) Kissa, E. *Fluorinated surfactants and repellents*, 2. ed., rev. and expanded.; Surfactants science series, Vol. 97; Dekker, 2001.

(22) Kim, H.-A. Water Repellency/Proof/Vapor Permeability Characteristics of Coated and Laminated Breathable Fabrics for Outdoor Clothing. *Coatings* **2022**, *12* (1), 12. DOI: 10.3390/coatings12010012.

(23) Friedrich, R. Fluorine compounds. 17/377,912.

(24) Quéré, D. Non-sticking drops. *Rep. Prog. Phys.* **2005**, *68* (11), 2495–2532. DOI: 10.1088/0034-4885/68/11/R01.

(25) Murata, H.; Chang, B.-J.; Prucker, O.; Dahm, M.; Rühe, J. Polymeric coatings for biomedical devices. *Surface Science* **2004**, *570* (1-2), 111–118. DOI: 10.1016/j.susc.2004.06.185.

(26) Pickard, H. M.; Criscitiello, A. S.; Persaud, D.; Spencer, C.; Muir, D. C. G.; Lehnherr, I.; Sharp, M. J.; Silva, A. O. de; Young, C. J. Ice Core Record of Persistent Short-Chain Fluorinated Alkyl Acids: Evidence of the Impact From Global Environmental Regulations. *Geophys. Res. Lett.* **2020**, *47* (10). DOI: 10.1029/2020GL087535.

(27) Pérez, F.; Nadal, M.; Navarro-Ortega, A.; Fàbrega, F.; Domingo, J. L.; Barceló, D.; Farré, M. Accumulation of perfluoroalkyl substances in human tissues.

Environment international **2013**, *59*, 354–362. DOI: 10.1016/j.envint.2013.06.004. Published Online: Jul. 25, 2013.

(28) Bartell, S. M.; Vieira, V. M. Critical review on PFOA, kidney cancer, and testicular cancer. *Journal of the Air & Waste Management Association (1995)* **2021**, *71* (6), 663–679. DOI: 10.1080/10962247.2021.1909668.

(29) US EPA. *Fact Sheet: 2010/2015 PFOA Stewardship Program* | *US EPA*. https://www.epa.gov/assessing-and-managing-chemicals-under-tsca/fact-sheet-20102015-pfoa-stewardship-program (accessed 2022-12-17).

(30) UN Stockholm Convention. *Listing of POPs in the Stockholm Convention*. http://www.pops.int/TheConvention/ThePOPs/AllPOPs/tabid/2509/Default.aspx (accessed 2022-12-18).

(31) Europoean Chemicals Agency. *Substances restricted under REACH - ECHA*. https://echa.europa.eu/substances-restricted-under-reach (accessed 2022-12-18).

(32) Ohmori, K.; Kudo, N.; Katayama, K.; Kawashima, Y. Comparison of the toxicokinetics between perfluorocarboxylic acids with different carbon chain length. *Toxicology* **2003**, *184* (2-3), 135–140. DOI: 10.1016/S0300-483X(02)00573-5.

(33) Martin, J. W.; Mabury, S. A.; Solomon, K. R.; Muir, D. C. G. Bioconcentration and tissue distribution of perfluorinated acids in rainbow trout (Oncorhynchus mykiss). *Environ Toxicol Chem* **2003**, *22* (1), 196–204. DOI: 10.1002/etc.5620220126.

(34) Peshoria, S.; Nandini, D.; Tanwar, R. K.; Narang, R. Short-chain and long-chain fluorosurfactants in firefighting foam: a review. *Environ Chem Lett* **2020**, *18* (4), 1277–1300. DOI: 10.1007/s10311-020-01015-8.

(35) Folkerson, A. P.; Joudan, S.; Mabury, S. A.; D'eon, J. C. In Vivo Transformation of a Novel Polyfluoroether Surfactant. *Environmental toxicology and chemistry* **2021**, *40* (12), 3328–3336. DOI: 10.1002/etc.5230. Published Online: Nov. 8, 2021.

(36) Friedrich, R.; Osthoff, J. Fluorinated tensides. 15/120,288.

(37) Kredel, J.; Gallei, M. Ozone-Degradable Fluoropolymers on Textile Surfaces for Water and Oil Repellency. *ACS Appl. Polym. Mater.* **2020**, *2* (7), 2867–2879. DOI: 10.1021/acsapm.0c00400.

(38) Friedrich, R.; Koch, F. Fluorine compounds. 17/357,193.

(39) Adams, J.; Gronski, W. LC side chain AB-block copolymers with an amorphous A-block and a liquid-crystalline B-block. *Die Makromolekulare Chemie, Rapid Communications* **1989**, *10*, 553–557.

(40) Hinkes, S. P. A.; Klein, C. D. P. Virtues of Volatility: A Facile Transesterification Approach to Boronic Acids. *Organic letters* **2019**, *21* (9), 3048–3052. DOI: 10.1021/acs.orglett.9b00584. Published Online: Apr. 23, 2019.

(41) Cambre, J. N.; Sumerlin, B. S. Biomedical applications of boronic acid polymers. *Polymer* **2011**, *52* (21), 4631–4643. DOI: 10.1016/j.polymer.2011.07.057.

(42) Yang, H.-S.; Cho, S.; Eom, Y.; Park, S.-A.; Hwang, S. Y.; Jeon, H.; Oh, D. X.; Park, J. Preparation of Self-Healable and Spinnable Hydrogel by Dynamic Boronate Ester Bond from Hyperbranched Polyglycerol and Boronic Acid-Containing Polymer. *Macromol. Res.* **2021**, *29* (2), 140–148. DOI: 10.1007/s13233-021-9016-5.

(43) Yang, X.; Guo, M.; Wu, Y.; Xue, S.; Li, Z.; Zhou, H.; Smith, A. T.; Sun, L. Biomimetic Boroxine-Based Multifunctional Thermosets via One-Pot Synthesis. *ACS applied materials & interfaces* **2020**, *12* (50), 56445–56453. DOI: 10.1021/acsami.0c16736. Published Online: Dec. 2, 2020.

(44) Zhang, D.; Boopathi, S. K.; Hadjichristidis, N.; Gnanou, Y.; Feng, X. Metal-Free Alternating Copolymerization of CO2 with Epoxides: Fulfilling "Green" Synthesis and Activity. *Journal of the American Chemical Society* **2016**, *138* (35), 11117–11120. DOI: 10.1021/jacs.6b06679. Published Online: Aug. 26, 2016.

(45) Xie, R.; Zhang, Y.-Y.; Yang, G.-W.; Zhu, X.-F.; Li, B.; Wu, G.-P. Record Productivity and Unprecedented Molecular Weight for Ring-Opening Copolymerization of Epoxides and Cyclic Anhydrides Enabled by Organoboron Catalysts. *Angewandte Chemie (International ed. in English)* **2021**, *60* (35), 19253–19261. DOI: 10.1002/anie.202104981. Published Online: Jul. 19, 2021.

(46) Müller, S. S.; Moers, C.; Frey, H. A Challenging Comonomer Pair: Copolymerization of Ethylene Oxide and Glycidyl Methyl Ether to Thermoresponsive Polyethers. *Macromolecules* **2014**, *47* (16), 5492–5500. DOI: 10.1021/ma501280k.

(47) Patil, N.; Bhoopathi, S.; Chidara, V.; Hadjichristidis, N.; Gnanou, Y.; Feng, X. Recycling a Borate Complex for Synthesis of Polycarbonate Polyols: Towards an Environmentally Friendly and Cost-Effective Process. *ChemSusChem* **2020**, *13* (18), 5080–5087. DOI: 10.1002/cssc.202001395. Published Online: Jul. 30, 2020.

Abstract

This work deals with the design, synthesis, and characterisation of application-oriented multifunctional polyethers. To this end, state of the art concepts in the areas of transfection agents, hydrate inhibitors, surface active polyfluoro-compounds, and organoborane compounds as polymerisation catalysts were developed further and applied in form of polyethers.

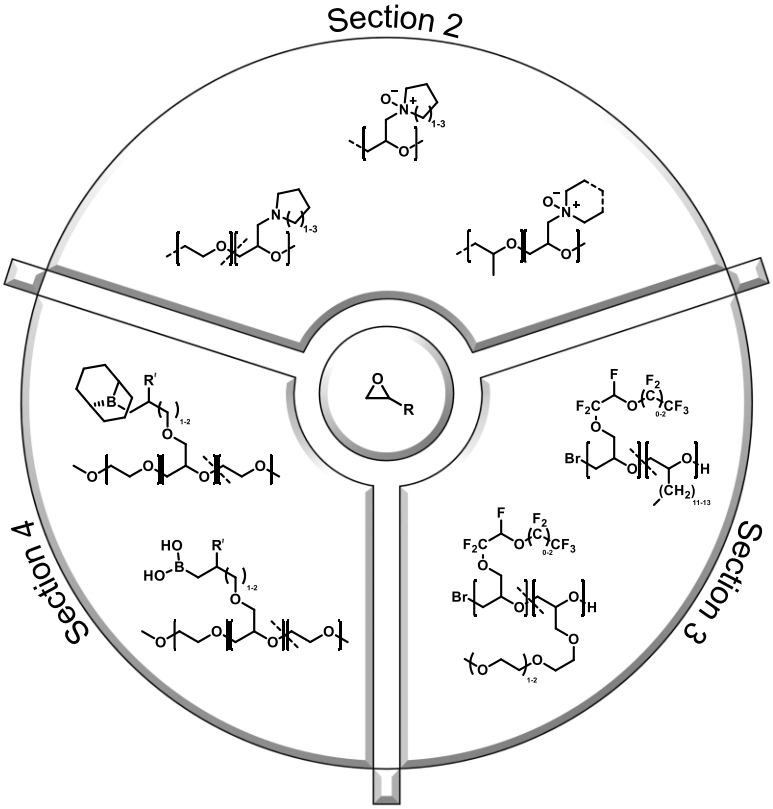

Scheme 1: Overview of the topics.

Beginning with the theoretical background of this work, section 1 first gives a brief introduction to polyethers and their, for this work relevant, synthesis strategies. The use of organoboranes in catalytic polymerisations and their chemical versatility is discussed. In the following, further targeted applications of in this work developed polymers are introduced. This part deals on the one hand with polyelectrolytes as cationic transfection agents as well as kinetic hydrate inhibitors (KHI) in fluid applications. On the other hand, organofluorine compounds are presented in the context of their properties, ecological risks, current development, and their application as surfactants as well as surface coatings.

Section 2 deals with amino-functional polyethers and is divided in their application as transfection agent and as KHI.

Chapter 2.1 investigates poly(glycidyl amine)s in a biomedical context. Series of copolymers with increasing ratio of amino-functionalities were synthesised via copolymerisation of ethylene oxide (EO) and a variety of glycidyl amines. This procedure enables adjustment of the amino group density and as a direct consequence the adjustment of the charge density, which is an important factor for transfection agents. Subsequently, the polymers toxicity as well as their abilities to complex desoxyribonucleic acid (DNA), transfer it into cells and allow protein synthesis were studied. The efficiency of complexation and transportation into cells increased with decreasing size of the amine substituents. Nonetheless, the ultimate aim of protein biosynthesis using the transfected DNA was not achieved with this system.

Chapter 2.2 introduces poly(glycidyl amine-*N*-oxide)s (PGAO) as kinetic hydrate inhibitors and chapter 2.3 develops this concept further by studying the structure-activity relationship of a variety of substituents. Both chapters begin with the synthesis of PGAO via anionic ring-opening polymerisation (AROP) and subsequent oxidation. Chapter 2.3 additionally introduces azepane glycidyl amine as a monomer for AROP. The PGAOs ability to delay gas hydrate formation and to decrease their growth rate was studied utilising a high-pressure rocking rig and a structure II hydrate-forming gas mixture. Chapter 2.2 focusses on diethylamino- and the 6-membered piperidine substituents and compares KHI-activities of homo- and blockcopolymer with polypropylene oxide as a synergistic block. Chapter 2.3 studies the influence of the substituent´s ring size (5- to 7-membered) as well as of the initiator (aromatic or aliphatic) and the necessity of the amine-oxidation itself.

Section 3 presents a collaboration with the German company Merck KGaA regarding surface active polyethers, which bear degradable polyfluorinated side chains. Utilising the monomer activated anionic ring-opening polymerisation (MAROP), series of copolymers derived from epoxides bearing the polyfluorinated side chain and either hydrophilic or hydrophobic epoxides were synthesised. This yielded on the one hand amphiphilic surfactant structures, which were studied for their ability to reduce the surface tension of water. On the other hand, omniphobic copolymers were gained, which were used to coat surfaces and were studied for their repellency of liquids. Furthermore, their thermal properties were studied. Systematic variation of

the comonomer ratio allowed tuning of the surface activity properties. *In situ* ^{1}H NMR kinetic studies revealed a weak gradient in the polymer microstructure.

In regard to the MAROP used in the previous section, section 4 studies organoborane bearing polyethers as alternative polymerisation catalysts. Initially, double bond bearing polyethers were synthesised via AROP. These double bonds were used in hydroboration reactions to yield either boronic esters or dialkylboranes. Acidic cleavage of the boronic esters yielded boronic acids, a versatile functional group. The dialkylborane bearing polyethers were studied as a polymeric alternative of small molecule aluminium or borane catalysts in polymerisations. The scope of the polymeric catalysts was examined by synthesising amorphous poly(propylene oxide) and crystalline poly (epoxytetradecane) as representatives of polyethers as well as poly(cyclohexane carbonate). Furthermore, the recyclability of the catalyst was demonstrated.

Appendix

Chapter A1 presents results based on section 3 in an industrial context. The invention of surface active polyethers bearing degradable polyfluorinated side chains has been filed for an European patent.

Zusammenfassung

Diese Arbeit behandelt das Design, die Synthese und die Charakterisierung von anwendungsbezogenen multifunktionellen Polyethern. Zu diesem Zweck wurden aktuelle Konzepte in den Bereichen der Transfektionsreagenzien, Hydratinhibitoren, oberflächenaktiven Polyfluorverbindungen, sowie bororganische Verbindungen als Polymerisationskatalysatoren weiterentwickelt und anhand von Polyethern praktisch umgesetzt.

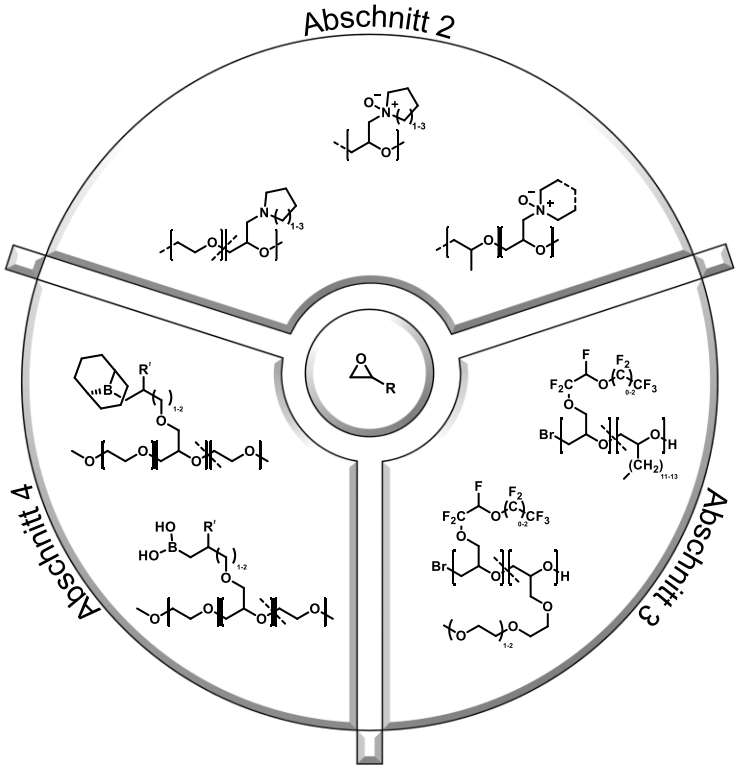

Schema 1: Übersicht der Themenabschnitte dieser Arbeit.

Abschnitt 1 erläutert die theoretischen Hintergründe dieser Arbeit. Zunächst wird eine kurze Einführung zu Polyethern und deren, in dieser Arbeit angewendeten, Synthesestrategien gegeben. In diesem Kontext wird zudem die Verwendung von Organoboranen in katalytischen Polymerisationen und ihre chemische Vielseitigkeit behandelt. Im Nachfolgenden wird auf weitere angezielte Anwendungen der in dieser Arbeit entwickelten Polyether eingegangen. Hierbei werden Polyelektrolyte anhand als kationischer Transfektionsreagenzien sowie als kinetische Hydratinhibitoren (KHI) in Flüssigkeitsanwendungen diskutiert. Nachfolgend wird auf organische Fluorverbindungen hinsichtlich ihrer Eigenschaften, Risiken, Weiterentwicklung und Anwendungen als Tenside und Oberflächenbeschichtungen eingegangen.

Abschnitt 2 behandelt aminofunktionelle Polyether und ist in die Anwendungen als Transfektionsreagenzien und als KHI aufgeteilt.

Kapitel 2.1 untersucht Poly(glycidylamin)e (PGA) im biomedizinischen Kontext. Durch Copolymerisation von verschiedener Glycidylaminen mit Ethylenoxid (EO) wurden Serien von Copolymeren mit steigendem Anteil an Amino-Funktionen im Polymer hergestellt. Dies ermöglichte eine direkte Beeinflussung der Aminogruppen- und damit der Ladungsdichte, was einen wichtigen Faktor für Transferreagenzien darstellt. Nachfolgend wurden diese Polymere hinsichtlich ihrer Toxizität als auch ihrer Fähigkeiten Desoxyribonucleinsäure (DNA) zu komplexieren, diese in Zellen zu transportieren und Proteinbiosynthese zu ermöglichen untersucht. Die Effizienz der DNA-Komplexierung als auch des Transports in Zellen stieg mit Abnahme der Größe der Aminsubstituenten. Nichtsdestotrotz wurde mit diesem System keine Proteinbiosynthese erreicht.

Kapitel 2.2 führt Poly(glycidylamin-*N*-oxid)e (PGAO) als kinetische Hydratinhibitoren ein. Nachfolgend entwickelt Kapitel 2.3 das Konzept anhand verschiedener Substitutionen weiter und untersucht Struktur-Wirkungsbeziehungen. Beide Kapitel behandeln zunächst die Synthese der PGAO mittels anionischer Ringöffnungs-Polymerisation (AROP) und nachfolgender Oxidation, wobei in Kapitel 2.3 Azepanglycidylamin als Monomer vorgestellt wird. Die PGAOs wurden mittels einer Hochdruckapparatur und einer Struktur II Hydrat-formenden Gasmischung hinsichtlich ihrer Fähigkeit zur Verzögerung der Ausbildung von Gashydraten und Verringerung deren Wachstumsgeschwindigkeit untersucht. Kapitel 2.2 fokussiert sich hierbei auf Diethylamin- und den 6-gliedrigen Piperidin-Substituenten und vergleicht KHI-Aktivitäten in Homo- und Blockcopolymerstrukturen mit Polypropylenoxid als synergistischen Block. Kapitel 2.3 untersucht die Einflüsse der Ringgröße des Substituenten (5- bis 7-gliedrig), des Initiators (aromatisch oder aliphatisch) sowie die Notwendigkeit der Oxidation des Amins.

Abschnitt 3 behandelt in Zusammenarbeit mit der deutschen Firma Merck KGaA hergestellte und untersuchte oberflächenaktive Polyether, die abbaubare polyfluorierte Seitenketten tragen. Mittels Monomer-aktivierter anionischer Ringöffnungs-Polymerisation (MAROP) wurden Copolymere aus Epoxiden mit fluorierten Seitenketten und aus hydrophilen oder hydrophoben Epoxiden synthetisiert. Die hierdurch einerseits entstandenen amphiphilen Tensidstrukturen

wurden hinsichtlich ihrer Fähigkeit die Oberflächenspannung von Wasser zu verringern untersucht. Die andererseits hergestellten omniphoben Copolymere wurden auf Oberflächen aufgetragen und hinsichtlich ihrer Eigenschaft der Flüssigkeitsabweisung getestet. Die oberflächenaktiven Eigenschaften konnten in beiden Anwendungsgebieten direkt durch die systematische Variation der Comonomeranteile eingestellt werden. Weiterhin wurde ein schwach ausgeprägter Gradient der Copolymer-Mikrostruktur mittels *in situ* 1H-NMR Kinetik Studien festgestellt.

Im Hinblick auf die in Abschnitt 3 verwendete MAROP wurden in Abschnitt 4 bororganische Polyether als alternative Katalysatoren untersucht. Zunächst wurden mittels AROP Doppelbindungs-funktionalisierte Polymere hergestellt. Anschließend wurden die Doppelbindungen durch Hydroborierung polymeranalog zu Borsäureestern oder Dialkylboranen umgesetzt. Die Borsäureester wurden anschließend zu Borsäuren hydrolysiert, eine vielseitig einsetzbare funktionelle Gruppe. Die Dialkylborane hingegen wurden als polymere Alternative zu niedermolekularen Aluminium- und Bor-Katalysatoren in Polymerisationen getestet. Um die Bandbreite des herstellten Katalysators zu zeigen, wurden das amorphe Polypropylenoxid und das kristalline Polyepoxytetradecan als Vertreter der Polyether sowie das Polycarbonat Poly(cyclohexancarbonat) hergestellt. Weiterhin wurde die gezeigt, dass die polymeren Katalysatoren für weitere Polymerisationen recycelt werden können.

Anhang

In Kapitel A1 werden auf Abschnittes 3 beruhende Ergebnisse zu oberflächenaktiven Polyethern mit abbaubaren polyfluorierten Seitenketten in einem industriellen Kontext als europäische Patentmeldung zusammengefasst.

Graphical Abstract

Graphical Abstract

Chapter 2.1

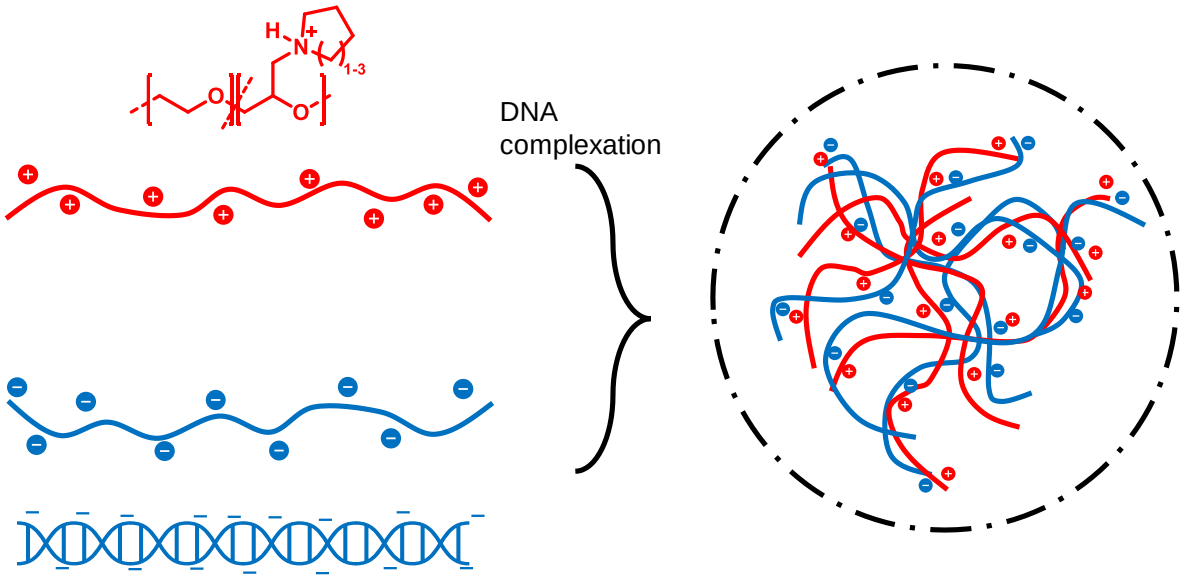

Chapter 2.2

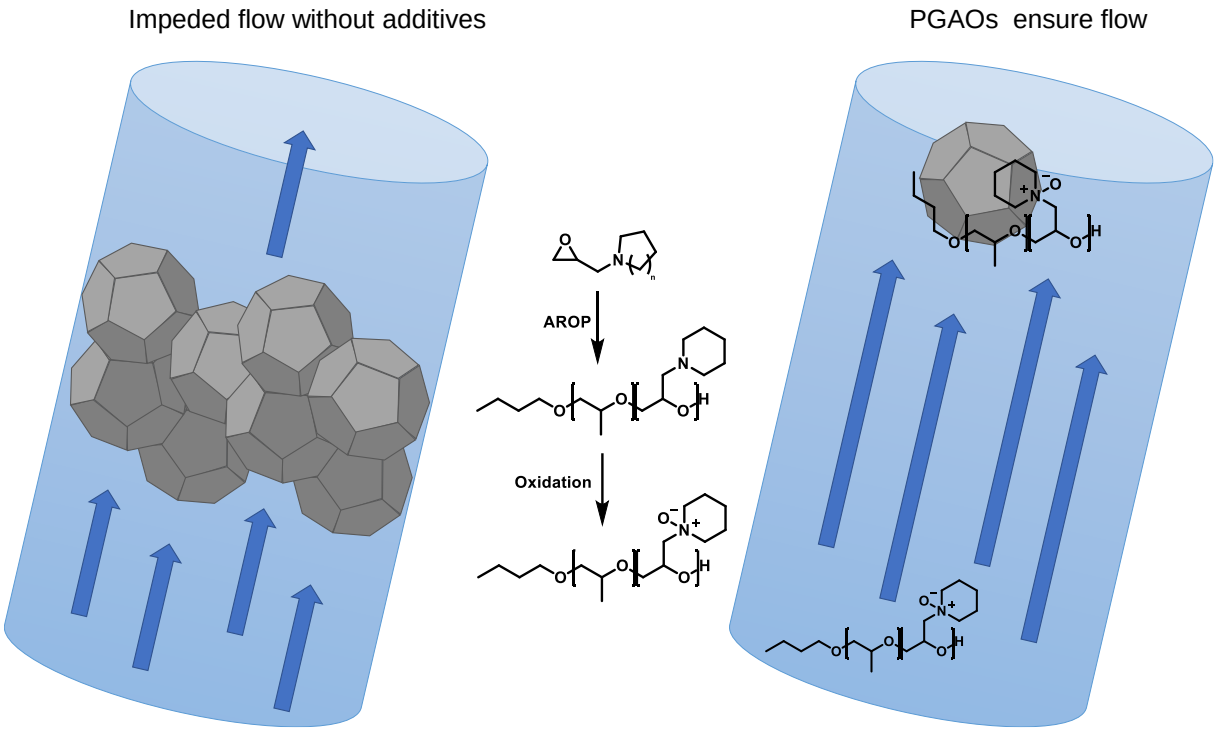

Chapter 2.3

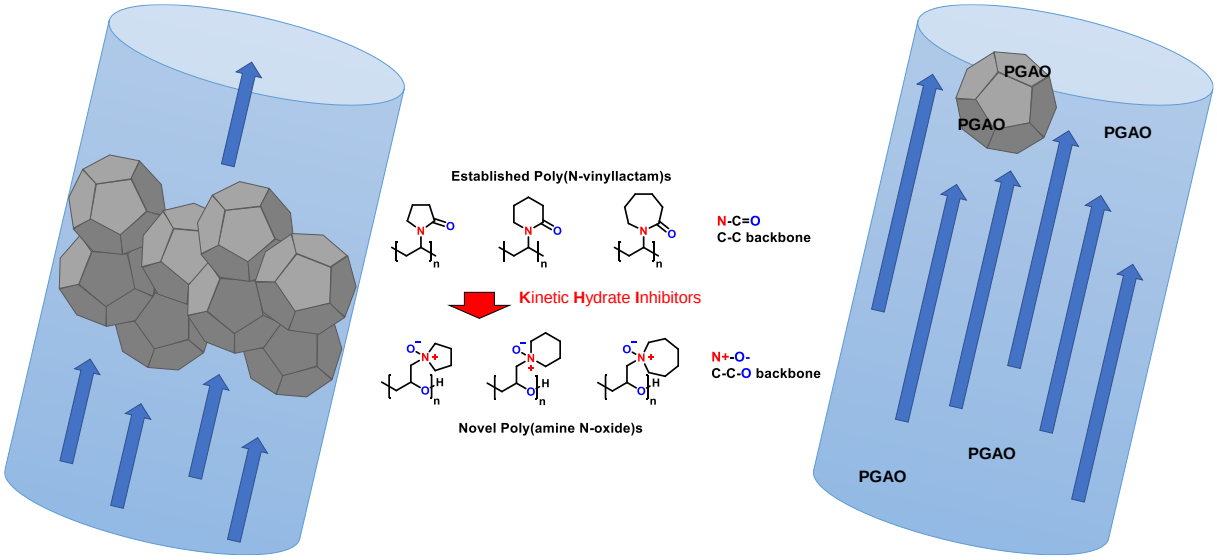

Chapter 3

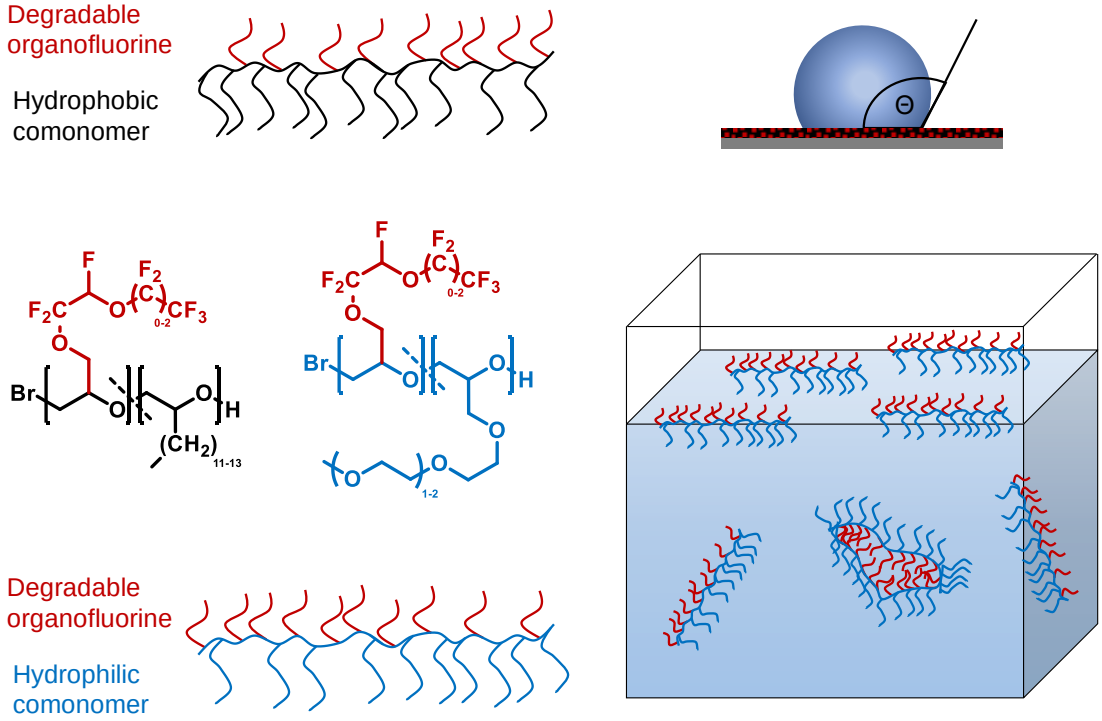

Chapter 4

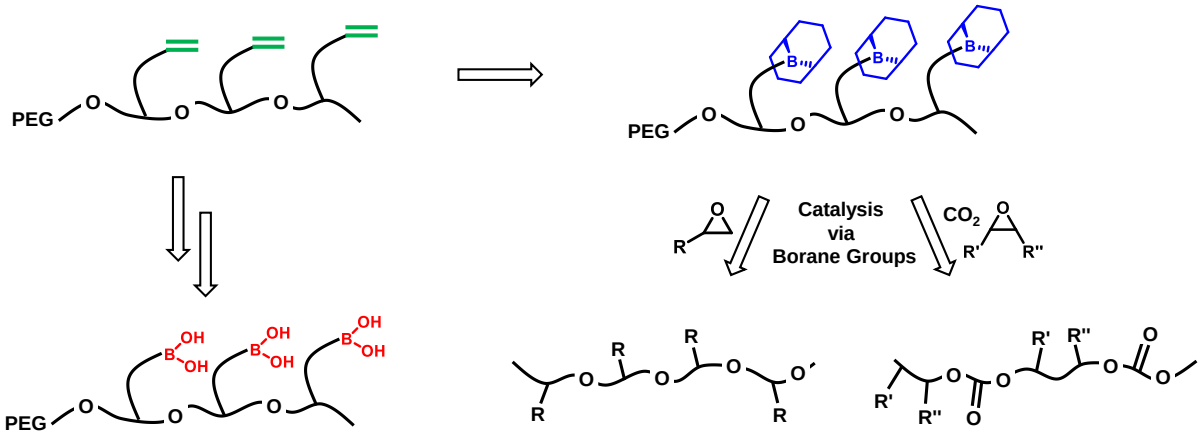
PEG
O
O
O
B
PEG
O
O
O
R
O
Catalysis
via
Borane Groups
CO2
O
R'
R''
PEG
O
O
O
OH
B
OH
OH
B
OH
OH
B
OH
R
O
R
O
O
O
R
R
R'
R''
O
O
O
R'
R''
O
O
O

1 – Introduction

This chapter gives an overview of the context and theoretical background of this thesis. First, a general introduction to polyethers and their polymerisation techniques as well as polymerisation behaviour is presented. Subsequently, the state of the art for the classes of polyethers specifically studied in this work are discussed regarding their synthesis, current applications, drawbacks, and opportunities.

1.1 Polyethers

Aliphatic polyethers are a wide class of polymers bearing an ether linkage in each repeating unit of the polymer backbone. These ether bonds grant the backbone high flexibility caused by the low rotation energy barrier of the carbon-oxygen bond (e.g. 11.3 kJ/mol for dimethyl ether in comparison to 13.8 kJ/mol for the carbon-carbon bond of propane) and a low excluded volume.[1] Common representatives are poly(ethylene glycol) (PEG), also well known as poly(ethylene oxide) (PEO), and poly(tetrahydrofuran). Substituted repeating units expend the spectra of polyethers of which poly(propylene oxide) (PPO), also known as poly(propylene glycol) (PPG) (Scheme 1) is of immense industrial relevance.

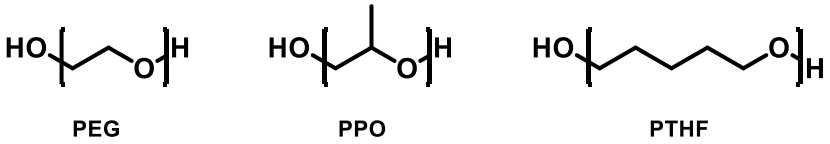

Scheme 1: Excerpt of industrial relevant polyethers.

The properties of the poly(epoxide)s are determined by their backbone substitution pattern. Characteristic for low molecular weight PEG is its excellent solubility in water caused by the oxygen distances in the backbone corresponding to those in liquid water.[2] Already the methylene groups of PPO impede the formation of hydrogen bonds with water, which leads to strongly reduced solubility. The polymer is not soluble above the so-called lower critical solution temperature (LCST).[2,3] Likewise, the thermal behaviour in bulk changes dramatically, when comparing PEO and PPO. For atactic PPO crystallisation is fully disabled, rendering it a viscous liquid with a glass transition temperature (T_g) of -73 °C.[4] Depending on the molecular weight, PEG itself possesses a T_g of -67 °C[5] and a melting temperature (T_m) of around 60 °C for high molecular weights[3,6].

PEG has a multitude of applications e.g., in pharmacy and cosmetics for the formulation of creams[3,6] and as a triblock copolymer with central PPO block, known

as poloxamer (tradename Pluronics®), it functions as a key polymer for non-ionic surfactants.[7] Furthermore, it is a gold standard in biomedical applications, e.g. for pegylation of active substances or proteins for the delivery in the human body. For a long time it was believed that PEG is highly biocompatible and either does not have any or exceptionally low toxicity or immunogenicity.[8] Nevertheless, in the last decades studies cast doubts on the immunogenicity, and anti-PEG antibodies were found with increasing abundance in human blood samples.[8–11]

1.2 Anionic ring-opening polymerisation

As early as in the 1860s it was known, that ethylene oxide (EO) can form consisting of multiple units.[12–14] Later it was found that either an alkaline, an acidic or a coordination catalyst could polymerise EO to yield PEG.[1] Especially the anionic ring-opening polymerisation (AROP) of EO is favourable. As early as 1940 Flory demonstrated a Poisson distribution for the molecular weight distribution of this reaction, which is an inherent characteristic of a “living” polymerisation.[15] A living polymerisation is characterised by the absence of termination or transfer reactions and an initiation reaction that is faster than the propagation. In consequence, all polymer chains grow simultaneously leading to a narrow dispersity given by M_w/M_n, where M_w is the weight average and M_n is the number average molar mass. Furthermore, the degree of polymerisation (P_n) is controlled solely by the initiator to monomer ratio.[16] The driving force of the polymerisation is the high ring strain of the epoxide monomers[17]: e.g. EO with 114.3 kJ mol^{-1} (for comparison: oxetane 106.7 kJ mol^{-1}, tetrahydrofuran 23.6 kJ mol^{-1}).[18,19]

The polymerisation of epoxides is typically carried out with a merely partially deprotonated initiator, leading to a major fraction of the initiator or respectively the propagating chain-ends being dormant. Nonetheless, because the proton transfer between the dormant and active sites I significantly faster than the propagation, chain growth of all polymers remains statistically identical.[20] In consequence these polymerisations are not strictly “living” but rather “controlled” polymerisations in analogy to controlled radical polymerisations.[16,21] Scheme 2 shows the general mechanism of the oxyanionic epoxide polymerisation: First, an alkoxide is formed, which opens an epoxide ring via nucleophilic attack, in consequence generating the propagating alkoxide species and ultimately leading to chain growth. The reaction can be terminated by addition of a protonating agent.

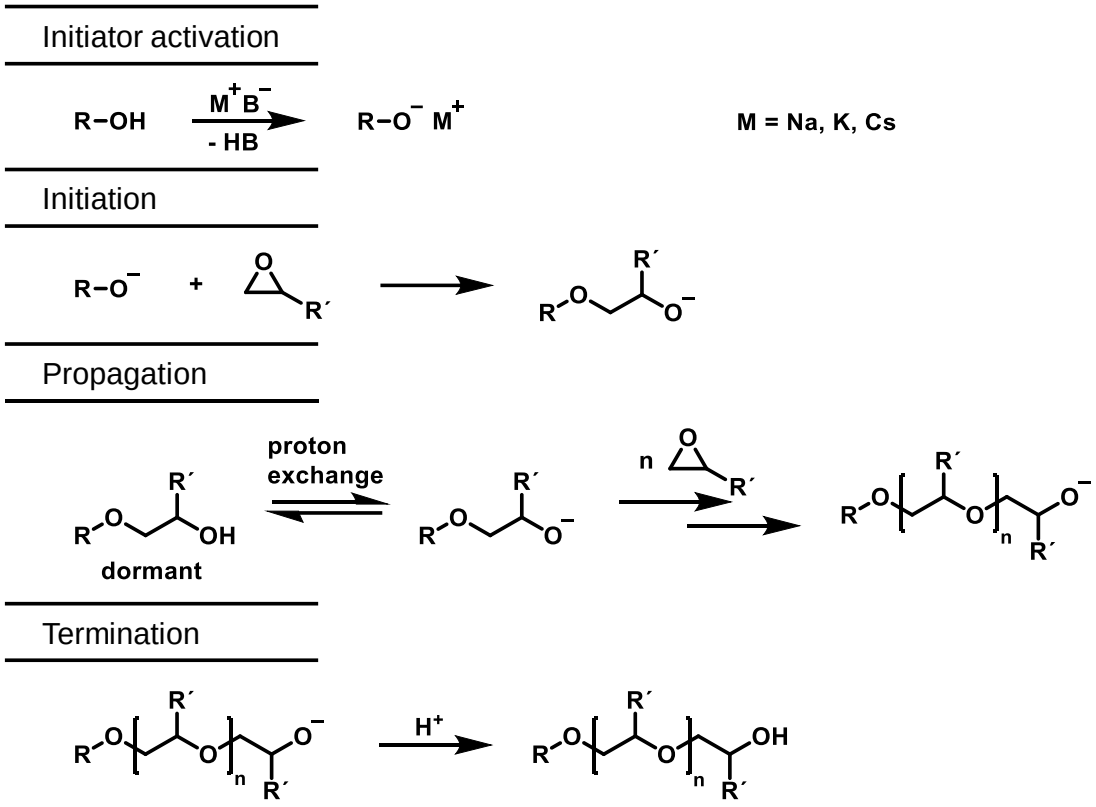

Scheme 2: General mechanism of the AROP of epoxides.

The reaction rate of the AROP is influenced by the binding strength of the counterion to the chain-end and increases with decreased binding strength. The Pearson[22] hard oxyanion forms a weaker bond to softer alkali metals like potassium or caesium, increasing the reaction rate. This effect is further enhanced through dissociation of the ions by the utilisation of a polar solvent or crown ether (Scheme 3). PEG itself also functions similar to crown ethers by complexing the counter ion with its backbone.[23]

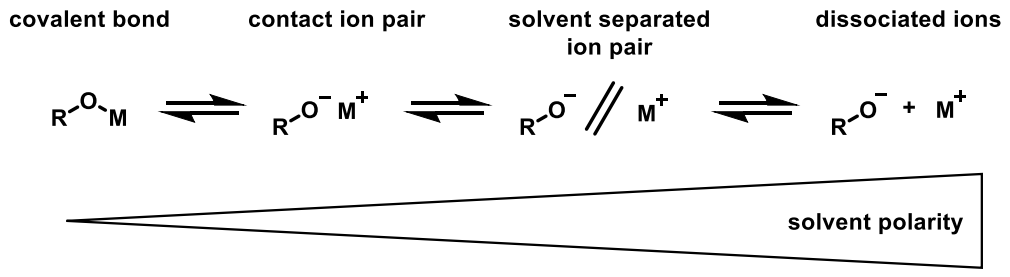

Scheme 3: Ion equilibrium of metal alkoxides in solvents.

A drawback of PEG is the absence of functional groups within the chain. The use of substituted epoxides allows for the synthesis of multifunctional polyethers with a high scope of side groups like ethers, tertiary amines (see chapter 1.5 Polyelectrolytes)

and more.[24,25] A prerequisite for the introduction of functional moieties is stability of the monomers under the harsh, basic AROP conditions. Less stable monomers like esters or monomers with fluorinated side chains can often be polymerised by the monomer-activated anionic ring-opening polymerisation (MAROP, see chapter 1.3 Monomer-activated anionic ring-opening polymerisation)[26,27], first reported by Deffieux and Carlotti, which proceeds under milder conditions.[28]

For substituted monomers the nucleophile typically attacks the sterically least hindered carbon of the epoxide ring, leading to a head-to-tail configuration of the polymer.[20,29] Besides this propagation a molecular weight limiting side reaction can occur for alkylene oxides and glycidyl ethers (Scheme 4): By abstraction of a proton from the α-carbon atom of the side chains, an allyl alkoxide serving as an initiator by itself is generated.[1,25] As a result, the molecular weight distribution broadens and the achievable maximum molecular weight of PPO synthesised by AROP is limited to approximately 6000 g/mol.[1] By reducing the reaction temperature as well as by activating the polymerisation without activating the undesired elimination reaction via a crown ether, the side reaction can be partially supressed.[30] However, higher molecular weights are achievable by MAROP[28] or by double metal cyanide (DMC) catalysis, which is commonly used in industry for the synthesis of PPO.[20,31]

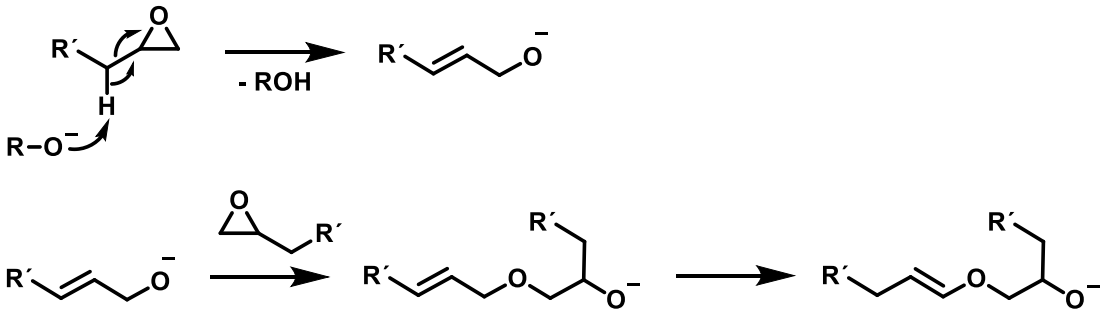

Scheme 4: General mechanism of the chain transfer.

1.3 Monomer-activated anionic ring-opening polymerisation

As mentioned before the monomer-activated anionic ring-opening polymerisation (MAROP) enables polymerisation of substituted monomers without chain transfer, permitting the synthesis of certain polyethers with high molecular weight that were previously unattainable by classical AROP. It also enables the polymerisation of monomers, which are unreactive or unstable under AROP conditions like epoxide esters[26] or monomers with fluorinated side chains.[27,32]

Deffieux and Carlotti implemented a polymerisation technique using an initiator-catalyst combination, which is now referred to as “activated monomer technique”.[28] In early MAROP studies trialkyl aluminium was used as a catalyst and an activator in combination with a metal alkoxide like sodium isopropoxide[27,28], which is nowadays typically exchanged for an onium salt like tetraoctylammonium[33] or methyltriphenylphosphonium bromide[34] to enable higher molar masses.[25]

Nevertheless, the use of organoaluminium species was known in this field before. For example, Vandenberg used aluminium-alkyl-water catalysts to polymerise epoxides and proposed the cyclic coordination shown in Scheme 5. As the ring opening of the (next) epoxide monomer proceeds, the growing chain end releases the bound aluminium and forms a new bond to the adjacent aluminium. The metal-oxygen bond of this aluminium shifts simultaneously to the aluminium of the original chain end.[35]

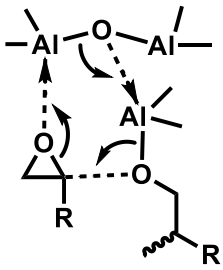

Scheme 5: Epoxide-aluminium coordination proposed by Vandenberg.[35]

In contrast to Vandenberg´s approach, the MAROP initiator and trialkyl aluminium generate an “ate” complex as active initiator with low nucleophilicity (Scheme 6). This also is one key difference to the classic oxyanionic ring-opening polymerisation, which uses stronger nucleophiles leading to the elimination side reaction shown in Scheme 4. Furthermore, the electrophilic aluminium species strongly activates the epoxide monomer by reducing the electron density in the ring, enabling ring-opening and smooth chain growth at mild conditions such as room temperature or even below 0 °C. The propagation by further activated epoxides occurs by head-tail linkage and is followed by active termination via a protic source like methanol. The combination of mild conditions and the reduced basicity of the alkoxide in the formed aluminate complex enables polymerisation without or at least with reduced chain transfer reactions in a “living-like” manner.[28,36]

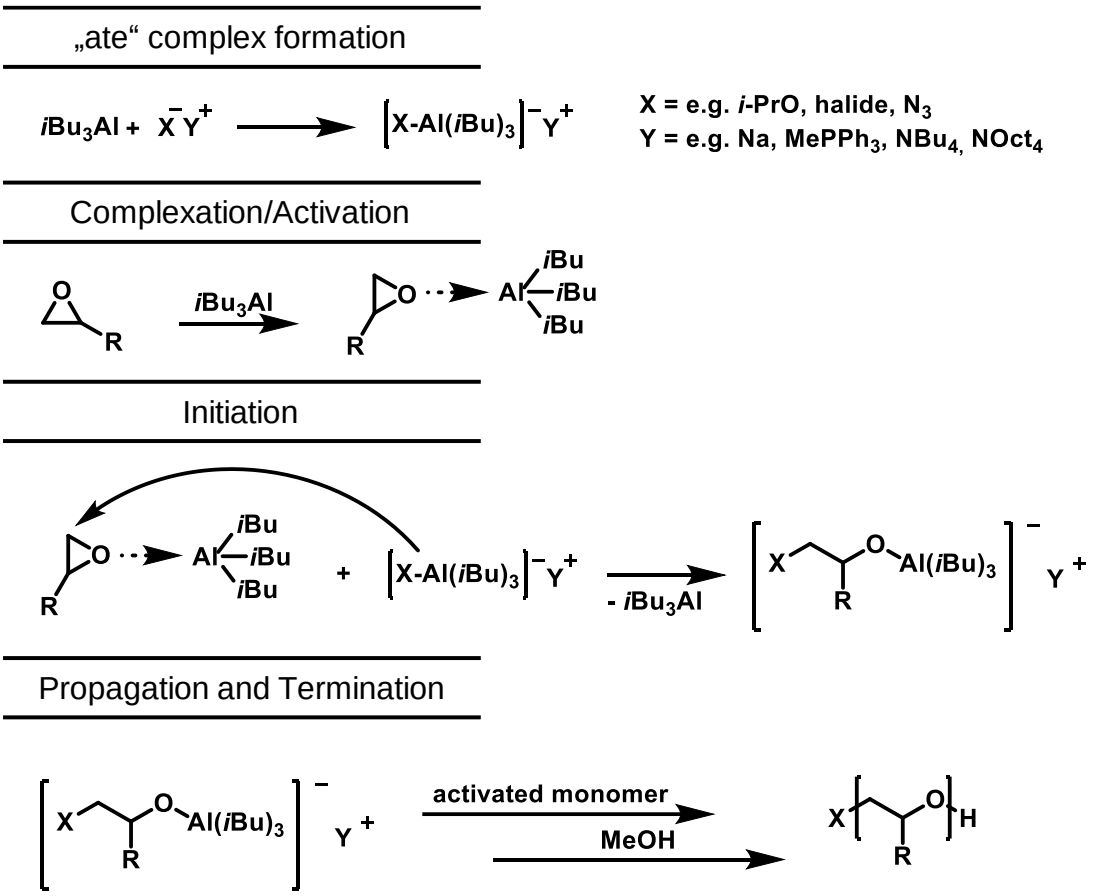

Scheme 6: General mechanism of the MAROP of epoxides.

A higher degree of control over the polymerisation is achievable by adjusting the polymerisation conditions, leading to narrow dispersity.[28] With increasing reaction temperatures or equivalents of the organoaluminium compound the probability for initiation side reactions through either a hydride or an alkyl group of the aluminium compound increases (Scheme 7). The molecular weight distribution is broadened by these side reactions.[27,37] Nevertheless, to enable the polymerisation a ratio of initiator to catalyst exceeding 1:1 is required.[28,36] The first equivalent is necessary to generate the “ate” complex with the initiator or growing chain, while only the excess is available to activate the monomers. The use of ammonium or phosphonium halide initiators reduces the side reactions in comparison to alkali metal alkoxides through a further decrease of basicity of the active complex.[25] The second disadvantage of the system isthat residual initiator and activator typically remain in the synthesised polymer, often requiring dialysis steps for complete purification and disabling biomedical applications.[33]

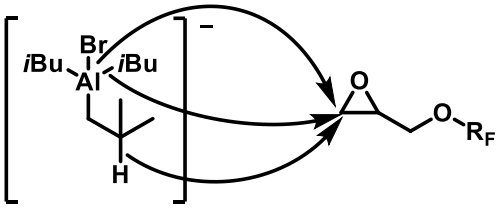

Scheme 7: Initiation side reaction of MAROP.

1.3.1 Organo boranes

Recently, organo boranes are intensely explored in (co)polymerisation of epoxides as an alternative to aluminium catalysts due to their metal-free character. The absence of metallic residues in the synthesised polymers can presumably open additional fields of application[38] for the polymers synthesised for example via MAROP (see chapter 1.3 Monomer-activated anionic ring-opening polymerisation). First studies were conducted using the relatively mild Lewis acid triethyl borane (TEB).[38] Zhang *et al*. gave an excellent review on development and state of the art of alkyl borane-mediated (co)polymerisations of oxygenated monomers.[39] While TEB is the most common reagent,[38,40–42] the catalytic activity can be tuned by changing the organic groups. In epoxide polymerisations activity increases with the Lewis acidity of the chosen borane, with for example tris(pentafluorophenoxy) borane (BCF) showing very high catalytic activity.[42,43] Recently boranes bearing different cyclic groups were explored and tertiary boranes with either a borinane (bora) or 9-borabicyclo[3.3.1]nonane (9-BBN) group showed activity in the polymerisation of epoxides. Weaker Lewis acids like dicyclohexylborane (BCy_2) or 4,4,5,5-tetramethyl-1,2,2-dioxoboryl (BPin) adducts conversely failed to polymerise epoxides (Scheme 9).[44,45] In catalytic copolymerisations of epoxides and carbon dioxide, on the other hand, contrary relationship between Lewis acidity and catalytic activity were found and in BCF catalysed reactions either cyclic carbonates or polyethers were obtained instead of polycarbonates.[46]

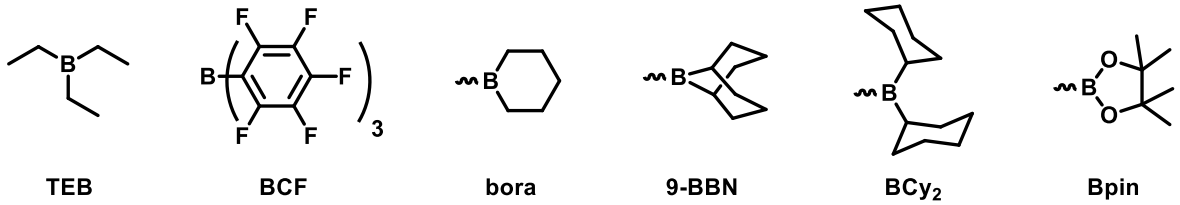

Scheme 8: Examples of organo boranes. TEB, BCF, bora as well as 9-BBN bearing molecules showed catalytic activity in polymerisations. BCy_2 and Bpin showed no significant catalytic activity.

In these copolymerisation reactions of epoxides and carbon dioxide Lewis acidic organo boranes are used in combination with a Lewis base to generate polycarbonates (Scheme 8). The borane centre activates the epoxide in the same manner as in the MAROP of epoxides, and the first ring-opening occurs via nucleophilic attack. In contrast to the polyether synthesis, carbon dioxide inserts into the oxygen-Lewis acid bond. A carbonate unit is formed, at which point either the polymerisation proceeds through chain growth by epoxide insertion or a cyclic carbonate is formed due to backbiting. A second side reaction is the formation of ether linkages due to subsequent insertion of epoxides. The selectivity between these reactions is adjusted by the catalyst system as well as the chosen reaction conditions.[47,48]

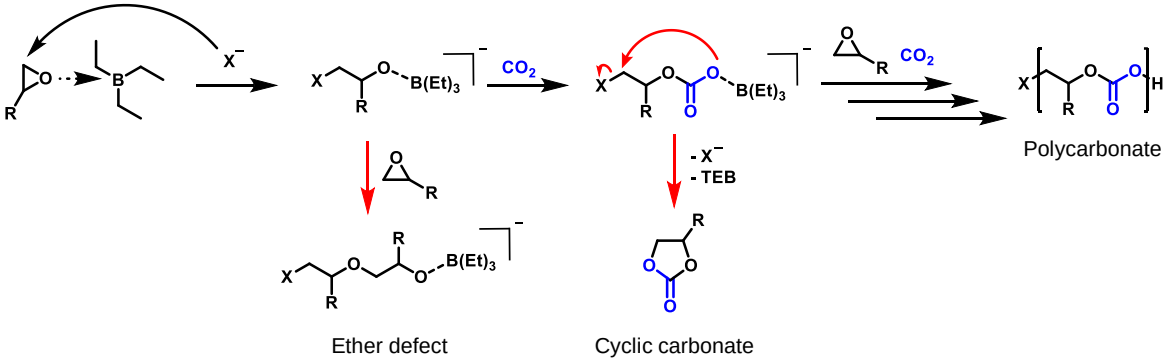

Scheme 9: Mechanism of polycarbonate synthesis and its side reactions leading to ether defects or cyclic carbonate formation.

One step to achieve sustainability is the recovery and reuse of catalysts. The borane alternatives bear similar problems as the aluminium catalysts regarding purification and recovery of the initiator-catalyst system. Recent publications are exploring this topic. In 2020 Patil *et al*. introduced a multistep system to recover TEB from synthesised polycarbonate. Following the addition of *n*-butylamine, TEB is trapped in a stable adduct. Simultaneous addition of succinic acid neutralises the “ate” complex and prevents backbiting reactions by the naked chain end. The synthesised polycarbonate is isolated via precipitation, while the trapped TEB remains in the mother liquor. Subsequent deblocking with tosyl-isocyanate and distillation yields the recovered TEB. The same work introduced a polymeric initiator salt for easy initiator isolation after polymerisation via filtration.[49] Nonetheless, the system suffered from large work effort and required multiple compounds.[44,49] Wu and Yang *et al*. introduced a bifunctional initiator-catalyst system combining an ammonium salt and borane

groups in one molecule. The synthesis was achieved by hydroboration of the pendant allyl groups of the ammonium salt.[44,50,51] Hydroboration with dialkoxyboranes requires catalysts like the ruthenium complex [Ru(*p*-cymene)Cl_2]$_2$, while dialkylboranes can react without a catalyst.[52] This system allowed for an increase in turn-over-frequency as well as purification via filtration.[44] Utilising a similar bifunctional system, Chen *et al*. were ultimately able to isolate and reuse their catalyst.[53] The bifunctional initiator-catalyst system was further developed to multinuclear catalysts, where one ammonium group was linked to up to four boron centres.[54,55] These multiple centres caused a synergistic effect indicated by high turnover frequencies.[56] Mechanisms were proposed (Scheme 10), where one boron centre (B_1) bears the active chain-end, and the others coordinate an epoxide each. For polyether synthesis propagation occurs via nucleophilic attack at the next epoxide. Consequently, the active chain-end shifts to this boron centre (B_2).[55] In copolymerisations with carbon dioxide this attack occurs subsequent to carbon dioxide insertion.[54]

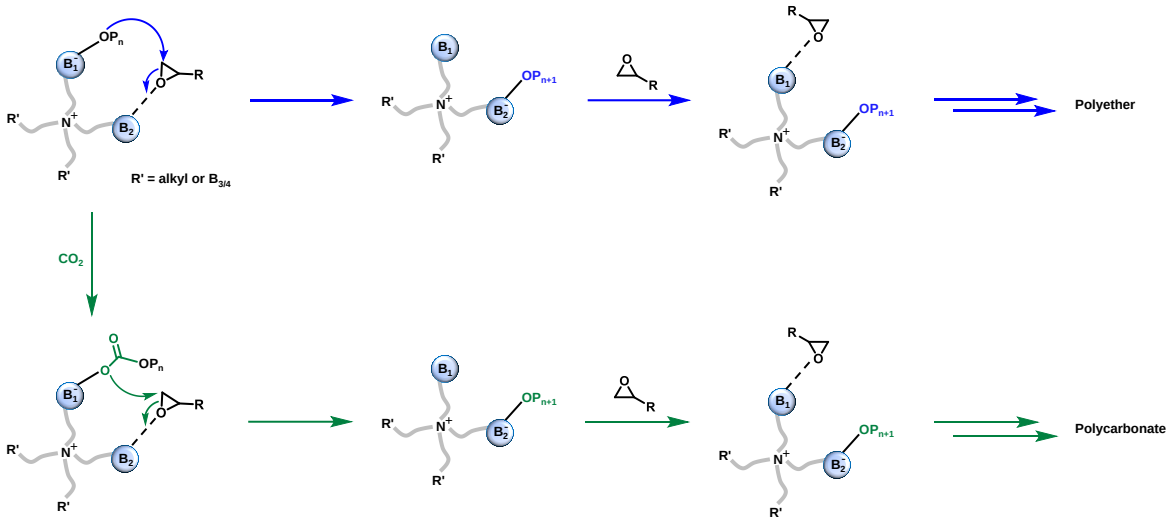

Scheme 10: Mechanisms of the cooperation between boron centres in polyether (top) and polycarbonate synthesis (bottom) as proposed by Yang and Wu et al.[54,55]

As a versatile group organo boranes offer more applications than the discussed high catalytic activity. While one of the main purposes of organo boranes is their usage as an intermediate and reagent for organic reactions like Suzuki coupling,[57,58] or hydroboration-oxidation[59,60] for C-C, C-X or C-O bond formation, they are also used in boron neutron capture therapy (BNCT) for cancer treatment.[61,62] Dialkoxyboranes are a precursor for the synthesis of small molecules or polymers bearing boronic

acid,[63] which have a multitude of application possibilities in biomedicine.[64,65] In this regard, they are, for example, used as enzyme inhibitors (e.g. lipase in obesity treatment)[66] and hydrogels (e.g. sensors for saccharides in diabetes treatment,[67] for HIV inhibition[68] or controlled drug-delivery[69]). Hydrogel networks can be obtained by capitalising on reversible boronic ester formation with polyalcohols.[70] Thermosets are also achievable via reversible boroxine formation.[71]

1.4 Copolymerisation models and architectures of linear copolymers

By combining different monomers, copolymers are obtained which inherit or combine the properties of the corresponding homopolymers. Depending on the order and timing of the comonomer addition, as well as their reactivity ratios, different polymer architectures are possible. Block copolymers are synthesised by either using a macroinitiator or via sequential monomer addition. Statistical copolymerisation on the other hand can lead to alternating, random or gradient structures depending on the reactivity ratios of the monomers in question.

Different methods to determine the polymer microstructure are known. For living copolymerisations, *in situ* ^{1}H NMR kinetics can be used to monitor monomer consumption in the ongoing polymerisation. This allows for calculation of the reactivity ratios.[72] The reactivity ratios, r_1 and r_2, for a comonomer pair are generally defined by the rate constants of the addition of the respective monomers to the polymer chain end, where homo-propagation is described by k_{xx} and cross-propagation by k_{xy} (1)(2).

$$r_1 = \frac{k_{11}}{k_{12}} \quad (1)$$

$$r_2 = \frac{k_{22}}{k_{21}} \quad (2)$$

Figure 1 gives an overview of prominent polymer architectures, which result from the relation of the reactivity ratios. If a reactivity ratio equals zero, the respective monomer does not add to an active chain end of the same monomer, and thus homopolymerisation is impossible. In consequence, if both reactivity ratios equal zero ($r_x = r_y = 0$) the polymer structure is strictly alternating. If both ratios are less than unity ($r_x < 1$, $r_y < 1$), the monomers also favour cross-propagation, resulting in a random copolymer. Furthermore, the polymerisation is random if one reactivity ratio is lower

than unity, while the other is larger ($r_x < 1$, $r_y > 1$). If in this case the values are strongly disparate, and a gradient structure is formed. The polymerisation is called ideal if the product of the reactivity ratios equals unity ($r_x < 1$, $r_y > 1$, $r_x r_y = 1$). While the chain ends are indiscriminate to the comonomers, one monomer can still have a higher reactivity than the other leading to a gradient. If both reactivity ratios equal unity ($r_x = r_y = 1$), the copolymer composes of the identical composition as the original comonomer mixture, and the polymerisation is called an ideal random copolymerisation. Polymers composed of blocks are the result of both reactivity ratios being larger than unity ($r_x > 1$, $r_y > 1$). The crossover from one monomer to the other can be impossible, leading to a blend of homopolymers. In this case both reactivity ratios are much larger than unity.[73]

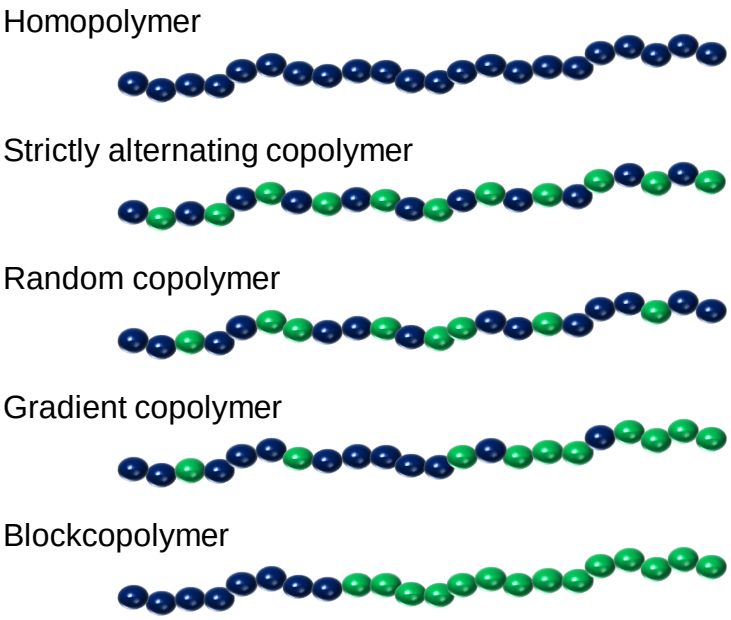

Figure 1: Polymer architectures.

To determine the polymer composition, different models can be used. One of the first models was the non-terminal model by Wall.[74] It did not take the chemical nature of the chain end into account, assuming that the selectivity towards comonomers *M* is independent of the chain end P^* ((3) and (4)).

$$P^* + M_1 \overset{k_1}{\rightarrow} P^* \tag{3}$$

$$P^* + M_2 \overset{k_2}{\rightarrow} P^* \tag{4}$$

In consequence, the rate of monomer consumption is defined by equation (5).

$$-\frac{[M_x]}{dt} = k_x[P^*][M_x] \tag{5}$$

Division of the rates of the respective comonomers gives equation (6).

$$\frac{d[M_1]}{d[M_2]} = \frac{k_1[M_1]}{k_2[M_2]} = \alpha\frac{[M_1]}{[M_2]} \tag{6}$$

Assuming the rate α is constant leads to equation (7) with initial concentration $M_{x,0}$

$$\frac{[M_1]}{[M_1]_0} = \left[\frac{[M_2]}{[M_2]_0}\right]^{\alpha} \tag{7}$$

Finally, Jaacks used the integrated equation (8) to describe the copolymerisation up to high conversion.[75,76]

$$\log\left[\frac{[M_1]}{[M_1]_0}\right] = r_1 \log\left[\frac{[M_2]}{[M_2]_0}\right] \tag{8}$$

Beckingham, Sanoja and Lynd developed the so-called BSL model[73] for ionic polymerisations, which tend to follow an ideal behaviour with chain end independency of the propagation.[73,77,78] In consequence, alternating and block copolymerisations cannot be described by this model, as they rely on the chain end reactivity. This integrated, non-terminal model allows determinations for high conversions like the Jaacks model.

The BSL model uses equation (5), where $[P^*]$ equals the initial initiator concentration X_0, and the assumption of livingness to receive the exponential equations for monomer and initiator X consumptions with time t (9) and (10).

$$[M_x](t) = [M_x]_0 e^{-k_x X_0 t} \tag{9}$$

$$X(t) = X_0 e^{\left[-\frac{1}{X_0}\right]\left[[M_1]_0 - [M_1](t) + [M_2]_0 - [M_2](t)\right]} \tag{10}$$

The total monomer conversion $p_{1,2}$ is now looked at as a function of time or conversion (11).

$$p_{1,2} = \frac{[M_1]_0 + [M_2]_0 - [M_1](t) - [M_2](t)}{[M_1]_0 + [M_2]_0} \tag{11}$$

Substituting these time-dependent monomer concentrations with (9) leads to (12), which can be simplified by using the initial mole fractions of the monomers n to equations (13) and (14).

$$p_{1,2} = \frac{[M_1]_0 + [M_2]_0 - [M_1]_0 e^{-k_1 X_0 t} - [M_2]_0 e^{-k_2 X_0 t}}{[M_1]_0 + [M_2]_0} \quad (12)$$

$$p_{1,2} = n_1 + n_2 - n_1 e^{-k_1 X_0 t} - n_2 e^{-k_2 X_0 t} \quad (13)$$

$$p_{1,2} = 1 - n_1 \frac{[M_1](t)}{[M_1]_0} - n_2 \frac{[M_2](t)}{[M_2]_0} \quad (14)$$

Using equation (7) and the definitions (15) and (16)

$$n_2 = 1 - n_1 \quad (15)$$

$$p_1 = 1 - \frac{[M_1](t)}{[M_1]_0} \quad (16)$$

the BSL equations (17) and (18) for the conversions of the respective comonomers are gained.

$$p_{1,2}(p_1) = 1 - n_1[1 - n_1] - [1 - n_1][1 - p_1]^{r_2} \quad (17)$$

$$p_{1,2}(p_2) = 1 - n_1[1 - p_2]^{r_1} - [1 - n_1][1 - p_2] \quad (18)$$

Three years after Wall´s non-terminal model, terminal models taking the influence of the last monomer in the growing chain into account were published independently by Alfrey and Goldfinger[79], by Mayo and Lewis[80], as well as by Wall[81] himself. The basis of the model are the equations (19) to (22), where *PM** is the growing chain and *M* is the monomer.

$$PM_1{}^* + M_1 \xrightarrow{k_{11}} PM_1M_1{}^* \quad (19)$$

$$PM_1{}^* + M_2 \xrightarrow{k_{12}} PM_1M_2{}^* \quad (20)$$

$$PM_2{}^* + M_2 \xrightarrow{k_{22}} PM_2M_2{}^* \quad (21)$$

$$PM_2{}^* + M_1 \xrightarrow{k_{21}} PM_2M_1{}^* \quad (22)$$

In this model, the rate of monomer consumption is defined by (23).

$$-\frac{[M_x]}{dt} = k_{xx}[PM_x{}^*][M_x] + k_{yx}\left[PM_y{}^*\right][M_x] \quad (23)$$

Consideration of both monomers leads to (24) and the simplified (25).

$$\frac{d[M_1]}{d[M_2]} = \frac{k_{11}[PM_1{}^*][M_1] + k_{21}[PM_2{}^*][M_1]}{k_{12}[PM_1{}^*][M_2] + k_{22}[PM_2{}^*][M_2]} \quad (24)$$

$$\frac{d[M_1]}{d[M_2]} = \frac{[M_1]}{[M_2]} \cdot \frac{k_{11}[PM_1{}^*] + k_{21}[PM_2{}^*]}{k_{12}[PM_1{}^*] + k_{22}[PM_2{}^*]} \quad (25)$$

Assuming a steady state for the active chain ends gives (26) and after rearrangement (27) and (28).

$$\frac{d[PM_2{}^*]}{dt} = k_{12}[PM_1{}^*][M_2] + k_{21}[PM_2{}^*][M_1] = 0 \quad (26)$$

$$k_{12}[PM_1{}^*][M_1] = k_{21}[PM_2{}^*][M_1] \quad (27)$$

$$[PM_1{}^*] = \frac{k_{21}[PM_2{}^*][M_1]}{k_{12}[M_1]} \quad (28)$$

Substitution of [PM_1*] in equation (25) gives (29).

$$\frac{d[M_1]}{d[M_2]} = \frac{[M_1]}{[M_2]} \cdot \frac{\frac{k_{11}}{k_{12}}[M_1] + [M_2]}{\frac{k_{22}}{k_{21}}[M_2] + [M_1]} \quad (29)$$

By using the definitions (1) and (2) the copolymerisation model (30) called the “Mayo-Lewis equation” is obtained.

$$\frac{d[M_1]}{d[M_2]} = \frac{[M_1]}{[M_2]} \cdot \frac{r_1[M_1] + [M_2]}{r_2[M_2] + [M_1]} \quad (30)$$

The Mayo-Lewis equation describes the copolymer composition in relation to the comonomer ratio. Due to the comonomer ratio changing throughout the copolymerisation, the copolymer composition is also changing. This effect is called “compositional drift”.[77,82] In consequence, this equation is only applicable at calculations for low conversions or in systems where the drift does not take place.

For a description of systems with high conversion the integrated (31) is needed.

$$\log\frac{[M_2]}{[M_2]_0} = \frac{r_2}{1-r_2}\log\frac{[M_2]_0[M_1]}{[M_1]_0[M_2]} - \frac{1-r_2r_1}{[1-r_2][1-r_1]}\log\frac{[r_1-1]\frac{[M_1]}{[M_2]} - r_2 + 1}{[r_1-1]\frac{[M_1]_0}{[M_2]_0} - r_2 + 1} \quad (31)$$

This equation is often used in the more convenient form describing the respective monomer as well as the total conversion. For this purpose, mole fractions are used to describe the concentrations of the monomers in the feed *f* (32) and in the polymer *F* (33).

$$f_1 = 1 - f_2 = \frac{[M_1]}{[M_1] + [M_2]} \quad (32)$$

$$F_1 = 1 - F_2 = \frac{d[M_1]}{d[M_1] + d[M_2]} \quad (33)$$

The definitions of (32) and (33) combined with (30) leads to equation (34), where f_2 can be described by 1-f_1.

$$F_1 = \frac{r_1 {f_1}^2 + f_1 f_2}{r_1 {f_1}^2 + 2 f_1 f_2 + r_2 {f_2}^2} = \frac{r_1 {f_1}^2 + f_1[1 - f_1]}{r_1 {f_1}^2 + 2 f_1[1 - f_1] + r_2[1 - f_1]^2} = \frac{[r_1 - 1]{f_1}^2 + f_1}{[r_1 + r_2 - 2]{f_1}^2 + 2[1 - r_2] f_1 + r_2} \quad (34)$$

Skeist[83] used (34) and the total monomer concentration (35) to develop the conversion-composition (36).

$$\frac{d[M]}{[M]} = \frac{df_1}{F_1 - f_1} \quad (35)$$

$$\ln \frac{d[M]}{[M]_0} = \int_{f_{1,0}}^{f_1} \frac{df_1}{F_1 - f_1} \quad (36)$$

Skeist´s equation requires graphical or numerical methods to solve the problem. Meyer and Lowry[84] further developed it to obtain an analytical solution for binary systems. Substituting (34) in (36), rearrangement and integration gives (37).

$$\frac{[M]}{[M_0]} = \left[\frac{f_1}{f_{1,0}}\right]^{\frac{r_2}{1-r_2}} \left[\frac{1 - f_1}{1 - f_{1,0}}\right]^{\frac{r_1}{1-r_1}} \left[\frac{f_{1,0} - \left[\frac{1 - r_2}{2 - r_1 - r_2}\right]}{f_1 - \left[\frac{1 - r_2}{2 - r_1 - r_2}\right]}\right]^{\frac{1 - r_1 r_2}{[1-r_1][1-r_2]}} \quad (37)$$

The Meyer-Lowry equation describes the copolymerisation behaviour in dependency of the conversion.

Ultimately, applying Ockham´s razor principle leads to the conclusion that the simplest model with the lowest number of assumptions should be used, provided that it fits the data.[85,86] In case of ionic epoxide polymerisation this principle would often lead to the non-terminal model with the Jaacks or the BSL equations, as stated by Beckingham, Sanoja and Lynd.[73]

1.5 Polyelectrolytes

Polyelectrolytes are a class of polymers bearing multiple charged atoms. The charge can be either positive, in case of a polycation, or negative, in case of a polyanion. Polyelectrolytes are pH-responsive polymers, classified as strong or weak depending on the dissociation constant (Scheme 10).

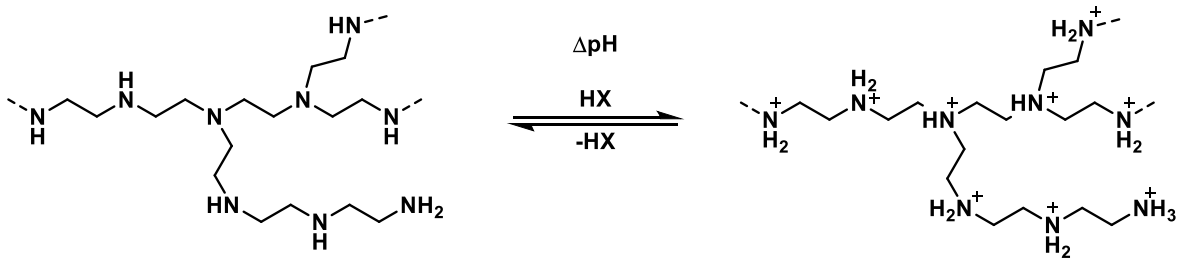

Scheme 11: Structure of branched polyethyleneimine. The degree of protonation is influenced by pH value.

Polycations are utilised in biomedical applications. Especially polyethyleneimine (PEI), which amine groups get protonated at low pH values, and its copolymers or derivatives are the gold standard in non-viral transfection for treatment or prophylaxis of diseases.[87,88] Transfection is the transfer of nucleic acids in a cell to achieve gene expression of the added genetic information. To transport the negatively charged nucleic acids through the negatively charged cell membranes, the nucleic acid is shielded in a complex with the positively charged PEI. The nucleic acid-polymer-complex binds to the cell surface via electrostatic interactions and undergoes endocytosis. Ultimately, DNA is released from the endosome or lysosome by the rupture of the compartment, due to the so-called proton sponge effect of the protonable nitrogen atoms of the polymer.[87,89,90] However, in consequence of its ability to disrupt and destroy membranes, PEI also bears an inherent toxicity.[91] Due to the correlation between toxicity and charge density as well as molecular weight, studies are conducted to balance these parameters.[92–95]

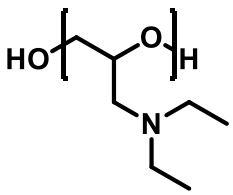

Scheme 12: Structure of a poly glycidyl amine: Poly diethyl glycidyl ether.

Another class of pH-responsive amino-functional polymers are poly(glycidyl amine)s. They combine the PEG backbone with side chain amino-functionalisation (Scheme 12). For the synthesis of amino-functional polyethers via AROP the use of a protected amino-functional monomer or post-polymerisation reactions e.g. thiol-ene click reaction of polymer allyl-groups is required.[96,97]

The established amino-functional monomers are distinguished in monomers for the incorporation of primary or secondary amines, which require subsequent

deprotection, and monomers for tertiary amines. These amino-functional monomers, called glycidyl amines, are accessible via nucleophilic substitution of epichlorohydrin and the corresponding secondary amine. Limitations are hereby imposed with regard to sterically demanding groups, which prevent the attack at the epoxide ring. Nevertheless, diethyl glycidyl amine (DEGA) is already achievable via this synthesis.[20,24,98]

First homopolymerisation attempts of DEGA or *N*,*N*-dibenzyl amino glycidol (DBAG) only led to oligomers,[99,100] presumably due to the complexation of the counterion by the oxygen and the nitrogen of the terminal repeating unit or due to transfer reactions. The following research showed that the use of crown ether suppresses the complexation and therefore enables the polymerisation in a controlled manner with low dispersities (Đ < 1.1).[99] Even so, Elter and Schacher *et al.* showed successful polymerisation of piperidine glycidyl amine (PiGA) without requiring crown ethers (1.16 < Đ < 1.23).[101]

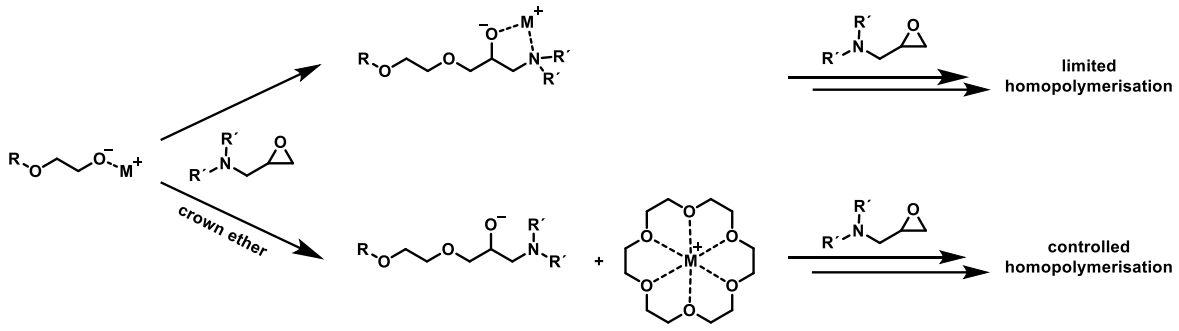

Scheme 13: Comparison of the homopolymerisation of glycidyl amines without (top) and with the addition of crown ether (bottom) as proposed by Blankenburg et al. Complexation of the counterion by the chain-end decreases the reactivity.[99]

In copolymerisation with comonomers without amino-functionalities, the glycidyl amine is preferably incorporated near the terminus, indicating lower reactivity of the amino-functionalised epoxide.[102] In contrast, glycidyl ethers are more likely to be incorporated at the initiation site due to an increased Lewis-basicity, which is caused by the counterion-coordination by the oxygen-atoms.[24,78,102]

The spectrum of monomers (Scheme 13) for tertiary amines was broadened by the higher homologues bearing *n*-butyl (DButGA), *n*-hexyl (DHexGA) and *n*-octyl groups (DOctGA)[102] as well as by the cyclic amines pyridine (PyrGA)[103] and PiGA.[104] Chapter 2 describes a novel polymer synthesised by azepane glycidyl amine (AzGA). Furthermore, compounds with a second heteroatom in the side chain were

introduced, namely *N*-glycidyl morpholine (GM), *N*,*N*-bis(2-methoxyethyl) glycidyl amine (BMEGA) and isopropyl-hexahydro-pyrimidine glycidyl amine (PyGA).[99,105]

Monomer for primary amines

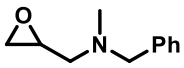

BMGA

Monomers for secondary amines

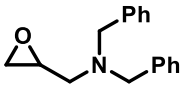

DBAG

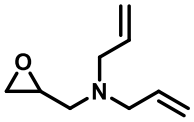

DAGA

Monomers for tertiary amines

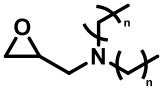

n=1: DEGA
n=3: DButGA
n=5: DHexGA
n=7: DOctGA

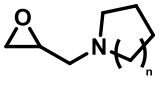

n=1: PyrGA
n=2: PiGA
n=3: AzGA

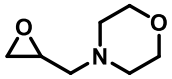

GM

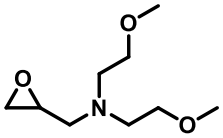

BMEGA

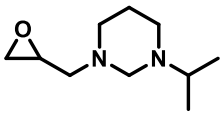

PyGA

Scheme 14: Overview of monomers for the synthesis of polyethers bearing primary amines (top),[105] secondary amines (middle),[100,106] and tertiary amines (bottom).[24,102–105,Chapter 2]

As mentioned before, the incorporation of a primary or a secondary amine requires the suppression of the nucleophilic attack of the amine at the epoxide-ring. This is avoided in the polymerisation of glycidyl amines bearing a tertiary amine. Different strategies for the protection of primary or secondary amines were established. DBAG was introduced as a precursor of an amino-analogue of polyglycerol.[100] To decrease the reaction times and increase to the polymer yield, *N*,*N*-diallyl glycidyl amine (DAGA) was developed subsequently.[106] The introduction of secondary amines can be achieved in an analogous manner if the amine bears only one cleavable group in combination with a permanent group, e.g. *N*-benzyl-*N*-methyl glycidyl amine (BMGA).[105]

1.5.1 Kinetic gas hydrate inhibitors

Different small molecules as well as polymers bearing nitrogen containing groups have found application in oil production as low-dosage hydrate inhibitors (LDHI), either as anti-agglomerant (AA) or as kinetic hydrate inhibitor (KHI). They are used to ensure, for example, the pipeline flow in cold climate regions and offshore, where gas hydrates tend to solidify and clog the transportation system. Gas hydrates are clathrates of water encapsulating small hydrocarbons that solidified at low temperatures and high pressures.[107,108] AAs prevent formed hydrates from agglomerating, while KHIs are anti-nucleators and delay the nucleation as well as often the crystal growth.

Before the development of LDHIs the flow was ensured by costly and elaborate methods like heating, insulation[108] or the use of 20 – 40wt% of an anti-freeze agent like methanol. In comparison LDHIs are used in 0.1 – 1.0wt%.[109] The system and the activity of the LDHIs are described by different temperatures. Below the hydrate equilibrium temperature T_{eq} the hydrates are stable, and their formation is thermodynamically favoured.[110] At the onset temperature T_o the hydrates start to form. The difference between T_{eq} and T_o is defined as the inhibitors ability to delay the gas hydrate formation and is described by the subcooling T_{sub} (Figure 2).[110] An abrupt decrease of the dissolved gas volume marks the rapid hydrate formation temperature T_a. Finally, the difference between T_o and T_a shows the KHI´s ability to delay rapid formation.

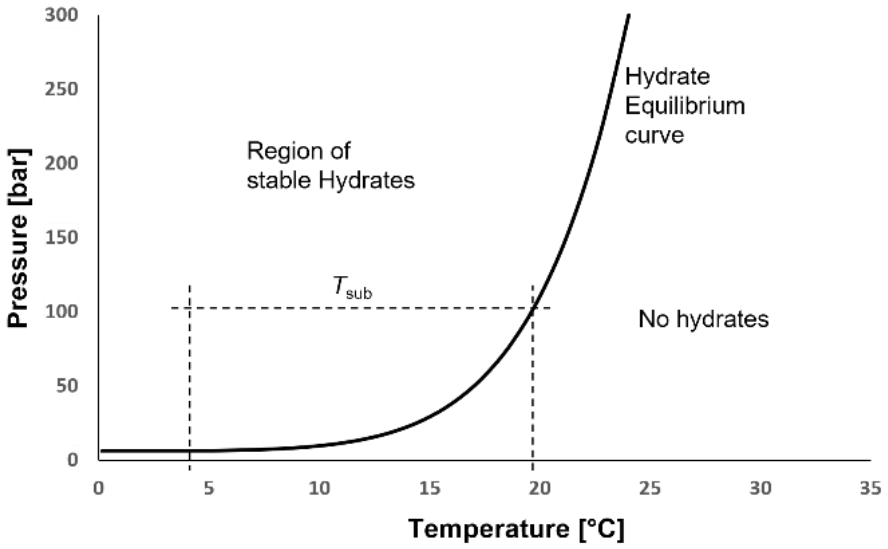

Figure 2: Pressure-temperature diagram for hydration formation. Adapted from Kelland.[109]

The main class of KHIs are (co)polymers containing amide functions. Typically used are poly(vinyl lactam)s like polyvinylcaprolactam (PVCap) or polyvinyl pyrrolidone (PVP). This group is extended by polyalkylacrylamides like polyacryloyl pyrrolidone (PolyNPyMA). The amides or lactams interact with the hydrate surface by entering the hydrate cavities with the alkyl group and bonding via the carbonyl group to the hydrogen bond network.[109] Sloan Jr. found additives consisting of PEG or PPO homo- and copolymers to have a synergistic effect on the KHI activity.[111] In a similar manner polypropoxylation increased the effectiveness of AAs, presumably by orientating at the aqueous and non-polar interface.[109] Furthermore, non-amide KHIs were identified. Representatives are ring-closed polyoxazolines and small molecule as well as polymeric amine-*N*-oxides (TBAO, HPEI-R-AO) (Scheme 14).[109,110,112]

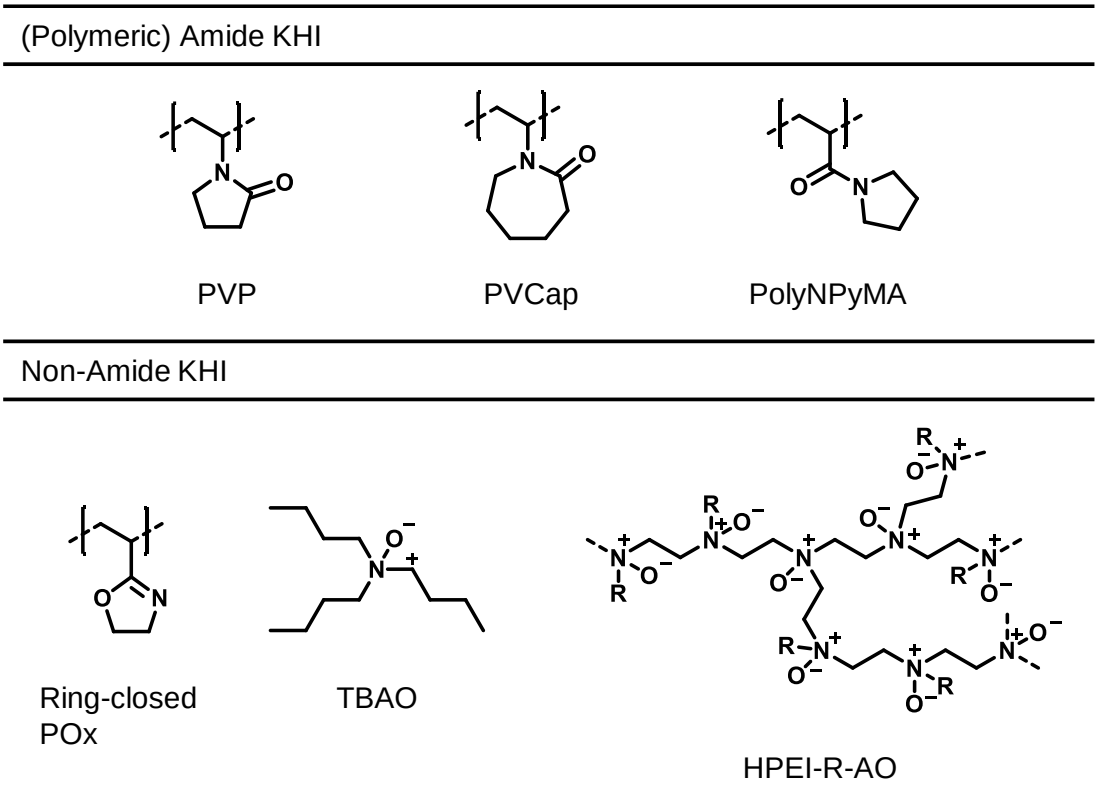

Scheme 15: Examples of KHIs. Typical polymeric amide-type KHIs (top),[109,110] non-amide KHIs (bottom).[109,110,112,113]

Given the application nature of KHIs it is necessary that they remain dissolved in the temperature and salinity range, which is defined by the cloud point T_{cl}. At the T_{cl}, phase separation of water and polymer occurs in consequence of increased polymer-polymer-interaction and decreased polymer-water-interactions. Typically, the deposition temperature lies 5 – 15 °C above the T_{cl}, representing the critical limit for KHIs.[108] Finally, with regard to the topic of ocean pollution, new offshore chemicals

are nowadays required to possess biodegradability, albeit the required level differs from legislation to legislation.[109]

The KHI activity can be measured using a high-pressure rocker rig. Cells containing the KHI, gas containing fluid and a steel or glass ball are placed in a cooling bath. Through rocking of the cells, turbulence is created by the moving balls leading to the fluids being mixed. Temperature as well as pressure are monitored over time, to determine T_o, T_a, T_{sub} and the delta of T_o and T_a.[114] Optimised KHIs are characterised by low T_o and T_a and high T_{sub} and T_o -T_a.

1.6 Fluorinated polymers

Another remarkable class of polymers are fluorinated polymers. The most famous material is polytetrafluoroethylene (PTFE), commercialised as Teflon® since 1946.[115] PTFE is known for its high thermal and mechanical durability originating from highly stable carbon-fluorine-bonds. The bond dissociation energies with typically over 400 kJ/mol increase with the number of fluorine atoms and are even higher than those of carbon-hydrogen-bonds (fluoromethane 485 kJ/mol, methane 439 kJ/mol[116]).[117] The carbon-backbone itself is also strengthened by electron withdrawal.[118,119] Low polarizability leads to low surface energies and exceptionally weak interactions. The consequence is its extraordinarily hydro- and oleophobicity making it highly interesting for antistick-coatings.[119] In combination with a hydrophilic headgroup, fluorinated compounds can become excellent surfactants.[120,121] Other fluorinated polymers often share these properties, highlighting them as high-performance polymers. Further characteristics are typically low dielectric constants as well as low refractive index, which qualifies the polymers for electronic insulation and optical applications.[122]

Fluorine-containing polyethers are often viscous liquids[123] resulting from the more flexible backbone in comparison to polymers with strict carbon backbones.[1] Consequently, they are be of interest for applications in elastomeric formulations[124] or for lubricants. Fluorine-containing polyethers are mainly known from perfluorinated epoxides (hexafluoropropylene oxide)[125] or epoxides bearing fluorinated alkyl chains (trifluoro epoxypropane).[27,123,126] Alternatively, glycidyl ethers with fluorinated side chains can be used.[27,123] Perfluoropolyethers like polyhexafluoropropylene oxide are used as lubricants known as Krytox.[127] Initially, fluorine-containing monomers were polymerised using iron chloride or aluminium chloride as catalyst, leading to low

polymerisation rates or degrees, respectively.[124] Later organozinc[126,128] and finally organoaluminium species[27] were used as initiator-catalyst systems. Monomer-activated ring-opening polymerisation (MAROP) (see chapter 1.3 Monomer-activated anionic ring-opening polymerisation) and cationic ring-opening polymerisation using a Lewis-acid, especially boron trifluoride etherate[129], were established for the polymerisation. A limiting factor for the polymerisation is the solvent, due to the compound´s low affinity for both organic and aqueous solvents. In consequence, fluorinated solvents are often required.[27,123]

1.6.1 Ecological considerations and restrictions for fluorine containing compounds

While the high stability is advantageous in many applications, it also bears negative ecological consequences. Fluorinated and especially poly- and perfluorinated organic compounds are almost unknown in nature.[117,124,130] In consequence, biodegradation mechanisms are limited, and the substances or their fluorinated degradation products accumulate in nature. Evich, Davis, and McCord *et al*. gave an extensive review on the fate of per- and polyfluoroalkyl substances (PFAS) in the environment.[131] PFAS were found ubiquitous, in the world for example in rainwater[132] and in human blood sera.[133] Ecological and health effects are still unknown for a high percentage of PFAS. Nevertheless, one of the major classes perfluoroalkyl carboxylic acids (PFCA) have known health impacts and are often the terminal transformation products of other PFAS.[134,135]

Nowadays, governments in North America, Europe and Asia have enacted guidelines to regulate the production and use of PFAS. In 2006, a voluntarily phase-out program encouraged by the United States Environmental Protection Agency (EPA) was introduced, in which major industrial producers are participating.[136] The Stockholm convention is a United Nations treaty concerning the elimination or restriction of persistent organic pollutants (POP). It listed perfluorooctanoic acid (PFOA), perfluorooctanesulfonic acid (PFOS) and related compounds in Annexes A and B for POPs to be banned or restricted in production and use. Nevertheless, there are defined exceptions from those restrictions.[137] The European Union took a similar approach to classify and restrict an excerpt of perfluorinated compounds in the Registration, Evaluation, Authorization, and Restriction of Chemicals (REACH) regulation.[138–140] PFAS are still a highly discussed topic, and the European

Chemicals Agency (ECHA) recently published a new proposal for further restrictions.[141,142]

In regard to the high global production volumes of fluoropolymers,[131,143] the environmental problems and the governmental restrictions, industry started to develop alternatives (Scheme 15). The two main strategies were to use shorter chain PFAS (≤6 perfluoroalkyl carbons in PFACs or ≤5 in perfluoroalkane sulfonic acids) or to use ether linkages in the perfluorinated chain (PFECA).[144] Short-chain PFAS were partially successful in reducing the bioaccumulation[145,146], but still remain persistent.[147] The ether linkage was used as a programmed breaking point for the biodegradation of PFAS, for example in GenX. Although the breakdown is possible to some degree for -CF_2-O-CF_2- motives by highly energy-consuming chemical approaches (combination of persulfate and ultrasonic irridation,[148] oxygen in subcritical water at 350 °C,[149] hydrated electrons[150]), these PFECAs were stable for example under total oxidisable pressures (TOP) assay conditions and are expected to be terminal and persistent products in the environment.[144,151] In comparison to the -O-CF_2- motive the reactivity of the adjacent hydrogen atom is increased in the -O-CHF- motive, rendering it a more suitable breaking point.[152,153] This group bearing chemical ADONA was oxidised in the TOP assay to perfluoro-3-methoxypropanoic acid as a new terminal product.[151]

Long-chain PFAS

PFOA

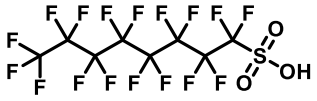

PFOS

Short-chain PFAS

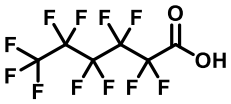

PFHxA

PFBS

Ether-linked PFAS

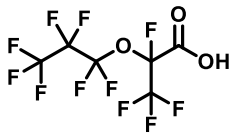

(Parent acid of)
GenX

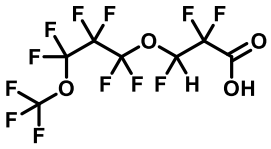

(Parent acid of)
ADONA

Recent development

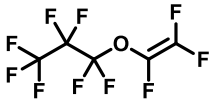

PPVE
Precursor for new PFAS

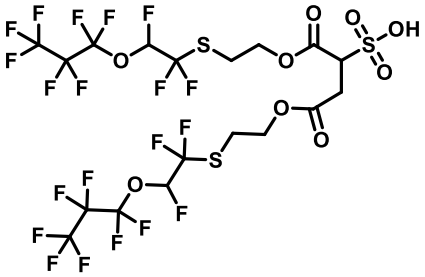

diFESOS

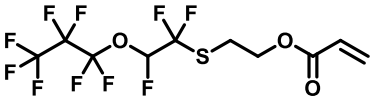

2-((1,1,2-trifluoro-2-(perfluoropropoxy)
ethyl)thio)ethyl acrylate

Scheme 16: Examples of PFAS. Legacy long-chain PFAS (top row). Established short-chain (second row), and ether-linked alternatives (third row). Recently developed PFAS from PPVE (bottom rows).

The surfactant diFESOS is derived from perfluoropropyl vinyl ether (PPVE) (Scheme 16). It bears two C3-perfluorinated chains and is bound to a hydrophilic

headgroup via -O-CHF-CF_2- ether linkages. The first degradation step of diFESOS is ester hydrolysis, yielding the alcohol FESOH.[154,155] The polyfluorinated FESOH is a semivolatile compound due to the low polarizability of the fluorine atoms (low interactions with molecules), and its atmospheric decomposition is a possible degradation pathway.[119,153] Joudan *et al*. discovered it to undergo a complex radical degradation pathway, which leads to carbonyl fluoride COF_2 and the perfluorated $C_3F_7OC(O)F$.[153] Carbonyl fluoride is unstable and hydrolyses to carbon dioxide and hydrogen fluoride upon contact with water.[156] Also in water, $C_3F_7OC(O)F$ undergoes a defluorination sequence, liberating hydrogen fluoride and perfluoropropionic acid (PFPrA) as a terminal product. PFPrA remains persistent in the environment,[147] but does not accumulate in animals.[154,157] Ultimately, the oxidation of FESOH mineralises 50% of its fluorine atoms. Furthermore, in consequence of low gas-phase lifetimes of FESOH (2.8 ± 1.3 days) and even lower lifetimes of its decomposition intermediates a decreased transport to remote regions is expected.[153]

In a follow-up paper Joudan *et al*. also studied the degradation of diFESOS in activated sludge as a model for wastewater treatment plants. After hydrolysis to FESOH and oxidation to the carboxylic acid FESCA the degradation starts from the functional group, and ultimately PFPrA is formed by defluorination.[155] Folkerson *et al*. studied the fate of diFESOS in rats and found it to be excreted via renal elimination after being metabolised via FESCA to a polyfluorinated ether sulfonate (2H 3:2 PFESA) and PFPrA.[154]

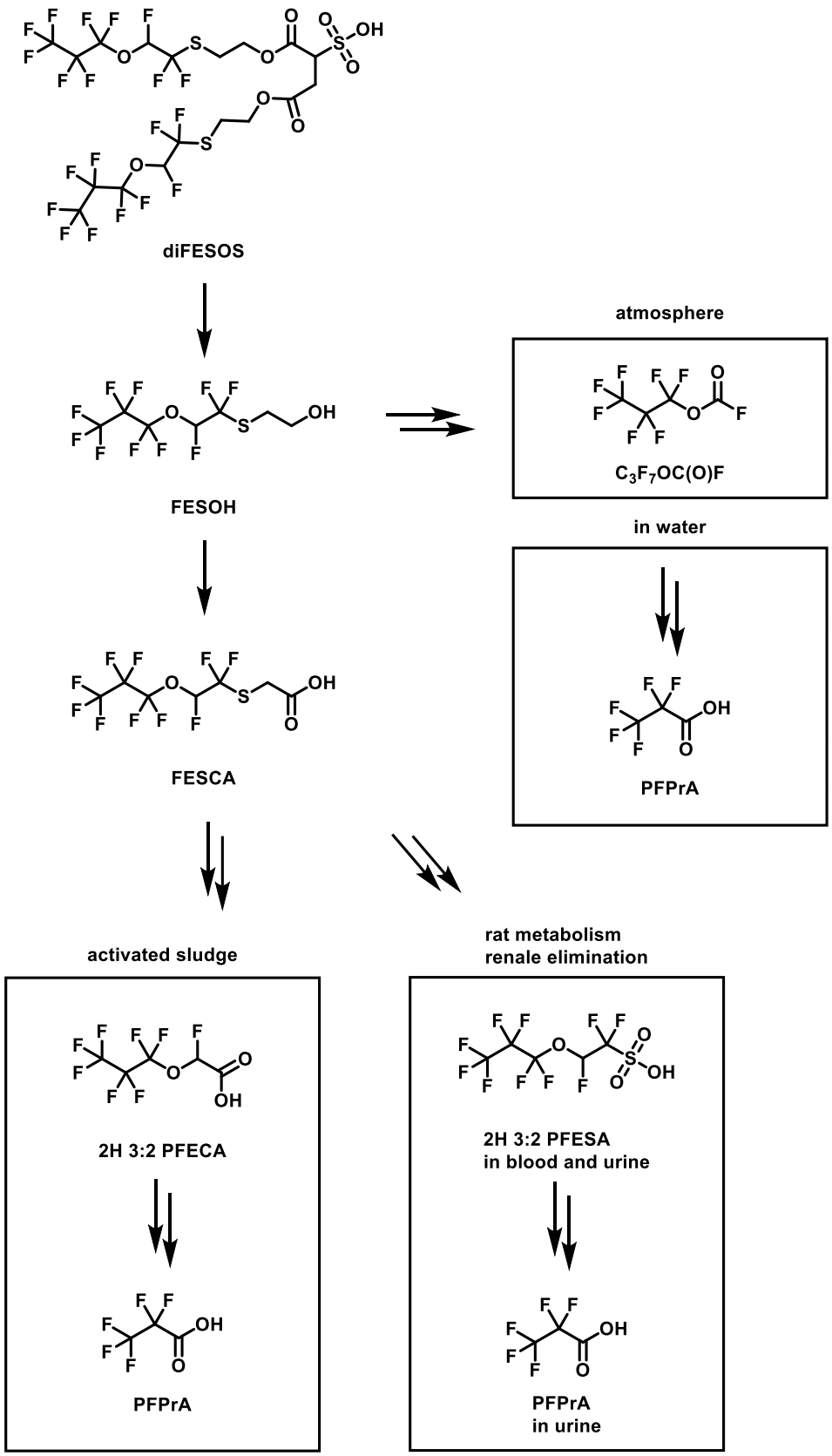

Scheme 17: Main degradation pathways of diFESOS as found by Joudan et al.[153,155] and Folkerson et al.[154]

1.6.2 Surfactants

Fluorosurfactants are employed in consumer products like shampoo[129] as well as in specialised applications like firefighting foam[121] or as additives in catalytical processes to enable micellar systems.[158] In consequence of the specific properties of fluorine and fluorine-carbon-bonds (see chapter 1.6 Fluorinated polymers), fluorosurfactants in general have especially high surface activities and lead to low surface tensions in aqueous media.[121] Their critical micelle concentration (cmc) is also lower than the cmc of comparable hydrocarbon surfactants due to a higher surface area. Classic surfactants consist of a hydrophilic head group (anionic, cationic, amphiphilic, or non-ionic polar) and a hydrophobic tail. In fluorosurfactants the tail is also oleophobic, leading to surface activity in aqueous as well as in hydrocarbon solvents.[120] L'Oréal developed oligomeric random and block copolymers with a multitude of ionic and non-ionic headgroups synthesised via cationic ring-opening polymerisation of epoxides bearing per- and polyfluorinated side chains. These surfactants were especially designed as shampoo additives for greasy hair to render the hair oil-repellent and to reduce re-greasing.[129]

The activity of surfactants can be evaluated via their cmc or via their surface tension. For the latter it may be distinguished between the static surface tension of a system at equilibrium and the dynamic surface tension of a changing system. The static surface tension γ_{stat} can be determined experimentally using the Wilhelmy plate method (DIN EN 14370) by inserting a metal plate into the surfactant solution and measuring the tension force F.[120,159] It is calculated by equation (38) using the wetted plate length L and the contact angle θ. If the plate is completely wetted, θ becomes zero and cos θ becomes one.[159]

$$\gamma_{stat} = \frac{F}{L \cos\theta} = \frac{F}{L} \qquad (38)$$

The dynamic surface tension γ_{dyn} can be determined by the bubble pressure method. Air bubbles are released from a capillary inside the surfactant solution and pressure changes are measured in combination with the bubble lifetime (39) with the capillary radius r, the maximal pressure p_{max}, the liquids density ρ, the gravity g and the immersion depth h.[159]

$$\gamma_{dyn} = \frac{r[p_{max} - \rho g h]}{2} \qquad (39)$$

Commercially available fluorosurfactants typically consist of C6 (e.g. S-103A-6 by chemguard) or C8 (e.g. perfluorooctane sulfonate) per- or polyfluorocarbon tails and show surface tensions between 15 and 33 mN m^{-1}.[121,160,161] The ecological considerations of per- and polyfluorinated compounds and their governmental regulations are discussed in chapter 1.6.1 Ecological considerations and restrictions of fluorine containing compounds.

More recently, eco-friendly fluorosurfactants have attracted high interest. The relevance of degradability and considerations regarding the perfluoropropyl vinyl ether (PPVE) derived diFESOS are also discussed in chapter 1.6.1. The TIVIDA® fluorosurfactants series by Merck KGaA uses ultrashort fluorinated alkyl groups (C2 and C3) that do not bioaccumulate and are non-toxic. Their surfactant profile is highly comparable to established compounds, as they reach static surface tensions of 17 to 23 mN m^{-1} and dynamic surface tensions of 17 to 20 mN m^{-1} after 60 s (0.1wt% of active ingredient).[162–164] Furthermore, Merck KGaA is currently investing in degradable fluorosurfactants derived from PPVE and similar structures, either as small molecules or coupled to polyethylene glycol or polypropylene glycol. Static surface tensions were reported to be between 18 and 28 mN m^{-1} and cmc values of 6 to 600 mg L^{-1} were achieved.[160,165–167] Besides Merck more companies are investing in this field, for example, Omnova Solutions Inc. with their fluorosurfactants series PolyFox achieving surface tensions down to 24 mN m^{-1} (0.1wt% of active ingredient).[168,169]

1.6.3 Coatings

A multitude of applications requires antistick, dirt-repellency and antifouling surfaces. Areas of interest are for example medical implants[170,171], outdoor-clothing[172], the automobile-industry[173] and optical elements[174]. These properties are typically achieved by cost- and resource-effective surface coatings in comparison to whole applications made of the repellent material. Silicon or long-chain alkylated polymers are used for water-repellent coatings[175,176] but are not suitable for oil-repellency for which fluorocarbon polymers are used[177,178] (Scheme 17). Application of the coating on the textile is done either via emulsion, chemical reaction, film formation on the fibre (typically procedure for silicone or fluorocarbon products) or utilising special fabric constructions like stretched PTFE films (Gore-Tex). To optimise the repellency properties the chains are oriented by heat curing.[177]

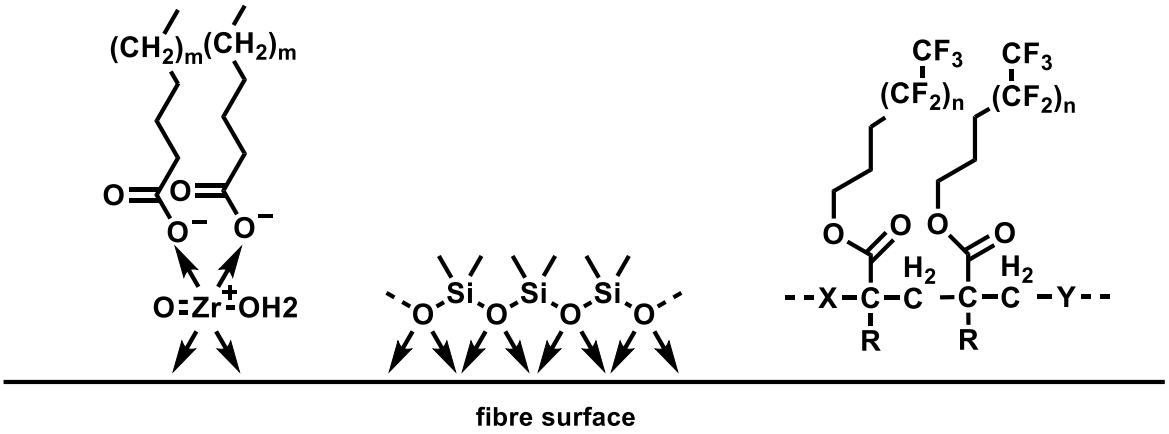

Scheme 18: Textile coatings. Water-repellent zirconium fatty acid (left) and polydimethylsiloxane (middle). Water- and oil-repellent fluorocarbon polyacrylate (right). R = H or CH_3; X and Y are comonomers. Adapted from Schindler.[177]

Repellent coating functions by decreasing the free energy at the surface. The internal interactions of the liquid drop must be higher than those of the drop (index: l) to the surface (index: s) for the drop to keep its shape. The critical surface energy γ_{sa} (index a: air; cellulose 100-120 mN m^{-1}, raw cotton 44 mN m^{-1}) (or tension for liquids γ_{la}) must be lower than the liquids γ_{liquid}. The wettability of a surface can be described by the spreading coefficient *S* with the interfacial tension γ_{sl} (40).[179]

$$S = \gamma_{sa} - (\gamma_{la} + \gamma_{sl}) \qquad (40)$$

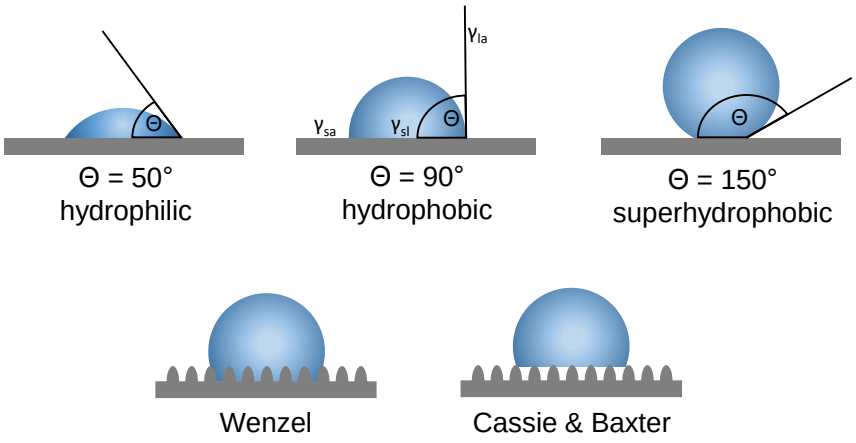

Figure 3: Wettability of surfaces. Top: Young's model showing from left to right hydrophilic, hydrophobic and superhydrophobic surfaces. Bottom: Wenzel and Cassie's (left) and Baxter's model (right) for rough surfaces.

Figure 3 shows the surface wettability models of Young, Wenzel and Cassie, and Baxter. Surfaces with contact angles over 90 ° are defined as hydrophobic (in the case of water) and will not wet. Surfaces with contact angles above 150° are called

superhydrophobic.[180] The relation between the energies and the contact angle between liquid and surface θ is described in the Young equation (41).[181,182]

$$\cos\theta = \frac{\gamma_{\mathrm{sa}} + \gamma_{\mathrm{sl}}}{\gamma_{\mathrm{la}}} \qquad (41)$$

Low γ_{sa} also enables dirt-repellency. γ_{la} of oils is with 20 – 35 mN m^{-1} multiple times lower than γ_{la} of water (72 mN m^{-1}).[179] While silicones (γ_{sa} = 24 – 30 mN m^{-1}) repel water, they will often not repel oil. Fluorocarbons, on the other hand, have a lower γ_{sa} (10 – 20 mN m^{-1}) and will repel oil. Ideal are close-packed arrays of CF_3-groups (6 mN m^{-1}, for comparison CH_3: 22 mN m^{-1}) as end groups of perfluorinated side chains.[179,183]

Porous materials like textiles composed of individual fibres are interspersed by capillaries. Whether the liquid is able to penetrate those, is furthermore dependent on the capillary pressure ΔP and the pore radius R (42).[179,184] A porous textile with a contact angle above 90° reaches a negative capillary pressure and capillary penetration is impossible.[179]

$$\Delta P = \frac{2\gamma_{sl}\cos\theta}{R} \qquad (42)$$

Wenzel advanced Young´s equation for rough (porous) surfaces, where the liquid penetrates the pores. In his theory the apparent θ_W and the real contact angle θ_F are connected with the roughness factor r (43).[185]

$$\cos\theta_W = r\cos\theta_F = r\frac{\gamma_{\mathrm{sa}} - \gamma_{\mathrm{sl}}}{\gamma_{\mathrm{la}}} \qquad (43)$$

Cassie and Baxter developed the apparent θ_{CA} equation for non-penetrated rough surfaces with the surface area Φ_s connected to the liquid (44).[186,187]

$$\cos\theta_{CA} = -1 + \phi_s\left[1 + \frac{\gamma_{\mathrm{sa}} - \gamma_{\mathrm{sl}}}{\gamma_{\mathrm{la}}}\right] \qquad (44)$$

Experimentally the contact angle is used to determine the hydrophobicity and the surface energy. In addition to the static contact angle, the dynamic contact angle of a moving drop can be measured. In this case the drop is, for example, either constantly increased and decreased in volume or moving down an inclined plane. Advancing (expanding, front) and receding (decreasing, back) angles are observed. The advancing contact angle is the maximum and the receding the minimum contact

angle of a surface. Their difference is called hysteresis.[188] The Wilhelmy plate method can be used to determine the dynamic contact angle.[120]

Standardised tests for the wettability determination of a surface were mostly developed by the American Association of Textile Chemists and Colorists (AATCC) and the International Organization for Standardization (ISO). Water resistance tests typically consist of spraying the textile with a fixed water pressure, followed by monitoring the wetting pattern and the absorbed as well as the permeated amount of water.[177,189,190] A typical oil resistance test is the method AATCC 118, in which a series of hydrocarbons with decreasing surface tension is placed on the fabric, and the wetting is monitored. The textile is graded with the number of the last non-wetting hydrocarbon (Table 1).[191]

Table 1: Grades and compounds of the oil resistance test AATCC 118.[191,192]

GRADE	HYDROCARBON	SURFACE TENSION
0	None	-
1	Kaydol (mineral oil)	31.5
2	65:35 Kaydol: n-hexadecane (by volume)	
3	n-hexadecane	27.3
4	n-tetradecane	26.4
5	n-dodecane	24.7
6	n-decane	23.5
7	n-octane	21.4
8	n-heptane	19.8

Alkylsiloxanes are typically used to achieve bonding to glass surfaces and methacrylates for bonding to textiles. Different methacrylate monomers with fluorinated side chains were developed by Merck KGaA in collaboration with academics using the knowledge described in chapter 1.6.1. In these cases, perfluoropropyl vinyl ether and derivatives were applied to achieve degradable textile coatings. An increase of the contact angles against water of glass from 44° to 94°, of polyurethane from 83° to 98° and of epoxyresin from 83° to 102° were reported.[174,192–194] Kredel and Gallei coated textiles with polymethacrylates derived from PPVE and stearyl, and achieved contact angles against water of 139-149° and oil repellency of

4-6, depending on the coated material. They found the repellencies to increase with the molar mass, influenced by the comonomer ratio.[195]

References

(1) Price, C. C. Polyethers. *Accounts of Chemical Research* **1974**, *7*, 294–301. DOI: 10.1021/ar50081a003.

(2) Kjellander, R.; Florin. Water Structure and Changes in Thermal Stability of the System Poly (et hylene oxide)-Water. *Journal of the Chemical Society, Faraday Transactions 1: Physical Chemistry in Condensed Phases* **1981**, *77* (9), 2053–2077.

(3) Dingels, C.; Schömer, M.; Frey, H. Die vielen Gesichter des Poly(ethylenglykol)s. *Chemie in unserer Zeit* **2011**, *45* (5), 338–349. DOI: 10.1002/ciuz.201100551.

(4) Johari, G. P.; Hallbrucker, A.; Mayer, E. Calorimetric relaxation and glass transition in poly(propylene glycols) and its monomer. *J. Polym. Sci. B Polym. Phys.* **1988**, *26* (9), 1923–1930. DOI: 10.1002/polb.1988.090260909.

(5) Allen, G.; Booth, C.; Price, C. VI-The Physical Properties of Poly(epoxides). *Polymer* **1967**, *8*, 414–418. DOI: 10.1016/0032-3861(67)90042-0.

(6) *Polyethylenglykole [MAK Value Documentation in German language, 1995]*. https://onlinelibrary.wiley.com/doi/pdf/10.1002/3527600418.mb2532268kskd0021 (accessed 2022-12-19).

(7) Zarrintaj, P.; Ramsey, J. D.; Samadi, A.; Atoufi, Z.; Yazdi, M. K.; Ganjali, M. R.; Amirabad, L. M.; Zangene, E.; Farokhi, M.; Formela, K.; Saeb, M. R.; Mozafari, M.; Thomas, S. Poloxamer: A versatile tri-block copolymer for biomedical applications. *Acta biomaterialia* **2020**, *110*, 37–67. DOI: 10.1016/j.actbio.2020.04.028. Published Online: May. 15, 2020.

(8) Knop, K.; Hoogenboom, R.; Fischer, D.; Schubert, U. S. Poly(ethylene glycol) in drug delivery: pros and cons as well as potential alternatives. *Angewandte Chemie (International ed. in English)* **2010**, *49* (36), 6288–6308. DOI: 10.1002/anie.200902672.

(9) Liu, Y.; Reidler, H.; Pan, J.; Milunic, D.; Qin, D.; Chen, D.; Vallejo, Y. R.; Yin, R. A double antigen bridging immunogenicity ELISA for the detection of antibodies to polyethylene glycol polymers. *Journal of pharmacological and toxicological methods* **2011**, *64* (3), 238–245. DOI: 10.1016/j.vascn.2011.07.003. Published Online: Jul. 29, 2011.

(10) Hamad, I.; Hunter, A. C.; Szebeni, J.; Moghimi, S. M. Poly(ethylene glycol)s generate complement activation products in human serum through increased alternative pathway turnover and a MASP-2-dependent process. *Molecular Immunology* **2008**, *46* (2), 225–232. DOI: 10.1016/j.molimm.2008.08.276. Published Online: Oct. 11, 2008.

(11) Armstrong, J. K. The occurrence, induction, specificity and potential effect of antibodies against poly(ethylene glycol). In *PEGylated Protein Drugs: Basic Science and Clinical Applications*; Birkhäuser Basel, 2009; pp 147–168. DOI: 10.1007/978-3-7643-8679-5_9.

(12) Würtz, A. Neue Untersuchungen über das Aethylenoxyd. *J. Prakt. Chem.* **1860**, *81* (1), 91–93. DOI: 10.1002/prac.18600810110.

(13) Lourenço, A. V. Intermediäre Aether des Glykols. *J. Prakt. Chem.* **1860**, *79* (1), 212–213. DOI: 10.1002/prac.18600790130.

(14) Lourenço, A. V. Ueber die Polyäthylenalkohole. *J. Prakt. Chem.* **1862**, *85* (1), 389–392. DOI: 10.1002/prac.18620850149.

(15) Flory, P. J. Molecular Size Distribution in Ethylene Oxide Polymers. *Journal of the American Chemical Society* **1940**, *62* (6), 1561–1565. DOI: 10.1021/ja01863a066.

(16) Szwarc, M. Living polymers. Their discovery, characterization, and properties. *J. Polym. Sci. A Polym. Chem.* **1998**, *36* (1), ix–xv. DOI: 10.1002/(SICI)1099-0518(19980115)36:1<IX:AID-POLA2>3.0.CO;2-9.

(17) Nuyken, O.; Pask, S. Ring-Opening Polymerization—An Introductory Review. *Polymers* **2013**, *5* (2), 361–403. DOI: 10.3390/polym5020361.

(18) Pell, A. S.; Pilcher, G. Measurements of heats of combustion by flame calorimetry. Part 3.—Ethylene oxide, trimethylene oxide, tetrahydrofuran and tetrahydropy. *Trans. Faraday Soc.* **1965**, *61* (0), 71–77. DOI: 10.1039/tf9656100071.

(19) Bednarek, M.; Kubisa, P.; Penczek, S. Coexistence of Activated Monomer and Active Chain End Mechanisms in Cationic Copolymerization of Tetrahydrofuran with Ethylene Oxide. *Macromolecules* **1999**, *32* (16), 5257–5263. DOI: 10.1021/ma9900939.

(20) Herzberger, J.; Niederer, K.; Pohlit, H.; Seiwert, J.; Worm, M.; Wurm, F. R.; Frey, H. Polymerization of Ethylene Oxide, Propylene Oxide, and Other Alkylene Oxides: Synthesis, Novel Polymer Architectures, and Bioconjugation. *Chemical*

reviews **2016**, *116* (4), 2170–2243. DOI: 10.1021/acs.chemrev.5b00441. Published Online: Dec. 29, 2015.

(21) Quirk, R. P.; Lee, B. Experimental Criteria for Living Polymerizations. *Polym. Int.* **1992**, *27* (4), 359–367. DOI: 10.1002/pi.4990270412.

(22) Pearson, R. G. Hard and Soft Acids and Bases. *J. Am. Chem. Soc.* **1963**, *85* (22), 3533–3539. DOI: 10.1021/ja00905a001.

(23) PENCZEK, S.; CYPRYK, M.; DUDA, A.; KUBISA, P.; SLOMKOWSKI, S. Living ring-opening polymerizations of heterocyclic monomers. *Progress in Polymer Science* **2007**, *32* (2), 247–282. DOI: 10.1016/j.progpolymsci.2007.01.002.

(24) Ponomarenko, V. A.; Khomutov, A. M.; Il'chenko, S. I.; Ignatenko, A. V. The effect of substituents of the anionic polymerization of α-oxides. *Polymer Science U.S.S.R.* **1971**, *13* (7), 1735–1740. DOI: 10.1016/0032-3950(71)90364-9.

(25) Brocas, A.-L.; Mantzaridis, C.; Tunc, D.; Carlotti, S. Polyether synthesis: From activated or metal-free anionic ring-opening polymerization of epoxides to functionalization. *Progress in Polymer Science* **2013**, *38* (6), 845–873. DOI: 10.1016/j.progpolymsci.2012.09.007.

(26) Linker, O.; Blankenburg, J.; Maciol, K.; Bros, M.; Frey, H. Ester Functional Epoxide Monomers for Random and Gradient Poly(ethylene glycol) Polyelectrolytes with Multiple Carboxylic Acid Moieties. *Macromolecules* **2020**, *53* (9), 3524–3534. DOI: 10.1021/acs.macromol.9b02320.

(27) Sakakibara, K.; Nakano, K.; Nozaki, K. Regio-controlled ring-opening polymerization of perfluoroalkyl-substituted epoxides. *Chemical communications (Cambridge, England)* **2006** (31), 3334–3336. DOI: 10.1039/b606693c. Published Online: Jun. 30, 2006.

(28) Billouard, C.; Carlotti, S.; Desbois, P.; Deffieux, A. “Controlled” High-Speed Anionic Polymerization of Propylene Oxide Initiated by Alkali Metal Alkoxide/Trialkylaluminum Systems. *Macromolecules* **2004**, *37* (11), 4038–4043. DOI: 10.1021/ma035768t.

(29) Oguni, N.; Lee, K.; Tani, H. Microstructure Analysis of Poly(propylene oxide) by 13C Nuclear Magnetic Resonance Spectroscopy. *Macromolecules* **1972**, *5* (6), 819–820.

(30) Allgaier, J.; Willbold, S.; Chang, T. Synthesis of Hydrophobic Poly(alkylene oxide)s and Amphiphilic Poly(alkylene oxide) Block Copolymers. *Macromolecules* **2007**, *40* (3), 518–525. DOI: 10.1021/ma062417g.

(31) Herold, R. J. Method of making a polyether using a double metal cyanide complex compound. 258,603.

(32) Gervais, M.; Brocas, A.-L.; Deffieux, A.; Ibarboure, E.; Carlotti, S. Rapid and controlled synthesis of hydrophobic polyethers by monomer activation. *Pure and Applied Chemistry* **2012**, *84* (10), 2103–2111. DOI: 10.1351/PAC-CON-11-11-16.

(33) Müller, S. S.; Moers, C.; Frey, H. A Challenging Comonomer Pair: Copolymerization of Ethylene Oxide and Glycidyl Methyl Ether to Thermoresponsive Polyethers. *Macromolecules* **2014**, *47* (16), 5492–5500. DOI: 10.1021/ma501280k.

(34) Maciol, K. Synthesis of Reactive Polyether Copolymers. Dissertation, Johannes Gutenberg-Universtität Mainz, Mainz, 2018.

(35) Vandenberg, E. J. Organometallic catalysts for polymerizing monosubstituted epoxides. *Journal of Polymer Science* **1960**, *47* (149), 486–489.

(36) Carlotti, S.; Desbois, P.; Billouard, C.; Deffieux, A. Reactivity control in anionic polymerization of ethylenic and heterocyclic monomers through formation of ‘ate’ complexes. *Polym. Int.* **2006**, *55* (10), 1126–1131. DOI: 10.1002/pi.1981.

(37) Eisch, J. J.; Liu, Z.-R.; Singh, M. Organometallic compounds of Group III. 48. High regioselectivity in the alternative, reductive cleavages of terminal epoxides with aluminum reagents. *Journal of Organic Chemistry* **1992**, *57* (5), 1618–1621.

(38) Zhang, D.; Boopathi, S. K.; Hadjichristidis, N.; Gnanou, Y.; Feng, X. Metal-Free Alternating Copolymerization of CO2 with Epoxides: Fulfilling "Green" Synthesis and Activity. *Journal of the American Chemical Society* **2016**, *138* (35), 11117–11120. DOI: 10.1021/jacs.6b06679. Published Online: Aug. 26, 2016.

(39) Zhang, C.; Geng, X.; Zhang, X.; Gnanou, Y.; Feng, X. Alkyl borane-mediated metal-free ring-opening (co)polymerizations of oxygenated monomers. *Progress in Polymer Science* **2023**, *136*, 101644. DOI: 10.1016/j.progpolymsci.2022.101644.

(40) Song, Q.; Zhao, J.; Zhang, G.; Taton, D.; Peruch, F.; Carlotti, S. N-Heterocyclic carbene/Lewis acid-mediated ring-opening polymerization of propylene oxide. Part 2: Toward dihydroxytelechelic polyethers using triethylborane. *European Polymer Journal* **2020**, *134*, 109839. DOI: 10.1016/j.eurpolymj.2020.109839.

(41) Zhang, C.-J.; Duan, H.-Y.; Hu, L.-F.; Zhang, C.-H.; Zhang, X.-H. Metal-Free Route to Precise Synthesis of Poly(propylene oxide) and Its Blocks with High Activity. *ChemSusChem* **2018**, *11* (24), 4209–4213. DOI: 10.1002/cssc.201802258. Published Online: Nov. 19, 2018.

(42) Andrea, K. A.; Plommer, H.; Kerton, F. M. Ring-opening polymerizations and copolymerizations of epoxides using aluminum- and boron-centered catalysts. *European Polymer Journal* **2019**, *120*, 109202. DOI: 10.1016/j.eurpolymj.2019.08.029.

(43) Chakraborty, D.; Rodriguez, A.; Chen, E. Y.-X. Catalytic Ring-Opening Polymerization of Propylene Oxide by Organoborane and Aluminum Lewis Acids. *Macromolecules* **2003**, *36* (15), 5470–5481. DOI: 10.1021/ma034050a.

(44) Yang, G.-W.; Zhang, Y.-Y.; Xie, R.; Wu, G.-P. Scalable Bifunctional Organoboron Catalysts for Copolymerization of CO2 and Epoxides with Unprecedented Efficiency. *Journal of the American Chemical Society* **2020**, *142* (28), 12245–12255. DOI: 10.1021/jacs.0c03651. Published Online: Jun. 30, 2020.

(45) Qi, H.; Xie, R.; Yang, G.-W.; Zhang, Y.-Y.; Xu, C.-K.; Wang, Y.; Wu, G.-P. Rational Optimization of Bifunctional Organoboron Catalysts for Versatile Polyethers via Ring-Opening Polymerization of Epoxides. *Macromolecules* **2022**, *55* (20), 9081–9090. DOI: 10.1021/acs.macromol.2c01596.

(46) Andrea, K. A.; Kerton, F. M. Triarylborane-Catalyzed Formation of Cyclic Organic Carbonates and Polycarbonates. *ACS Catal.* **2019**, *9* (3), 1799–1809. DOI: 10.1021/acscatal.8b04282.

(47) Taherimehr, M.; Al-Amsyar, S. M.; Whiteoak, C. J.; Kleij, A. W.; Pescarmona, P. P. High activity and switchable selectivity in the synthesis of cyclic and polymeric cyclohexene carbonates with iron amino triphenolate catalysts. *Green Chem.* **2013**, *15* (11), 3083. DOI: 10.1039/c3gc41303a.

(48) Chen, Z.; Yang, J.-L.; Lu, X.-Y.; Hu, L.-F.; Cao, X.-H.; Wu, G.-P.; Zhang, X.-H. Triethyl borane-regulated selective production of polycarbonates and cyclic carbonates for the coupling reaction of CO 2 with epoxides. *Polym. Chem.* **2019**, *10* (26), 3621–3628. DOI: 10.1039/C9PY00398C.

(49) Patil, N.; Bhoopathi, S.; Chidara, V.; Hadjichristidis, N.; Gnanou, Y.; Feng, X. Recycling a Borate Complex for Synthesis of Polycarbonate Polyols: Towards an Environmentally Friendly and Cost-Effective Process. *ChemSusChem* **2020**, *13* (18), 5080–5087. DOI: 10.1002/cssc.202001395. Published Online: Jul. 30, 2020.

(50) Wu, G.-P.; Yang, G.-W.; Zhang, Y.-Y. An organic metal-free catalyst with electrophilic and nucleophilic dual functions, its preparation method and application. An organic metal-free catalyst with electrophilic and nucleophilic dual functions, its preparation method and application. CN112387307A.

(51) Wu, G.; Yang, G.; Zhang, Y. Organic metal-free catalysts with electrophilic and nucleophilic dual-functions, preparation methods of making the same, and thereof. 17/278,327.

(52) Kisan, S.; Krishnakumar, V.; Gunanathan, C. Ruthenium-Catalyzed Anti-Markovnikov Selective Hydroboration of Olefins. *ACS Catal.* **2017**, *7* (9), 5950–5954. DOI: 10.1021/acscatal.7b01750.

(53) Chen, C.; Gnanou, Y.; Feng, X. Borinane-based organoboron catalysts for alternating copolymerization of CO 2 with cyclic ethers: improved productivity and facile recovery. *Polym. Chem.* **2022**, *13* (45), 6312–6321. DOI: 10.1039/D2PY01161A.

(54) Yang, G.-W.; Xu, C.-K.; Xie, R.; Zhang, Y.-Y.; Zhu, X.-F.; Wu, G.-P. Pinwheel-Shaped Tetranuclear Organoboron Catalysts for Perfectly Alternating Copolymerization of CO2 and Epichlorohydrin. *Journal of the American Chemical Society* **2021**, *143* (9), 3455–3465. DOI: 10.1021/jacs.0c12425. Published Online: Feb. 16, 2021.

(55) Yang, G.-W.; Zhang, Y.-Y.; Xie, R.; Wu, G.-P. High-Activity Organocatalysts for Polyether Synthesis via Intramolecular Ammonium Cation Assisted SN 2 Ring-Opening Polymerization. *Angew. Chem. Int. Ed.* **2020**, *59* (39), 16910–16917. DOI: 10.1002/anie.202002815. Published Online: Jul. 27, 2020.

(56) Yang, G.-W.; Zhang, Y.-Y.; Wu, G.-P. Modular Organoboron Catalysts Enable Transformations with Unprecedented Reactivity. *Accounts of Chemical Research* **2021**, *54* (23), 4434–4448. DOI: 10.1021/acs.accounts.1c00620. Published Online: Nov. 21, 2021.

(57) Morrill, C.; Grubbs, R. H. Synthesis of functionalized vinyl boronates via ruthenium-catalyzed olefin cross-metathesis and subsequent conversion to vinyl halides. *The Journal of organic chemistry* **2003**, *68* (15), 6031–6034. DOI: 10.1021/jo0345345.

(58) Martin, R.; Buchwald, S. L. Palladium-catalyzed Suzuki-Miyaura cross-coupling reactions employing dialkylbiaryl phosphine ligands. *Accounts of Chemical Research* **2008**, *41* (11), 1461–1473. DOI: 10.1021/ar800036s.

(59) Brown, H. C.; Zweifel, G. A Stereospecific cis Hydration of the Double Bond in Cyclic Derivatives. *J. Am. Chem. Soc.* **1959**, *81* (1), 247. DOI: 10.1021/ja01510a059.

(60) Chung, T. C.; Rhubright, D. Functionalization of polypropylene by hydroboration. *J. Polym. Sci. A Polym. Chem.* **1993**, *31* (11), 2759–2763. DOI: 10.1002/pola.1993.080311112.

(61) Soloway, A. H.; Tjarks, W.; Barnum, B. A.; Rong, F.-G.; Barth, R. F.; Codogni, I. M.; Wilson, J. G. The Chemistry of Neutron Capture Therapy. *Chemical reviews* **1998**, *98*, 1515–1562.

(62) Pitto-Barry, A. Polymers and boron neutron capture therapy (BNCT): a potent combination. *Polym. Chem.* **2021**, *12* (14), 2035–2044. DOI: 10.1039/D0PY01392G.

(63) Hinkes, S. P. A.; Klein, C. D. P. Virtues of Volatility: A Facile Transesterification Approach to Boronic Acids. *Organic letters* **2019**, *21* (9), 3048–3052. DOI: 10.1021/acs.orglett.9b00584. Published Online: Apr. 23, 2019.

(64) Cambre, J. N.; Sumerlin, B. S. Biomedical applications of boronic acid polymers. *Polymer* **2011**, *52* (21), 4631–4643. DOI: 10.1016/j.polymer.2011.07.057.

(65) Yang, W.; Gao, X.; Wang, B. Boronic acid compounds as potential pharmaceutical agents. *Medicinal research reviews* **2003**, *23* (3), 346–368. DOI: 10.1002/med.10043.

(66) Huval, C. C.; Li, X.; Holmes-Farley. Stephen Randall; Dhal, P. K. Polymeric boronic acid derivatives as lipase inhibitors. 10/535,639.

(67) Schneider, H.-J.; Kato, K.; Strongin, R. M. Chemomechanical Polymers as Sensors and Actuators for Biological and Medicinal Applications. *Sensors (Basel, Switzerland)* **2007**, *7* (8), 1578–1611. DOI: 10.3390/s7081578.

(68) Jay, J. I.; Lai, B. E.; Myszka, D. G.; Mahalingam, A.; Langheinrich, K.; Katz, D. F.; Kiser, P. F. Multivalent benzoboroxole functionalized polymers as gp120 glycan targeted microbicide entry inhibitors. *Molecular pharmaceutics* **2010**, *7* (1), 116–129. DOI: 10.1021/mp900159n.

(69) Shiino, D.; Murata, Y.; Kataoka, K.; Koyama, Y.; Yokoyama, M.; Okano, T.; Sakurai, Y. Preparation and characterization of a glucose-responsive insulin-releasing polymer device. *Biomaterials* **1994**, *15* (2), 121–128. DOI: 10.1016/0142-9612(94)90261-5.

(70) Yang, H.-S.; Cho, S.; Eom, Y.; Park, S.-A.; Hwang, S. Y.; Jeon, H.; Oh, D. X.; Park, J. Preparation of Self-Healable and Spinnable Hydrogel by Dynamic Boronate Ester Bond from Hyperbranched Polyglycerol and Boronic Acid-Containing Polymer. *Macromol. Res.* **2021**, *29* (2), 140–148. DOI: 10.1007/s13233-021-9016-5.

(71) Yang, X.; Guo, M.; Wu, Y.; Xue, S.; Li, Z.; Zhou, H.; Smith, A. T.; Sun, L. Biomimetic Boroxine-Based Multifunctional Thermosets via One-Pot Synthesis. *ACS applied materials & interfaces* **2020**, *12* (50), 56445–56453. DOI: 10.1021/acsami.0c16736. Published Online: Dec. 2, 2020.

(72) Natansohn, A. Method for reactivity ratio determination in high-conversion copolymerisations by means of 1H-n.m.r. spectroscopy. *Brit. Poly.J.* **1978**, *10* (3), 218–220. DOI: 10.1002/pi.4980100313.

(73) Beckingham, B. S.; Sanoja, G. E.; Lynd, N. A. Simple and Accurate Determination of Reactivity Ratios Using a Nonterminal Model of Chain Copolymerization. *Macromolecules* **2015**, *48* (19), 6922–6930. DOI: 10.1021/acs.macromol.5b01631.

(74) Wall, F. T. The Structure of Vinyl Copolymers. *Journal of the American Chemical Society* **1941**, *63* (7), 1862–1866.

(75) Jaacks, V. A novel method of determination of reactivity ratios in binary and ternary copolymerizations. *Makromol. Chem.* **1972**, *161* (1), 161–172. DOI: 10.1002/macp.1972.021610110.

(76) Jaacks, V. Eine neuartige Methode zur Bestimmung von Copolymerisationsparametern. *Angew. Chem.* **1967**, *79* (9), 419. DOI: 10.1002/ange.19670790927.

(77) Odian, G. G. *Principles of polymerization*, Fourth edition; Wiley, 2010. DOI: 10.1002/047147875X.

(78) Lee, B. F.; Wolffs, M.; Delaney, K. T.; Sprafke, J. K.; Leibfarth, F. A.; Hawker, C. J.; Lynd, N. A. Reactivity ratios, and mechanistic insight for anionic ring-opening copolymerization of epoxides. *Macromolecules* **2012**, *45* (9), 3722–3731. DOI: 10.1021/ma300634d. Published Online: Apr. 17, 2012.

(79) Alfrey, T.; Goldfinger, G. The Mechanism of Copolymerization. *The Journal of Chemical Physics* **1944**, *12* (6), 205–209. DOI: 10.1063/1.1723934.

(80) Mayo, F. R.; Lewis, F. M. Copolymerization. I. A Basis for Comparing the Behavior of Monomers in Copolymerization; The Copolymerization of Styrene and Methyl Methacrylate. *J. Am. Chem. Soc.* **1944**, *66* (9), 1594–1601. DOI: 10.1021/ja01237a052.

(81) Wall, F. T. The Structure of Copolymers. II. *Journal of American Chemical Society* **1944**, *66*, 2030–2057.

(82) Molau, G. E. Heterogeneous polymer systems. I. Polymeric oil-in-oil emulsions. *J. Polym. Sci. A Gen. Pap.* **1965**, *3* (4), 1267–1278. DOI: 10.1002/pol.1965.100030402.

(83) Skeist, I. Copolymerization: the composition distribution curve. *Journal of the American Chemical Society* **1946**, *68* (9), 1781–1784. DOI: 10.1021/ja01213a031.

(84) Meyer, V. E.; Lowry, G. G. Integral and differential binary copolymerization equations. *J. Polym. Sci. A Gen. Pap.* **1965**, *3* (8), 2843–2851. DOI: 10.1002/pol.1965.100030811.

(85) Roald Hoffmann; Vladimir I Minkin; Barry K Carpenter. Ockham's Razor and chemistry. *Bulletin de la Societe Chimique de France* **1996**, *2* (133), 117–130.

(86) Blankenburg, J.; Kersten, E.; Maciol, K.; Wagner, M.; Zarbakhsh, S.; Frey, H. The poly(propylene oxide- co -ethylene oxide) gradient is controlled by the polymerization method: determination of reactivity ratios by direct comparison of different copolymerization models. *Polym. Chem.* **2019**, *10* (22), 2863–2871. DOI: 10.1039/C9PY00500E.

(87) Patil, S. D.; Rhodes, D. G.; Burgess, D. J. DNA-based therapeutics and DNA delivery systems: a comprehensive review. *The AAPS journal* **2005**, *7* (1), E61-77. DOI: 10.1208/aapsj070109. Published Online: Apr. 8, 2005.

(88) Luo, D.; Saltzman, W. M. Synthetic DNA delivery systems. *Nat Biotechnol* **2000**, *18* (1), 33–37. DOI: 10.1038/71889.

(89) Akinc, A.; Thomas, M.; Klibanov, Alexander, M.; Langer, R. Exploring polyethylenimine-mediated DNA transfection and the proton sponge hypothesis. *The journal of gene medicine* **2005**, *7*, 657–663.

(90) Godbey, W. T.; Wu, K. K.; Mikos, A. G. Poly(ethylenimine) and its role in gene delivery. *Journal of controlled release : official journal of the Controlled Release Society* **1999**, *60* (2-3), 149–160. DOI: 10.1016/s0168-3659(99)00090-5.

(91) Florea, B. I.; Meaney, C.; Junginger, H. E.; Borchard, G. Transfection efficiency and toxicity of polyethylenimine in differentiated Calu-3 and nondifferentiated COS-1 cell cultures. *AAPS J* **2002**, *4* (3), E12. DOI: 10.1208/ps040312.

(92) Leclercq, F.; Dubertret, C.; Pitard, B.; Scherman, D.; Herscovici, J. Synthesis of glycosylated polyethylenimine with reduced toxicity and high transfecting efficiency. *Bioorganic & medicinal chemistry letters* **2000**, *10* (11), 1233–1235. DOI: 10.1016/s0960-894x(00)00195-5.

(93) Petersen, H.; Fechner, P. M.; Fischer, D.; Kissel, T. Synthesis, Characterization, and Biocompatibility of Polyethylenimine- graft -poly(ethylene glycol) Block Copolymers. *Macromolecules* **2002**, *35* (18), 6867–6874. DOI: 10.1021/ma012060a.

(94) Boussif, O.; Lezoualc'h, F.; Zanta, M. A.; Mergny, M. D.; Scherman, D.; Demeneix, B.; Behr, J.-P. A versatile vector for gene and oligonucleotide transfer into cells in culture and in vivo: Polyethyleneimine. *Proceedings of the National Academy of Sciences of the United States of America* **1995**, *92*, 7297–7301.

(95) Gosselin, M. A.; Guo, W.; Lee, R. J. Efficient gene transfer using reversibly cross-linked low molecular weight polyethylenimine. *Bioconjugate chemistry* **2001**, *12* (6), 989–994. DOI: 10.1021/bc0100455.

(96) Koyama, Y.; Umehara, M.; Mizuno, A.; Itaba, M.; Yasukouchi, T.; Natsume, K.; Suginaka, A. Synthesis of novel poly(ethylene glycol) derivatives having pendant amino groups and aggregating behavior of its mixture with fatty acid in water. *Bioconjugate chemistry* **1996**, *7* (3), 298–301. DOI: 10.1021/bc9600123.

(97) Verkoyen, P.; Frey, H. Amino-functional polyethers: versatile, stimuli-responsive polymers. *Polym. Chem.* **2020**, *11* (24), 3940–3950. DOI: 10.1039/d0py00466a.

(98) Burness, D. M.; Bayer, H. O. Synthesis and Reactions of Quaternary Salts of Glyeidyl Amines. *The Journal of organic chemistry* **1963**, *28* (9), 2283–2288. DOI: 10.1021/jo01044a031.

(99) Blankenburg, J.; Wagner, M.; Frey, H. Well-Defined Multi-Amino-Functional and Stimuli-Responsive Poly(propylene oxide) by Crown Ether Assisted Anionic Ring-Opening Polymerization. *Macromolecules* **2017**, *50* (22), 8885–8893. DOI: 10.1021/acs.macromol.7b01324.

(100) Obermeier, B.; Wurm, F.; Frey, H. Amino Functional Poly(ethylene glycol) Copolymers via Protected Amino Glycidol. *Macromolecules* **2010**, *43* (5), 2244–2251. DOI: 10.1021/ma902245d.

(101) Elter, J. K.; Eichhorn, J.; Ringleb, M.; Schacher, F. H. Amine-containing diblock terpolymers via AROP: a versatile method for the generation of multifunctional micelles. *Polym. Chem.* **2021**, *12* (27), 3900–3916. DOI: 10.1039/D1PY00666E.

(102) Herzberger, J.; Kurzbach, D.; Werre, M.; Fischer, K.; Hinderberger, D.; Frey, H. Stimuli-Responsive Tertiary Amine Functional PEGs Based on N , N -Dialkylglycidylamines. *Macromolecules* **2014**, *47* (22), 7679–7690. DOI: 10.1021/ma501367b.

(103) Verkoyen, P. Long-chain alkyl glycidyl ethers: Amphiphilic polyether architectures and non-covalent hydrogels. Dissertation, Johannes Gutenberg-Universtität Mainz, Mainz, 2020.

(104) Blankenburg, J.; Stark, M.; Frey, H. Oxidation-responsive polyether block copolymers lead to non-ionic polymer surfactants with multiple amine N -oxides. *Polym. Chem.* **2019**, *10* (13), 1569–1574. DOI: 10.1039/C9PY00093C.

(105) Isono, T.; Asai, S.; Satoh, Y.; Takaoka, T.; Tajima, K.; Kakuchi, T.; Satoh, T. Controlled/Living Ring-Opening Polymerization of Glycidylamine Derivatives Using t -Bu-P 4 /Alcohol Initiating System Leading to Polyethers with Pendant Primary, Secondary, and Tertiary Amino Groups. *Macromolecules* **2015**, *48* (10), 3217–3229. DOI: 10.1021/acs.macromol.5b00556.

(106) Reuss, V. S.; Obermeier, B.; Dingels, C.; Frey, H. N,N -Diallylglycidylamine: A Key Monomer for Amino-Functional Poly(ethylene glycol) Architectures. *Macromolecules* **2012**, *45* (11), 4581–4589. DOI: 10.1021/ma300292m.

(107) Kelland, M.; Svartaas, T. M.; Dybvik, L. A. Control of Hydrate Formation by Surfactants and Polymers. In *SPE Annual Technical Conference and Exhibition*; Society of Petroleum Engineers, 1994. DOI: 10.2118/28506-MS.

(108) Kelland, M.; Svartaas, T. M.; Øvsthus, J.; Namba, T. A New Class of Kinetic Hydrate Inhibitor. *Annals of the New York Academy of Sciences* **2000**, *912* (1), 281–293.

(109) Kelland, M. A. History of the Development of Low Dosage Hydrate Inhibitors. *Energy Fuels* **2006**, *20* (3), 825–847. DOI: 10.1021/ef050427x.

(110) Colle, K. S.; Costello, C. A.; Oelfke, H. R.; Talley, L. D.; Longo, J. M.; Berluche, E. Method for inhibiting hydrate formation. 449,151.

(111) Sloan Jr., E. D. Method for controlling clathrate hydrates in fluid systems. 248,477.

(112) Magnusson, C. D.; Kelland, M. A. Nonpolymeric Kinetic Hydrate Inhibitors: Alkylated Ethyleneamine Oxides. *Energy Fuels* **2015**, *29* (10), 6347–6354. DOI: 10.1021/acs.energyfuels.5b01592.

(113) Zhang, Q.; Kelland, M. A. Kinetic inhibition performance of alkylated polyamine oxides on structure I methane hydrate. *Chemical Engineering Science* **2020**, *220*, 115652. DOI: 10.1016/j.ces.2020.115652.

(114) Lone, A.; Kelland, M. A. Exploring Kinetic Hydrate Inhibitor Test Methods and Conditions Using a Multicell Steel Rocker Rig. *Energy Fuels* **2013**, *27* (5), 2536–2547. DOI: 10.1021/ef400321z.

(115) Chemours. *The History of Teflon™ Fluoropolymers*. https://www.teflon.com/en/news-events/history (accessed 2023-02-11).

(116) Blanksby, S. J.; Ellison, G. B. Bond dissociation energies of organic molecules. *Accounts of Chemical Research* **2003**, *36* (4), 255–263. DOI: 10.1021/ar020230d.

(117) O'Hagan, D. Understanding organofluorine chemistry. An introduction to the C-F bond. *Chemical Society reviews* **2008**, *37* (2), 308–319. DOI: 10.1039/b711844a. Published Online: Oct. 17, 2007.

(118) Leroy, G.; Sana, M.; Wilante, C.; Nemba, R. M. Bond-dissociation energies of organic compounds. A tentative rationalization based on the concept of stabilization energy. *Journal of Molecular Structure* **1989**, *198*, 159–173. DOI: 10.1016/0022-2860(89)80036-5.

(119) Lemal, D. M. Perspective on fluorocarbon chemistry. *The Journal of organic chemistry* **2004**, *69* (1), 1–11. DOI: 10.1021/jo0302556.

(120) Kissa, E. *Fluorinated surfactants and repellents*, 2. ed., rev. and expanded.; Surfactants science series, Vol. 97; Dekker, 2001.

(121) Peshoria, S.; Nandini, D.; Tanwar, R. K.; Narang, R. Short-chain and long-chain fluorosurfactants in firefighting foam: a review. *Environ Chem Lett* **2020**, *18* (4), 1277–1300. DOI: 10.1007/s10311-020-01015-8.

(122) Améduri, B.; Boutevin, B. *Well-architectured fluoropolymers*:*Synthesis, properties and applications*; Elsevier, 2004.

(123) Sakakibara, K.; Nakano, K.; Nozaki, K. Regioregular Polymerization of Fluorine-Containing Epoxides. *Macromolecules* **2007**, *40* (17), 6136–6142. DOI: 10.1021/ma070428j.

(124) Smith, D. D.; Murch R. M.; Pierce, O. R. Fluorine-Containing Polyethers. *Industrial and Engineering Chemistry* **1957**, *49* (8), 1241–1246.

(125) Koyama, M.; Akiyama, M.; Kashiwagi, K.; Nozaki, K.; Okazoe, T. Synthesis of Crystalline CF3 -Rich Perfluoropolyethers from Hexafluoropropylene Oxide and (Trifluoromethyl)Trimethylsilane. *Macromolecular Rapid Communications* **2022**, *43* (9), e2200038. DOI: 10.1002/marc.202200038. Published Online: Mar. 20, 2022.

(126) Hagiwara, T.; Terasaki, Y.; Hamana, H.; Narita, T. Polymerization of 3,3,3-trifluoro-1,2-epoxypropane with organozinc compounds and alkali metal alkoxides. *Macromolecular Rapid Communications* **1992**, *13* (8), 363–370.

(127) Banks, R. E.; Smart, B. E.; Tatlow, J. C. *Organofluorine Chemistry*:*Principles and Commercial Applications*; Topics in Applied Chemistry Ser; Springer, 2013.

(128) Umezawa, J.; Hagiwara, T.; Hamana, H.; Narita, T.; Furuhashi, K.; Nohira, H. Ring-Opening Polymerization of 3,3,3-Trifluoro-1,2-epoxypropane. Studies on Monomer Reactivity and Polymer Structure. *Polymer Journal* **1994**, *26* (6), 715–721.

(129) Vanleberghe, G.; Sebag, H. Grenzflächenaktive perfluorierte Oligomere, Verfahren zu ihrer Herstellung und diese Oligomere enthaltende Mittel. C07 C 147/14.

(130) Dolbier, W. R. Fluorine chemistry at the millennium. *Journal of Fluorine Chemistry* **2005**, *126* (2), 157–163. DOI: 10.1016/j.jfluchem.2004.09.033.

(131) Evich, M. G.; Davis, M. J. B.; McCord, J. P.; Acrey, B.; Awkerman, J. A.; Knappe, D. R. U.; Lindstrom, A. B.; Speth, T. F.; Tebes-Stevens, C.; Strynar, M. J.; Wang, Z.; Weber, E. J.; Henderson, W. M.; Washington, J. W. Per- and polyfluoroalkyl substances in the environment. *Science (New York, N.Y.)* **2022**, *375* (6580), eabg9065. DOI: 10.1126/science.abg9065. Published Online: Feb. 4, 2022.

(132) Cousins, I. T.; Johansson, J. H.; Salter, M. E.; Sha, B.; Scheringer, M. Outside the Safe Operating Space of a New Planetary Boundary for Per- and Polyfluoroalkyl Substances (PFAS). *Environmental science & technology* **2022**, *56* (16), 11172–11179. DOI: 10.1021/acs.est.2c02765. Published Online: Aug. 2, 2022.

(133) Kärrman, A.; Harada, K. H.; Inoue, K.; Takasuga, T.; Ohi, E.; Koizumi, A. Relationship between dietary exposure and serum perfluorochemical (PFC) levels--a case study. *Environment international* **2009**, *35* (4), 712–717. DOI: 10.1016/j.envint.2009.01.010. Published Online: Feb. 27, 2009.

(134) Bartell, S. M.; Vieira, V. M. Critical review on PFOA, kidney cancer, and testicular cancer. *Journal of the Air & Waste Management Association (1995)* **2021**, *71* (6), 663–679. DOI: 10.1080/10962247.2021.1909668.

(135) Fenton, S. E.; Ducatman, A.; Boobis, A.; DeWitt, J. C.; Lau, C.; Ng, C.; Smith, J. S.; Roberts, S. M. Per- and Polyfluoroalkyl Substance Toxicity and Human Health Review: Current State of Knowledge and Strategies for Informing Future Research. *Environmental toxicology and chemistry* **2021**, *40* (3), 606–630. DOI: 10.1002/etc.4890. Published Online: Dec. 7, 2020.

(136) US EPA. *Fact Sheet: 2010/2015 PFOA Stewardship Program | US EPA*. https://www.epa.gov/assessing-and-managing-chemicals-under-tsca/fact-sheet-20102015-pfoa-stewardship-program (accessed 2022-12-17).

(137) UN Stockholm Convention. *Listing of POPs in the Stockholm Convention*. http://www.pops.int/TheConvention/ThePOPs/AllPOPs/tabid/2509/Default.aspx (accessed 2022-12-18).

(138) Europoean Chemicals Agency. *Candidate List of substances of very high concern for Authorisation - ECHA*. https://echa.europa.eu/candidate-list-table (accessed 2022-12-18).

(139) Europoean Chemicals Agency. *Substances restricted under REACH - ECHA*. https://echa.europa.eu/substances-restricted-under-reach (accessed 2022-12-18).

(140) European Environment Agency. *Emerging chemical risks in Europe- 'PFAS'*. https://www.eea.europa.eu/publications/emerging-chemical-risks-in-europe/emerging-chemical-risks-in-europe (accessed 2022-12-18).

(141) Europoean Chemicals Agency. *Registry of restriction intentions until outcome*. https://echa.europa.eu/registry-of-restriction-intentions/-/dislist/details/0b0236e18663449b (accessed 2023-03-08).

(142) Europoean Chemicals Agency. *ECHA publishes PFAS restriction proposal*. https://echa.europa.eu/-/echa-publishes-pfas-restriction-proposal (accessed 2023-03-08).

(143) Glüge, J.; Scheringer, M.; Cousins, I. T.; DeWitt, J. C.; Goldenman, G.; Herzke, D.; Lohmann, R.; Ng, C. A.; Trier, X.; Wang, Z. An overview of the uses of per- and polyfluoroalkyl substances (PFAS). *Environmental science. Processes & impacts* **2020**, *22* (12), 2345–2373. DOI: 10.1039/d0em00291g. Published Online: Oct. 30, 2020.

(144) Wang, Z.; Cousins, I. T.; Scheringer, M.; Hungerbuehler, K. Hazard assessment of fluorinated alternatives to long-chain perfluoroalkyl acids (PFAAs) and their precursors: status quo, ongoing challenges and possible solutions. *Environment international* **2015**, *75*, 172–179. DOI: 10.1016/j.envint.2014.11.013. Published Online: Nov. 27, 2014.

(145) Pérez, F.; Nadal, M.; Navarro-Ortega, A.; Fàbrega, F.; Domingo, J. L.; Barceló, D.; Farré, M. Accumulation of perfluoroalkyl substances in human tissues. *Environment international* **2013**, *59*, 354–362. DOI: 10.1016/j.envint.2013.06.004. Published Online: Jul. 25, 2013.

(146) Martin, J. W.; Mabury, S. A.; Solomon, K. R.; Muir, D. C. G. Bioconcentration and tissue distribution of perfluorinated acids in rainbow trout (Oncorhynchus mykiss). *Environ Toxicol Chem* **2003**, *22* (1), 196–204. DOI: 10.1002/etc.5620220126.

(147) Pickard, H. M.; Criscitiello, A. S.; Persaud, D.; Spencer, C.; Muir, D. C. G.; Lehnherr, I.; Sharp, M. J.; Silva, A. O. de; Young, C. J. Ice Core Record of Persistent Short-Chain Fluorinated Alkyl Acids: Evidence of the Impact From Global Environmental Regulations. *Geophys. Res. Lett.* **2020**, *47* (10). DOI: 10.1029/2020GL087535.

(148) Hori, H.; Nagano, Y.; Murayama, M.; Koike, K.; Kutsuna, S. Efficient decomposition of perfluoroether carboxylic acids in water with a combination of persulfate oxidant and ultrasonic irradiation. *Journal of Fluorine Chemistry* **2012**, *141*, 5–10. DOI: 10.1016/j.jfluchem.2012.05.012.

(149) Hori, H.; Murayama, M.; Kutsuna, S. Oxygen-induced efficient mineralization of perfluoroalkylether sulfonates in subcritical water. *Chemosphere* **2009**, *77* (10), 1400–1405. DOI: 10.1016/j.chemosphere.2009.09.013. Published Online: Oct. 2, 2009.

(150) Bentel, M. J.; Yu, Y.; Xu, L.; Kwon, H.; Li, Z.; Wong, B. M.; Men, Y.; Liu, J. Degradation of Perfluoroalkyl Ether Carboxylic Acids with Hydrated Electrons: Structure-Reactivity Relationships and Environmental Implications. *Environmental science & technology* **2020**, *54* (4), 2489–2499. DOI: 10.1021/acs.est.9b05869. Published Online: Jan. 30, 2020.

(151) Zhang, C.; Hopkins, Z. R.; McCord, J.; Strynar, M. J.; Knappe, D. R. U. Fate of Per- and Polyfluoroalkyl Ether Acids in the Total Oxidizable Precursor Assay and Implications for the Analysis of Impacted Water. *Environmental science & technology letters* **2019**, *6* (11), 662–668. DOI: 10.1021/acs.estlett.9b00525.

(152) Kwok, E. S. C.; Atkinson, R. Estimation of hydroxyl radical reaction rate constants for gas-phase organix compounds using a structure-reactivity relationship: an update. *Atmospheric Environment* **1995**, *29* (14), 1685–1695.

(153) Joudan, S.; Orlando, J. J.; Tyndall, G. S.; Furlani, T. C.; Young, C. J.; Mabury, S. A. Atmospheric Fate of a New Polyfluoroalkyl Building Block, C3F7OCHFCF2SCH2CH2OH. *Environmental science & technology* **2022**, *56* (10), 6027–6035. DOI: 10.1021/acs.est.0c07584. Published Online: Apr. 22, 2021.

(154) Folkerson, A. P.; Joudan, S.; Mabury, S. A.; D'eon, J. C. In Vivo Transformation of a Novel Polyfluoroether Surfactant. *Environmental toxicology and chemistry* **2021**, *40* (12), 3328–3336. DOI: 10.1002/etc.5230. Published Online: Nov. 8, 2021.

(155) Joudan, S.; Mabury, S. A. Aerobic biotransformation of a novel highly functionalized polyfluoroether-based surfactant using activated sludge from a wastewater treatment plant. *Environmental science. Processes & impacts* **2022**, *24* (1), 62–71. DOI: 10.1039/d1em00358e. Published Online: Jan. 26, 2022.

(156) Farlow, M. W.; Man, E. H.; Tullock, C. W.; Richardson, R. D. Carbonyl Fluoride. In *Inorganic syntheses*; Rochow, E. G., Ed.; Inorganic Syntheses; McGraw Hill, 1960; pp 155–158. DOI: 10.1002/9780470132371.ch48.

(157) Conder, J. M.; Hoke, R. A.; Wolf, W. de; Russell, M. H.; Buck, R. C. Are PFCAs bioaccumulative? A critical review and comparison with regulatory criteria and persistent lipophilic compounds. *Environmental science & technology* **2008**, *42* (4), 995–1003. DOI: 10.1021/es070895g.

(158) Jochyms, Q.; Mignard, E.; Vincent, J.-M. Fluorosurfactants for applications in catalysis. *Journal of Fluorine Chemistry* **2015**, *177*, 11–18. DOI: 10.1016/j.jfluchem.2015.01.011.

(159) Friedrich, R.; Jonschker, G.; Schooren, F.; Depner, C.; Schellenberger, S. Fluorosurfactants. 14/416,003.

(160) Friedrich, R.; Osthoff, J. Fluorinated tensides. 15/120,288.

(161) Chemguard. *Data sheet S-103A-6*. http://www.sintal.de/tdblatt/chemguard/S-103A-6.pdf (accessed 2022-12-16).

(162) Merck KGaA. *Technical datasheet TIVIDA FL 2300*. https://www.merckgroup.com/de/products/pm/101724.html (accessed 2022-12-16).

(163) Merck KGaA. *Technical datasheet TIVIDA FL 2500*. https://www.merckgroup.com/de/products/pm/102458.html (accessed 2022-12-16).

(164) Merck KGaA. *Technical datasheet TIVIDA FL 2700*. https://www.merckgroup.com/de/products/pm/140013.html (accessed 2022-12-16).

(165) Friedrich, R.; Koch, F. Fluorinated tensides. 16/347,424.

(166) Friedrich, R.; Jonschker, G. Fluorinated tensides. 15/500,368.

(167) Friedrich, R.; Schooren, F. Fluorinated tensides. 15/120,696.

(168) OMNOVA Solutions - Investors. *OMNOVA Solutions Introduces New Line of Design for the Environment Compatible Fluorosurfactants*. https://omnova.investorroom.com/index.php?s=43&item=26 (accessed 2023-01-12).

(169) Guangzhou Haoyi New Material Technology Co., Ltd. *Omnova PolyFox PF-136A, PF-156A, PF-151N Fluorosurfactants*. https://www.pudchem.com/detail-640.html (accessed 2023-01-12).

(170) McKeen, L. W. Plastics Used in Medical Devices. In *Handbook of polymer applications in medicine and medical devices*; Modjarrad, K., Ebnesajjad, S., Eds.; Plastics design library; William Andrew, 2014; pp 21–53. DOI: 10.1016/B978-0-323-22805-3.00003-7.

(171) Murata, H.; Chang, B.-J.; Prucker, O.; Dahm, M.; Rühe, J. Polymeric coatings for biomedical devices. *Surface Science* **2004**, *570* (1-2), 111–118. DOI: 10.1016/j.susc.2004.06.185.

(172) Kim, H.-A. Water Repellency/Proof/Vapor Permeability Characteristics of Coated and Laminated Breathable Fabrics for Outdoor Clothing. *Coatings* **2022**, *12* (1), 12. DOI: 10.3390/coatings12010012.

(173) Quéré, D. Non-sticking drops. *Rep. Prog. Phys.* **2005**, *68* (11), 2495–2532. DOI: 10.1088/0034-4885/68/11/R01.

(174) Friedrich, R. Fluorine compounds. 17/377,912.

(175) Barroso, G.; Li, Q.; Bordia, R. K.; Motz, G. Polymeric and ceramic silicon-based coatings – a review. *J. Mater. Chem. A* **2019**, *7* (5), 1936–1963. DOI: 10.1039/C8TA09054H.

(176) Sawatari, C.; Sekiguchi, Y.; Yagi, T. Durable Water-Repellent Cotton Fabrics Prepared by Low-Degree Substitution of Long Chain Alkyl Groups. *Textile Research Journal* **1998**, *68* (7), 508–514. DOI: 10.1177/004051759806800707.

(177) Schindler, W. D.; Hauser, P. J. Repellent finishes. In *Chemical finishing of textiles*; Schindler, W. D., Hauser, P. J., Eds.; Woodhead publishing in textiles; Woodhead Publishing, 2004; pp 74–86. DOI: 10.1533/9781845690373.74.

(178) Smet, D. de; Weydts, D.; Vanneste, M. Environmentally friendly fabric finishes. In *Sustainable Apparel*; Elsevier, 2015; pp 3–33. DOI: 10.1016/B978-1-78242-339-3.00001-7.

(179) Audenaert, F.; Lens, H.; Rolly, D.; Vander Elst, P. Fluorochemical Textile Repellents—Synthesis and Applications: A 3M Perspective. *Journal of the Textile Institute* **1999**, *90* (3), 76–94. DOI: 10.1080/00405009908659480.

(180) Kim, J.; Choi, S.-O. Superhydrophobicity. In *Waterproof and water repellent textiles and clothing*; Williams, J. T., Ed.; Woodhead Publishing is an imprint of Elsevier, 2018; pp 267–297. DOI: 10.1016/B978-0-08-101212-3.00010-1.

(181) Young, T. An essay on the cohesion of fluids. *Philosophical Transactions of the Royal Society of London* **1805**, *95*, 65–87. DOI: 10.1098/rstl.1805.0005.

(182) Fox, H.; Zisman, W. The spreading of liquids on low energy surfaces. I. polytetrafluoroethylene. *Journal of Colloid Science* **1950**, *5* (6), 514–531. DOI: 10.1016/0095-8522(50)90044-4.

(183) Hopken, J.; Moller, M. Low-surface-energy polystyrene. *Macromolecules* **1992**, *25* (5), 1461–1467. DOI: 10.1021/ma00031a016.

(184) Fanchi, J. R. Measures of Rock-Fluid Interactions. In *Shared Earth Modeling*; Elsevier, 2002; pp 108–132. DOI: 10.1016/B978-075067522-2/50007-0.

(185) Wenzel, R. N. Resistance of solid surfaces to wetting by water. *Industrial & Engineering Chemistry* **1936**, *28* (8), 988–994. DOI: 10.1021/ie50320a024.

(186) Cassie, A. B. D.; Baxter, S. Wettability of porous surfaces. *Trans. Faraday Soc.* **1944**, *40*, 546. DOI: 10.1039/tf9444000546.

(187) Chu, Z.; Feng, Y.; Seeger, S. Öl/Wasser-Trennung mit selektiven superabweisenden/superbenetzbaren Oberflächenmaterialien. *Angew. Chem.* **2015**, *127* (8), 2358–2368. DOI: 10.1002/ange.201405785.

(188) Johnson, R. E.; Dettre, R. H.; Brandreth, D. A. Dynamic Conatct Angles and Contact Angle Hysteresis. *Journal of Colloid and Interface Science* **1977**, *62* (2), 205–212.

(189) AATCC. *AATCC*. https://www.aatcc.org/ (accessed 2022-12-17).

(190) ISO. *ISO - International Organization for Standardization*. https://www.iso.org/home.html (accessed 2022-12-17).

(191) AATCC. *Oil Repellency: Hydrocarbon Resistance Test Method 118*, 1997.

(192) Fang, H.; Friedrich, R. Fluorine containing polymers. 16/310,709.

(193) Fang, H.; Friedrich, R. Fluorine containing polymers. 16/310,709.

(194) Friedrich, R. Fluorine compounds. 15/536,700.

(195) Kredel, J.; Gallei, M. Ozone-Degradable Fluoropolymers on Textile Surfaces for Water and Oil Repellency. *ACS Appl. Polym. Mater.* **2020**, *2* (7), 2867–2879. DOI: 10.1021/acsapm.0c00400.

2 – Nitrogen bearing polyethers

2.1 Copolymers of glycidyl amines and ethylene oxide as transfection agents with controllable charge density

Larissa Limmer,[a] Matthias Bros,[b] Holger Frey[a*]

[a] Johannes Gutenberg-Universität Mainz, Department of Chemistry, Duesbergweg 10 - 14, 55128 Mainz, Germany

[b] University Medical Center, Department of Dermatology, 55131 Mainz, Germany

To be submitted

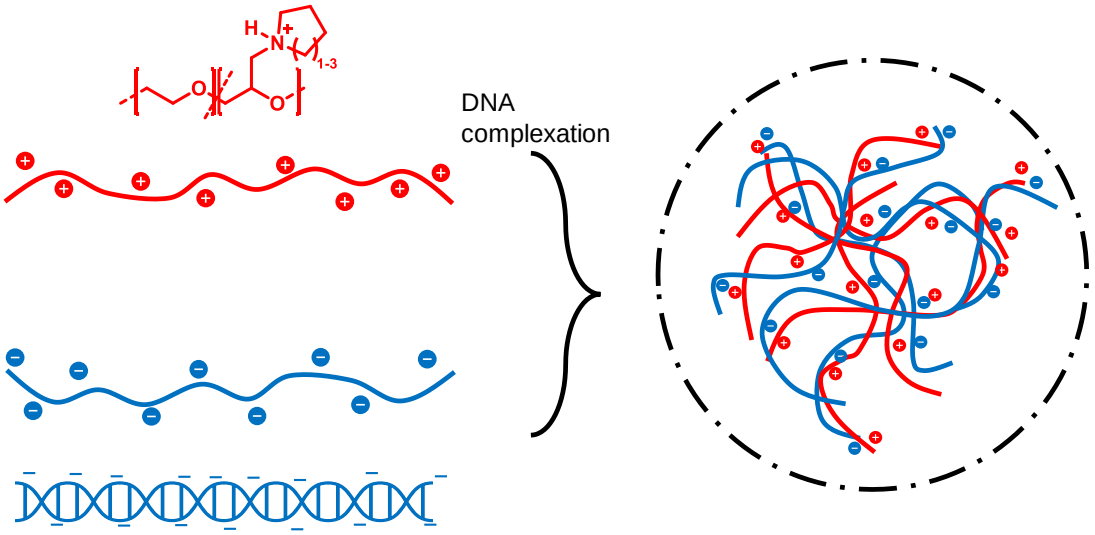

Contributions

L.L. – Concept; performance and evaluation of experiments; writing of manuscript. M.B. – performance and evaluation of experiments; writing of manuscript. H.F. – supervision; editing.

Abstract

Amino-functional polycations are highly interesting for biomedical research and therapy utilising their transfection abilities. Here we describe the syntheses and transfection properties of copolymers obtained from glycidyl amines and ethylene oxide. Albeit no major breakthrough was achieved, several compounds showed potential for this purpose. Three series of polymers containing glycidyl amines (GA) were synthesised in a controlled manner ($Đ$ < 1.14) and studied for their ability to interact with DNA and cells. With increasing ring size of the amino substituents the copolymers of pyrrolidine-, piperidine- and azepane- glycidyl amines showed a decreasing ability to bind DNA. The best performing polymer series had pyrrolidine glycidyl amine incorporated and showed a high efficiency in pDNA transportation, where the relative mean fluorescence intensity (MFI) increased with the GA share of 34 to 69 mol% from 1.04 to 2.68 (normalised to DOTAP). Nonetheless, none of the used polymer/nucleic acid complexes led to biosynthesis of proteins.

Introduction

Transfection is a viable method for *in vitro* and *in vivo* studies and utilised in genetic engineering as well as in gene therapy.[1,2] To achieve successful transfection a series of events is required: Complexation of nucleic acid by a transport vector, binding to the cellular surface, uptake via endocytosis, shielding against degradation, escape from endosome (or lysosome) and, in case of DNA transfection, transport into the nucleus.[2,3] Various techniques were developed, of which cationic vectors were found to be favourable, due to simple preparation, low immunogenicity and lack of need of receptors. Electrostatic interactions of the cationic vectors with a negatively charged nucleic acid and cellular surface enables the binding and transport into the endosome.[1,2] Early work studied and established polylysine and 2-(diethylamino)ether (DEAE)-dextran. However, these linear polycations showed relatively high cytotoxicity and low efficiency. To achieve a higher degree of efficiency, the polycations can be linked to a targeting ligand, e.g. transferrin, resulting in a higher cellular uptake via receptor-mediated endocytosis. On the other hand, this method leads to a hindered endosomal escape. Endosome disrupting agents bound to the vector are able to counter this effect.[1,4,5]

Polyamidoamide (PAMAM) cascade polymers[4] and lipopolyamines,[6] both bearing residual amino groups, were developed as well-tolerated and efficient transfection agents. In comparison to lipids bearing quaternary ammonium groups the elevated efficiency was attributed to the high charge density in the polymers,[1] the buffering capability in the endosome as well as the lysomothrophic effect.[4,7] The buffering enables protection against degradation. Furthermore, the proton sponge effect of the protonable nitrogen-atoms leads to osmotic swelling and rupture of the endosome, ultimately releasing the vector into the cell.[8] Consequently, Boussif *et al*. studied polyethyleneimine (PEI), which bears an especially high charge density potential, and showed high transfection efficiency.[7] The ratio of amino groups to nucleotide phosphates influences efficiency as well as cytotoxicity through organelle damage and necrosis.[3,7,9] Despite the mechanism of the polycations' toxicity has not been fully explained as of yet, evidence for the opening of pores leading to disruption of the cellular membranes was found. These pores are presumably formed via hydrolysis of phospholipids either through the cationic polymer itself or through released endo/lysosomal enzymes after rupture thereof.[7,9,10] Furthermore, efficiency

and toxicity are increasing with charge density as well as with the polymers molecular weight.[9,11,12] Recently, research has been conducted to balance between efficiency and toxicity via modified PEI. *N*-glycosylation[13] or -acylation, quaternisation via alkylation[14] as well as the use of block- and graft copolymers with poly(ethylene glycol) (PEG)[15,16] or poly(oxazoline)[17] led to an improved balance.

Intrigued by the high transfection efficiency of PEI, while being cytotoxic, we wondered if multiamino-functional PEG could be a suitable alternative. Copolymerisation of ethylene oxide and glycidyl amines leads to a controllable and defined positive charge density along the polymer. In consequence, the balance between transfection and toxicity could be adjustable via monomer ratio.

Experimental Section

Materials

Epichlorohydrine and pyrrolidine were obtained in 99% purity from Acros Organics; piperidine was obtained in 99% purity from Sigma-Aldrich; azepane was obtained in 98% purity from Alfa Aesar. Benzyloxyethanol was purchased from TCI in 98%. THF was dried via sodium/benzophenone and distillation. HEK293 cells used in this study were obtained from ATCC (no. CRL-1573). DMEM, L-glutamine, penicillin, and streptomycin were purchased from Sigma-Aldrich. ß-mercaptoethanol and DOTAP were purchased from Roth. Fetal bovine serum was obtained from PAN-Biotech, Cy5 from Mirus and FVD-eFL450 from ThermoFisher. All other chemicals were purchased from Acros Organics, Fisher Scientific, Roth, Sigma-Aldrich, TCI, VWR or Deutero GmbH.

Instrumentation

^{1}H NMR (300 MHz) and ^{13}C NMR (75 MHz) spectra were recorded on a Bruker Avance III HD 300 (5 mm BBFO-Probe with *z*-Gradient and ATM). Size exclusion chromatography (SEC) was performed at 50 °C in *N*,*N*-dimethylformamide (DMF), containing 1 g/mL lithium bromide (flow rate of 1 mL/min) on an Agilent 1100 Series, HEMA columns with 300/100/40 Å porosity and an Agilent G1362A RID detector. Calibration was done with poly(ethylene oxide) (PEG) standards by Polymer Standards Service (PSS, Mainz, Germany) and toluene as an internal standard.

Samples were assayed by flow cytometry for Cy5 intensity and viability using an Attune Nxt flow cytometer equipped with Attune Attune NxT Software (both from Thermo Fisher, Waltham, MA).

Monomer synthesis

Monomer synthesis and characterisation data are literature known.[18–20] A typical synthesis of pyrrolidine glycidyl amine (PyrGA) is described exemplarily.

Pyrrolidine (1 eq, 0.49 mol, 40.0 mL) and a 40 wt% solution of NaOH (1.5 eq) were mixed and kept at 0 °C, while epichlorohydrin (1.5 eq, 0.73 mol, 57.3 mL) was added dropwise under vigorous stirring. After complete addition, cooling was removed and stirred for an additional 30 min. The product was separated in the organic phase via extraction with petroleum ether and water, dried over $MgSO_4$ and isolated via distillation under reduced pressure in typical yields of 60-70%.

For the synthesis of piperidine glycidyl amine (PiGA) the NaOH solution was added 3 h after epichlorohydrin addition and the mixture was stirred overnight, for azepane glycidyl amine (AzGA) the NaOH solution was added 1.5 h after epichlorohydrin addition, and the mixture was stirred overnight. PiGA and AzGA were purified via extraction with diethyl ether instead of petroleum ether.

Polymer synthesis

Homo- and copolymerisation were initiated by partially deprotonated 2-benzyloxyethanol (BnO). BnO (1 eq) and KO^{t}Bu (0.5 eq) were combined and dissolved in 12:1 benzene:methanol mixture. After stirring at 60 °C for 30 min in a dried Schlenk flask, the initiator was dried under reduced pressure. For homopolymerisations, the monomer was added, and the polymerisation was performed in bulk at 40 °C for 48-71 h. For copolymerisations, a 6:2 THF: DMSO mixture and the glycidyl amine monomer were added via syringe. Ethylene oxide was transferred into the at -80 °C cooled flask via condensation from a graduate ampule. The mixture was slowly heated to 55 °C under stirring and the polymerisation was performed for 48-72 h. Polymers were purified via extraction with DCM and water and subsequent dialysis using 1 kDa tubing and an initial 9:1 methanol:DCM mixture, which was changed to pure methanol. The purified polymers were dried under reduced pressure.

P(EG-*co*-PyrGA): ^{1}H NMR (300 MHz, C*D*Cl$_3$): δ [ppm] = 7.34–7.28 (m, Bn), 4,56 (s, Bn-C*H*$_2$), 3.66–3.53 (m, backbone), 2.64–2.53 (m, C*H*$_2$-N-C*H*$_2$), 1.74 (dt, N-CH$_2$-C*H*$_2$). ^{13}C NMR (75 MHz, C*D*Cl$_3$): δ [ppm] = 128.37–127.60 (Bn), 72.70 (Bn-*C*H$_2$), 70.71 (backbone), 69.41 (*C*H$_2$-OH), 57.60 (*C*H$_2$-N), 54.81 (N-*C*H$_2$-CH$_2$), 23.58 (N-CH$_2$-*C*H$_2$).

P(EG-*co*-PiGA): ^{1}H NMR (300 MHz, C*D*Cl$_3$): δ [ppm] = 7.31–7.24 (m, Bn), 4.53 (s, Bn-C*H*$_2$), 3.76–3.39 (m, backbone), 2.37 (dq, C*H*$_2$-N-C*H*$_2$), 1.52 (h, N-CH$_2$-C*H*$_2$), 1.37 (q, N-(CH$_2$)$_2$-C*H*$_2$). ^{13}C NMR (75 MHz, C*D*Cl$_3$): δ [ppm] = 128.42–127.62 (Bn), 72.95 (Bn-*C*H$_2$), 70.79 (backbone), 69.40 (*C*H$_2$-OH), 60.61 (*C*H$_2$-N), 55.35 (N-*C*H$_2$-CH$_2$), 26.19 (N-CH$_2$-*C*H$_2$), 24.40 (N-(CH$_2$)$_2$-*C*H$_2$).

P(EG-*co*-AzGA): ^{1}H NMR (300 MHz, C*D*Cl$_3$): δ [ppm] = 7.32–7.26 (m, Bn), 4.54 (s, Bn-C*H*$_2$), 3.85–3.33 (m, backbone), 2.70–2.44 (m, C*H*$_2$-N-C*H*$_2$), 1.61–1.55 (m, N-CH$_2$-(*CH*$_2$)$_2$). ^{13}C NMR (75 MHz, C*D*Cl$_3$): δ [ppm] = 128.04–127.56 (Bn), 72.75 (Bn-*C*H$_2$), 70.72 (backbone), 69.42 (*C*H$_2$-OH), 59.04 (*C*H$_2$-N), 56.15 (N-*C*H$_2$-CH$_2$), 28.32 (N-CH$_2$-*C*H$_2$), 27.07 (N-(CH$_2$)$_2$-*C*H$_2$)

DNA retardation assay

A dilution series of polymer in aqua bidest (aq. bid.) was prepared to yield agent solutions with 100, 20, 10, 2, 1, 0.2 and 0.1 µg µL^{-1}. 1 µL of agent solution, 1 µL of pDNA (1 µg µL^{-1}, pGL3-Control from Promega, Fitchburg, Wi, USA) and 13 µL of aq. bid. were mixed and incubated for 30 min. 4 µL of TRIS-Acetat-EDTA-loading buffer was added, and the solution was loaded into a agarose gel (prepared with GelRed from Biotium, Fremont, CA, USA. Dilution: 1:10000). Subsequently, electrophoresis was performed.

pDNA transport

The capability of various pDNA complexing copolymers for intracellular pDNA transport was assessed using human embryonic kidney (HEK)293 cells. HEK293 cells were kept in DMEM-based culture medium containing 2 mM L-glutamine, 100 U mL^{-1} penicillin, 100 µg mL^{-1} streptomycin, and 50 µM ß-mercaptoethanol containing 5% fetal bovine serum at 5% CO_2 and 37°C. pDNA was labeled with Cy5 as recommended by the manufacturer and was mixed with unlabeled pDNA (1:9). Copolymer/pDNA complexes were set up at the indicated ratios. Complexes composed of DOTAP and pDNA served as an internal control. For cellular studies,

HEK293 cells (10^5 cells $1ml^{-1}$) were seeded in 12-well cell cluster replicate plates. After 2h, one replicate plate was put in a fridge (4 °C) to allow for subsequent differentiation between temperature-independent cell binding and temperature-dependent cellular uptake of differentially complexed pDNA. After 30 min, pDNA and differentially complexed pDNA (each 1 µg) was applied in parallel to seeded HEK293 cells kept in a fridge and at 37 °C, respectively. On the next day, samples were harvested, washed with PBS buffer and incubated with membrane-impermeable FVD-eFL450 to delineate living and dead cells. Subsequently, samples were assayed by flow cytometry for Cy5 intensity and viability.

Results and Discussion

We synthesised copolymers consisting of EO and an amino-functional comonomer: pyrrolidine glycidyl amine (PyrGA), piperidine glycidyl amine (PiGA) or azepane glycidyl amine (AzGA), for which the side chain ring size increases from 5- to 7-membered. As a consequence of the increasing ring size the amine density and ultimately the charge density decreases.

To demonstrate the controllability and adjustability of the comonomer system copolymer series with glycidyl amine (GA) share increasing in 10 mol% steps were synthesised (full data is given in Table S1 and Figure S1). Due to decreasing water solubility with increasing GA share as well as with increasing ring size only an excerpt of these copolymers were studied for their cytotoxicity and transfection ability (Table 1).

Table 1: Characterisation data of the synthesised and tested copolymers.

Polymer	*%(GA)*[a]	M_n[a] (g mol^{-1})	M_n[b] (g mol^{-1})	*Đ*[b]
P(EG_{29}-*co*-$PyrGA_{15}$)	34	3340	1340	1.10
P(EG_{20}-*co*-$PyrGA_{19}$)	48	3450	1210	1.10
P(EG_{11}-*co*-$PyrGA_{24}$)	69	3690	950	1.08
P(EG_{31}-*co*-$PiGA_{12}$)	28	3210	1740	1,08
P(EG_{53}-*co*-$AzGA_{4}$)	7	3110	2330	1.05
P(EG_{25}-*co*-$AzGA_{11}$)	31	2960	1810	1.06

[a]Determined by ^1H NMR spectroscopy (300 MHz, $CDCl_3$). [b]Determined by SEC (DMF, RI detector, PEG standards).

SEC shows monomodal and narrow dispersities (Figure 1). Underestimation of molecular weight by SEC is a known phenomenon and caused by reduced hydrodynamic radii of the substituted polymer in comparison to the PEG calibration.[21] Molecular weights and monomer ratios determined via ^{1}H NMR spectroscopy were typically in good agreement with the targeted values (exemplarily ^{1}H and ^{13}C spectra are given in SI).

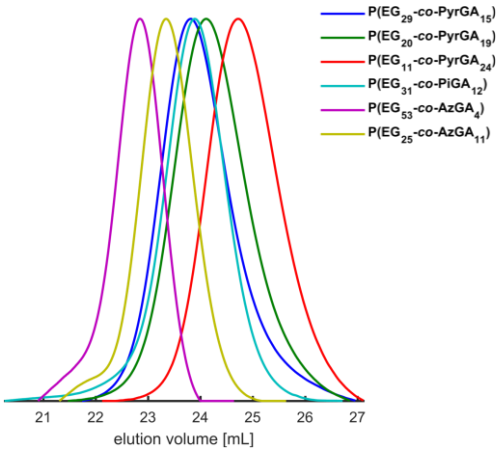

Figure 1: SEC traces of the tested polymers (DMF, PEG calibration, RI signal).

DNA retardation: First, the ability to bind DNA was studied for an excerpt of the polymers. Electrophoresis was performed subsequent to incubation of DNA with the polymer (Figure 2).

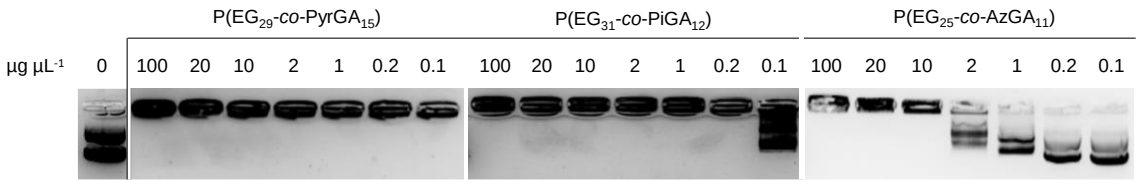

Figure 2: DNA retardation assays of copolymers with 34, 28 and 31% of GA content, respectively. From left to rigth: PyrGA, PiGA, AzGA. Additional assays are given in Figure S8.

PyrGA copolymers with at least 34% of GA were able to bind the DNA completely in the tested concentration region of 100 to 0.1 µg µL^{-1}. While 0.2 µg µL^{-1} of 28% containing PiGA was able to fully bind the DNA, the DNA was released at a concentration of 0.1 µg µL^{-1}. Using the copolymer with 31% of AzGA complete DNA binding required a 10 µg µL^{-1} polymer solution. The aforementioned effect of an increasing ring size of the amine leading to a reduced DNA binding ability was presumably caused by the decreased amine density of the substituents with bigger rings. On the other hand, the degree of polymerisation of GA in the copolymers was adjusted to the increasing molecular weight of the GAs to keep the molecular weight

constant. The resulting decreased number of amines could also affect the DNA binding. Finally, the different steric environments could influence the DNA binding.

Transfection: Evaluation of pDNA transport activity of a representative excerpt of the synthesised polymers were studied via flow cytometric analysis subsequent to incubation of HEK-293 cells with differentially complexed Cy5-labeled pDNA. To allow differentiation between pDNA transportation across the cell membrane into cells or simple attachment to the outside of the membrane, the experiments were repeated at different temperatures (Table 2, Figures 3, S9-S10). In a first set-up, incubation was performed at 0 °C, at which no significant transportation should occur. In a second set-up, incubation was performed at 37 °C to allow optimal transfection conditions.

Table 2: Flow cytometry analysis data of HEK293 cells after incubation at 4 and 37 °C, respectively: Percentage of Cy5 positive cells and mean fluorescence intensity (MFI).

	Incubated at 4 °C			Incubated at 37 °C		
Treatment[a]	Cy5+ cells % of singlets	MFI	Relative MFI[b]	Cy5+ cells % of singlets	MFI	Relative MFI[b]
Negative control	3.42	520	0.10	0.47	283	0.03
Cy5 pDNA	16.80	1827	0.34	81.72	4961	0.59
DOTAP	79.60	5373	1	84.41	8410	1
P(EG_{29}-*co*-$PyrGA_{15}$)	22.03	3210	0.60	68.35	8799	1.05
P(EG_{20}-*co*-$PyrGA_{19}$)	35.68	6138	1.14	84.49	22566	2.68
P(EG_{11}-*co*-$PyrGA_{24}$)	44.70	9866	1.84	79.0	21896	2.60
P(EG_{31}-*co*-$PiGA_{12}$)	18.37	2232	0.42	52.91	2712	0.32
P(EG_{53}-*co*-$AzGA_4$)	17.38	2002	0.37	89.08	6566	0.78
P(EG_{25}-*co*-$AzGA_{11}$)	18.84	2156	0.40	52.06	2665	0.32

[a]The originally used dilution for the polymers were determined using the respective lowest concentration, which showed efficient DNA binding in the DNA retardation assays: PyrGA copolymers: 1:500; PiGA copolymer: 1:100, P(EG_{53}-co-$AzGA_4$): 1:5; P(EG_{25}-co-$AzGA_{11}$): 1:25. [b] Normalised to DOTAP control.

The control sample, which was incubated with Cy5 and pDNA but without polymer, showed unexpectedly an increase in Cy5 positive cells and MFI. Nonetheless, the MFI was relatively low in comparison to cells treated with DOTAP, indicating a low transport presumably via pinocytosis.

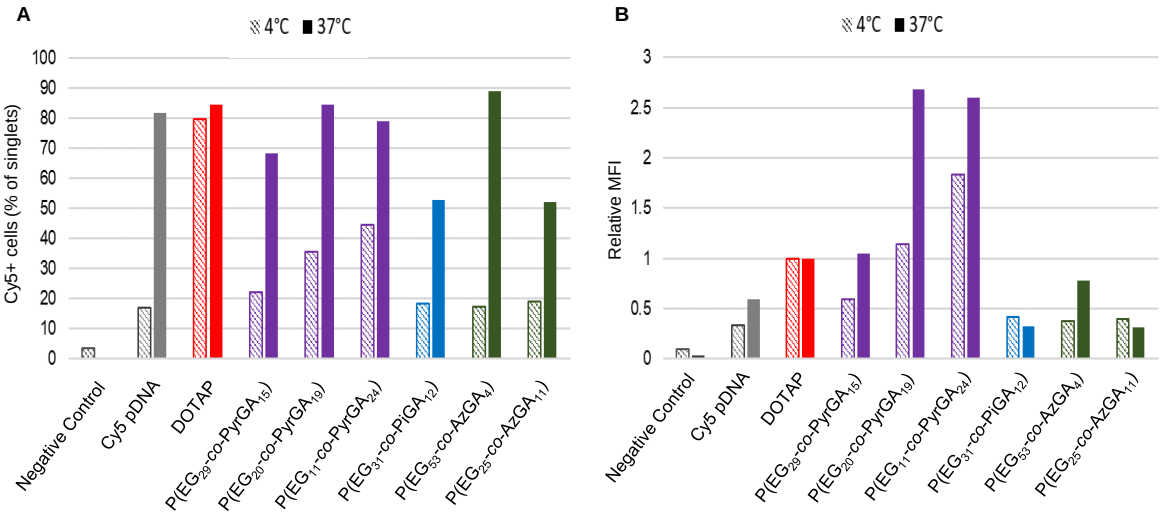

Figure 3: Flow cytometric analysis results of the studies at 4 (dashed) and 37 °C (filled). A: Cy5 positive cell percentage of singlets. B: Relative MFI normalised to DOTAP.

A comparison of the results obtained by cells incubated at 4 and 37 °C discloses generally higher values for cells incubated at higher temperature, verifying the successful transport of pDNA into the cells. The DOTAP control displayed high membrane attachment at 4 °C. Copolymers of the PyrGA series showed high Cy5 positive percentages as well as high MFIs. Especially the copolymers with PyrGA shares of 34 and 69 mol% (P(EG$_{20}$-*co*-PyrGA$_{19}$) and P(EG$_{11}$-*co*-PyrGA$_{24}$)) exhibited high MFIs, indicating an efficiency increase with higher shares of GA. Furthermore, comparing Cy5 positive percentage and MFI for these samples indicates high pDNA concentrations inside the single cells and consequently a high transport efficiency. The tested PiGA copolymer showed the lowest Cy5 positive percentage and MFI of the tested substances. The piperidine substituent presumably hindered complex/membrane interactions, while simultaneously showing a lower amine density than PyrGA copolymers. The tested AzGA copolymers similarly showed low MFIs, albeit P(EG$_{53}$-*co*-AzGA$_{4}$) exhibited a high Cy5 positive percentage of 89.08 mol% (37 °C). This polymer promoted the pDNA transport into the cells but led to lower concentrations inside the cells in comparison to P(EG$_{20}$-*co*-PyrGA$_{19}$) and P(EG$_{11}$-*co*-PyrGA$_{24}$), presumably due to the sterically hindered amine group and reduced amine density.

Finally, the expression of enhanced green fluorescent protein (EGFP) was studied using via flow cytometric analysis. After treatment of HEK-293 cells with either polymer/pDNA (Figure S11) or polymer/mRNA complexes (Figure S12), no

significant expression was observed in contrast to the DOTAP control. Consequently, none of the herein synthesised and tested polymers were able to successfully lead to protein biosynthesis. As mentioned in the introduction a certain series of events is required for successful transfection and biosynthesis of the targeted proteins. The negative results obtained by treatment with mRNA indicated the transportation inside the cell to the nucleus not to be the critical step, which is not needed for mRNA. Consequently, the absence of biosynthesis was presumably caused by entrapment of the nucleic acids in cell compartments, which prevented their further processing. On the other hand, a lack of dissociation of the complexes as well as destruction of either the nucleic acids or the cells could prevent biosynthesis.

Cytotoxicity: Potential cytotoxicity was evaluated using a similar approach to the transportation experiments via flow cytometric analysis utilising a live-dead cell dye (FVD eFluor450) (Figure 4).

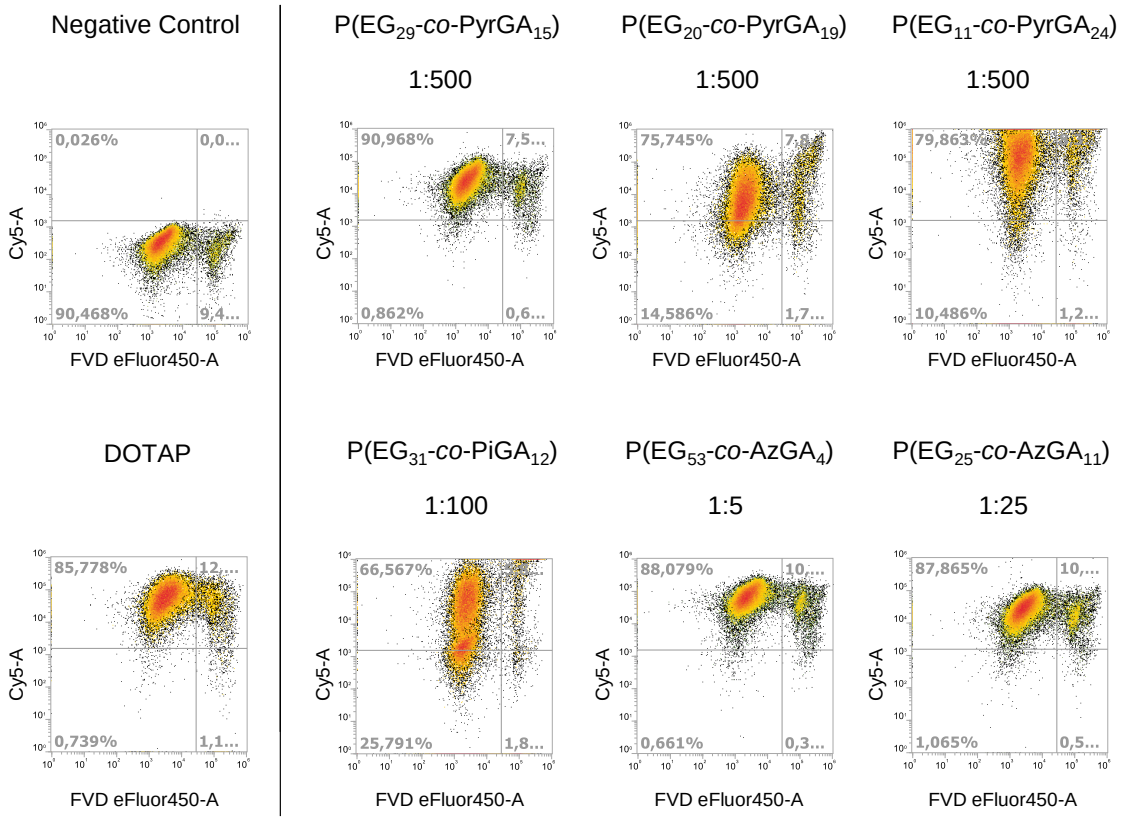

Figure 4: FACS scan of with polymer/DNA complex and dye incubated HEK-293 cells. Marked limits were determined in additional scans and are indicating living (left) and dead (right) cells as well as the presence (top) or absence (bottom) of DNA at the cell. Control experiments were performed using HEK cells without transfection agent (negative control) and DOTAP as the transfection agent (positive control). The marked dilutions of the polymer samples were determined using the respective lowest concentration, which showed DNA binding in the DNA retardation assays.

Figure 4 shows the results of the viability assay, where dead cells are located on the right side of the cross mark. The cell viability was not significantly affected by the incubation with the polymer/DNA complexes (Figure 5). The results represented in Figure 4 furthermore support the results of the flow cytometric temperature studies: All tested polymers transported pDNA, with the PiGA-copolymer being the least efficient.

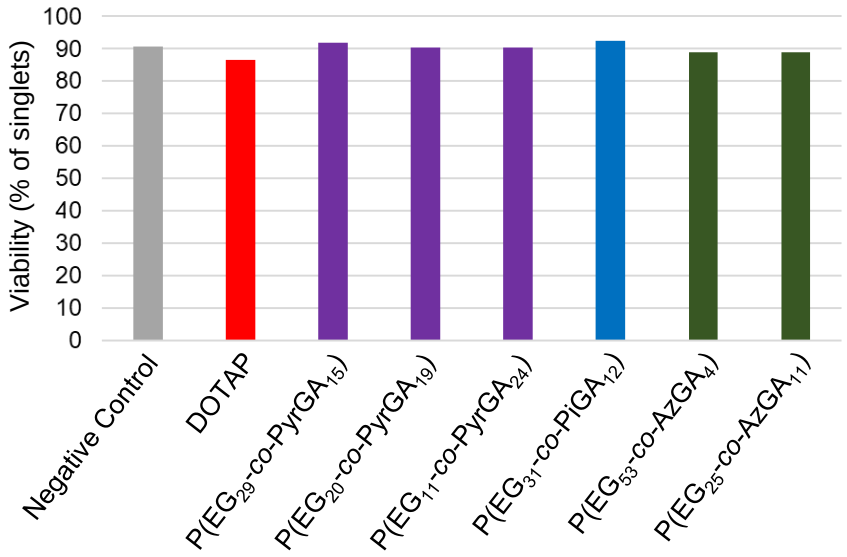

Figure 5: Plot of the cell viability after treatment with polymer/pDNA complexes and dye.

Conclusion

Copolymers of EO and glycidyl amines with varying ring sizes (5- to 7-membered: PyrGA, PiGA and AzGA) were synthesised with narrow dispersities ($Đ$ < 1.14) and studied for their transfection ability and biocompatibility, whereas none of the polymers exhibited cytotoxicity. While all of the tested polymers were able to bind DNA, the efficiency decreased with increasing ring size of the amine substituent presumably due to steric hindrance and a decreased amine density. PyrGA copolymers further exhibited the highest pDNA transport efficiency into HEK293 cells, which increased for higher PyrGA shares in the polymer (up to 84.49% of Cy5 positive cells and relative MFI up to 2.68 normalised to DOTAP). Ultimately, no protein biosynthesis was achieved using this system, presumably due to entrapment inside cell compartments. Further research will focus on evaluation of the entrapment

hypothesis and prevention of thereof utilising the proton sponge effect of amino groups.

References

(1) Behr, J.-P. Gene Transfer with Synthetic Cationic Amphiphiles: Prospects for Gene Therapy. *Bioconjugate chemistry* **1994**, *5*, 382–389.

(2) Kumar, V. V.; Singh, R. S.; Chaudhuri, A. Cationic transfection lipids in gene therapy: successes, set-backs, challenges and promises. *Current medicinal chemistry* **2003**, *10* (14), 1297–1306. DOI: 10.2174/0929867033457458.

(3) Godbey, W. T.; Wu, K. K.; Mikos, A. G. Poly(ethylenimine) and its role in gene delivery. *Journal of controlled release : official journal of the Controlled Release Society* **1999**, *60* (2-3), 149–160. DOI: 10.1016/s0168-3659(99)00090-5.

(4) Haensler, J.; Szoka, F. C., JR. Polyamidoamine cascade polymers mediate efficient transfection of cells in culture. *Bioconjugate chemistry* **1993**, *4*, 372–379.

(5) Luo, D.; Saltzman, W. M. Synthetic DNA delivery systems. *Nature Biotechnology* **2000**, *18*.

(6) Behr, J. P.; Demeneix, B.; Loeffler, J. P.; Perez-Mutul, J. Efficient gene transfer into mammalian primary endocrine cells with lipopolyamine-coated DNA. *Proceedings of the National Academy of Sciences of the United States of America* **1989**, *86* (18), 6982–6986. DOI: 10.1073/pnas.86.18.6982.

(7) Boussif, O.; Lezoualc'h, F.; Zanta, M. A.; Mergny, M. D.; Scherman, D.; Demeneix, B.; Behr, J.-P. A versatile vector for gene and oligonucleotide transfer into cells in culture and in vivo: Polyethyleneimine. *Proceedings of the National Academy of Sciences of the United States of America* **1995**, *92*, 7297–7301.

(8) Akinc, A.; Thomas, M.; Klibanov, Alexander, M.; Langer, R. Exploring polyethylenimine-mediated DNA transfection and the proton sponge hypothesis. *The journal of gene medicine* **2005**, *7*, 657–663.

(9) Monnery, B. D.; Wright, M.; Cavill, R.; Hoogenboom, R.; Shaunak, S.; Steinke, J. H. G.; Thanou, M. Cytotoxicity of polycations: Relationship of molecular weight and the hydrolytic theory of the mechanism of toxicity. *International journal of pharmaceutics* **2017**, *521* (1-2), 249–258. DOI: 10.1016/j.ijpharm.2017.02.048. Published Online: Feb. 21, 2017.

(10) Baciu, M.; Sebai, S. C.; Ces, O.; Mulet, X.; Clarke, J. A.; Shearman, G. C.; Law, R. V.; Templer, R. H.; Plisson, C.; Parker, C. A.; Gee, A. Degradative transport of cationic amphiphilic drugs across phospholipid bilayers. *Philosophical transactions. Series A, Mathematical, physical, and engineering sciences* **2006**, *364* (1847), 2597–2614. DOI: 10.1098/rsta.2006.1842.

(11) Gosselin, M. A.; Guo, W.; Lee, R. J. Efficient gene transfer using reversibly cross-linked low molecular weight polyethylenimine. *Bioconjugate chemistry* **2001**, *12* (6), 989–994. DOI: 10.1021/bc0100455.

(12) Godbey, W. T.; Wu, K. K.; Mikos, A. G. Size matters: Molecular weight affects the efficiency of poly(ethylenimine) as a gene delivery vehicle. *J. Biomed. Mater. Res.* **1999**, *45* (3), 268–275. DOI: 10.1002/(SICI)1097-4636(19990605)45:3<268:AID-JBM15>3.0.CO;2-Q.

(13) Leclercq, F.; Dubertret, C.; Pitard, B.; Scherman, D.; Herscovici, J. Synthesis of glycosylated polyethylenimine with reduced toxicity and high transfecting efficiency. *Bioorganic & medicinal chemistry letters* **2000**, *10* (11), 1233–1235. DOI: 10.1016/s0960-894x(00)00195-5.

(14) Thomas, M.; Klibanov, A. M. Enhancing polyethylenimine's delivery of plasmid DNA into mammalian cells. *Proceedings of the National Academy of Sciences of the United States of America* **2002**, *99* (23), 14640–14645. DOI: 10.1073/pnas.192581499. Published Online: Oct. 25, 2002.

(15) Zhong, Z.; Feijen, J.; Lok, M. C.; Hennink, W. E.; Christensen, L. V.; Yockman, J. W.; Kim, Y.-H.; Kim, S. W. Low molecular weight linear polyethylenimine-b-poly(ethylene glycol)-b-polyethylenimine triblock copolymers: synthesis, characterization, and in vitro gene transfer properties. *Biomacromolecules* **2005**, *6* (6), 3440–3448. DOI: 10.1021/bm050505n.

(16) Petersen, H.; Fechner, P. M.; Martin, A. L.; Kunath, K.; Stolnik, S.; Roberts, C. J.; Fischer, D.; Davies, M. C.; Kissel, T. Polyethylenimine-graft-poly(ethylene glycol) copolymers: influence of copolymer block structure on DNA complexation and biological activities as gene delivery system. *Bioconjugate chemistry* **2002**, *13* (4), 845–854. DOI: 10.1021/bc025529v.

(17) Hsiue, G.-H.; Chiang, H.-Z.; Wang, C.-H.; Juang, T.-M. Nonviral gene carriers based on diblock copolymers of poly(2-ethyl-2-oxazoline) and linear polyethylenimine. *Bioconjugate chemistry* **2006**, *17* (3), 781–786. DOI: 10.1021/bc050317u.

(18) Blankenburg, J.; Stark, M.; Frey, H. Oxidation-responsive polyether block copolymers lead to non-ionic polymer surfactants with multiple amine N -oxides. *Polym. Chem.* **2019**, *10* (13), 1569–1574. DOI: 10.1039/C9PY00093C.

(19) Verkoyen, P. Long-chain alkyl glycidyl ethers: Amphiphilic polyether architectures and non-covalent hydrogels. Dissertation, Johannes Gutenberg-Universtität Mainz, Mainz, 2020.

(20) Zhang, Q.; Limmer, L.; Frey, H.; Kelland, M. A. N -Oxide Polyethers as Kinetic Hydrate Inhibitors: Side Chain Ring Size Makes the Difference. *Energy Fuels* **2021**, *35* (5), 4067–4074. DOI: 10.1021/acs.energyfuels.0c04333.

(21) Blankenburg, J.; Wagner, M.; Frey, H. Well-Defined Multi-Amino-Functional and Stimuli-Responsive Poly(propylene oxide) by Crown Ether Assisted Anionic Ring-Opening Polymerization. *Macromolecules* **2017**, *50* (22), 8885–8893. DOI: 10.1021/acs.macromol.7b01324.

Supporting Information

Table S1: Characterisation data of the synthesised copolymers.

Polymer	*mol%(GA)*[a]	M_n[a] (g mol^{-1})	M_n[b] (g mol^{-1})	$Đ$[b]
P(EG$_{49}$-*co*-PyrGA$_6$)	11	3070	2030	1.09
P(EG$_{37}$-*co*-PyrGA$_{10}$)	21	3050	1620	1.08
P(EG$_{29}$-*co*-PyrGA$_{15}$)	34	3340	1340	1.10
P(EG$_{19}$-*co*-PyrGA$_{15}$)	44	2900	1050	1.10
P(EG$_{20}$-*co*-PyrGA$_{19}$)	48	3450	1210	1.10
P(EG$_{14}$-*co*-PyrGA$_{20}$)	59	3310	1080	1.08
P(EG$_{11}$-*co*-PyrGA$_{24}$)	69	3690	950	1.08
P(EG$_6$-*co*-PyrGA$_{23}$)	79	3340	950	1.08
PPyrGA$_{30}$	100	3970	1000	1.10
P(EG$_{51}$-*co*-PiGA$_5$)	9	3100	1690	1.09
P(EG$_{34}$-*co*-PiGA$_8$)	19	2780	1640	1.07
P(EG$_{31}$-*co*-PiGA$_{12}$)	28	3210	1740	1,08
P(EG$_{24}$-*co*-PiGA$_{15}$)	38	3330	1730	1.11
P(EG$_{14}$-*co*-PiGA$_{16}$)	53	3030	1400	1.14
P(EG$_{12}$-*co*-PiGA$_{17}$)	59	3080	1390	1.11

Table S1: Characterisation data of the synthesised copolymers (continued).

Polymer	*mol%(GA)*[a]	M_n[a] (g mol^{-1})	M_n[b] (g mol^{-1})	$Đ$[b]
P(EG$_{10}$-*co*-PiGA$_{19}$)	66	3270	1440	1.09
P(EG$_{6}$-*co*-PiGA$_{19}$)	76	3100	1350	1.05
PPiGA$_{20}$	100	2970	1330	1.03
P(EG$_{53}$-*co*-AzGA$_{4}$)	7	3110	2330	1.05
P(EG$_{37}$-*co*-AzGA$_{9}$)	20	3180	1960	1.06
P(EG$_{25}$-*co*-AzGA$_{11}$)	31	2960	1810	1.06
P(EG$_{19}$-*co*-AzGA$_{12}$)	39	2850	1690	1.08
P(EG$_{16}$-*co*-AzGA$_{14}$)	47	3030	1500	1.10
P(EG$_{10}$-*co*-AzGA$_{15}$)	60	2920	1380	1.09
P(EG$_{8}$-*co*-AzGA$_{16}$)	67	2990	1290	1.08
P(EG$_{5}$-*co*-AzGA$_{16}$)	76	2850	1320	1.05
PAzGA$_{17}$	100	2790	1020	1.06

We targeted copolymer series of 3000 g mol^{-1} with glycidyl amine (GA) share increasing in 10 mol% steps. Exception were not synthesised polymers bearing 90% GA, due to used apparatus not allowing the low EO content. [a]Determined by ^{1}H NMR spectroscopy (300 MHz, C*D*Cl$_3$). [b]Determined by SEC (DMF, RI detector, PEG standards).

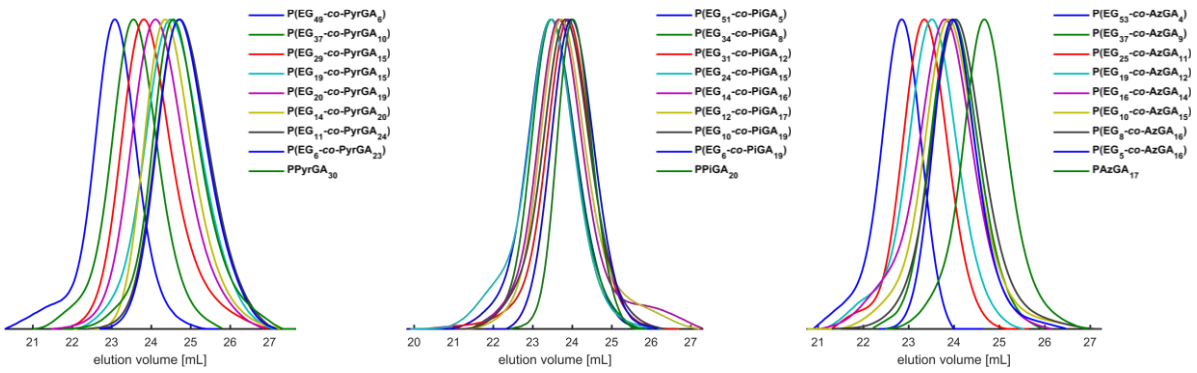

Figure S1: SEC traces of the PyrGA (left), PiGA (middle) and AzGA series (right) (DMF, PEG calibration, RI signal).

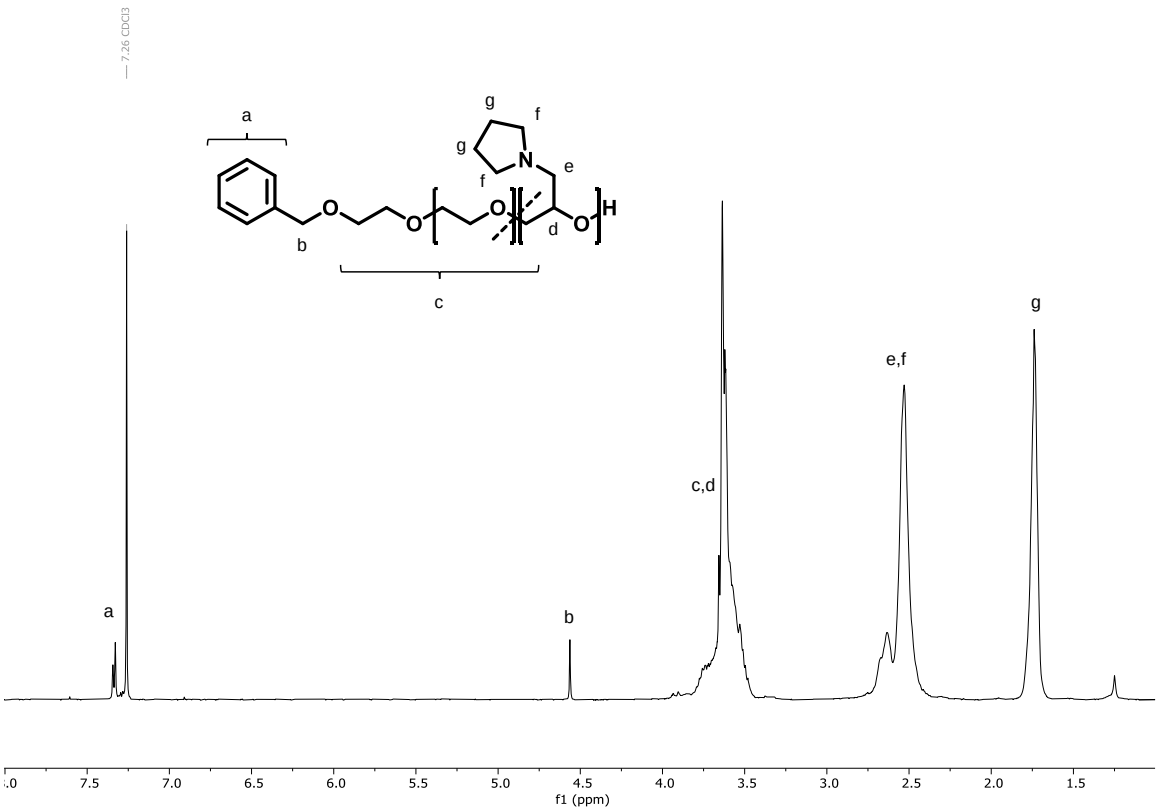

Figure S2: ^{1}H NMR spectrum ($CDCl_3$, 300 MHz) of $P(EG_{20}$-co-$PyrGA_{19})$.

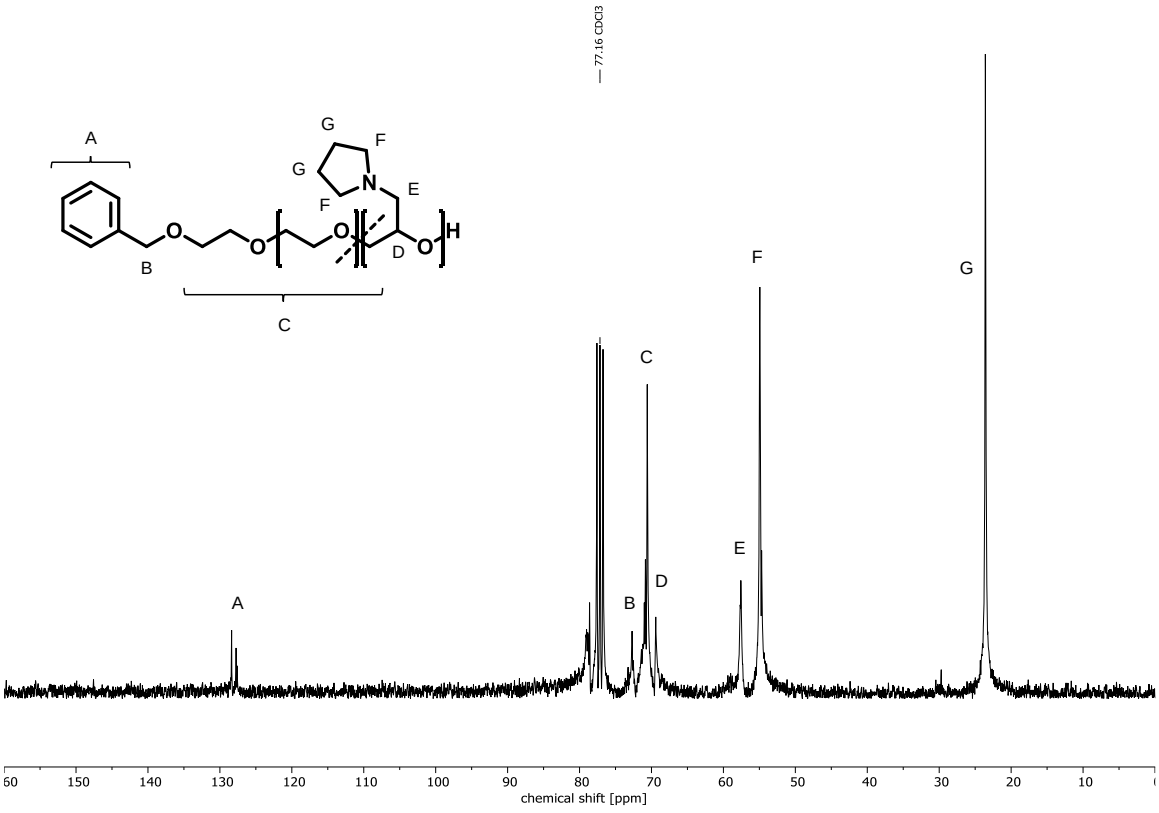

Figure S3: ^{13}C NMR spectrum ($CDCl_3$, 75 MHz) of $P(EG_{20}$-co-$PyrGA_{19})$.

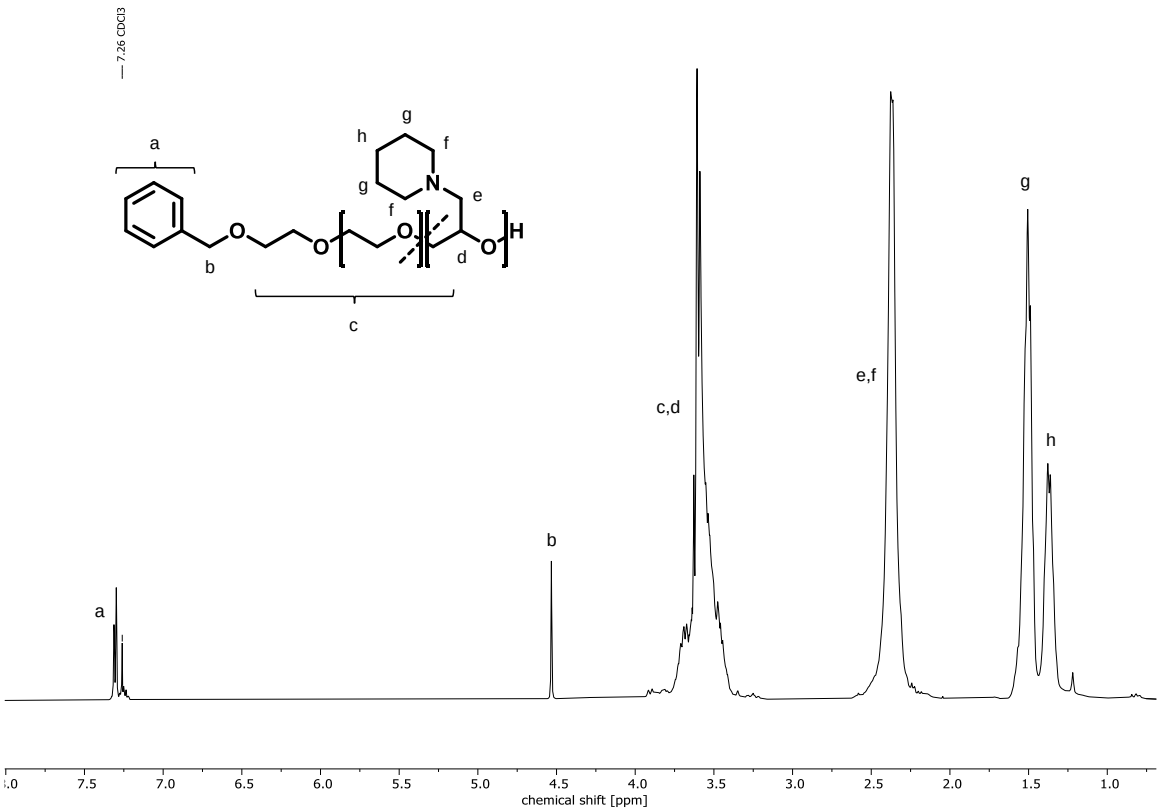

Figure S4: ^{1}H NMR spectrum ($CDCl_3$, 300 MHz) of P(EG_{14}-co-$PiGA_{16}$).

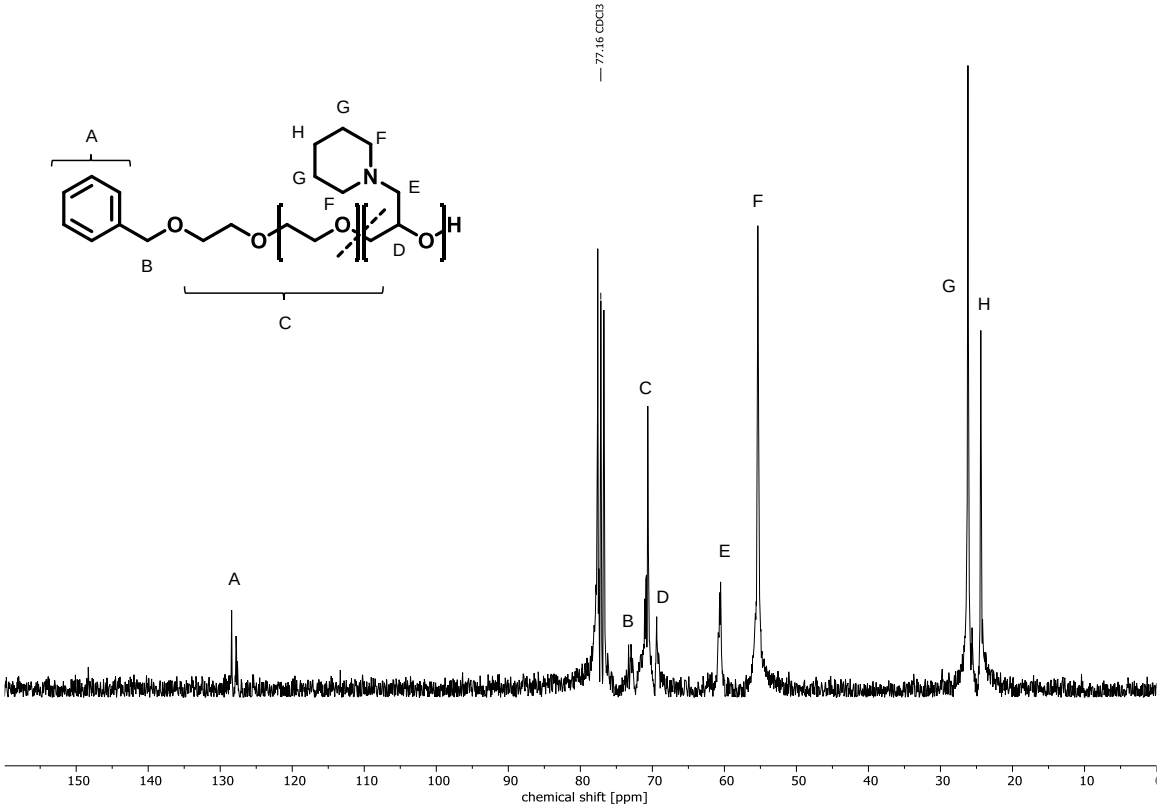

Figure S5: ^{13}C NMR spectrum ($CDCl_3$, 75 MHz) of P(EG_{14}-co-$PiGA_{16}$).

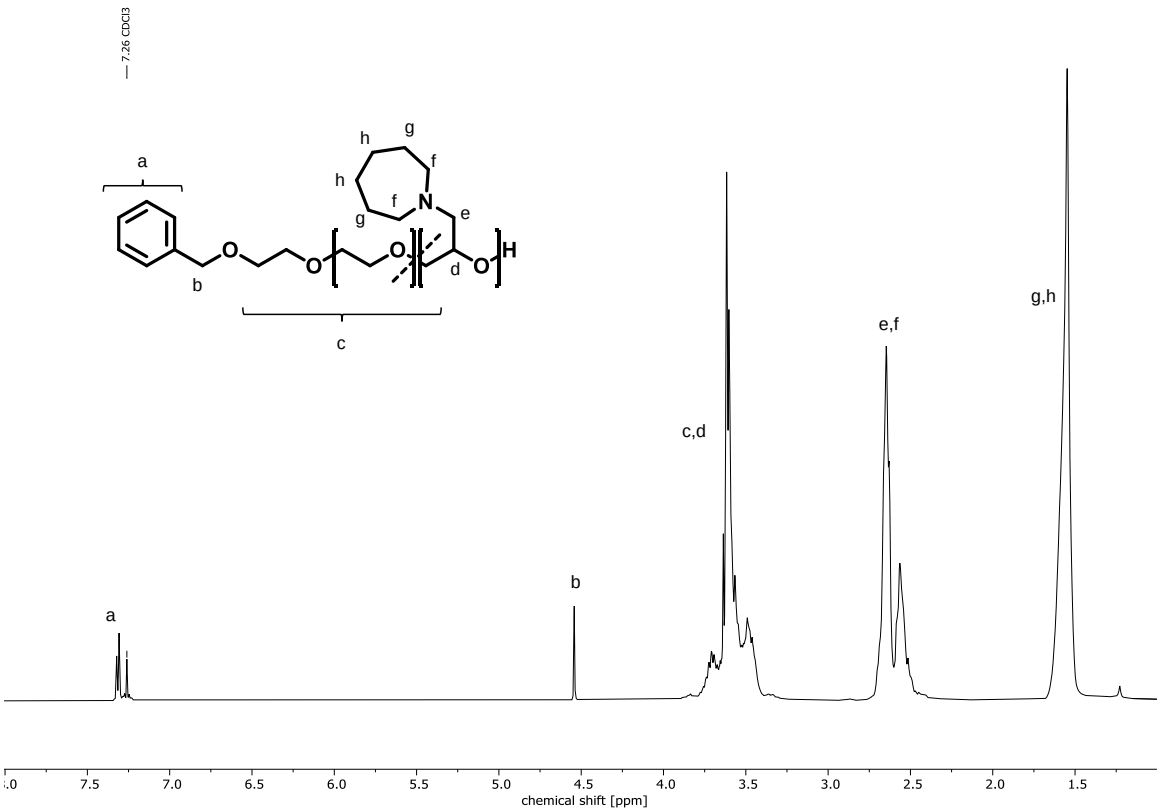

Figure S6: ^{1}H NMR spectrum ($CDCl_3$, 300 MHz) of P(EG_{16}-co-$AzGA_{14}$).

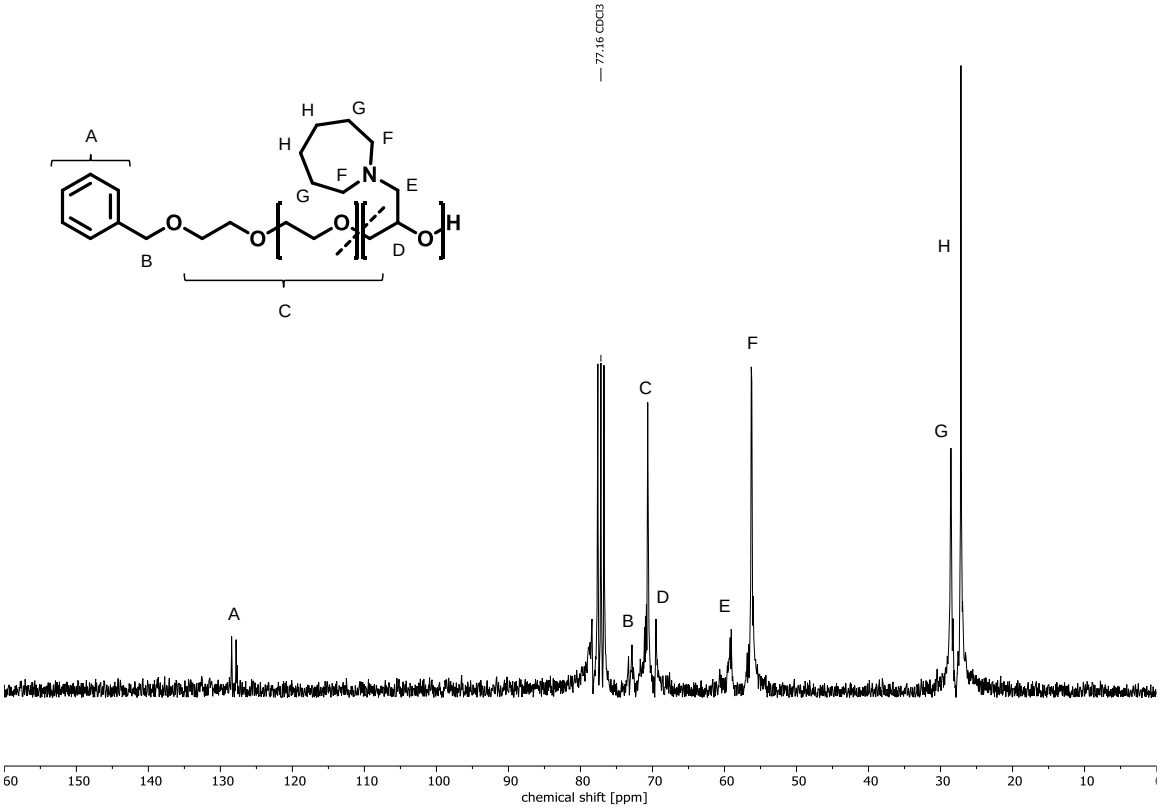

Figure S7: ^{13}C NMR spectrum ($CDCl_3$, 75 MHz) of P(EG_{16}-co-$AzGA_{14}$).

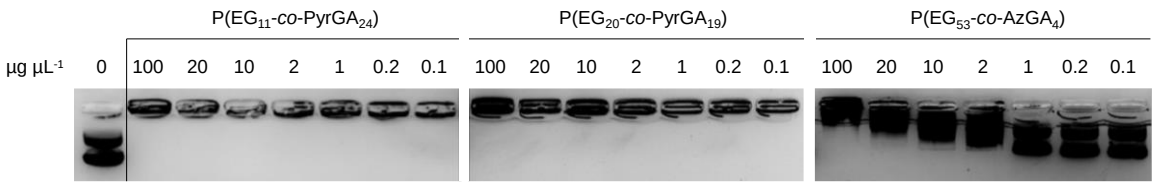

Figure S8: Additional DNA retardation assays. From left to right: copolymers with 69 and 48% of PyrGA and 7% of AzGA. The tested PyrGA copolymers show full retardation of DNA. While some DNA binding is observable for P(EG53-co-AzGA4), even high concentrations of up to 100 µg µL-1 did not achieve full retardation.

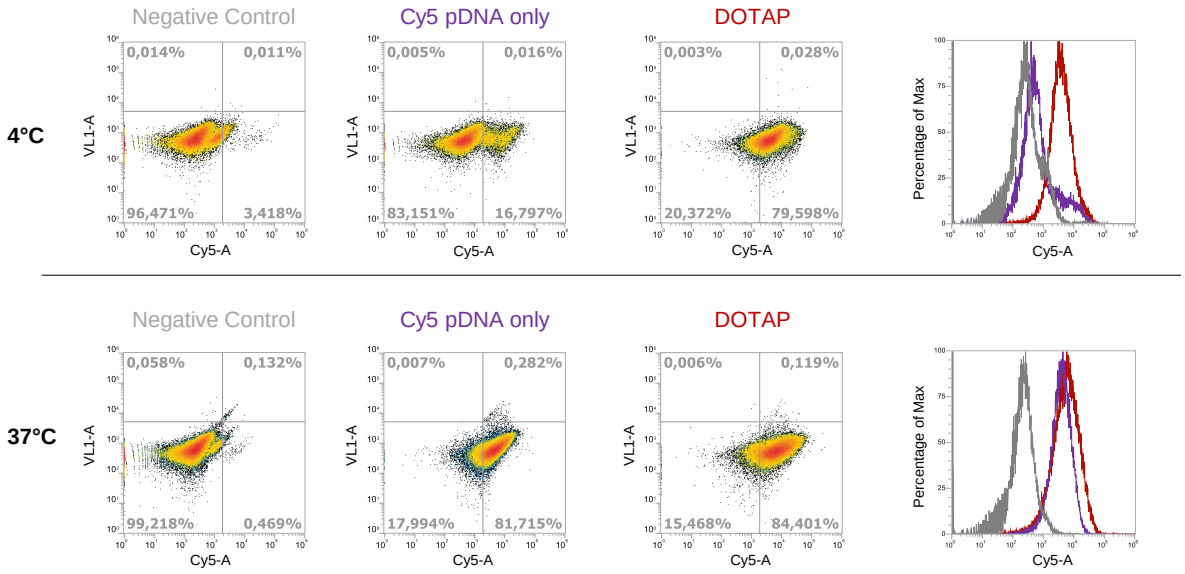

Figure S9: FACS scan of the control HEK-293 cells. Marked limits were determined in additional scans and are indicating the presence (right) or absence (left) of DNA at the cell.

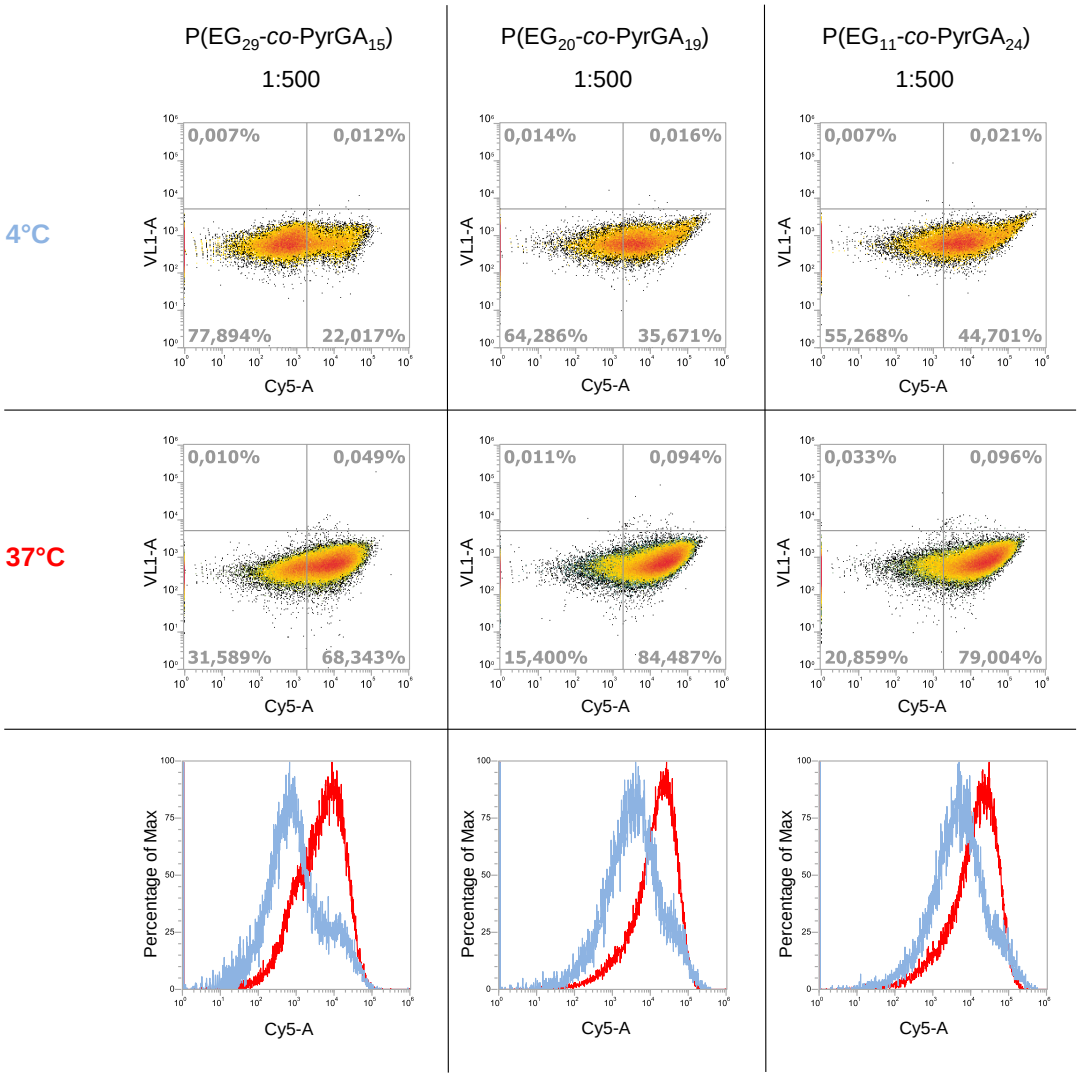

Figure S10: FACS scan of with polymer/DNA complex and dye incubated HEK-293 cells. Marked limits were determined in additional scans and are indicating the presence (right) or absence (left) of DNA at the cell. The marked dilutions of the polymer samples were determined using the respective lowest concentration, which showed efficient DNA binding in the DNA retardation assays.

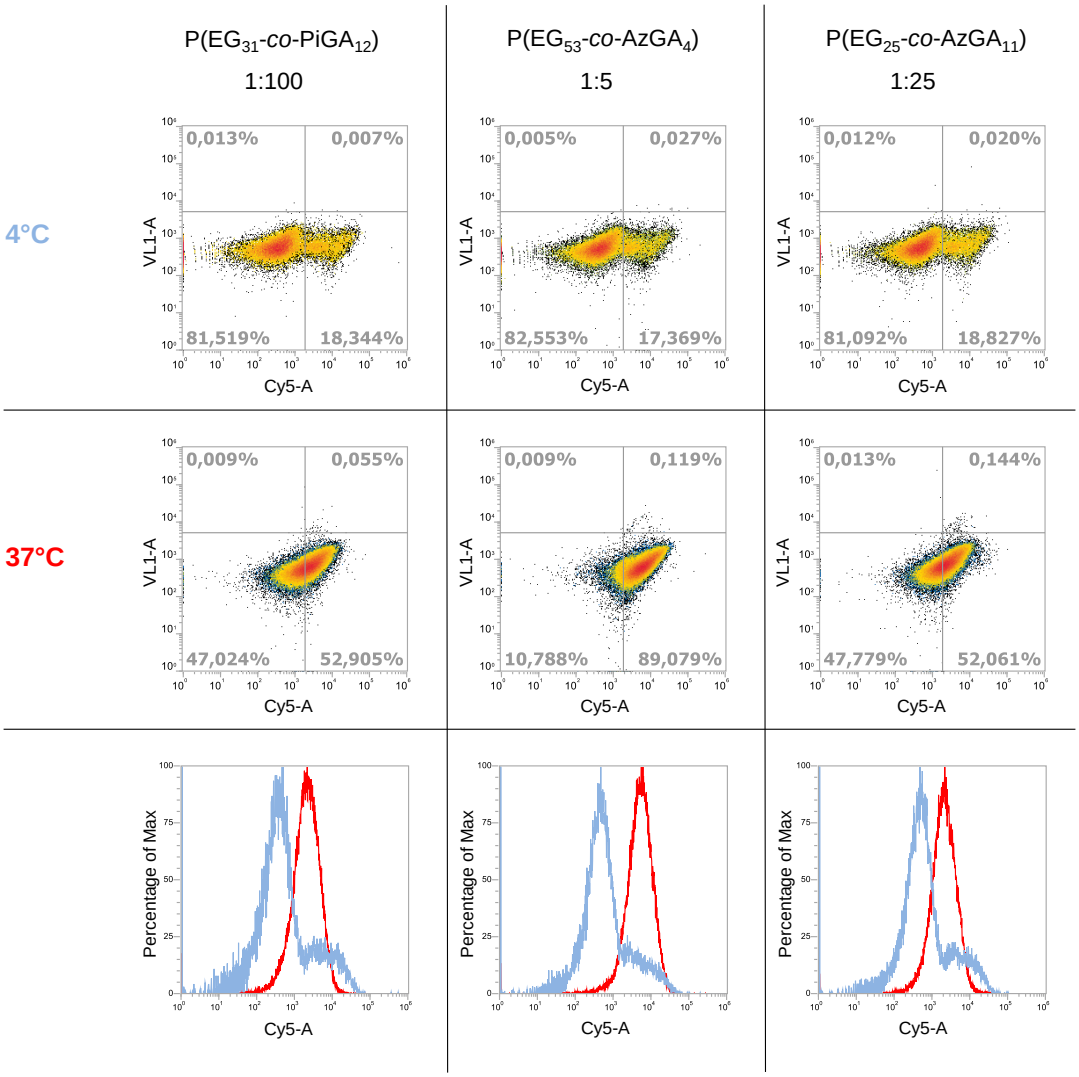

Figure S10: FACS scan of with polymer/DNA complex and dye incubated HEK-293 cells (continued). Marked limits were determined in additional scans and are indicating the presence (right) or absence (left) of DNA at the cell. The marked dilutions of the polymer samples were determined using the respective lowest concentration, which showed efficient DNA binding in the DNA retardation assays.

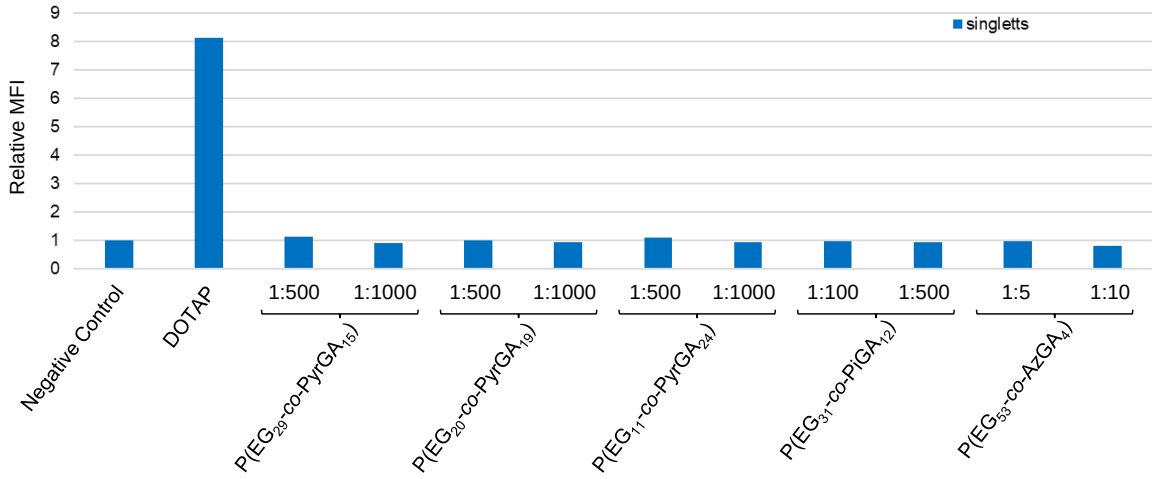

Figure S11: MFI of HEK-293 cells after incubation with agent and EGFP-pDNA in different dilutions.

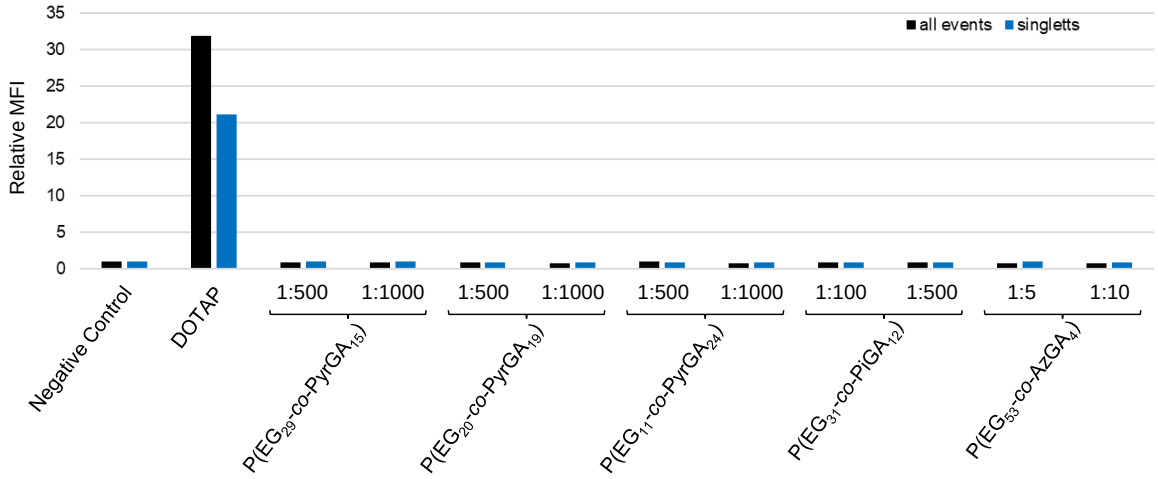

Figure S12: MFI of HEK-293 cells after incubation with agent and EGFP-mRNA in different dilutions.

2.2 Amine *N*-oxide Kinetic Hydrate Inhibitor Polymers for High-Salinity Applications

Qian Zhang,[1]* Malcolm A. Kelland,[1] Holger Frey,[2] Jan Blankenburg,[2] Larissa Limmer[2]

[1] Department of Chemistry, Bioscience and Environmental Engineering, Faculty of Science and Technology, University of Stavanger, N-4036 Stavanger, Norway

[2] Johannes Gutenberg-Universität Mainz, Department of Chemistry, Duesbergweg 10 - 14, 55128 Mainz, Germany

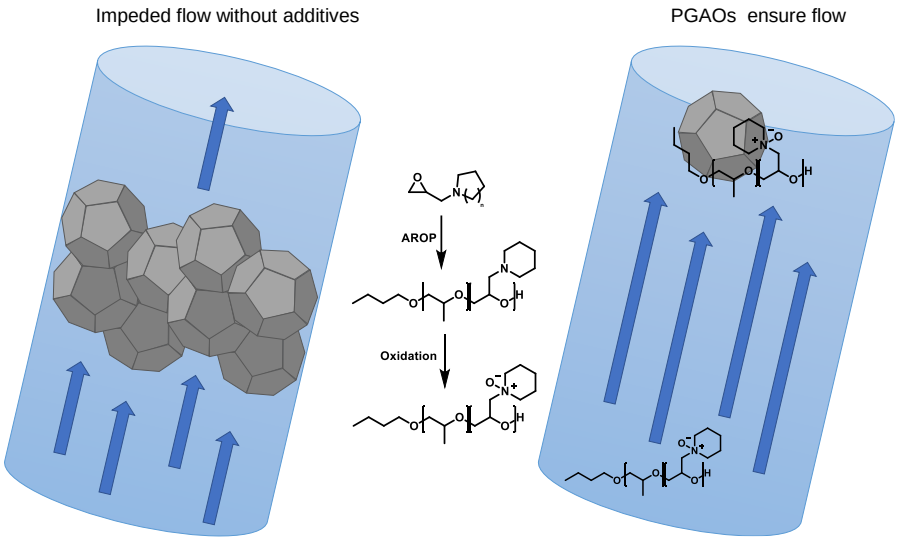

Contributions

Q.Z. – Performance and Evaluation of experiments; writing of manuscript. M.A.K. – Concept; Supervision; Editing. H.F. – Supervision; editing. J.B. – Performance and evaluation of experiments. L.L. – Performance and Evaluation of experiments; writing of manuscript.

Abstract

A series of glycidyl amine *N*-oxide polyethers with cyclic and acyclic amine *N*-oxide side groups and their block copolymers with poly(propylene) oxide (Mn in the range of 1.8 to 6.4 kg/mol) have been synthesised and investigated as kinetic hydrate inhibitors using a structure II hydrate-forming gas mixture. Polymers based on cyclic amine *N*-oxides, containing poly(piperidine glycidyl amine *N*-oxide) units gave a remarkable KHI performance. The best polymers gave similar KHI performance to commercial poly(N-vinylcaprolactam) (PVCap) at the same concentration of 2500 ppm. In addition, upon heating to 95 ^{o}C, the best polymers had no cloud point at 2500 ppm (0.25 wt%), even in 15 wt% sodium chloride solution. Thus, these polymers possess excellent potential for injection into high-salinity-, high-temperature-produced fluids.

Introduction

Gas clathrate hydrates (or gas hydrates) are crystalline compounds comprising light hydrocarbon gases trapped by water molecule lattices, which easily form in gas and oil production flow lines under the situation of subsea and/or cold climate. The formation of gas hydrates in pipelines can cause great potential risk to the flow assurance.[1,2] The deployment of kinetic hydrate inhibitor (KHI) is one of the most efficient and money-saving methods to avoid the formation of gas hydrate in flow lines. Because a very low dosage (1000-30000 ppm or 0.1-3.0 wt%) of a KHI can give considerable gas hydrate inhibition performance, KHIs are classified as low-dosage hydrate inhibitors (LDHIs).[3,4]

Hundreds of KHIs have been studied and reported since the early 1990s.[5] KHIs are based on one or more water-soluble polymers as the main active ingredient. From past studies, it has been shown that there are two key structural elements for a polymer to be a good KHI: (i) the presence of hydrophilic groups to render the polymer water-soluble, and (ii) the presence of appropriately-sized hydrophobic groups, for example alkyl groups, preferably attached to the hydrophilic group.[6,7] The amide moiety is a useful hydrophilic group, much used in commercial KHI polymers. This group offers three covalent bonds (two from the nitrogen atom and one from the carbon atom) that can in principle be used to connect hydrophobic groups. Immense structural variation is possible in the case of amide-based KHIs. This may be the reason why most reported KHIs at present are water-soluble amide-containing polymers. The amine oxide group (N=O, also written as N^{+}-O^{-}) is highly hydrophilic as a result of its strong polarity and it also possesses three covalent bonds for connecting with hydrophobic groups. Recently, studies showed that amine oxide compounds can perform well as KHIs, which was demonstrated for linear or hyperbranched alkylated ethylene-amine oxides.[8–10] In addition, the amine oxide group has been proven to be rather biocompatible, which meets the criteria of designing environmentally friendly KHI.[11,12] Thus, further investigation of amine oxide-containing polymers as KHIs is of particular interest, which motivated the studies presented here.

N-vinyl lactam and *N*-alkyl(meth)acrylamide are the most common monomer units employed in KHI polymers. Several of their polymers and copolymers have already been commercialised in this field, such as poly(*N*-vinylcaprolactam) (PVCap) and

poly(*N*-isopropylmethacrylamide) (PNIPMAM) (Figure 1). PVCap is a member of the poly(*N*-vinyl lactam) series with 7-membered pendant rings. PVCap was reported to be an efficient KHI back in the early 1990s and is still regarded today as an industry standard for comparison to newly developed KHIs in laboratory studies. Commercial PVCaps are available either as a 41.1 wt% in monoethylene glycol solution named Luviap® EG or as 50 wt. % in 2-butoxyethanol solution named Inhibex™ 101. The hydrate onset temperature (T_o) of 2500 ppm (0.25 wt%) Luvicap® EG is approximately 8 ^oC on structure II gas hydrate obtained from constant cooling tests and that for Inhibex 101 is approximately 5 ^oC.[13] For the poly(*N*-vinyl lactam) series, an increase in the KHI performance can be seen with the ring size enlarging from 5-membered to 8-membered. At 2500 ppm, poly(*N*-vinyl pyrrolidone) (PVP), poly(*N*-vinyl piperidone) (PVPip), PVCap, and poly(*N*-vinyl azacyclooctanone) (PVACO) with similar molecular weight (Mw) of approximately 4000 g/mol gave an average T_o value of 11.3, 10.5, 10.1, and 9.7 respectively.[14] In another series of ring-based KHI polymers, poly(3-methylene-2-piperidone) (3M2Pip) with six-membered rings gave better inhibition performance than the poly(3-methylene-2-pyrrolidone) (3M2P) with five-membered rings.[15]

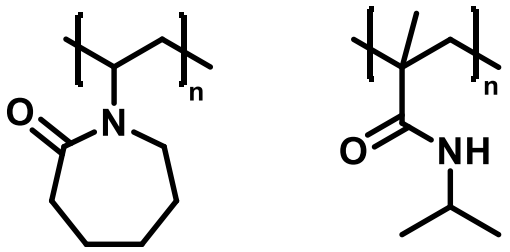

Figure 1: KHI polymers: poly(*N*-vinyl caprolactam) (PVCap) and poly(*N*-isopropylmethacrylamide) (PNIPMAM).

ExxonMobil showed that poly(*N*,*N*-diethylacrylamide) (PDEAM) gave worse KHI performance than poly(acryloylpyrrolidine) (PAPYD), suggesting that the cyclic pyrrolidino group is more efficient than the ring-opened diethylamino group.[16,17] In more recent studies with hydrazide polymethacrylamides, poly(*N*-(pyrrolidin-1-yl)methacrylamide) (PolyNPyMA) with a heterocyclic end group exhibited better performance than poly(*N*,*N*-dimethylhydrazido methacrylamide) (PDMHMAM) (Figure 2).[18,19]

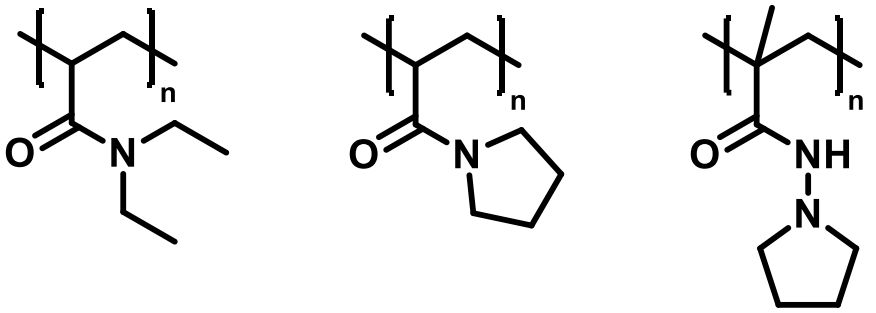

Figure 2: From left to right: poly(*N*,*N*-diethylacrylamide) (PDEAM), poly(acryloylpyrrolidine) (PAPYD), and poly(*N*-(pyrrolidin-1-yl)methacrylamide) (PolyNPyMA).

Amine *N*-oxide polyethers based on cyclic imines have not previously been investigated. Therefore, we were interested to explore this class of polymers as KHIs and compare them to amine oxides with diethylamine groups (i.e. “open” imine rings). Here we report the synthesis of a series of ring imine and diethylamine *N*-oxide polyethers. They include poly(piperidine glycidyl amine *N*-oxide) homopolymers, block copolymers containing poly(propylene oxide) and poly(*N*,*N*-diethyl glycidyl amine *N*-oxide), and block copolymers containing poly(propylene oxide) and poly(piperidine glycidyl amine *N*-oxide). The molecular weight of these polymers ranged from 2.1 to 6.4 kg/mol. Normally, the optimum molecular weight for a KHI polymer is approximately from 1.0 to 3.0 kg/mol.[3,10,14] The synthesised polymers were investigated for their KHI performance in high-pressure rocking cells using a synthetic natural gas mixture.

While the amine *N*-oxide group is the active component of these novel KHIs, we aimed at an evaluation of the possible synergistic effects of a hydrophobic comonomer. Propylene oxide stands out as an attractive comonomer because it is widely available and established industrially. The resulting polyether, poly(propylene oxide) (PPO), is characterised by its high chain flexibility and apolar character. Despite the LCST (lower critical solution temperature) behaviour of short PPO chains below 18 °C,[20] an adjustable water solubility can be introduced into this hydrophobic polymer by copolymerisation with glycidyl amines,[21] rendering it a promising material for use as a KHI.

Experimental Section

Terminology

In this work the monomers *N*,*N*-diethyl glycidyl amine (DEGA) and piperidine glycidyl amine (PiGA) were used to synthesise poly(glycidyl amines) (PGA). The oxidised form is termed as poly(glycidyl amine *N*-oxide) (PGAO).

Synthesis of PPO-*b*-PDEGAO and PPO-*b*-PPiGAO block copolymers and PPiGAO homopolymers.

Details of the synthesis procedure have been reported previously.[22] A summary is given here. The synthesising procedure of the amine *N*-oxides polymers includes two main steps: (i) Synthesis of PPO-b-PDEGA and PPO-b-PPiGA block copolymers and PPiGA homopolymers: In a dried Schlenk flask the initiator poly(propylene oxide) monobutyl ether was combined with a solution of KO^{t}Bu and 18-crown-6 in a benzene/methanol mixture. The solvent was removed; DEGA was added; and the polymerisation was carried out for 48 h at 70 °C. The product was purified by liquid-liquid extraction and dried to yield the polymer in typical yields of 70 - 90%. (ii) Oxidation of the amines to amine-*N*-oxides: The polymer was oxidised by H_2O_2 and dried to yield the poly(glycidyl amine *N*-oxide).

Using two different PPO macroinitiators (molecular weight of 1300 or 2800) as well as the low-molecular-weight initiator 2-(benzyloxy)ethanol a series of block copolymers and homopolymers were synthesised (Table 1, Figure 3). The degrees of polymerisation of the glycidyl amines were targeted to be 5, 10 and 20 units for the copolymers, and 20 and 25 for the homopolymers.

Table 1: Characterisation data of PPO-*b*-PDEGA, PPO-*b*-PPiGA and PPiGA and the corresponding amine oxide polymers (PGAO) [size exclusion chromatography (SEC) and nuclear magnetic resonance (NMR)].

Sample	GA (mol %)	M_n[a] (kg/mol)	M_n[b] (kg/mol)	$Đ$[b]	M_n(PGAO)[a] (kg/mol)
PPO_{21}-*b*-$PDEGA_6$	22	2.1	1.4	1.08	2.2
PPO_{21}-*b*-$PDEGA_{12}$	36	2.9	1.5	1.10	3.0
PPO_{47}-*b*-$PDEGA_{11}$	23	4.3	2.6	1.17	4.4
PPO_{47}-*b*-$PDEGA_{20}$	30	5.4	2.7	1.19	5.7
PPO_{21}-*b*-$PPiGA_3$	13	1.8	1.4	1.05	1.8

Table 1: Characterisation data of PPO-*b*-PDEGA, PPO-*b*-PPiGA and PPiGA and the corresponding amine oxide polymers (PGAO) [size exclusion chromatography (SEC) and nuclear magnetic resonance (NMR)] (continued).

Sample	GA (mol %)	M_n[a] (kg/mol)	M_n[b] (kg/mol)	$Đ$[b]	M_n(PGAO)[a] (kg/mol)
PPO_{21}-*b*-$PPiGA_{13}$	38	3.1	1.7	1.05	3.3
PPO_{21}-*b*-$PPiGA_{20}$	49	4.2	1.7	1.08	4.4
PPO_{47}-*b*-$PPiGA_{14}$	23	4.7	2.5	1.18	5.0
PPO_{47}-*b*-$PPiGA_{25}$	35	6.4	2.3	1.25	6.7
$PPiGA_{20}$	100	3.0	1.1	1.03	3.3
$PPiGA_{24}$	100	3.5	1.4	1.03	3.9

[a]Composition and molecular weights determined by ^{1}H NMR (400 MHz, C*D*Cl_3). [b]Determined by SEC (DMF, PEO calibration).

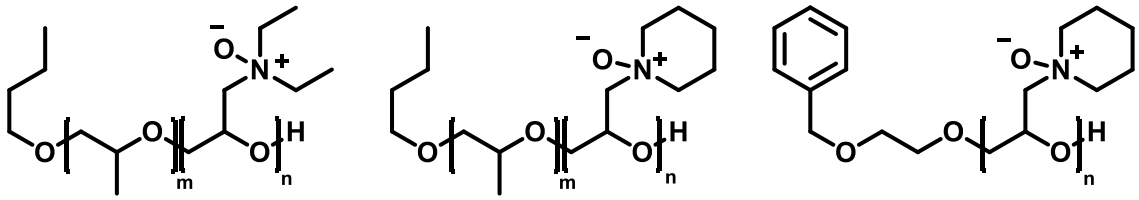

Figure 3: From left to right, structures of PPO-*b*-PDEGAO, PPO-*b*-PPiGAO, and PPiGAO.

Kinetic Hydrate Inhibitor Performance Tests in High Pressure Rocker Rig.

The KHI performance tests were carried out in a rocker rig with five steel high-pressure rocking cells (Figure 4), as reported in our previous studies.[23,24] The rocker rig was supplied by PSL Systemtechnik, Germany. A synthetic natural gas mixture (Table 2) was used to provide the high-pressure atmosphere for gas hydrate formation, which theoretically forms structure II hydrate as the most stable phase.

Figure 4: High-pressure rocking cells for testing KHI performance.

Table 2: Composition of synthetic nature gas mixture.

Component	mol %
methane	80.67
ethane	10.20
propane	4.90
CO_2	1.84
isobutane	1.53
n-butane	0.76
N_2	0.10

The slow constant cooling (SCC) test method was deployed to measure the KHI performance of the amine oxide-containing polymers. This is a suitable and reliable method to screen KHIs at laboratory scales, that has been used in many published studies.[25–27] The procedure of the SCC method was as follows:

1. The five cells with 20 ml KHI aqueous solution and a steel ball in each were set sequentially in the cooling bath.

2. The air in the cells was removed by vacuuming, purging with the synthetic natural gas mixture, and vacuuming once more.

3. Approximately 76 bar of synthetic natural gas mixture was loaded into each of the cells at 20.5 ^{o}C.

4. The system was continuously cooled from 20.5 ^{o}C to 2 ^{o}C over 18.5 hours. The cells were rocked at a rate of 20 full swings/min with the maximum rocking angle of 40° during the cooling period.

5. The data of pressure and temperature for each cell, and the temperature data of the cooling bath were recorded by a local computer through sensors.

Figure 5 shows typical pressure and temperature graphs from a SCC program. The individual temperature traces are all very close so they look like a single line. From Figure 5, we can see that in the beginning of the test, there was approximately 1 bar of pressure drop as a result of the gas dissolved in the KHI solution during initial rocking. Then the pressure decreased linearly as the temperature decreased at a constant rate in the closed cells. When the temperature cooled to 11.4 ^{o}C, which can be seen more clearly from Figure 6, there was a second pressure drop, indicating the formation of gas hydrate at this temperature. The value of 11.4 ^{o}C was treated as the hydrate onset temperature (T_o) of the 2500 ppm of $PPiGAO_{24}$ solution. The T_o value is an important temperature parameter for field application, because it refers to the first macroscopically detectable gas hydrate formation, although the gas hydrate nucleation process might have started in the system before reaching T_o.[28] With temperature cooling down continuously, when the temperature reached 10.3 ^{o}C, at which the corresponding pressure graph had the maximum slope, indicating rapid gas hydrate formation. This temperature was taken as the T_a value of the 2500 ppm $PPiGAO_{24}$ solution. The difference between T_o and T_a refers to the ability of a KHI to delay gas hydrate rapid formation. Normally 8 - 10 tests were repeated and averaged to obtain better statistical information for comparison of the performance ranking of the KHI polymers. A *t*-test was carried out to evaluate statistics, and it is considered as a statistical significant difference in KHI performance of two polymers when *p* value of their T_o values is less than 0.05.[29]

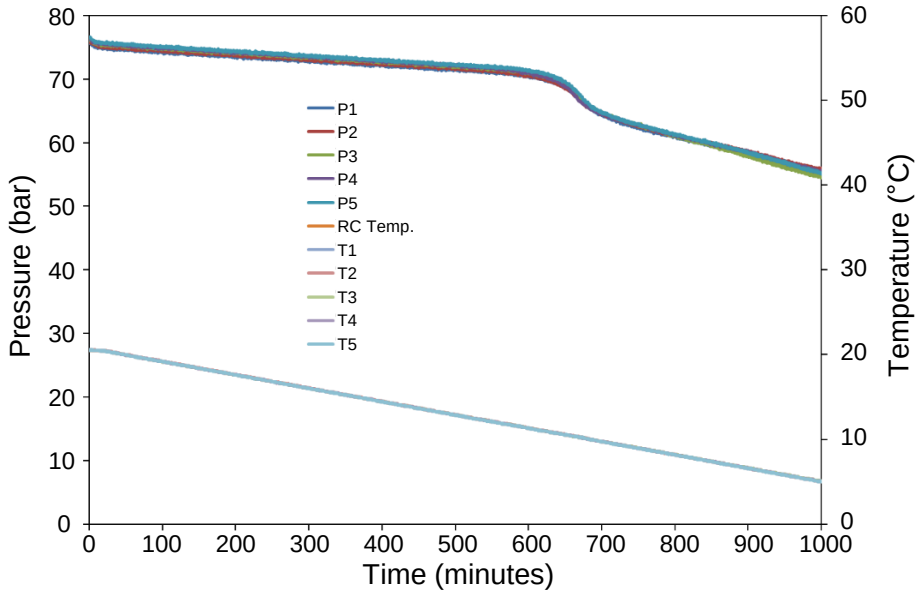

Figure 5: Temperature and pressure graphs from a constant cooling test for five cells. 2500 ppm of $PPiGAO_{24}$ solution was used in each cell.

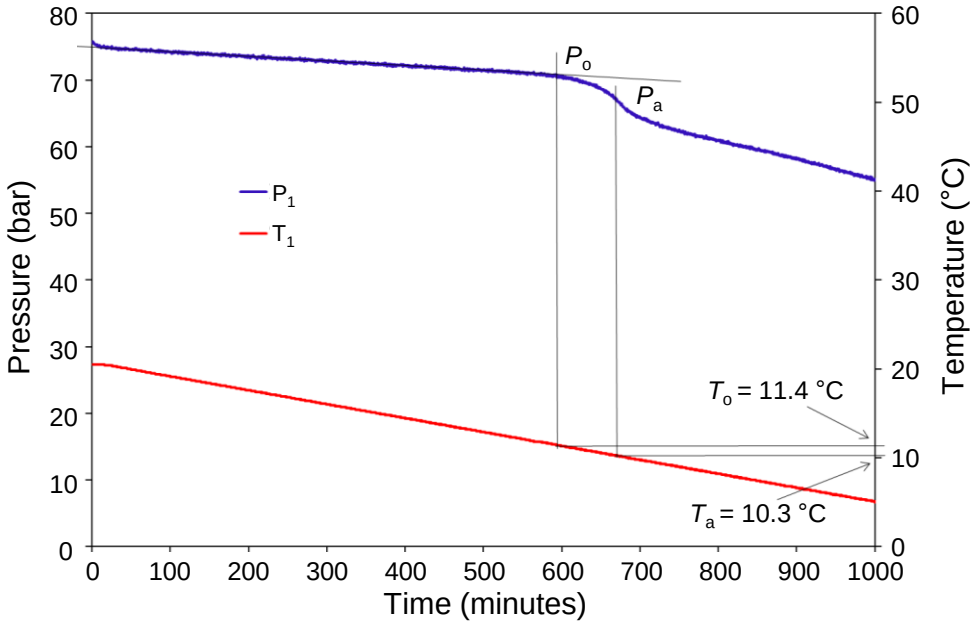

Figure 6: Determination of the onset temperature (T_o) and rapid hydrate formation temperature (T_a) for cell 1. 2500 ppm of $PPiGAO_{24}$ solution was used in cell 1.

Results and Discussion

Table 3 summarised the KHI performance results of each polymer at the concentration of 2500 ppm in water from SCC tests. The results of pure deionised water (DIW) and 2500 ppm of PVCap solution are also included in this table for

comparison. PVCap solid with a molecular weight of 2000 - 4000 g/mol was made from Luvicap® EG using multiple precipitations and high vacuum evaporation. Each average T_o [T_o (av.)] value and average T_a [T_a (av.)] value was calculated from 8 - 10 SCC tests. The subcooling degree (ΔT) at T_o was the difference between the predicted gas hydrate equilibrium temperature (T_{eq}) and the corresponding T_o value. We are aware that, with sufficient subcooling, structure I will also form, even from a natural gas mixture like ours, as you also pass the structure I phase boundary.[13] Because the T_o value refers to the first macroscopic detectable gas hydrate formation in a solution, we have compared the KHI performance of polymers mainly based on their T_o values. The KHI performance improves with a decreasing T_o value (or increasing subcooling). From Table 2, all the solutions with polymer additives gave lower T_o values than the deionised water. This means that all of the polymers have inhibition effect on gas hydrate. At a concentration of 2500 ppm, none of the new amine *N*-oxide polymers had a cloud point in deionised water, when heated up to 95 °C.

Table 3: Summary of the KHI performance results of each polymer at the concentration of 2500 ppm in water from SCC tests.

Name	T_o (av.) (°C)	ΔT (av.) at T_o (°C)	T_a (av.) (°C)	T_o (av.) − T_a (av.) (°C)
DIW	16.6	3.8	16.5	0.1
PVCap	10.4	9.8	9.9	0.5
PPO_{21}-*b*-$PDEGAO_6$	15.2	5.2	15.1	0.1
PPO_{21}-*b*-$PDEGAO_{12}$	15.7	4.7	15.6	0.1
PPO_{47}-*b*-$PDEGAO_{11}$	14.9	5.5	14.8	0.1
PPO_{47}-*b*-$PDEGAO_{20}$	14.8	5.6	14.7	0.1
PPO_{21}-*b*-$PPiGAO_3$	12.5	7.8	11.1	1.4
PPO_{21}-*b*-$PPiGAO_{13}$	10.6	9.6	10.0	0.6
PPO_{21}-*b*-$PPiGAO_{20}$	11.3	8.9	10.8	0.5
PPO_{47}-*b*-$PPiGAO_{14}$	9.8	10.4	9.7	0.1
PPO_{47}-*b*-$PPiGAO_{25}$	10.8	9.4	10.6	0.2
$PPiGAO_{20}$	9.9	10.3	8.7	1.2
$PPiGAO_{24}$	11.4	8.8	10.3	1.1

The four block copolymers combining poly(propylene oxide) and poly(*N*,*N*-diethyl glycidyl amine *N*-oxide) blocks showed little inhibition performance regarding gas hydrate formation, as they gave T_o values just a little lower than pure water. Copolymer PPO_{21}-*b*-$PDEGAO_6$ and copolymer PPO_{21}-*b*-$PDEGAO_{12}$ have the same number of poly(propylene oxide) units, but different number of poly(*N*,*N*-diethyl glycidyl amine *N*-oxide) repeating units. Although copolymer PPO_{21}-*b*-$PDEGAO_6$ and copolymer PPO_{21}-*b*-$PDEGAO_{12}$ gave T_o (av.) values of 15.2 ^oC and 15.7 ^oC, respectively, they showed the same KHI performance as a result of the *p* value more than 0.05 from *t*-test analysis. $p > 0.05$ means that there is no statistically significant difference between the results of the two samples.[29] This same KHI performance of PPO_{21}-*b*-$PDEGAO_6$ and PPO_{21}-*b*-$PDEGAO_{12}$ indicates that the poly(*N*,*N*-diethyl glycidyl amine *N*-oxide) block in copolymers had a negligible effect on KHI performance, because an increased number of these moieties in the copolymers did not increase the KHI performance. Copolymer PPO_{47}-*b*-$PDEGAO_{11}$ and copolymer PPO_{47}-*b*-$PDEGAO_{20}$ also gave similar T_o (av.) values, which further confirmed the weaker ability of the poly(*N*,*N*-diethyl glycidyl amine *N*-oxide) block polymers in inhibiting gas hydrate formation. Nevertheless, the number of the poly(propylene oxide) units affected the KHI performance of the block copolymer, because from the *t*-test, copolymer PPO_{47}-*b*-$PDEGAO_{11}$ showed a statistically significant better KHI performance than the copolymer PPO_{21}-*b*-$PDEGAO_{12}$ with less number of poly(propylene oxide) units but similar number of poly(*N*,*N*-diethyl glycidyl amine *N*-oxide) units. However, the KHI effect of poly(propylene oxide) block in copolymer is very limited, because this group is not sufficiently hydrophobic.[30] Previous studies showed that the size and shape of the hydrophobic groups in a polymer are critical for optimal KHI performance.[15,31,32] Therefore we investigated block copolymers containing poly(propylene oxide) units and the more hydrophobic poly(piperidine glycidyl amine *N*-oxide) units.

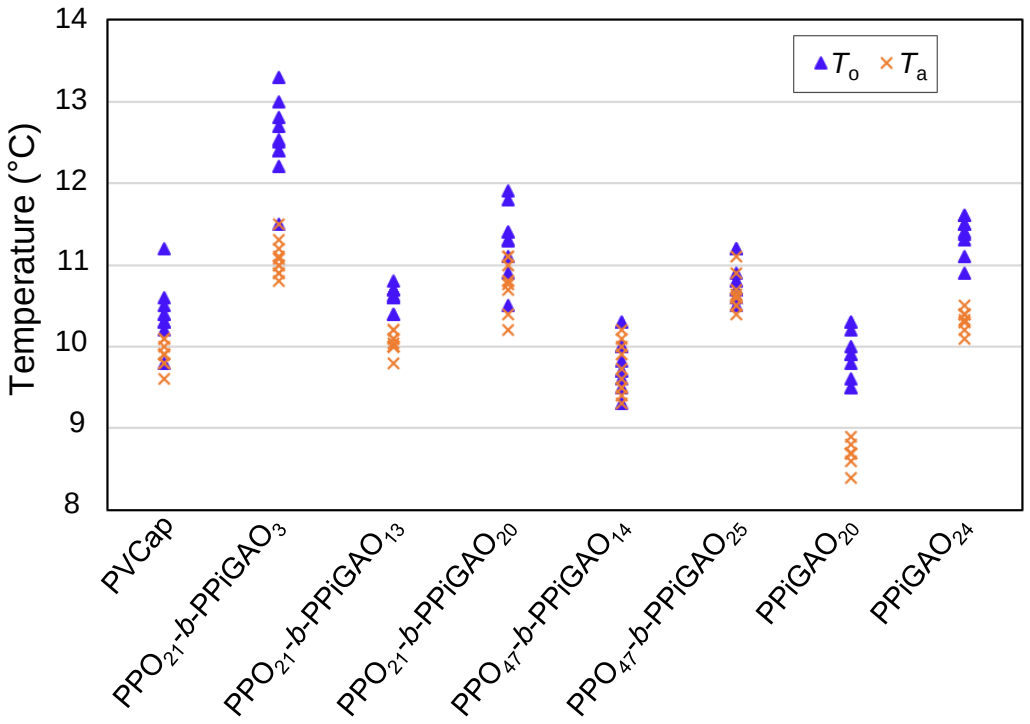

Figure 7: Summary of the KHI performance results of polymers with poly(piperidine glycidyl amine *N*-oxide) units at 2500 ppm.

The polymers with poly(piperidine glycidyl amine *N*-oxide) units showed significantly better KHI performance (Table 3 and Figure 7) than those with diethylamine *N*-oxide groups. Although the difference in performance between the 7 polymers containing poly(piperidine glycidyl amine *N*-oxide) is not large, only varying from 9.8 to 12.5 ^{o}C for the T_o average values, statistical significance can be obtained from *t*-tests to rank the KHI performance of these polymers. The copolymer PPO_{21}-*b*-$PPiGAO_3$, which contains 21 poly(propylene oxide) units and 3 poly(piperidine glycidyl amine *N*-oxide) units, gave an average T_o value of 12.5 ^{o}C. The copolymer PPO_{21}-*b*-$PPiGAO_{13}$ gave an average T_o value of 10.6 ^{o}C, which is a KHI performance on a par with the commercialised PVCap. The number of poly(propylene oxide) units in copolymer PPO_{21}-*b*-$PPiGAO_{13}$ is the same as that in copolymer PPO_{21}-*b*-$PPiGAO_3$, but the number of poly(piperidine glycidyl amine *N*-oxide) units in the former is higher than that in the latter. This means that the better KHI performance of the copolymer PPO_{21}-*b*-$PPiGAO_{13}$ is attributed to a greater number of poly(piperidine glycidyl amine *N*-oxide) units. However, the copolymer PPO_{21}-*b*-$PPiGAO_{20}$ with 20 poly(piperidine glycidyl amine *N*-oxide) units gave larger T_o values ($p < 0.05$ from the *t*-test) than the copolymer PPO_{21}-*b*-$PPiGAO_{13}$ with 13 poly(piperidine glycidyl amine *N*-oxide) units indicating that too many poly(piperidine glycidyl amine *N*-oxide) units in a copolymer

can lead to worse KHI performance. The same is true for copolymer PPO_{47}-*b*-$PPiGAO_{14}$ and copolymer PPO_{47}-*b*-$PPiGAO_{25}$. Both of them contain 47 poly(propylene oxide) units, but copolymer PPO_{47}-*b*-$PPiGAO_{14}$ has 14 poly(piperidine glycidyl amine *N*-oxide) units and it gave a T_o (av.) value of 9.8 °C while copolymer PPO_{47}-*b*-$PPiGAO_{25}$ has 25 poly(piperidine glycidyl amine *N*-oxide) units and it gave a T_o (av.) value of 10.8 °C. Therefore, it appears that there is an optimal number of the poly(piperidine glycidyl amine N-oxide) units between 3 and 20 to lead to the best copolymer performance. This may also explain why the homopolymer $PPiGAO_{24}$ with 24 poly(piperidine glycidyl amine *N*-oxide) units gave worse KHI performance than the homopolymer $PPiGAO_{20}$ with 20 poly(piperidine glycidyl amine *N*-oxide) units, because 24 is not within the optimal number of the poly(piperidine glycidyl amine *N*-oxide) units.

In comparison of the results of copolymer PPO_{21}-*b*-$PPiGAO_{13}$ (T_o (av.) = 10.6 °C) and copolymer PPO_{47}-*b*-$PPiGAO_{14}$ (T_o (av.) = 9.8 °C) with a similar number of poly(piperidine glycidyl amine *N*-oxide) units but greater number of poly(propylene oxide) units in the latter, we further confirm that a greater number of poly(propylene oxide) units in the polymer gives advantage to the KHI performance. Copolymer PPO_{47}-*b*-$PPiGAO_{25}$ and homopolymer $PPiGAO_{24}$ contain similar number of poly(piperidine glycidyl amine *N*-oxide) units, and the copolymer with 47 poly(propylene oxide) units performed better ($p < 0.05$ from *t*-test), which means that the copolymerisation is beneficial to the KHI performance. To our surprise, the copolymer PPO_{21}-*b*-$PPiGAO_{20}$ with 21 poly(propylene oxide) units and 20 poly(piperidine glycidyl amine *N*-oxide) units gave worse KHI performance ($p < 0.05$ from *t*-test) than the homopolymer $PPiGAO_{20}$ with only 20 poly(piperidine glycidyl amine *N*-oxide) units. This is tentatively ascribed to the mole ratio of the two compositions in copolymer PPO_{21}-*b*-$PPiGAO_{20}$, which does not represent the optimal value. This relates to previous studies that showed that the KHI performance could be affected by the mole fraction of the monomers in copolymers.[33–35] The reason why the polymers with piperidine glycidyl amine *N*-oxide units gave better KHI performance than those with diethylamine *N*-oxide groups may be as follows: We believe that the large cone angle produced by two ethyl groups compared to piperidine is crucial. Thus, two ethyl groups are not as effective as the six-membered ring for disrupting (or entering, depending on how you view the KHI mechanism)

hydrate cavities in hydrate nuclei. Two ethyl groups will also lose more rotational entropy when entering cavities because this rotation is not available to a cyclic group. Yagasaki *et al*. reported that the entropic stabilisation caused by the cavities at the hydrate surface is preferential for absorption from cyclic rather than acyclic groups as long as they have a suitable size.[36] Thus, the six-membered ring can be accommodated in open cavities on the gas hydrate surface. Therefore, probably the most active hydrophobic group in our series of amine *N*-oxide polymers is the cyclic piperidine ring.

We knew already that the homopolymer $PPiGAO_{20}$ gave no cloud point in deionised water; therefore, we wanted to see if it was compatible with brines. We found that this homopolymer gave no cloud point in 15 wt% sodium chloride solution up to 95 ^{o}C. This polymer is therefore suitable for injection at high well temperatures and high salinity brines, which is not possible for many established, commercial KHI polymers. The poor compatibility of high-performance commercial KHI polymers, such as PVCap, was reported in the literature.[37–39]

The problem relates to the salting out effect of electrolytes according to the Hofmeister series. Most salts show a salting out effect, including sodium chloride.[40–43] The excellent compatible behaviour of $PPIGAO_{20}$ with a high concentration of sodium chloride solution may be due to the amine *N*-oxide group. The amine *N*-oxide groups with greater polarity than the amide groups that exist in commercial KHI polymers allow for high solubility of the $PPIGAO_{20}$ polymer in brine solutions at a high temperature, despite the hydrophobic effect from the rest of the six-membered ring piperidine group.[44]

We also aimed at exploring the change in performance of the respective homopolymer at varying concentrations. It is generally accepted that the performance of a KHI polymer improves with an increasing concentration in the typical deployment window of 1000-10000 ppm (0.1-1.0 wt%). However, the rate of improvement varies considerable between polymer classes.[45–47] Table 4 and Figure 8 summarised the KHI performance of homopolymer $PPiGAO_{24}$ at varying concentrations ranging from 1250 ppm to 7500 ppm. We chose homopolymer $PPiGAO_{24}$ to evaluate the KHI performance with varying concentrations, because this was the only sample that was available for making higher concentration solutions. At a concentration of 1250 ppm, the homopolymer $PPiGAO_{24}$ gave an average T_o value of 13 ^{o}C and T_a value of 12.2

°C. When the concentration increased to 2500 ppm, the corresponding T_o (av.) ad T_a (av.) values decreased to 11.4 °C and 10.3 °C, respectively, indicating that a higher concentration leads to better KHI performance. The same trend is true for solutions at 5000 ppm and 7500 ppm. Although some individual results of the PPiGAO$_{24}$ solutions at the highest two concentrations overlapped in Figure 8, the T_o and T_a values of 5000 ppm solution are statistically significant higher ($p < 0.05$) than those of the 7500 ppm solution based on *t*-tests (10 tests at each concentration).

Table 4: Summary of the KHI Performance Results of PPiGAO$_{24}$ at Varying Concentrations in Water from SCC tests.

Name	*Conc.* (ppm)	T_o (av.) (°C)	ΔT (av.) at T_o (°C)	T_a (av.) (°C)	T_o (av.) − T_a (av.) (°C)
PPiGAO$_{24}$	1250	13.0	7.3	12.2	0.8
	2500	11.4	8.8	10.3	1.0
	5000	8.9	11.3	8.0	0.9
	7500	8.0	12.2	6.9	1.1

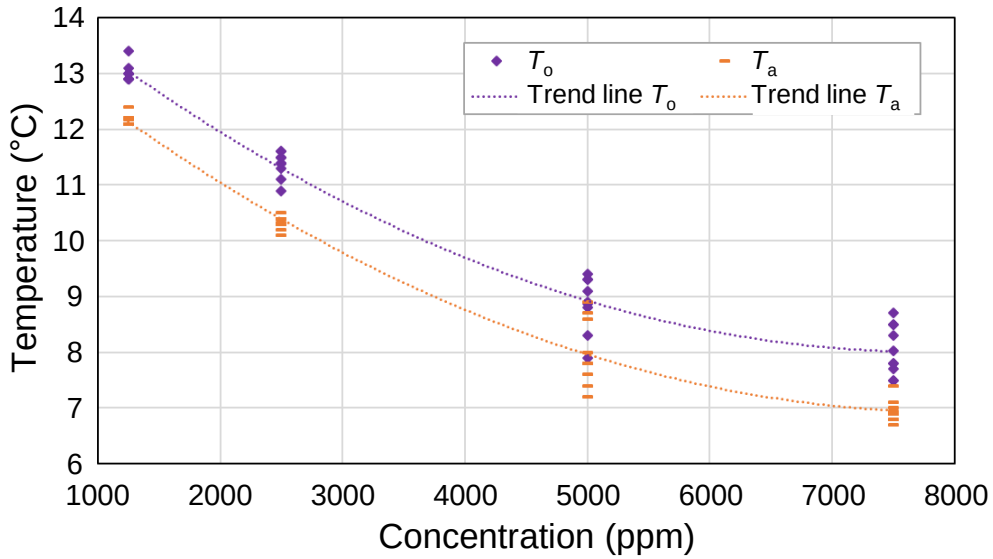

Figure 8: KHI performance results for PPiGAO$_{24}$ at varying concentrations.

Conclusion

In this study we introduce a series of poly(piperidine glycidyl amine *N*-oxide) homopolymers, block copolymers with poly(propylene oxide) and poly(*N*,*N*-diethyl

glycidyl amine *N*-oxide), and block copolymers containing poly(propylene oxide) and poly(piperidine glycidyl amine *N*-oxide) and investigate them as kinetic hydrate inhibitors in the high-pressure rocking cells using synthetic nature gas mixture. The copolymer with best KHI performance is the one containing 47 poly(propylene oxide) units and 14 poly(piperidine glycidyl amine *N*-oxide) units, gave an average T_o value of 9.8 ^oC. The best homopolymer with 20 poly(piperidine glycidyl amine *N*-oxide) units also gave an average T_o value of 9.9 ^oC.

We have also chosen one of the most efficient polymers in this study to evaluate the KHI performance at varying concentrations. The average T_o value of the homopolymer containing 24 piperidine glycidyl amine *N*-oxide units decreased from 13.0 ^oC to 8.0 ^oC when the concentration of this polymer increased from 1250 ppm to 7500 ppm.

This study has shown that polymers with piperidine glycidyl amine *N*-oxide groups are KHIs with both good inhibition performance and excellent compatibility with high salinity brines. Because these polymers have such good compatibility with high salinity brines, there is room to explore polymers with more hydrophobic groups, as this may improve the performance. We will be reporting on this in our next study, particularly polymers with varying size cyclic amine groups.[48] In addition, there is a benzyl end-cap on the best amine *N*-oxide homopolymer, and we know that aromatic rings as end-caps are detrimental to the KHI performance.[24] Future polymers will also explore other end-capping groups.

References

(1) Sloan, E. D.; Koh, C. A. *Clathrate hydrates of natural gases*, 3rd ed.; Chemical industries, Vol. 119; CRC Press, 2008. DOI: 10.1201/9781420008494.

(2) Kelland, M. A. Gas Hydrate Control. In *Production Chemicals for the Oil and Gas Industry,* 2nd ed.; Kelland, M. A., Ed.; CRC Press, 2014; pp 219–245.

(3) Kelland, M. A. History of the Development of Low Dosage Hydrate Inhibitors. *Energy Fuels* **2006**, *20* (3), 825–847. DOI: 10.1021/ef050427x.

(4) Perrin, A.; Musa, O. M.; Steed, J. W. The chemistry of low dosage clathrate hydrate inhibitors. *Chemical Society reviews* **2013**, *42* (5), 1996–2015. DOI: 10.1039/c2cs35340g. Published Online: Jan. 10, 2013.

(5) Wang, Y.; Fan, S.; Lang, X. Reviews of gas hydrate inhibitors in gas-dominant pipelines and application of kinetic hydrate inhibitors in China. *Chinese Journal of Chemical Engineering* **2019**, *27* (9), 2118–2132. DOI: 10.1016/j.cjche.2019.02.023.

(6) Ree, L. H. S.; Opsahl, E.; Kelland, M. A. N -Alkyl Methacrylamide Polymers as High Performing Kinetic Hydrate Inhibitors. *Energy Fuels* **2019**, *33* (5), 4190–4201. DOI: 10.1021/acs.energyfuels.9b00573.

(7) Zhang, Q.; Kawatani, R.; Ajiro, H.; Kelland, M. A. Optimizing the Kinetic Hydrate Inhibition Performance of N -Alkyl- N -vinylamide Copolymers. *Energy Fuels* **2018**, *32* (4), 4925–4931. DOI: 10.1021/acs.energyfuels.8b00251.

(8) Kelland, M. A.; Magnusson, C.; Lin, H.; Abrahamsen, E.; Mady, M. F. Acylamide and Amine Oxide Derivatives of Linear and Hyperbranched Polyethylenimine. Part 2: Comparison of Gas Kinetic Hydrate Inhibition Performance. *Energy Fuels* **2016**, *30* (7), 5665–5671. DOI: 10.1021/acs.energyfuels.6b01519.

(9) Kelland, M. A.; Mady, M. F. Acylamide and Amine Oxide Derivatives of Linear and Hyperbranched Polyethylenimines. Part 1: Comparison of Tetrahydrofuran Hydrate Crystal Growth Inhibition Performance. *Energy Fuels* **2016**, *30* (5), 3934–3940. DOI: 10.1021/acs.energyfuels.6b00386.

(10) Magnusson, C. D.; Kelland, M. A. Nonpolymeric Kinetic Hydrate Inhibitors: Alkylated Ethyleneamine Oxides. *Energy Fuels* **2015**, *29* (10), 6347–6354. DOI: 10.1021/acs.energyfuels.5b01592.

(11) Singh, S. K.; Bajpai, M.; Tyagi, V. K. Amine Oxides: A Review. *J. Oleo Sci.* **2006**, *55* (3), 99–119. DOI: 10.5650/jos.55.99.

(12) Gram, L.; Huss, H. H. Microbiological spoilage of fish and fish products. *International Journal of Food Microbiology* **1996**, *33* (1), 121–137. DOI: 10.1016/0168-1605(96)01134-8.

(13) Abrahamsen, E.; Kelland, M. A. Comparison of Kinetic Hydrate Inhibitor Performance on Structure I and Structure II Hydrate-Forming Gases for a Range of Polymer Classes. *Energy Fuels* **2018**, *32* (1), 342–351. DOI: 10.1021/acs.energyfuels.7b03318.

(14) Chua, P. C.; Kelland, M. A. Poly(N -vinyl azacyclooctanone): A More Powerful Structure II Kinetic Hydrate Inhibitor than Poly(N -vinyl caprolactam). *Energy Fuels* **2012**, *26* (7), 4481–4485. DOI: 10.1021/ef300688x.

(15) Zhang, Q.; Heyns, I. M.; Pfukwa, R.; Klumperman, B.; Kelland, M. A. Improving the Kinetic Hydrate Inhibition Performance of 3-Methylene-2-pyrrolidone Polymers

by N-Alkylation, Ring Expansion, and Copolymerization. *Energy Fuels* **2018**, *32* (12), 12337–12344. DOI: 10.1021/acs.energyfuels.8b03103.

(16) Colle, K. S.; Costello, C. A.; Talley, L. D.; Oelfke, H. R.; Berluche, E. Method for Inhibiting Hydrate Formation. PCT/US96/10003.

(17) Colle, K. S.; Costello, C. A.; Oelfke, H. R.; Talley, L. D.; Longo, J. M. A Method for Inhibiting Hydrate Formation. PCT/US95/11065.

(18) Ree, L. H. S.; Mady, M. F.; Kelland, M. A. N , N -Dimethylhydrazidoacrylamides. Part 3: Improving Kinetic Hydrate Inhibitor Performance Using Polymers of N , N -Dimethylhydrazidomethacrylamide. *Energy Fuels* **2015**, *29* (12), 7923–7930. DOI: 10.1021/acs.energyfuels.5b02079.

(19) Mady, M. F.; Kelland, M. A. N , N -Dimethylhydrazidoacrylamides. Part 1: Copolymers with N -Isopropylacrylamide as Novel High-Cloud-Point Kinetic Hydrate Inhibitors. *Energy Fuels* **2014**, *28* (9), 5714–5720. DOI: 10.1021/ef501391g.

(20) Mortensen, K.; Schwahn, D.; Janssen, S. Pressure-induced melting of micellar crystal. *Physical Review Letters* **1993**, *71* (11), 1728–1731. DOI: 10.1103/PhysRevLett.71.1728.

(21) Blankenburg, J.; Wagner, M.; Frey, H. Well-Defined Multi-Amino-Functional and Stimuli-Responsive Poly(propylene oxide) by Crown Ether Assisted Anionic Ring-Opening Polymerization. *Macromolecules* **2017**, *50* (22), 8885–8893. DOI: 10.1021/acs.macromol.7b01324.

(22) Blankenburg, J.; Stark, M.; Frey, H. Oxidation-responsive polyether block copolymers lead to non-ionic polymer surfactants with multiple amine N -oxides. *Polym. Chem.* **2019**, *10* (13), 1569–1574. DOI: 10.1039/C9PY00093C.

(23) Abrahamsen, E.; Heyns, I. M.; Solms, N. von; Pfukwa, R.; Klumperman, B.; Kelland, M. A. First Study of Poly(3-methylene-2-pyrrolidone) as a Kinetic Hydrate Inhibitor. *Energy Fuels* **2017**, *31* (12), 13572–13577. DOI: 10.1021/acs.energyfuels.7b03006.

(24) Zhang, Q.; Kelland, M. A. Study of the Kinetic Hydrate Inhibitor Performance of Poly(N -vinylcaprolactam) and poly(N -isopropylmethacrylamide) with Varying End Caps. *Energy Fuels* **2018**, *32* (9), 9211–9219. DOI: 10.1021/acs.energyfuels.8b01985.

(25) Ree, L. H. S.; Sirianni, Q. E. A.; Gillies, E. R.; Kelland, M. A. Systematic Study of Polyglyoxylamides as Powerful, High-Cloud-Point Kinetic Hydrate Inhibitors. *Energy Fuels* **2019**, *33* (3), 2067–2075. DOI: 10.1021/acs.energyfuels.8b04335.

(26) Ke, W.; Kelland, M. A. Kinetic Hydrate Inhibitor Studies for Gas Hydrate Systems: A Review of Experimental Equipment and Test Methods. *Energy Fuels* **2016**, *30* (12), 10015–10028. DOI: 10.1021/acs.energyfuels.6b02739.

(27) Zhang, Q.; Shen, X.; Zhou, X.; Liang, D. Inhibition Effect Study of Carboxyl-Terminated Polyvinyl Caprolactam on Methane Hydrate Formation. *Energy Fuels* **2017**, *31* (1), 839–846. DOI: 10.1021/acs.energyfuels.6b02603.

(28) Semenov, A. P.; Medvedev, V. I.; Gushchin, P. A.; Vinokurov, V. A. Kinetic Inhibition of Hydrate Formation by Polymeric Reagents: Effect of Pressure and Structure of Gas Hydrates. *Chem Technol Fuels Oils* **2016**, *51* (6), 679–687. DOI: 10.1007/s10553-016-0658-5.

(29) Walpole, R. E.; Myers, R. H.; Myers, S. L. *Statistics for Engineers & Scientists*; Prentice Hall/Pearson Education, Inc, 2012.

(30) Kelland, M. A.; Svartås, T. M.; Andersen, L. D. Gas hydrate anti-agglomerant properties of polypropoxylates and some other demulsifiers. *Journal of Petroleum Science and Engineering* **2009**, *64* (1-4), 1–10. DOI: 10.1016/j.petrol.2008.12.001.

(31) Abrahamsen, E.; Kelland, M. A. Carbamate Polymers as Kinetic Hydrate Inhibitors. *Energy Fuels* **2016**, *30* (10), 8134–8140. DOI: 10.1021/acs.energyfuels.6b01349.

(32) Ajiro, H.; Takemoto, Y.; Akashi, M.; Chua, P. C.; Kelland, M. A. Study of the Kinetic Hydrate Inhibitor Performance of a Series of Poly(N -alkyl- N -vinylacetamide)s. *Energy Fuels* **2010**, *24* (12), 6400–6410. DOI: 10.1021/ef101107r.

(33) Kamal, M. S.; Hussein, I. A.; Sultan, A. S.; Solms, N. von. Application of various water soluble polymers in gas hydrate inhibition. *Renewable and Sustainable Energy Reviews* **2016**, *60*, 206–225. DOI: 10.1016/j.rser.2016.01.092.

(34) Thieu, V.; Bakeev, K. N.; Shih, J. S. Gas Hydrate Inhibitor. 09/812,504.

(35) Colle, K. S.; Oelfke, H. R.; Kelland, M. A. Method for inhibiting hydrate formation:United States Patent. 539,033.

(36) Yagasaki, T.; Matsumoto, M.; Tanaka, H. Adsorption Mechanism of Inhibitor and Guest Molecules on the Surface of Gas Hydrates. *J. Am. Chem. Soc.* **2015**, *137* (37), 12079–12085. DOI: 10.1021/jacs.5b07417. Published Online: Sep. 11, 2015.

(37) Kelland, M. A.; Mønig, K.; Iversen, J. E.; Lekvam, K. Feasibility Study for the Use of Kinetic Hydrate Inhibitors in Deep-Water Drilling Fluids. *Energy Fuels* **2008**, *22* (4), 2405–2410. DOI: 10.1021/ef800109e.

(38) Kelland, M. A. Additives for Kinetic Hydrate Inhibitor Formulations To Avoid Polymer Fouling at High Injection Temperatures: Part 1. A Review of Possible Methods. *Energy Fuels* **2020**, *34* (3), 2643–2653. DOI: 10.1021/acs.energyfuels.9b04040.

(39) Kelland, M. A.; Iversen, J. E. Kinetic Hydrate Inhibition at Pressures up to 760 Bar in Deep Water Drilling Fluids. *Energy Fuels* **2010**, *24* (5), 3003–3013. DOI: 10.1021/ef9016152.

(40) Cacace, M. G.; Landau, E. M.; Ramsden, J. J. The Hofmeister series: salt and solvent effects on interfacial phenomena. *Quarterly reviews of biophysics* **1997**, *30* (3), 241–277. DOI: 10.1017/S0033583597003363.

(41) Güner, A.; Ataman, M. Effects of inorganic salts on the properties of aqueous poly(vinylpyrrolidone) solutions. *Colloid Polym Sci* **1994**, *272* (2), 175–180. DOI: 10.1007/BF00658844.

(42) Moghaddam, S. Z.; Thormann, E. The Hofmeister series: Specific ion effects in aqueous polymer solutions. *Journal of Colloid and Interface Science* **2019**, *555*, 615–635. DOI: 10.1016/j.jcis.2019.07.067. Published Online: Jul. 25, 2019.

(43) Hofmeister, F. Zur Lehre von der Wirkung der Salze. *Archiv f. experiment. Pathol. u. Pharmakol* **1888**, *24* (4-5), 247–260. DOI: 10.1007/BF01918191.

(44) Bernier, D.; Wefelscheid, U. K.; Woodward, S. Properties, Preparation and Synthetic Uses of Amine N -Oxides. An Update. *Organic Preparations and Procedures International* **2009**, *41* (3), 173–210. DOI: 10.1080/00304940902955756.

(45) Magnusson, C.; Abrahamsen, E.; Kelland, M. A.; Cely, A.; Kinnari, K.; Li, X.; Askvik, K. M. As Green As It Gets: An Abundant Kinetic Hydrate Inhibitor from Nature. *Energy Fuels* **2018**, *32* (5), 5772–5778. DOI: 10.1021/acs.energyfuels.8b00367.

(46) Ree, L. H.; Kelland, M. A.; Roth, P. J.; Batchelor, R. First investigation of modified poly(2-vinyl-4,4-dimethylazlactone)s as kinetic hydrate inhibitors. *Chemical Engineering Science* **2016**, *152*, 248–254. DOI: 10.1016/j.ces.2016.06.031.

(47) Kelland, M. A.; Abrahamsen, E.; Ajiro, H.; Akashi, M. Kinetic Hydrate Inhibition with N -Alkyl- N -vinylformamide Polymers: Comparison of Polymers to n -Propyl and Isopropyl Groups. *Energy Fuels* **2015**, *29* (8), 4941–4946. DOI: 10.1021/acs.energyfuels.5b01251.

(48) Dirdal, E. G.; Kelland, M. A. Does the Cloud Point Temperature of a Polymer Correlate with Its Kinetic Hydrate Inhibitor Performance? *Energy Fuels* **2019**, *33* (8), 7127–7137. DOI: 10.1021/acs.energyfuels.9b01185.

Supporting Information

Reagents

All chemicals were purchased from Acros Organics, Fisher Scientific, Roth, Sigma-Aldrich, TCI, VWR, Fluka or Deutero GmbH. Glycidyl amines were synthesised in accordance with literature.[1,2] PPO (2800 g/mol) was synthesised in accordance to literature.[3]

Instrumentation

^{1}H NMR (300 MHz) spectra were recorded on a Bruker Avance III HD 300 (5 mm BBFO-Probe with *z*-Gradient and ATM). Size exclusion chromatography (SEC) was performed in *N*,*N*-dimethylformamide (DMF), containing 1 g/mL lithium bromide, at 50 °C with a flow rate of 1 mL/min. The system consisted of an Agilent 1100 Series, HEMA columns with 300/100/40 Å porosity and Agilent G1362A RID as refractive index detector (Agilent Technologies, Santa Clara, CA, USA). The system was calibrated with poly(ethylene oxide) (PEG) standards by Polymer Standards Service (PSS, Mainz, Germany). Toluene was used as an internal reference.

References

(1) Reuss, V. S.; Werre, M.; Frey, H. Thermoresponsive copolymers of ethylene oxide and N,N-diethyl glycidyl amine: polyether polyelectrolytes and PEGylated gold nanoparticle formation. *Macromol. Rapid Commun.* **2012**, *33* (18), 1556–1561. DOI: 10.1002/marc.201200307. Published Online: Jun. 25, 2012.

(2) Blankenburg, J.; Wagner, M.; Frey, H. Well-Defined Multi-Amino-Functional and Stimuli-Responsive Poly(propylene oxide) by Crown Ether Assisted Anionic Ring-Opening Polymerization. *Macromolecules* **2017**, *50* (22), 8885–8893. DOI: 10.1021/acs.macromol.7b01324.

(3) Blankenburg, J.; Stark, M.; Frey, H. Oxidation-responsive polyether block copolymers lead to non-ionic polymer surfactants with multiple amine N -oxides. *Polym. Chem.* **2019**, *10* (13), 1569–1574. DOI: 10.1039/C9PY00093C.

2.3 N-oxide polyethers as Kinetic Hydrate Inhibitors: Side Chain Ring Size Makes the Difference

Qian Zhang,[1,2#*] Larissa Limmer,[3#] Holger Frey,[3] Malcolm A. Kelland[1]

# First two authors contributed equally.

[1] Department of Chemistry, Bioscience and Environmental Engineering, Faculty of Science and Technology, University of Stavanger, N-4036 Stavanger, Norway

[2] Beijing International Center for Gas Hydrate & College of Engineering, Peking University, Beijing, 100871, China

Reprinted with permission from Energy Fuels 2021, 35, 5, 4067–4074.

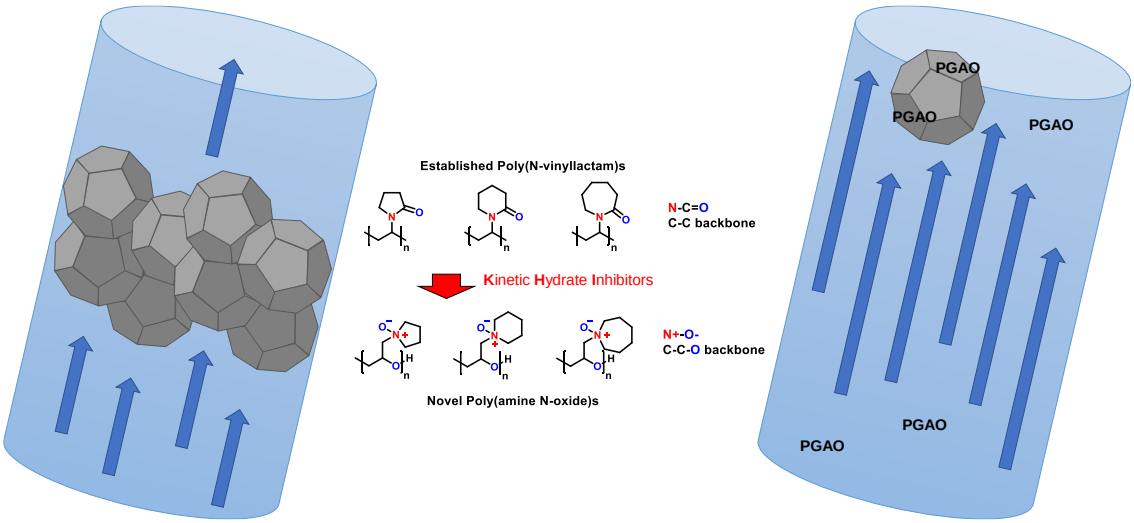

Contributions

Q.Z. – Concept, performance, and evaluation of experiments; writing of manuscript. L.L. – Concept, performance, and evaluation of experiments; writing of manuscript. M.A.K. – Concept; supervision; editing. H.F. – Supervision; editing.

Abstract

The formation of gas hydrates in flow lines is one of the most severe problems for flow assurance in gas and oil industry. Developing effective kinetic hydrate inhibitors (KHI) to avoid the problem of gas hydrate formation has attracted widespread attention. In this study, a series of poly(glycidyl amine *N*-oxide)s (PGAO) with 5-7-membered rings as side chains, poly(pyrrolidine glycidyl amine *N*-oxide)s (PPyrGAO), poly(piperidine glycidyl amine *N*-oxide)s (PPiGAO) and poly(azepane glycidyl amine *N*-oxide)s (PAzGAO), with varying molecular weights have been synthesised. The KHI performance of these glycidyl amine *N*-oxide polyethers has been evaluated in high-pressure rocking cells with synthetic natural gas (SNG) mixture. The PGAOs with lower molecular weights gave better KHI performance, and at 2500 ppm the best one gave an average T_o value of 9.8 ^{o}C (ΔT = 10.4 ^{o}C), which is on a par with polyvinylcaprolactam (PVCap). Even in high concentration of brine solution, none of the PGAOs showed a cloud point up to 95 ^{o}C. Employing molecular weights of around 4 kg/mol, the KHI performance of the PGAOs follows the following trend, correlating with the ring size: PPyrGAO < PPiGAO < PAzGAO. However, at higher molecular weight, the ring size of the pendant group did not affect the KHI performance of the PGAOs. PPiGAO with the smaller piperidine ring groups gave better inhibition effect than PAzGAO when the molecular weights were at approximately 8 kg/mol. In addition, the KHI performance of one of the best PAzGAOs was tested in the concentration range from 1000 to 5000 ppm, and an increase of the KHI performance with increasing concentration of polymer was observed. The amine *N*-oxide functional group is critical for the KHI performance of these polymers, as poly(pyrrolidine glycidyl amine)s (PPyrGA) and poly(azepane glycidyl amine)s (PAzGA) with amine groups instead of the *N*-oxide gave a negligible inhibitory effect.

Introduction

Gas hydrates are clathrate crystalline solids consisting of water crystal structures as well as physically trapped gas molecules, such as nitrogen, carbon dioxide and light hydrocarbons like methane, ethane, and propane.[1-3] Structure I (sI) hydrate, structure II (sII) hydrate, and structure H (sH) hydrate can be formed at conditions of low temperature and high pressure. The temperature-pressure phase boundaries and type of gas hydrates formed will depend on the gas composition.[4]

The formation of gas hydrates is one of the biggest problems of gas and oil flow assurance, especially in offshore development.[5-7] If the temperature is low, such as in the subsea and cold climate operation area, gas hydrates are easy to form. Once gas hydrates form in the flow line or any other place in the production and transportation system, they tend to be difficult to remove. Thus, to avoid the problem of gas hydrate formation in gas and oil industry, the best strategy is to prevent gas hydrates from forming.

Many methods, including hydraulic methods, water removal, thermal methods, and chemical methods, have been proposed to prevent the formation of gas hydrates. Among these mentioned gas hydrate prevention methods, chemical methods, especially the method of injecting low dosage-hydrate inhibitors (LDHI), are relatively more efficient and cost-saving.[8-10] Kinetic hydrate inhibitors (KHI) belong to LDHI, as the effective dosage of KHI can be less than 5 wt. %. Since the early 1990s, when the very first efficient KHI polyvinylpyrrolidone (PVP) was reported, hundreds of KHIs have been discovered. A few kinds of KHIs have been commercialised, such as N-vinylcaprolactam (VCap)-based homo- and copolymers, *N-iso*-propylmethacrylamide (NiPMAM) homo- and copolymers, hyperbranched polyesteramides and polyester pyroglutamates are also available commercially. (Figure 1). Most reported KHIs and nearly all the current commercial KHIs are amide group-containing polymers.[11, 12]

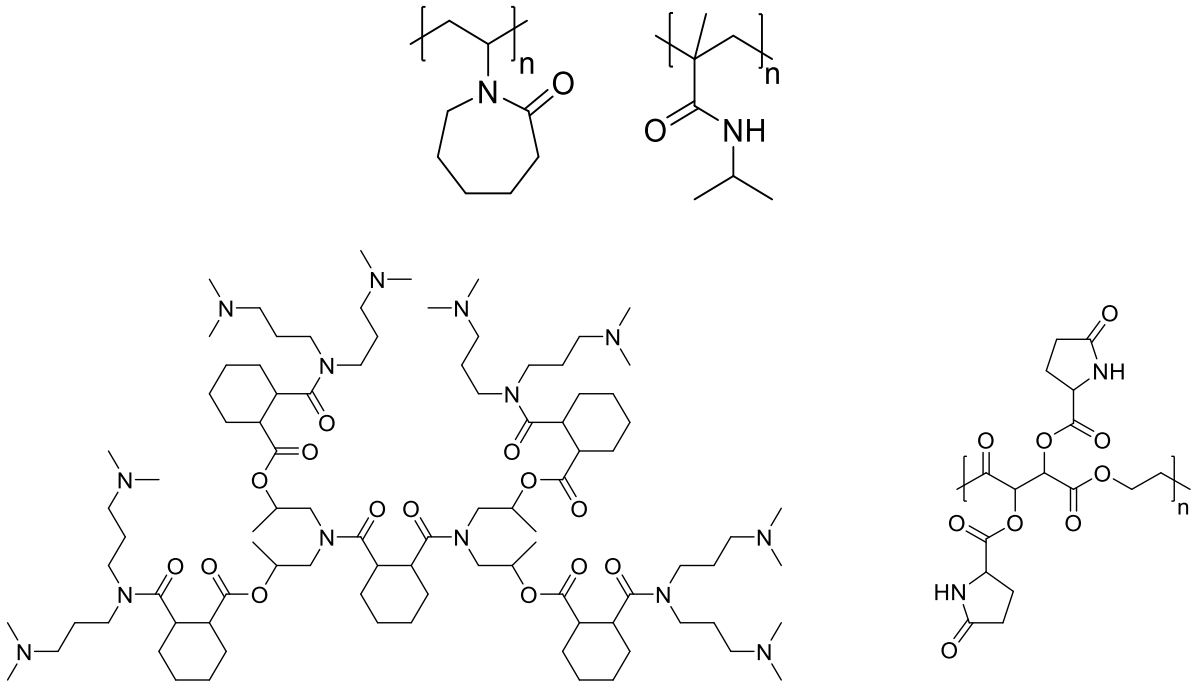

Figure 1: Structures of various commercial KHIs. Poly(*N*-vinylcaprolactam), PVCap (top left); poly(*N*-*iso*-propylmethacrylamide), PNiPMAM (top right); hyperbranched polyesteramide (bottom left); polyester pyroglutamate (bottom right).

Recently, several series of non-amide polymers, such as poly(isopropenyloxazoline),[13] poly(vinylphosphonate) diesters,[14] poly(alkyl ethylene phosphonate)s,[15] poly(amine *N*-oxide)s,[16-18] poly(vinylsulfonamide)s,[19] poly(vinylaminal)s,[20] poly(sulfobetaine methacrylate)s[21] and polysaccharides like starch, chitosan and pectin,[11] have been reported to be excellent KHIs (Figure 2). Poly(amine *N*-oxide) non-amide KHIs have attracted increasing attention, due to the immense structural variability, their superior hydrophilicity, and, most importantly, the remarkable inhibition performance of amine *N*-oxide polymers. Reports showed that hyperbranched polyethyleneimine-alkyl-amine *N*-oxides (HPEI-R-AO), especially those with large alkyl groups, can inhibit the formation of both sI and sII hydrates effectively.[17, 22] Lately, Zhang et al. reported that poly(piperidine glycidyl amine *N*-oxide) (PIGAO) showed considerable KHI performance on sII hydrate. The best results were on a par with the highly established commercial PVCap.[23] In addition, even in high-salinity solution, the PIGAOs gave no cloud point when heated up to 95 ^{o}C, while the cloud point of PVCap in aqueous solution is around 35 ^{o}C.[10, 24, 25] For many KHI series, the polymer with lower cloud point gave better inhibition performance.[26] Ring expansion to a 7-membered azepane ring for the pendant group is a key strategy to decrease the cloud point of the KHI polymer.[27, 28] Thus, enlarging

the six-membered ring of the PIGAOs may improve the inhibition performance of this poly(amine *N*-oxide) KHI series, which motivated this study. We also included polymers with the 5-membered pyrrolidine ring for comparison to the pyrrolidone ring found in several commercial N-vinyl pyrrolidone-based KHI polymers.

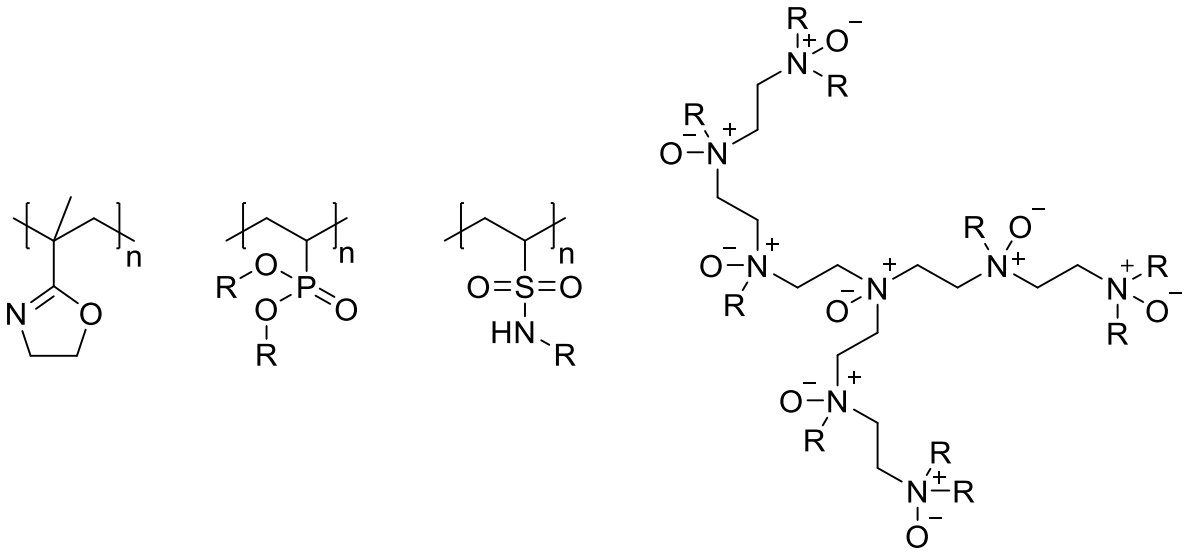

Figure 2: Structures of non-amide KHIs. From left to right: polyisopropenyloxazoline, poly (dialkyl vinylphosphonate)s, poly(vinylsulfonamide)s, and hyperbranched polyethyleneimine-alkyl-amine *N*-oxides (HPEI-R-AO). R = alkyl group.

In addition, previous studies showed that a larger size of the pendant cyclic groups of a KHI polymer can lead to better inhibition performance. For example, with the molecular weights (M_n) at around 4 kg/mol, poly(*N*-vinyl lactam)s gave an improved inhibition performance, when the size of the pendant ring groups increased from five to eight members.[28] Also, poly(3-methylene-2-piperidone) (3M2Pip) containing larger cyclic pendant groups was reported to be a better KHI inhibitor than poly(3-methylene-2-pyrrolidone) (3M2P).[27] At a molecular weight of approximately 20 kg/mol the polyvinylaminal with cyclohexyl groups gave better inhibition performance than its analogue with cyclopentyl groups.[20]

In this study we have synthesised a series of poly(glycidyl amine *N*-oxide)s (PGAO) with varied cyclic imines, namely poly(pyrrolidine glycidyl amine *N*-oxide)s (PPyrGAO), poly(piperidine glycidyl amine *N*-oxide)s (PPiGAO) and poly(azepane glycidyl amine *N*-oxide)s (PAzGAO), respectively (Figure 3). The molecular weights (*Mn* value) of these PGAOs range from 1.4 to 8.5 kg/mol. The inhibition performance on sII hydrates of these synthesised PGAOs was evaluated by using synthetic natural gas (SNG) mixture in high-pressure rocking cells.

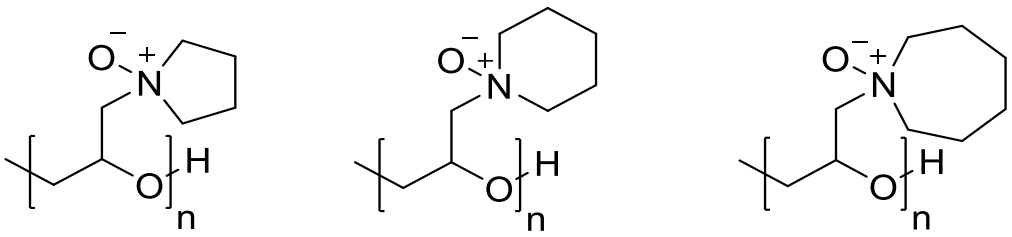

Figure 3: Structures of PPyrGAO (left), PPiGAO (middle) and PAzGAO (right).

Experimental Section

Materials

All chemicals for the syntheses and characterisation of monomers and polymers were purchased from Acros Organics, Fisher Scientific, Roth, Sigma-Aldrich, TCI, VWR or Deutero GmbH. Epichlorohydrine and pyrrolidine were obtained in 99% purity from Acros Organics; piperidine was obtained in 99% purity from Sigma-Aldrich; azepane was obtained in 98% purity from Alfa Aesar. Benzyloxyethanol and ethylene glycol monobutyl ether with purities of 98% or 99%, respectively, were purchased from TCI.

Instrumentation

^{1}H NMR (300 MHz) and ^{13}C NMR (75 MHz) spectra were recorded on a Bruker Avance III HD 300 (5 mm BBFO-Probe with *z*-Gradient and ATM). Size exclusion chromatography (SEC) was typically carried out in *N*,*N*-dimethylformamide (DMF) at 50 °C, containing 1 g/mL lithium bromide with a flow rate of 1 mL/min on an Agilent 1100 Series, HEMA columns with 300/100/40 Å porosity and Agilent G1362A RID as refractive index detector. Calibration was performed with poly(ethylene oxide) (PEG) standards by Polymer Standards Service (PSS, Mainz, Germany). SEC of in DMF-insoluble polymers was done at 40 °C in hexafluoroisopropanol containing 3 g/L potassium trifluoroacetate with a flow rate of 0.8 mL/min, using columns packed with modified silica (PFG columns) 100/1000 Å porosity and calibrated with Poly(methyl methacrylate) (PMMA) standards by PSS.

Synthesis of Monomers

The syntheses of the glycidyl amine monomers were adapted from the literature synthesis of piperidine glycidyl amine.[29] In the following, the synthesis of azepane glycidyl amine (AzGA) is described exemplarily.

Azepane (15.0 mL, 1 eq, 0.13 mol) was kept at 0 °C by a water/ice bath, while 10.2 mL epichlorohydrin (1 eq, 0.13 mol) was added dropwise under vigorous stirring. After addition, the mixture was stirred for 90 minutes at 0 °C. While the mixture was slowly allowed to reach room temperature, a cooled solution of 5.2 g NaOH (1 eq, 0.13 mol) in 12 mL of water was added. After stirring overnight, the mixture was diluted with 50 mL of water and extracted three times with 50 mL of diethyl ether each time. The combined organic phases were dried over $MgSO_4$, and the solvent was removed under reduced pressure; subsequently, the product was isolated in high purity by distillation under reduced pressure in typical yields of 60-70%. AzGA was identified as a colourless liquid. ^{1}H NMR (300 MHz, C*D*Cl_3) δ 3.01 (dtd, *J* = 6.5, 3.8, 2.7 Hz, 1H, C*H*), 2.78 – 2.54 (m, 1H, C*H*$_2$-CH; 1 H, CH-C*H*$_2$-N; 4H, N(-C*H*$_2$-CH_2)$_2$), 2.48 – 2.38 (m, 1H, C*H*$_2$-CH and 1H, CH-C*H*$_2$-N), 1.69 – 1.43 (m, 8H, (C*H*$_2$)$_4$). ^{13}C NMR (75 MHz, C*D*Cl_3) δ 60.66 (CH-*C*H_2-N), 56.06 (N-(*C*H_2-CH_2)$_2$), 50.99 (*C*H), 45.13 (*C*H_2-CH), 27.97 (N-(CH_2-*C*H_2)$_2$), 26.94 (N-(CH_2-CH_2-*C*H_2)$_2$).

Pyrrolidine glycidyl amine (PyrGA) and piperidine glycidyl amine (PiGA) were synthesised in a similar manner. However, for PyrGA 1.5 equivalents of epichlorohydrin and NaOH were used in the reaction, and stirring was reduced from overnight to 30 minutes; petroleum ether was used for the extraction procedure. In the synthesis of PiGA the mixture was stirred for 2 hours at 0 °C, and the NaOH solution was added after the mixture reached room temperature. The characterisation data for PiGA was reported previously.[29] PyrGA was identified as a colourless liquid. ^{1}H NMR (300 MHz, C*D*Cl_3) δ 3.05 (dtd, *J* = 6.7, 4.0, 2.7 Hz, 1H, C*H*), 2.77 – 2.68 (m, 1H, C*H*$_2$-CH and 1 H, CH-C*H*$_2$-N), 2.53 (tdd, *J* = 6.5, 4.7, 3.3 Hz, 4H, N(-C*H*$_2$-CH_2)$_2$), 2.46 (dd, *J* = 5.0, 2.7 Hz, 1H, C*H*$_2$-CH), 2.37 (dd, *J* = 12.8, 6.5 Hz, 1H, CH-C*H*$_2$-N), 1.79 – 1.71 (m, 4H, N-(CH_2-C*H*$_2$)$_2$). ^{13}C NMR (75 MHz, $CDCl_3$) δ 58.50 (CH-*C*H_2-N), 54.50 (N-(*C*H_2-CH_2)$_2$), 50.86 (*C*H), 45.36 (*C*H_2-CH), 23.36 (N-(CH_2-*C*H_2)$_2$).

Polyether Synthesis

The synthesis of the novel polyethers consisted of two steps, adapted from a literature protocol for poly(piperidine glycidyl amine-*N*-oxide).[29] (1) The initiator ethylene glycol monobutyl ether (EGBE) (1 eq), or benzyloxyethanol (BnO) (1 eq), respectively, was combined with a solution of KO^{t}Bu (0.5 eq) and 18-crown-6 (1 eq) in a benzene/methanol 5:1 mixture in a dried Schlenk flask. After removal of the solvents, monomer was added, and the polymerisation was carried out at 40 °C for 48-72 hours. After purification by liquid-liquid extraction and removal of the solvents the polymer poly(glycidyl amine) (PGA) was isolated. (2) The oxidation of PGA (1 eq) was performed by addition of aqueous H_2O_2 solution (1.2 eq) and stirring overnight at room temperature. After drying, fully oxidised poly(glycidyl amine *N*-oxide) (PGAO) was obtained in typical yields of 70-90%.

Kinetic Hydrate Inhibitor Performance Tests

The kinetic hydrate inhibitor performance tests of the synthesised glycidyl amine *N*-oxide polyethers were carried out in a high-pressure rocker rig, provided by PSL Systemtechnik, Germany. This high-pressure equipment contains five separate cells, so five parallel experimental results can be obtained from one testing process.[30,31] A synthetic natural gas (SNG) mixture (Table 1), which theoretically forms sII hydrate as the most stable phase, was used to supply the high pressure in the cells.

Table 1: Composition of SNG mixture.

Component	mol %
nitrogen	0.11
n-butane	0.72
isobutane	1.65
propane	5
CO_2	1.82
ethane	10.3
methane	80.4

The hydrate onset temperature (T_o) and the rapid hydrate formation temperature (T_a) obtained from the slow constant cooling (SCC) tests were used to evaluate the kinetic hydrate inhibitor performance of the polymers in this study. The brief procedure of

the SCC test is as follows: 20 ml of KHI solution was loaded into the five test cells, each of which has a maximum inner volume of 40 ml. Usually, KHI solutions were made at least 24 hrs before the SCC tests to ensure complete dissolution of the polymers. The five cells were placed sequentially in the water bath of the rocker rig. A procedure of vacuum - purge with SNG mixture - vacuum was applied to remove air from the cells. Approximately 76 bars of SNG mixture was added to each cell when the temperature for each cell had stabilised at 20.5 ^{o}C. The inlet/outlet value of each cell was then switched off. Subsequently, the temperature of the cooling bath was slowly decreased with the cooling rate set at 1 ^{o}C/h. During the constant cooling period, the cells were rocked (20 full swings/min, maximum 40°) for agitation. The temperature and pressure data for each cell were recorded and saved in a local computer. Figure 4 shows an example of the temperature-time and pressure-time curves for all the five cells from one SCC test process.

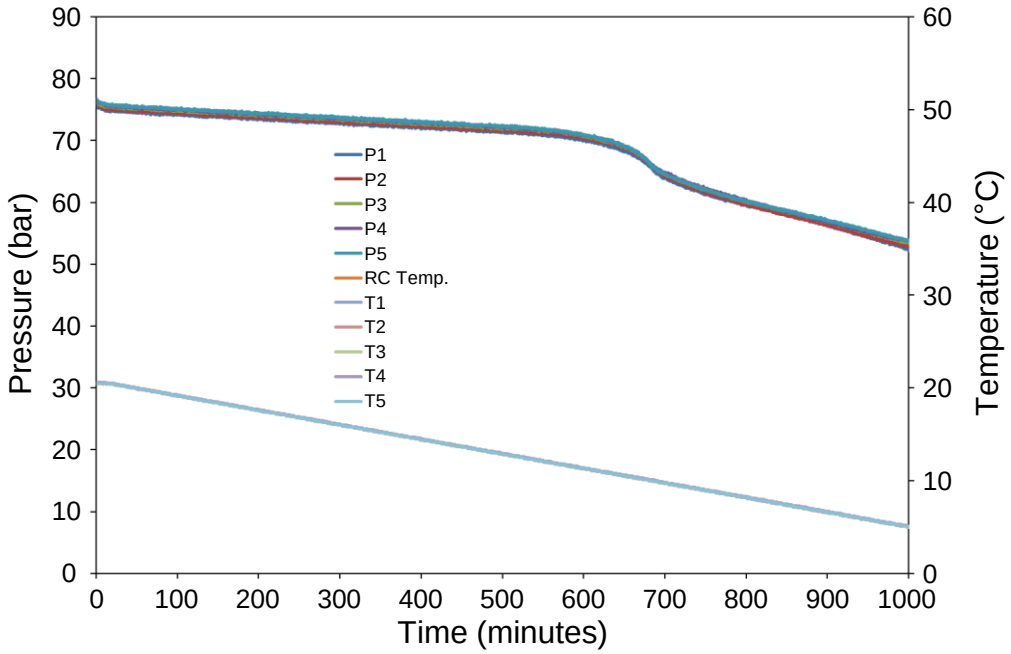

Figure 4: Example of the temperature-time and pressure-time curves for all the five cells from one SCC test process. Each cell contained 20 ml of EGBE-PAzGAO$_{38}$ solution at 2500 ppm. RC Temp. means the temperature of the cooling bath of RC5.

Figure 5 shows an example of how to analyse the hydrate onset temperature (T_o) and the rapid hydrate formation temperature (T_a) from the pressure and temperature curves. As the temperature constantly decreased, the pressure in the cell also decreased linearly. When the gas molecules in the cell were consumed to form gas hydrates, the pressure curve deviated from the original linear track. The temperature

at the point of the first pressure deviation (P_o) was identified as T_o. The temperature at the point of the fastest pressure deviation (P_a) was called T_a.

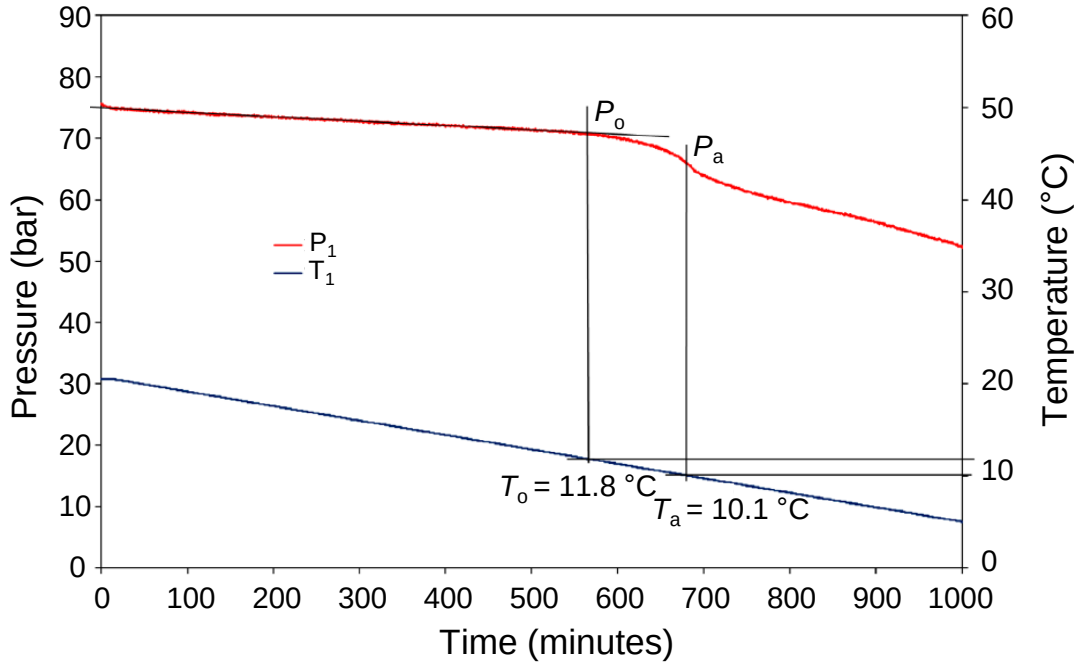

Figure 5: Example of analysing the hydrate onset temperature (T_o) and the rapid hydrate formation temperature (T_a) for one cell. The cell contained 20 ml of EGBE-PAzGAO$_{38}$ solution at 2500 ppm.

Results and Discussion

Utilising the anionic ring opening polymerisation (AROP) of the epoxide monomers pyrrolidine glycidyl amine (PyrGA), piperidine glycidyl amine (PiGA) and azepane glycidyl amine (AzGA) as well as the two different initiators benzyloxyethanol (BnO) and ethylene glycol monobutyl ether (EGBE) a series of poly(glycidyl amine)s were prepared and oxidised to obtain poly(glycidyl amine *N*-oxide)s (PGAO). The preparation of the monomers was performed in analogy to known literature procedures by the reaction of epichlorohydrin with the corresponding amine.[29] To the best of our knowledge, PyrGA and AzGA were used as intermediates in organic reactions but have never been polymerised to date.[32] Both ^{1}H NMR and ^{13}C NMR spectra of PyrGA and AzGA are given in Figures S1-S3. Via the crown ether-assisted AROP of the monomers, the corresponding polyethers were synthesised in yields of 70-90% with narrow dispersity, typically below 1.23 (Table 2). The molecular weights determined by ^{1}H NMR spectroscopy (spectra before and after oxidation in Figures S5 and S6) show discrepancies to the molecular weights calculated by size exclusion

chromatography (SEC), caused by the different elution behaviour of the functionalised polyethers in comparison to the PEG standards used for calibration. (We note that Mn was measured by NMR using two different solvents because of the solubility change due to the oxidation step). This effect was reported previously by different authors.[33,34] While the SEC curves of polymers insoluble in *N*,*N*-dimethylformamide show a monomodal distribution, the molecular weights and dispersities are not comparable due to the PMMA standard used for these measurements.

Table 2: Characterisation data of PGA and PGAO.

Name	M_n[a] kg/mol	M_n[b] kg/mol	$Đ$[b]	M_n(PGAO)[c] kg/mol
EGBE-PPyrGA$_9$	1.3	0.6	1.17	-
EGBE-PPyrGA$_{18}$	2.4	1.0	1.09	2.7
BnO-PPyrGA$_{20}$	2.7	1.3	1.04	3.0
EGBE-PPiGA$_{10}$	1.5	0.8	1.10	1.7
EGBE-PPiGA$_{24}$	3.5	1.2	1,07	3.9
EGBE-PPiGA$_{49}$	7.0	-	1.19[d]	7.8
EGBE-PAzGA$_{14}$	2.3	0.9	1.06	2.5
EGBE-PAzGA$_{23}$	3.7	0.8	1.23	4.1
EGBE-PAzGA$_{38}$	6.0	-	1.87[d]	6.6
EGBE-PAzGA$_{49}$	7.7	-	1.21[d]	8.5

[a]Molecular weights determined by ^{1}H NMR (300 MHz, C*D*Cl$_3$). [b]Determined by SEC (DMF, PEG-calibration). [c]Determined by ^{1}H NMR (300 MHz, D_2O) [d]Determined by SEC (HFIP, PMMA-calibration). Not comparable data due to different calibrations and solvents.

Table 3 summarises the results of the KHI performance for the synthesised PGAOs at the concentration of 2500 ppm. The results of deionised water (DIW) and polyvinylcaprolactam (PVCap) were also listed in this table for comparison. The PVCap (2~4 kg/mol) solid used in this study was obtained from the commercial Luvicap EG by removing the monoethylene glycol solvent. The average T_o (T_o (av.)) and average T_a (T_a (av.)) values for each polymer were calculated from at least five repeated tests. Subcooling (ΔT) was calculated by using the equilibrium temperature at the pressure of P_o (see Figure 5) minus the value of T_o. The difference between T_o (av.) and T_a (av.) indicates the degree of how a KHI polymer stops the rapid hydrate formation once the detectable gas hydrates occurs. As T_o value refers to the first detectable gas hydrate formation, which is the most important parameter for

evaluating the KHI performance of a polymer, we will focus on discussing T_o values. In addition, as seen in Table 3, when comparing the performance of the KHI polymers, their T_a values almost follow the same trend as the T_o values. Generally, lower T_o values translate to better KHI performance.

Table 3: Summarised results of the KHI performance obtained from the SCC tests.[a]

Name	M_n[b] kg/mol	T_o (av.) (°C)	ΔT (av.) at T_o (°C)	T_a (av.) (°C)	T_o (av.) − T_a (av.) (°C)
DIW	-	16.3	4.1	16.2	0.1
PVCap	2-4	10.4	9.8	9.9	0.5
EGBE-PPyrGAO$_{18}$	2.7	13.5	6.8	11.2	2.3
BnO-PPyrGAO$_{20}$	3.0	13.2	7.1	12.0	1.1
EGBE-PPiGAO$_{10}$	1.7	9.8	10.4	8.7	1.0
EGBE-PPiGAO$_{24}$	3.9	11.7	8.5	10.6	1.1
EGBE-PPiGAO$_{49}$	7.8	13.3	7.0	12.2	1.1
EGBE-PAzGAO$_{14}$	2.5	9.8	10.4	9.1	0.6
EGBE-PAzGAO$_{23}$	4.1	10.0	10.2	9.2	0.8
EGBE-PAzGAO$_{38}$	6.6	11.7	8.5	10.1	1.6
EGBE-PAzGAO$_{49}$	8.5	13.6	6.7	12.2	1.4
EGBE-PPyrGA$_9$	1.3	17.0	3.4	16.5	0.5
EGBE-PAzGA$_{14}$	2.3	17.1	3.3	16.7	0.4
EGBE-PAzGA$_{23}$	3.7	16.8	3.6	16.4	0.4

[a]Concentration at 2500 ppm. [b]Determined by ^{1}H NMR (300 MHz, D_2O).

All PGAOs gave better KHI performance than DIW. EGBE-PPyrGAO$_{18}$ and BnO-PPyrGAO$_{20}$ are poly(pyrrolidine glycidyl amine *N*-oxide)s with a similar number of monomer units, and they gave similar KHI performance despite the varying initiators with an aliphatic or aromatic group, respectively. BnO-PPyrGAO$_{20}$, EGBE-PPiGAO$_{24}$ and EGBE-PAzGAO$_{23}$ gave a T_o (av.) value of 13.2, 11.7 and 10.0 °C, respectively, indicating that the poly(pyrrolidine glycidyl amine *N*-oxide), poly(piperidine glycidyl amine *N*-oxide) and poly(azepane glycidyl amine *N*-oxide) with similar number of monomer units at around 20 gave different KHI performances. EGBE-PAzGAO$_{23}$ gave better KHI performance than EGBE-PPiGAO$_{24}$, while EGBE-PPiGAO$_{24}$ was superior to BnO-PPyrGAO$_{20}$. This means when M_n (which is around equal to M_w, for

the three polymers mentioned here) is around 4 kg/mol, the PGAOs with larger size of the pendant ring groups gave better KHI performance. Interestingly, in 2012, Chua and Kelland already reported that an increasing ring size leads to improved KHI performance for the poly(*N*-vinyl lactam)s at $M_w \approx 4$ kg/mol, and they presumed that the reason for this tendency may involve polymer tacticity.[28, 35, 36] They hypothesised that the increasing steric bulk of the *N*-vinyl lactam probably leads to a more syndiotactic structure of the polymer when polymerised, and syndiotactic structures can maximise the polymer surface/volume ratio. It is the pendant amphiphilic groups of the polymer that interfere with the hydrate nucleation and crystal growth processes. Therefore, at a given concentration, maximising the surface area to volume ratio will make the best use of the polymer. However, this is not the case for polyethers, as there is no evidence for a change of tacticity. However, a large surface/volume ratio may enhance the KHI performance of a polymer. Thus, the polymer with the largest pendant ring groups performed the best. In addition, according to the adsorption mechanism reported by Yagasaki et al.,[37] the azepane ring could have the suitable size for the KHI polymer to stabilise at the hydrate surface, thus providing stronger adsorption affinity for preventing gas hydrates from further growth.

To see how the molecular weight affects the KHI performance of the PGAOs, the performance of a series of EGBE-PPiGAOs and EGBE-PAzGAOs with different degrees of polymerisation ranging from 10 to 49 was tested. The results of the PPiGAOs with varying monomer units, showed a trend that the larger the molecular weight, the worse KHI performance of the polymer. The same was observed for the PAzGAO series (Table 3 and Figure 6). This trend can be found in many of previously reported KHI series.[18, 38, 39] The PGAOs with the lowest molecular weight were on a par with PVCap regarding inhibition of sII gas hydrate formation.

However, when comparing the PGAOs with similar degree of polymerisation, the KHI performance of the EGBE-PAzGAOs with larger ring size were not always better than the EGBE-PPiGAOs. For example, EGBE-PPiGAO$_{10}$ and EGBE-PAzGAO$_{14}$ gave the same T_o (av.) value of 9.8 ^{o}C. To our surprise, EGBE-PPiGAO$_{49}$ and EGBE-PAzGAO$_{49}$ with higher molecular weights gave T_o *(av.)* values of 13.3 and 13.6 ^{o}C, respectively. The *P* value between the average T_o values of PPiGAO$_{49}$ and PAzGAO$_{49}$ is 0.001 calculated from a *t*-test, which means that the confidence of a significant difference between them is as high as 99.9%, i.e. the KHI performance of

$PPiGAO_{49}$ is statistically significantly better than that of $PAzGAO_{49}$.[43] A possible reason why, at high molecular weights, EGBE-$PAzGAO_{49}$ gave worse KHI performance than EGBE-$PPiGAO_{49}$ might be that there is more overlapping area for the larger azepane groups to curve the hydrate surface region, so the coverage area per monomer unit is reduced. Reduced coverage area renders weak adsorption effect, thus causing poor inhibition performance.[40]

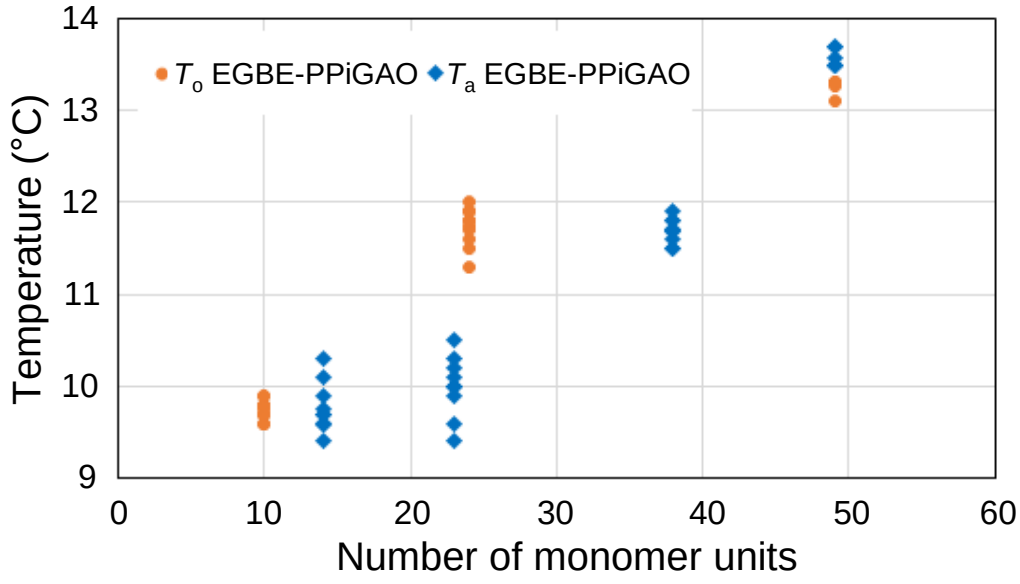

Figure 6: T_o values of EGBE-PPiGAO and EGBE-PAzGA with varying degrees of polymerisation.

At the concentration of 2500 ppm, none of the PGAOs showed a cloud point when heated up to 95 °C. To determine a possible cloud point, each polymer solution was slowly heated to 95 °C, and visual observations were made. No turbidity was observed at any stage of the heating process indicating no cloud point up to this temperature. The test was repeated for assurance of the result. In addition, no cloud point occurred for the two best PGAOs EGBE-$PPiGAO_{10}$ and EGBE-$PAzGAO_{14}$ in 15 wt% (150000 ppm) sodium chloride solution upon heating to 95 °C. Usually, the polymer with lower cloud point is expected to give better KHI performance,[26] and the amine polyethers without being oxidised are more hydrophobic than the corresponding PGAOs. Therefore, the KHI performance of three amine polyethers EGBE-$PPyrGA_9$, EGBE-$PAzGA_{14}$ and EGBE-$PAzGA_{23}$ were measured. All of them are very poor KHIs, which means that the amine is not a suitable functional group to inhibit gas hydrate formation.

The KHI performance of one of the best PGAOs EGBE-PAzGAO$_{23}$ was determined at varying concentrations. The results are summarised in Table 4 and Figure 7. Similar to many other KHI polymers with hydrogen-bonding functional groups,[27, 41, 42] the KHI performance of poly(azepane glycidyl amine *N*-oxide) increased dramatically with the concentration increasing.

Table 4: Summary of the KHI performance results of EGBE-PAzGAO$_{23}$ at different concentrations.

Name	Conc. (ppm)	T_o (av.) (°C)	ΔT (av.) at T_o (°C)	T_a (av.) (°C)	T_o (av.) − T_a (av.) (°C)
EGBE-PAzGAO$_{23}$	1000	12.3	8.0	11.7	0.6
	2500	10.0	10.2	9.2	0.8
	5000	7.9	12.3	6.6	1.3

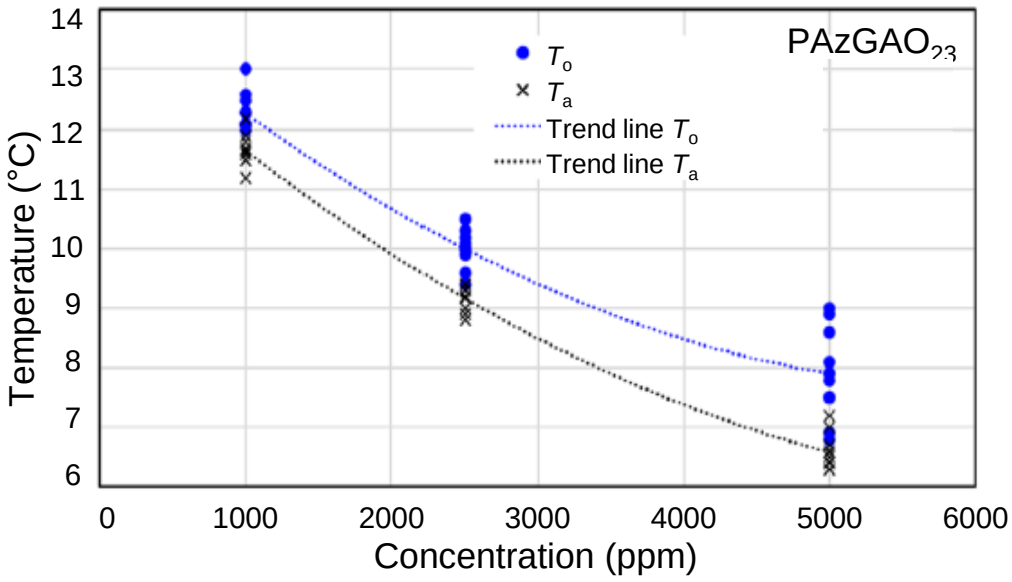

Figure 7: T_o and T_a values of EGBE-PAzGAO$_{23}$ at varying concentrations.

Conclusion

In this study we have synthesised and tested the KHI performance of a series of novel polyethers with cyclic amine side chains and oxidised these compounds to the corresponding amine N-oxides. Poly(pyrrolidine glycidyl amine *N*-oxide)s (PPyrGAO), poly(piperidine glycidyl amine *N*-oxide)s (PPiGAO) and poly(azepane glycidyl amine *N*-oxide)s (PAzGAO) with different molecular weights and degrees of polymerisation have been introduced. At a molecular weight (M_n value) of

approximately 2 kg/mol, translating to degrees of polymerisation (P_n) of 10 and 14, respectively, PPiGAO gave the same KHI performance as PAzGAO. When *Mn* increased to around 4 kg/mol (P_n of 20 to 24), the trend of the KHI performance of the glycidyl amine *N*-oxide polyethers can be summarised in this order: PPyrGAO < PPiGAO < PAzGAO. However, at a higher molecular weight $M_n \approx 8$ kg/mol (P_n of 49), PAzGAO with larger azepane ring groups resulted in slightly worse KHI performance in comparison to that of PPiGAO.

Within each poly(glycidyl amine *N*-oxide) series with the same monomer units, there is a clear trend, showing that the polymer with higher molecular weight gave worse KHI performance. With the concentration range from 1000 to 5000 ppm, the KHI performance was better, when the concentration of the polyether was increased.

Poly(pyrrolidine glycidyl amine)s (PPyrGA) and poly(azepane glycidyl amine)s (PAzGA) gave very poor KHI performance on sII gas hydrate, while their corresponding glycidyl amine *N*-oxide polyethers showed considerable performance as well as excellent compatibility with 15 wt.% NaCl brine solution. Thus, not only the ring size affects the inhibition effect, but also the proper functional groups are critical for KHI performance.

References

(1) Englezos, P., Clathrate hydrates. *Industrial & engineering chemistry research* **1993,** *32* (7), 1251-1274.
(2) Kvenvolden, K. A. J. R. o. g., Gas hydrates—geological perspective and global change. **1993,** *31* (2), 173-187.
(3) Sloan, E. D. Jr.; Koh, C. A., *Clathrate hydrates of natural gases. 3rd Ed.* CRC Press: Boca Raton, Florida, 2008.
(4) Jr, E. D. S., Fundamental principles and applications of natural gas hydrates. *Nature* **2003,** *426*.
(5) Sloan, E. D., A changing hydrate paradigm - from apprehension to avoidance to risk management. *Fluid Phase Equilib.* **2005,** *228*, 67-74.
(6) Sloan, E. D., Koh, C.; Sum, A. K., *Natural gas hydrates in flow assurance*. Gulf Professional Publishing: 2010.

(7) Creek, J. L., Efficient Hydrate Plug Prevention. *Energy & Fuels* **2012,** *26* (7), 4112-4116.

(8) Kelland, M. A., *Production Chemicals for the Oil and Gas Industry. 2nd Ed.* CRC Press: Boca Raton, Florida, **2014**; p 219-245.

(9) Kelland, M. A., History of the Development of Low Dosage Hydrate Inhibitors. *Energy & Fuels* **2006,** *20* (3), 825-847.

(10) Perrin, A.; Musa, O. M.; Steed, J. W., The chemistry of low dosage clathrate hydrate inhibitors. *Chem Soc Rev* **2013,** *42* (5), 1996-2015.

(11) Wang, Y.; Fan, S.; Lang, X., Reviews of gas hydrate inhibitors in gas-dominant pipelines and application of kinetic hydrate inhibitors in China. *Chinese Journal of Chemical Engineering* **2019,** *27* (9), 2118-2132.

(12) Kelland, M. A., A Review of Kinetic Hydrate Inhibitors from an Environmental Perspective. *Energy & Fuels* **2018,** *32* (12), 12001-12012.

(13) Reyes, F. T.; Malins, E. L.; Becer, C. R.; Kelland, M. A. J. E.; Fuels, Non-amide kinetic hydrate inhibitors: Performance of a series of polymers of isopropenyloxazoline on structure II gas hydrates. **2013,** *27* (6), 3154-3160.

(14) Magnusson, C. D.; Liu, D. J.; Chen, E. Y. X.; Kelland, M. A., Non-Amide Kinetic Hydrate Inhibitors: Investigation of the Performance of a Series of Poly(vinylphosphonate) Diesters. *Energy & Fuels* **2015,** *29* (4), 2336-2341.

(15) Lin, H.; Wolf, T.; Wurm, F. R.; Kelland, M. A., Poly(alkyl ethylene phosphonate)s: A New Class of Non-amide Kinetic Hydrate Inhibitor Polymers. *Energy & Fuels* **2017,** *31* (4), 3843-3848.

(16) Kelland, M. A.; Mady, M. F., Acylamide and Amine Oxide Derivatives of Linear and Hyperbranched Polyethylenimines. Part 1: Comparison of Tetrahydrofuran Hydrate Crystal Growth Inhibition Performance. *Energy & Fuels* **2016,** *30* (5), 3934-3940.

(17) Kelland, M. A.; Magnusson, C.; Lin, H.; Abrahamsen, E.; Mady, M. F., Acylamide and Amine Oxide Derivatives of Linear and Hyperbranched Polyethylenimine. Part 2: Comparison of Gas Kinetic Hydrate Inhibition Performance. *Energy & Fuels* **2016,** *30* (7), 5665-5671.

(18) Magnusson, C. D.; Kelland, M. A., Nonpolymeric Kinetic Hydrate Inhibitors: Alkylated Ethyleneamine Oxides. *Energy & Fuels* **2015,** *29* (10), 6347-6354.

(19) Zhang, Q.; Kelland, M. A.; Ajiro, H., Polyvinylsulfonamides as Kinetic Hydrate Inhibitors. *Energy & Fuels* **2020,** *34* (2), 2230-2237.

(20) Kelland, M. A.; Dirdal, E. G.; Zhang, Q., High Cloud Point Polyvinylaminals as Non-Amide-Based Kinetic Gas Hydrate Inhibitors. *Energy & Fuels* **2020,** *34* (7), 8301-8307.

(21) Zhang, Q.; Kelland, M. A.; Lewoczko, E. M.; Bohannon, C. A.; Zhao, B., Non-amide based zwitterionic poly (sulfobetaine methacrylate) s as kinetic hydrate inhibitors. *Chemical Engineering Science* **2021,** *229*, 116031-116037.

(22) Zhang, Q.; Kelland, M. A., Kinetic inhibition performance of alkylated polyamine oxides on structure I methane hydrate. *Chemical Engineering Science* **2020,** *220*.

(23) Zhang, Q.; Kelland, M. A.; Frey, H.; Blankenburg, J.; Limmer, L., Amine N-Oxide Kinetic Hydrate Inhibitor Polymers for High-Salinity Applications. *Energy & Fuels* **2020**, 34, 6298-6305.

(24) Zhang, Q.; Shen, X.; Zhou, X.; Liang, D., Inhibition Effect Study of Carboxyl-Terminated Polyvinyl Caprolactam on Methane Hydrate Formation. *Energy & Fuels* **2017,** *31* (1), 839-846.

(25) Zhang, Q.; Kelland, M. A., Study of the Kinetic Hydrate Inhibitor Performance of Poly(N-vinylcaprolactam) and poly(N-isopropylmethacrylamide) with Varying End Caps. *Energy & Fuels* **2018,** *32* (9), 9211-9219.

(26) Dirdal, E. G.; Kelland, M. A., Does the Cloud Point Temperature of a Polymer Correlate with Its Kinetic Hydrate Inhibitor Performance? *Energy & Fuels* **2019,** *33* (8), 7127-7137.

(27) Zhang, Q.; Heyns, I. M.; Pfukwa, R.; Klumperman, B.; Kelland, M. A., Improving the Kinetic Hydrate Inhibition Performance of 3-Methylene-2-pyrrolidone Polymers by N-Alkylation, Ring Expansion, and Copolymerization. *Energy & Fuels* **2018,** *32* (12), 12337-12344.

(28) Chua, P. C.; Kelland, M. A., Poly(N-vinyl azacyclooctanone): A More Powerful Structure II Kinetic Hydrate Inhibitor than Poly(N-vinyl caprolactam). *Energy & Fuels* **2012,** *26* (7), 4481-4485.

(29) Blankenburg, J.; Stark, M.; Frey, H. Oxidation-responsive polyether block copolymers lead to non-ionic polymer surfactants with multiple amine N-oxides. *Polym. Chem.* **2019**, *10*, 1569–1574.

(30) Chua, P. C.; Kelland, M. A., Tetra(iso-hexyl)ammonium Bromide-The Most Powerful Quaternary Ammonium-Based Tetrahydrofuran Crystal Growth Inhibitor and Synergist with Polyvinylcaprolactam Kinetic Gas Hydrate Inhibitor. *Energy & Fuels* **2012,** *26* (2), 1160-1168.

(31) Mady, M. F.; Kelland, M. A., N,N-Dimethylhydrazidoacrylamides. Part 2: High-Cloud-Point Kinetic Hydrate Inhibitor Copolymers with N-Vinylcaprolactam and Effect of pH on Performance. *Energy & Fuels* **2015,** *29* (2), 678-685.

(32) Mandalapu, D.; Lal, N.; Kumar, L.;Kushwaha, B.; Gupta, S.; Kumar, L.; Bala,V.; Yadav, S. K.; Singh, P.; Singh,N.; Maikhuri, J P.; Sankhwar, S. N.; Shukla, P. K.; Siddiqi, I.; Gupta, G.; Sharma, V. L. Innovative Disulfide Esters of Dithiocarbamic Acid as Women-Controlled Contraceptive Microbicides: A Bioisosterism Approach. *ChemMedChem* **2015**, *10*, 1739-1753.

(33) Isono, T.; Asai, S.; Satoh, Y.; Takaoka, T.; Tajima, K.; Kakuchi, T.; Satoh, T. Controlled/Living Ring-Opening Polymerization of Glycidylamine Derivatives Using t-Bu-P_4/Alcohol Initiating System Leading to Polyethers with Pendant Primary, Secondary, and Tertiary Amino Groups. *Macromolecules*, **2015**, *48*, 3217–3229.

(34) Blankenburg, J.; Wagner, M.; Frey, H. Well-Defined Multi-Amino-Functional and Stimuli-Responsive Poly(propylene oxide) by Crown Ether Assisted Anionic Ring-Opening Polymerization. *Macromolecules* **2017**, *50*, 8885–8893.

(35) Chua, P. C.; Kelland, M. A.; Hirano, T.; Yamamoto, H., Kinetic Hydrate Inhibition of Poly(N-isopropylacrylamide)s with Different Tacticities. *Energy & Fuels* **2012,** *26* (8), 4961-4967.

(36) Del Villano, L.; Kelland, M. A.; Miyake, G. M.; Chen, E. Y. X., Effect of Polymer Tacticity on the Performance of Poly(N,N-dialkylacrylamide)s as Kinetic Hydrate Inhibitors. *Energy & Fuels* **2010,** *24* (4), 2554-2562.

(37) Yagasaki, T.; Matsumoto, M.; Tanaka, H., Adsorption Mechanism of Inhibitor and Guest Molecules on the Surface of Gas Hydrates. *J Am Chem Soc* **2015,** *137* (37), 12079-85.

(38) Seo, S. D.; Paik, H. J.; Lim, D. H.; Lee, J. D., Effects of Poly(N-vinylcaprolactam) Molecular Weight and Molecular Weight Distribution on Methane Hydrate Formation. *Energy & Fuels* **2017,** *31* (6), 6358-6363.

(39) Chua, P. C.; Kelland, M. A.; Ajiro, H.; Sugihara, F.; Akashi, M., Poly(vinylalkanamide)s as Kinetic Hydrate Inhibitors: Comparison of Poly(N-vinylisobutyramide) with Poly(N-isopropylacrylamide). *Energy & Fuels* **2013,** *27* (1), 183-188.

(40) Yagasaki, T.; Matsumoto, M.; Tanaka, H., Molecular Dynamics Study of Kinetic Hydrate Inhibitors: The Optimal Inhibitor Size and Effect of Guest Species. *The Journal of Physical Chemistry C* **2018,** *123* (3), 1806-1816.

(41) Abrahamsen, E.; Kelland, M. A., Carbamate Polymers as Kinetic Hydrate Inhibitors. *Energy & Fuels* **2016,** *30* (10), 8134-8140.

(42) Reyes, F. T.; Guo, L.; Hedgepeth, J. W.; Zhang, D.; Kelland, M. A., First Investigation of the Kinetic Hydrate Inhibitor Performance of Poly(N-alkylglycine)s. *Energy & Fuels* **2014,** *28* (11), 6889-6896.

(43) Walpole, R. E. Probability & Statistics for Engineers & Scientists, 9th ed.; Pearson: Boston, MA, 2012.

Supporting Information

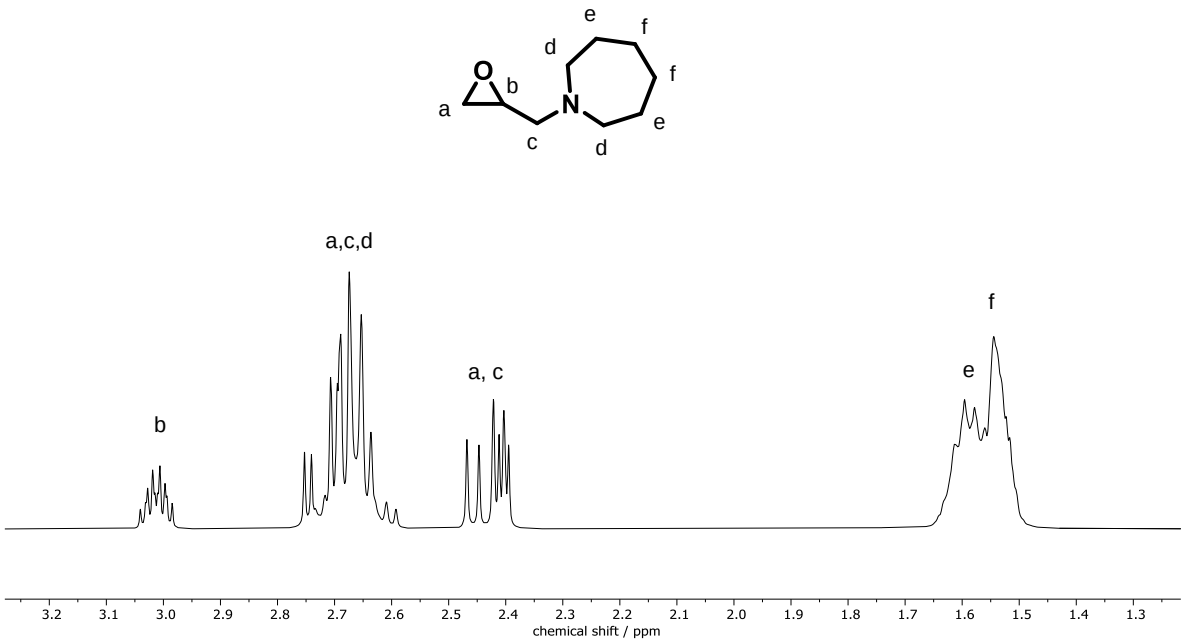

Figure S1: ^{1}H NMR spectrum (300 MHz, CDCl3) of AzGA monomer.

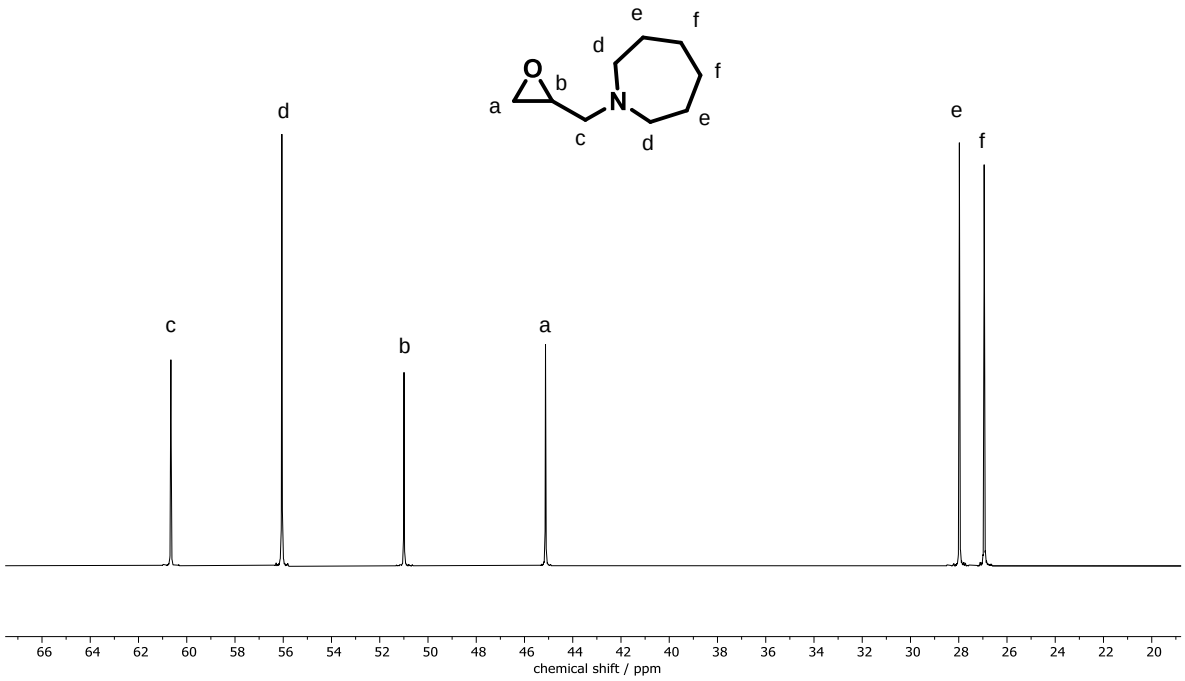

Figure S2: ^{13}C NMR spectrum (75 MHz, CDCl3) of AzGA monomer.

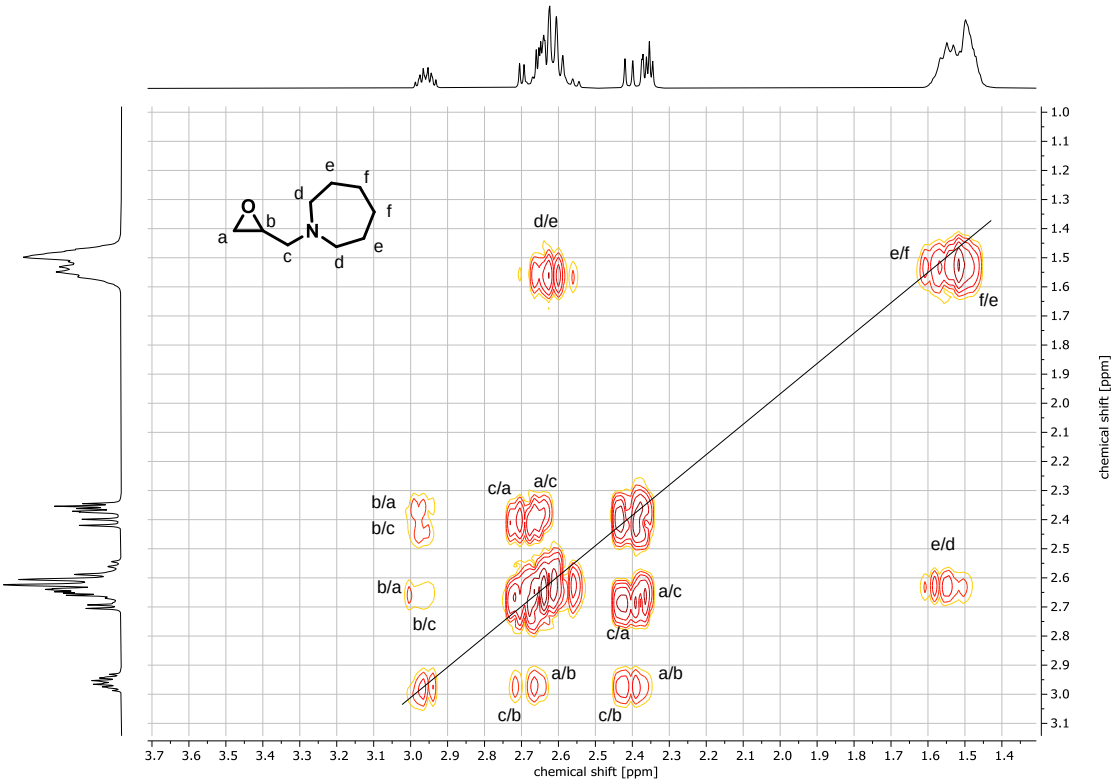

Figure S3: ^{1}H 1H COSY NMR spectrum (300 MHz, CDCl3) of AzGA monomer.

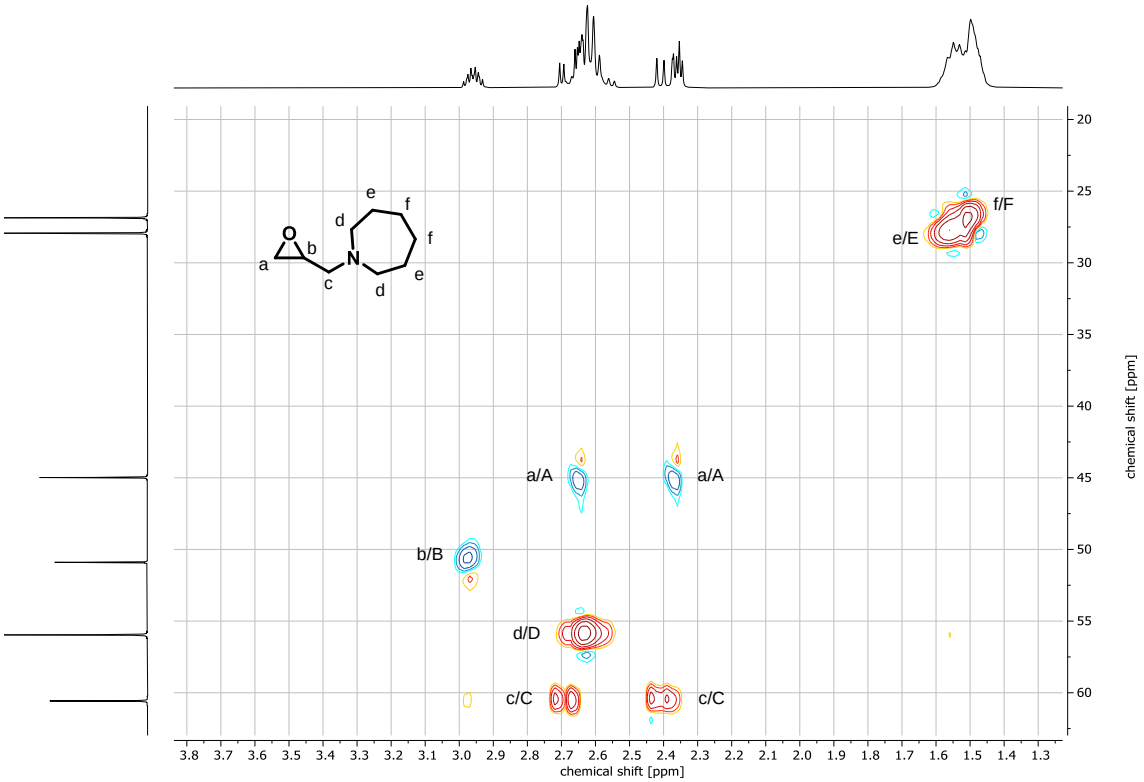

Figure S4: ^{1}H 13C HSQC NMR spectrum (CDCl3) of AzGA monomer.

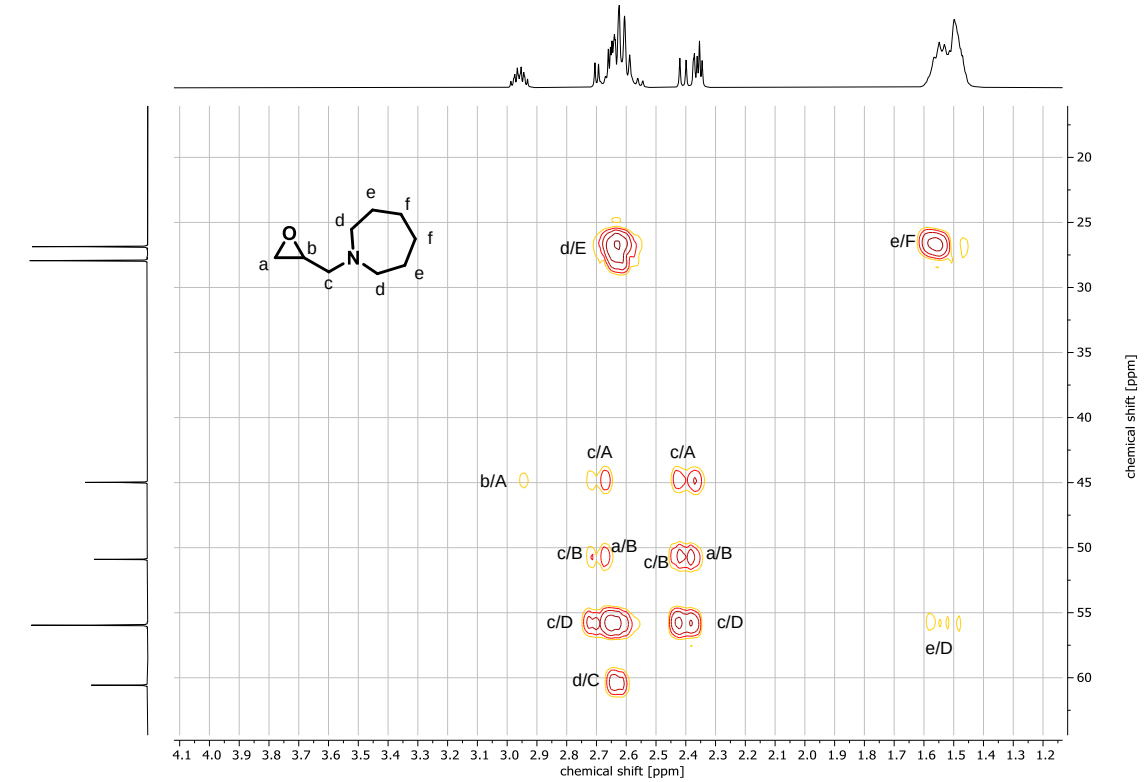

Figure S5: ^{1}H 13C HMBC NMR spectrum (CDCl3) of AzGA monomer.

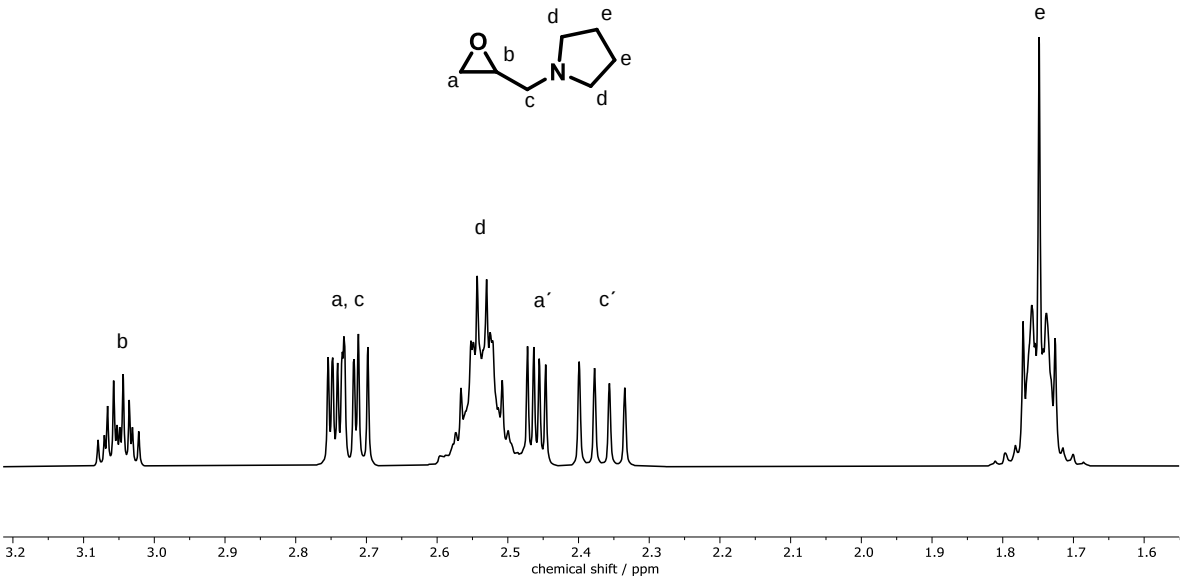

Figure S6: [1]H NMR spectrum (300 MHz, CDCl3) of PyrGA monomer.

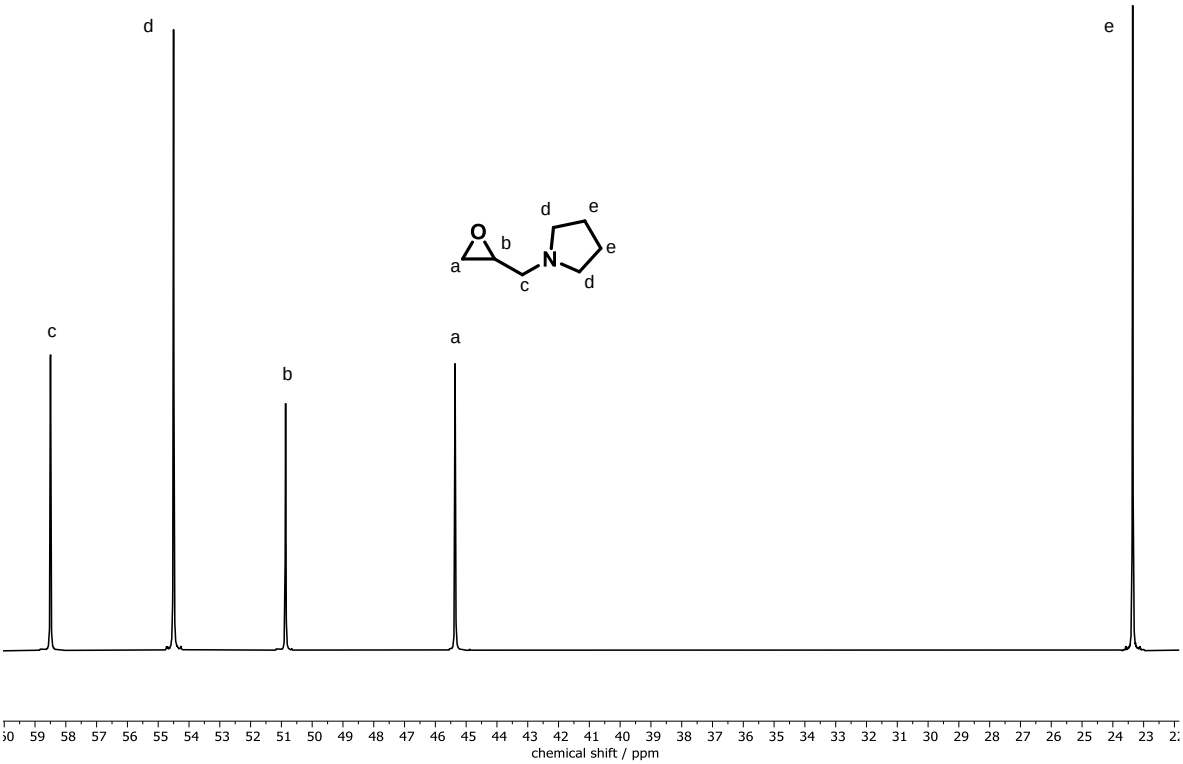

Figure S7: [13]C NMR spectrum (75 MHz, CDCl3) of PyrGA monomer.

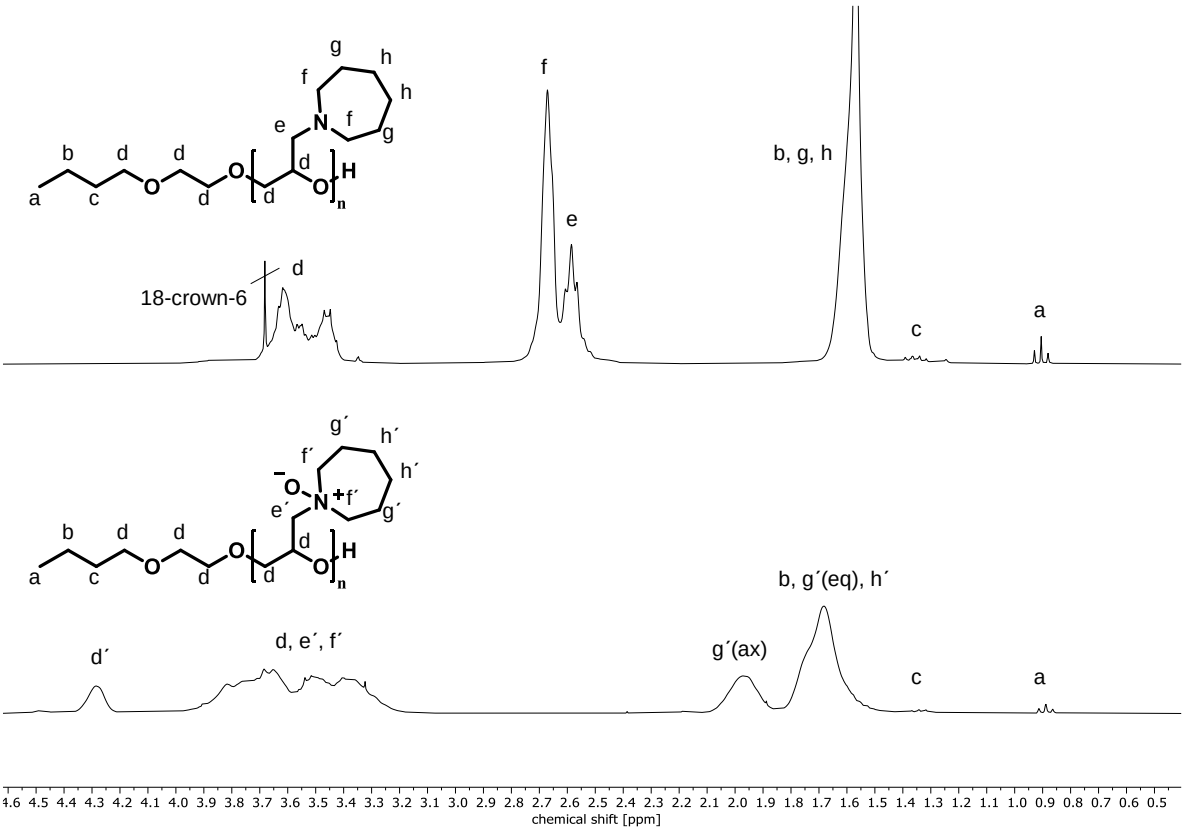

Figure S8: ^{1}H NMR spectra (300 MHz) of PAzGA$_{38}$ in CDCl$_3$ (top) and PAzGAO$_{38}$ in D$_2$O (bottom).

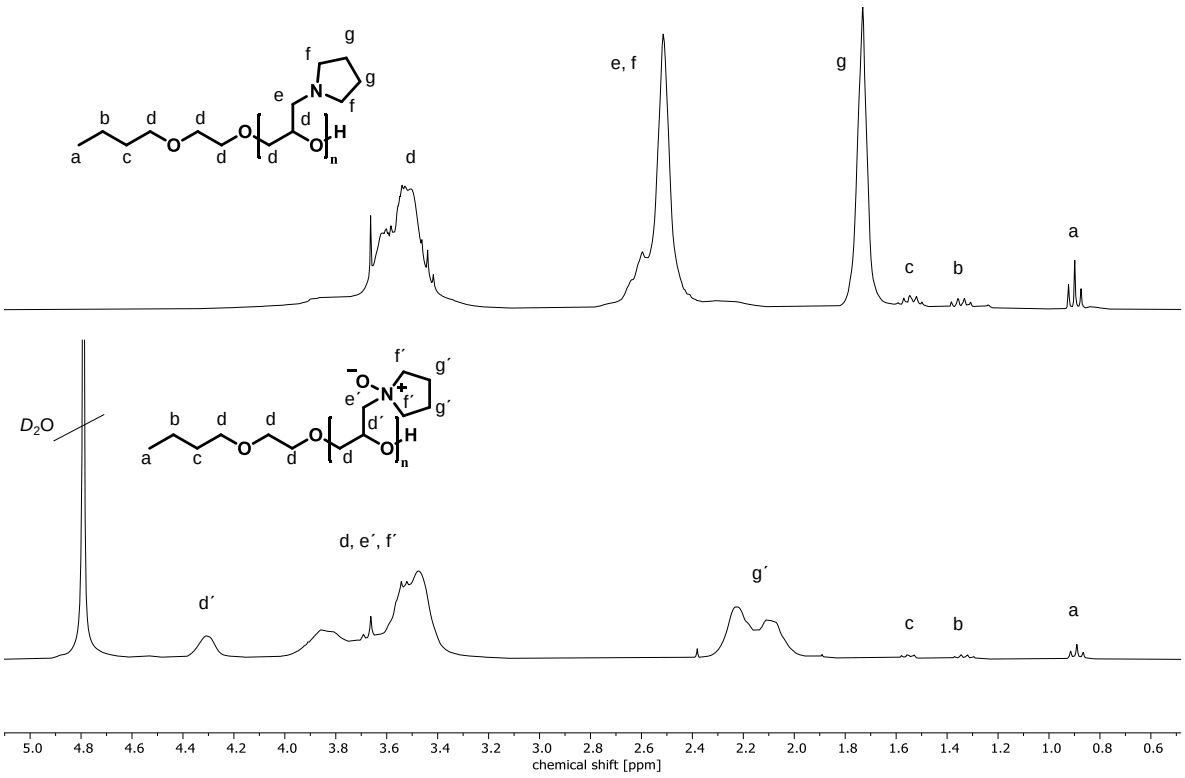

Figure S9: ^{1}H NMR spectra (300 MHz) of PPyrGA$_{18}$ in CDCl$_3$ (top) and PPyrGAO$_{18}$ in D$_2$O (bottom).

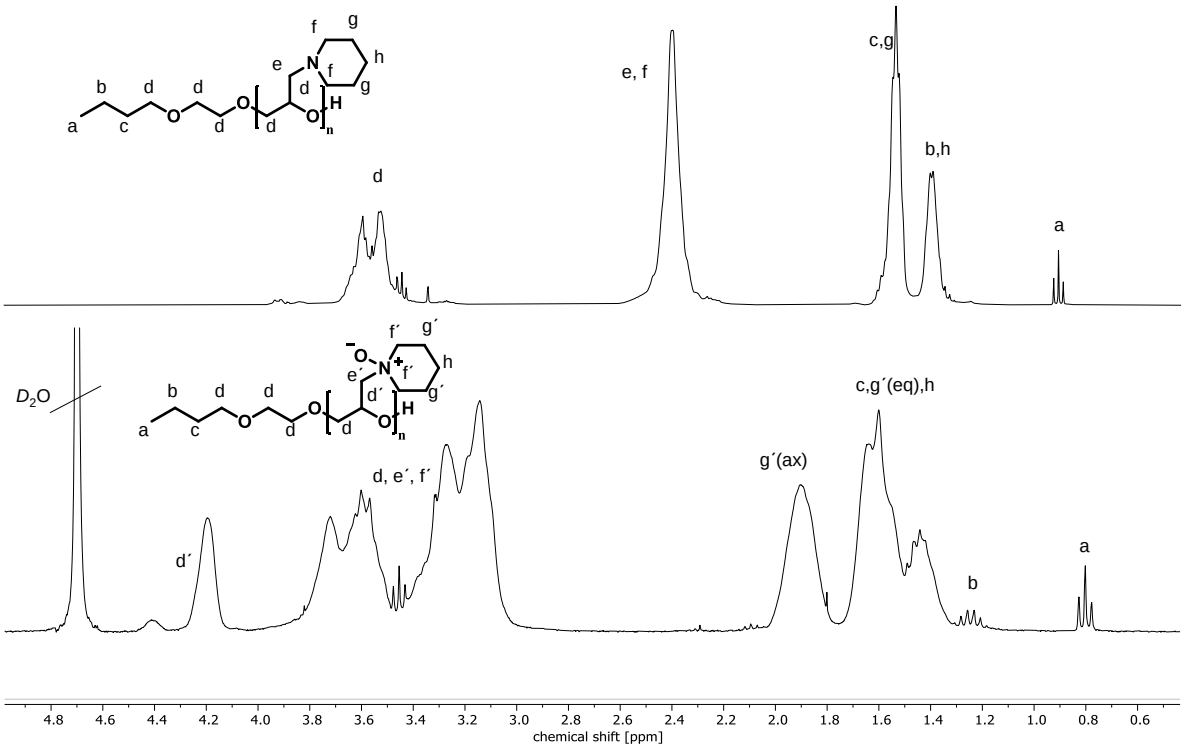

Figure S10: ^{1}H NMR spectra (300 MHz) of $PPiGA_{24}$ in $CDCl_3$ (top) and $PPiGAO_{24}$ in D_2O (bottom).

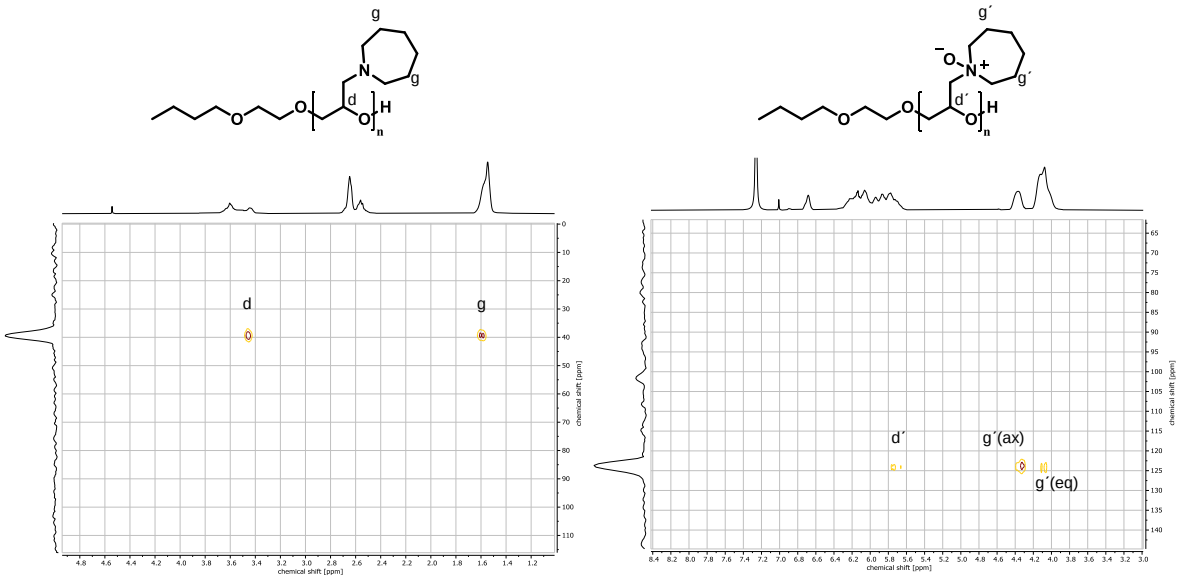

Figure S11: ^{1}H, ^{15}N HMBC NMR spectra ($CDCl_3$) of $PAzGA_{18}$ (left) and $PAzGAO_{18}$ (right).

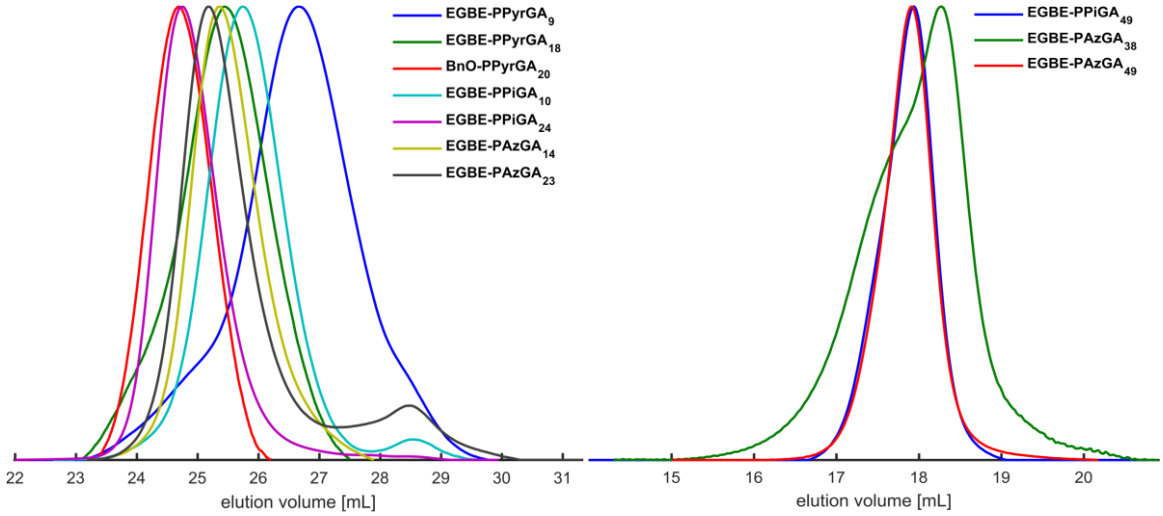

Figure S12: SEC traces of the synthesised polymers (RI signal). Left: DMF, PEG calibration. Right: Polymers with higher molecular weight were insoluble in DMF: HFIP, PMMA calibration.

3 – Fluorine bearing polyethers

3.1 Surface Active Polyethers with Degradable Fluorinated Side Chains

Larissa Limmer,[a] Tom Reimers,[a] Gregor M. Linden,[a] Johannes Liermann,[a] Reiner Friedrich,[b] Holger Frey*,[a]

[a] Johannes Gutenberg-Universität Mainz, Department of Chemistry, Duesbergweg 10 - 14, 55128 Mainz, Germany

[b] Merck KGaA, Frankfurter Straße 250, 64293 Darmstadt, Germany

To be submitted, patent pending

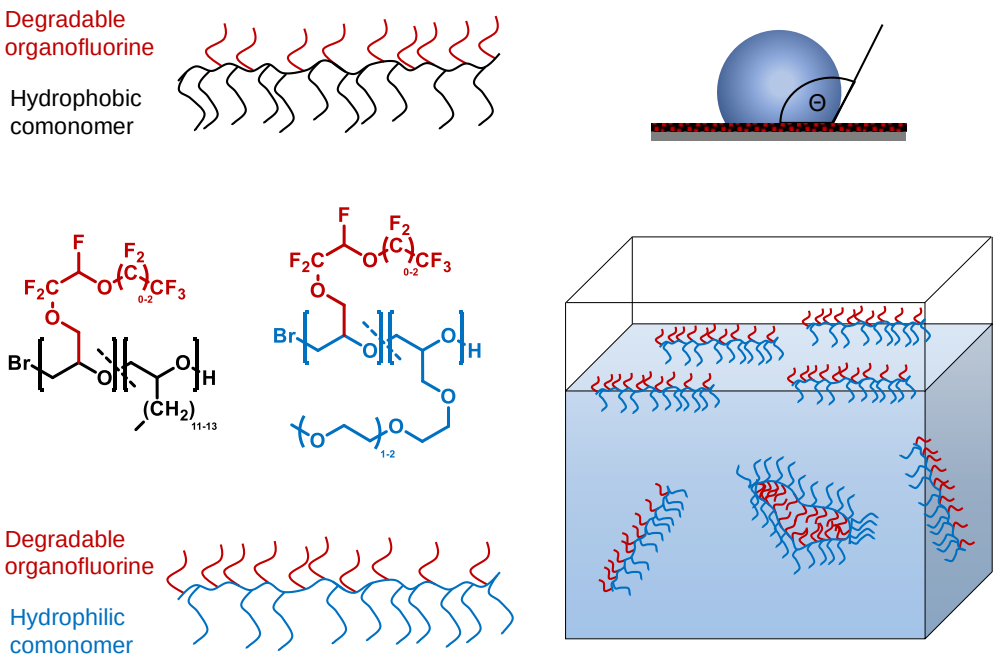

Contributions

L.L. – Concept; performance and evaluation of experiments; writing of manuscript. T.R. – performance and evaluation of experiments. G.L. – Support for NMR experiments and evaluation. J.L. – Support for NMR measurements. R.F. – Concept; performance and evaluation of experiments. H.F. – Concept; supervision; editing.

Abstract

Per- and polyfluorinated substances are highly established compounds as antistick coatings, for textile modification or as surfactants, but have evoked ecological and health concerns and are increasingly restricted by governments. In the search for alternatives, perfluoropropyl vinyl ether is a promising building block with improved ecological profile regarding degradation and accumulation. Synthesis and surface properties of polyethers bearing comonomers with side chains derived from perfluoropropyl vinyl ether or perfluoromethyl vinyl ether are described. Amphiphilic copolymers with 2-(2-methoxyethoxy)ethylglycidylether, 2-[2-(2-methoxyethoxy)-ethoxy]ethylglycidylether or ethylene oxide (3–56 mol% of fluorinated monomer) as well as copolymers with 1,2-epoxytretradecane or 1,2-epoxyhexadecane and allyl glycidyl ether as a functional comonomer (17–65 mol% of fluorinated monomer) were synthesised. *In situ* ^{1}H NMR kinetic studies indicated random polymer microstructures with slight gradients. Surfactant properties of the best performing amphiphilic copolymers ($\gamma_{stat} \geq 20.35$ mN m^{-1}) were on par or even outperformed perfluorooctanesulfonic acid and recently developed degradable fluorosurfactants. The copolymers bearing hydrophobic comonomers did not lead to high water and oil-repellency simultaneously. Depending on molecular weight and comonomer ratios either hydrophobicity (contact angle on cellulose ≤ 115°; on glass ≤ 96°) or oleophobicity (grade 0.5; homopolymer: ≤ 3.5) was achieved.

Introduction

Organofluorines are used all around us in a multitude of applications as antistick coatings e.g. in the automobile industry[1], water- and dirt-repellent coatings for outdoor clothing[2] or as surfactants[3] and stabilizers in paints[4] and firefighting foams.[5] Fluorosurfactants used as stabilizers and emulsifiers in organic reactions can make it possible to omit organic solvents[6] and enable emulsion polymerisations.[7] All these uses have their origin in the low polarizability of fluorine, which leads to low interactions with aqueous as well as organic surroundings.[8] Fluorosurfactants are typically more efficient than their hydrocarbon homologues. They show lower surface tensions (≥10 mN m^{-1}, commercially available typically ≥15 mN m^{-1} vs. hydrocarbons ≥24 mN m^{-1})[5,9] and critical micelle concentrations (cmc) due to their increased stiffness, surface area and decreased interactions.[3,6] As a consequence of the strong carbon-fluorine bond the compounds furthermore exhibit excellent thermal and chemical stability.[5,10] While this may be desirable and targeted for some applications, their persistency has become an ecological problem. Highly persistent per- and polyfluorinated substances (PFAS) have been found all over the world[11,12] and accumulate in the food chain,[13] with a percentage of PFAS showing toxicity.[14,15] A majority of the used PFAS were based on the nowadays restricted perfluorooctanoic acid (PFOA) or perfluorooctanesulfonic acid (PFOS)[16–18], which motivates an intense search for less persistent alternatives.[5,19] Because of their exceptional properties, it is challenging to identify non-fluorinated alternatives with similar profile, and in consequence degradable and non-toxic PFAS are in the focus of current studies.[5,19] Two strategies have been introduced for fluorinated alternatives: small-chain PFAS and long-chain PFAS with an incorporated ether linkage as a breaking point. Small-chain PFAS show reduced bioaccumulation,[20,21] but are still persistent in the environment.[22] Long-chain ether-bearing PFAS are degradable to small-chain PFAS, albeit using highly energy-consuming processes like ultrasonication with strong oxidants[23] or treatment with oxygen in subcritical water at 350 °C.[24] The combination of an ether linkage with a neighbouring carbon-hydrogen bond increased the reactivity further,[25] enabling degradation under environmental conditions for perfluoropropyl vinyl ether (PPVE) derivatives. Joudan *et al*. found this compound to undergo degradation in the atmosphere as well as in activated sludge to perfluoropropionic acid (PFPrA).[26,27] Folkerson *et al*. observed renal excretion of PFPrA as the terminal product of rat metabolism.[28] PPVE and perfluoromethyl vinyl

ether (PMVE) derived epoxides 2-((1,1,2-trifluoro-2-(perfluoropropoxy)-ethoxy)methyl)oxirane (PPVEGLY) and 2-((1,1,2-trifluoro-2-(trifluoromethoxy)-ethoxy)methyl)oxirane (PMVEGLY) (Figure 1) have recently been developed as a degradable and ecological friendlier alternative for classic building blocks,[29] due to the -O-CHF-CF_2- motive as an initial point for degradation.[26–28]

Long-chain PFAS, particularly C_8-based structures, generally show superior performance in both surfactant and surface treatment applications compared to their short-chain homologues.[30] Incorporating short-chain fluorinated units in a polymer provides efficient means to increase the overall fluorine content per molecule while leaving the degradability of each individual unit essentially unaltered. Consequently, Kredel and Gallei investigated polyacrylate copolymers bearing a PPVE derived comonomer in textile coatings.[31]

In this work we aim at exploring, whether short-chain PFAS, bearing the -O-CHF- degradation bond, are able to compete with long-chain PFAS, when incorporated in a polymer multiple times, potentially leading to a synergistic effect.

Series of copolymers composed of PPVEGLY or PMVEGLY and either hydrophilic or hydrophobic comonomers were synthesised. To study the surface properties in aqueous media hydrophilic oligoethylene glycol monomethyl ether bearing epoxide comonomers were chosen. We expected the long hydrophilic side chains to be highly immiscible with the fluorinated side chains, leading to a hydrophilicity gradient. Furthermore, we synthesised copolymers by combining the fluorinated epoxide monomers with ethylene oxide as the hydrophilic component as a more established approach for surfactants. Aiming at application as surface coating, comonomers with hydrophobic alkylene side chains were incorporated in the polyethers. High alkane homologues are suitable for water-repellent applications, but are oleophilic.[9] In consequence, alkylene oxides were used to boost water-repellency and a copolymer series with different monomer ratios was prepared. Functional comonomers bearing allyl or methacrylate groups were used in terpolymerisations to incorporate an anchor group, e.g. for future textile modification. The synthesised polymers were used to coat cellulose as well as glass slides and investigated for their water- and oil-repellency. *In situ* ^{1}H NMR kinetic studies were performed to determine the polymers microstructure, which has a key impact on the surface properties.

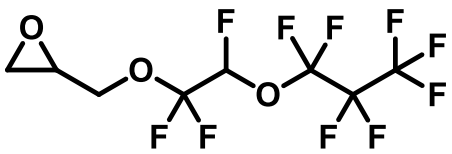

PPVEGLY

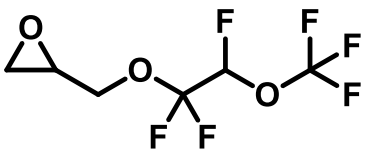

PMVEGLY

Figure 1: Structures of the studied polyfluorinated monomers PPVEGLY and PMVEGLY.

Experimental Section

Monomer synthesis

The synthesis of fluorinated monomers was conducted in a modified literature procedure.[29] An exemplary synthesis of PMVEGLY is given here. A 300 mL dried pressure-reactor was evacuated and flushed with argon three times. Potassium carbonate (0.3 eq, 2.77), dioxane (5 eq, 28,7 mL), and glycidol (1 eq, 4.97 g), which was previously distilled over calcium hydride, were added. The reactor was closed and evacuated. Gaseous PMVE was added until a pressure of 4.8 bar was established. The reaction mixture was stirred for 16 h at 110 °C and cooled to room temperature. The reactor was opened to release the excess PMVE into a slurry of calcium chloride (0.75 M) and potassium hydroxide (0.5 M). The in the reactor remaining mixture was inertisied with nitrogen. 30 mL of water and of methyl *tert*-butyl ether each was added, and the phases separated. The organic phase was washed twice with water and once with brine and subsequently dried over sodium sulfate. The solvent was removed under reduced pressure and the product isolated via fractional distillation as a colourless liquid and typical yields of 60-70% (7 mbar, T_{head} = 25 °C).

PMVEGLY:

^{1}H NMR (300 MHz, C*D*Cl$_3$) δ [ppm] = 5.78 (m, 1H, C*H*F), 4.20 (dd, J = 11.6, 3.4 Hz, 1H, C*H*$_2$-O), 3.92 (ddd, J = 11.6, 6.0, 0.8 Hz, 1H, C*H*$_2$-O), 3.24 (dq, J = 6.4, 3.3 Hz, 1H, O-C*H*), 2.88 (dd, J = 6.4, 3.3 Hz, 1H, O-CH-C*H*$_2$), 2.67 (dd, J = 4.8, 2.6 Hz, 1H, O-CH-C*H*$_2$).

^{13}C NMR, (75 MHz, C*D*Cl$_3$): 125.98–113.64 (*C*F$_3$ and *C*F$_2$), 100.99–96.63 (*C*HF), 65.53 (*C*H$_2$-O), 49.01 (O-CH-*C*H$_2$), 44.34 (O-CH-*C*H$_2$).

^{19}F-NMR (282 MHz, C*D*Cl3): -59.76 (dd, C*F*$_3$), -88.61– -90.31 (m, C*F*$_2$), -144.95 (dtt, C*F*).

PPVEGLY:

^{1}H NMR (300 MHz, C*D*Cl$_3$) δ [ppm] = 6.00–5.81 (m, C*H*F), 4.18 (dd, J = 11.6, 3.4 Hz, 1H, C*H*$_2$-O), 3.92 (ddd, J = 11.6, 6.0, 2.0 Hz, 1H, C*H*$_2$-O), 3.21 (dtd, J = 6.1, 4.0, 2.5 Hz, 1H, O-C*H*), 2.87 (dd, J = 4.8, 4.1 Hz, 1H, O-CH-C*H*$_2$), 2.65 (ddd, J = 4.8, 2.6, 1.0 Hz, 1H, O-CH-C*H*$_2$).

^{13}C NMR, (75 MHz, C*D*Cl$_3$): 121.16–115.18 (*C*F$_3$ and *C*F$_2$), 99.90–95.6 (*C*HF), 65.45 (*C*H$_2$-O), 48.99 (O-CH-*C*H$_2$), 44.32 (O-CH-*C*H$_2$).

^{19}F-NMR (282 MHz, C*D*Cl3): -81.70 (t, C*F*$_3$), -84.84– -87.57 (m, O-C*F*$_2$-CF$_2$), -89.92 – -90.08 (m, O-C*F*$_2$-CFH), -130.08 (q, C*F*$_2$-CF$_3$), -144.52– -144.84 (m, CH*F*).

The synthesis of ME$_3$GE and ME$_2$GE was adapted from literature[32] and is described in the supplementary information.

Polymer synthesis

All polymers were synthesised using the monomer-activated ring-opening polymerisation. An exemplary statistical copolymerisation of PPVEGLY and Me$_3$GE is given in the following. Tetrabutylammonium bromide (TBAB, 1 eq, 0.15 g) in 6 mL benzene was added to a dried Schlenk flask and dried under reduced pressure for 16 h. All additions were done via syringe. TBAB was suspended in 4 mL 2-methyltetrahydrofurane (2MeTHF) and the flask was filled with argon. The monomers PPVEGLY (4 eq, 0.63 g) and Me$_3$GE (12 eq, 1.23 g) were added and the flask was cooled to -30 °C using an ethanol-nitrogen bath. Triisobutylaluminum (1.1 M in toluene, 2 eq, 0.85 mL) was added. After 2-16 h of stirring the polymerisation was terminated by addition of 1 mL of methanol. The polymer was isolated in the organic phase by liquid-liquid extraction using DCM and water and subsequent drying (quantitative yields). Copolymerisations with glycidyl methacrylate were performed in toluene at 0 °C and under exclusion of light to prevent crosslinking reactions.

Block copolymers were synthesised using a deprotonated mPEG-macroinitiator. mPEG 5000 (1 eq, 0.28 mmol,1.5 g) and KO^{t}Bu (0.9 eq, 0.25 mmol, 28 mg) or

tetrabutylammonium chloride (0.9 eq, 2.5 mmol, 69 mg) were dissolved in 1 mL methanol and 12 mL benzene and stirred for 3 h at 60 °C. The solvents were removed, and the polymerisation was carried out in analog to the statistical copolymerisations for at least 2 d.

^{1}H-NMR (400 MHz, C*D*Cl$_3$):

P(ME$_3$GE-*co*-PMVEGLY) δ [ppm] = 5.85–5.70 (m, C*H*F), 4.25–3.86 (m, C*H*$_2$-O-CF$_2$), 3.86–3.42 (m, backbone and oligoethylene), 3.38 (s, C*H*$_3$).

P(ME$_2$GE-*co*-PMVEGLY) δ [ppm] = 5.82–5.68 (m, C*H*F), 4.19–3.90 (m, C*H*$_2$-O-CF$_2$), 3.83–3.55 (m, backbone and oligoethylene), 3.36 (s, C*H*$_3$).

^{1}H-NMR (300 MHz, C*D*Cl$_3$):

P(ME$_3$GE-*co*-PPVEGLY) δ [ppm] = 6.04–5.86 (m, C*H*F), 4.23–3.98 (m, C*H*$_2$-O-CF$_2$), 3.87–3.47 (m, backbone and oligoethylene), 3.37 (s, C*H*$_3$).

P(EO-*co*-PPVEGLY) δ [ppm] = 5.99–5.77 (m, C*H*F), 4.13–4.00 (m, C*H*$_2$-O-CF$_2$), 3.83–3.35 (m, backbone).

P(ETD-*co*-PPVEGLY) δ [ppm] = 5.95–5.77 (m, C*H*F), 4.12–3.97 (m, C*H*$_2$-O-CF$_2$), 3.63–3.34 (m, backbone), 1.47–1.25 (m, C*H*$_2$), 0.87 (t, C*H*$_3$).

P(EHD-*co*-PMVEGLY) δ [ppm] = 5.81–5.63 (m, C*H*F), 4.13–3.99 (m, C*H*$_2$-O-CF$_2$), 3.61–3.34 (m, backbone), 1.57–1.17 (m, C*H*$_2$), 0.87 (t, C*H*$_3$).

P(EHD-*co*-PPVEGLY) δ [ppm] = 5.95–5.77 (m, C*H*F), 4.12–3.99 (m, C*H*$_2$-O-CF$_2$), 3.59–3.34 (m, backbone), 1.57–1.25 (m, C*H*$_2$), 0.88 (t, C*H*$_3$).

P(EHD-*co*-PMVEGLY-*co*-AGE) δ [ppm] = 5.81–5.63 (m, C*H*F, C*H*=CH$_2$), 5.28–5.13 (m, CH=C*H*$_2$), 4.12–3.98 (m, C*H*$_2$-O-CF$_2$), 3.63–3.34 (m, backbone), 1.57–1.25 (m, C*H*$_2$), 0.87 (t, C*H*$_3$).

P(EHD-*co*-PPVEGLY-*co*-AGE) δ [ppm] = 5.93–5.80 (m, C*H*F, C*H*=CH$_2$), 5.30–5.13 (m, CH=C*H*$_2$), 4.13–3.98 (m, C*H*$_2$-O-CF$_2$), 3.75–3.34 (m, backbone), 1.57–1.18 (m, C*H*$_2$), 0.88 (t, C*H*$_3$).

^{1}H NMR kinetic studies

An exemplarily setup is described in the following. TBAB (10 eq, 0.11 mmol, 34 mg) in 3 mL benzene was added to a Schlenk flask and dried under reduced pressure.

All following steps were carried out under argon atmosphere or vacuum using the Schlenk technique. Subsequently, TBAB was dissolved in 1 mL dry benzene, of which 0.1 mL (1 eq) were added to a dried Norell S-5-400 NMR tube equipped with a flame-sealed acetone-D_6 capillary. Benzene was removed under reduced pressure and TBAB dissolved in a dry solvent (2-methyltetrahydrofurane (2-MeTHF) or THF) and TIBAL (1.1 M in toluene, for polymerisation in 2-MeTHF: 2 eq, 0.02 mL; in THF: 19 eq, 0.18 mL). The tube was shaken to homogenise the solution, cooled to -80 °C to prevent initiation and the monomers ME_3GE (24 eq, 0.25 mmol, 55.8 mg) and PPVEGLY (12 eq, 0.13 mmol, 43 mg) were added. The NMR tube was sealed by a Teflon stop-cock and the mixture was only allowed to thaw immediately before the measurement was conducted. The tube was shaken beforehand to ensure homogeneity. The measurement was performed at 10 °C for 6 h. Sample spinning was turned off. If the system was not able to lock on acetone-D_6, lock was turned off and shimming was performed using the solvents signal. Spectra were recorded every 30 s.

Static surface tension

The static surface tensions were measured using the Wilhelmy plate method (DIN EN 14370) on a model DCAT 11 tensiometer from dataphysics, Filderstadt Germany. 0.1 wt% aqueous solutions were measured at 20 ± 0.2 °C using a 19.9 mm platin plate. Full wetting was ensured to eliminate the contact angle from the equation used for calculations: $\gamma_{stat} = F \cos\theta \; L^{-1} = F \; L^{-1}$ (γ = tension, F = tension force, Θ = contact angle, L = wetted plate length).

Dynamic surface tension

The bubble pressure method was used to determine the dynamic surface tension. 0.05 wt% (PPVEGLY copolymers) or 0.1 wt% (PMVEGLY copolymers) aqueous solutions were measured at 21 ± 0.9 °C using a model t60 tensiometer from SITA, Dresden, Germany. The dynamic surface tension was calculated using the equation $\gamma_{dyn} = r(p_{max} - \rho g h) \; 2^{-1}$ (γ = tension, r = capillary radius, p_{max} = pressure maximum, ρ = liquid density, g = gravity, h = immersion depth)

Static contact angle

For the determination of water-repellency, contact angle measurements were conducted using the sessile drop technique on a OCA20 from dataphysics,

Filderstadt Germany. 4 µL of Milli-Q water were placed on top of a coated surface and the contact angles were determined using the SCA20 software (dataphysics). Measurements were repeated at least 5 times and the results were averaged. Coating of cellulose was performed by immersion with 100 mg mL^{-1} polymer solutions in DCM or THF. The coated cellulose was dried for 4 h at 65 °C. Glass slides were coated by either covering with 3–10 mg mL^{-1} polymer solutions or by covering with the pure viscous polymer using a scraper. The glass slides were subsequently dried under reduced pressure for at least 16 h.

Oil-repellency

Blotting paper was immersed with 100 mg mL^{-1} solutions of polymer in DCM or THF and dried for 4 h at 65 °C under reduced pressure. Oil-repellency was evaluated using the AATCC method 118.[33] 50 µL drops of a series of hydrocarbons (see table S1 for more information) are discarded on the coated surface and the wetting behaviour is observed after 30 s.

Results and Discussion

Part A: Synthesis and characterisation of the copolymers

Utilising the monomer-activated ring-opening polymerisation (MAROP, first described by Deffieux and Carlotti)[34] of fluorine containing epoxides and non-fluorinated comonomers series of copolymers were synthesised.

Amphiphilic copolymers

Amphiphilic copolymers with surfactant properties were synthesised by statistical copolymerisation of PMVEGLY or PPVEGLY with hydrophilic epoxides.

On the one hand, 2-(2-methoxyethoxy)ethylglycidylether (ME_2GE) and 2-[2-(2-methoxyethoxy)ethoxy]ethylglycidylether (ME_3GE) were used, due to their oligoethylene glycol monomethyl ether side chain. The orientation of the side chain was expected to lead to a hydrophilicity gradient orthogonal to the backbone. ME_2GE was used in copolymers with PMVEGLY in particular, to match the shorter polyfluorinated chain of PMVEGLY with respect to PPVEGLY. On the other hand, ethylene oxide (EO) was studied as a comonomer either in a statistical

copolymerisation or via utilising mPEG macroinitiators, which results in block copolymers. These copolymers were synthesised as comparable compounds to classic surfactants, which often consist of PEG as hydrophilic segment. Characterisation data of the copolymers is listed in Table 1.

Table 1: Characterisation data of the polymers synthesised for application as surfactant.

No.	Polymer[a]	Ratio[th] / units[th]	M_n[th] (g mol^{-1})	M_n[b] (g mol^{-1})	$Đ$[b]
S1	P(ME$_3$GE $_{0.80}$-*co*-PPVEGLY$_{0.20}$)	80:20 / 8:2	2520	2340	1.11
S2	P(ME$_3$GE $_{0.44}$-*co*-PPVEGLY$_{0.56}$)	50:50 / 4:4	2320	2720	1.16
S3	P(ME$_3$GE $_{0.73}$-*co*-PPVEGLY$_{0.27}$)	67:33 / 8:4	3200	2640	1.07
S4	P(ME$_3$GE$_{0.77}$-*co*-PPVEGL $_{0.23}$)	75:25 / 12:4	4080	3920	1.10
S5	P(ME$_3$GE$_{0.88}$-*co*-PPVEGLY$_{0.12}$)	86:14 / 24:4	6730	4350	1.09
S6	P(ME$_3$GE$_{0.91}$-*co*-PPVEGLY$_{0.09}$)	90:10 / 36:4	9370	4520	1.14
S7	P(ME$_3$GE$_{0.71}$-*co*-PMVEGLY$_{0.29}$)	67:33 / 4:2	1440	1880	1.09
S8	P(ME$_3$GE$_{0.80}$-*co*-PMVEGLY$_{0.20}$)	80:20 / 8:2	2320	2210	1.16
S9	P(ME$_3$GE$_{0.84}$-*co*-PMVEGLY$_{0.16}$)	86:14 / 12:2	3200	3240	1.11
S10	P(ME$_3$GE$_{0.47}$-*co*-PMVEGLY$_{0.53}$)	50:50 / 4:4	1920	1960	1.09
S11	P(ME$_3$GE$_{0.67}$-*co*-PMVEGLY$_{0.33}$)	67:33 / 8:4	2800	2910	1.09
S12	P(ME$_3$GE$_{0.75}$-*co*-PMVEGLY$_{0.25}$)	75:25 / 12:4	3680	3300	1.14
S13	P(ME$_3$GE$_{0.86}$-*co*-PMVEGLY$_{0.14}$)	86:14 / 24:4	6330	5060	1.13
S14	P(ME$_3$GE$_{0.91}$-*co*-PMVEGLY$_{0.09}$)	90:10 / 36:4	8970	6130	1.14
S15	P(ME$_3$GE$_{0.52}$-*co*-PMVEGLY$_{0.48}$)	50:50 / 6:6	2840	2410	1.10
S16	P(ME$_3$GE$_{0.67}$-*co*-PMVEGLY$_{0.33}$)	67:33 / 12:6	4160	3620	1.14
S17	P(ME$_2$GE$_{0.78}$-*co*-PMVEGLY$_{0.22}$)	80:20 / 8:2	1970	2000	1.08
S18	P(ME$_2$GE$_{0.53}$-*co*-PMVEGLY$_{0.47}$)	50:50 / 4:4	1750	1560	1.13
S19	P(ME$_2$GE$_{0.65}$ -*co*-PMVEGLY$_{0.35}$)	67:33 / 8:4	2450	2760	1.08

Table 1: Characterisation data of the polymers synthesised for application as surfactant (continued).

No.	Polymer[a]	Ratio[th] / units[th]	M_n[th] (g mol^{-1})	M_n[b] (g mol^{-1})	$Đ$[b]
S20	P($ME_2GE_{0.73}$-*co*-$PMVEGLY_{0.27}$)	75:25 / 12:4	3160	2640	1.18
S21	P($ME_2GE_{0.85}$-*co*-$PMVEGLY_{0.15}$)	86:14 / 24:4	5270	3620	1.15
S22	P($ME_2GE_{0.47}$-*co*-$PMVEGLY_{0.53}$)	50:50 / 6:6	2580	2400	1.18
S23	P($ME_2GE_{0.67}$-*co*-$PMVEGLY_{0.33}$)	67:33 / 12:6	3640	3330	1.09
S24	P($EG_{0.94}$-*co*-$PPVEGLY_{0.06}$)	80:20 / 20:5	2660	2570	1.15
S25	P($EG_{0.97}$-*co*-$PPVEGLY_{0.03}$)	85:15 / 45:8	4780	2240	1.07
S26	$mPEG_{0.81}$-*b*-$PPVEGLY_{0.19}$	76:24 / 13:4	1940	1810	1.10
S27	$mPEG_{0.94}$-*b*-$PPVEGLY_{0.06}$[c]	93:7 / 50:4	3580	2290[c]	1.41[c]
S28	$mPEG_{0.97}$-*b*-$PPVEGLY_{0.03}$[c]	97:3 / 123:4	6770	4310[c]	1.10[c]
S29	$mPEG_{0.76}$-*b*-$PPVEGLY_{0.24}$	68:32 / 13:6	2620	1920	1.09
S30	$mPEG_{0.91}$-*b*-$PPVEGLY_{0.09}$[c]	88:12 / 50:7	4600	2540[c]	2.25[c]
S31	$mPEG_{0.61}$-*b*-$PPVEGLY_{0.39}$	50:50 / 13:13	5000	2310	1.12

[a]Compositions in mole% calculated by ^{1}H NMR spectroscopy (300 MHz, C*D*Cl_3). [b]Determined by SEC (RI detector, PEG standards). PPVEGLY-copolymers in THF, PMVEGLY-copolymers in DMF [c]Incomplete initiation led to the formation of a blend composed of unmodified mPEG and the block copolymer.

The experimental composition was calculated using ^{1}H NMR spectroscopy by normalisation to the (O-C*H*F-CF_2) ether proton and comparison of the monomer signals. SEC showed narrow to moderate dispersities (***Đ*** = 1.07–1.18) and monomodal molecular weight distributions with tailing to lower molecular weight (Figure 2), which is typical for MAROP due to initiation side reactions (exemplarily shown in MALDI-ToF spectrum S18). Exceptions were S24 showing a low molecular weight shoulder and block copolymers with 2 kg mol^{-1} and 5 kg mol^{-1} mPEG, which were bimodal due to incomplete initiation by the mPEG macroinitiator (***Đ*** = 1.10–2.25). Thus, blends of unmodified mPEG and the corresponding copolymer were obtained. In consequence, the resulting copolymers have a higher molecular weight than expected. Discrepancies between theoretical and experimental molecular weight can be attributed to the PEG calibration, which shows

different hydrodynamic radii in comparison to substituted polyethers. Sakakibara *et. al*. reported an underestimation of the molecular weight for polyethers with fluorinated side chains and attributed it to the high molecular weight-volume ratio of fluorine atoms.[35]

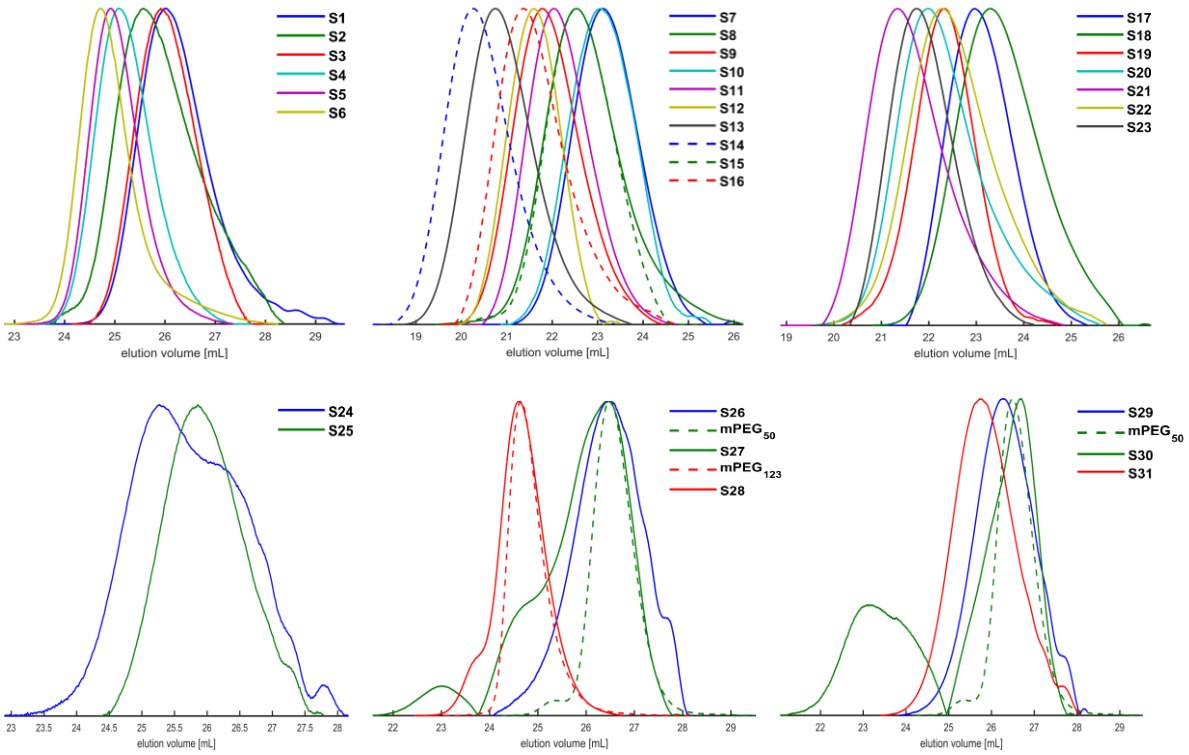

Figure 2: SEC traces (RI signal) of the copolymer series. Top row from left to right: P(ME$_3$GE-co-PPVEGLY), P(ME$_3$GE-co-PMVEGLY), P(ME$_2$GE-co-PMVEGLY). Bottom row from left to right: P(EO-co-PPVEGLY), PEG-b-PPPVEGLY$_4$, PEG-b-PPPVEGLY$_{6\text{-}13}$.

Microstructure determination for the statistical copolymerisation of glycidyl ethers: Typical surfactants consist of a hydrophilic head and a hydrophobic tail. In our system, these elements are distributed all over the backbone via the side chains. Nevertheless, gradient and blocklike structures are expected to support the surface activity, due to an eased orientation at the phase boundary. Hence, ^{1}H NMR kinetic studies were conducted to investigate the polymers microstructure. The studied polymers were synthesised in 2Me-THF, due to the shielding of the oxygen atom preventing catalyst complexation. Consequently, kinetic studies for the comonomer pairs ME$_3$GE-PPVEGLY, ME$_3$GE-PMVEGLY and ME$_2$GE-PMVEGLY were performed in 2-MeTHF. Copolymerisation of ME$_3$GE and PPVEGLY was furthermore studied in THF as a cheaper and more industrially relevant solvent. For the polymerisation in THF more equivalents of TIBAL were required, probably to overcome the complexation of the catalyst. The polymerisations were performed in

sealed Norell S-5-400 NMR tubes at 10 °C. The decreasing monomer conversions were monitored and used to determine the reactivity ratios.

Because both comonomers were glycidyl ethers, we expected the individual reactivity ratios to be only influenced by the strength of electron withdrawal through the substituents as well as the complexation of TIBAL by the multiple oxygen atoms of the ME_3GE side chain. Figure 3 shows the decrease of the monomer signal with time, which was used for the calculations, and the simulated microstructure of the polymer (see SI regarding kinetic models and plots).

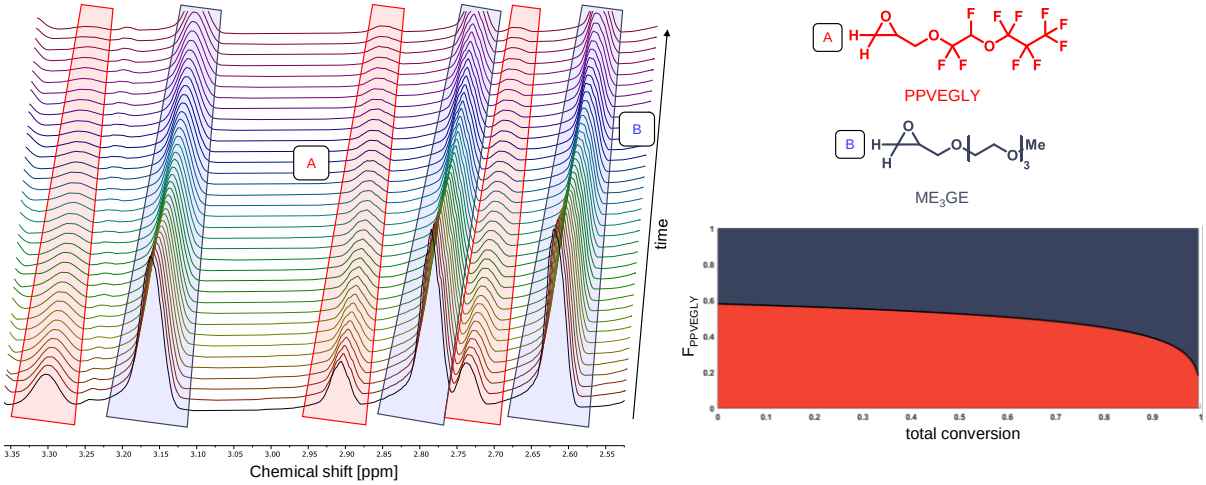

Figure 3: Left: zoom in of the ^1H NMR spectra for synthesis of P($ME_3GE_{0.67}$-co-$PPVEGLY_{0.33}$) in 2-MeTHF at 10 °C employing the monomer-activated ring-opening method. The epoxide signals were assigned to the corresponding monomers. Signals marked with A and B were used for the calculations. Bottom right: Microstructure simulation od P(ME_3GE-co-PPVEGLY) using the reactivity ratios determined via the Jaacks method.

Indeed, ^1H NMR kinetic evaluation showed a slight incorporation preference of the fluorinated monomer in the first chain segment close to the initiator, which could promote the desired surfactant properties. Reactivity ratios in 2-MeTHF of $r_{PPVEGLY} = 1.38 \pm 0.01$ and $r_{ME_3GE} = 0.72 \pm 0.01$ were calculated using the non-terminal Jaacks model. Values calculated via the Jaacks method were in good agreement with the values fitted via BSL and Meyer-Lowry ideal. The product of the reactivity ratios equalling 1 shows an ideal copolymerisation behaviour, which was not influenced by the chain end. Nevertheless, the orientation of the side chains is presumably the predominant cause of the polymer's hydrophilicity gradient. The kinetic studies in THF also revealed an ideal copolymerisation behaviour with reactivity ratios of $r_{PPVEGLY} = 1.54 \pm 0.01$ and $r_{ME_3GE} = 0.65 \pm 0.01$. The slightly

increased difference between the values shows that the more reactive PPVEGLY is stronger influenced by the reaction conditions than ME_3GE.

The comonomer pair with the less electron withdrawing PMVEGLY shows a similar ideal behaviour, with a slightly less pronounced gradient: $r_{PMVEGLY} = 1.22 \pm 0.04$ and $r_{ME_3GE} = 0.82 \pm 0.03$. In combination with ME_2GE the gradient was found to be stronger: $r_{PMVEGLY} = 1.60 \pm 0.02$ and $r_{ME_2GE} = 0.63 \pm 0.01$. We assume, that ME_3GE is more reactive than ME_2GE, due to the higher number of oxygen atoms leading to a stronger complexation of the Lewis acid. On the other hand, Herzberger *et. al.* found an opposite behaviour for the comonomer pair of ethylene oxide and ethoxy ethyl glycidyl ether (EEGE) in MAROP, albeit the reaction conditions are not comparable, and differences could be caused by the non-complexing solvent toluene.

Hydrophobic and oleophobic copolymers

Comonomers bearing long alkyl side chains, 1,2-epoxytetradecane (ETD) and 1,2-epoxyhexadecane (EHD), were used to enhance the hydrophobicity in hydrophobic and oleophobic coatings. Although their corresponding homopolymers are suitable for hydrophobic coatings, they are not suitable for oleophobic coatings due to their oleophilicity. In consequence, they were used to balance hydro- and oleophobicity in series of copolymers with the fluorinated monomers. Allyl glycidyl ether (AGE) was used in terpolymerisations to incorporate a functional group as an anchor for textile modification. Table 2 summarises the characterisation data for the polymers synthesised for the intended application as surface coatings. These monomers as well as 1,2-epoxydodecane (EDD) and (3-glycidoxypropyl)-bis(trimethyl-siloxy)methylsilane were used in homopolymerisations (Table S2). Because the two latter polymers showed water-repellency that was lower than targeted, no copolymers were synthesised using these monomers. Furthermore, glycidyl methacrylate (GMA) was used exemplarily in a copolymerisation with PPVEGLY as an alternative functional group to AGE (see SI).

Table 2: Characterisation data of the copolymers synthesised for coatings applications.

No.	Polymer[a]	Ratio[th] / units[th]	M_n^{th} (g mol^{-1})	M_n^{b} (g mol^{-1})	Đ[b]
C1	P(ETD$_{0.83}$-*co*-PPVEGLY$_{0.17}$)	80:20 / 20:5	6030	8460	1.28
C2	P(ETD$_{0.57}$-*co*-PPVEGLY$_{0.43}$)	50:50 / 8:8	4500	3650[c]	1.49[c]
C3	P(ETD$_{0.70}$-*co*-PPVEGLY$_{0.30}$)	67:33 / 16:8	6200	7690	1.27
C4	P(ETD$_{0.81}$-*co*-PPVEGLY$_{0.19}$)	79:21 / 30:8	9170	14140	1.15
C5	P(ETD$_{0.70}$-*co*-PPVEGLY$_{0.30}$)	67:33 / 24:12	9260	12050	1.23
C6	P(ETD$_{0.35}$-*co*-PPVEGLY$_{0.65}$)	33:67 / 8:16	7220	4820	1.37
C7	P(EHD$_{0.76}$-*co*-PPVEGLY$_{0.24}$)	75:25 / 15:5	5390	7000	1.33
C8	P(EHD$_{0.79}$-*co*-PPVEGLY$_{0.21}$)	80:20 / 20:5	6590	9720	1.34
C9	P(EHD$_{0.79}$-*co*-PPVEGLY$_{0.21}$)	79:21 / 30:8	10010	11030	1.30
C10	P(EHD$_{0.67}$-*co*-PPVEGLY$_{0.33}$)	67:33 / 24:12	9930	11040	1.30
C11	P(EHD$_{0.78}$-*co*-PMVEGLY$_{0.22}$)	80:20 / 20:5	6090	7910	1.29
C12	P(EHD$_{0.77}$-*co*-PMVEGLY$_{0.23}$)	79:21 / 30:8	9210	11030	1.32
C13	P(EHD$_{0.66}$-*co*-PMVEGLY$_{0.34}$)	67:33 / 24:12	8730	9270	1.34
C14	P(EHD$_{0.72}$-*co*-PPVEGLY$_{0.15}$-*co*-AGE$_{0.12}$)	69:17:14 / 20:5:4	7050	7790	1.36
C15	P(EHD$_{0.69}$-*co*-PPVEGLY$_{0.21}$-*co*-AGE$_{0.10}$)	68:23:9 / 30:10:4	11150	11690	1.36
C16	P(EHD$_{0.74}$-*co*-PPVEGLY$_{0.18}$-*co*-AGE$_{0.8}$)	74:19:7 / 40:10:4	13550	13660	1.45
C17	P(EHD$_{0.66}$-*co*-PPVEGLY$_{0.28}$-*co*-AGE$_{0.06}$)	68:27:5 / 50:20:4	19369	17120	1.47
C18	P(EHD$_{0.49}$-*co*-PPVEGLY$_{0.45}$-*co*-AGE$_{0.06}$)	47:47:6 / 30:30:4	17950	11810[c]	1.49[c]
C19	P(EHD$_{0.75}$-*co*-PPVEGLY$_{0.20}$-*co*-AGE$_{0.05}$)	73:24:3 / 90:30:4	32380	20280	1.55
C20	P(EHD$_{0.69}$-*co*-PMVEGLY$_{0.23}$-*co*-AGE$_{0.9}$)	68:23:9 / 30:10:4	10060	10490	1.47
C21	P(EHD$_{0.74}$-*co*-PMVEGLY$_{0.19}$-*co*-AGE$_{0.7}$)	74:19:7 / 40:10:4	12560	11370	1.49

[a]Compositions in mole% calculated by ^{1}H NMR spectroscopy (300 MHz, C*D*Cl$_3$). [b]Determined by SEC (THF, RI detector, PEG standards). [c]Copolymers of a composition near 50:50 showed unexpected behaviour in SEC measurements, where the area switched from a higher RI signal than the eluents to a lower signal. Signals lower than the eluents signal are characteristic for fluorinated polymers. MALDI-ToF and ^{1}H DOSY spectra showed the presence of copolymers (Figure S20 and S21).

The experimental composition of terpolymers was calculated using the signal of the terminal alkene protons of AGE for normalisation, due to an overlap of the fluorinated monomer´s proton signal (-O-C*H*F-) and AGE. No isomerisation of the AGE double bonds was observed under the reaction conditions chosen. SEC (Figure 4) typically showed monomodal distributions with tailing to lower molecular weights. Exceptions

were C2 and C18 with ratios of fluorinated and alkylated side chains close to 50:50. For these polymers a switch of the curve area was found, where the RI signal changed from higher than the eluents RI signal to lower (Figure 4 shows both signals plotted to be positive). Lower RI signals are characteristic for fluorinated polymers due to the low refractive index of fluorine. An explanation for this bimodal behaviour is that the monomer ratio is around the point where the low RI of the fluorinated side chains becomes dominant and changes the polymer RI signal to lower values than for the eluents. MALDI-ToF and ^{1}H DOSY NMR spectroscopy verified the presence of copolymers (Figure S20 and S21 exemplarily).

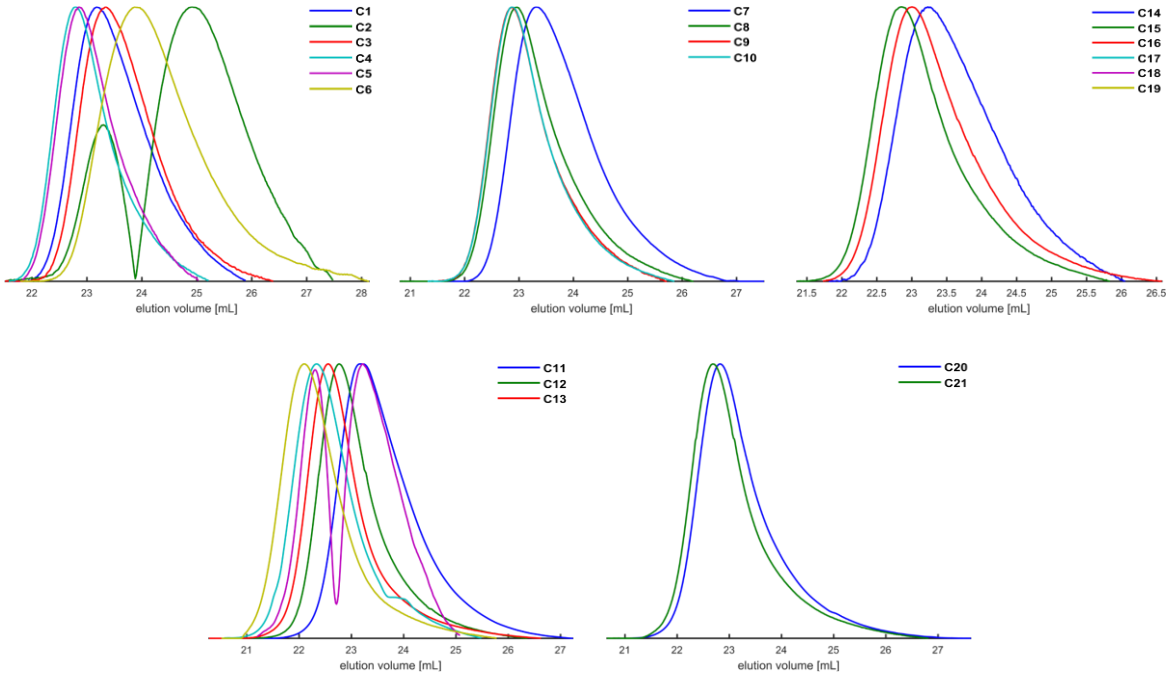

Figure 4: SEC traces (THF, RI signal) of the copolymer series. Top row from left to right: P(ETD-co-PPVEGLY), P(EHD-co-PPVEGLY), P(EHD-co-PMVEGLY). Bottom row from left to right: P(EHD-co-PPVEGLY-co-AGE), P(EHD-co-PMVEGLY-co-AGE).

Microstructure determination for the statistical copolymerisation of fluorinated glycidyl ethers with alkylene oxides: ^{1}H NMR kinetic studies were conducted to investigate the comonomer distribution along the backbone. Gradient and block(like) structure are expected to boost both the water- and oil-repellency, due to separation of the monomers yielding highly hydrophobic and highly oleophobic chain segments. The synthesis of P(ETD$_{0.67}$-*co*-PPVEGLY$_{0.33}$) was performed in 2-MeTHF in a sealed Norell S-5-400 NMR tube at 10 °C. The decreasing monomer conversions were used to determine the reactivity ratios. The combination of a glycidyl ether and an alkylene oxide was expected to yield (slight) gradients, as Carlotti, Deffieux and co-workers

reported for the combination of ethoxyethyl glycidyl ether (EEGE) and propylene oxide (PO) reactivity ratios of r_{EEGE} = 0.18 and r_{PO} = 1.58 (Kelen-Tüdös method).[36]

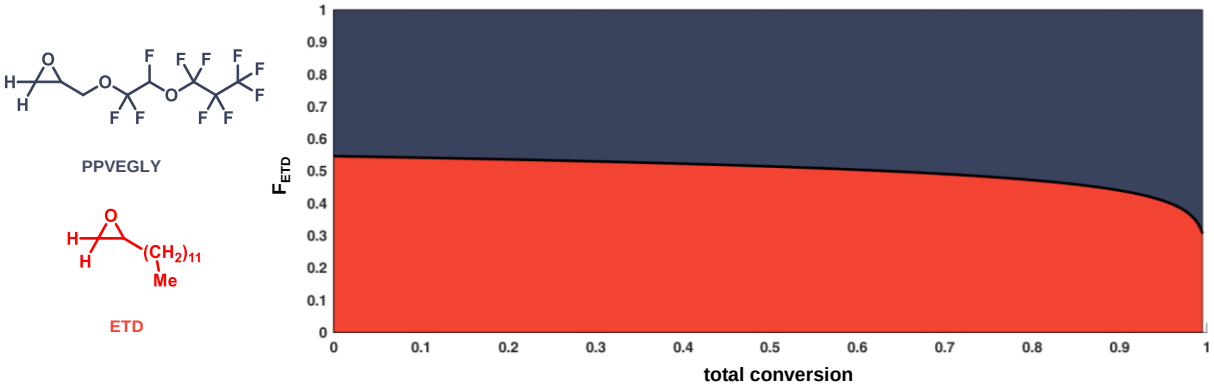

Figure 5: Microstructure simulation of P(ETD-co-PPVEGLY).

Indeed, ^{1}H NMR kinetic evaluation showed a slight incorporation preference of the non-fluorinated monomer in the initiation region in comparison to the respective monomer content (Figure 5): Using the non-terminal Jaacks model we calculated reactivity ratios of $r_{PPVEGLY}$ = 0.83 ± 0.01 and r_{ETD} = 1.20 ± 0.01 (SI for more details), which were in good agreement with the BSL and Meyer-Lowry ideal models.

Part B: Properties of the copolymers

Thermal properties: The thermal properties of the hydrophobic and oleophobic copolymers were investigated via DSC measurements. The results are listed in Table 3. The results of the homopolymers can be found in the Supporting Information (Table S2). Copolymerisation of the alkylene oxides with the fluorinated monomers lowered the melting temperatures T_m below room temperature leading the copolymers to be viscous liquids. Increasing content of the fluorinated monomer further reduced the melting temperature as well as the enthalpy. The glass transition temperature (T_g) of the fluorinated monomer was typically not observable for the copolymers, although different cooling and heating rates were used for the investigation (10, 20 and 40 °C min^{-1}). Exceptions were C7 and C12, which sowed higher T_gs than the respective homopolymers due to the long-chain comonomers.

Table 3: Thermal characterisation of the copolymers synthesised for coating applications.

No.	Polymer[a]	M_n[b] (g mol^{-1})	T_m (°C)[c]	ΔH_m (J g^{-1})[c]
C1	P(ETD$_{0.83}$-*co*-PPVEGLY$_{0.17}$)	8460	4	47
C2	P(ETD$_{0.57}$-*co*-PPVEGLY$_{0.43}$)	3650	-3	33
C3	P(ETD$_{0.70}$-*co*-PPVEGLY$_{0.30}$)	7690	0	38
C4	P(ETD$_{0.81}$-*co*-PPVEGLY$_{0.19}$)	14140	4	61
C5	P(ETD$_{0.70}$-*co*-PPVEGLY$_{0.30}$)	12050	0	40
C6	P(ETD$_{0.35}$-*co*-PPVEGLY$_{0.65}$)	4820	-6	29
C7	P(EHD$_{0.76}$-*co*-PPVEGLY$_{0.24}$)	7000	18 T_g -45[d]	53
C8	P(EHD$_{0.79}$-*co*-PPVEGLY$_{0.21}$)	9720	21	61
C9	P(EHD$_{0.79}$-*co*-PPVEGLY$_{0.21}$)	11030	21	74
C10	P(EHD$_{0.67}$-*co*-PPVEGLY$_{0.33}$)	11040	18	47
C11	P(EHD$_{0.78}$-*co*-PMVEGLY$_{0.22}$)	7910	24	78
C12	P(EHD$_{0.77}$-*co*-PMVEGLY$_{0.23}$)	11030	22 T_g -47[d]	73
C13	P(EHD$_{0.66}$-*co*-PMVEGLY$_{0.34}$)	9270	16	61
C14	P(EHD$_{0.72}$-*co*-PPVEGLY$_{0.15}$-*co*-AGE$_{0.12}$)	7790	18	47
C15	P(EHD$_{0.69}$-*co*-PPVEGLY$_{0.21}$-*co*-AGE$_{0.10}$)	11690	17	46
C16	P(EHD$_{0.74}$-*co*-PPVEGLY$_{0.18}$-*co*-AGE$_{0.8}$)	13660	19	53
C17	P(EHD$_{0.66}$-*co*-PPVEGLY$_{0.28}$-*co*-AGE$_{0.06}$)	17120	18	51
C18	P(EHD$_{0.49}$-*co*-PPVEGLY$_{0.45}$-*co*-AGE$_{0.06}$)	11810	14	35
C19	P(EHD$_{0.75}$-*co*-PPVEGLY$_{0.20}$-*co*-AGE$_{0.05}$)	20280	20	56
C20	P(EHD$_{0.69}$-*co*-PMVEGLY$_{0.23}$-*co*-AGE$_{0.9}$)	10060	17	67
C21	P(EHD$_{0.74}$-*co*-PMVEGLY$_{0.19}$-*co*-AGE$_{0.7}$)	11370	18	76

[a]Compositions calculated by ^{1}H NMR spectroscopy (300 MHz, C*D*Cl$_3$). [b]Determined by SEC (THF, RI detector, PEG standards). [c]Determined by DSC: second heat curve, 10 °C min^{-1}, 5 min isothermal between steps. [d]Heating and cooling rate 20 °C min^{-1}.

Degradation: The successful degradation of the polymer side chain was verified in a simple experimental set-up via heat-treatment of a PMVEGLY homopolymer either with diethylenetriamine (approx. 1.9 M) or with KOH and subsequent analysis via ^{19}F NMR spectroscopy (Figures S22 and S23). Degradation of PPVEGLY as well as PMVEGLY occurs via a combination of oxidation and hydrolysis. While degradation of PPVE, which bears a CF_3-CF_2-CF_2- group, yields PFPrA as a terminal product (see Introduction),[26,27] the degradation of PMVE ultimately leads to the formation of fluoride anions due to the absence of this perfluorinated group.

Surfactant properties of amphiphilic copolymers: The synthesised copolymers combine hydrophilic comonomers with hydrophobic and oleophobic comonomers and were evaluated for their activity as surfactants by measurement of static and dynamic surface tension.

Static surface tension: The static surface tension γ_{stat} of a 0.1 wt% aqueous polymer solution in equilibrium was measured by the Wilhelmy method. The results are shown in Table 4 and Figure 6.

Table 4: Static surface tensions of the polymers synthesised for application as surfactant.

No.	Polymer[a]	Ratio[th] / units[th]	M_n[b] (g mol^{-1})	γ_{stat}[c] (mN m^{-1})
S1	P(ME$_3$GE $_{0.80}$-*co*-PPVEGLY$_{0.20}$)	80:20 / 8:2	2340	21.67 ± 0.03
S2	P(ME$_3$GE $_{0.44}$-*co*-PPVEGLY$_{0.56}$)	50:50 / 4:4	2720	20.35 ± 0.03
S3	P(ME$_3$GE $_{0.73}$-*co*-PPVEGLY$_{0.27}$)	67:33 / 8:4	2640	21.94 ± 0.03
S4	P(ME$_3$GE$_{0.77}$-*co*-PPVEGL $_{0.23}$)	75:25 / 12:4	3920	23.34 ± 0.03
S5	P(ME$_3$GE$_{0.88}$-*co*-PPVEGLY$_{0.12}$)	86:14 / 24:4	4350	25.02 ± 0.03
S6	P(ME$_3$GE$_{0.91}$-*co*-PPVEGLY$_{0.09}$)	90:10 / 36:4	4520	30.53 ± 0.03
S7	P(ME$_3$GE$_{0.71}$-*co*-PMVEGLY$_{0.29}$)	67:33 / 4:2	1880	25.61 ± 0.03
S8	P(ME$_3$GE$_{0.80}$-*co*-PMVEGLY$_{0.20}$)	80:20 / 8:2	2210	27.23 ± 0.03
S9	P(ME$_3$GE$_{0.84}$-*co*-PMVEGLY$_{0.16}$)	86:14 / 12:2	3240	29.22 ± 0.03
S10	P(ME$_3$GE$_{0.47}$-*co*-PMVEGLY$_{0.53}$)	50:50 / 4:4	1960	27.84 ± 0.03
S11	P(ME$_3$GE$_{0.67}$-*co*-PMVEGLY$_{0.33}$)	67:33 / 8:4	2910	25.23 ± 0.03
S12	P(ME$_3$GE$_{0.75}$-*co*-PMVEGLY$_{0.25}$)	75:25 / 12:4	3300	26.05 ± 0.03
S13	P(ME$_3$GE$_{0.86}$-*co*-PMVEGLY$_{0.14}$)	86:14 / 24:4	5060	31.79 ± 0.03
S14	P(ME$_3$GE$_{0.91}$-*co*-PMVEGLY$_{0.09}$)	90:10 / 36:4	6130	33.35 ± 0.03
S15	P(ME$_3$GE$_{0.52}$-*co*-PMVEGLY$_{0.48}$)	50:50 / 6:6	2410	26.46 ± 0.03
S16	P(ME$_3$GE$_{0.67}$-*co*-PMVEGLY$_{0.33}$)	67:33 / 12:6	3620	25.70 ± 0.03
S17	P(ME$_2$GE$_{0.78}$-*co*-PMVEGLY$_{0.22}$)	80:20 / 8:2	2000	26.92 ± 0.03

Table 4: Static surface tensions of the polymers synthesised for application as surfactant (continued).

No.	Polymer[a]	Ratio[th] / units[th]	M_n[b] (g mol^{-1})	γ_{stat}[c] (mN m^{-1})
S18	P(ME$_2$GE$_{0.53}$-*co*-PMVEGLY$_{0.47}$)	50:50 / 4:4	1560	27.68 ± 0.03
S19	P(ME$_2$GE$_{0.65}$ -*co*-PMVEGLY$_{0.35}$)	67:33 / 8:4	2760	26.54 ± 0.03
S20	P(ME$_2$GE$_{0.73}$-*co*-PMVEGLY$_{0.27}$)	75:25 / 12:4	2640	26.42 ± 0.03
S21	P(ME$_2$GE$_{0.85}$-*co*-PMVEGLY$_{0.15}$)	86:14 / 24:4	3620	28.41 ± 0.03
S22	P(ME$_2$GE$_{0.47}$-*co*-PMVEGLY$_{0.53}$)	50:50 / 6:6	2400	27.27 ± 0.03
S23	P(ME$_2$GE$_{0.67}$-*co*-PMVEGLY$_{0.33}$)	67:33 / 12:6	3330	26.36 ± 0.03
S24	P(EG$_{0.94}$-*co*-PPVEGLY$_{0.06}$)	80:20 / 20:5	2570	23.87 ± 0.03[e]
S25	P(EG$_{0.97}$-*co*-PPVEGLY$_{0.03}$)	85:15 / 45:8	2240	25.03 ± 0.03[e]
S26	mPEG$_{0.81}$-*b*-PPVEGLY$_{0.19}$	76:24 / 13:4	1810	21.51 ± 0.03
S27	mPEG$_{0.94}$-*b*-PPVEGLY$_{0.06}$[d]	93:7 / 50:4	2290[d]	31.68 ± 0.03
S28	mPEG$_{0.97}$-*b*-PPVEGLY$_{0.03}$[d]	97:3 / 123:4	4310[d]	42.62 ± 0.03
S29	mPEG$_{0.76}$-*b*-PPVEGLY$_{0.24}$	68:32 / 13:6	1920	21.83 ± 0.03
S30	mPEG$_{0.91}$-*b*-PPVEGLY$_{0.09}$[d]	88:12 / 50:7	2540[d]	28.53 ± 0.03
S31	mPEG$_{0.61}$-*b*-PPVEGLY$_{0.39}$	50:50 / 13:13	2310	25.08 ± 0.03

[a]Compositions in mole% calculated by ^{1}H NMR spectroscopy (300 MHz, C*D*Cl$_3$). [b]Determined by SEC (RI detector, PEG standards). PPVEGLY-copolymers in THF, PMVEGLY-copolymers in DMF [c]Surface tensions of 0.1 wt% aqueous solution measured with the Wilhelmy method. [d]Incomplete initiation led to the formation of a blend composed of unmodified mPEG and the blockcopolymer. [e]Slow equilibration.

Comparing the P(ME$_3$GE-*co*-PPVEGLY) copolymers S1 to S6 (marked green in Figure 6) a γ_{stat} increase, translating to worse surfactant activity, is observable with decreasing percentage of PPVEGLY. The polyfluorinated chain of PPVEGLY reduces the polymers polarizability leading to reduced interactions with water and thus increases hydrophobicity. Molar ratios of fluorinated monomer were not raised above 56% on the one hand to compromise between surfactant performance and ecological profile and on the other hand to guarantee water solubility, which decreases with increasing ratio.

P(ME$_3$GE-*co*-PMVEGLY) copolymers (blue, S7-S9: circle, S11-S14: triangle, S15-S16: square) showed a similar trend as PPVEGLY copolymers: increased surfactant activity with increasing percentage of PMVEGLY. However, S10 with a ratio of 47:53 showed higher γ_{stat} then the next copolymers in the series. For S10 the effective surfactant concentration in solution was decreased, due to reduced solubility in water, indicated by a noticeable turbidity of prepared aqueous solution. The reduced concentration led to a higher γ_{stat} value. Copolymers with the same comonomer ratios but different molecular weights, showed similar γ_{stat} (e.g. S7, S11 and S16). In consequence, the surface activity of these polymeric surfactants seems to be affected predominantly by the appropriate balance between fluorinated (hydrophobic) and hydrophilic portions of the molecule.

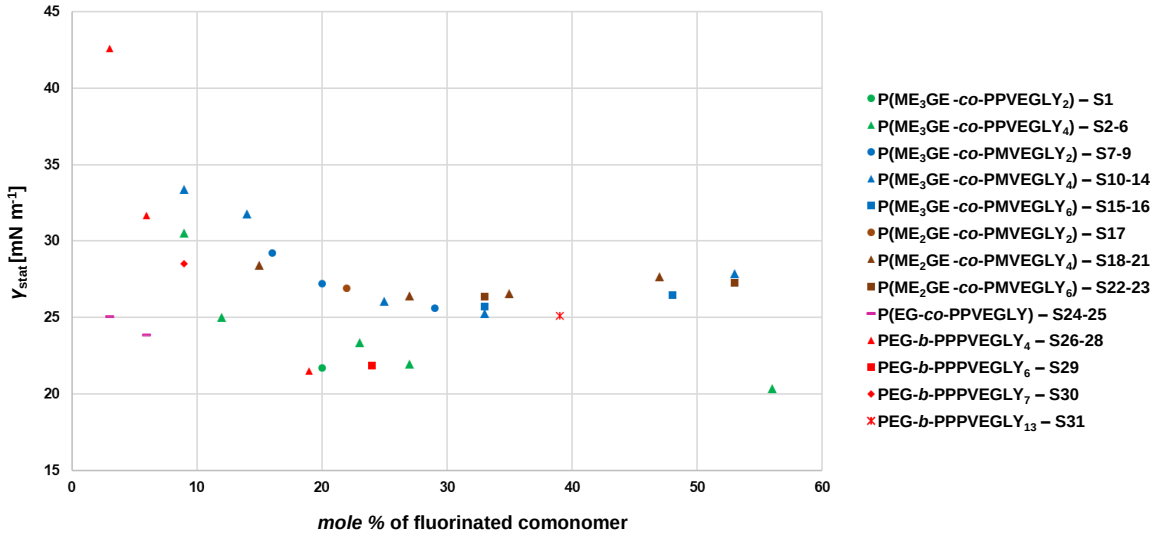

Figure 6: Static surface tension against the mole percentage of the fluorinated monomer of the copolymer series. Same colours are indicating series of the same comonomers. Shapes indicate series with constant targeted repeating units of the fluorinated monomer.

A general trend between PPVEGLY and PMVEGLY is evident, showing lower γ_{stat} for PPVEGLY bearing copolymers. This is observable for polymers with the same ratios as well as for polymers with similar molecular weight. For example, in the pair S2 and S10, where both polymers were targeted to bear 4 units of the comonomers each (50:50), S2 is superior to S10. S2 is also superior to S15, with S15 consisting of 6 units each (50:50) yielding a higher molecular weight. The same is true for the pairs S3 and S11 with 4 fluorinated and 8 oligoether units (67:33) as well as for S3 in comparison with polymers of the same ratios but different molecular weights: S16, bearing 6 and 12 units, and S7, bearing 2 and 4 units. Furthermore, S4 is superior to

S12 with 4 and 12 units (75:25); S1 to S8 with 2 and 8 units (80:20); S5 to S13 with 4 and 24 units (86:14); and finally, S6 to S14 with 4 and 36 units (90:10). The longer polyfluorinated chain of PPVGLY has a stronger impact on the hydrophobicity. This enables more pronounced surface tension reduction even at lower degrees of polymerisation (e.g. S1 with 4 units each vs. S15 with 6 units each) or fluorinated monomer percentage (e.g. S4 ratio: 77:23 and S11 ratio: 67:33), respectively. From another point of view, units of PMVEGLY consist only of 6 fluorine atoms, while PPVEGLY has 10 fluorine atoms. A comparison of the best PMVEGLY copolymer S11 bearing 24 fluorine atoms (6 units) did not perform better than S4 with 20 fluorine atoms (2 units).

The substitution of ME_3GE with ME_2GE (brown, S17: circle, S18-21: triangle, S22-23: square) in copolymers with PMVEGLY did not lead to improved surface activity. The P(ME_3GE-*co*-PMVEGLY) copolymer with the highest surface activity achieved a γ_{stat} of 25.23 ± 0.03 mN m^{-1}, comparable to 26.36 ± 0.03 mN m^{-1} in the ME_2GE copolymer series (polymers S11 and S23, respectively). Interestingly, both polymers had a comonomer ratio of 67:33, which seems to be the nearly ideal composition for PMVEGLY copolymers. Although a similar composition also led to good surfactant activity for the PPVEGLY copolymer (S3 21.94 ± 0.03 mN m^{-1}), the best result was obtained with a ratio of 44:56 (S2 20.35 ± 0.03 mN m^{-1}). S22 like S10 (both 47:53) showed reduced solubility (indicated by turbidity) and increased γ_{stat}, indicating the usable comonomer ratio range.

P(EG-*co*-PPVEGLY) (S24 and S25, pink) showed moderate activity (≥ 23.87 mN m^{-1}), presumably due to no significant separation between hydrophilic and hydrophobic segments. Accordingly, higher activities were achieved with block copolymers (S26-S31, red; ≥ 21.51 mN m^{-1}). EO and PPVEGLY copolymer series generally showed the same behaviour of increased γ_{stat} with decreasing percentage of the fluorinated PPVEGLY in the same manner as copolymers with oligoethylene side chains. Comparing block copolymers where the mPEG block was kept constant at 13 discloses an unexpected decrease of the activity with increasing PPVEGLY ratio. These polymers showed at higher ratios decreased aqueous solubility, indicated by turbidity of the prepared solution. In consequence, the amount of active surfactant was decreased. Nonetheless, especially solutions of these lower molecular weight copolymers reached low surface tensions.

Dynamic surface tension: The dynamic surface tension of a non-equilibrium system was measured using the bubble pressure method. Figure 7 shows the surface tension against the bubble pressure lifetime.

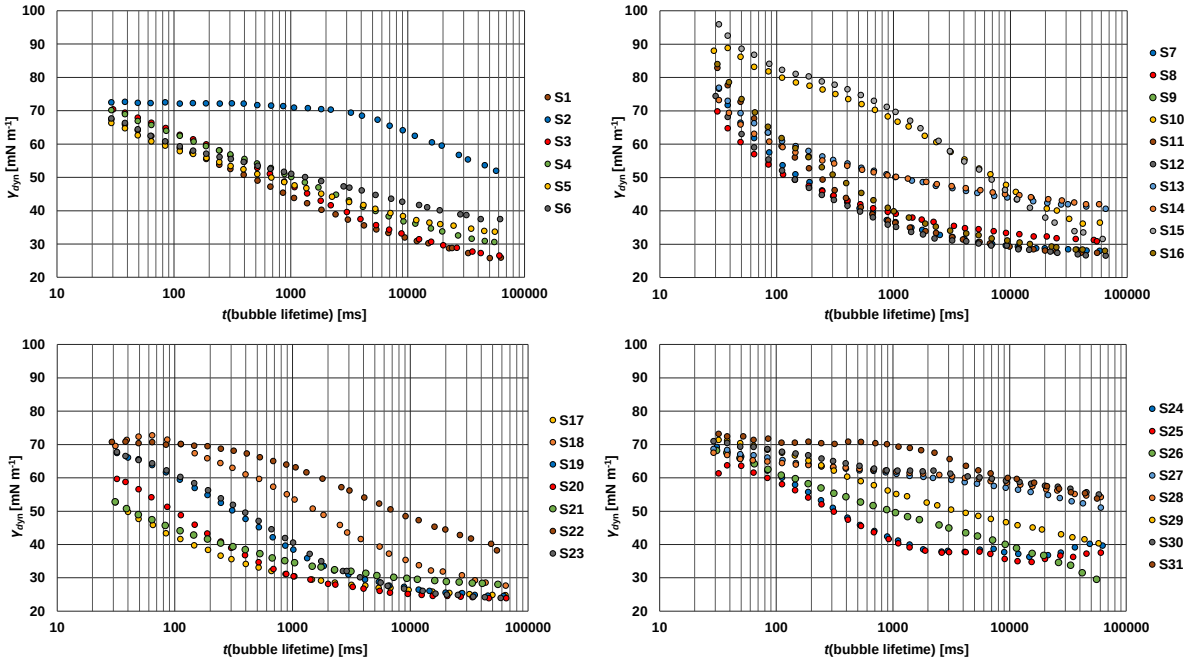

Figure 7: Surface tensions against bubble lifetime. P(ME$_3$GE-co-PPVEGLY) (top left), P(ME$_3$GE-co-PMVEGLY) (top right), P(ME$_2$GE-co-PMVEGLY) (bottom left) and EO-PPVEGLY copolymers (bottom right).

The dynamic surface tensions γ_{dyn} of solutions derived from the ME$_3$GE and ME$_2$GE series constantly decreased and typically approached a plateau. For the ME$_3$GE series, the γ_{dyn} values did not reach the γ_{stat} values in the measured time frame of one minute. The P(ME$_2$GE-*co*-PMVEGLY) series typically surpassed the measured values for γ_{stat} except for the 50:50 copolymer S15. For the 50:50 copolymers S2 and S15 γ_{dyn} first stayed constant at a plateau, before starting to decrease after roughly 2 and 1 s, respectively. This ratio seems to impede the mutual orientation of the side chains at the phase boundary. Generally, P(ME$_2$GE-*co*-PMVEGLY) led to a faster decrease of γ_{dyn} than P(ME$_3$GE-*co*-PMVEGLY), probably in consequence of the shorter chain length. The same trend is evident when comparing P(ME$_3$GE-*co*-PMVEGLY) with P(ME$_3$GE-*co*-PPVEGLY), with the latter series showing the slowest decrease of γ_{dyn}. The trend is more apparent, when comparing the polymeric fluorosurfactants to the small molecule fluorosurfactants series TIVIDA® FL (0.1 % solutions, see data sheets).[37–39] The polymers required more time to orientate at the surface boundary approaching the systems equilibrium. Statistical EO copolymers (S24 and S25) showed fluctuations at their plateau, which was higher than their γ_{stat}

values. Orientation seems impeded due to missing side chain support. Noticeably, mPEG block copolymers S26-S31 also differed from the behaviour and decreased γ_{dyn} in an almost linear manner even slower than the other copolymer series. The copolymer near a 50:50 ratio, S31, showed a plateau like the 50:50 ME_3GE as well as ME_2GE copolymers. This supports the assumption of hindered orientation resulting from this specific comonomer ratio.

Surface properties of hydrophobic and oleophobic copolymers: Different surfaces were treated with the copolymers, which were synthesised for the application as coatings, to further investigate surface properties of the polymers.

Water-repellency: Cellulose blotting paper as well as glass surfaces were coated with the synthesised polymers (Table 5). With a few exceptions, the polymer coatings incorporated suitable water-repellency on cellulose surfaces as shown by contact angle measurements. To ensure persistent non-wetting properties the drops were monitored over at least 30 min. With the marked exceptions all coatings were stable. The results are listed in Table 5 and Figure 8.

Table 5: Contact angle (Θ) against water of coated cellulose and glass surfaces with standard deviation.

No.	Polymer[a]	M_n[b] (g mol^{-1})	Θ(cellulose) (°)	Θ(glass) (°)
C1	P(ETD$_{0.83}$-*co*-PPVEGLY$_{0.17}$)	8460	97 ± 4	71 ± 3
C2	P(ETD$_{0.57}$-*co*-PPVEGLY$_{0.43}$)	3650	66 ± 3[d]	64 ± 3
C3	P(ETD$_{0.70}$-*co*-PPVEGLY$_{0.30}$)	7690	67 ± 3[d]	72 ± 3
C4	P(ETD$_{0.81}$-*co*-PPVEGLY$_{0.19}$)	14140	104 ± 3	62 ± 4
C5	P(ETD$_{0.70}$-*co*-PPVEGLY$_{0.30}$)	12050	104 ± 5	58 ± 6[d]
C6	P(ETD$_{0.35}$-*co*-PPVEGLY$_{0.65}$)	4820	57 ± 7[c]	66 ± 2 [d]
C7	P(EHD$_{0.76}$-*co*-PPVEGLY$_{0.24}$)	7000	108 ± 5	66 ± 2
C8	P(EHD$_{0.79}$-*co*-PPVEGLY$_{0.21}$)	9720	115 ± 3	96 ± 2
C9	P(EHD$_{0.79}$-*co*-PPVEGLY$_{0.21}$)	11030	109 ± 3	92 ± 4
C10	P(EHD$_{0.67}$-*co*-PPVEGLY$_{0.33}$)	11040	88 ± 4[c]	77 ± 3 [d]
C11	P(EHD$_{0.78}$-*co*-PMVEGLY$_{0.22}$)	7910	105 ± 3	95 ± 3

Table 5: Contact angle (Θ) against water of coated cellulose and glass surfaces with standard deviation (continued).

No.	Polymer[a]	M_n[b] (g mol^{-1})	Θ(cellulose) (°)	Θ(glass) (°)
C12	P(EHD$_{0.77}$-*co*-PMVEGLY$_{0.23}$)	11030	112 ± 5	94 ± 5
C13	P(EHD$_{0.66}$-*co*-PMVEGLY$_{0.34}$)	9270	97 ± 6[c]	74 ± 2 [d]
C14	P(EHD$_{0.72}$-*co*-PPVEGLY$_{0.15}$-*co*-AGE$_{0.12}$)	7790	108 ± 2	77 ± 5
C15	P(EHD$_{0.69}$-*co*-PPVEGLY$_{0.21}$-*co*-AGE$_{0.10}$)	11690	106 ± 3	78 ± 4
C16	P(EHD$_{0.74}$-*co*-PPVEGLY$_{0.18}$-*co*-AGE$_{0.8}$)	13660	112 ± 3	82 ± 4
C17	P(EHD$_{0.66}$-*co*-PPVEGLY$_{0.28}$-*co*-AGE$_{0.06}$)	17120	109 ± 3	78 ± 5
C18	P(EHD$_{0.49}$-*co*-PPVEGLY$_{0.45}$-*co*-AGE$_{0.06}$)	11810	97 ± 3[d]	81 ± 2
C19	P(EHD$_{0.75}$-*co*-PPVEGLY$_{0.20}$-*co*-AGE$_{0.05}$)	20280	114 ± 3	87 ± 2
C20	P(EHD$_{0.69}$-*co*-PMVEGLY$_{0.23}$-*co*-AGE$_{0.9}$)	10060	99 ± 4	73 ± 5
C21	P(EHD$_{0.74}$-*co*-PMVEGLY$_{0.19}$-*co*-AGE$_{0.7}$)	11370	99 ± 2	92 ± 2

[a]Compositions calculated by ^{1}H NMR spectroscopy (300 MHz, C*D*Cl$_3$). [b]Determined by SEC (THF, RI detector, PEG standards). [c]Water drops lost their form in less than 5 min. [d]Half of the water drops lost their form in less than 15 min.

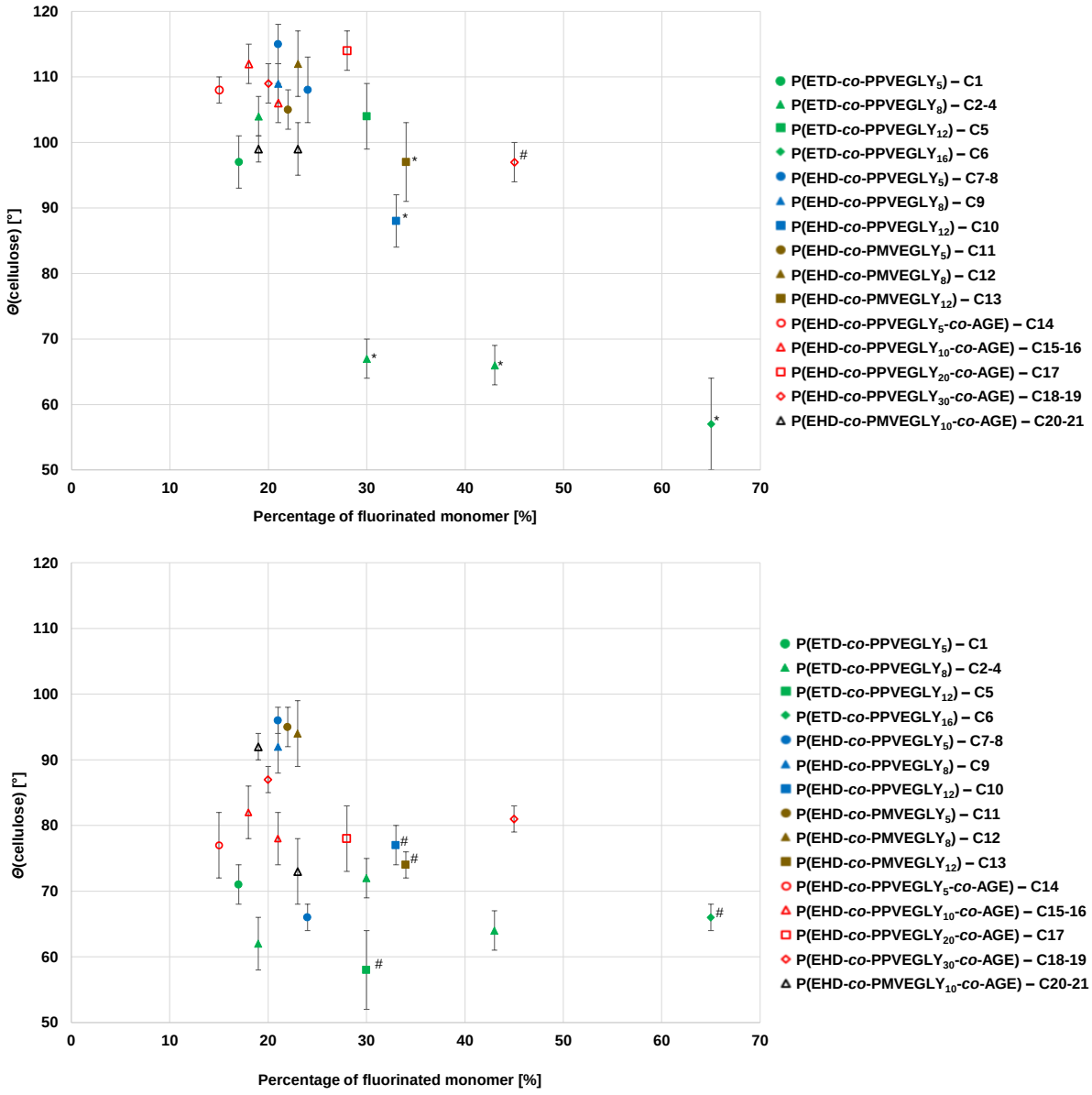

Figure 8: Contact angles of water on coated cellulose (top) and coated glass (bottom) against the percentage of fluorinated monomer in the copolymers. P(ETD-co-PPVEGLY) (green), P(EHD-co-PPVEGLY) (blue), P(EHD-co-PMVEGLY) (brown), P(EHD-co-PPVEGLY-co-AGE) (red), and P(EHD-co-PMVEGLY-co-AGE) (black). Shapes represent series where the degree of polymerisation of the fluorinated monomer were kept constant at 5 (circle), 8 (triangle), 12 (square), 16 (rhombus), 10 (hollow triangle), 20 (hollow square), and 30 (hollow rhombus). Asterisks mark unstable coatings leading to wetting within 5 min. Hashtag marks a coating, where half the drops were unstable.

Copolymers consisting of different monomers are represented with different colours, in which the same shapes represent series with constant fluorinated monomer percentage. Terpolymers are represented by hollow shapes. Contact angels were decreasing with increasing fluorinated monomer percentage (e.g. C2 to C4, green triangles). This trend reproduces the results of the corresponding homopolymers: Unsuitable hydrophobisation of cellulose by the fluorinated homopolymers leading to

wetting, and hydrophobisation by alkyl side chains. Interestingly, Kredel and Gallei found the contact angle to increase with increasing percentage of fluorinated monomer in polyacrylate copolymers bearing side chains of stearyl and PPVE derivatives. Furthermore, they found the contact angle to increase with the molecular weight.[31] A similar behaviour of increasing contact angle with increasing molecular weight was found in this study (e.g. C3 and C5, green triangle and rhombus). The polyether copolymers of this work showed lower contact angles than the polyacrylates of Kredel and Gallei[31] except for their lowest molecular weight polymer with 183 kg mol^{-1}. In consequence, an explanation for the reduced repellency of the polyethers is the lower molecular weights in comparison to the polyacrylates.

A third trend was the contact angle increase with either of the monomers side chain-lengths, which translates to an increased hydrophobic percentage in comparison to the hydrophilic backbone (e.g. C1 and C8 and C11, circles). The incorporation of AGE as a third monomer led to a slight decrease of the contact angle (e.g. C15 with C8 and C9, filled and hollow). To summarise, high molecular weights, long side chains, and a high percentage of the alkylated monomer are favourable for the hydrophobisation of cellulose. Antistick properties of the fluoropolymers are caused by the low polarizability of fluorine leading to only weak interaction with water and organic compounds. Presumably in consequence of their hydrophilic polyether backbone, the polymers did not reach the repellency of Teflon (measured $\Theta = 128 \pm 6$).

The observed contact angles on coated glass surfaces indicated successful hydrophobisation and similar trends as the coated cellulose. Nonetheless, they were generally lower than the contact angles of coated cellulose (Table 5, Figure 9). An explanation for this is the low interaction of polymer and glass, which caused an insufficient coating and unfavourable orientation. Especially for polymer coatings with high percentage of fluorinated monomer, the film formation was difficult and led to uneven coatings.

Figure 9: Water drops on uncoated and coated surfaces. From left to right: uncoated glass (42°), C8 coated glass (96°), C8 coated cellulose (115°), uncoated Teflon (128°).

Oil-repellency: Oil-repellency tests were conducted using the AATCC test method 118[33] for the fluorinated homopolymers of PMVEGLY and PPVEGLY as well as the most promising copolymers. Grades are assigned as the corresponding number of the last successfully repelled liquid (see Table S1). In consequence the repellency is increasing with increasing number. A borderline pass in consequence of a rounding drop with partial darkening is represented by subtracting 0.5 from the liquids number.[33]

Homopolymers of the fluorinated monomers showed an increased oil-repellency with increased molecular weight. PPPVEGLY achieved grades of 1.5 for 10 to 30 targeted repeating units, 2 for 50 units, 2.5 for 70 to 90 units, and 3.5 for 120 units (Figure 10). PPMVEGLY with 10 targeted repeating units, did not show oil-repellency, while the polymer with 30 targeted repeating units achieved grade 1.

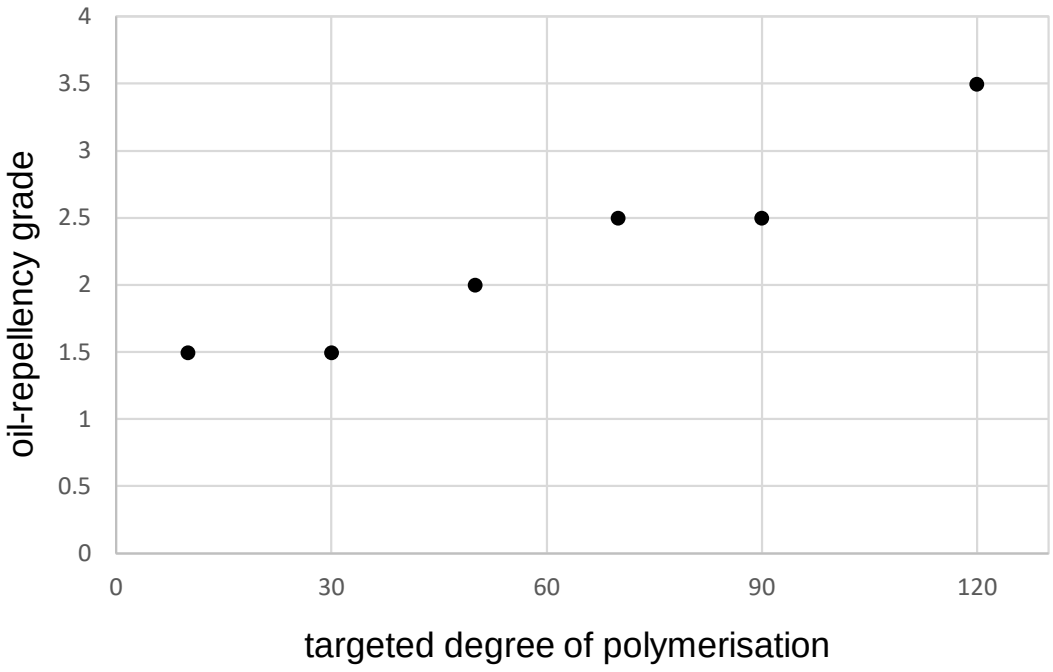

Figure 10: Oil-repellency grade plotted against the targeted degree of polymerisation of PPVEGLY homopolymers.

PPVEGLY copolymers C3, C10, C15 and C18 yielded grade 0.5, only achieving a borderline pass with the mineral oil Kaydol. Expectedly, incorporation of non-fluorinated comonomers is decreasing the oil-repellency of the copolymer. PMVEGLY copolymers C13 and C20 failed the oil-repellency test. The smaller fluorinated side chain of PMVEGLY is at least in this molecular weight of ≤12 kg mol^{-1} not suitable for oil-repellency.

Polymethacrylates bearing PPVE side chains are literature known. Homopolymers on cotton achieved with grade 5[40] a higher repellency than the synthesised homopolyethers (up to grade 3.5) of this study. This difference can either be caused by the different chemical nature of the backbones or by different molecular weights. As discussed earlier, higher molecular weights led to better water-repellency as well as better oil-repellency. Kredel and Gallei achieved with PPVE and stearyl derived copolymers on cotton grade 4 and on cellulose grade 3 to 6 with an increasing molecular weight from 183 kg mol^{-1} to 760 kg mol^{-1} (coating conditions also influenced the grade).[31] The polymers of this study also showed an increased repellency with increased molecular weight, but did not reach either molecular weight or grade as the polymethacrylates bearing PPVE derived groups.

Conclusion

Series of copolymers consisting of PMVEGLY or PPVEGLY as degradable and ecological friendlier alternatives for classic fluorinated monomers and either a hydrophilic or hydrophobic comonomer were synthesised and studied with respect to their surface properties. The copolymers of the structures PEG-*b*-PPVEGLY as well as ME_3GE-*co*-PPVEGLY, ME_3GE-*co*-PMVEGLY and ME_2GE-*co*-PMVEGLY were found to be suitable surfactants. The improved solubility and easy preparation of the statistical copolymers in comparison to the block copolymers renders them especially suitable. The best synthesised polymers ($\gamma_{stat} \geq 20.35$ mN m^{-1}) were on par or outperformed the legacy compound perfluorooctanesulfonic acid (21.9 mN m^{-1})[5] as well as the recently developed commercially available ionic fluorosurfactants TIVIDA® FL 2300 ($\gamma_{stat} \leq 22.9$ mN m^{-1}, 0.1% active ingredient)[37] and PolyFox from Omnova Solutions Inc. (e.g. PolyFox PF 151N: $\gamma_{stat} = 24$ mN m^{-1}, 0.1% active ingredient).[41,42] On the other hand, the polymers did not achieve the activity of TIVIDA® FL 2500 ($\gamma_{stat} \leq 18.9$ mN m^{-1})[38] and FL 2700 ($\gamma_{stat} \leq 16.8$ mN m^{-1})[39]. Investigation of the dynamic surface tensions indicated rather slow equilibration. Copolymers with hydrophobic comonomers showed hydrophobicity (contact angles on coated cellulose ≤ 115°, on coated glass ≤ 96°), but only low oleophobicity (AATCC 118 grade 0.5). PPVEGLY homopolymers yielded higher oil-repellency (grade 3.5), but no sufficient hydrophobicity. As higher molecular weight polymers yielded higher repellencies, a further increase in the polyethers molecular weight

could be promising. PPVEGLY copolymers outperformed PMVEGLY copolymers in both applications, as a result of its higher fluorine content. Nonetheless, PMVEGLY showed a better degradation profile, rendering it ecological friendlier.

In situ ^{1}H NMR kinetic studies revealed a slight gradient structure for copolymers with oligoethylene bearing comonomers as well as with alkylene oxide comonomers. In consequence, the hydrophilicity gradient of the surfactants is predominantly formed due to orientation of the side chains and not the microstructure of the polymer. A clear separation of the comonomers within the copolymer structure could lead to increased surface activity for both applications and is the focus of our further research as well as the introduction of ionic groups to further boost the surfactant efficiency.

Acknowledgements

The authors thank Merck KGaA for providing the fluorine containing compounds PPVEGLY and PMVE. The authors thank Sabine Hennig for practical support and Dr. Elena Berger-Nicoletti for MALDI-ToF measurements.

References

(1) Quéré, D. Non-sticking drops. *Rep. Prog. Phys.* **2005**, *68* (11), 2495–2532. DOI: 10.1088/0034-4885/68/11/R01.

(2) Kim, H.-A. Water Repellency/Proof/Vapor Permeability Characteristics of Coated and Laminated Breathable Fabrics for Outdoor Clothing. *Coatings* **2022**, *12* (1), 12. DOI: 10.3390/coatings12010012.

(3) Kissa, E. *Fluorinated surfactants and repellents*, 2. ed., rev. and expanded.; Surfactants science series, Vol. 97; Dekker, 2001.

(4) Chemours. *Technical datasheet Capstone FS-22*:*Fluorosurfactant*. https://www.chemours.de/brands-and-products/capstone/products/fluorosurfactants (accessed 2022-12-28).

(5) Peshoria, S.; Nandini, D.; Tanwar, R. K.; Narang, R. Short-chain and long-chain fluorosurfactants in firefighting foam: a review. *Environ Chem Lett* **2020**, *18* (4), 1277–1300. DOI: 10.1007/s10311-020-01015-8.

(6) Jochyms, Q.; Mignard, E.; Vincent, J.-M. Fluorosurfactants for applications in catalysis. *Journal of Fluorine Chemistry* **2015**, *177*, 11–18. DOI: 10.1016/j.jfluchem.2015.01.011.

(7) Banerjee, S.; Tawade, B. V.; Ladmiral, V.; Dupuy, L. X.; MacDonald, M. P.; Améduri, B. Poly(fluoroacrylate)s with tunable surface hydrophobicity via radical copolymerization of 2,2,2-trifluoroethyl α-fluoroacrylate and 2-(trifluoromethyl)acrylic acid. *Polym. Chem.* **2017**, *8* (12), 1978–1988. DOI: 10.1039/C7PY00209B.

(8) Lemal, D. M. Perspective on fluorocarbon chemistry. *The Journal of organic chemistry* **2004**, *69* (1), 1–11. DOI: 10.1021/jo0302556.

(9) Schindler, W. D.; Hauser, P. J. Repellent finishes. In *Chemical finishing of textiles*; Schindler, W. D., Hauser, P. J., Eds.; Woodhead publishing in textiles; Woodhead Publishing, 2004; pp 74–86. DOI: 10.1533/9781845690373.74.

(10) O'Hagan, D. Understanding organofluorine chemistry. An introduction to the C-F bond. *Chemical Society reviews* **2008**, *37* (2), 308–319. DOI: 10.1039/b711844a.

(11) Cousins, I. T.; Johansson, J. H.; Salter, M. E.; Sha, B.; Scheringer, M. Outside the Safe Operating Space of a New Planetary Boundary for Per- and Polyfluoroalkyl Substances (PFAS). *Environmental science & technology* **2022**, *56* (16), 11172–11179. DOI: 10.1021/acs.est.2c02765.

(12) Kärrman, A.; Harada, K. H.; Inoue, K.; Takasuga, T.; Ohi, E.; Koizumi, A. Relationship between dietary exposure and serum perfluorochemical (PFC) levels--a case study. *Environment international* **2009**, *35* (4), 712–717. DOI: 10.1016/j.envint.2009.01.010.

(13) Evich, M. G.; Davis, M. J. B.; McCord, J. P.; Acrey, B.; Awkerman, J. A.; Knappe, D. R. U.; Lindstrom, A. B.; Speth, T. F.; Tebes-Stevens, C.; Strynar, M. J.; Wang, Z.; Weber, E. J.; Henderson, W. M.; Washington, J. W. Per- and polyfluoroalkyl substances in the environment. *Science (New York, N.Y.)* **2022**, *375* (6580), eabg9065. DOI: 10.1126/science.abg9065.

(14) Bartell, S. M.; Vieira, V. M. Critical review on PFOA, kidney cancer, and testicular cancer. *Journal of the Air & Waste Management Association (1995)* **2021**, *71* (6), 663–679. DOI: 10.1080/10962247.2021.1909668.

(15) Fenton, S. E.; Ducatman, A.; Boobis, A.; DeWitt, J. C.; Lau, C.; Ng, C.; Smith, J. S.; Roberts, S. M. Per- and Polyfluoroalkyl Substance Toxicity and Human Health Review: Current State of Knowledge and Strategies for Informing Future Research.

Environmental toxicology and chemistry **2021**, *40* (3), 606–630. DOI: 10.1002/etc.4890.

(16) Olsavsky, N. J.; Kearns, V. M.; Beckman, C. P.; Sheehan, P. L.; F. John Burpo, F. John; Bahaghighat H. Daniel; Nagelli, E. A. Research and Regulatory Advancements on Remediation and Degradation of Fluorinated Polymer Compounds. *Applied Sciences* **2020**, *10* (19), 6921.

(17) US EPA. *Fact Sheet: 2010/2015 PFOA Stewardship Program* | *US EPA*. https://www.epa.gov/assessing-and-managing-chemicals-under-tsca/fact-sheet-20102015-pfoa-stewardship-program (accessed 2022-12-17).

(18) UN Stockholm Convention. *Listing of POPs in the Stockholm Convention*. http://www.pops.int/TheConvention/ThePOPs/AllPOPs/tabid/2509/Default.aspx (accessed 2022-12-18).

(19) Wang, Z.; Cousins, I. T.; Scheringer, M.; Hungerbuehler, K. Hazard assessment of fluorinated alternatives to long-chain perfluoroalkyl acids (PFAAs) and their precursors: status quo, ongoing challenges and possible solutions. *Environment international* **2015**, *75*, 172–179. DOI: 10.1016/j.envint.2014.11.013.

(20) Pérez, F.; Nadal, M.; Navarro-Ortega, A.; Fàbrega, F.; Domingo, J. L.; Barceló, D.; Farré, M. Accumulation of perfluoroalkyl substances in human tissues. *Environment international* **2013**, *59*, 354–362. DOI: 10.1016/j.envint.2013.06.004.

(21) Martin, J. W.; Mabury, S. A.; Solomon, K. R.; Muir, D. C. G. Bioconcentration and tissue distribution of perfluorinated acids in rainbow trout (Oncorhynchus mykiss). *Environ Toxicol Chem* **2003**, *22* (1), 196–204. DOI: 10.1002/etc.5620220126.

(22) Pickard, H. M.; Criscitiello, A. S.; Persaud, D.; Spencer, C.; Muir, D. C. G.; Lehnherr, I.; Sharp, M. J.; Silva, A. O. de; Young, C. J. Ice Core Record of Persistent Short-Chain Fluorinated Alkyl Acids: Evidence of the Impact From Global Environmental Regulations. *Geophys. Res. Lett.* **2020**, *47* (10). DOI: 10.1029/2020GL087535.

(23) Hori, H.; Nagano, Y.; Murayama, M.; Koike, K.; Kutsuna, S. Efficient decomposition of perfluoroether carboxylic acids in water with a combination of persulfate oxidant and ultrasonic irradiation. *Journal of Fluorine Chemistry* **2012**, *141*, 5–10. DOI: 10.1016/j.jfluchem.2012.05.012.

(24) Hori, H.; Murayama, M.; Kutsuna, S. Oxygen-induced efficient mineralization of perfluoroalkylether sulfonates in subcritical water. *Chemosphere* **2009**, *77* (10), 1400–1405. DOI: 10.1016/j.chemosphere.2009.09.013.

(25) Kwok, E. S. C.; Atkinson, R. Estimation of hydroxyl radical reaction rate constants for gas-phase organix compounds using a structure-reactivity relationship: an update. *Atmospheric Environment* **1995**, *29* (14), 1685–1695.

(26) Joudan, S.; Mabury, S. A. Aerobic biotransformation of a novel highly functionalized polyfluoroether-based surfactant using activated sludge from a wastewater treatment plant. *Environmental science. Processes & impacts* **2022**, *24* (1), 62–71. DOI: 10.1039/d1em00358e.

(27) Joudan, S.; Orlando, J. J.; Tyndall, G. S.; Furlani, T. C.; Young, C. J.; Mabury, S. A. Atmospheric Fate of a New Polyfluoroalkyl Building Block, C3F7OCHFCF2SCH2CH2OH. *Environmental science & technology* **2022**, *56* (10), 6027–6035. DOI: 10.1021/acs.est.0c07584.

(28) Folkerson, A. P.; Joudan, S.; Mabury, S. A.; D'eon, J. C. In Vivo Transformation of a Novel Polyfluoroether Surfactant. *Environmental toxicology and chemistry* **2021**, *40* (12), 3328–3336. DOI: 10.1002/etc.5230.

(29) Friedrich, R.; Koch, F. Fluorine compounds. 17/357,193.

(30) Lindstrom, A. B.; Strynar, M. J.; Libelo, E. L. Polyfluorinated compounds: past, present, and future. *Environmental science & technology* **2011**, *45* (19), 7954–7961. DOI: 10.1021/es2011622.

(31) Kredel, J.; Gallei, M. Ozone-Degradable Fluoropolymers on Textile Surfaces for Water and Oil Repellency. *ACS Appl. Polym. Mater.* **2020**, *2* (7), 2867–2879. DOI: 10.1021/acsapm.0c00400.

(32) Motogami, K.; Kono, M.; Mori, S.; Watanabe, M.; Ogata, N. A new polymer electrolyte based on polyglycidylether. *Electrochimica Acta* **1992**, *37* (9), 1725–1727. DOI: 10.1016/0013-4686(92)80147-E.

(33) AATCC. *Oil Repellency: Hydrocarbon Resistance Test Method 118*, 1997.

(34) Billouard, C.; Carlotti, S.; Desbois, P.; Deffieux, A. “Controlled” High-Speed Anionic Polymerization of Propylene Oxide Initiated by Alkali Metal Alkoxide/Trialkylaluminum Systems. *Macromolecules* **2004**, *37* (11), 4038–4043. DOI: 10.1021/ma035768t.

(35) Sakakibara, K.; Nakano, K.; Nozaki, K. Regioregular Polymerization of Fluorine-Containing Epoxides. *Macromolecules* **2007**, *40* (17), 6136–6142. DOI: 10.1021/ma070428j.

(36) Gervais, M.; Brocas, A.-L.; Cendejas, G.; Deffieux, A.; Carlotti, S. Synthesis of Linear High Molar Mass Glycidol-Based Polymers by Monomer-Activated Anionic

Polymerization. *Macromolecules* **2010**, *43* (4), 1778–1784. DOI: 10.1021/ma902286a.

(37) Merck KGaA. *Technical datasheet TIVIDA FL 2300*. https://www.merckgroup.com/de/products/pm/101724.html (accessed 2022-12-16).

(38) Merck KGaA. *Technical datasheet TIVIDA FL 2500*. https://www.merckgroup.com/de/products/pm/102458.html (accessed 2022-12-16).

(39) Merck KGaA. *Technical datasheet TIVIDA FL 2700*. https://www.merckgroup.com/de/products/pm/140013.html (accessed 2022-12-16).

(40) Fang, H.; Friedrich, R. Fluorine containing polymers. 16/310,709.

(41) OMNOVA Solutions - Investors. *OMNOVA Solutions Introduces New Line of Design for the Environment Compatible Fluorosurfactants*. https://omnova.investorroom.com/index.php?s=43&item=26 (accessed 2023-01-12).

(42) Guangzhou Haoyi New Material Technology Co., Ltd. *Omnova PolyFox PF-136A, PF-156A, PF-151N Fluorosurfactants*. https://www.pudchem.com/detail-640.html (accessed 2023-01-12).

Supporting Information

Table of Contents

Materials

PPVEGLY was provided by Merck KGaA. PMVE was obtained in >99% purity from Chemours; diethyleneglycol monomethyl ether was obtained in 99% purity from TCI; trithyleneglycol monomethyl ether was obtained in >97% purity from Sigma-Aldrich. Alkylene oxides were purchased from TCI (EDD and ETD in >95%, EHD in >80% purity). (3-Glycidoxypropyl)bis(trimethylsiloxy)methylsilane was obtained in 97% purity from Gelest. TBAB was obtained in >98% purity from Alfa Aesar. TIBAL was obtained as a 1.1 M solution in toluene from Acros Organics. The AATCC test kit and blotting paper were purchased from SDL Atlas. All remaining chemicals were purchased from Acros Organics, Fisher Scientific, Roth, Sigma-Aldrich, TCI, VWR, or Deutero GmbH. All compounds were used as received.

Instrumentation

^{1}H NMR (300 or 400 MHz), ^{13}C NMR (75 MHz) and ^{19}F NMR (282 MHz) spectra were recorded on a Bruker Avance III HD 300 (5 mm BBFO-Probe with z-Gradient and ATM). ^{1}H NMR and ^{13}C NMR spectra were referenced internally with the proton signal of the deuterated solvent. ^{19}F NMR spectra were not referenced. Size exclusion chromatography (SEC) was carried out either in tetrahydrofurane (THF) at 35 °C with a flow rate of 1 mL/min on an Agilent 1100 series (Agilent Technologies, Santa Clara, CA, USA), SDV columns of 100/1000/10000 Å porosity (Polymer Standards Service (PSS), Mainz, Germany) or in *N*,*N*-dimethylformamide (DMF) containing 1 g/mL lithium bromide at 50 °C with a flow rate of 1 mL/min with HEMA columns with 300/100/40 Å porosity. Detection was done with an Agilent G1362A RID as refractive index detector. Toluene was used as an internal standard and PEG standards from PSS were used for calibration. MALDI-ToF measurements were performed on a Bruker Autoflex maX. Samples were prepared with Dithranol (DIT) and either sodium or silver trifluoroacetate. DSC measurements were performed using a DSC250 from TA instruments (New Castle, DE, USA) and the TRIOS software.

Synthesis of oligoethylene chain monomers

The synthesis of ME_3GE and ME_2GE was adapted from literature.[1] Epichlorohydrine (1 eq, 0.32 mol, 29.5 g) and sodium hydroxide (1.5 eq, 0.48 mol, 19.1 g) were combined in a round bottom flask and cooled with a water bath. Triethylene glycol monomethyl ether (1 eq, 0.32 mol, 52.3 g) or diethylene glycol monomethyl ether (1 eq, 0.32 mol, 28.5 g) was added dropwise and stirred for 2 h. The reaction mixture

was cooled to precipitate salts, filtrated under reduced pressure and dried with magnesium sulfate. The product was isolated via distillation in typical yields of 80-90% (ME_3GE 0.02 mbar, T_{head} = 102 °C; ME_2GE 0.03 mbar, T_{head} = 80 °C). Characterization data is given in literature.[1]

AATCC 118 test method

Table S1: Test substances of the AATCC 118 test method.[2,3]

Grade	Hydrocarbon	Surface tension
0	None	-
1	Kaydol (mineral oil)	31.5
2	65:35 Kaydol: n-hexadecane (by volume)	
3	n-hexadecane	27.3
4	n-tetradecane	26.4
5	n-dodecane	24.7
6	n-decane	23.5
7	n-octane	21.4
8	n-heptane	19.8

Supplementary characterisation data

Table S2: Characterisation data of polymers.

Polymer[th]	M_n[th] (g mol^{-1})	M_n[a] (g mol^{-1})	$Đ$[a]	T_m[c] T_g[c] (°C)	ΔH_m[c] (J g^{-1})	Θ (cellu-lose) (°)	Θ (glass) (°)
$PPMVEGLY_8$	2000	2090	1.09	/ -54	/	-	-
$PPMVEGLY_{10}$	2530	2470	1.12	-	-	-	-
$PPMVEGLY_{30}$	7280	5320	1.12	-	-	-	-
$PPPVEGLY_8$	2800	2700	1.14	/ -54	/	wetting	63 ± 1
$PPPVEGLY_{10}$	3480	2640	1.09	-	-	-	-
$PPPVEGLY_{30}$	10280	7740	1.14	-	-	-	-
$PPPVEGLY_{50}$	17080	9730	1.24	-	-	-	-
$PPPVEGLY_{70}$	23880	11740	1.26	-	-	-	-

Table S2: Characterisation data of polymers (continued).

Polymer[th]	M_n[th] (g mol^{-1})	M_n[a] (g mol^{-1})	$Đ$[a]	T_m[c] T_g[c] (°C)	ΔH_m[c] (J g^{-1})	Θ (cellu-lose) (°)	Θ (glass) (°)
$PPPVEGLY_{90}$	30680	11510	1.50	-	-	-	-
$PPPVEGLY_{120}$	40880	n.a.[b]	n.a.[b]	-48 /	/	wetting	63 ± 6
$PEDD_{10}$	1920	3640	1.15	22 /	68	wetting	81 ± 6
$PEDD_{30}$	5610	5960	1.22	27 /	70	wetting	87 ± 2
$PETD_{10}$	2200	3490	1.16	44 /	96	88 ± 3	103 ± 1
$PETD_{30}$	6450	6420	1.23	44 /	86	100 ± 5	104 ±1
$PEHD_{10}$	2490	3030	1.17	40 /	96	105 ± 7	112 ± 2
$PEHD_{30}$	7290	7010	1.24	54 /	112	122 ± 2	103 ± 1
P[(3-glycidoxy-propyl)bis(tri-methylsiloxy)-methylsilane]$_{10}$	3350	3370	1.08	-	-	wetting	-
P($PPVEGLY_{16}$-*co*-GMA_4)[d]	6090	5150	1.20	-	-	-	-

[a]Determined by SEC (THF, PEG calibration, RI detector) [b]Insufficient solubility for SEC measurement. [c]Determined by DSC: second heating curve, 10 °C min^{-1}, 5 min isothermal between steps. [d]Theoretical composition: $PPVEGLY_{0.80}$-*co*-$GMA_{0.20}$; experimental composition determined via ^{1}H NMR spectroscopy (C*D*Cl$_3$, 300 MHz): $PPVEGLY_{0.77}$-*co*-$GMA_{0.23}$.

Representative characterisation of monomers

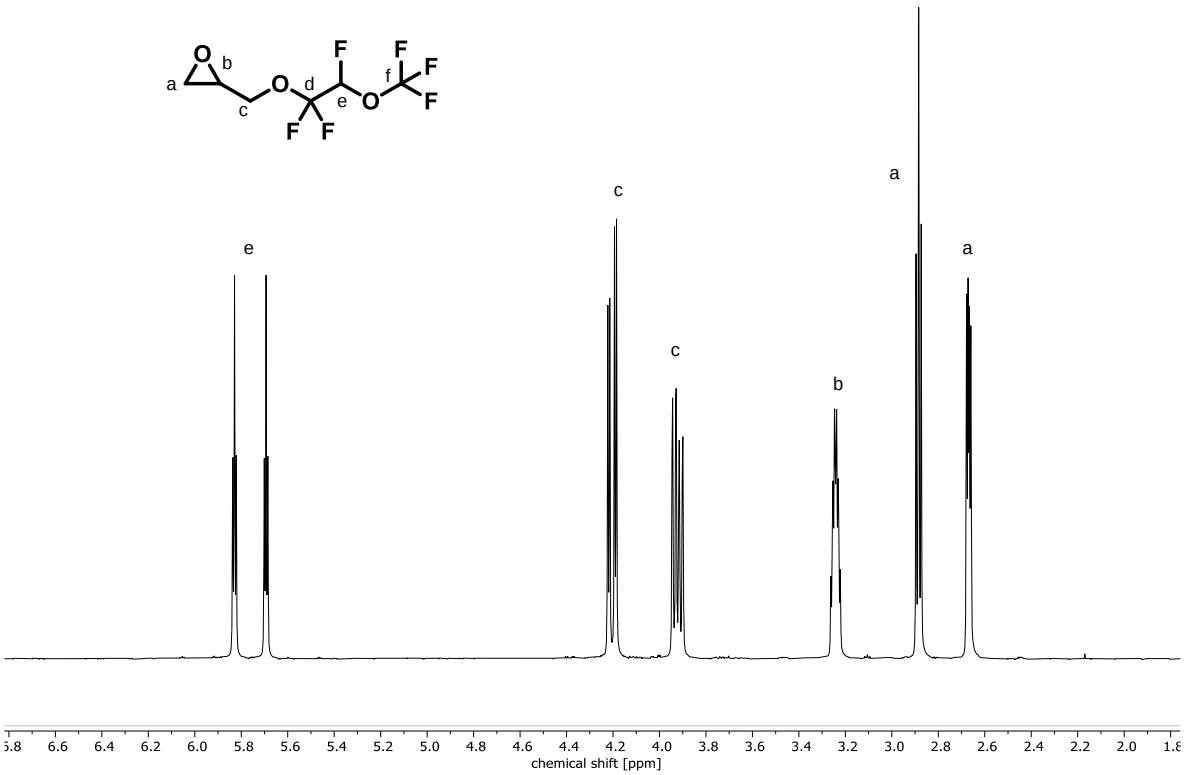

Figure S1: ^{1}H NMR spectrum ($CDCl_3$, 300 MHz) of PMVEGLY.

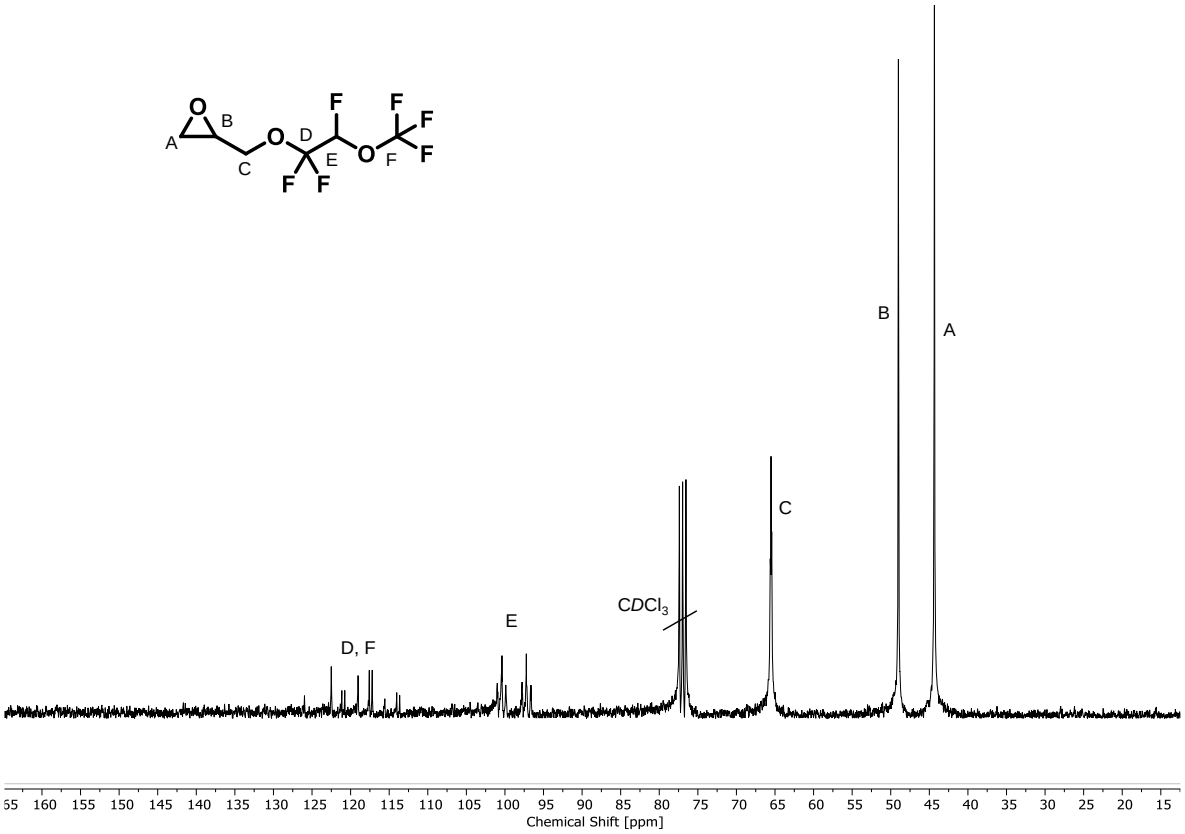

Figure S2: ^{13}C NMR spectrum ($CDCl_3$, 75 MHz) of PMVEGLY.

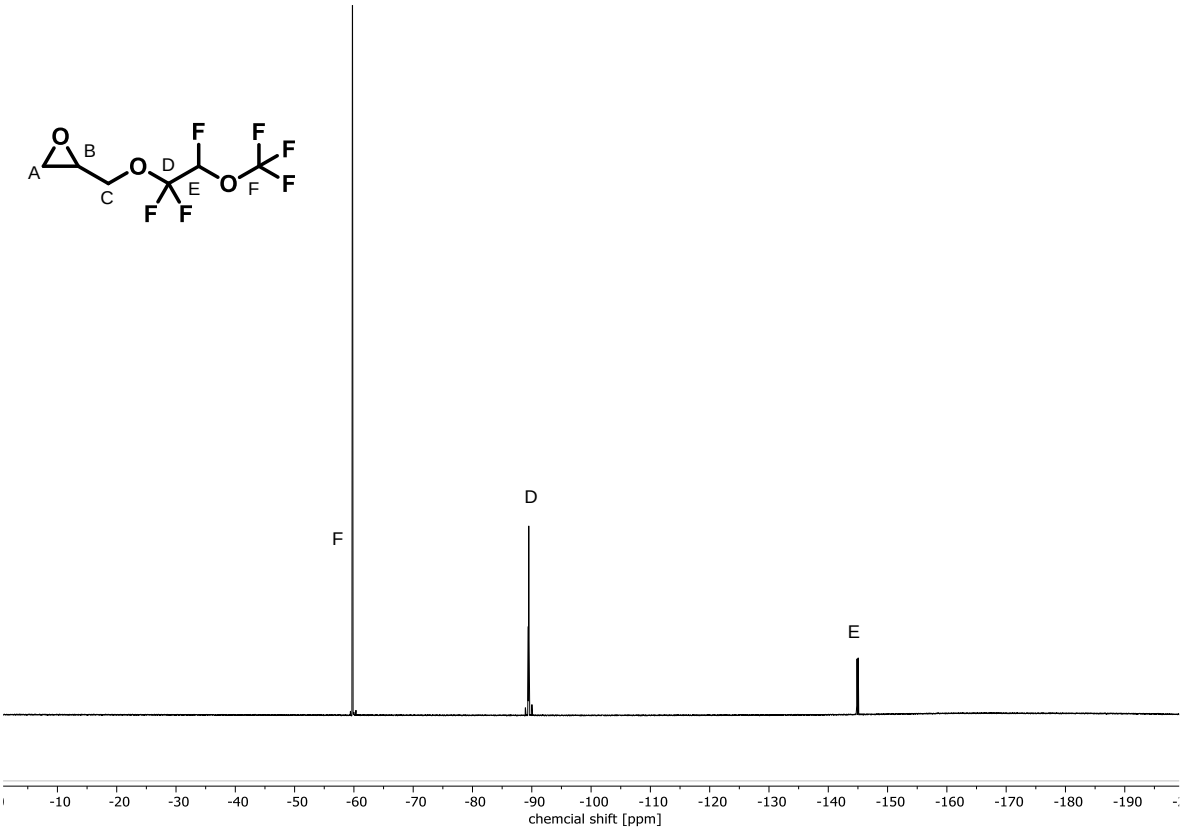

Figure S3: ^{19}F NMR spectrum ($CDCl_3$, 282 MHz) of PMVEGLY.

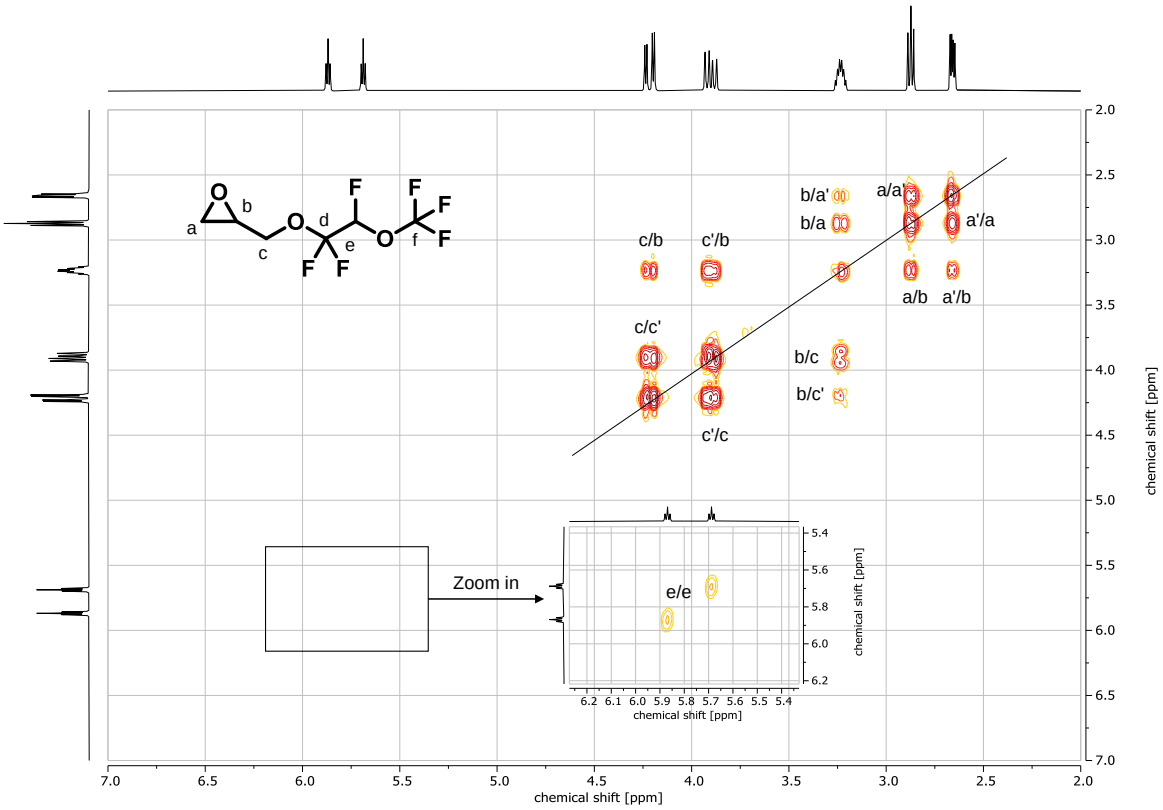

Figure S4: ^{1}H, ^{1}H COSY NMR spectrum ($CDCl_3$, 300 MHz) of PMVEGLY.

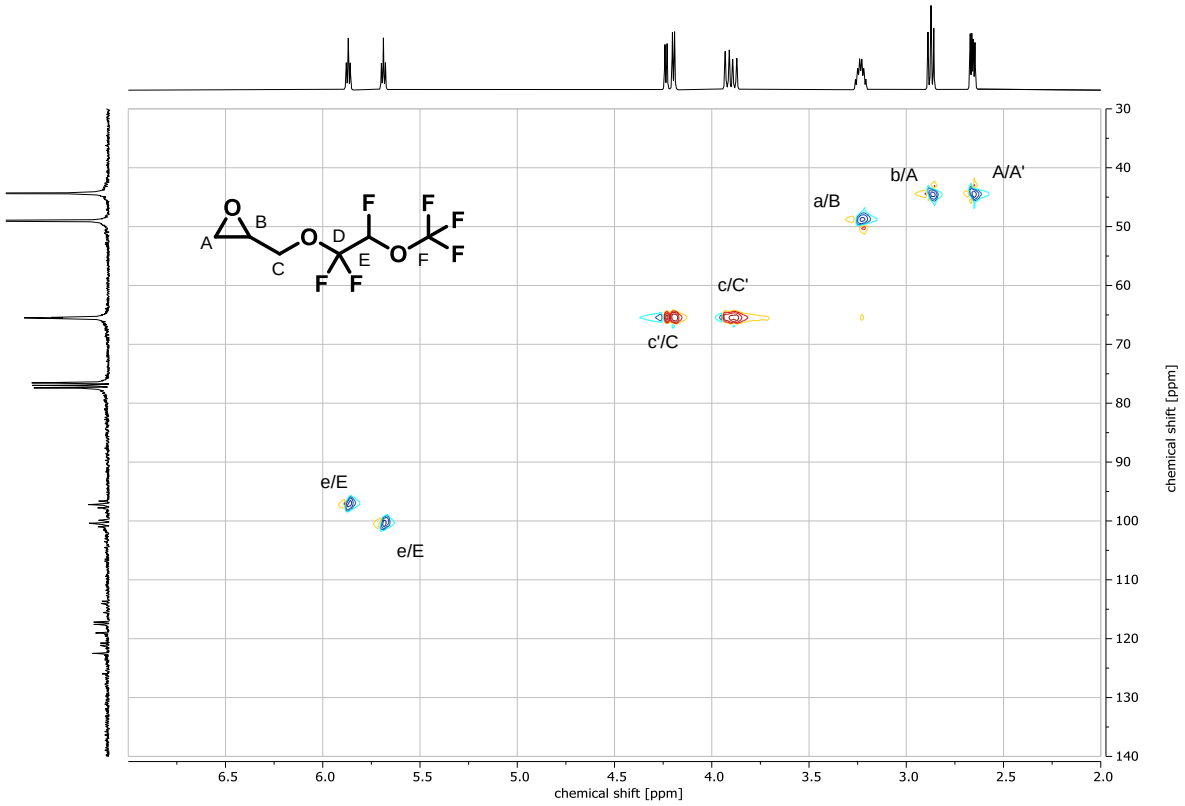

Figure S5: ^{1}H, ^{13}C HSQC NMR spectrum ($CDCl_3$) of PMVEGLY.

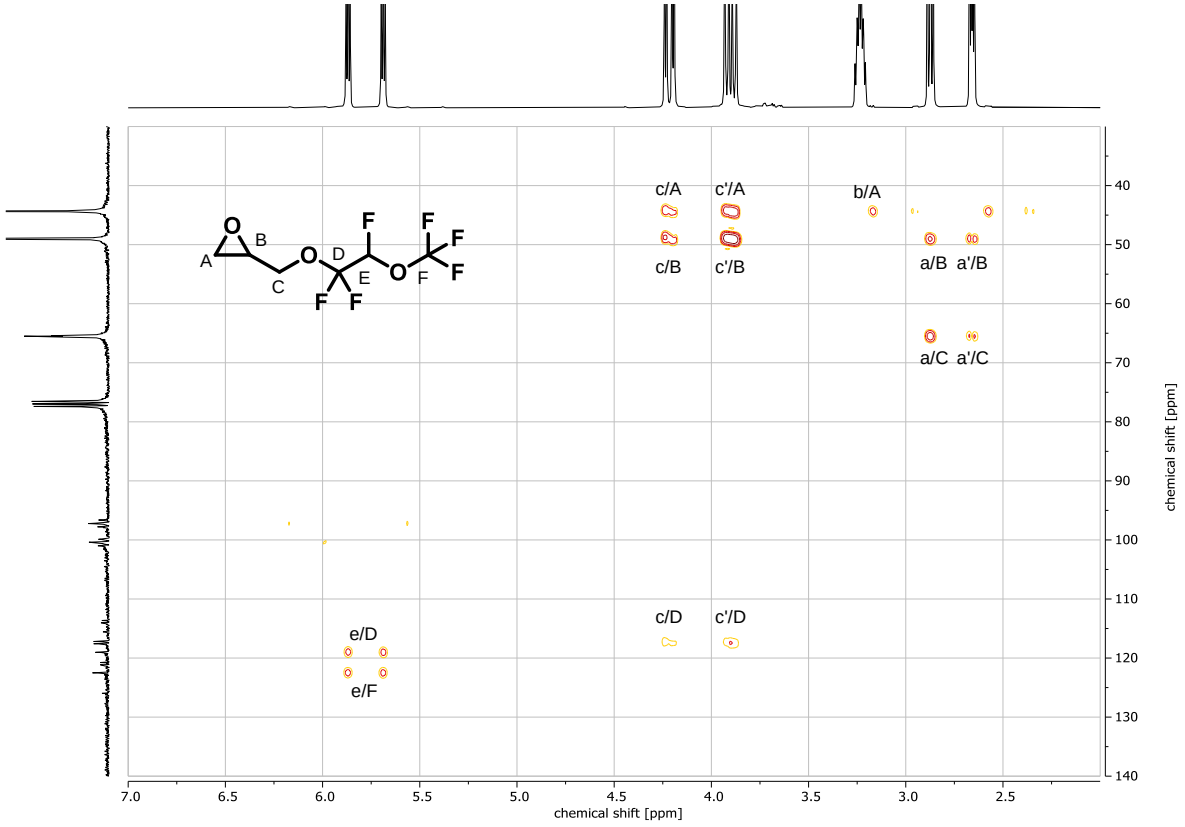

Figure S6: ^{1}H, ^{13}C HMBC NMR spectrum ($CDCl_3$) of PMVEGLY.

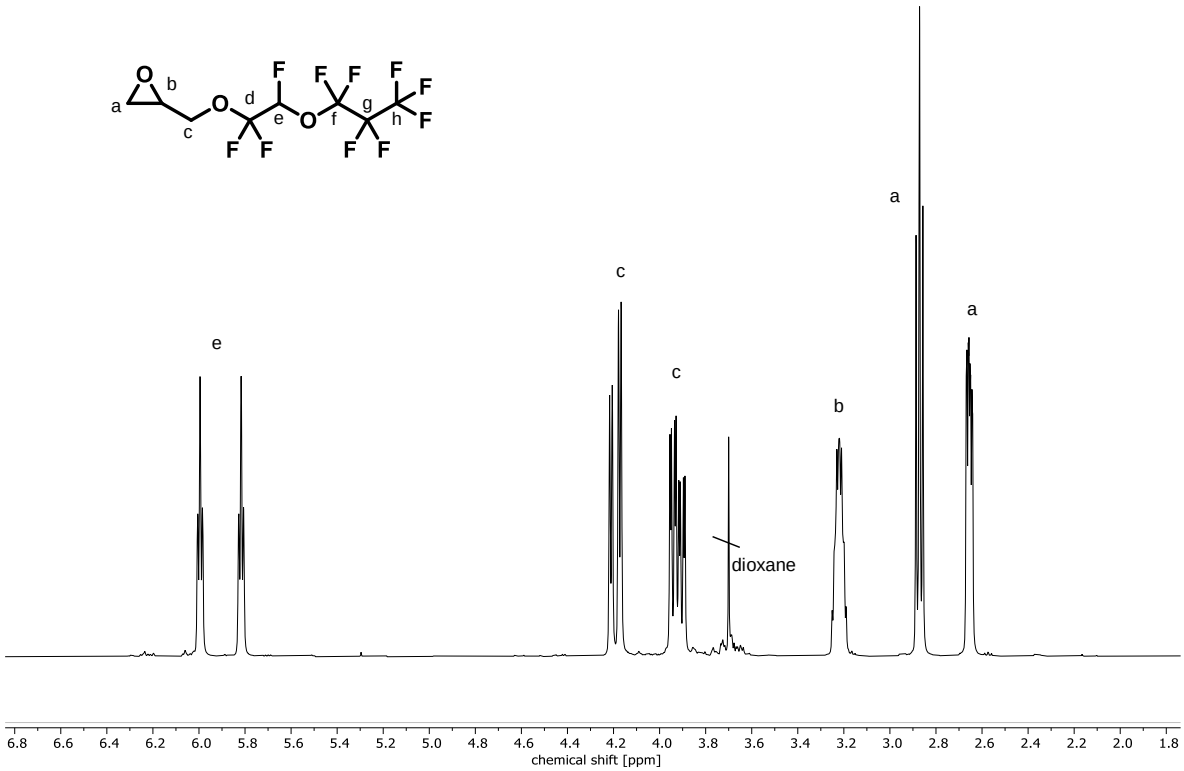

Figure S7: ^{1}H NMR spectrum ($CDCl_3$, 300 MHz) of PPVEGLY.

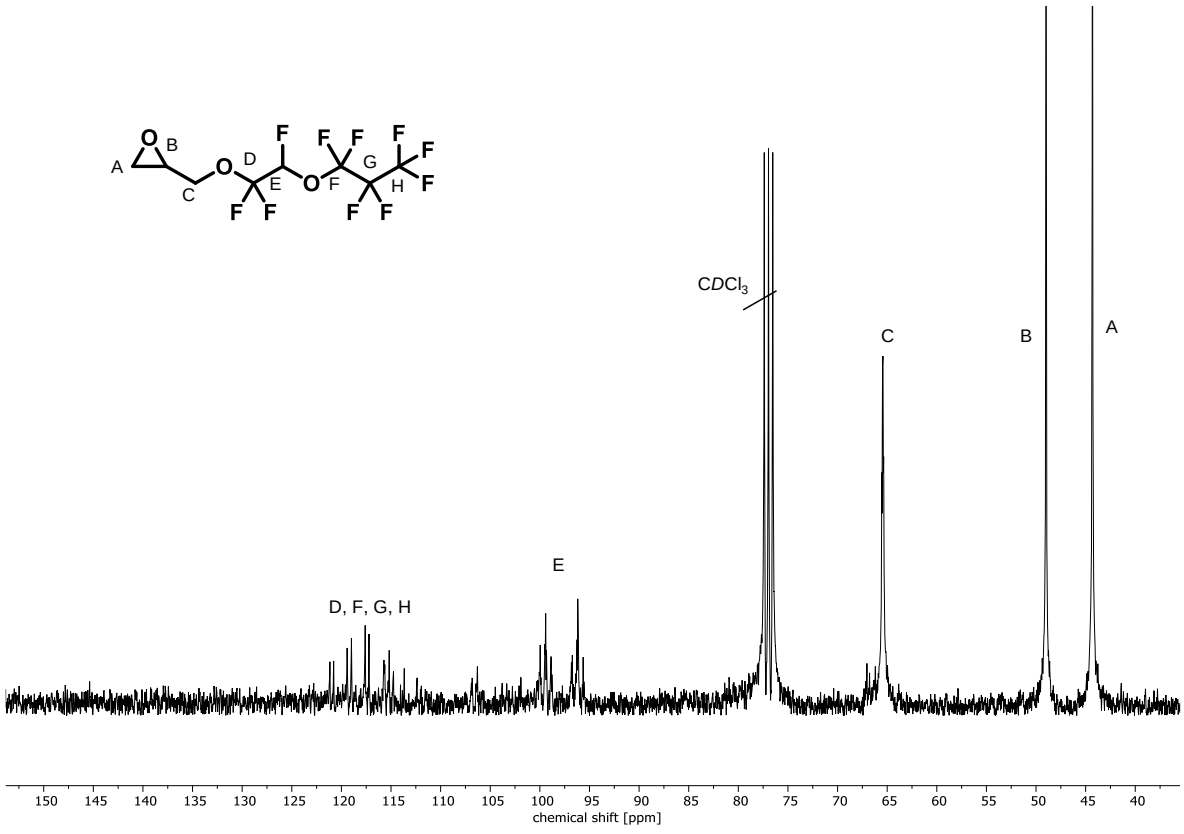

Figure S8: ^{13}C NMR spectrum ($CDCl_3$, 75 MHz) of PPVEGLY.

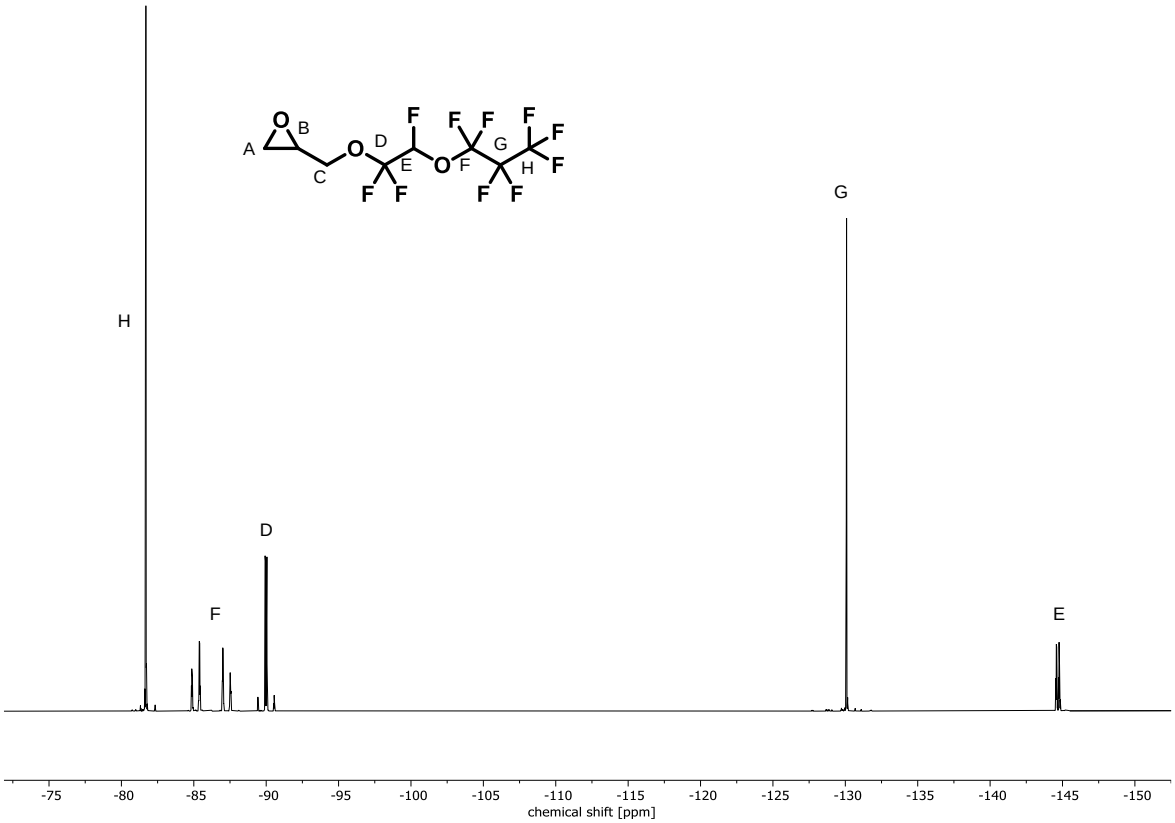

Figure S9: ^{19}F NMR spectrum ($CDCl_3$, 282 MHz) of PPVEGLY.

Representative characterisation of polymers

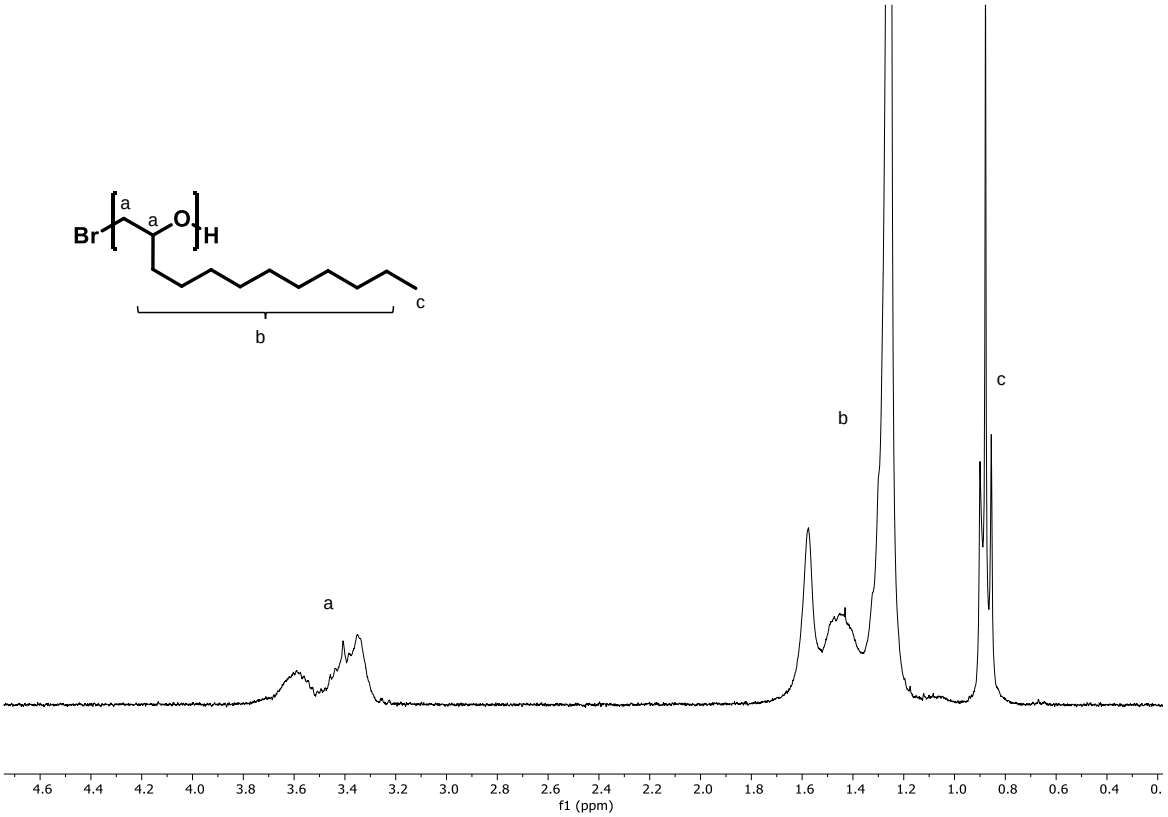

Figure S10: ^{1}H NMR spectrum ($CDCl_3$, 300 MHz) of $PEDD_{10}$ (δ [ppm] = 3.59–3.35 (m, a), 1.57–1.26 (m, b), 0.88 (t, c)).

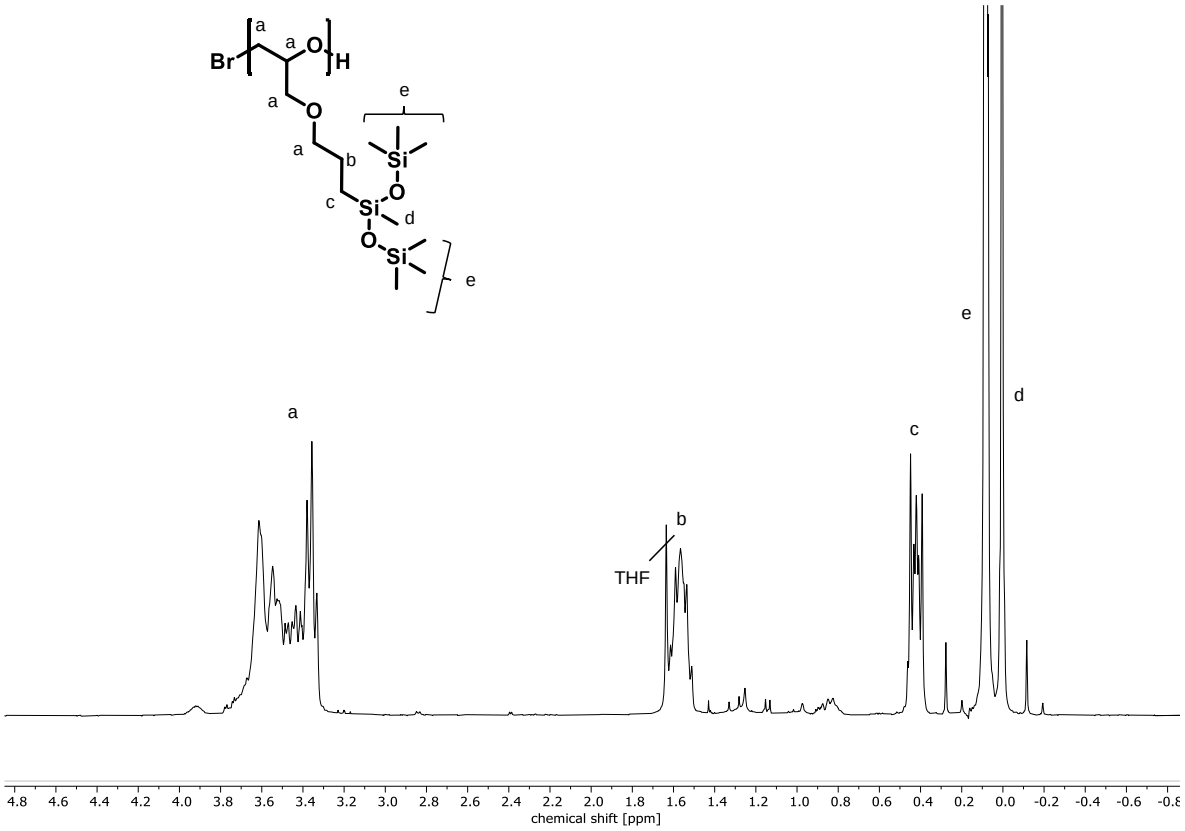

Figure S11: ^{1}H NMR spectrum ($CDCl_3$, 300 MHz) of P[(3-glycidoxypropyl)bis(trimethyl-siloxy)methylsilane]$_{10}$ (δ [ppm] = 3.61–3.33 (m, a), 1.57 (td, b), 0.43 (dt, c), 0.08 (s, e), 0.00 (s, d)).

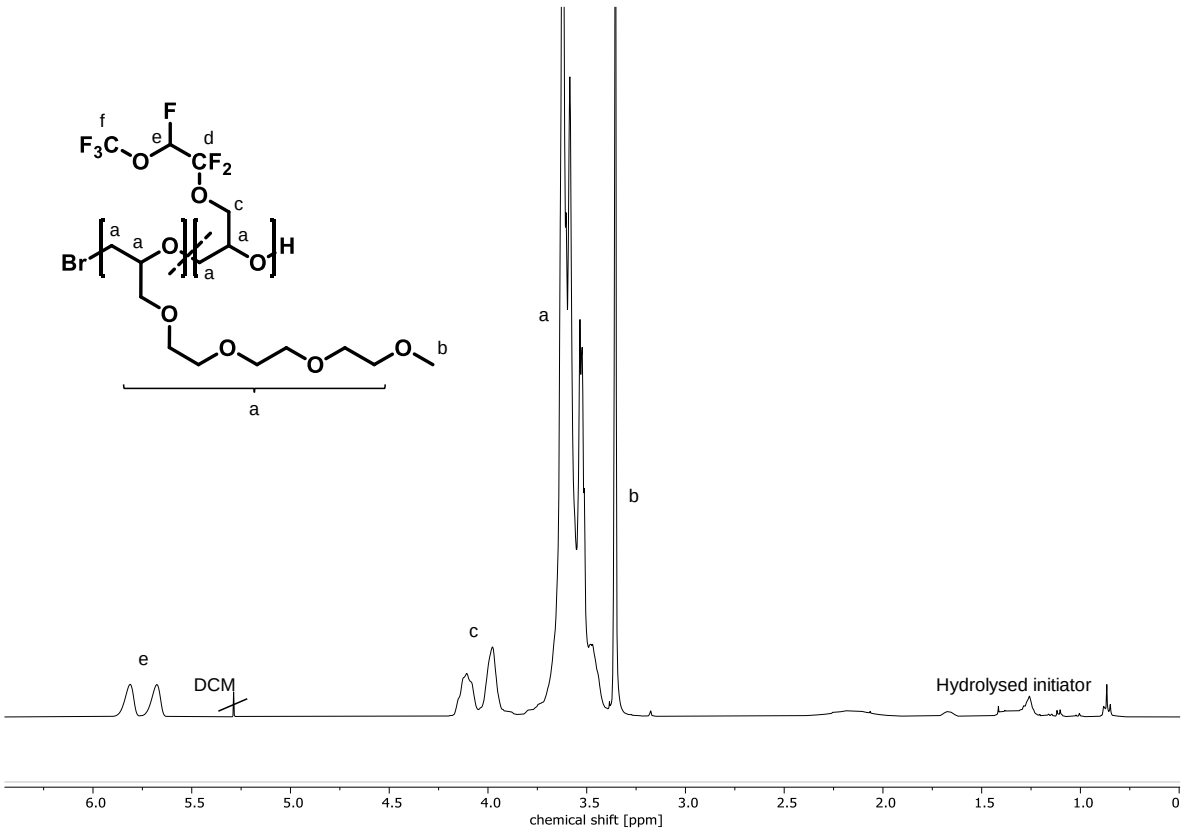

Figure S12: ^{1}H NMR spectrum ($CDCl_3$, 300 MHz) of S15.

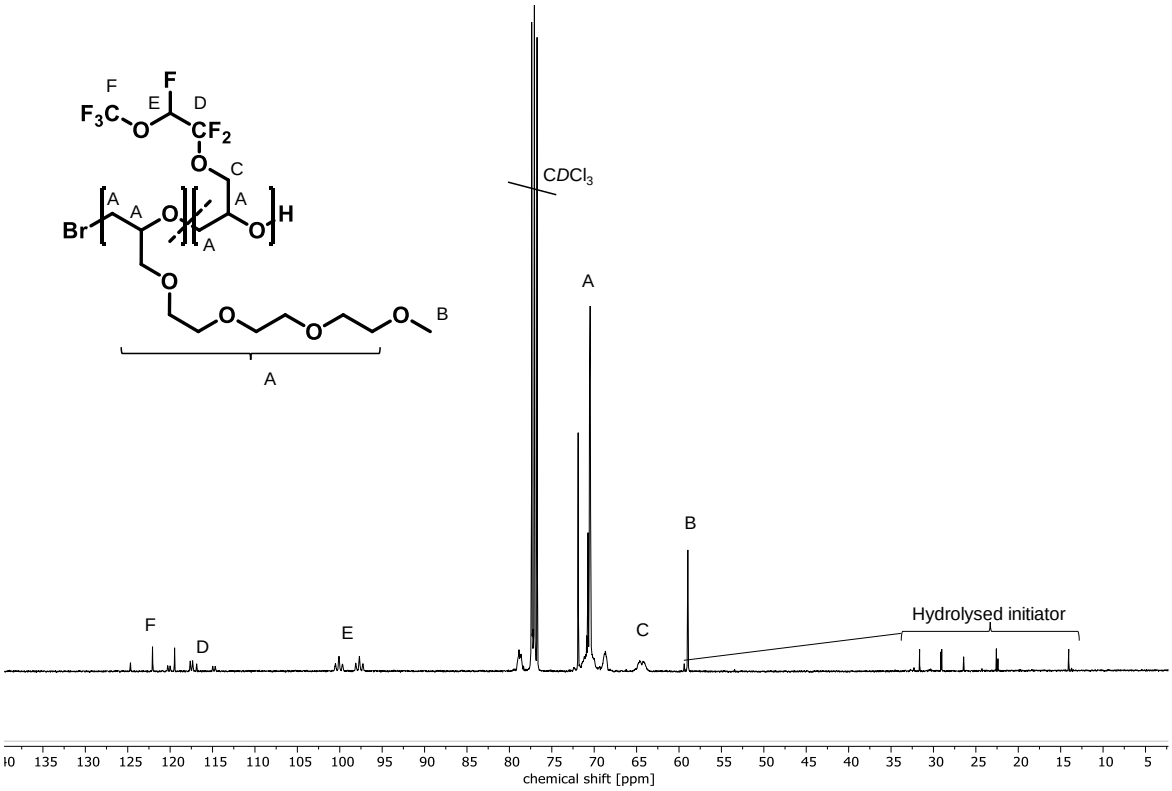

Figure S13: ^{13}C NMR spectrum ($CDCl_3$, 75 MHz) of S15.

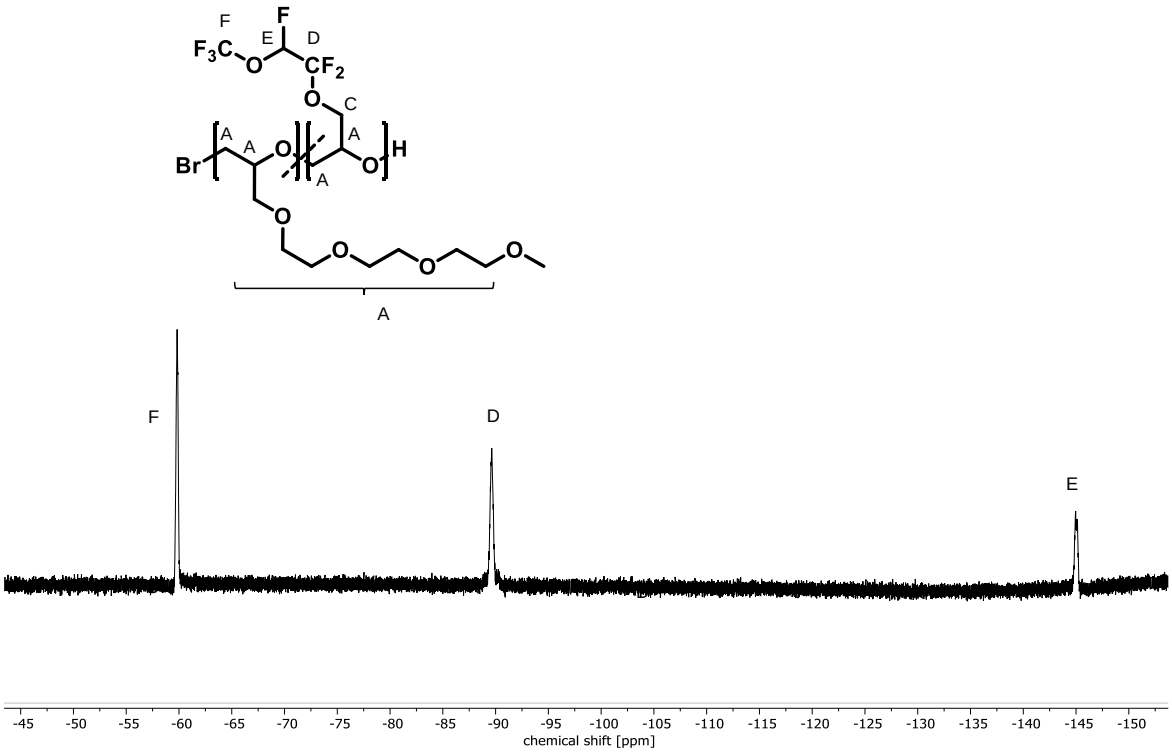

Figure S14: ^{19}F NMR spectrum ($CDCl_3$, 282 MHz) of S15.

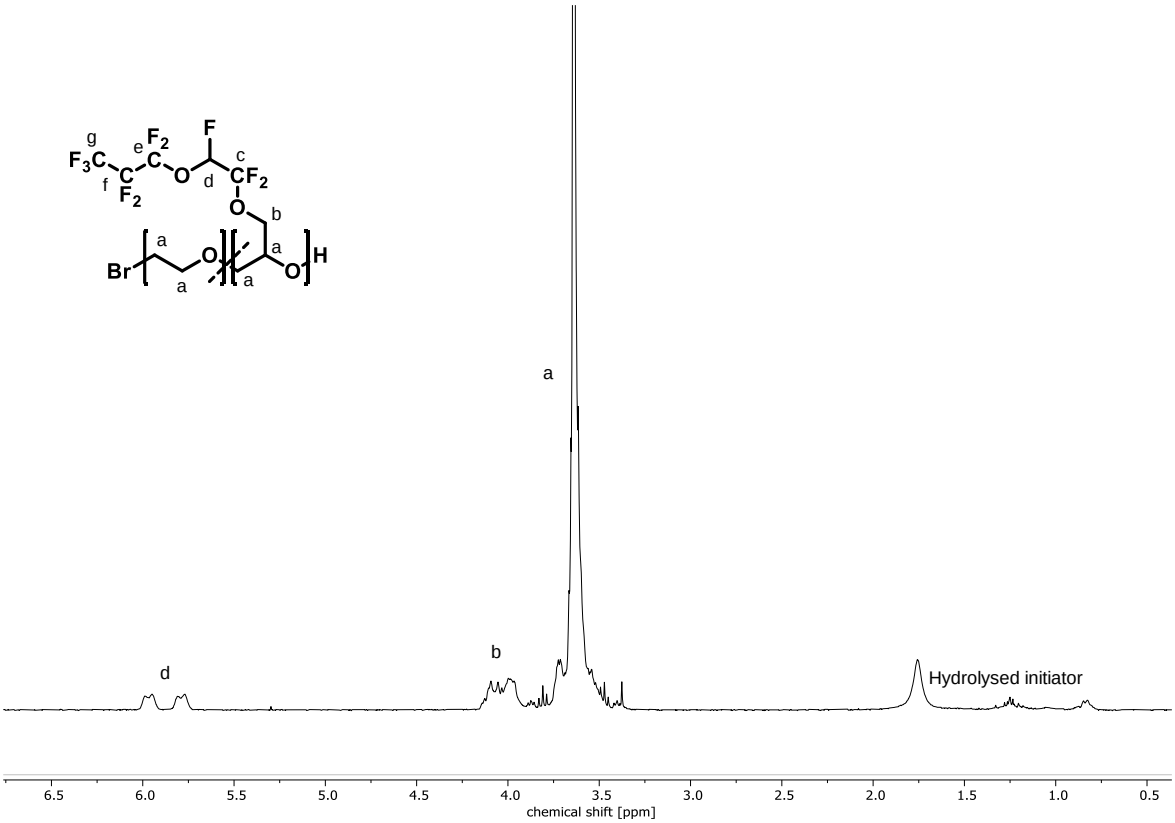

Figure S15: ^{1}H NMR spectrum ($CDCl_3$, 300 MHz) of S25.

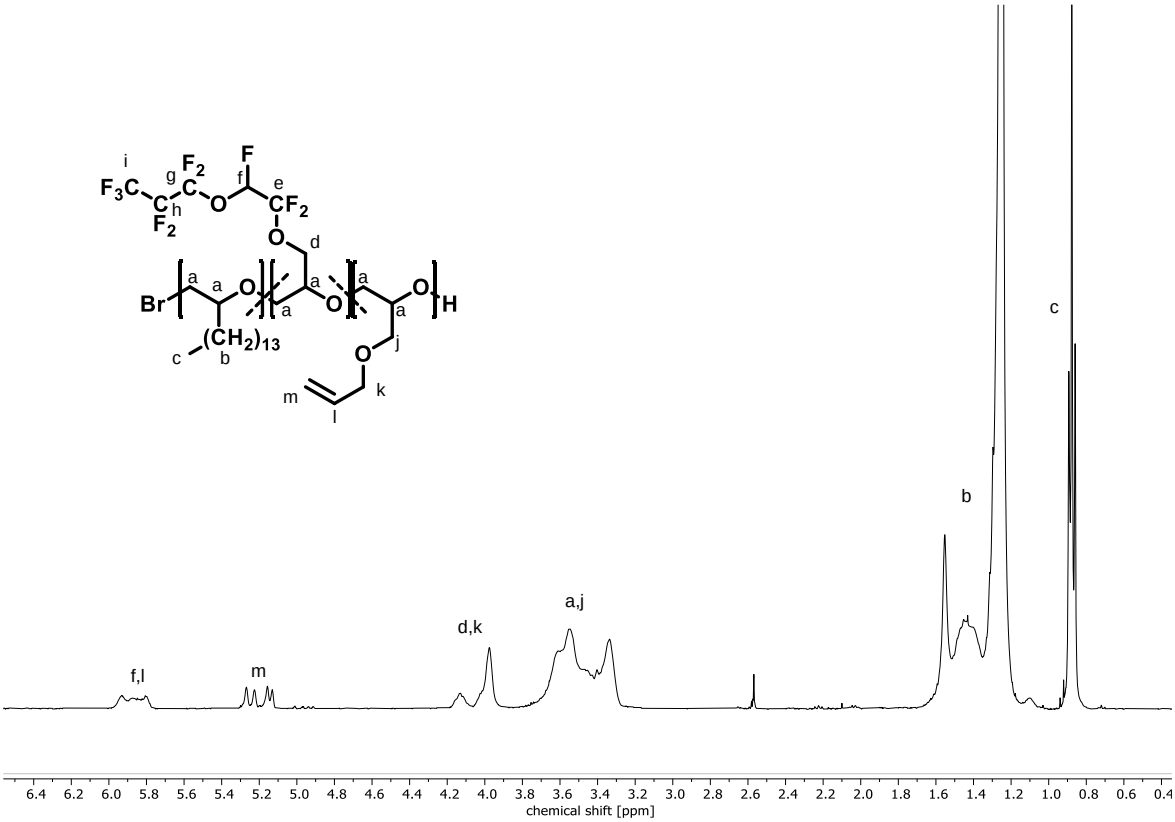

Figure S16: ^{1}H NMR spectrum ($CDCl_3$, 300 MHz) of C14.

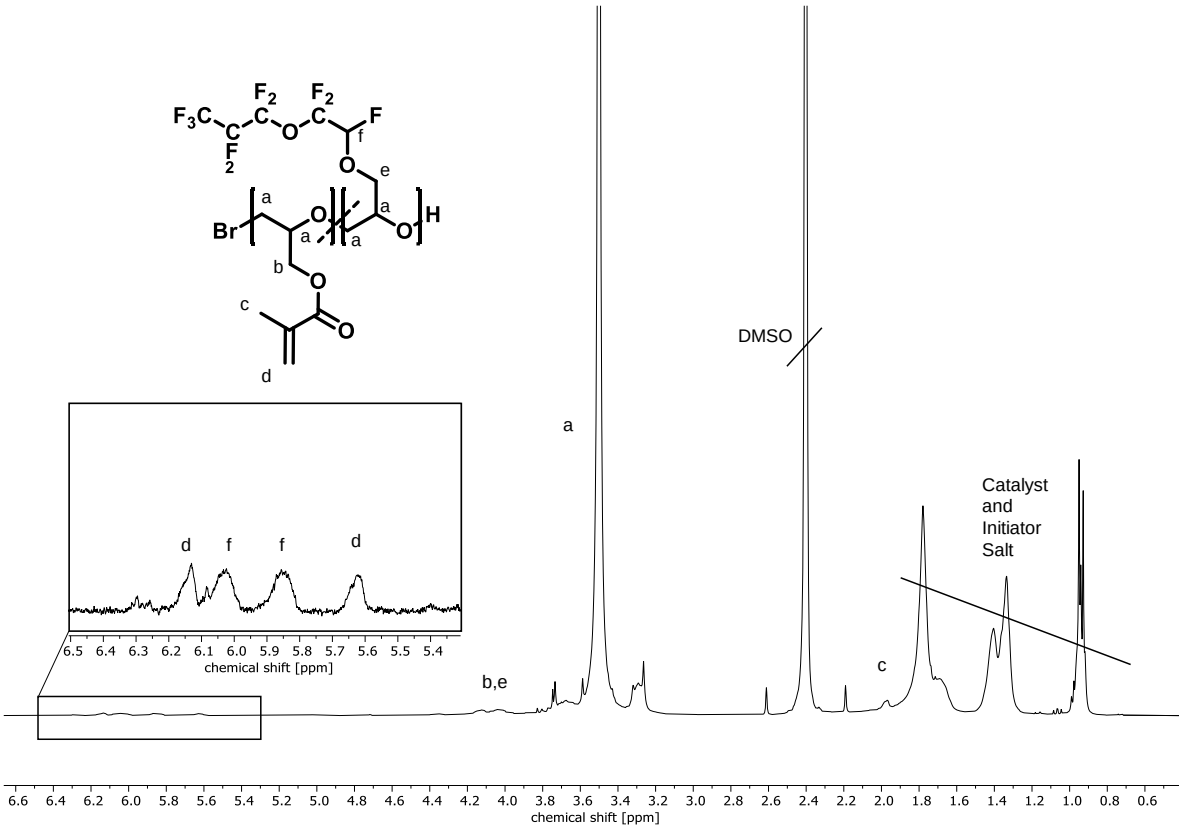

Figure S17: ^{1}H NMR spectrum ($CDCl_3$, 300 MHz) of P(GMA_4-co-$PPVEGLY_{16}$).

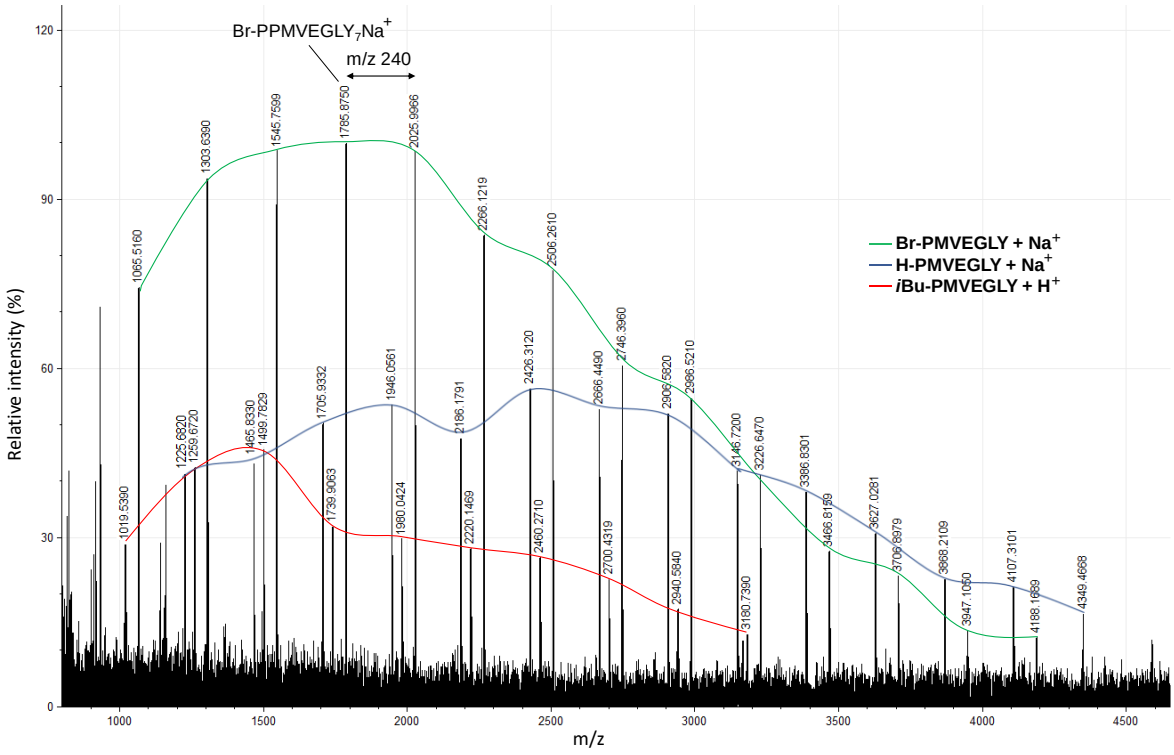

Figure S18: MALDI-ToF spectrum of $PPMVEGLY_8$.

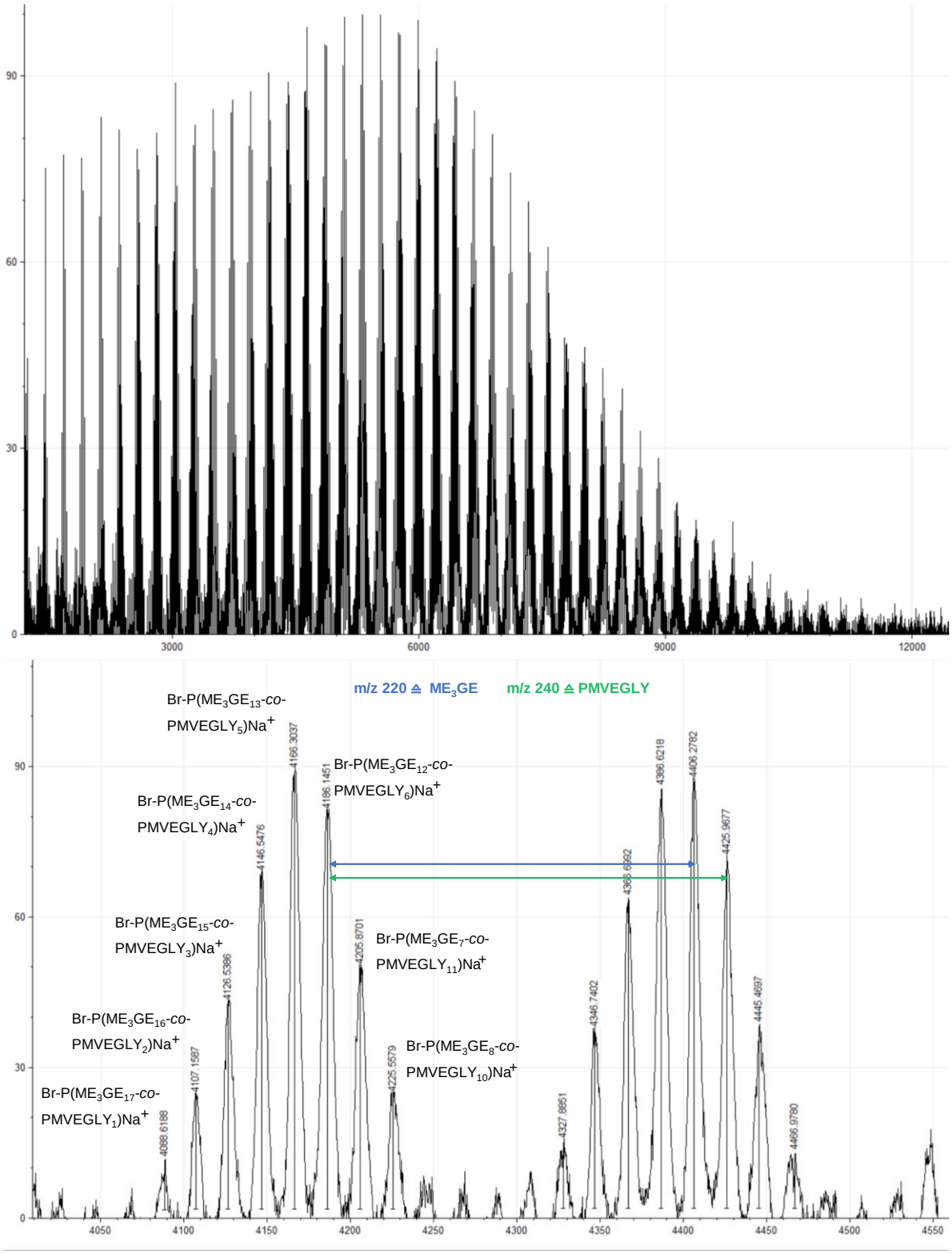

Figure S19: MALDI-ToF spectrum of S16 (top) and zoom in (bottom).

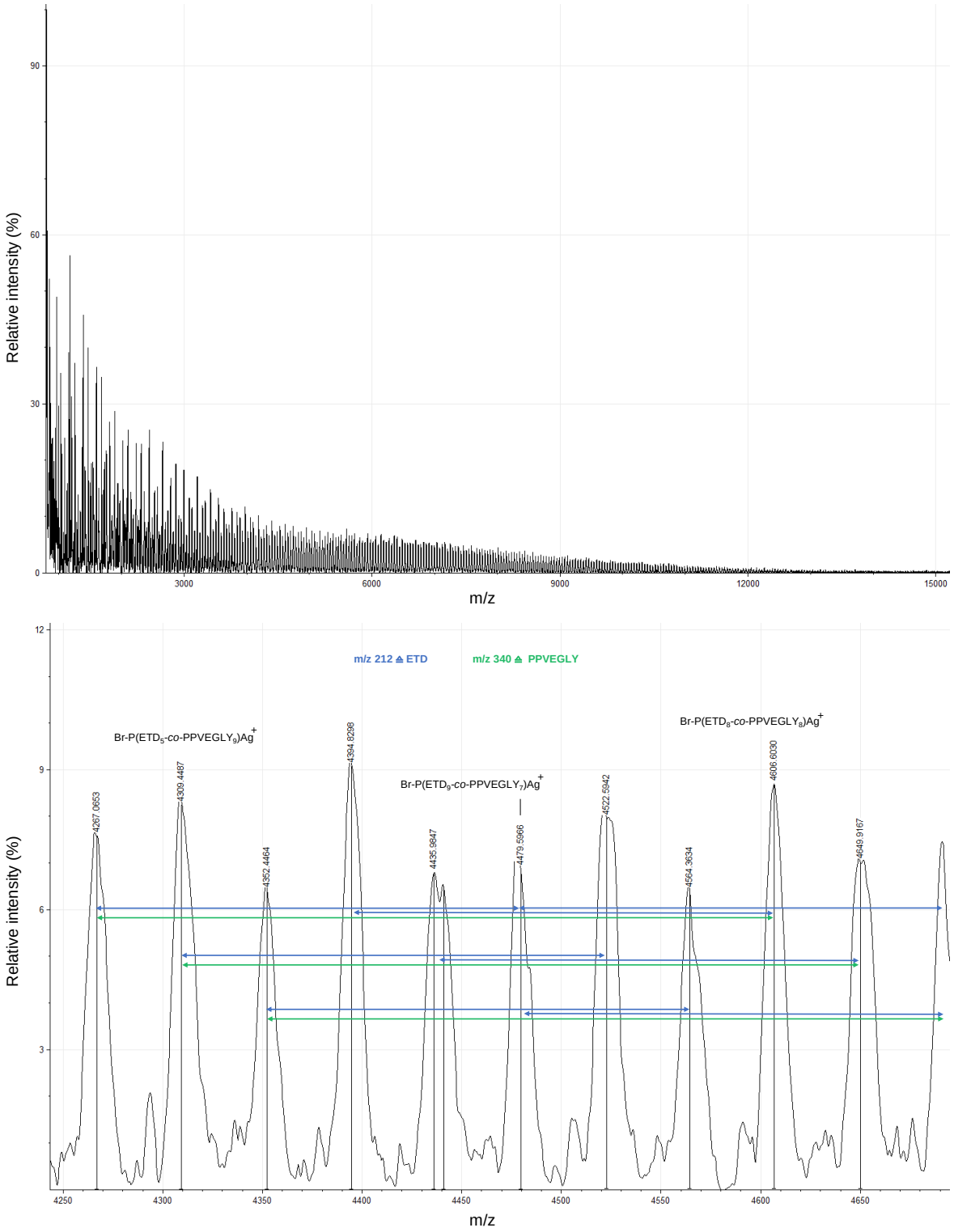

Figure S20: MALDI-ToF spectrum of C2 (top) and zoom in (bottom). In consequence of the low resolution and broad peaks, each of the peaks can be assigned to two polymer species: e.g. m/z of 4394.8298 can be assigned to Br-P(ETD$_7$-co-PPVEGLY$_8$)Ag$^+$ and Br-P(ETD$_{15}$-co-PPVEGLY$_3$)Ag$^+$.

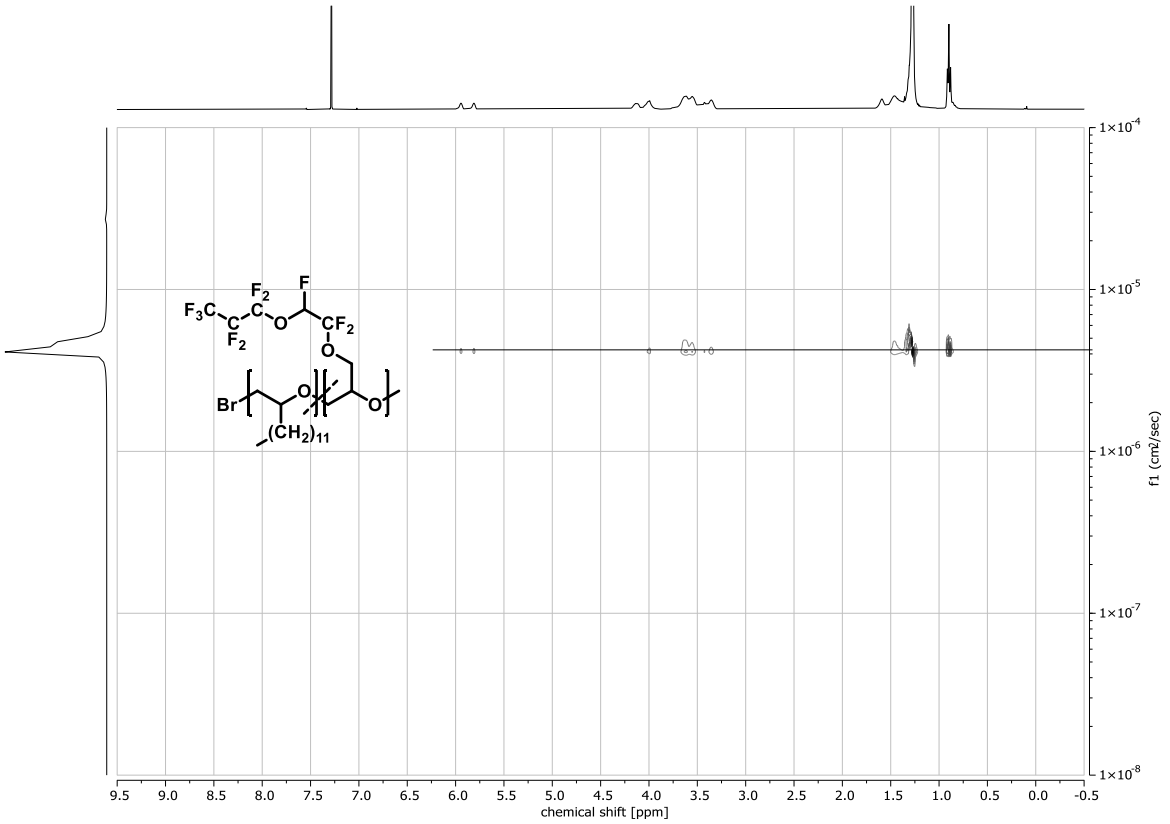

Figure S21: ^{1}H DOSY NMR ($CDCl_3$, 400 MHz) of C2.

^{1}H NMR spectra of degradation studies

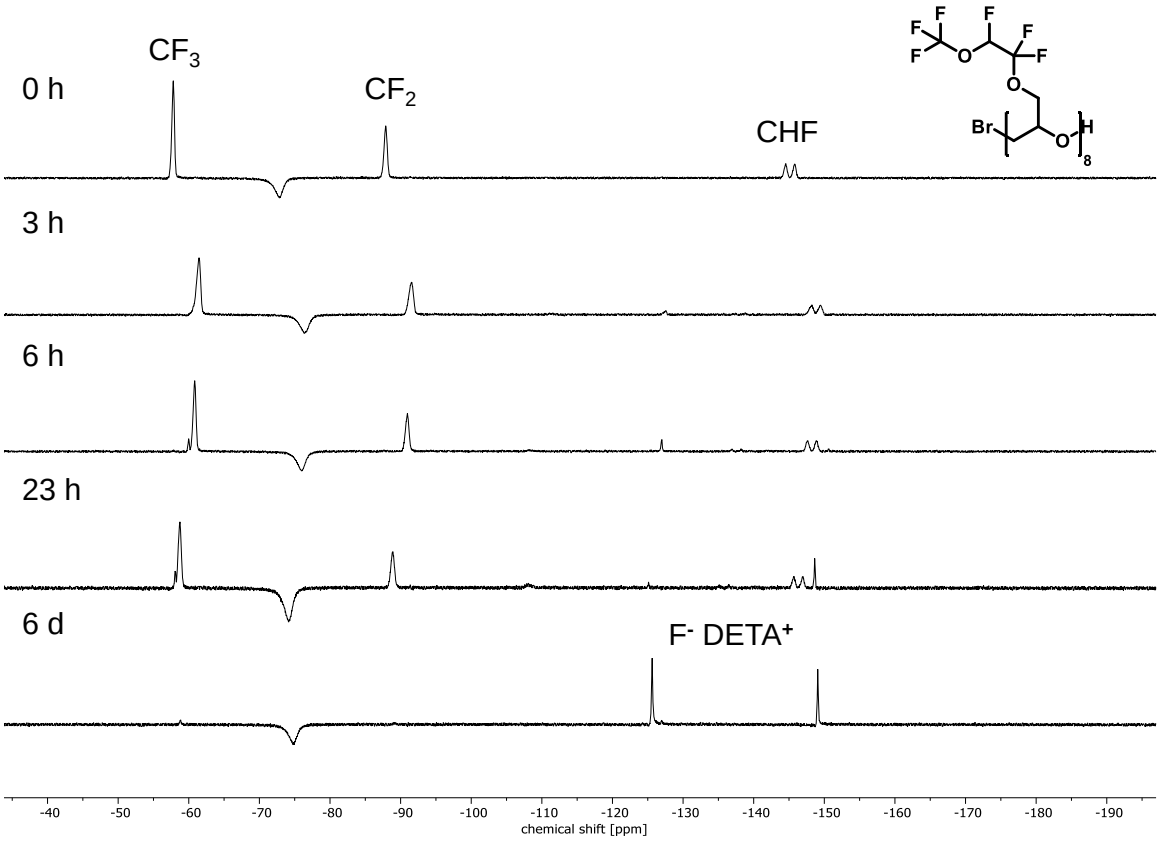

Figure S22: ^{19}F NMR spectra (DMSO-d_6, 41 MHz) of PMVEGLY$_8$ degradation study with diethylenetriamine. Reaction set-up: 0.12 g polymer, 0.8 mL d_6-DMSO, 0.2 mL diethylenetriamine (DETA), 120 °C. CF_3, CF_2 and CHF signals are decreasing with advancing time, while signals of the generated fluoride anions are evolving. The observation of two species is presumably the result of the different interactions with the primary and the secondary amines of DETA.

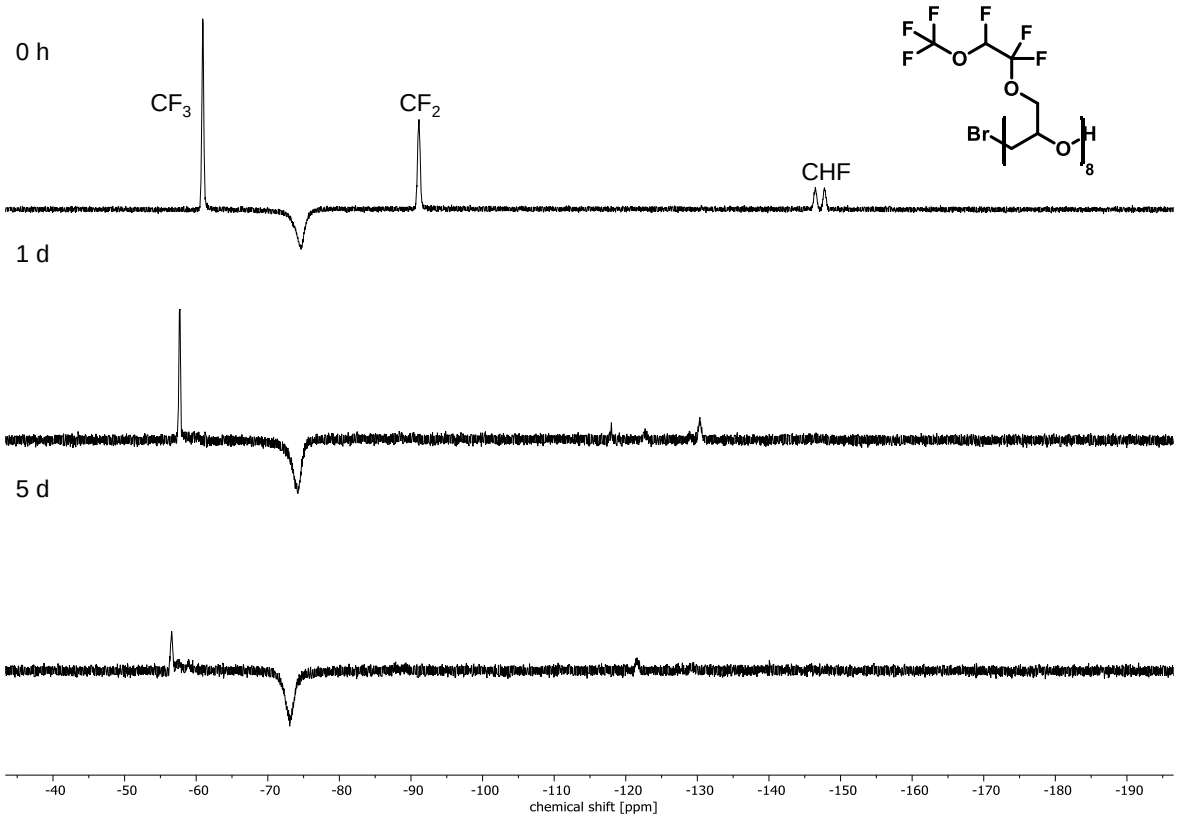

Figure S23: ^{19}F NMR spectra (DMSO-d_6, 41 MHz) of PMVEGLY$_8$ degradation study with potassium hydroxide. The signals of the fluoride anions are comparably weak due to precipitation of the KF salt.

Dynamic Surface tension measurements

The listed data were obtained using the bubble pressure method.

Table S3: Dynamic surface tensions of copolymers S1 to S31.

S1		S2		S3		S4	
t	γ_{dyn}	t	γ_{dyn}	t	γ_{dyn}	t	γ_{dyn}
0.029	67.4	0.029	72.5	0.030	70.4	0.029	70.2
0.038	65.9	0.038	72.7	0.038	69.4	0.038	69.0
0.049	64.1	0.049	72.4	0.049	67.9	0.049	66.9
0.064	62.4	0.063	72.3	0.064	66.4	0.064	65.7
0.084	60.6	0.084	72.5	0.085	64.8	0.086	64.0
0.112	58.8	0.112	72.1	0.112	62.8	0.112	62.5
0.144	57.4	0.145	72.3	0.146	61.4	0.147	60.7
0.189	55.5	0.188	72.2	0.189	59.9	0.188	59.4
0.244	53.8	0.246	72.1	0.245	58.1	0.243	58.1
0.303	52.5	0.313	72.2	0.303	56.6	0.303	56.9
0.394	50.8	0.394	72.1	0.400	54.8	0.400	55.5
0.518	49.0	0.516	71.7	0.517	52.9	0.514	54.2
0.669	47.2	0.679	71.5	0.660	51.1	0.675	52.8
0.855	45.4	0.861	71.4	0.876	48.7	0.880	51.0
1.064	43.8	1.066	70.9	1.077	47.1	1.010	50.1
1.380	42.2	1.400	70.8	1.376	45.2	1.315	48.5
1.827	40.3	1.821	70.5	1.804	43.0	1.719	47.0
2.408	38.9	2.198	70.3	2.198	41.6	2.433	44.8
3.079	37.3	3.270	69.4	3.019	39.6	3.140	43.1
4.214	35.6	4.057	68.5	3.947	37.5	4.147	41.2
5.378	34.4	5.512	67.3	5.363	35.7	5.292	39.9
6.824	33.3	7.013	65.5	6.928	34.3	6.859	38.3
9.427	32.0	9.038	64.1	8.819	33.2	9.203	36.8
11.956	30.9	11.484	62.5	12.521	31.4	11.592	36.1
14.981	30.2	16.108	60.5	15.821	30.7	15.753	34.7
22.561	28.7	19.562	59.5	20.085	29.6	19.728	33.8
23.899	28.8	27.306	56.7	26.324	28.9	26.921	32.6
32.912	27.3	32.659	55.4	35.713	27.7	35.190	31.6
50.214	25.8	45.618	53.6	42.167	27.3	45.527	30.9
62.552	25.9	57.026	52.0	60.808	26.5	54.936	30.6

Table S3 continued: Dynamic surface tensions of copolymers S1 to S31.

S5		S6		S7		S8	
t	γ_{dyn}	t	γ_{dyn}	t	γ_{dyn}	t	γ_{dyn}
0.029	66.3	0.029	67.7	0.032	76.6	0.031	69.8
0.038	64.7	0.038	66.3	0.038	71.7	0.038	64.8
0.049	62.6	0.049	64.4	0.049	66.4	0.049	60.6
0.064	60.8	0.063	62.5	0.064	61.8	0.064	57.0
0.084	59.5	0.084	60.8	0.086	57.5	0.085	53.9
0.112	57.9	0.112	59.3	0.112	53.7	0.113	50.9
0.146	57.0	0.146	58.0	0.144	51.0	0.143	49.3
0.190	55.8	0.189	57.1	0.190	48.6	0.188	47.5
0.244	54.6	0.245	56.1	0.244	46.1	0.245	45.9
0.305	53.4	0.306	55.5	0.303	44.4	0.306	44.6
0.393	52.4	0.394	54.6	0.400	42.6	0.403	43.1
0.516	51.0	0.521	53.5	0.510	40.8	0.518	42.0
0.680	49.9	0.668	52.6	0.666	39.5	0.668	40.8
0.878	48.6	0.871	51.7	0.874	37.2	0.89	39.7
1.077	47.6	1.008	51.1	1.037	36.6	1.043	39.1
1.360	46.8	1.322	50.1	1.416	35.0	1.447	38.0
1.821	45.1	1.819	48.9	1.753	34.3	1.742	37.4
2.250	44.2	2.824	47.3	2.484	32.8	2.196	36.7
3.148	42.6	3.172	46.9	3.185	32.2	3.277	35.5
4.174	41.7	4.039	46.1	4.041	31.6	4.081	34.8
5.278	40.6	5.311	44.7	5.316	30.6	5.326	34.5
7.087	39.3	7.220	43.6	6.984	30.1	7.178	33.9
9.089	38.4	8.960	42.7	9.111	29.6	9.141	33.4
11.842	37.2	12.498	41.7	11.569	29.3	11.895	33.0
15.316	36.4	14.661	41.0	16.645	28.8	15.785	32.3
18.948	36.0	18.740	40.1	19.661	28.8	20.461	32.3
24.654	35.5	28.118	38.9	31.229	28.5	24.857	31.8
34.852	34.6	31.684	38.7	37.289	28.3	36.132	31.6
45.062	33.9	42.158	37.5	44.884	28.1	51.817	31.3
55.449	33.7	61.824	37.5	57.888	28.0	54.853	30.9

Table S3 continued: Dynamic surface tensions of copolymers S1 to S31.

S9		S10		S11		S12	
t	γ_{dyn}	t	γ_{dyn}	t	γ_{dyn}	t	γ_{dyn}
0.032	74.6	0.029	88.0	0.031	82.9	0.030	74.4
0.038	70.4	0.038	88.8	0.038	77.7	0.038	68.2
0.049	66.4	0.049	86.2	0.049	72.7	0.050	63.0
0.065	63.2	0.064	83.2	0.064	67.7	0.064	59.0
0.085	60.1	0.085	81.8	0.084	63.5	0.085	55.4
0.112	57.7	0.111	79.9	0.110	59.4	0.111	52.1
0.145	55.9	0.146	78.5	0.143	56.0	0.143	49.4
0.191	54.7	0.190	77.5	0.189	52.8	0.189	46.9
0.243	53.0	0.247	76.4	0.246	49.4	0.243	44.8
0.310	51.9	0.317	75.0	0.312	46.2	0.308	43.3
0.403	50.7	0.408	73.5	0.391	43.9	0.402	41.5
0.525	49.6	0.531	72.0	0.523	41.1	0.517	39.8
0.678	48.6	0.691	70.3	0.658	39.0	0.664	38.1
0.871	47.7	0.892	68.3	0.897	37.1	0.891	35.9
1.056	46.9	1.082	66.7	1.031	36.4	1.049	35.2
1.312	46.1	1.347	65.3	1.380	35.0	1.414	33.7
1.891	44.9	1.844	62.5	1.878	33.9	1.783	32.9
2.302	44.5	2.318	60.6	2.303	33.4	2.236	31.7
3.230	43.5	3.077	57.7	3.165	32.1	3.172	31.1
4.137	43.0	4.048	55.4	3.927	31.4	4.184	30.9
5.316	42.2	5.381	52.7	5.446	30.7	5.344	30.2
6.975	41.7	6.740	51.0	6.665	30.2	6.848	29.6
9.189	41.1	9.167	47.8	9.821	29.3	9.320	29.6
12.080	40.4	11.125	45.7	11.822	28.9	11.675	28.5
14.568	40.5	15.161	43.8	15.700	28.5	14.483	28.3
21.589	39.5	20.499	40.7	19.760	28.1	21.980	27.8
28.642	39.5	24.958	40.1	24.572	27.8	25.174	27.4
33.371	38.1	31.767	37.6	39.602	27.5	37.564	27.0
47.377	38.1	41.544	36.2	40.352	27.5	44.138	26.7
59.676	36.7	58.218	36.5	55.118	27.4	65.267	26.6

Table S3 continued: Dynamic surface tensions of copolymers S1 to S31.

S13		S14		S15		S16	
t	γ_{dyn}	t	γ_{dyn}	t	γ_{dyn}	t	γ_{dyn}
0.032	76.9	0.032	73.2	0.032	95.9	0.031	84.0
0.038	73.0	0.039	69.4	0.038	92.5	0.039	78.6
0.049	69.3	0.049	65.9	0.050	88.6	0.050	73.5
0.064	66.3	0.064	63.1	0.064	86.8	0.065	69.5
0.084	63.5	0.086	60.8	0.086	84.1	0.084	65.2
0.111	60.9	0.112	59.1	0.111	82.3	0.110	61.8
0.145	59.4	0.144	57.5	0.145	81.1	0.144	58.8
0.187	58.0	0.188	56.3	0.188	80.3	0.187	56.1
0.245	56.3	0.245	55.1	0.243	78.8	0.243	53.1
0.303	55.3	0.310	54.2	0.313	77.8	0.300	50.9
0.403	54.2	0.400	53.5	0.403	76.5	0.392	48.3
0.529	52.9	0.536	52.3	0.525	74.7	0.530	45.4
0.678	52.0	0.674	51.6	0.678	73.0	0.670	43.2
0.870	51.0	0.885	50.7	0.873	71.2	0.890	40.9
1.032	50.1	1.050	50.2	1.041	69.7	1.005	39.9
1.434	49.1	1.324	49.7	1.382	67.0	1.352	38.0
1.776	48.6	1.905	48.7	1.693	64.8	1.860	36.2
2.300	47.5	2.346	48.0	2.421	61.0	2.297	35.3
3.188	46.8	3.144	47.4	3.037	57.9	3.049	34.1
4.168	46.0	4.148	46.8	4.028	54.8	4.186	33.2
5.205	45.4	5.515	46.2	5.380	52.4	5.326	32.7
7.266	44.5	7.035	45.5	6.892	49.4	6.898	31.7
9.374	44.0	8.960	45.0	8.986	46.3	9.382	31.1
11.327	43.4	11.923	44.7	11.372	43.5	11.963	30.5
15.667	42.9	14.943	44.1	14.639	40.9	14.660	30.1
20.622	42.4	21.098	43.5	19.830	38.0	22.438	29.3
27.097	41.9	27.552	43.1	23.876	36.5	24.646	29.1
31.083	42.0	35.048	42.5	35.340	33.9	36.273	28.4
44.584	41.3	44.436	42.0	41.965	33.5	41.348	28.4

Table S3 continued: Dynamic surface tensions of copolymers S1 to S31.

S17		S18		S19		S20	
t	γ_{dyn}	t	γ_{dyn}	t	γ_{dyn}	t	γ_{dyn}
0.031	52.7	0.032	69.6	0.032	67.5	0.032	59.7
0.040	49.8	0.038	71.4	0.040	66.1	0.038	58.8
0.049	47.7	0.051	72.4	0.049	65.6	0.049	56.6
0.065	45.9	0.065	72.8	0.064	63.9	0.063	54.2
0.084	43.4	0.084	71.5	0.084	61.7	0.086	51.3
0.111	41.7	0.112	70.1	0.110	59.5	0.112	48.8
0.146	39.8	0.145	67.4	0.147	57.0	0.147	46.0
0.191	38.4	0.189	65.9	0.189	54.9	0.188	43.3
0.244	36.7	0.245	64.5	0.245	52.5	0.246	40.9
0.302	35.6	0.315	63.0	0.306	50.3	0.301	39.0
0.400	34.2	0.414	61.1	0.398	47.7	0.394	36.8
0.514	33.1	0.521	59.7	0.515	45.2	0.514	34.7
0.660	32.1	0.688	57.4	0.678	42.2	0.685	32.7
0.868	31.2	0.888	55.1	0.866	39.7	0.883	31.2
1.034	30.5	1.073	53.5	1.015	38.5	1.016	30.5
1.457	29.5	1.424	50.8	1.327	35.9	1.413	29.5
1.744	29.2	1.699	48.9	1.837	33.6	1.998	28.2
2.286	28.6	2.397	45.9	2.246	32.2	2.301	28.0
3.158	27.9	3.191	43.6	2.970	31.0	3.231	27.3
4.139	27.7	4.008	41.7	4.110	29.5	3.997	26.8
5.383	27.0	5.337	39.4	5.399	28.8	5.484	26.1
6.764	27.0	6.983	37.3	6.593	27.7	6.718	25.6
9.644	26.4	8.642	35.4	8.808	27.3	9.512	25.2
12.311	26.1	11.613	33.8	11.751	26.5	12.443	24.9
15.424	25.9	15.457	32.2	14.533	26.1	15.483	24.6
21.387	25.5	19.375	31.9	19.905	25.6	20.542	24.6
26.975	25.3	25.816	30.8	27.470	25.4	26.739	24.4
31.702	25.1	33.238	29.3	35.215	24.9	33.642	24.2
49.590	24.9	46.492	28.6	45.423	24.7	46.325	23.9

Table S3 continued: Dynamic surface tensions of copolymers S1 to S31.

S21		S22		S23		S24	
t	γ_{dyn}	t	γ_{dyn}	t	γ_{dyn}	t	γ_{dyn}
0.031	52.8	0.029	70.8	0.032	67.8	0.031	69.3
0.039	50.7	0.038	70.9	0.038	66.6	0.038	67.9
0.049	48.9	0.049	70.4	0.049	65.4	0.050	66.4
0.064	47.4	0.064	70.7	0.064	64.4	0.064	64.4
0.083	45.7	0.084	70.0	0.085	62.3	0.084	62.2
0.111	44.1	0.112	70.2	0.111	60.3	0.112	60.1
0.145	42.8	0.146	69.7	0.146	58.4	0.145	58.0
0.190	41.6	0.189	69.5	0.191	56.3	0.188	55.8
0.245	40.4	0.245	68.8	0.245	53.9	0.242	53.3
0.313	39.3	0.315	68.2	0.311	51.9	0.305	51.0
0.398	38.4	0.408	67.3	0.396	49.6	0.407	48.1
0.530	37.2	0.527	66.2	0.513	47.1	0.521	45.9
0.674	35.9	0.684	65.1	0.661	44.6	0.694	44.1
0.862	35.1	0.883	64.0	0.861	42.0	0.893	42.4
1.045	34.5	1.057	63.2	1.010	40.6	1.102	41.2
1.470	33.4	1.309	61.7	1.393	37.2	1.390	40.0
1.747	33.2	1.796	59.8	1.747	35.0	1.816	38.6
2.277	32.4	2.598	57.2	2.671	32.1	2.608	37.9
3.138	31.9	3.040	56.2	2.874	32.1	2.953	38.1
4.195	31.3	4.052	54.1	3.740	30.2	4.118	37.8
5.219	30.6	5.425	52.3	5.591	28.6	5.537	38.5
7.234	30.1	6.775	50.6	6.422	27.6	7.280	38.7
9.353	29.8	9.093	48.5	8.809	26.8	8.991	37.7
11.533	29.5	11.732	47.3	12.684	26.1	11.868	37.2
16.153	29.1	16.052	45.4	16.354	25.3	14.741	36.3
20.315	28.8	19.816	44.5	20.370	25.0	21.308	36.8
26.045	28.7	26.299	42.9	25.298	24.9	27.439	37.6
33.626	28.4	32.679	41.8	34.160	24.4	36.311	39.2
41.019	28.3	48.524	40.2	42.939	24.2	48.511	40.2

Table S3 continued: Dynamic surface tensions of copolymers S1 to S31.

S25		S26		S27		S28	
t	γ_{dyn}	t	γ_{dyn}	t	γ_{dyn}	t	γ_{dyn}
0.032	61.4	0.031	68.2	0.029	68.7	0.029	67.6
0.038	63.8	0.038	67.5	0.038	68.4	0.038	66.9
0.050	63.6	0.049	65.9	0.049	67.1	0.049	65.7
0.064	61.6	0.065	64.2	0.064	66.8	0.063	65.3
0.084	60.0	0.085	62.5	0.084	66.1	0.084	64.9
0.112	58.1	0.111	60.8	0.113	65.4	0.112	64.5
0.145	56.3	0.146	59.7	0.147	64.5	0.147	64.0
0.188	54.1	0.189	58.2	0.189	64.1	0.189	63.9
0.244	52.1	0.243	56.9	0.243	63.5	0.244	63.5
0.312	49.9	0.313	55.3	0.307	63.2	0.308	63.3
0.412	47.5	0.397	54.3	0.395	62.8	0.393	63.1
0.532	45.6	0.529	52.7	0.517	62.3	0.516	62.7
0.687	43.7	0.679	51.6	0.681	62.1	0.678	62.5
0.919	41.7	0.887	50.4	0.865	61.7	0.865	62.2
1.109	40.4	1.057	49.5	1.071	61.2	1.066	61.9
1.391	39.2	1.339	48.3	1.385	60.6	1.390	61.5
1.890	38.2	1.691	47.4	1.822	60.3	1.815	61.3
2.625	37.6	2.499	45.8	2.203	60.0	2.496	60.9
3.033	37.7	3.029	44.9	3.165	59.4	3.211	60.5
4.201	37.7	4.216	43.5	4.121	58.7	4.143	60.0
5.515	37.9	5.328	42.5	5.247	58.3	5.433	59.7
6.844	37.2	7.192	41.3	7.316	57.6	6.853	59.0
9.064	35.7	9.200	40.0	9.269	57.1	9.465	58.6
11.653	35.0	11.490	38.9	11.806	56.5	12.337	58.0
15.418	34.8	15.636	37.3	15.150	55.8	15.682	57.5
20.046	35.7	19.630	36.7	21.291	54.9	20.586	56.6
27.190	36.7	26.428	34.6	26.946	54.0	25.572	56.2
35.055	36.3	33.424	33.7	33.949	53.0	36.117	55.2
45.630	37.3	42.082	31.5	42.510	52.4	45.280	54.7

Table S3 continued: Dynamic surface tensions of copolymers S1 to S31.

S29		S30		S31	
t	γ_{dyn}	t	γ_{dyn}	t	γ_{dyn}
0.032	71.4	0.029	71.0	0.032	73.2
0.038	71.2	0.038	70.5	0.038	72.5
0.049	70.4	0.049	69.4	0.052	72.5
0.064	69.7	0.064	69.3	0.064	71.4
0.084	68.5	0.084	68.7	0.085	71.8
0.112	67.6	0.112	67.9	0.111	70.6
0.144	66.7	0.146	67.3	0.144	70.6
0.189	65.2	0.188	66.8	0.189	70.9
0.243	63.8	0.244	65.8	0.243	70.4
0.311	62.2	0.306	65.1	0.316	70.2
0.405	60.4	0.394	64.4	0.413	70.9
0.530	59.0	0.516	63.6	0.533	70.8
0.686	57.8	0.688	62.8	0.706	70.4
0.902	56.2	0.883	62.3	0.888	70.1
1.069	55.2	1.091	62.2	1.118	69.4
1.321	54.5	1.402	62.2	1.393	69.0
1.947	52.6	1.794	62.0	1.740	68.3
2.399	51.8	2.221	62.2	2.266	67.6
3.155	50.5	3.106	61.3	3.062	65.7
4.208	49.5	4.362	60.5	4.230	63.6
5.395	48.6	5.507	60.2	5.371	62.3
6.910	47.7	7.032	59.8	6.853	61.4
9.313	46.7	9.273	59.2	9.628	60.0
11.696	45.8	12.125	58.8	11.494	59.7
15.717	45.1	15.280	58.3	16.218	58.6
18.947	44.5	20.021	57.7	20.866	57.5
27.551	43.1	25.830	57.4	26.497	56.8
34.520	42.2	33.132	56.8	33.387	55.7
43.757	41.6	45.505	55.7	44.181	55.4

Thermal analysis

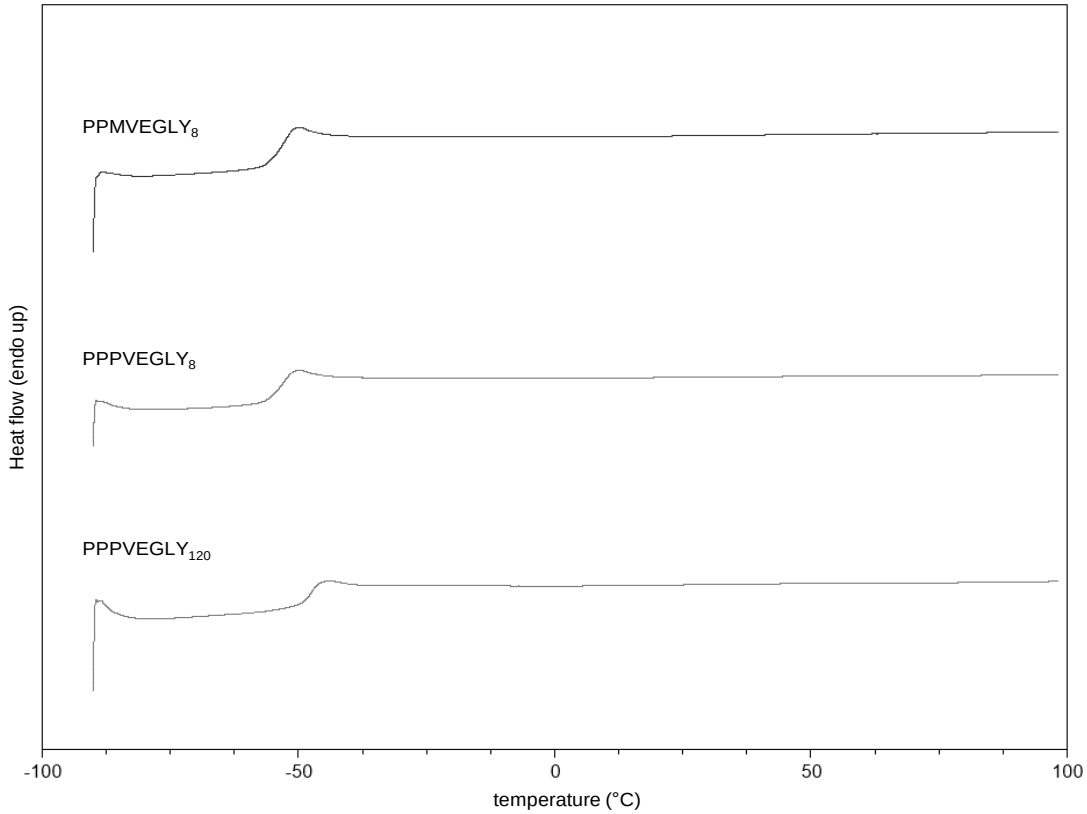

Figure S24: DSC measurement of polyfluorinated homopolymers (2nd heating curve, heating and cooling rate 10 °C min-1).

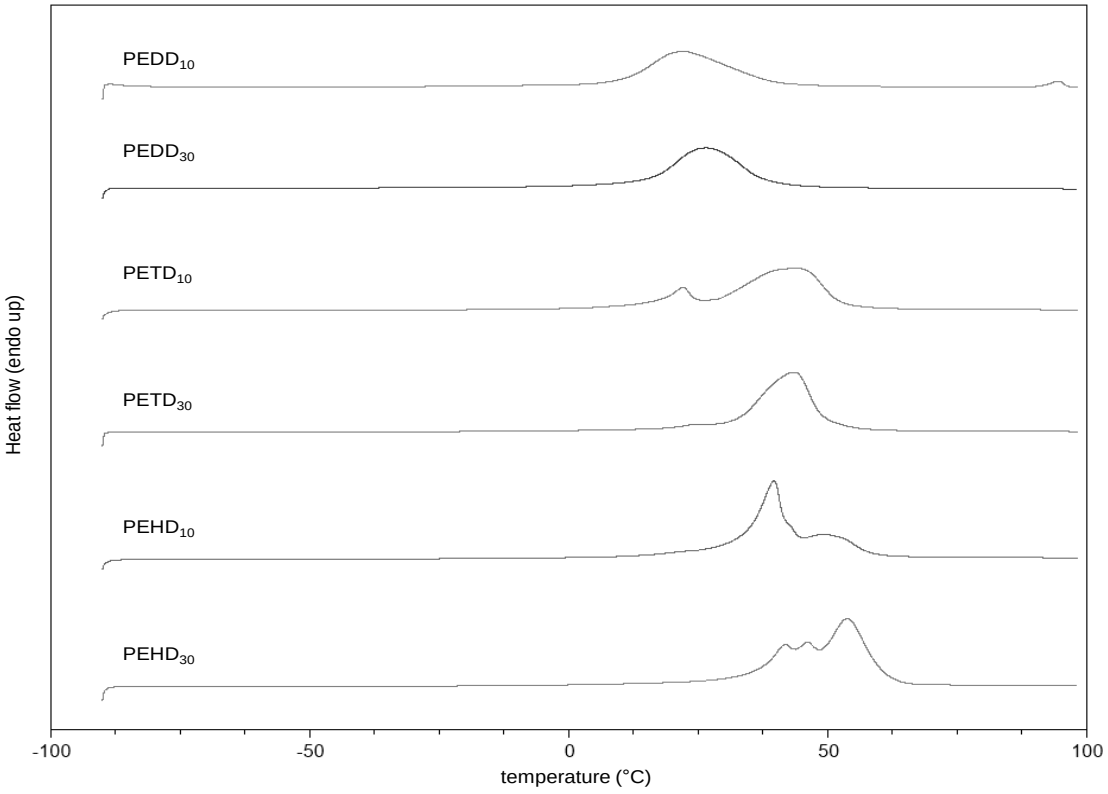

Figure S25: DSC measurement of homo alkylene oxides (2nd heating curve, heating and cooling rate 10 °C min-1).

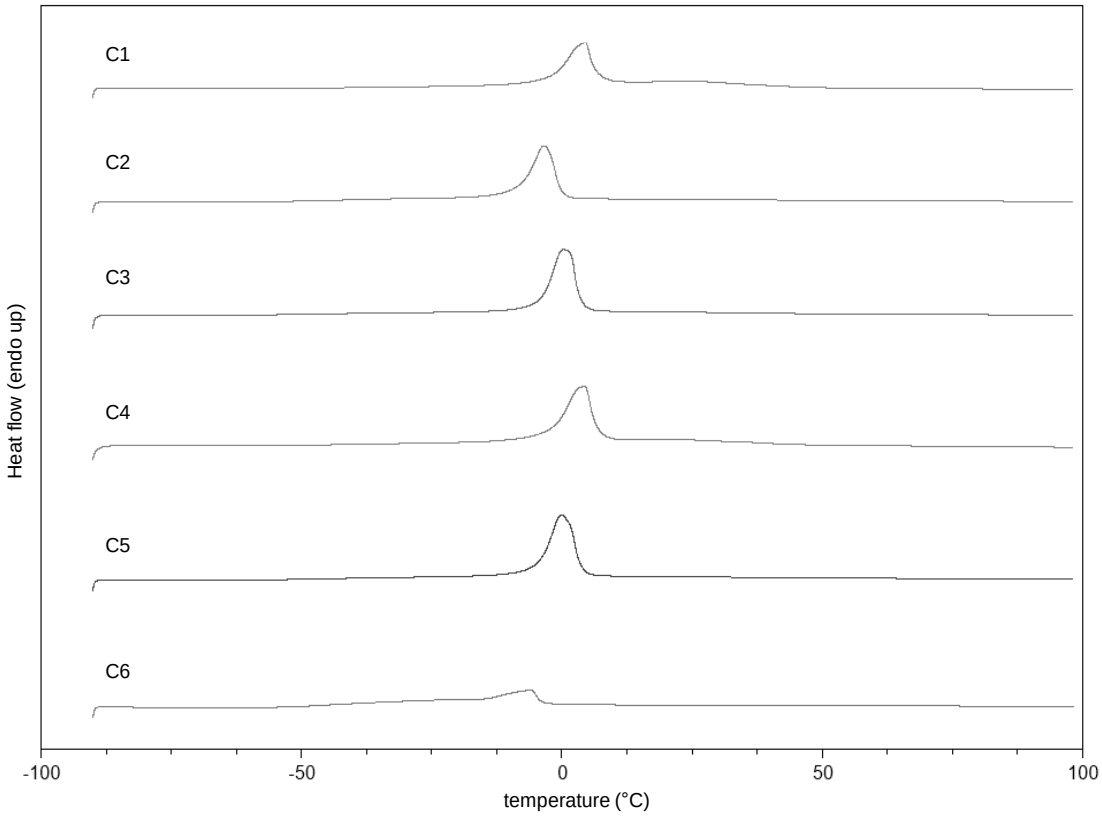

Figure S26: DSC measurement of P(ETD-co-PPVEGLY) series (2nd heating curve, heating and cooling rate 10 °C min-1).

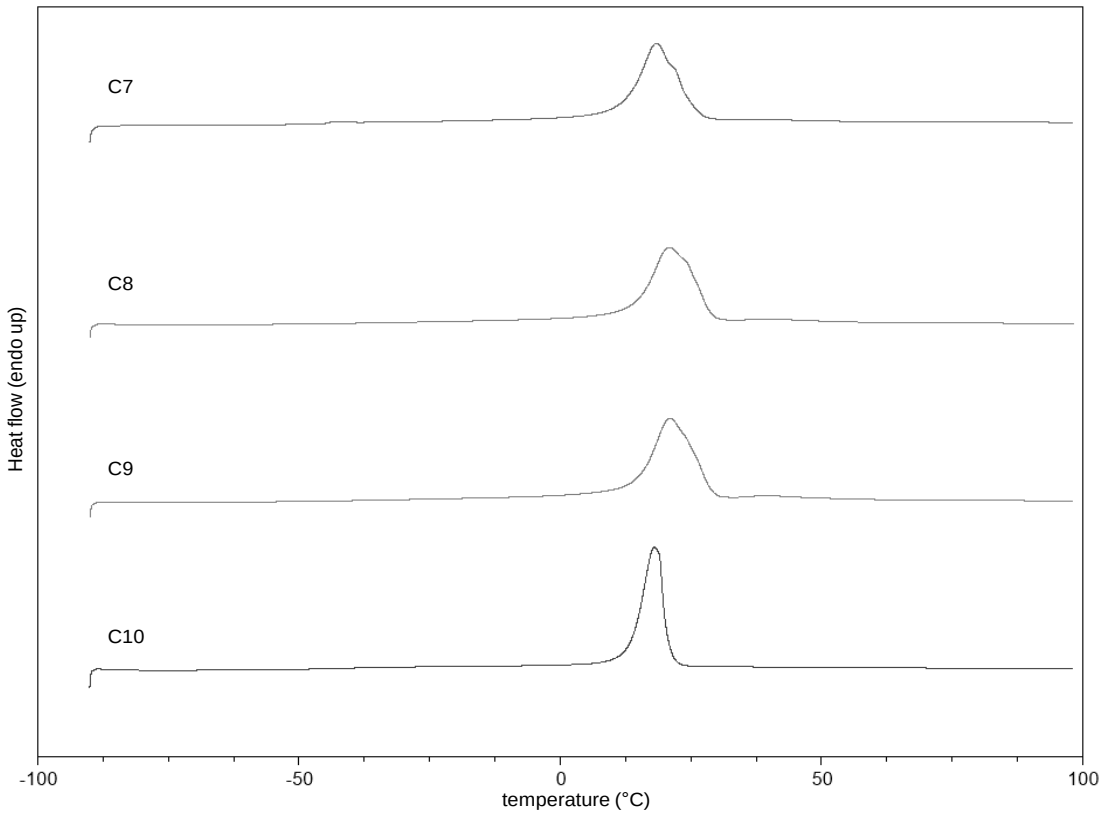

Figure S27: DSC measurement of P(EHD-co-PPVEGLY) series (2nd heating curve, heating and cooling rate 10 °C min-1).

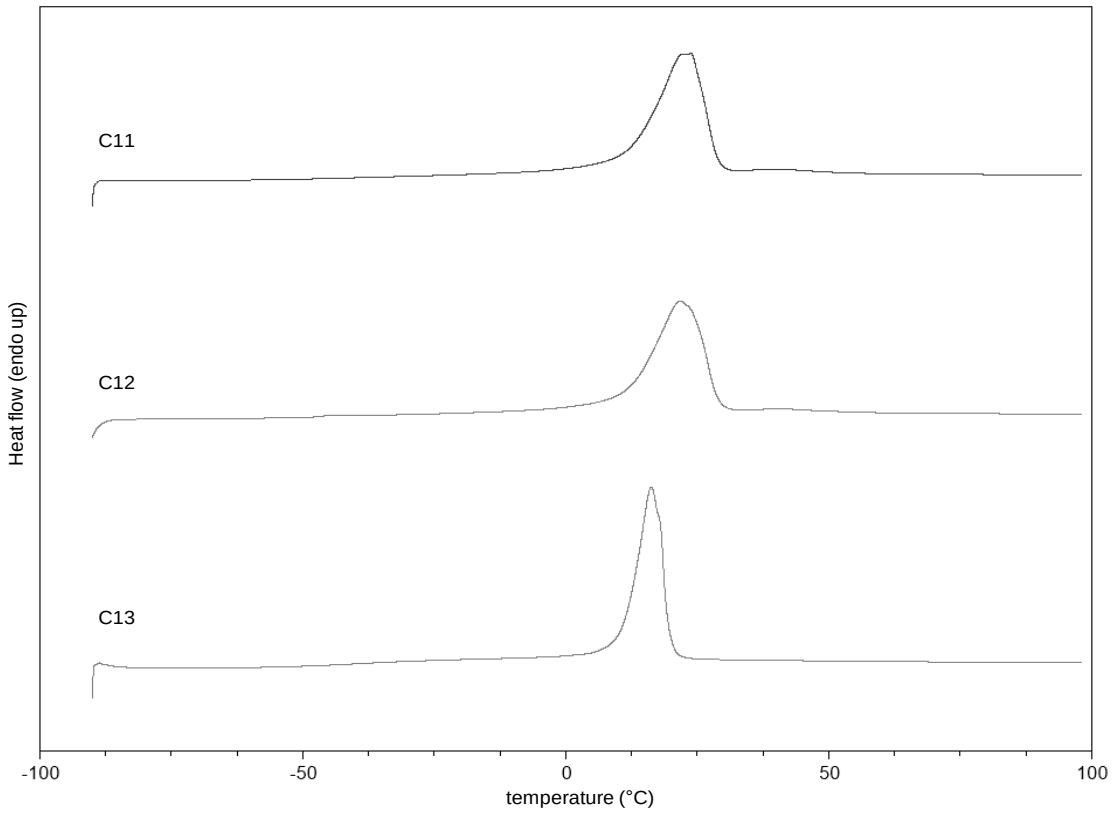

Figure S28: DSC measurement of P(EHD-co-PMVEGLY) series (2nd heating curve, heating and cooling rate 10 °C min-1).

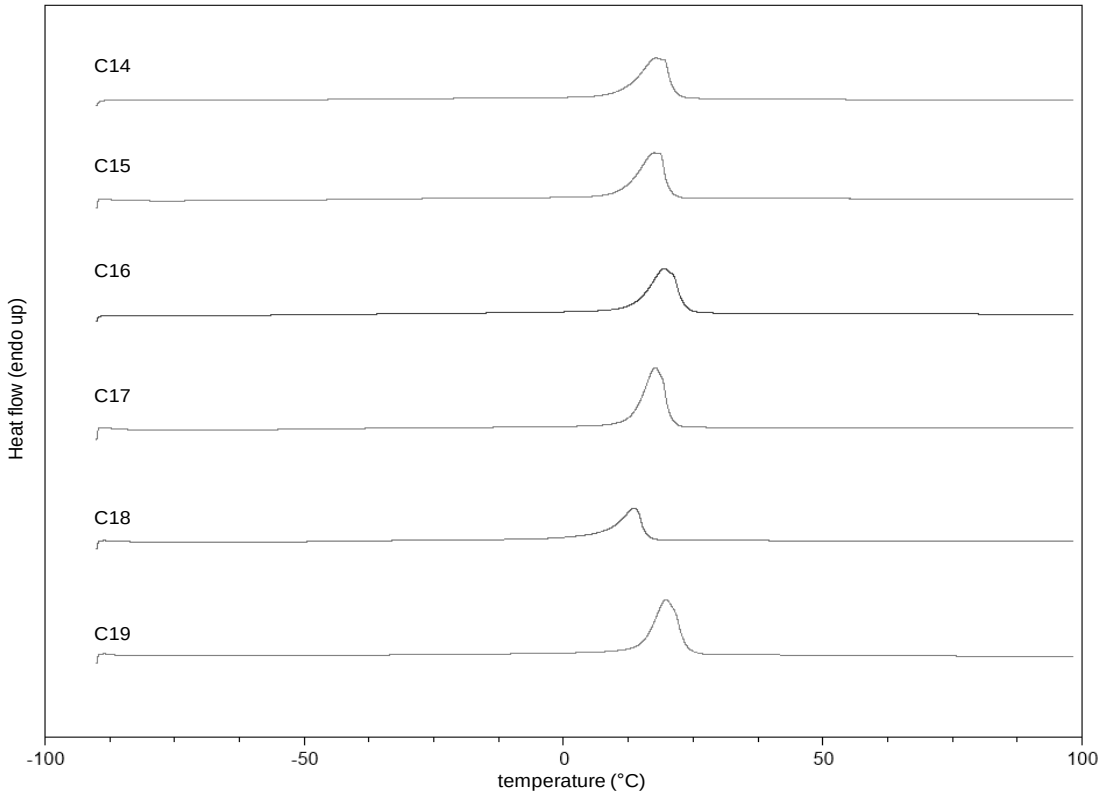

Figure S29: DSC measurement of P(EHD-co-PPVEGLY-co-AGE) series (2nd heating curve, heating and cooling rate 10 °C min-1).

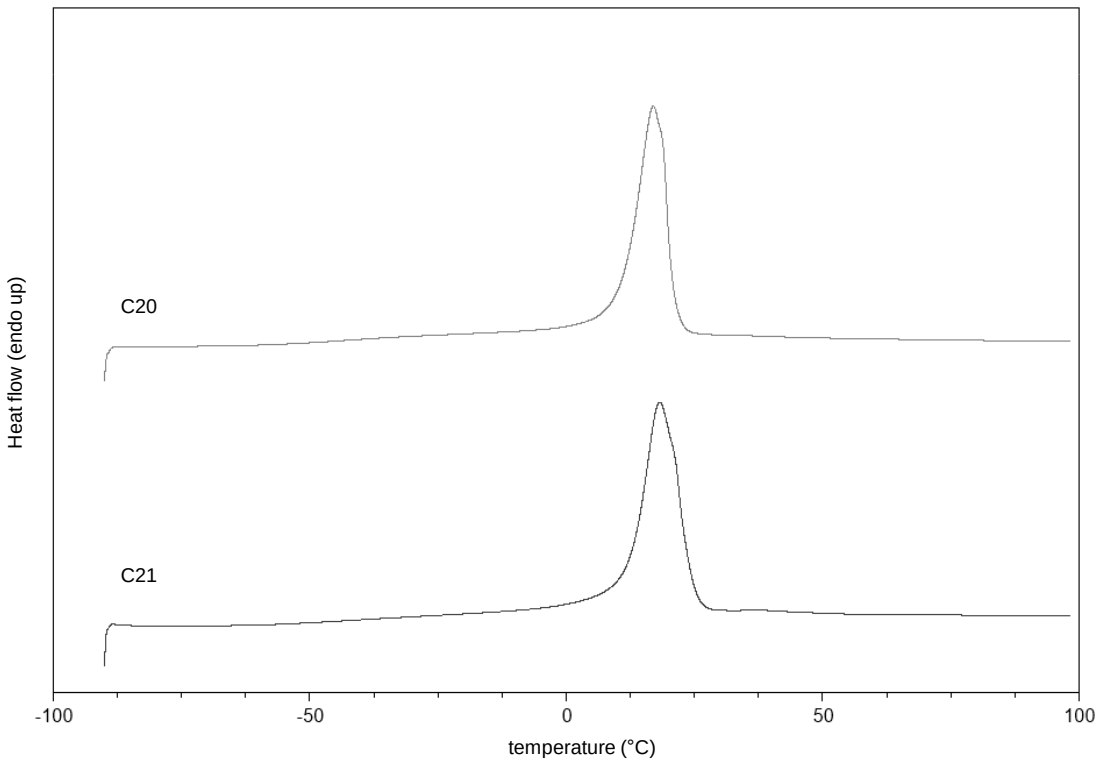

Figure S30: DSC measurement of P(EHD-co-PMVEGLY-co-AGE) series (2nd heating curve, heating and cooling rate 10 °C min-1).

In situ ^{1}H NMR kinetic studies

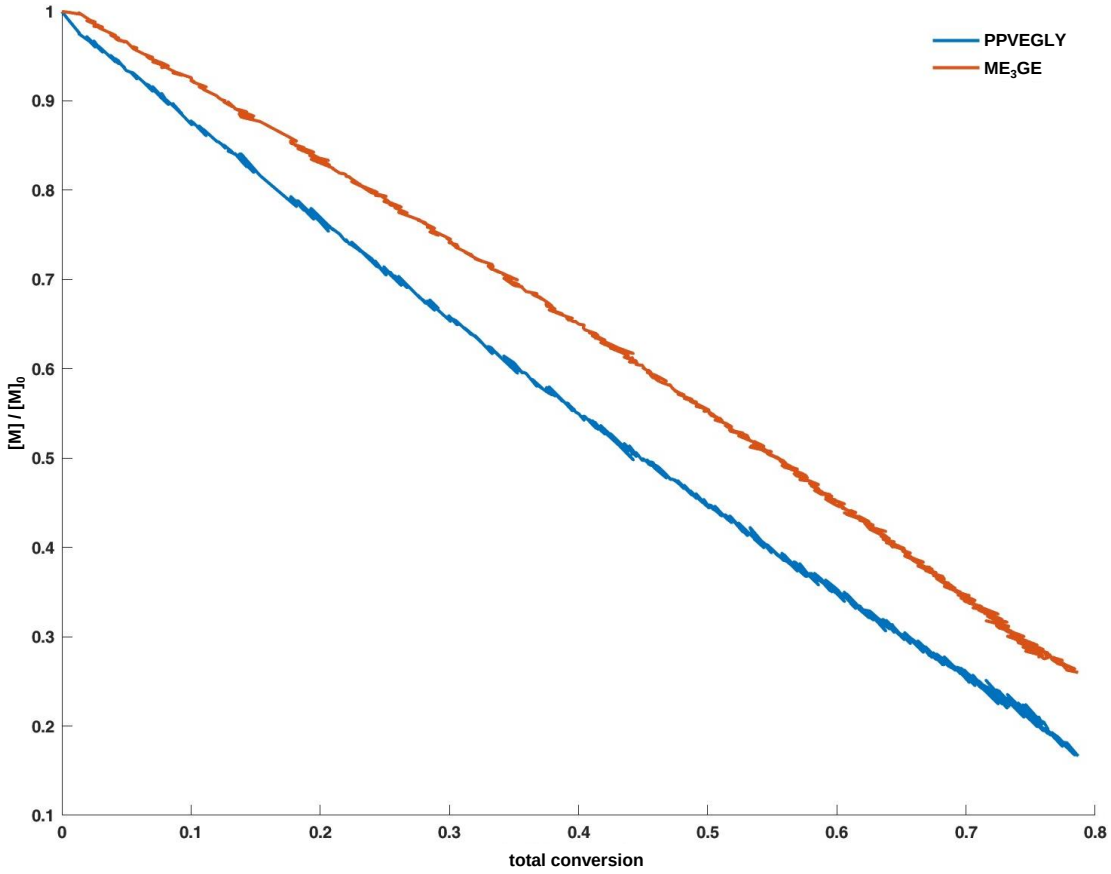

Figure S31: P(ME$_3$GE-co-PPVEGLY): Comonomer concentration plotted versus the total conversion.

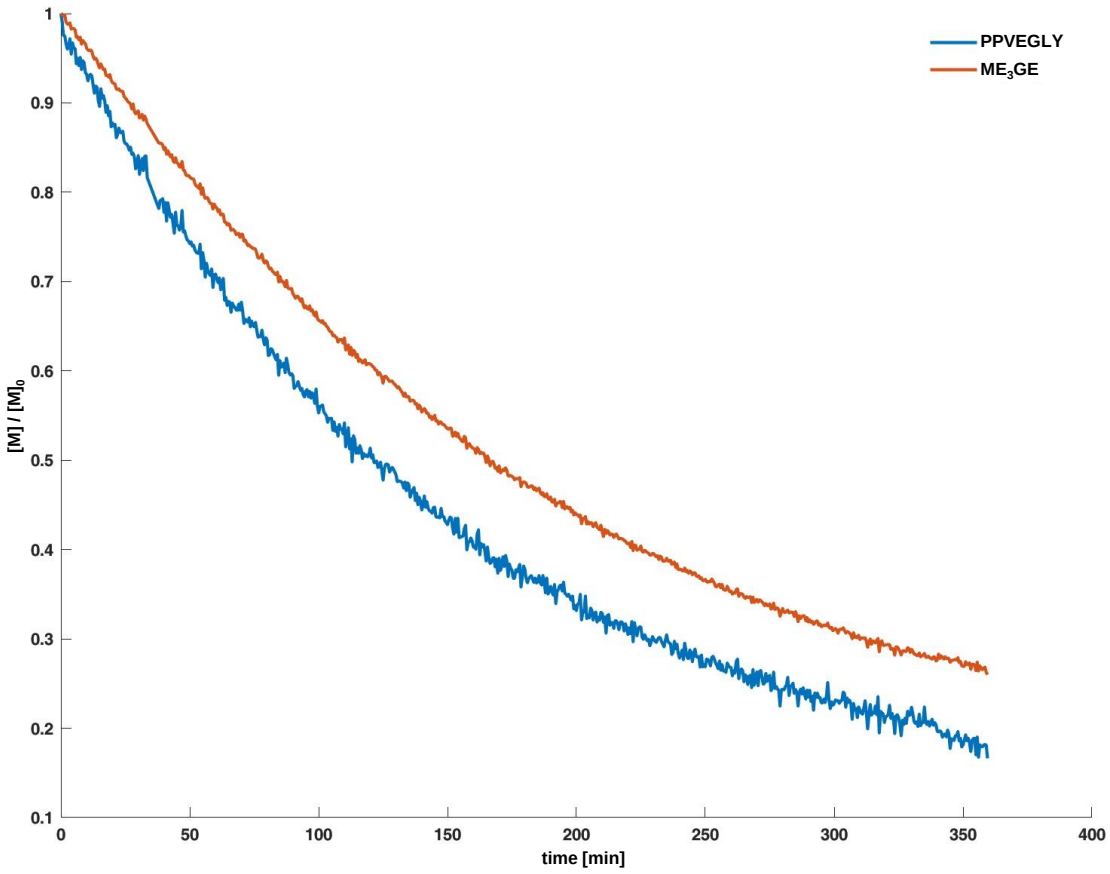

Figure S32: P(ME$_3$GE-co-PPVEGLY): Comonomer concentration plotted versus the time.

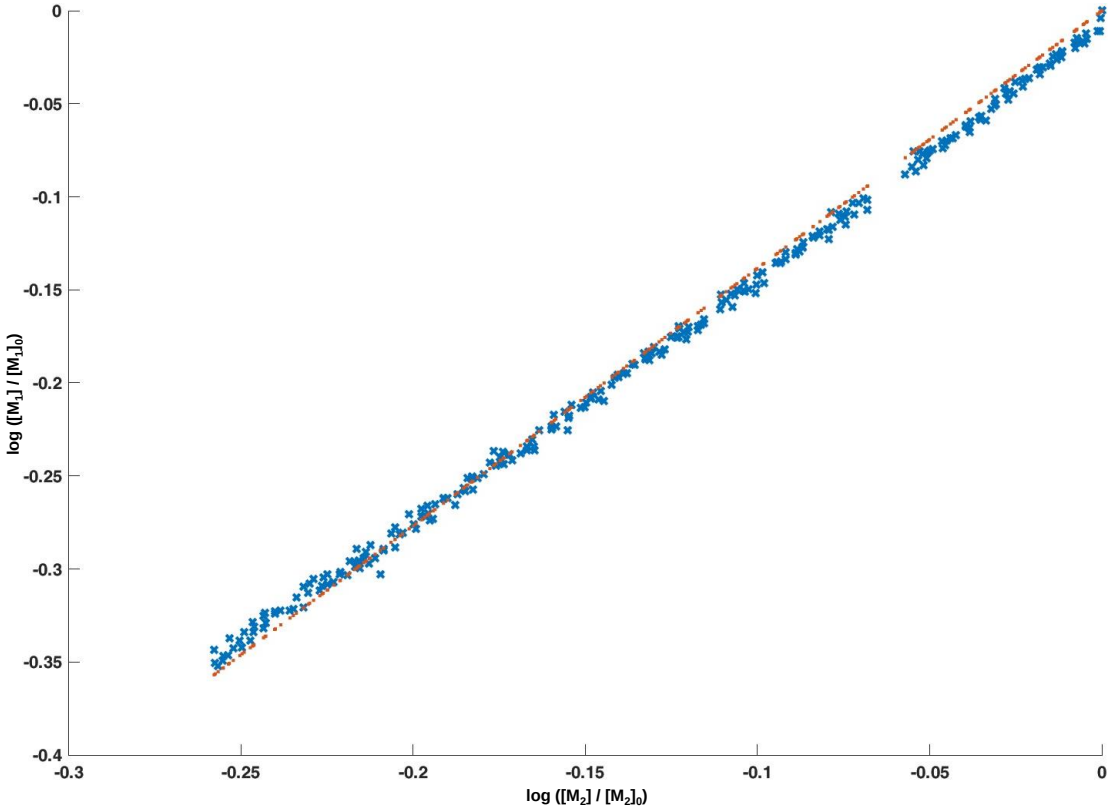

Figure S33: P(ME$_3$GE-co-PPVEGLY): Jaacks fit for the determination of reactivity ratios.

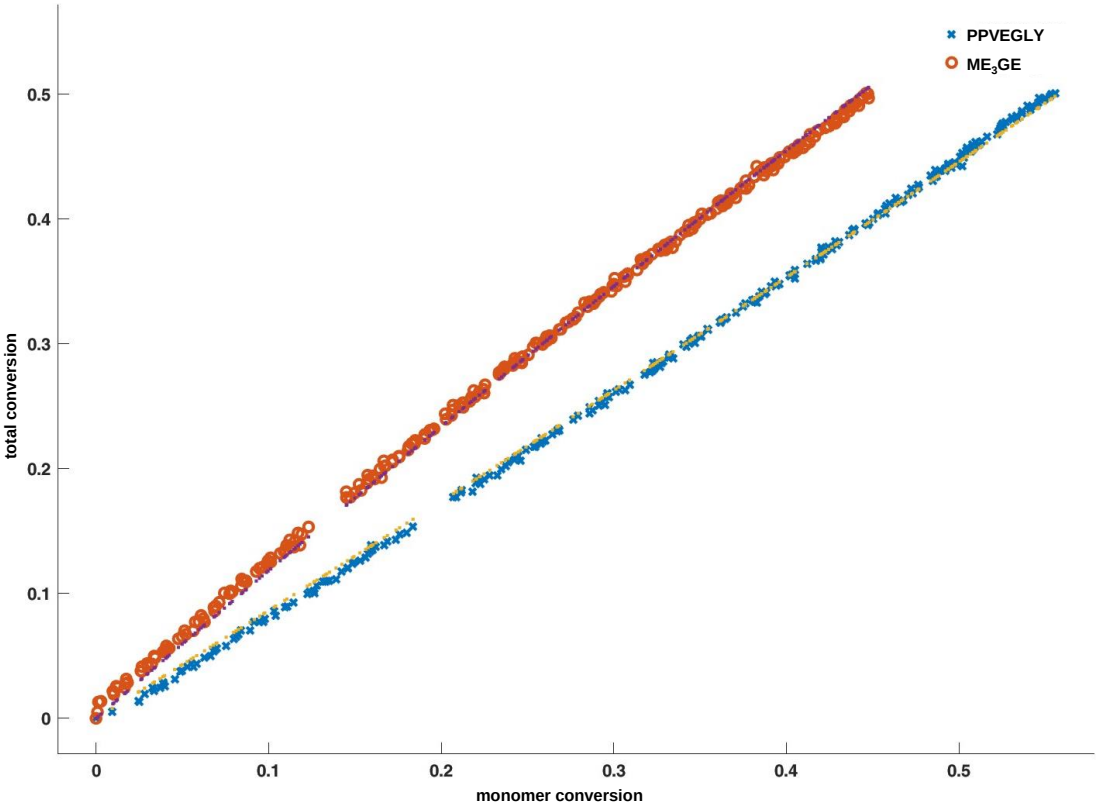

Figure S34: P(ME₃GE-co-PPVEGLY): BSL fit for the determination of reactivity ratios.

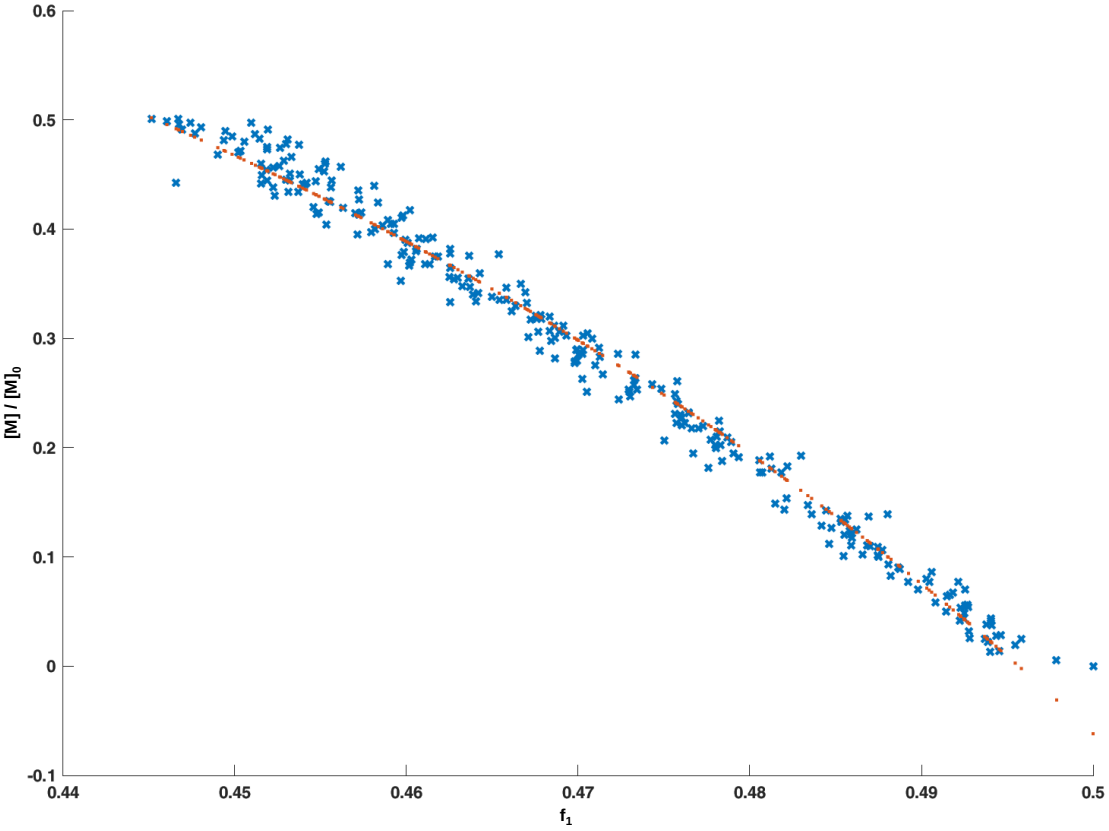

Figure S35: P(ME₃GE-co-PPVEGLY): Meyer-Lowry ideal fit for the determination of reactivity ratios with f_1 = PPVEGLY.

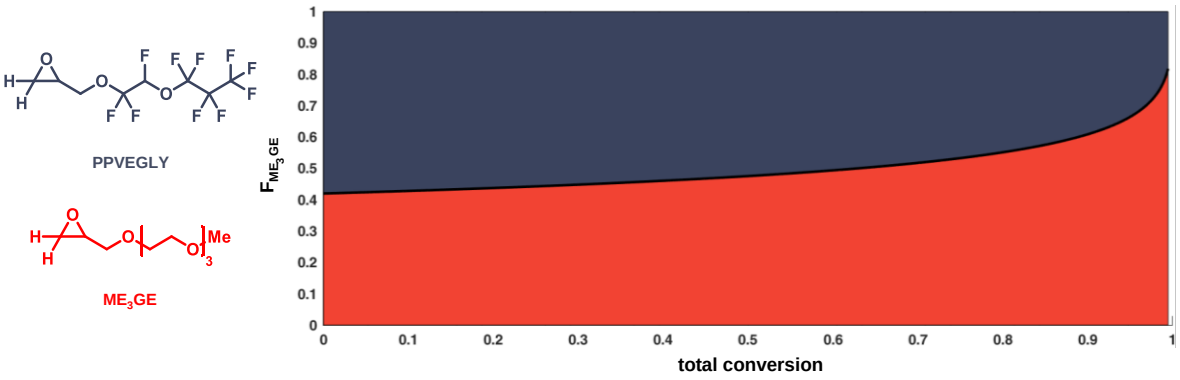

Figure S36: Simulation of the microstructure of P(ME₃GE-co-PPVEGLY synthesised in 2-MeTHF).

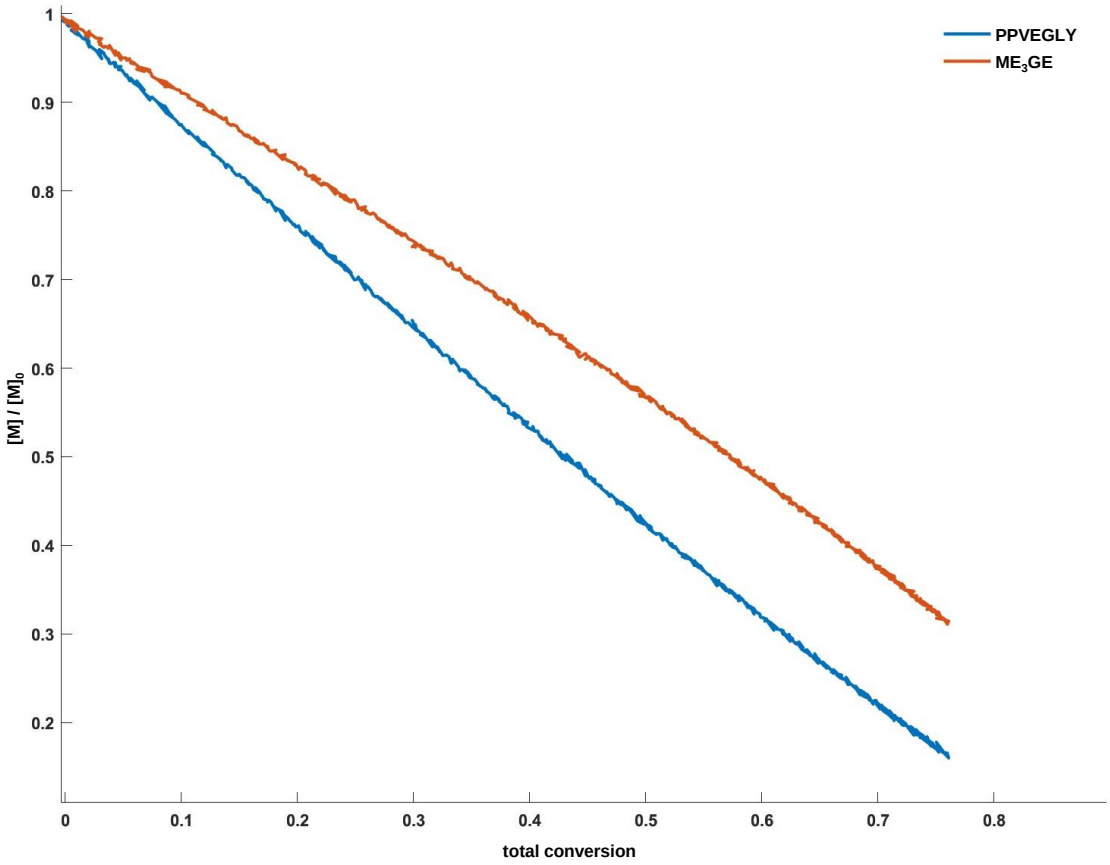

Figure S37: P(ME₃GE-co-PPVEGLY) in THF: Comonomer concentration plotted versus the total conversion.

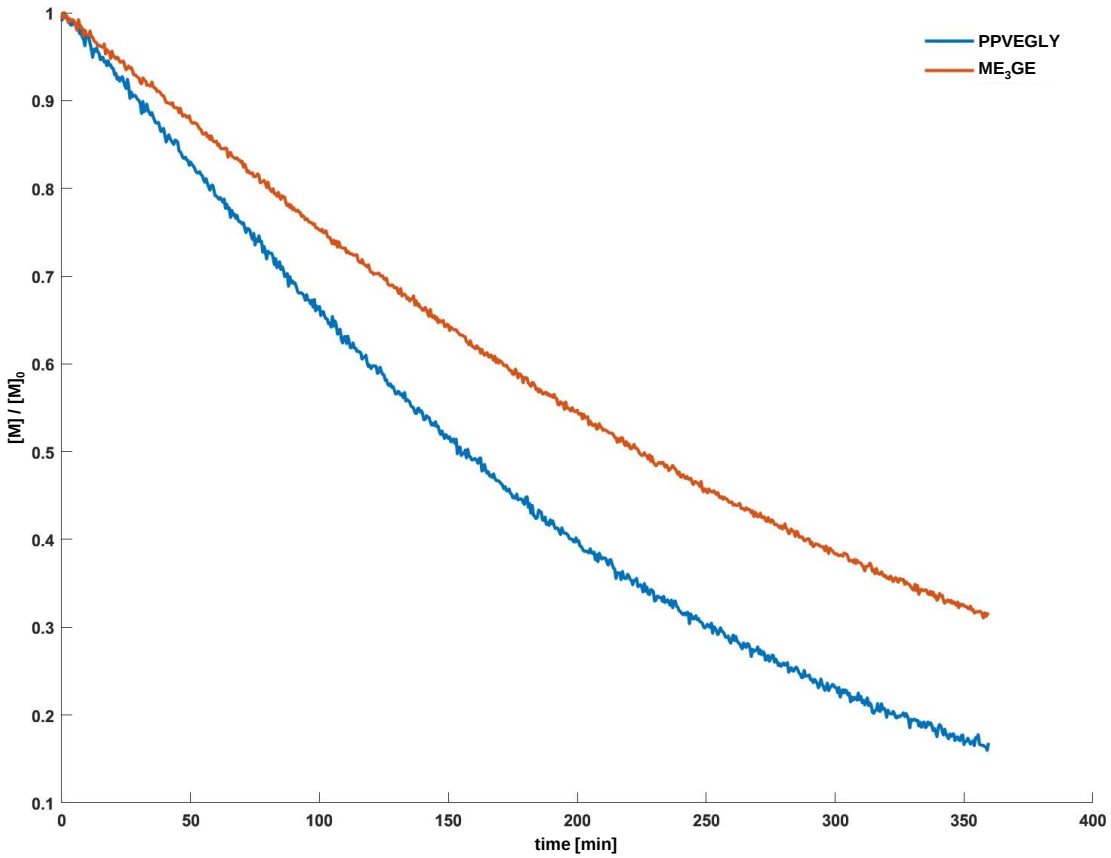

Figure S38: P(ME3GE-co-PPVEGLY) in THF: Comonomer concentration plotted versus time.

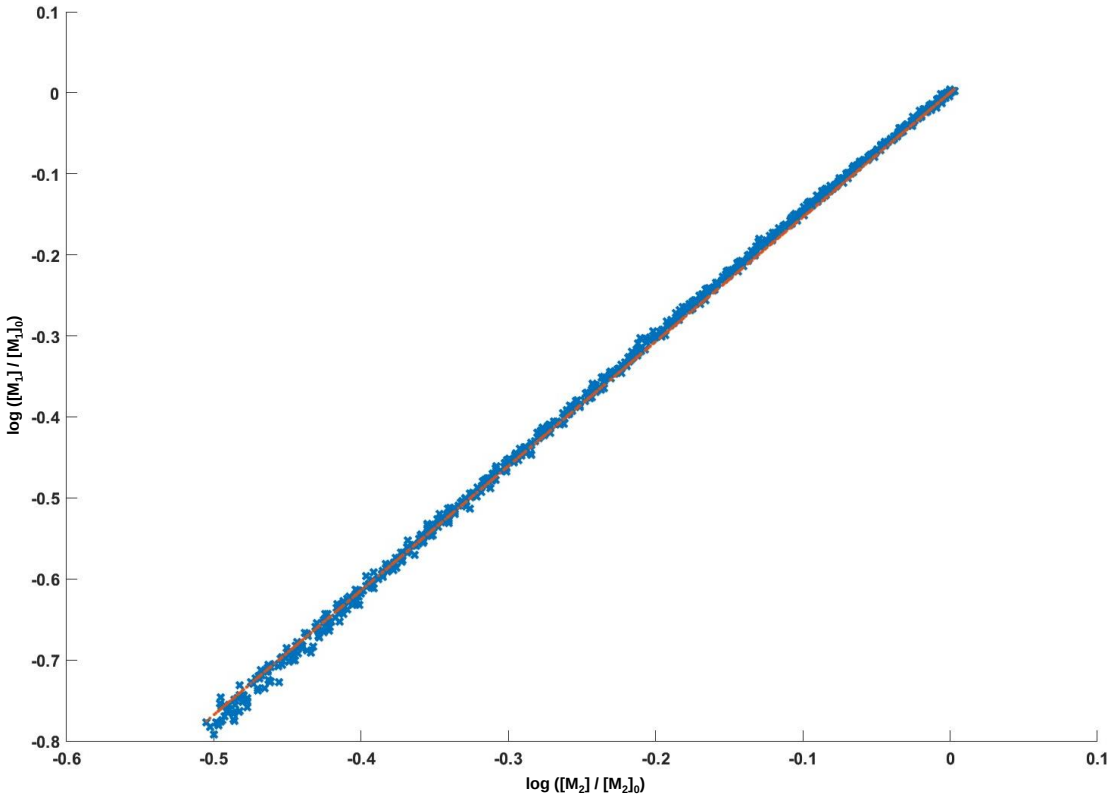

Figure S39: P(ME3GE-co-PPVEGLY) in THF: Jaacks fit for the determination of reactivity ratios.

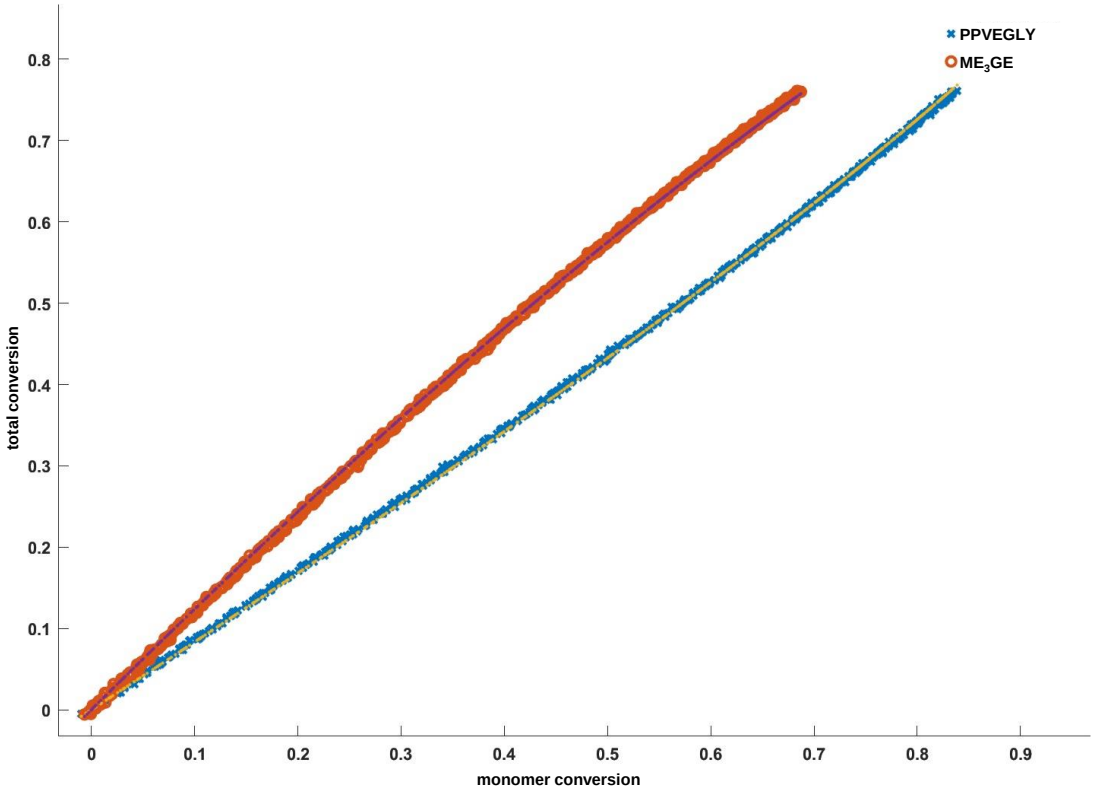

Figure S 40: P(ME$_3$GE-co-PPVEGLY) in THF: BSL fit for the determination of reactivity ratios.

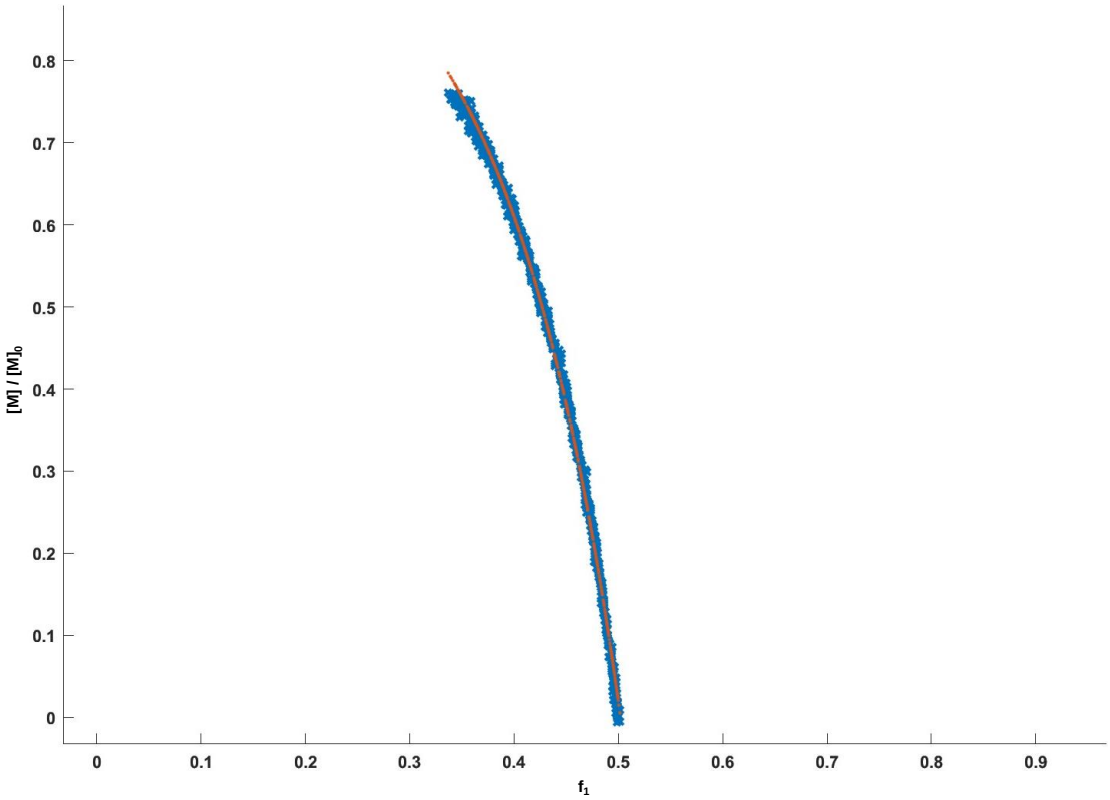

Figure S41: P(ME$_3$GE-co-PPVEGLY) in THF: Meyer-Lowry ideal fit for the determination of reactivity ratios with f_1 = PPVEGLY.

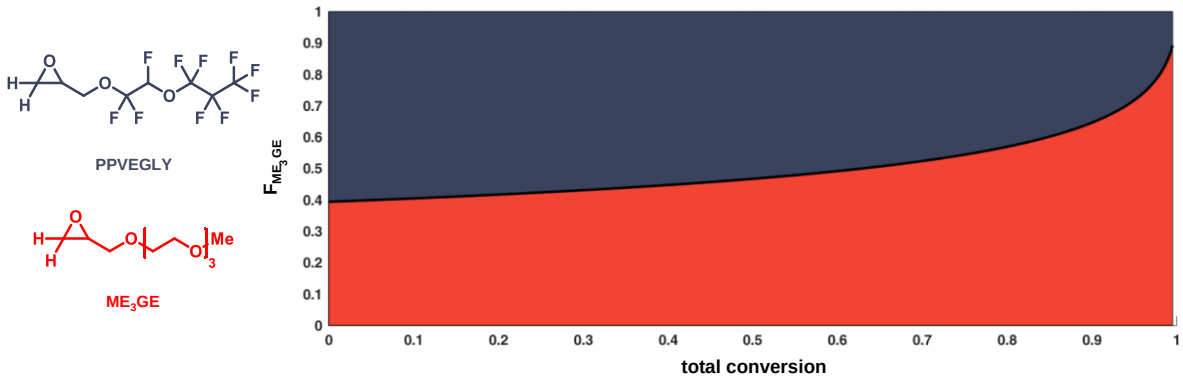

Figure S42: Simulation of the microstructure of P(ME$_3$GE-co-PPVEGLY) synthesised in THF.

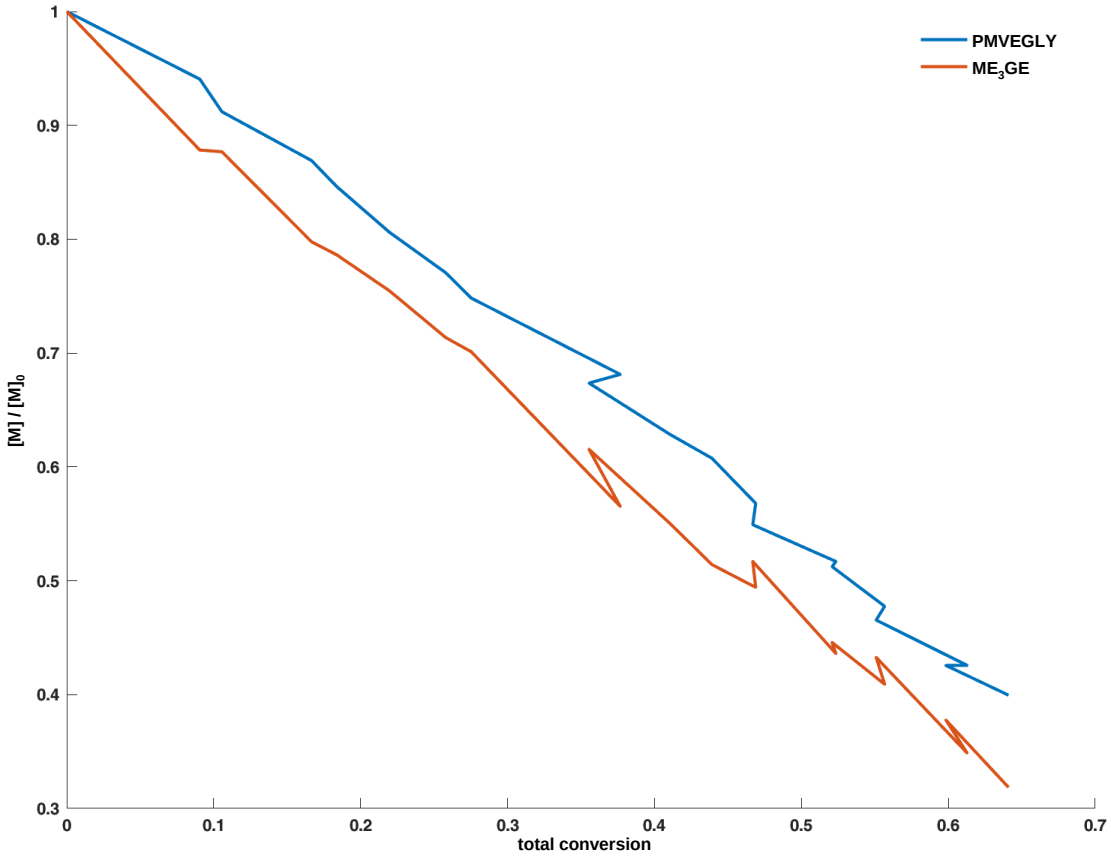

Figure S43: P(ME$_3$GE-co-PMVEGLY): Comonomer concentration plotted versus the total conversion. Data points were acquired every 120 s.

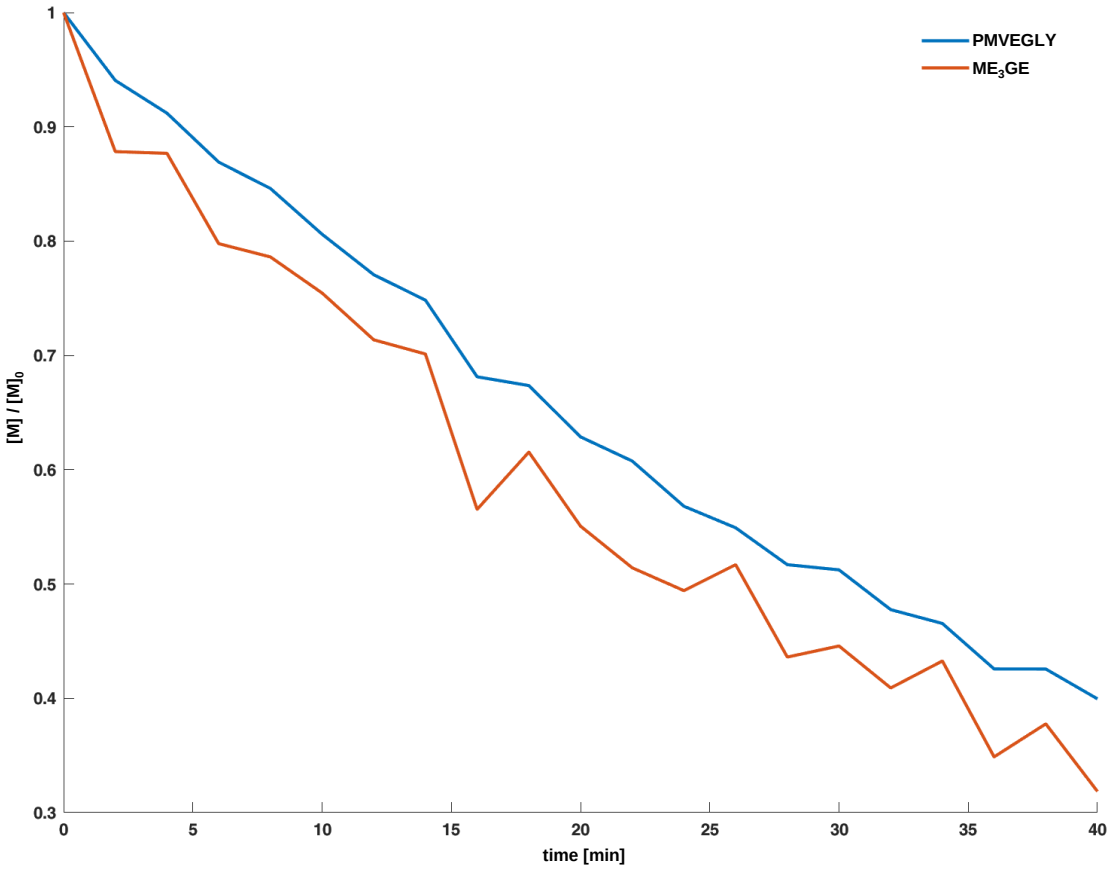

Figure S44: P(ME$_3$GE-co-PMVEGLY): Comonomer concentration plotted versus the time. Data points were acquired every 120 s.

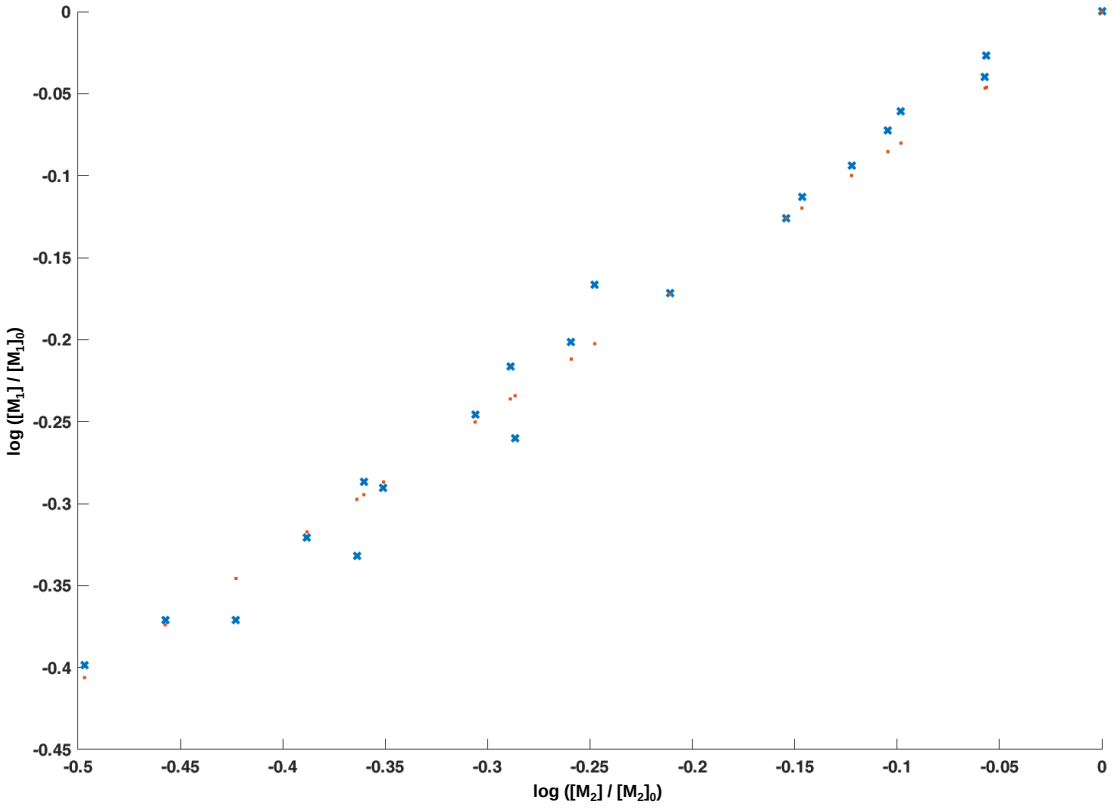

Figure S45: P(ME$_3$GE-co-PMVEGLY): Jaacks fit for the determination of reactivity ratios. Data points were acquired every 120 s.

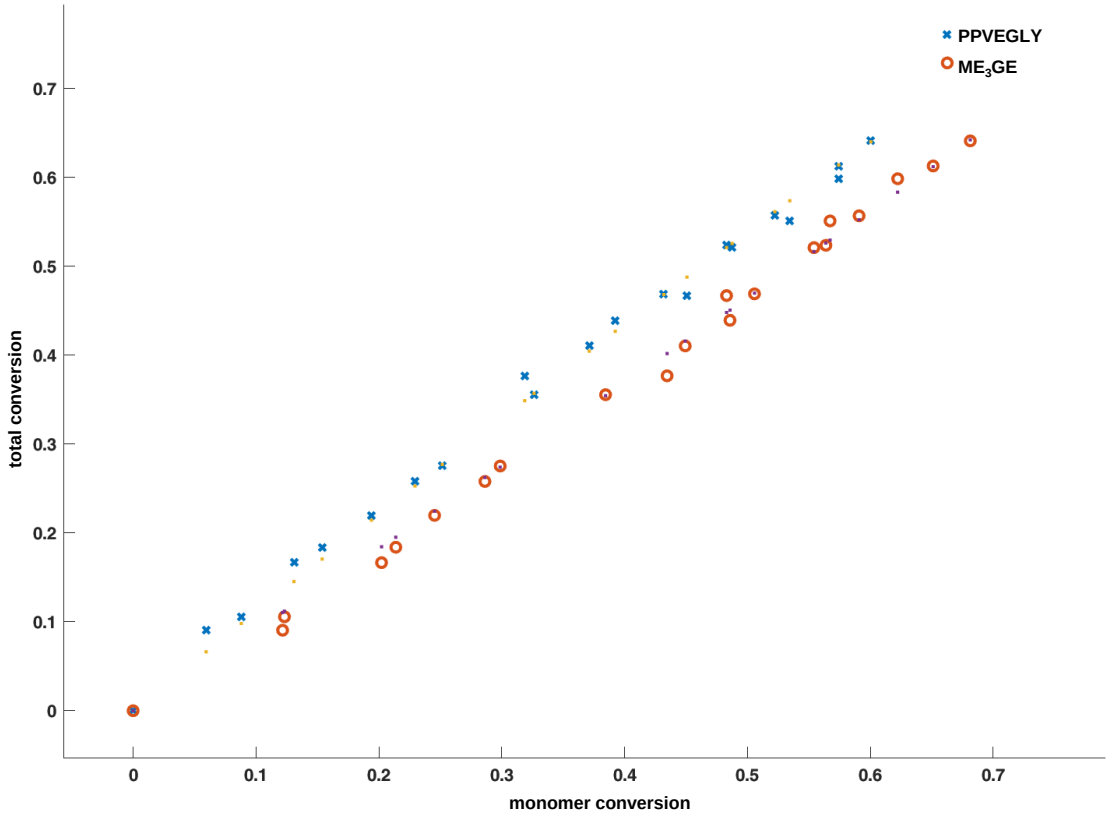

Figure S46: P(ME$_3$GE-co-PMVEGLY): BSL fit for the determination of reactivity ratios. Data points were acquired every 120 s.

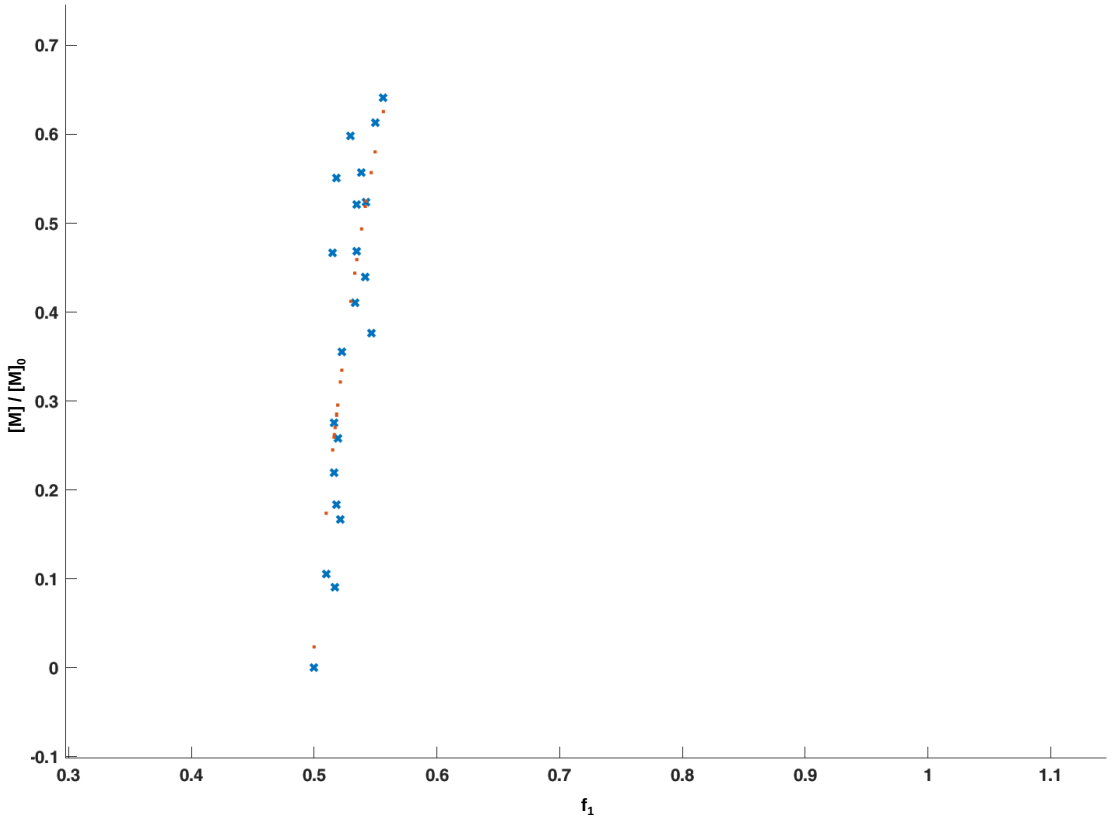

Figure S47: P(ME$_3$GE-co-PMVEGLY): Meyer-Lowry ideal fit for the determination of reactivity ratios with f_1 = PMVEGLY. Data points were acquired every 120 s.

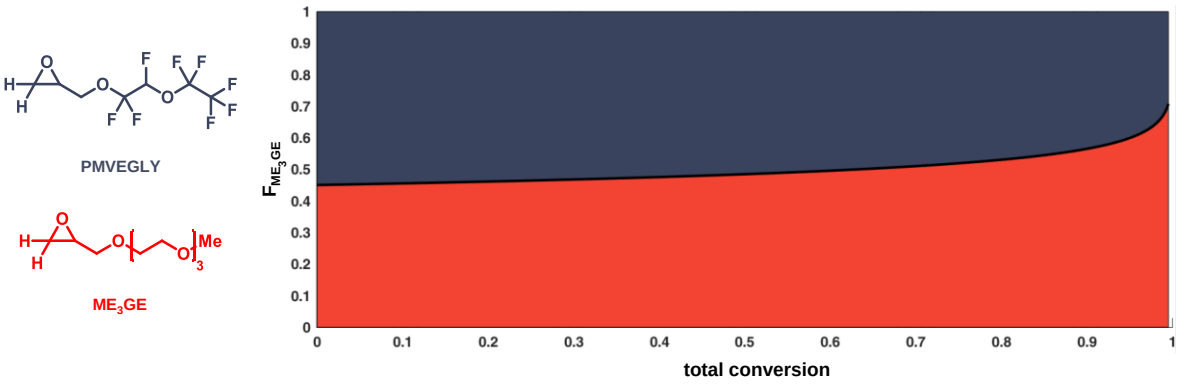

Figure S48: Simulation of the microstructure of P(ME$_3$GE-co-PMVEGLY). Data points were acquired every 120 s.

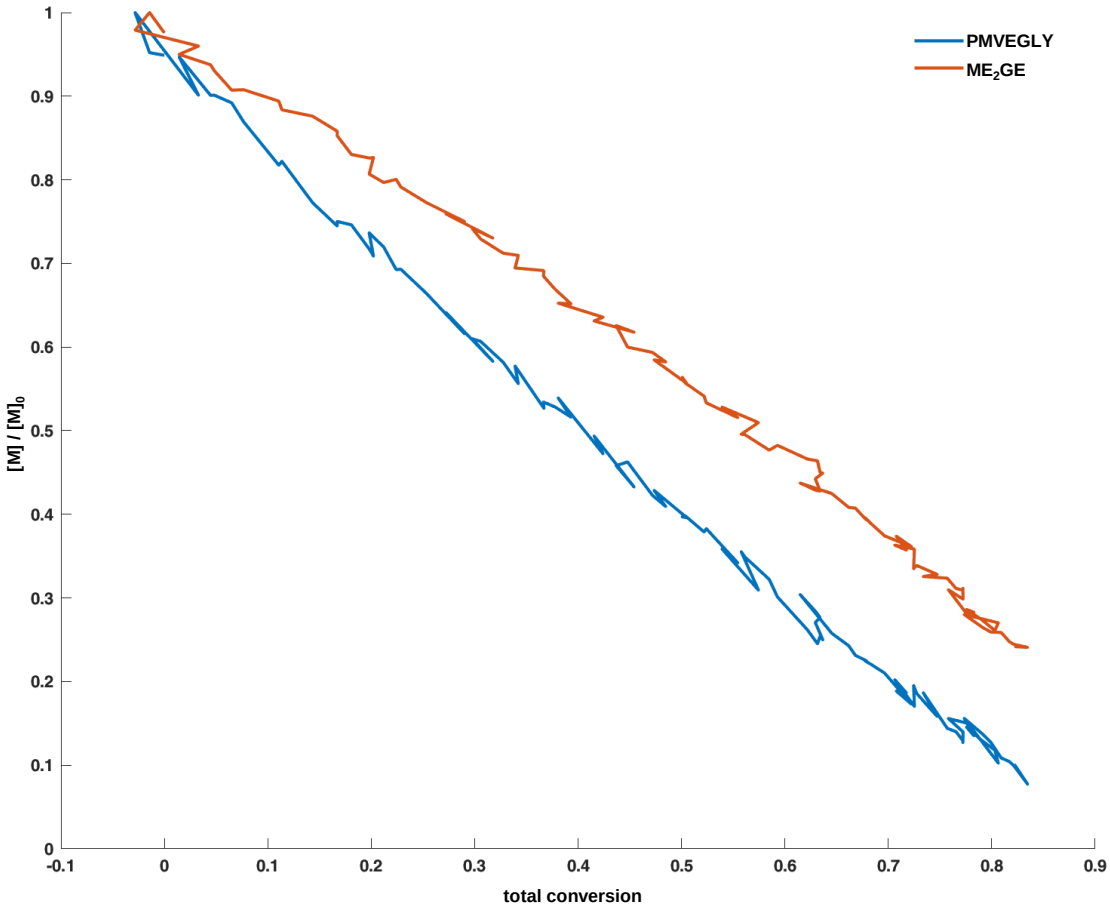

Figure S49: P(ME$_2$GE-co-PMVEGLY): Comonomer concentration plotted versus the total conversion.

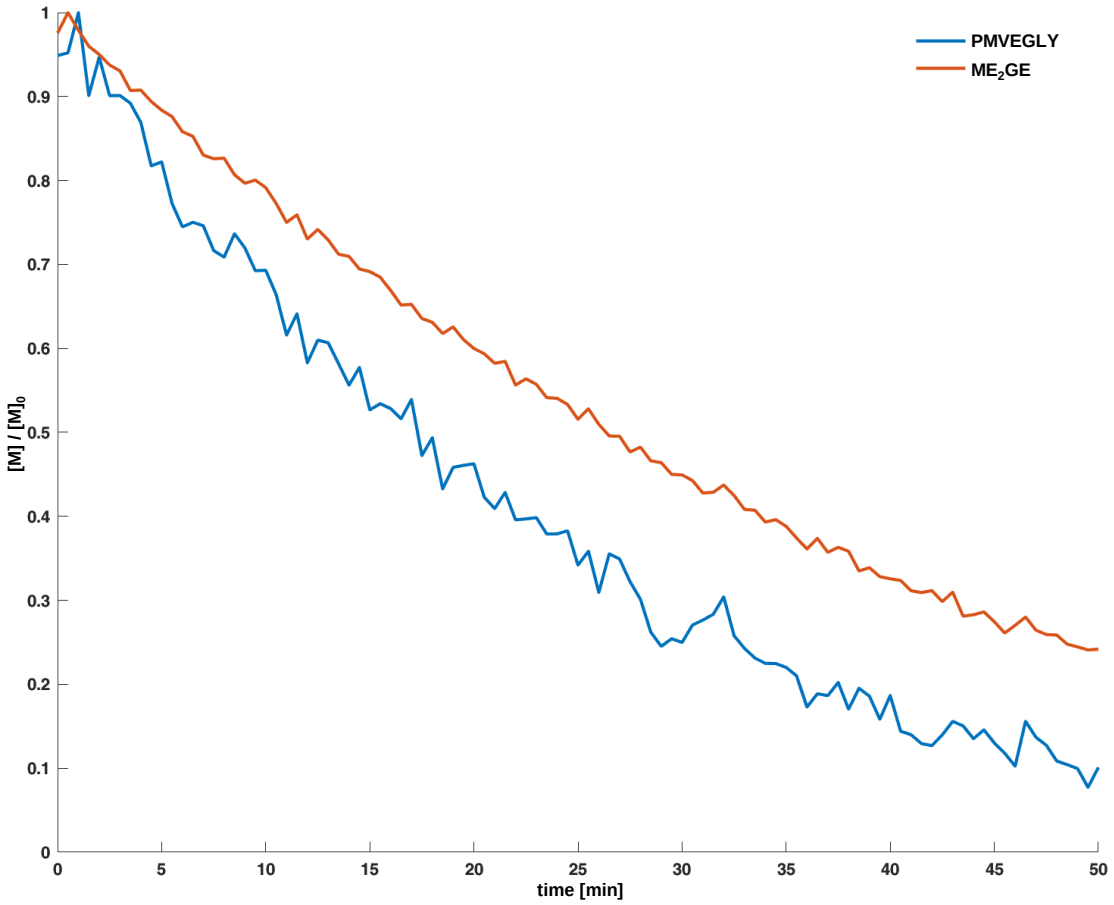

Figure S50: P(ME₂GE-co-PMVEGLY): Comonomer concentration plotted versus the time.

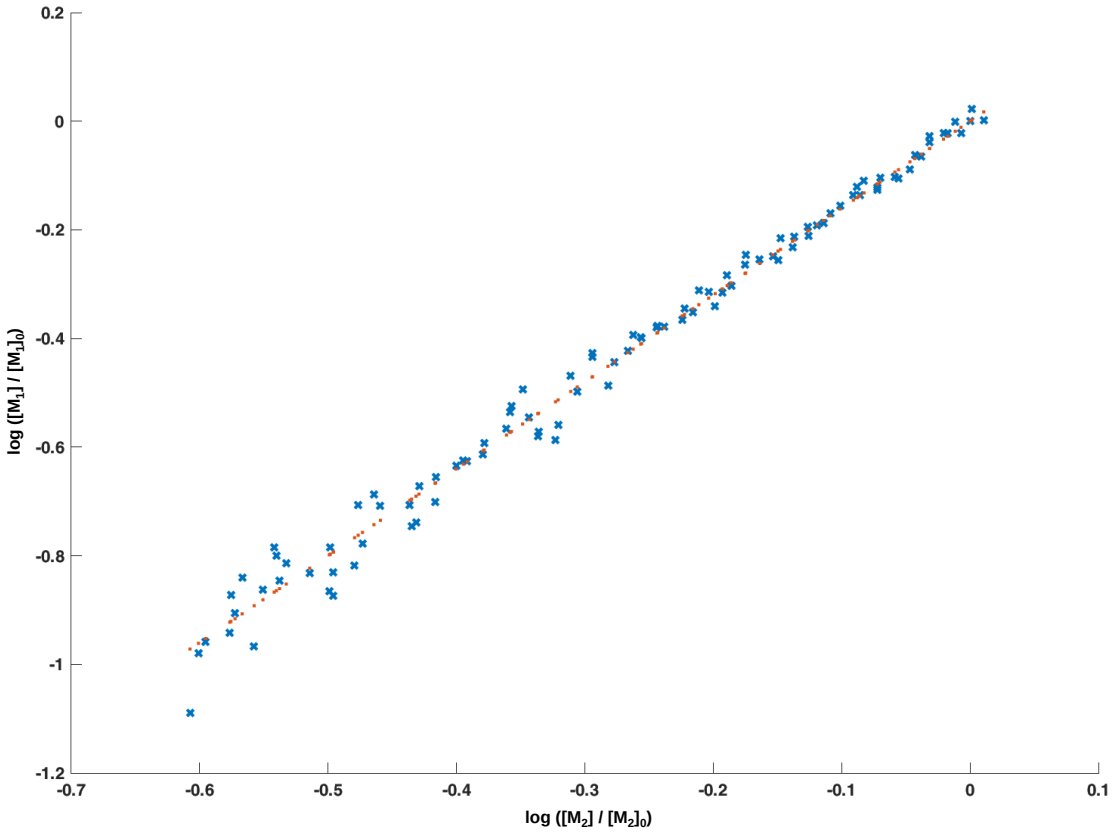

Figure S51: P(ME₂GE-co-PMVEGLY): Jaacks fit for the determination of reactivity ratios.

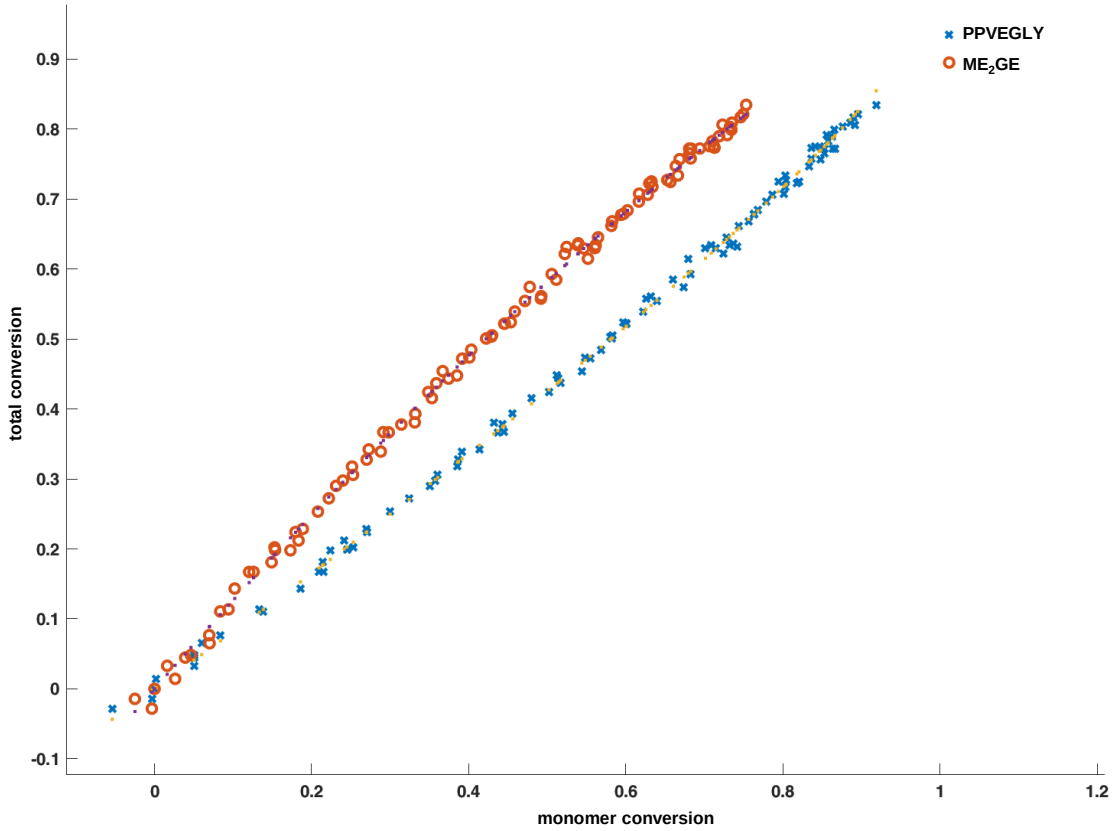

Figure S52: P(ME₂GE-co-PMVEGLY): BSL fit for the determination of reactivity ratios.

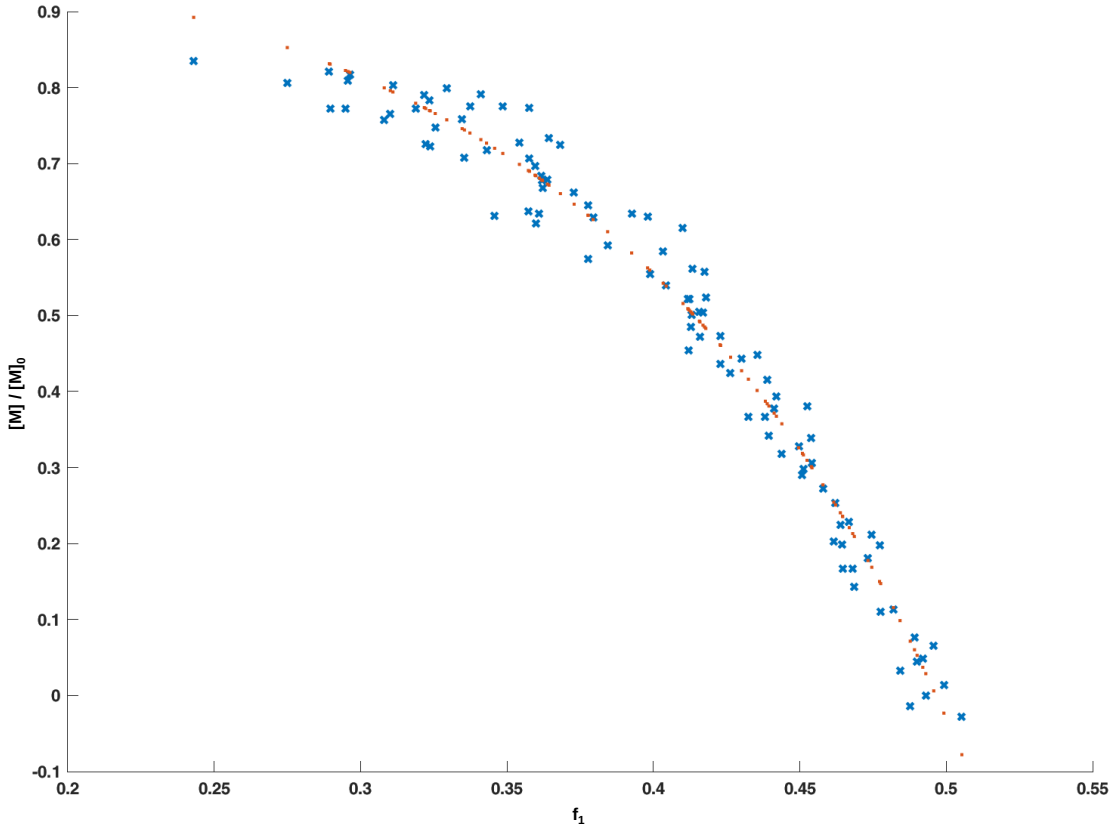

Figure S53: P(ME₂GE-co-PMVEGLY): Meyer-Lowry ideal fit for the determination of reactivity ratios with f_1 = PMVEGLY.

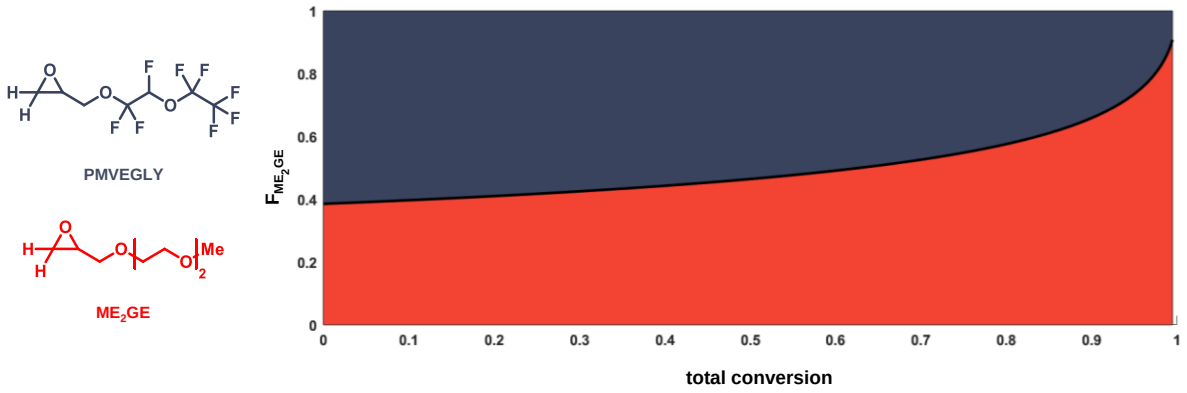

Figure S54: Simulation of the microstructure of P(ME_2GE-co-PMVEGLY).

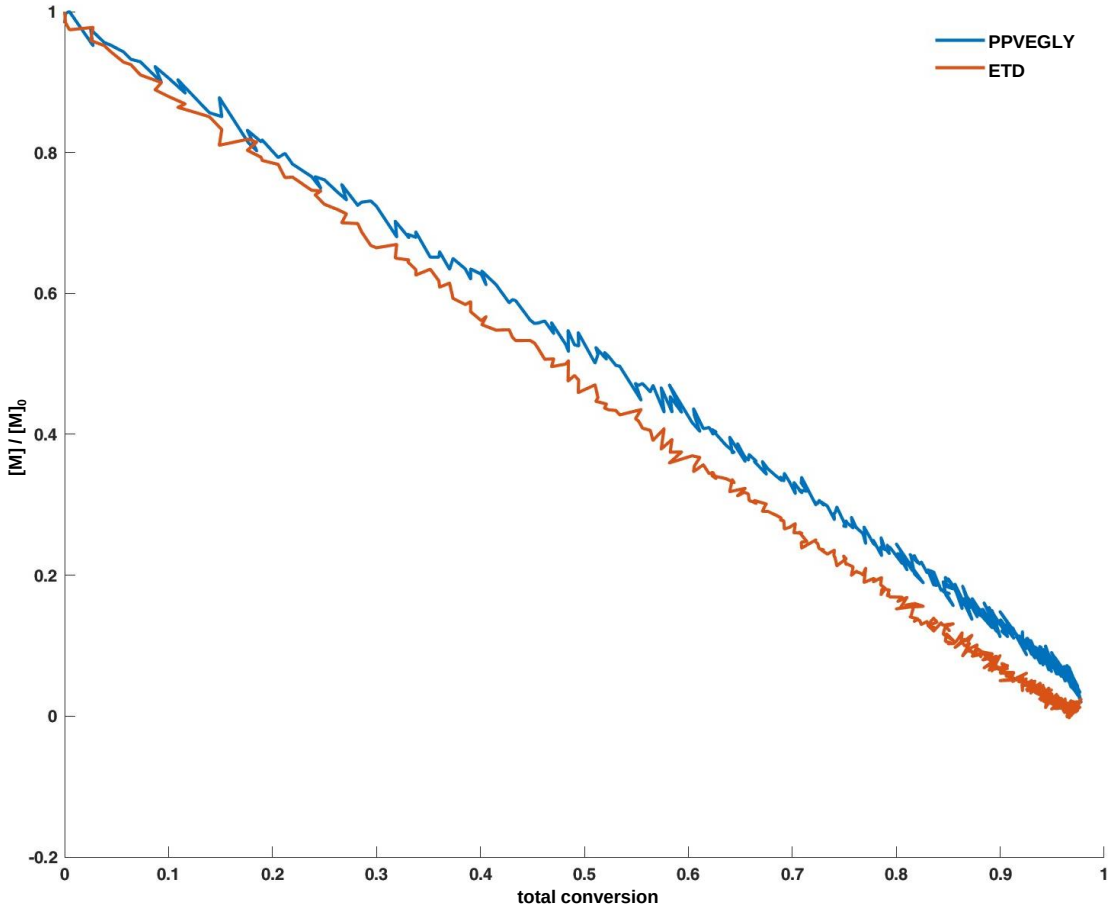

Figure S55: P(ETD-co-PPVEGLY): Comonomer concentration plotted versus the total conversion.

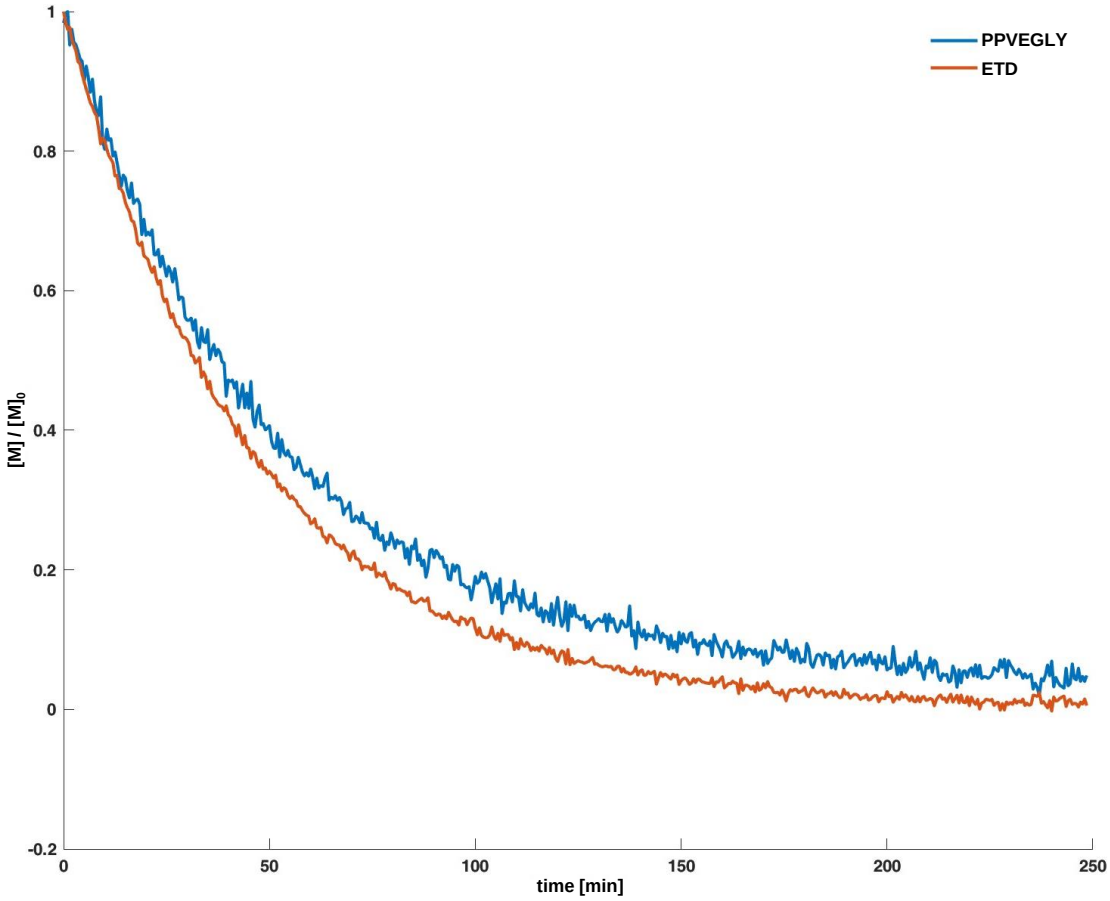

Figure S56: P(ETD-co-PPVEGLY): Comonomer concentration plotted versus the time.

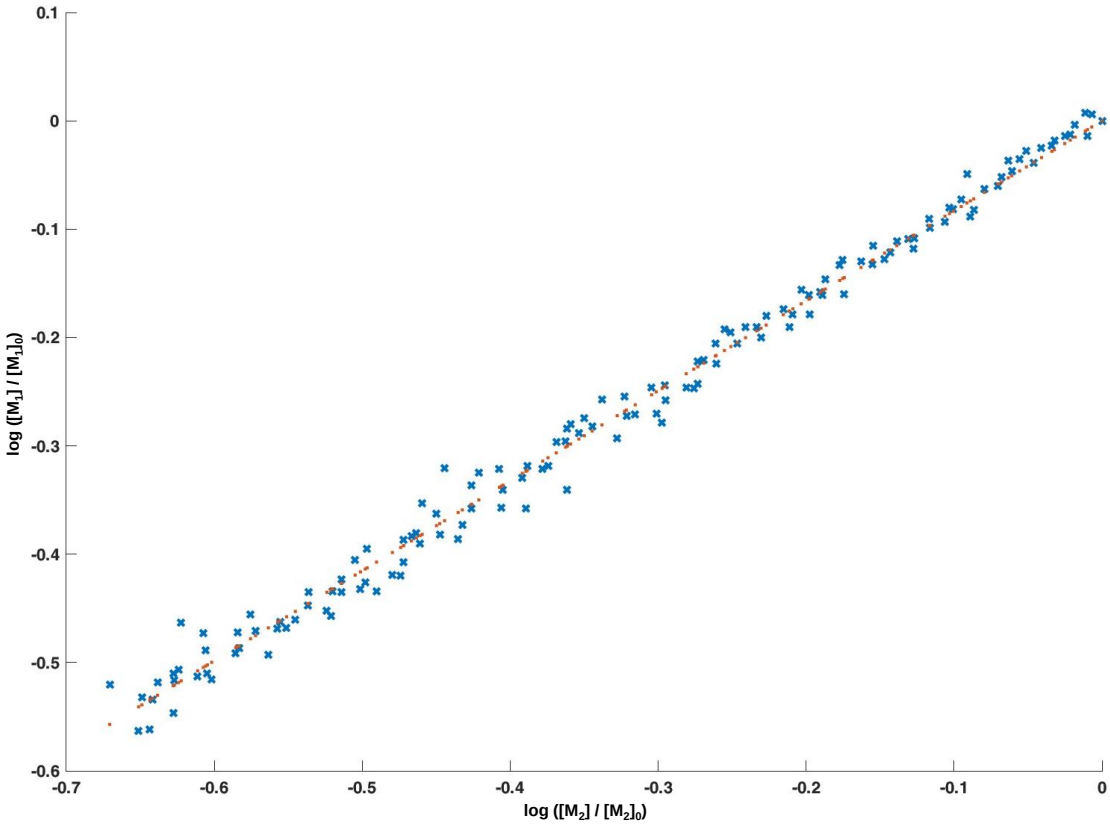

Figure S57: P(ETD-co-PPVEGLY): Jaacks fit for the determination of reactivity ratios.

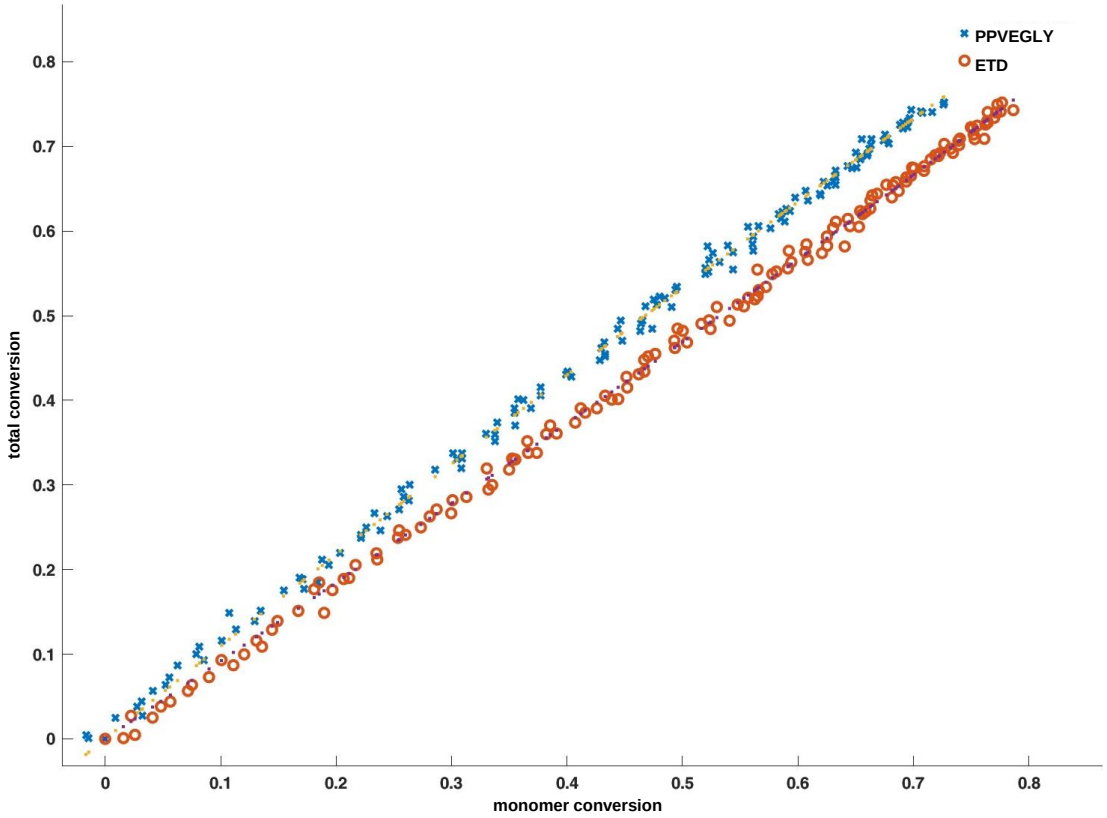

Figure S58: P(ETD-co-PPVEGLY): BSL fit for the determination of reactivity ratios.

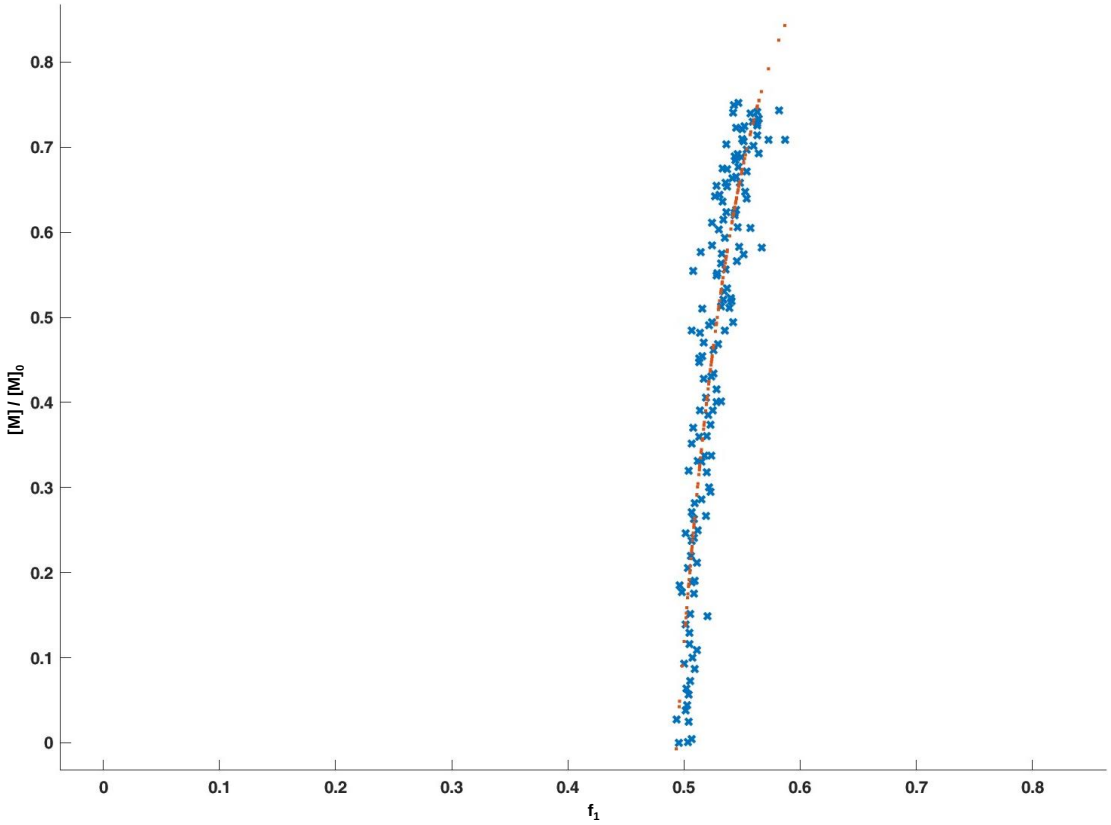

Figure S59: P(ETD-co-PPVEGLY): Meyer-Lowry ideal fit for the determination of reactivity ratios with f_1 = PPVEGLY.

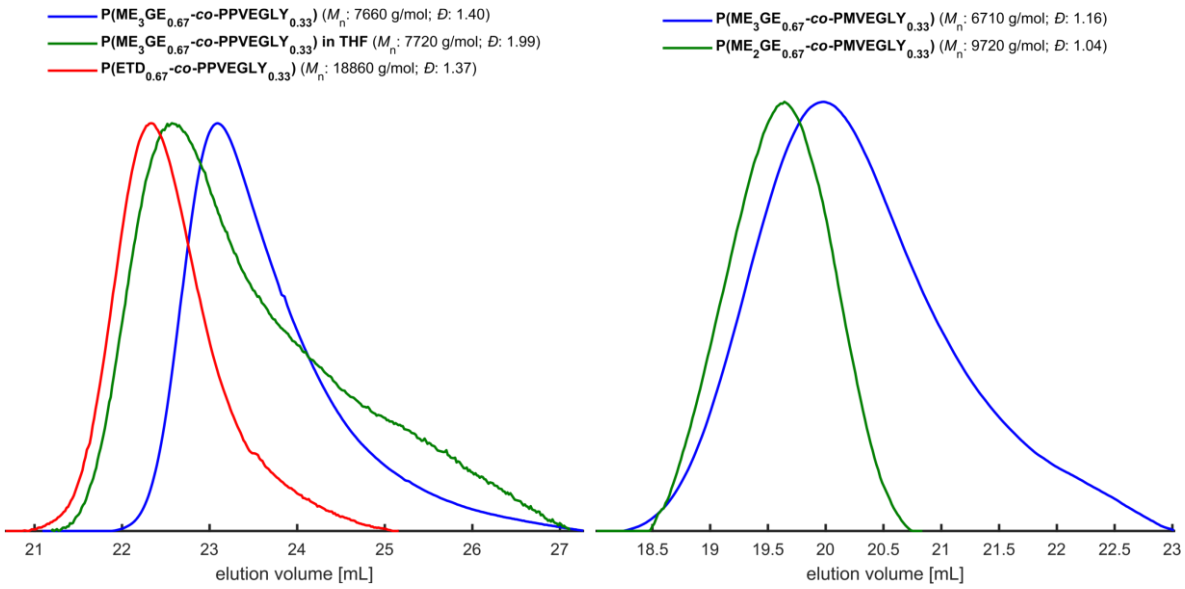

Figure S60: SEC traces (PEG calibration, RI signal). Left: PPVEGLY copolymers measured in THF as eluent; Right: PMVEGLY copolymers measured in DMF as eluent.

Table S4: Calculated reactivity ratios of the comonomer pairs in 2-MeTHF at 10 °C. Data was fitted by using NIREVAL Software from Tobias Johann, Marvin Steube and Holger Frey.[4]

Polymer	parameter	Jaacks	BSL	Meyer-Lowry ideal
P(ME_3GE-*co*-PPVEGLY)	r_{ME_3GE}	0.72 ± 0.01	0.72 ± 0.01	0.75 ± 0.01
	$r_{PPVEGLY}$	1.38 ± 0.01	1.40 ± 0.01	1.34 ± 0.01
	R^2 / *NormRes (NR)*	R^2 = 0.996	*NR* = 0.006	*NR* = 0.078
P(ME_3GE-*co*-PPVEGLY) in THF	r_{ME_3GE}	0.65 ± 0.01	0.66 ± 0.01	0.65 ± 0.01
	$r_{PPVEGLY}$	1.54 ± 0.01	1.52 ± 0.01	1.55 ± 0.01
	R^2 / *NormRes (NR)*	R^2 = 0.999	*NR* = 0.009	*NR* = 0.103
P(ME_3GE-*co*-PMVEGLY)	r_{ME_3GE}	0.82 ± 0.03	0.81 ± 0.03	Insufficient fitting
	$r_{PMVEGLY}$	1.22 ± 0.04	1.24 ± 0.05	
	R^2 / *NormRes (NR)*	R^2 = 0.982	*NR* = 0.003	
P(ME_2GE-*co*-PMVEGLY)	r_{ME_2GE}	0.63 ± 0.01	0.63 ± 0.01	0.62 ± 0.01
	$r_{PMVEGLY}$	1.60 ± 0.02	1.58 ± 0.02	1.62 ± 0.03
	R^2 / *NormRes (NR)*	R^2 = 0.988	*NR* = 0.010	*NR* = 0.163
P(ETD-*co*-PPVEGLY)	r_{ETD}	1.20 ± 0.01	1.20 ± 0.01	1.22 ± 0.02
	$r_{PPVEGLY}$	0.83 ± 0.01	0.83 ± 0.01	0.82 ± 0.02
	R^2 / *NormRes (NR)*	R^2 = 0.991	*NR* = 0.012	*NR* = 1.341

References

(1) Motogami, K.; Kono, M.; Mori, S.; Watanabe, M.; Ogata, N. A new polymer electrolyte based on polyglycidylether. *Electrochimica Acta* **1992**, *37* (9), 1725–1727. DOI: 10.1016/0013-4686(92)80147-E.

(2) AATCC. *Oil Repellency: Hydrocarbon Resistance Test Method 118*, 1997.

(3) Fang, H.; Friedrich, R. Fluorine containing polymers. 16/310,709.

(4) Steube, M.; Johann, T.; Plank, M.; Tjaberings, S.; Gröschel, A. H.; Gallei, M.; Frey, H.; Müller, A. H. E. Kinetics of Anionic Living Copolymerization of Isoprene

and Styrene Using in Situ NIR Spectroscopy: Temperature Effects on Monomer Sequence and Morphology. *Macromolecules* **2019**, *52* (23), 9299–9310. DOI: 10.1021/acs.macromol.9b01790.

4 – Boron bearing polyethers

4.1 Versatile borane polyethers as recyclable catalysts for the synthesis of polyethers and CO_2 based polycarbonates

Larissa Limmer,[a] Philipp Holzmüller,[a] Sandra Schüttner,[a] M. Kevin Brown,[b] Holger Frey[a*]

[a] Johannes Gutenberg-Universität Mainz, Department of Chemistry, Duesbergweg 10 - 14, 55128 Mainz, Germany

[b] Indiana University, Department of Chemistry, Bloomington, Indiana 47405, United States

To be submitted

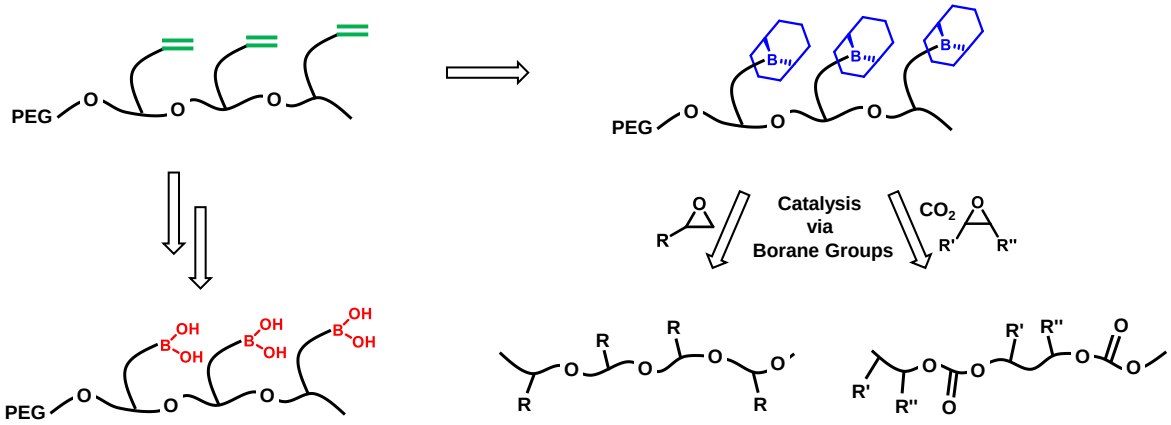

Contributions

L.L. – Concept; performance and evaluation of experiments; writing of manuscript. P.H. – Performance and evaluation of carbon dioxide experiments, writing of manuscript. S.S. – Synthesis of IsoPreGE copolymers. M.K.B. – Support for hydroboration experiments. H.F. – Concept; supervision; editing.

Abstract

Organo boranes are used in a multitude of applications due to their specific properties. Boronic acids are applied in medicine, while trialkyl boranes have gained high interest as catalysts in polymerisations of oxygenated monomers. For this study, borane bearing polymers were prepared by oxyanionic polymerisation starting from allyl glycidyl ether or isoprenol glycidyl ether and ethylene oxide followed by hydroboration, yielding an adaptable polymer class. On the one hand, versatile polymeric boronic acids were achieved after cleavage of boronic esters. On the other hand, 9-BBN bearing polymers were synthesised and studied for their catalytic activity in homo- and copolymerisations as well as their removability via precipitation. Catalysed homopolymerisation of propylene oxide permitted synthesis and purification of poly propylene oxide (*Đ* = 1.10–1.16). Long-chain alkylene oxides were successfully synthesised (*Đ* = 1.22 – 1.58; or bimodal *Đ* = 3.14), but purification was not achieved completely. The catalyst was shown to be recyclable by separation via precipitation and subsequent introduction to the next polymerisation batch. Additionally, the 9-BBN based polymer was able to copolymerise carbon dioxide with cyclohexene oxide to provide poly carbonates with >99% carbonate linkages and polymer selectivity and up to 100% monomer conversion. Separation of the polymer catalyst from the targeted polycarbonate was almost fully possible due to solubility tailoring.

Introduction

Side chain functionalisation enables a broad scope of properties and applications for polyethers. These functionalities can either be incorporated by direct polymerisation of substituted epoxides or by post-polymerisation modifications. The latter is utilised if the functionality is unstable under polymerisation conditions. Double bonds represent a versatile platform for modifications, being readily available for thiol-ene-click[1,2] or hydroboration reactions. Hydroboration of double bonds enables the synthesis of polymers with organo borane side chains.[3,4] One the one hand, alkyl boranes find applications in medicine for example in boron neutron capturing therapy (BNCT)[5,6] or in catalytic polymerisations.[7,8] On the other hand, they are a precursor for other organic reactions like C-C, C-O or C-X bond formation.[9–13] Dialkoxyboranes can be converted to boronic acids,[14] which also found application in medicine. Cambre *et al*. published a review of biomedical applications of boronic acid containing polymers, which include for example sensors for saccharides, controlled drug release and inhibitors for enzymes.[15] These polymers either act by interaction with a target molecule or by reversible formation of thermosets via boroxine formation or hydrogels via esterification with hydroxy bearing polymers.[15–17]

Lewis acidic organo boranes are known as a more sustainable alternative for metal catalysts in the (co)polymerisation of oxygenated monomers such as epoxides and carbon dioxide. Extensive reviews were given recently by Naumann[18] as well as by Zhang, Gnanou and Feng *et al*.[19] In these polymerisations the catalyst forms on the one hand an “ate” complex with the initiator or growing chain and on the other hand activates the monomer, which permits mild polymerisation conditions. Due to the mild conditions and the low basicity of the “ate” complex the polymerisation runs with reduced side reactions.[20–22] As a consequence of this duality, high catalyst amounts in respect to initiator are needed.[23,24] To counter this, multinuclear systems consisting of the initiating onium salt and multiple organo boron groups in one molecule were developed.[25,26] Recent focus came to the removal and recycling of the catalyst. Feng, Gnanou and co-workers first reported a complex multistep recycling system for triethyl borane[27] and later a simple recycling system for a bifunctional catalyst combining the borane and the initiator in one molecule.[23]

Hydroboration of alkenes is often realised by catalysis with Rh, Ir, Fe or Co ligand complexes leading to anti-Markovnikov products, with typically a minor yield of

Markovnikov by-products.[28–32] Ru catalysed hydroboration was studied, but hydrogenation, isomerisation and dehydrogenative borylation occurred as side reactions.[33–35] Kisan *et al*. developed an anti-Markovnikov Ru catalysed hydroboration, which does not suffer from these side reactions and reported a broad scope of alkenes including allyl glycidyl ether (AGE).[32] Hinkes *et al*. reported a monophasic and mild strategy for transesterification of boronic esters to yield boronic acids. They used methyl boronic acid and acidic or basic conditions, in respect to the educt stability and easy purification via evaporation of reagents and byproducts.[14]

Motivated by the versatility of organo boranes it was intriguing to investigate polymeric organo boranes, allowing multiple borane groups per molecule. In this work the synthesis of multifunctional polyethers bearing organo boranes or boronic esters yielding boronic acids after hydrolysis is demonstrated. The organo boranes were furthermore used as catalysts in activated homopolymerisation of epoxides as well as copolymerisation of epoxides and carbon dioxide to obtain polycarbonates. To the best of our knowledge, this is the first time a polymeric catalyst based on organo boranes was used for these applications. In addition, recyclability was demonstrated.

Experimental Section

Materials

Isoprenol (≥97% purity), epichlorohydrin (99% purity) and pinacolborane (97% purity) were obtained from Thermo Fisher Scientific. Ethylene glycol monobutyl ether (99% purity), allyl glycidyl ether (>99% purity), epoxytetradecane (>95% purity), epoxyhexadecane (>80% purity), mPEG2000 and tetraoctylammonium bromide (>98% purity) were purchased from TCI. Ethylene oxide was obtained in 99.8% purity from Air Liquide. 9-Borabicyclo[3.3.1]nonane (0.5 M in THF) and dichloro(p-cymene)ruthenium(II) dimer (97% purity) were obtained from Sigma-Aldrich. Carbon dioxide 5.0 was purchased from Westfalen AG (Münster, Germany) and dried over molecular sieve for three days prior to use. Bis(triphenylphosphine)iminium chloride ([PPN]Cl) was received from abcr GmbH in 97% purity. Cyclohexene oxide (CHO) was purchased from Alfa Aesar in 98+% purity. All remaining chemicals were purchased from Acros Organics, Fisher Scientific, Roth, Sigma-Aldrich, TCI, VWR, or Deutero GmbH.

Instrumentation

NMR spectra were measured on a Bruker Avance III HD 300 (5 mm BBFOProbe with z-Gradient and ATM) and referenced internally with the deuterated solvent. Size exclusion chromatography (SEC) of polyethers was carried out in *N*,*N*-dimethylformamide (DMF) containing 1 g/mL lithium bromide at 50 °C with a flow rate of 1 mL/min on an Agilent1100 series (Agilent Technologies, Santa Clara, CA, USA), with HEMA columns with 300/100/40 Å porosity (Polymer Standards Service (PSS), Mainz, Germany) and Agilent G1362A RID as refractive index detector. Polycarbonates were measured in tetrahydrofurane (THF) at 35 °C on an Agilent 1100 series using SDV columns of 100/1000/10000 Å porosity (PSS). Calibration was done via the internal standard toluene and PEG or PS standards from PSS. MALDI ToF measurements were performed on a Bruker Autoflex maX. Samples were prepared with Dithranol (DIT) if not otherwise noted.

Monomer synthesis

IsoPreGE was performed analogous to literature.[36]

Polymer synthesis

Homo- and block- copolymerisation: Ethylene glycol monobutyl ether (1 eq) or mPEG macroinitiator (1 eq) and KO^{t}Bu (0.8-0.9 eq) were dissolved in a benzene:methanol 6:1 mixture in a dried Schlenk flask and stirring while heating at 50-70 °C for 30-60 min. Subsequently, they were dried under reduced pressure at room temperature or 70 °C, respectively. Homopolymerisations were performed in bulk, while block copolymerisations were performed in DMSO or at 66 °C in melt. The monomer was dried over CaH_2, distilled, and added to the reaction via syringe. The polymerisation was performed over night at 45 °C. The homopolymer was extracted via liquid-liquid extraction with DCM and water and dried under reduced pressure. Typical yields: 90%. Block copolymers were purified via precipitation in cold diethyl ether. Typical yields: 80%.

^{1}H NMR (300 MHz, C*D*Cl$_3$):

EGBE-PAGE δ [ppm] = 5.88 (ddt, C*H*=CH$_2$), 5.30–5.12 (m, CH=C*H*$_2$), 4.06–3.96 (m, C*H*$_2$-CH=CH$_2$), 3.77–3.41 (m, backbone and C*H*$_2$-O), 1.60–1.51 (m, CH$_3$-CH$_2$-C*H*$_2$), 1.39–1.32 (m, CH$_3$-C*H*$_2$-CH$_2$), 0.91 (t, C*H*$_3$-CH$_2$-CH$_2$).

mPEG-*b*-PAGE δ [ppm] = 5.88–5.75 (m, C*H*=CH_2), 5.22–5.05 (m, CH=CH_2), 3.90 (dd, CH_2-CH=CH_2), 3.78–3.38 (m, backbone and CH_2-O), 3.30 (s, CH_3-O).

Statistical copolymerisation: The polymerisation was done analogous to the block copolymerisation. Ethylene oxide was cryo-transferred to the to -80 °C cooled flask containing the reaction mixture and the polymerisation was allowed to take place over 3 d at 40 °C. Typical yields: 80%.

^{1}H NMR (300 MHz, C*D*Cl_3):

mPEG-*b*-P(EG-*co*-AGE) analogous to mPEG-*b*-PAGE

mPEG-*b*-P(EG-*co*-IsoPreGE) δ [ppm] = 4.70 (d, =CH_2), 3.97–3.38 (m, backbone and CH_2-O), 3.35 (s, CH_3-O), 2.34 (s, O*H*), 2.25 (t, CH_2-C_q), 1.71 (s, CH_3).

Methylation of hydroxy group: The synthesised double bond bearing polymer (1 eq) was dissolved in benzene and dried under reduced pressure in a dried Schlenk flask. The polymer was dissolved in dry THF and sodium hydride (3 eq) was added. After 4 h of stirring methyl iodide (3 eq) was added and the mixture was stirred for 1 d. Ammonia solution (25%$_{aq}$, 9 eq) was added and stirred for 4 h more to ensure complete neutralisation of excess methyl iodide. The mixture was filtrated, extracted with DCM and water and dried. Typical yields: 60%. ^{1}H NMR: analogous to mPEG-copolymers without the OH singlet.

Synthesis of polymers bearing boronic acids

The synthesis consisted of two synthesis steps. 1) Pinacolborane synthesis was adapted from Kisan *et al*.:[32] The synthesised polymer was combined with dichloro(p-cymene)ruthenium(II) dimer (0.002 eq per double bond), dissolved in benzene and dried under reduced pressure in a dried Schlenk flask. The mixture was dissolved in dry THF and pinacolborane (1.2 eq per double bond) was added. After stirring for 1 d the mixture was filtrated over silica, washed with THF and dried. The polymer was obtained in quantitative yields after drying. In reactions of PAGE hydrogenation side reactions led to formation of propoxymethyl side chains (PGE) in typical yields of <21% of the double bonds. In reactions with PIsoPreGE hydrogenation was with 57% the main reaction (HydPreGE), while 14% of the double bonds remained.

^{1}H NMR (300 MHz, C*D*Cl$_3$):

EGBE-P(PGE-*co*-BpinAGE) δ [ppm] = 3.59–3.34 (m, backbone and C*H*$_2$-O), 1.73–1.53 (m, C*H*$_2$-CH$_2$-B and CH$_3$-CH$_2$-C*H*$_2$ and CH$_3$-C*H*$_2$), 1.40–1.32 (m, hydrogenated C*H*$_2$), 1.25–1.21 (m, C*H*$_3$,), 0.99 (t, hydrogenated C*H*$_3$), 0.90 (t, C*H*$_3$-CH$_2$), 0.75 (t, C*H*$_2$-B).

mPEG$_{123}$-*b*-P(EG$_{32}$-*co*-IsoPreGE$_2$-*co*-HydPreGE$_8$-*co*-BpinIsoPreGE$_4$)Me δ [ppm] = 4.66 (d, =C*H*$_2$), 3.92–3.34 (m, backbone and C*H*$_2$-O), 3.31 (s, C*H*$_3$-O), 2.21 (t, C*H*$_2$-C$_q$), 1.79–1.67 (m, C*H*-(CH$_3$)$_2$), 1.70–1.64 (m, C*H*-CH$_3$ and C$_q$-C*H*$_3$), 1.59 (s, CH-C*H*$_3$), 1.55–1.43 (m, C*H*$_2$-CH-CH$_3$), 1.44–1.32 (m, C*H*$_2$-CH-(CH$_3$)$_2$), 1.17–1.15 (m, C*H*$_3$(pinacol)), 0.87–0.75 (m, CH-(C*H*$_2$)$_2$), 0.63–0.55 (m, C*H*$_2$-B).

^{13}C NMR (75 MHz, C*D*Cl$_3$):

EGBE-P(PGE-*co*-BpinAGE) δ [ppm] = 82.93 (s, *C*$_q$), 78.84 (s, *C*H), 73.39–70.03 (m, backbone and *C*H$_2$-O), 24.89 (s, *C*H$_3$), 24.81 (s, CH$_3$-CH$_2$-*C*H$_2$), 24.63 (s, *C*H$_2$-CH$_2$-B), 24.14 (s, CH$_3$-*C*H$_2$), 12.62 (s, hydrogenated *C*H$_3$), 10.73 (s, *C*H$_3$-CH$_2$), 7.38 (s, *C*H$_2$-B).

mPEG$_{123}$-*b*-P(EG$_{32}$-*co*-IsoPreGE$_2$-*co*-HydPreGE$_8$-*co*-BpinIsoPreGE$_4$)Me δ [ppm] = 111.42 (s, =*C*H$_2$), 82.71 (d, *C*$_q$), 71.42–69.91 (m, backbone and *C*H$_2$-O), 59.99 (s, C*H*$_3$-O), 38.93 (s, *C*H$_2$-CH-CH$_3$), 38.42 (s, *C*H$_2$-CH-(CH$_3$)$_2$), 37.69 (s, C*H*$_2$-C$_q$), 26.58 (*C*H-(CH$_3$)$_2$), 25.79 (s, *C*H-CH$_3$), 24.81 (d, *C*H$_3$(pinacol)), 24.58 (*C*H$_2$-B), 22.64 (s, C$_q$-*C*H$_3$), 22.30 (s, CH-(*C*H$_2$)$_2$), 18.03 (s, CH-*C*H$_3$).

2) Boronic acid synthesis was adapted from Hinkes *et al*.[14]: The polymeric pinacol borane was combined with methylboronic acid (MBA, 5 eq per ester) and stirred in 5% trifluoro acetic acid solution in DCM for 1 d. Volatile compounds and solvents were removed under reduced pressure. The polymer was dissolved or suspended in 1 N HCl, to prevent mixed anhydride formation. BpinAGE containing polymers showed full conversions; BpinIsoPreGE conversions of 94%.

^{1}H NMR (300 MHz, *D*$_2$O):

EGBE-P(PGE-*co*-HOBAGE) δ [ppm] = 3.71–3.37 (m, backbone and C*H*$_2$-O), 1.89–1.55 (m, CH$_3$-CH$_2$-C*H*$_2$), 1.71–1.61 (m, C*H*$_2$-CH$_2$-B), 1.62–1.53 (m, CH$_3$-C*H*$_2$), 1.37–1.31 (m, hydrogenated C*H*$_2$), 0.92–0.88 (m, C*H*$_3$ and hydrogenated C*H*$_3$), 0.78 (t, C*H*$_2$-B).

mPEG$_{123}$-*b*-P(EG$_{32}$-*co*-IsoPreGE$_{2}$-*co*-HydPreGE$_{8}$-*co*-(HOBIsoPreGE$_{0.94}$-*co*-BpinIsoPreGE$_{0.06}$)$_{4}$)Me δ [ppm] = 3.94–3.40 (m, backbone and *C*H$_2$-O), 3.36 (s, *C*H$_3$-O), 1.82–1.39 (m, C*H*$_2$-CH-CH$_3$; C*H*-CH$_3$; C*H*$_2$-C$_q$; C$_q$-C*H*$_3$; C*H*$_2$-CH-(CH$_3$)$_2$; C*H*-(CH$_3$)$_2$; linker to Bpin), 1.20 (s, C*H*$_3$(pinacol), 0.93–0.83 (m, CH-C*H*$_3$, CH-(C*H*$_2$)$_2$), 0.68–0.60 (m, C*H*$_2$-B), not visible =*C*H$_2$.

^{13}C NMR (75 MHz, *D*$_2$O):

EGBE-P(PGE-*co*-HOBAGE δ [ppm] (not referenced) = 78.87 (d, *C*H), 73.16–58.62 (m, backbone and C*H*$_2$-O), 31.28 (s, CH$_3$-CH$_2$-*C*H$_2$), 23.58 (s, *C*H$_2$-CH$_2$-B), 22.03 (s, CH$_3$-C*H*$_2$), 18.7 (s, hydrogenated *C*H$_2$), 13.1 (s, hydrogenated *C*H$_3$), 10.68 (s, *C*H$_3$), 9.85 (s, *C*H$_2$-B).

mPEG$_{123}$-*b*-P(EG$_{32}$-*co*-IsoPreGE$_{2}$-*co*-HydPreGE$_{8}$-*co*-(HOBIsoPreGE$_{0.94}$-*co*-BpinIsoPreGE$_{0.06}$)$_{4}$)Me: no full analysis was possible due to signal intensities. δ [ppm] (not referenced) = 70.06–69.54 (backbone and *C*H$_2$-O), 58.01 (C*H*$_3$-O), 37.90 (*C*H$_2$-CH-CH$_3$), 25.94 (*C*H-CH$_3$), 21.82 (CH-(*C*H$_3$)$_2$), 15.63 (CH-*C*H$_3$).

Synthesis of the polymeric catalyst for polymerisations

Hydroboration was adapted from Kisan *et al*.:[32] The polymer was combined with dichloro(p-cymene)ruthenium(II) dimer (0.002 eq per double bond), dissolved in benzene and dried under reduced pressure in a dried Schlenk flask. 9-Borabicyclo[3.3.1]nonane (0.5 M in THF, 0.6-1 eq per double bond) was added via syringe and the solution was stirred for 1 d. The polymer was dried and used directly or stored in the glovebox. No further characterisation was done due to the instability of the organo borane.

Catalytic polymerisation of epoxides

Tetraoctylammonium bromide (1 eq) was dissolved in benzene and dried under reduced pressure in a dried Schlenk flask. The in dry THF dissolved polymeric catalyst (8 eq of 9-BBN) and the previously with calcium hydride dried monomer were added via syringe. Polymerisation took place over 24–72 h. Separation of the product from polymeric catalyst was achieved, by exploiting solubility differences of catalyst and synthesised polymer. Isolation was done via precipitation either in ice cold diethyl ether or methanol or via extraction. For recycling studies, precipitation in diethylether was conducted inside the glove box. The recovered catalyst was dried under Schlenk

conditions, redissolved in THF, and introduced into a new polymerisation. Characterisation data are literature known.

Catalytic polymerisation of epoxides with carbon dioxide

The general polymerisation procedure for polycarbonates is described in the following. Prior to polymerisation, [PPN]Cl was suspended in benzene and dried under reduced pressure and CHO was dried over calcium hydride. CHO (1.0 mL, 59 mmol) polymeric catalyst (15 mg, 0.040 mmol 9-BBN units), [PPN]Cl (4.4 mg, 0.0075 mmol) and toluene (0.3 mL) were placed in an autoclave, equipped with a stirring bar, in an inert argon atmosphere. The reaction mixture was stirred at a carbon dioxide pressure of 50 bar at 60 °C for 48 hours. The crude product was dissolved in dichloromethane, and the catalyst was deactivated with a 5% volume HCl solution in methanol. The product was precipitated using ice-cold methanol as a non-solvent. The obtained colourless solid was dried under reduced pressure. The polymer yields ranged between 30 and 76%.

1H NMR (300 MHz, C*D*Cl_3):

PCHC δ [ppm] = 4.80 (m, 2H, CH-CH polymer backbone), 2.10 (m, 2H, CH-C*H*$_2$-CH_2), 1.70 (m, 2H, CH-C*H*$_2$-CH_2), 1.61−1.23 (m, 4H, C*H*$_2$-C*H*$_2$).

Results and Discussion

First, functional homo- and copolymers bearing double bonds were synthesised via anionic ring-opening polymerisation (AROP) and were utilised in post-polymerisation modifications to obtain borane group side-functionalisation. Allyl glycidyl ether was chosen as a precursor, as a cheap and industrial relevant compound. Furthermore, isoprenol glycidyl ether was studied as a potentially biobased alternative. mPEG macroinitiators were used to improve solubility in various solvents and to exploit its crystallinity as a possibility for purification via precipitation. Additionally, ethylene oxide (EO) was used for copolymerisations to adjust the density of functionalisation. Polymeric pinacolboranes (PBpin) were synthesised and cleaved to yield boronic acids, a promising functional group for biomedical applications. Alternatively, polymers bearing 9-borabicyclo[3.3.1]nonane (9-BBN) were synthesised and

ultimately used as polymeric catalysts in subsequent catalytic polymerisations of oxygenated monomers. An overview over the reaction pathway is given in Scheme 1.

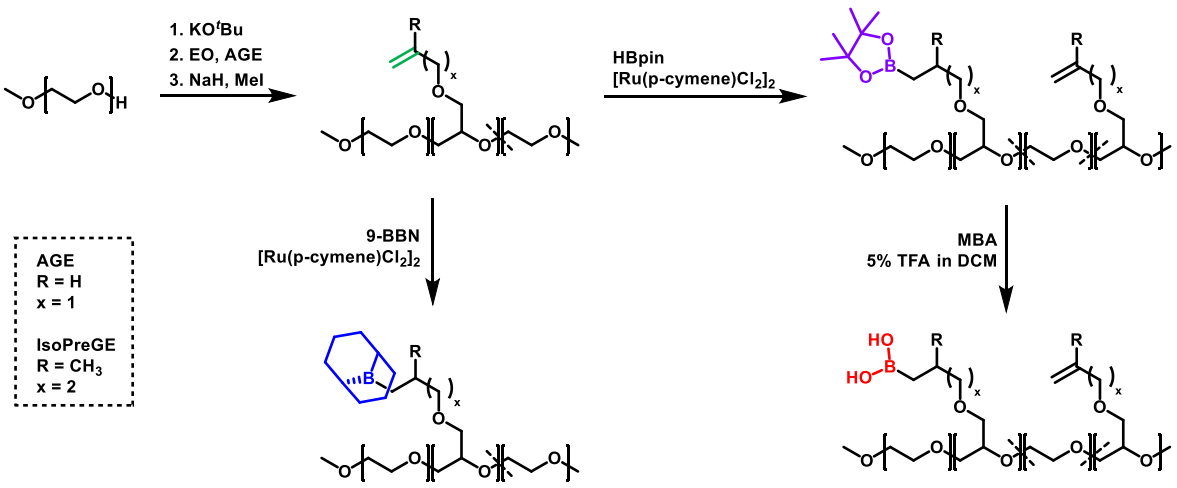

Scheme 1: Overview of exemplary synthesis pathways for organo boranes as well as boronic esters and acids.

Monomer-activated anionic ring-opening polymerisation (MAROP) of epoxides as well as copolymerisation of cyclohexene oxide with carbon dioxide were performed, to test the scope of the catalytic polymers in representative systems (Scheme 2).

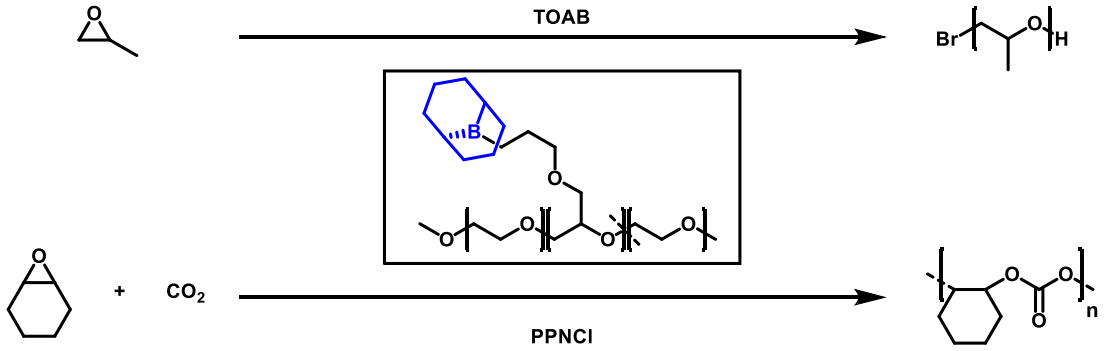

Scheme 2: Catalytic polymerisations utilising the synthesised polymers as catalyst.

Polymeric precursors: Poly (allyl glycidyl ether) (PAGE) and Poly (isoprenol glycidyl ether) (PIsoPreGE) as well as their block and statistical copolymers with ethylene oxide (EO) were synthesised via anionic ring-opening polymerisation (AROP) in bulk or in DMSO. Polymerisations in THF or toluene were significantly slower or needed higher reaction temperatures. Polymers designed for the use as a catalyst were methylated to prevent the hydroxy term from serving as an initiator in subsequent catalytic polymerisations (Figure S2). The characterisation data of polymers further used for modification are listed in Table 1. To investigate achievable comonomer ratios, extended series of polymers were synthesised (see SI Table S1 for more information).

Table 1: Characterisation data for the synthesised precursor polymers.

Polymer	P_n^{th}*(GE)*	M_n^a (g mol^{-1})	M_n^b (g mol^{-1})	$Đ^b$
EGBE-PAGE$_{32}$	37	3770	2110	1.09
EGBE-PAGE$_{32}$Me	37	3790	2070	1.12
mPEG$_{51}$-*b*-PAGE$_{13}$Me	15	3780	2840	1.04
mPEG$_{51}$-*b*-PAGE$_{28}$Me	29	5580	3250	1.11
mPEG$_{123}$-*b*-P(EG$_{25}$-*co*-AGE$_{24}$)Me	32	9360	7440	1.04
mPEG$_{123}$-*b*-P(EG$_{32}$-*co*-IsoPreGE$_{14}$)Me	23	8770	7530	1.05

[a]Determined by ^{1}H NMR spectroscopy (C*D*Cl$_3$, 300 MHz). [b]Determined by SEC (DMF, RI detector, PEG standards).

The synthesis of block copolymers yielded typically two polymeric species. After isolating the block copolymer via precipitation, the second species remained in the mother liquor and was identified via ^{1}H NMR spectroscopy as the homopolymer of the substituted monomer (exemplary spectra of both fractions is given in Figure S1), presumably formed due to monomer initiation. In consequence, the degree of polymerisation and the molecular weight of the block copolymer is lower than targeted. SEC of the isolated polymers showed monomodal and narrow distributions (Figure 1). Underestimation of the molecular weight by SEC is caused by different hydrodynamic radii for the substituted polyethers in comparison to the PEG standards and the underestimation consequently increased with increasing percentage of substituted comonomer.

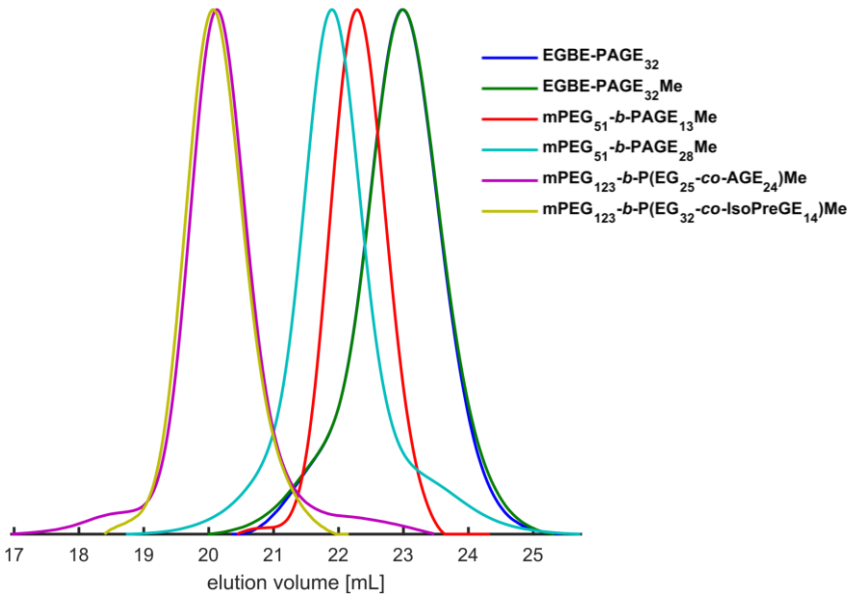

Figure 1: SEC traces (DMF, RI signal) of the synthesised precursor polymers.

Polymeric boronic acids: Subsequently, the polymers were used in catalytic hydroboration reactions to yield polymeric organo boranes. Hydroboration without the dichloro(p-cymene)ruthenium(II) dimer catalyst remained unsuccessful, albeit reported in the literature for different systems.[4,37] The boronic esters were cleaved to yield boronic acids. Characterisation data of the stable Bpin as well as boronic acid bearing polymers is given in Table 2 (NMR spectra are given in SI).

Table 2: Characterisation data for esterified and hydrolysed polymers.

Boronic ester				Boronic acid	
Polymer[a]	M_n[a] (g mol^{-1})	M_n[b] (g mol^{-1})	$Đ$[b]	Conversion (%)	M_n[a] (g mol^{-1})
EGBE-P(PGE$_7$-*co*-BpinAGE$_{25}$)	6980	3220	1.10	100	4930
EGBE-P(PGE$_6$-*co*-BpinAGE$_{26}$Me	7130	3100	1.10	100	5000
mPEG$_{51}$-*b*-BpinPAGE$_{13}$Me	5430	3370	1.24	100	4360
mPEG$_{123}$-*b*-P(EG$_{32}$-*co*-IsoPreGE$_2$-*co*-HydPreGE$_8$-*co*-BpinIsoPreGE$_4$)Me	9300	7470	1.14	94	8970

[a]Determined by ^{1}H NMR spectroscopy (C*D*Cl$_3$, 300 MHz). [b]Determined by SEC (DMF, RI detector, PEG standards).

The conversions was monitored via ^{1}H NMR spectroscopy. The double bonds of AGE (co)polymers were fully consumed, albeit up to 21% were hydrogenated instead of hydroborated. Analogous signals are observable in previous work by Kisan *et al.*[32] Expectedly, SEC measurements showed an increase of the molecular weight after hydroboration (Figure 2). Subsequently, the boronic esters were cleaved via acidic hydrolysis to yield the versatile polymeric boronic acids. Full conversion was verified via NMR spectroscopy (Figure S3). IsoPreGE copolymers showed reduced reactivity in the hydroboration reaction with pinacolborane (HBpin). However, mPEG$_{51}$-*b*-IsoPreGE$_{6}$ did not react in hydroboration and was recovered. The polymer mPEG$_{123}$-*b*-P(EG$_{32}$-*co*-IsoPreGE$_{14}$)Me has a reduced density of functional groups. For this polymer 29% of the double bonds were successfully hydroborated, while 14% remained unaltered and 57% underwent hydrogenation (HydPreGE). Broadening of the molecular weight distribution was observed in SEC, as a result of the product mixture. The additional substitution of IsoPreGE in comparison to AGE presumably hinders the HBPin-catalyst-alkene intermediate formation. Kisan *et al*. reported the catalyst to sterically discriminate monosubstituted alkenes, while being able to accommodate sterically hindered alkenes. Furthermore, Kisan *et al*. reported slightly lower conversions for alkenes bearing electron-donating substituents.[32]

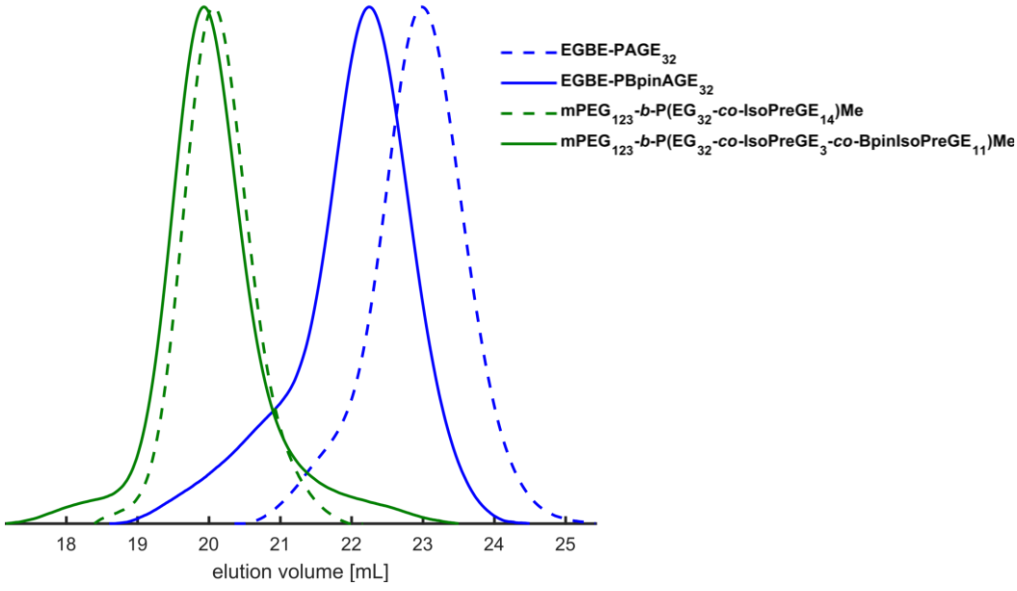

Figure 2: SEC traces (DMF, RI signal) of exemplarily hydroboration reaction with HBpin.

Polymeric catalysis: EGBE-PBBNAGE$_{32}$Me, mPEG$_{51}$-*b*-PAGE$_{28}$Me, mPEG$_{123}$-*b*-P(EG$_{25}$-*co*-PAGE$_{24}$)Me and mPEG$_{123}$-*b*-P(EG$_{32}$-*co*-IsoPreGE$_{14}$)Me were used in hydroboration reactions with 9-BBN. Dialkylboranes show in hydroboration reactions

generally a higher reactivities than dialkoxyboranes. Consequently, hydroboration with 9-BBN yielded full conversions for AGE as well as IsoPreGE copolymers. For the synthesis of catalyst mPEG$_{123}$-*b*-P(EG$_{25}$-*co*-BBNAGE$_{6}$-*co*-BBNAGE$_{18}$)Me an excess of double bonds was used to ensure the absence of residual 9-BBN. In this case, successful hydroboration was verified by decreased intensity of the double bond signals. The polymers were not characterised further in respect to their instability in air.

Polyethers: The 9-BBN functional polymers were used as the Lewis acid catalyst in catalytic polymerisations of epoxides. To demonstrate the scope of this polymeric catalyst, amorphous poly (propylene oxide) (PPO) as well as crystalline poly (epoxytetradecane) (PETD) or poly (epoxyhexadecane) (PEHD) were synthesised via MAROP. In control experiments, MAROP was performed using no Lewis acid catalyst, pure 9-BBN or the Bpin modified polymer mPEG$_{51}$-*b*-PBpinAGE$_{13}$Me instead of the 9-BBN modified polymer. All control experiments did not lead to monomer conversion, verifying the necessity of the trialkylborane group. In agreement to our results, the less Lewis acidic Bpin was found beforehand by Qi *et al*. to not facilitate polymerisation reactions significantly.[38] Results are listed in Table 3.

Table 3: Characterisation data for polyethers synthesised by polymeric catalysts.

Polymer	Catalyst	Pnth	M_n^{th} (g mol^{-1})	M_n^{a} (g mol^{-1})	$Đ^{a}$
PPO-1	EGBE-PBBNAGE$_{32}$Me	30	1820	1080	1.10
PPO-2	mPEG$_{51}$-b-P(AGE$_{6}$-co-BBNAGE$_{22}$)Me	30	1820	1190	1.16
PPO-3	mPEG$_{123}$-*b*-P(EG$_{25}$-*co*-AGE$_{1}$-*co*-BBNAGE$_{23}$)Me	30	1820	620	1.11
PETD-1	EGBE-PBBNAGE$_{32}$Me	34	7300	5660	1.22
PEHD	mPEG$_{51}$-*b*-P(AGE$_{4}$-*co*-BBNAGE$_{24}$)Me	30	7300	4540	1.58
PETD-2	mPEG$_{123}$-*b*-P(EG$_{25}$-*co*-AGE$_{6}$-*co*-BBNAGE$_{18}$)Me	34	7300	bimodal: 2310; 21110	3.14: 1.10; 1.15

[a]Determined by SEC (RI detector, PEG standards): PPO in DMF, PETD and PHD in THF.

Homo-, block- and copolymer architectures of the polymeric 9BBN catalyst were all successfully used to synthesise PPO and PETD or PEHD, respectively. Purification of PPO was performed through precipitation of the polymeric 9BBN-catalyst in diethyl ether. The synthesised PPOs show low to moderate dispersities (Figure 3). Discrepancies between theoretical and experimental molecular weight can partially be attributed to the PEG calibration, due to different hydrodynamic radii of substituted polyethers. Nonetheless, PPO-3 showed a lower molecular weight, than PPO-1 and PPO-2. ^{1}H NMR spectroscopy verified the absence of residual monomer in all reaction mixtures immediately prior to termination. Consequently, no discrepancies should be observable within the series. The lower molecular weight of PPO-3 is presumably caused by evaporation of PO through the septum, of which more suitable were not obtainable at the time. Proofing the presence or absence of excess catalyst was not possible via SEC due to the generally reduced solubility of the air-exposed catalysts and their consequential lack of signal. ^{1}H NMR spectroscopy of the PPOs after three precipitations was used to check for residual polymeric 9BBN-catalyst (Figure S23). PPO-1 was synthesised using the 9BBN bearing homopolymer EGBE-PBBNAGE$_{32}$Me. No residual catalyst was found in the NMR spectrum. Nonetheless, due to a lack of a strong characteristic signal of the catalyst, its presence cannot be ruled out. PPO-2 showed a PEG backbone signal, corresponding residual polymeric 9BBN-catalyst. While ^{1}H DOSY NMR spectroscopy disclosed a different diffusion coefficient for the PEG backbone, with a further zoom the PEG signal also arose parallel to PPO (Figure S24). This is either an artefact or a minor fraction of the catalyst was incorporated into the synthesised PPO presumably due to incomplete methylation of the polymeric precursor. Nonetheless, the PEG2000 block of mPEG$_{51}$-*b*-PBBNAGE$_{28}$Me is not sufficient for complete recovery of the copolymer via precipitation in diethyl ether. mPEG$_{123}$-*b*-P(EG$_{25}$-*co*-AGE$_{1}$-*co*-BBNAGE$_{23}$)Me consisted of a higher molecular weight PEG 5000 block and was used for the synthesis of PPO-3. No PEG signal and consequently no catalyst was found in PPO-3, indicating its suitability for the synthesis of diethyl ether soluble polyethers. MALDI ToF analysis verified the presence of bromide-initiated homo-PPO as well as a small fraction of hydroxy-initiated PPO. A third species of PPO with unknown end groups was found in a higher molecular weight region (Figure S25). Consequently, the targeted molecular weights were not achieved.

The long-chain poly (alkylene oxide)s PETD and PEHD were purified via precipitation in methanol. SEC showed high molecular weight shoulders for PETD-1 and PEHD, while PETD-2 was bimodal. MALDI ToF analysis of PETD and PEHD showed bromide-initiated homo-PETD or homo-PEHD, respectively, as well as hydroxy-initiated species (exemplarily shown for PETD-1: Figure S27). The high molecular weight species in PETD-2 is assumingly formed via the initiation by the polymeric 9BBN-catalyst, which is possible if methylation of hydroxy terminus was not achieved quantitatively. Nonetheless, this high molecular weight species was neither observable in ^{1}H NMR DOSY spectroscopy nor MALDI ToF spectrometry (Figures S28 and S29). ^{1}H NMR spectroscopy was used to check for the presence of residual polymeric 9BBN-catylst in the polymerisation products (Figure S26). PETD-1, which was synthesised with the homopolymeric 9BBN-catalyst, did not show a catalyst signal in the ^{1}H NMR spectrum. Nonetheless, similarly to the synthesised PPO-1 catalyst presence cannot be ruled out. The long-chain poly (alkylene oxide)s synthesised with copolymeric catalysts both show the backbone signal of residual catalyst in the ^{1}H NMR spectra. This signal is stronger in PETD-2, due to the higher amount of PEG in the catalyst structure and possibly due to initiation by the catalyst itself. While all used polymeric 9BBN-catalysts successfully catalysed the MAROP of alkylene oxides, removal of at least the copolymeric catalysts was not completely possible via three precipitation steps in methanol.

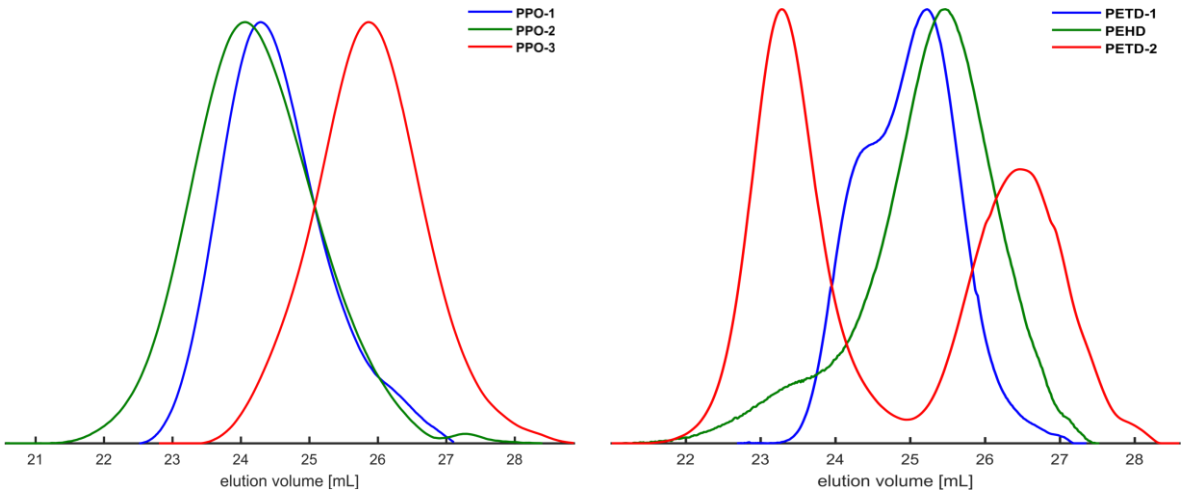

Figure 3: SEC traces of the final products (RI signal): PPO (left, DMF); PETD and PEHD (right, THF).

Recycling: Recyclability studies were conducted on PPO polymerisation, due to the polymer isolation via an aprotic solvent/antisolvent, which is compatible with the 9-BBN group of the catalyst. After the full conversion of the first PO polymerisation was

verified via ^{1}H NMR spectroscopy, the batch was dried under Schlenk conditions, moved inside the glovebox, and precipitated to yield the catalyst as precipitate and the synthesised PPO in the mother liquor. Subsequently, the recovered catalyst was introduced in a second polymerisation of PO. Characterisation data of the runs is given in Table 4.

Table 4: Characterisation data of PPO synthesised using fresh (run 1) and recycled (run 2) mPEG$_{123}$-*b*-P(EG$_{25}$-*co*-AGE$_{6}$-*co*-BBNAGE$_{18}$)Me catalyst.

Run	Pnth	M_n^{th} (g mol^{-1})	M_n^{a} (g mol^{-1})	$Đ^{a}$
1	40	2400	470	1.15
2	130	7630	1240	1.12

[a]Determined by SEC (DMF, RI detector, PEG standards).

^{1}H NMR spectroscopy (Figure S30) and SEC (Figure 4) verified the successful polymerisation of PO with fresh as well as with recycled catalyst. Determination of the molecular weight via SEC disclosed for both polymers lower molecular weights than targeted, albeit the polymerisations were conducted until ^{1}H NMR spectroscopy verified the absence of residual monomer. SEC furthermore showed a shoulder in the lower molecular weight area for both polymers. This indicates a second initiation species, ultimately leading to a reduced molecular weight of the polymer and decreasing M_n. Evaporation of PO through the septa presumably decreased the achievable molecular weight further, as noted previously for PPO-3.

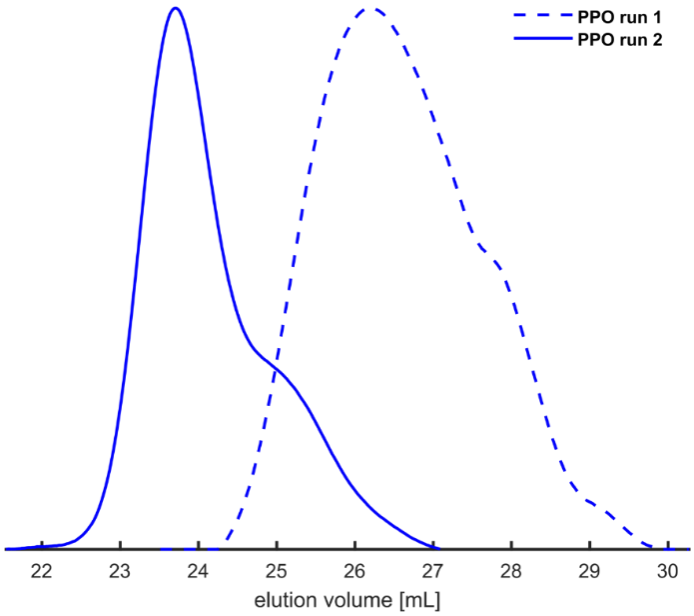

Figure 4: SEC traces (RI gingal, DMF) of PPO synthesised with fresh catalyst (dashed) and recycled catalyst (bold).

Polycarbonates: In addition to polyethers, the polymeric 9-BBN catalyst $mPEG_{51}$-b-P(AGE_6-co-$BBNAGE_{22}$)Me was examined for the copolymerisation of cyclohexene oxide (CHO) and CO_2 to poly (cyclohexene carbonate) (PCHC). An overview of the different experiments conducted are presented in Table 5.

Table 5: Characterisation data for polycarbonates synthesised by using the $mPEG_{51}$-b-P(AGE_6-co-$BBNAGE_{22}$)Me catalyst.[a]

Polymer	*[Cat]:[In]:[Epoxide]*[b]	*Con.*[c] *(%)*	*Selectivity (polymer %)*[c]	*Carbonate linkages (%)*[d]	M_n[e] (g mol^{-1})	*Đ*[e]	*Catalyst efficiency (mg g^{-1})*[f]
PC-1	16:1:1000	97	100	>99	17.1	1.27	59
PC-2	8:1:1000	100	100	>99	24.1	1.27	24
PC-3	4:1:1000	87	100	>99	22.2	1.22	--
PC-4	8:0.5:1000	87	100	>99	23.9	1.27	25
PC-5	4:0.75:1000	92	100	>99	35.4	1.26	14
PC-6	2.7:0.75:1000	62	100	>99	24.1	1.29	21
PC-7	2:0.75:1000	55	100	>99	24.3	1.28	13
PC-8[g]	8:0.5:1000	0	--	--	--	--	--

[a]All of the polymerisations were carried out in autoclaves under 45 bar of CO_2 at 60 °C for 48 hours unless otherwise mentioned. [b]Equivalents of borane centres per polymeric 9-BBN catalyst compared to epoxide and initiator. [c]Conversion (con.) determined by ^{1}H NMR spectroscopy (C*D*Cl$_3$, 300 MHz) of the crude polymerisation mixture after opening the reactor. [d]Determined by ^{1}H NMR spectroscopy (C*D*Cl$_3$, 300 MHz) of the final polymer. [e]Determined by SEC (THF, RI detector, PS standard). [f]Catalyst required (mg) to produce 1 g of polymer. [g]Conducted at room temperature.

The effect on CO_2 pressure and reaction time were not further investigated, due to the literature known improvement of polymerisation of CHO and CO_2 by higher CO_2 pressure and longer reaction times in borane catalyst-based systems.[39,40] The co-catalyst PPNCl was chosen as standard initiator based on well-known borane catalyst systems in literature.[41,42] The main focus was to find the optimised ratio between catalyst, monomer and initiator to achieve high molecular weights of the resulting PCHC with as less catalyst as possible. Lower catalyst loading led to increased molecular weight (PC-1, PC-2, PC-3) presumably due to fewer impurities in the system. These impurities can originate either from water in the CO_2 hydrolysing the borane group or from incomplete conversion in the methylation step of the catalyst synthesis. Both cases generate a second initiating group, leading to lower molecular weights of the polymer overall. A high zoom in in the ^{1}H DOSY NMR spectrum indeed indicated the presence of a polyether backbone in the polymer, but

at this zoom in artefacts started to appear, making the origin of this peak uncertain (Figure S32). SEC showed bimodal distributions due to the water traces present in the reaction system typical for this kind of reaction as well as presumably due to the discussed impurities (Figure 5).[8,39,43]

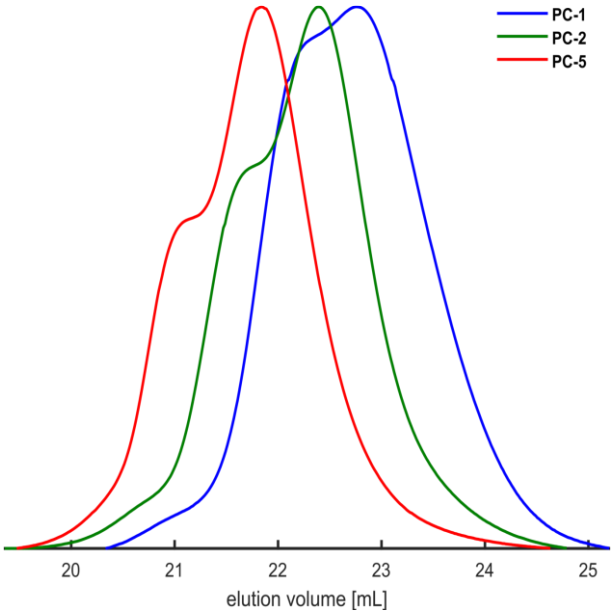

Figure 5: Exemplarily SEC traces of PCHC (THF, RI signal).

100% conversion was achieved with a catalyst loading of 1000/8 after 48 hours which is unusual for the CHO/CO_2 copolymerisation with borane catalysts. From our knowledge, 100% conversion is quite unusual for the CHO/CO_2 copolymerisation with borane catalysts indicating a good efficiency of the catalyst.[8,25,44] The conversion was determined by the crude reaction mixture in which the typical PPC peak at 4.66 ppm and the CHO peak at 3.12 ppm were analysed (figure S31 in Supporting Information). The cyclic carbonate as typical side product for the copolymerisation of epoxides and CO_2 was not identified in the crude product for all reactions supporting the good selectivity of the borane catalyst. When the catalyst loading got too small, too few active borane centres were present to catalyse the copolymerisation and the conversion dropped (PC-3). To increase the molecular weight, the amount of PPNCl was reduced leading to a decreased number of Cl^- initiators in the reaction mixture. PC-5 with a catalyst:initiator:monomer ratio of 4:0.75:1000 led to the highest molecular weight polymer with 35.4 kg mol^{-1} at conditions of 60 °C and 48 hours. By decreasing the catalyst and initiator ratios even lower (PC-6, PC-7), no higher molecular weights of the resulting polymer were achieved, in consequence to the significantly dropped conversion due to few borane centres present in the catalysis.

The copolymerisation showed no reaction at ambient temperature indicating that a certain initiation energy is required for the catalyst (PC-8). The catalytic system showed high carbonate linkage selectivity as shown by ^{1}H NMR spectroscopy (figure S31 in Supporting Information) comparable to other borane based catalysts.[25,40] The major advantage of the borane polymer catalyst is the possibility to separate the catalyst from the resulting polycarbonate and to use the catalyst again (which was already shown for polyethers earlier). As shown in figure S31 in the Supporting Information, most of the catalyst can be removed from the final PC compared to the crude product, but some traces remain. The separation of the polyether-based catalyst and the PCHC can be achieved due to their different solubility in methanol. Regardless of some catalyst residues, the properties of the resulting PCHC were not affected as shown by the glass transition temperature (T_g) of 118 °C (Figure S33), which is in line with literature known values.[45] The PDIs were in the range of 1.22 – 1.29 for all polymers (Table 5). As for the polymerisation optimisation only the borane centres were considered, but the PEG block has high mass influence and is required for solubility reasons, the total catalyst efficiency by mass was determined in Table 5. The trend shows similar results as for the borane centre loading: The polymer yields increased with lower catalyst loading and high conversion, resulting in improved mass efficiency (see Table 5).

Conclusion

Series of organo borane bearing polyethers were synthesised via anionic ring-opening polymerisation and subsequent hydroboration. Hydroboration of AGE containing polymers with HBpin showed hydrogenation side reaction for up to 21% of the double bonds. For IsoPreGE bearing copolymers the hydrogenation was the main reaction and no full conversion of the double bonds was achieved, presumably due to the double bonds being sterically hindered. This hydroboration yielded polymeric boronic esters, which were cleaved to yield polymeric boronic acids. Boronic acids are a versatile and widely used group of high potential. The introduction of 9-BBN as side chain functionality yielded a polymer with the ability to polymerise epoxides under mild conditions as well as copolymerise epoxides and carbon dioxide. Firstly, using this new catalyst we demonstrated the successful synthesis of amorphous PPO ($Đ$ = 1.10 – 1.16) and crystalline PETD and PEHD ($Đ$ = 1.22 – 1.58;

or bimodal $Đ = 3.14$) followed by purification via precipitation. The products purity was influenced by the polymer architecture of the catalyst. Copolymers bearing a PEG block generally increased the solubility of the catalyst but hindered full purification of synthesised long-chain poly (alkylene oxide)s. Secondly, successful recycling of the catalyst was shown for the polymerisation of PO. And finally, the catalyst was used to copolymerise cyclohexene oxide and carbon dioxide yielding polycarbonates with conversions up to 100%, carbonate linkages >99%, good PDIs (1.22 – 1.29) and high molecular weights (17.1 – 35.4 kg mol^{-1}). Additionally, the polymer catalyst was almost fully removed from the resulting polycarbonate.

Outlook

The final goal of our research is the exploration of a bifunctional polymer catalyst with the initiator- (ammonium or phosphonium centres) and catalyst- functions in one molecule to get one fully recyclable system for the polymerisation of oxygenated monomers. In the next steps, the understanding of the multi centred borane catalyst is in the focus to derive additional optimisation opportunities. Therefore, comprehensive studies on turn over frequency (TOF) as well as turn over number (TON) will be conducted to get a better understanding of the mechanistics behind the polymeric catalyst. This will be the starting point for further investigations on the number of catalytic centres per polymer and different borane centre structures. By adjusting the solubility of the catalyst, full recyclability and removal can be achieved.

Acknowledgement

The authors thank Sabine Hennig for practical support and Dr. Elena Berger-Nicoletti for measurements of MALDI ToF spectra.

References

(1) Koyama, Y.; Umehara, M.; Mizuno, A.; Itaba, M.; Yasukouchi, T.; Natsume, K.; Suginaka, A. Synthesis of novel poly(ethylene glycol) derivatives having pendant

amino groups and aggregating behavior of its mixture with fatty acid in water. *Bioconjugate chemistry* **1996**, *7* (3), 298–301. DOI: 10.1021/bc9600123.

(2) Verkoyen, P.; Frey, H. Amino-functional polyethers: versatile, stimuli-responsive polymers. *Polym. Chem.* **2020**, *11* (24), 3940–3950. DOI: 10.1039/d0py00466a.

(3) Adams, J.; Gronski, W. LC side chain AB-block copolymers with an amorphous A-block and a liquid-crystalline B-block. *Die Makromolekulare Chemie, Rapid Communications* **1989**, *10*, 553–557.

(4) Chung, T. C.; Raate, M.; Berluche, E.; Schulz, D. N. Synthesis of functional hydrocarbon polymers with well-defined molecular structures. *Macromolecules* **1988**, *21* (7), 1903–1907. DOI: 10.1021/ma00185a003.

(5) Soloway, A. H.; Tjarks, W.; Barnum, B. A.; Rong, F.-G.; Barth, R. F.; Codogni, I. M.; Wilson, J. G. The Chemistry of Neutron Capture Therapy. *Chemical reviews* **1998**, *98*, 1515–1562.

(6) Pitto-Barry, A. Polymers and boron neutron capture therapy (BNCT): a potent combination. *Polym. Chem.* **2021**, *12* (14), 2035–2044. DOI: 10.1039/D0PY01392G.

(7) Chakraborty, D.; Rodriguez, A.; Chen, E. Y.-X. Catalytic Ring-Opening Polymerization of Propylene Oxide by Organoborane and Aluminum Lewis Acids. *Macromolecules* **2003**, *36* (15), 5470–5481. DOI: 10.1021/ma034050a.

(8) Zhang, D.; Boopathi, S. K.; Hadjichristidis, N.; Gnanou, Y.; Feng, X. Metal-Free Alternating Copolymerization of CO2 with Epoxides: Fulfilling "Green" Synthesis and Activity. *Journal of the American Chemical Society* **2016**, *138* (35), 11117–11120. DOI: 10.1021/jacs.6b06679. Published Online: Aug. 26, 2016.

(9) Martin, R.; Buchwald, S. L. Palladium-catalyzed Suzuki-Miyaura cross-coupling reactions employing dialkylbiaryl phosphine ligands. *Accounts of Chemical Research* **2008**, *41* (11), 1461–1473. DOI: 10.1021/ar800036s.

(10) Morrill, C.; Grubbs, R. H. Synthesis of functionalized vinyl boronates via ruthenium-catalyzed olefin cross-metathesis and subsequent conversion to vinyl halides. *The Journal of organic chemistry* **2003**, *68* (15), 6031–6034. DOI: 10.1021/jo0345345.

(11) Chung, T. C.; Rhubright, D. Functionalization of polypropylene by hydroboration. *J. Polym. Sci. A Polym. Chem.* **1993**, *31* (11), 2759–2763. DOI: 10.1002/pola.1993.080311112.

(12) Crudden, C. M.; Edwards, D. Catalytic Asymmetric Hydroboration: Recent Advances and Applications in Carbon−Carbon Bond-Forming Reactions. *Eur. J. Org. Chem.* **2003**, *2003* (24), 4695–4712. DOI: 10.1002/ejoc.200300433.

(13) Brown, H. C.; Zweifel, G. A Stereospecific cis Hydration of the Double Bond in Cyclic Derivatives. *J. Am. Chem. Soc.* **1959**, *81* (1), 247. DOI: 10.1021/ja01510a059.

(14) Hinkes, S. P. A.; Klein, C. D. P. Virtues of Volatility: A Facile Transesterification Approach to Boronic Acids. *Organic letters* **2019**, *21* (9), 3048–3052. DOI: 10.1021/acs.orglett.9b00584. Published Online: Apr. 23, 2019.

(15) Cambre, J. N.; Sumerlin, B. S. Biomedical applications of boronic acid polymers. *Polymer* **2011**, *52* (21), 4631–4643. DOI: 10.1016/j.polymer.2011.07.057.

(16) Yang, X.; Guo, M.; Wu, Y.; Xue, S.; Li, Z.; Zhou, H.; Smith, A. T.; Sun, L. Biomimetic Boroxine-Based Multifunctional Thermosets via One-Pot Synthesis. *ACS applied materials & interfaces* **2020**, *12* (50), 56445–56453. DOI: 10.1021/acsami.0c16736. Published Online: Dec. 2, 2020.

(17) Tang, S.; Ma, H.; Tu, H.-C.; Wang, H.-R.; Lin, P.-C.; Anseth, K. S. Adaptable Fast Relaxing Boronate-Based Hydrogels for Probing Cell-Matrix Interactions. *Advanced science (Weinheim, Baden-Wurttemberg, Germany)* **2018**, *5* (9), 1800638. DOI: 10.1002/advs.201800638. Published Online: Jul. 26, 2018.

(18) Naumann, S. Borane Catalysis for Epoxide (Co)Polymerization. *Polym. Chem.* **2023.** DOI: 10.1039/D3PY00018D.

(19) Zhang, C.; Geng, X.; Zhang, X.; Gnanou, Y.; Feng, X. Alkyl borane-mediated metal-free ring-opening (co)polymerizations of oxygenated monomers. *Progress in Polymer Science* **2023**, *136*, 101644. DOI: 10.1016/j.progpolymsci.2022.101644.

(20) Billouard, C.; Carlotti, S.; Desbois, P.; Deffieux, A. “Controlled” High-Speed Anionic Polymerization of Propylene Oxide Initiated by Alkali Metal Alkoxide/Trialkylaluminum Systems. *Macromolecules* **2004**, *37* (11), 4038–4043. DOI: 10.1021/ma035768t.

(21) Carlotti, S.; Desbois, P.; Billouard, C.; Deffieux, A. Reactivity control in anionic polymerization of ethylenic and heterocyclic monomers through formation of ‘ate’ complexes. *Polym. Int.* **2006**, *55* (10), 1126–1131. DOI: 10.1002/pi.1981.

(22) Zhang, D.-D.; Feng, X.; Gnanou, Y.; Huang, K.-W. Theoretical Mechanistic Investigation into Metal-Free Alternating Copolymerization of CO 2 and Epoxides: The Key Role of Triethylborane. *Macromolecules* **2018**, *51* (15), 5600–5607. DOI: 10.1021/acs.macromol.8b00471.

(23) Chen, C.; Gnanou, Y.; Feng, X. Borinane-based organoboron catalysts for alternating copolymerization of CO 2 with cyclic ethers: improved productivity and facile recovery. *Polym. Chem.* **2022**, *13* (45), 6312–6321. DOI: 10.1039/D2PY01161A.

(24) Brocas, A.-L.; Mantzaridis, C.; Tunc, D.; Carlotti, S. Polyether synthesis: From activated or metal-free anionic ring-opening polymerization of epoxides to functionalization. *Progress in Polymer Science* **2013**, *38* (6), 845–873. DOI: 10.1016/j.progpolymsci.2012.09.007.

(25) Yang, G.-W.; Zhang, Y.-Y.; Xie, R.; Wu, G.-P. Scalable Bifunctional Organoboron Catalysts for Copolymerization of CO2 and Epoxides with Unprecedented Efficiency. *Journal of the American Chemical Society* **2020**, *142* (28), 12245–12255. DOI: 10.1021/jacs.0c03651. Published Online: Jun. 30, 2020.

(26) Yang, G.-W.; Zhang, Y.-Y.; Wu, G.-P. Modular Organoboron Catalysts Enable Transformations with Unprecedented Reactivity. *Accounts of Chemical Research* **2021**, *54* (23), 4434–4448. DOI: 10.1021/acs.accounts.1c00620. Published Online: Nov. 21, 2021.

(27) Patil, N.; Bhoopathi, S.; Chidara, V.; Hadjichristidis, N.; Gnanou, Y.; Feng, X. Recycling a Borate Complex for Synthesis of Polycarbonate Polyols: Towards an Environmentally Friendly and Cost-Effective Process. *ChemSusChem* **2020**, *13* (18), 5080–5087. DOI: 10.1002/cssc.202001395. Published Online: Jul. 30, 2020.

(28) Männig, D.; Nöth, h. Catalytic Hydroboration with Rhodium Complexes. *Angewandte Chemie (International ed. in English)* **1985**, *24* (10), 878–879.

(29) Mkhalid, I. A. I.; Barnard, J. H.; Marder, T. B.; Murphy, J. M.; Hartwig, J. F. C-H activation for the construction of C-B bonds. *Chemical reviews* **2010**, *110* (2), 890–931. DOI: 10.1021/cr900206p.

(30) Chen; Schlecht; Semple; Hartwig. Thermal, catalytic, regiospecific functionalization of alkanes. *Science (New York, N.Y.)* **2000**, *287* (5460), 1995–1997. DOI: 10.1126/science.287.5460.1995.

(31) Shimada, S.; Batsanov, A. S.; Howard, J. A. K.; Marder, T. B. Formation of Aryl- and Benzylboronate Esters by Rhodium-Catalyzed C−H Bond Functionalization with Pinacolborane. *Angew. Chem. Int. Ed.* **2001**, *40* (11), 2168–2171. DOI: 10.1002/1521-3773(20010601)40:11<2168:AID-ANIE2168>3.0.CO;2-0.

(32) Kisan, S.; Krishnakumar, V.; Gunanathan, C. Ruthenium-Catalyzed Anti-Markovnikov Selective Hydroboration of Olefins. *ACS Catal.* **2017**, *7* (9), 5950–5954. DOI: 10.1021/acscatal.7b01750.

(33) Burgess, K.; Jaspars, M. Ruthenium-catalyzed hydroborations of alkenes. *Organometallics* **1993**, *12* (10), 4197–4200. DOI: 10.1021/om00034a065.

(34) Caballero, A.; Sabo-Etienne, S. Ruthenium-Catalyzed Hydroboration and Dehydrogenative Borylation of Linear and Cyclic Alkenes with Pinacolborane. *Organometallics* **2007**, *26* (5), 1191–1195. DOI: 10.1021/om0610851.

(35) Riddlestone, I. M.; McKay, D.; Gutmann, M. J.; Macgregor, S. A.; Mahon, M. F.; Sparkes, H. A.; Whittlesey, M. K. Isolation of [Ru(IPr) 2 (CO)H] + (IPr = 1,3-Bis(2,6-diisopropylphenyl)imidazol-2-ylidene) and Reactivity toward E–H (E = H, B) Bonds. *Organometallics* **2016**, *35* (9), 1301–1312. DOI: 10.1021/acs.organomet.6b00173.

(36) Schüttner, S.; Linden, G. M.; Hoffmann, E. C.; Holzmüller, P.; Frey, H. Poly(Terpenyl Glycidyl Ethers): Copolymerization with Ethylene Oxide, Properties, and Functionalization. *to be submitted*.

(37) Crombie, A. L.; Kane, J. L.; Shea, K. M.; Danheiser, R. L. Ring expansion-annulation strategy for the synthesis of substituted azulenes and oligoazulenes. 2. Synthesis of azulenyl halides, sulfonates, and azulenylmetal compounds and their application in transition-metal-mediated coupling reactions. *The Journal of organic chemistry* **2004**, *69* (25), 8652–8667. DOI: 10.1021/jo048698c.

(38) Qi, H.; Xie, R.; Yang, G.-W.; Zhang, Y.-Y.; Xu, C.-K.; Wang, Y.; Wu, G.-P. Rational Optimization of Bifunctional Organoboron Catalysts for Versatile Polyethers via Ring-Opening Polymerization of Epoxides. *Macromolecules* **2022**, *55* (20), 9081–9090. DOI: 10.1021/acs.macromol.2c01596.

(39) Sengoden, M.; Bhat, G. A.; Darensbourg, D. J. Bifunctional organoboron-phosphonium catalysts for coupling reactions of CO2 and epoxides. *RSC advances* **2022**, *12* (50), 32440–32447. DOI: 10.1039/d2ra06358a. Published Online: Nov. 14, 2022.

(40) Zhang, Y.-Y.; Lu, C.; Yang, G.-W.; Xie, R.; Fang, Y.-B.; Wang, Y.; Wu, G.-P. Mechanism-Inspired Upgradation of Phosphonium-Containing Organoboron Catalysts for Epoxide-Involved Copolymerization and Homopolymerization. *Macromolecules* **2022**, *55* (15), 6443–6452. DOI: 10.1021/acs.macromol.2c01180.

(41) Jia, M.; Hadjichristidis, N.; Gnanou, Y.; Feng, X. Monomodal Ultrahigh-Molar-Mass Polycarbonate Homopolymers and Diblock Copolymers by Anionic

Copolymerization of Epoxides with CO2. *ACS Macro Lett.* **2019**, *8* (12), 1594–1598. DOI: 10.1021/acsmacrolett.9b00854. Published Online: Nov. 21, 2019.

(42) Jia, M.; Zhang, D.; Kort, G. W. de; Wilsens, C. H. R. M.; Rastogi, S.; Hadjichristidis, N.; Gnanou, Y.; Feng, X. All-Polycarbonate Thermoplastic Elastomers Based on Triblock Copolymers Derived from Triethylborane-Mediated Sequential Copolymerization of CO2 with Various Epoxides. *Macromolecules* **2020**, *53* (13), 5297–5307. DOI: 10.1021/acs.macromol.0c01068. Published Online: Jun. 29, 2020.

(43) Tong, Y.; Cheng, R.; Dong, H.; Liu, Z.; Ye, J.; Liu, B. Highly active bifunctional dual-arm organoboron catalysts bearing cooperative intramolecular structures for the copolymerization of CO2 and epoxides. *Journal of CO2 Utilization* **2022**, *60*, 101979. DOI: 10.1016/j.jcou.2022.101979.

(44) Wang, X.-W.; Hui, J.-W.; Li, Y.-T.; Gu, Y.-R.; Li, Z.-B. Facile Synthesis of Polycarbonate Diol via Copolymerization of CO2 and Cyclohexene Oxide Catalysed by a Combination of One-Component Phosphonium Borane Lewis Pair and Water. *Chin J Polym Sci* **2023.** DOI: 10.1007/s10118-023-2925-3.

(45) Bailer, J.; Feth, S.; Bretschneider, F.; Rosenfeldt, S.; Drechsler, M.; Abetz, V.; Schmalz, H.; Greiner, A. Synthesis and self-assembly of biobased poly(limonene carbonate)- block -poly(cyclohexene carbonate) diblock copolymers prepared by sequential ring-opening copolymerization. *Green Chem.* **2019**, *21* (9), 2266–2272. DOI: 10.1039/C9GC00250B.

Supporting Information

Table of Contents

Characterisation Table of supporting polymers

Table S1: Scope of polymerisation: Conditions and characterisation data.

Polymer	*Conditions*[a]	P_n^{th}*(PGE)*	M_n[b] (g mol^{-1})	M_n[c] (g mol^{-1})	$Đ$[c]
No conversion	THF, 3d	37	-	-	-
mPEG$_{123}$-*b*-PAGE$_{18}$	Toluene, CsOHxH$_2$O,14 d at 45 °C, 3 d at 65 °C	37	7510	5940	1.05
mPEG$_{123}$-*b*-PAGE$_{22}$	12:3 THF:DMSO, 6 d 50°C, 3 d 60 °C	37	7970	6310	1.04
mPEG$_{123}$-*b*-PAGE$_{14}$	1 d	22	7050	5810	1.05
mPEG$_{123}$-*b*-PAGE$_{25}$	6 d 50°C, 3 d 60 °C	37	8310	6390	1.06
mPEG$_{123}$-*b*-PAGE$_{25}$	Bulk, 3 d, 66 °C	37	8310	6780	1.06
mPEG$_{123}$-*b*-PAGE$_{35}$	35 °C, 1 d	60	9450	7380	1.05
mPEG$_{51}$-*b*-PAGE$_{7}$	1 d	9	3170	2400	1.05
mPEG$_{51}$-*b*-PAGE$_{11}$	1 d	15	3620	2820	1.07
mPEG$_{51}$-*b*-PAGE$_{52}$	1 d	62	8300	3940	1.12
mPEG$_{51}$-*b*-P(EG$_{37}$-*co*-PAGE$_{6}$)	40 °C, 3 d	9, P_n(EO): 22	4680	3020	1.06
mPEG$_{51}$-*b*-P(EG$_{19}$-*co*-PAGE$_{7}$)	40 °C, 3 d	13, P_n(EO): 13	4000	2960	1.05
mPEG$_{123}$-*b*-P(EG$_{42}$-*co*-PAGE$_{16}$)	40 °C, 3 d	23, P_n(EO): 54	8680	7210	1.06
mPEG$_{51}$-*b*-PIsoPreGE$_{9}$	RT, 3 d	13	3650	2630	1.09
mPEG$_{51}$-*b*-PIsoPreGE$_{6}$	RT, 3 d	7	3220	2340	1.07
mPEG$_{123}$-*b*-PIsoPreGE$_{19}$	RT, 3 d	37	5020	6030	1.08
mPEG$_{123}$-*b*-PIsoPreGE$_{13}$	RT, 3 d	21	5190	5750	1.05
mPEG$_{132}$-*b*-P(EG$_{16}$-*co*-PIsoPreGE$_{18}$)	RT, 3 d	32, P_n(EO): 32	6130	6980	1.08

[a]If not specifically noted KO^{t}Bu, DMSO and 45 °C were used. [b]Determined by ^{1}H NMR spectroscopy (C*D*Cl$_3$, 300 MHz). [c]Determined by SEC (DMF, RI detector, PEG standards).

Representative ^{1}H NMR spectra of polymeric precursors

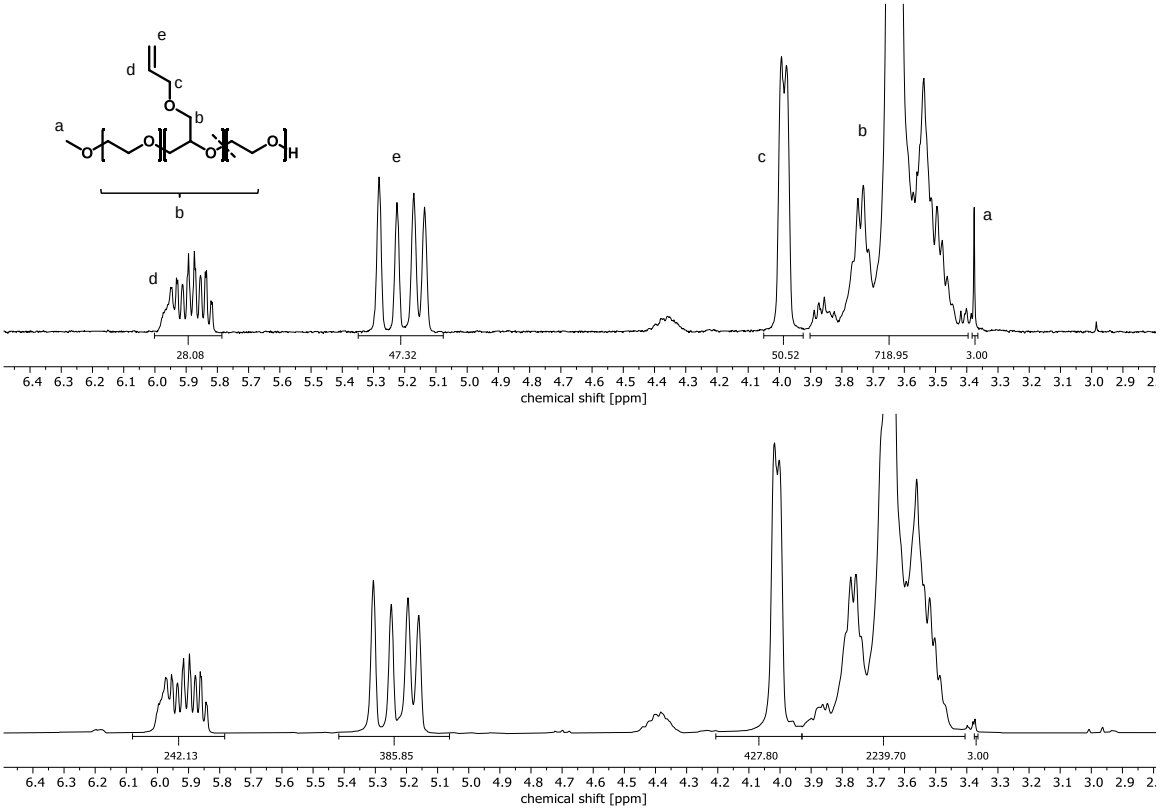

Figure S1: ^{1}H NMR spectrum ($CDCl_3$, 300 MHz) of $mPEG_{123}$-b-P(EG_{25}-co-$PAGE_{24}$) precipitate (top) and mother liquor (bottom).

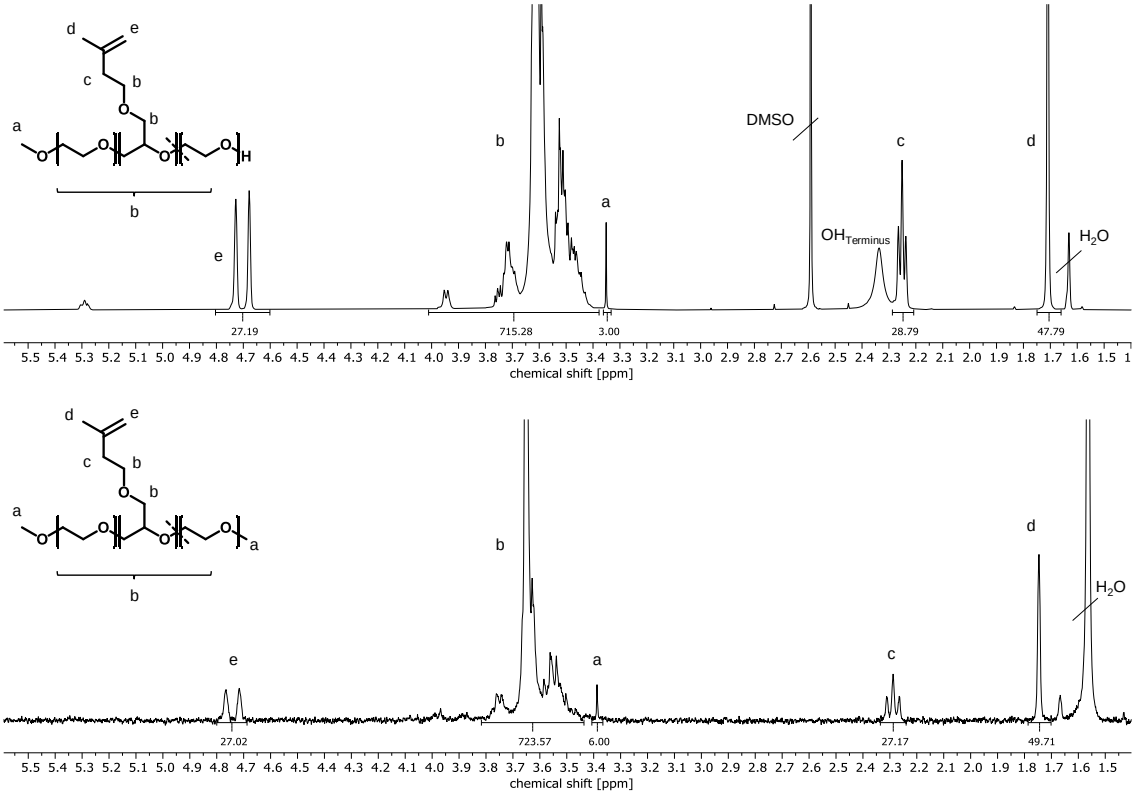

Figure S2: ^{1}H NMR spectrum (CDCl$_3$, 300 MHz) of mPEG$_{123}$-b-P(EG$_{32}$-co-PIsoPreGE$_{14}$) (top) and the methylated mPEG$_{123}$-b-P(EG$_{32}$-co-PIsoPreGE$_{14}$)Me (bottom).

Representative NMR spectra of hydroborated and hydrolysed polymers

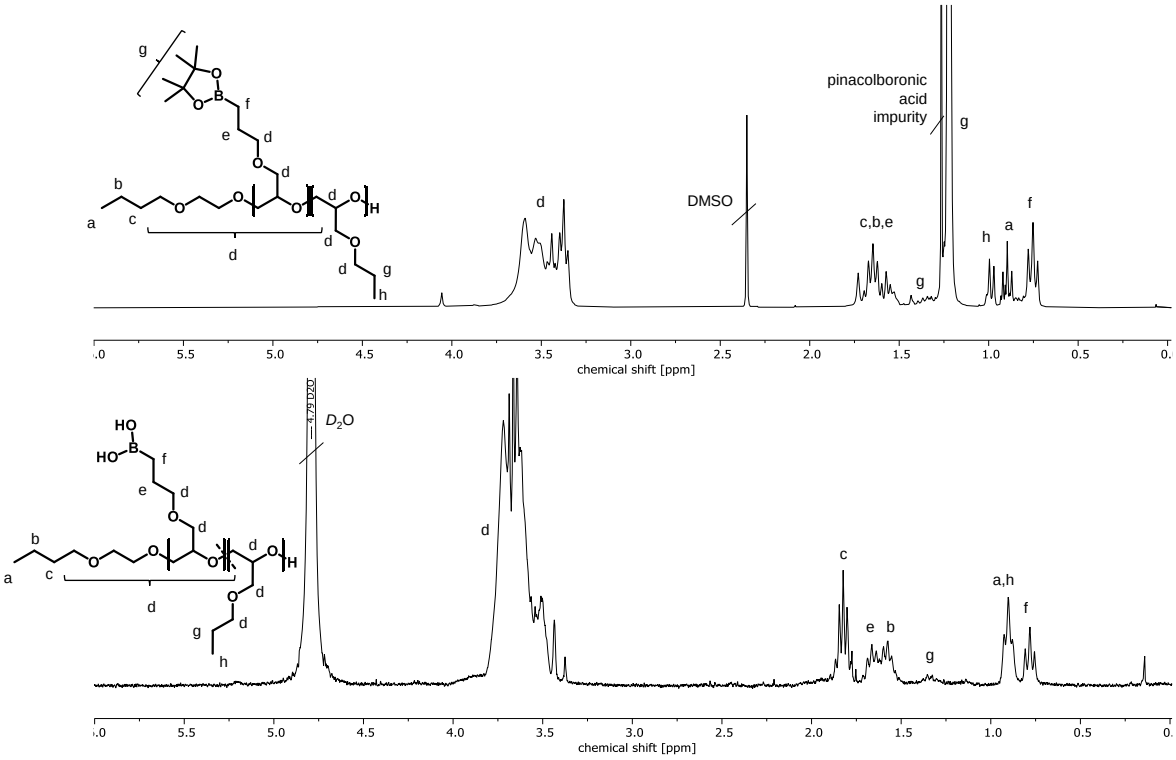

Figure S3: ^{1}H NMR spectrum of EGBE-P(PGE$_7$-co-BpinAGE$_{25}$) (top, CDCl$_3$, 300 MHz) and the hydrolysed EGBE-P(PGE$_7$-co-HOBpinAGE$_{25}$) (bottom, D$_2$O, 300 MHz).

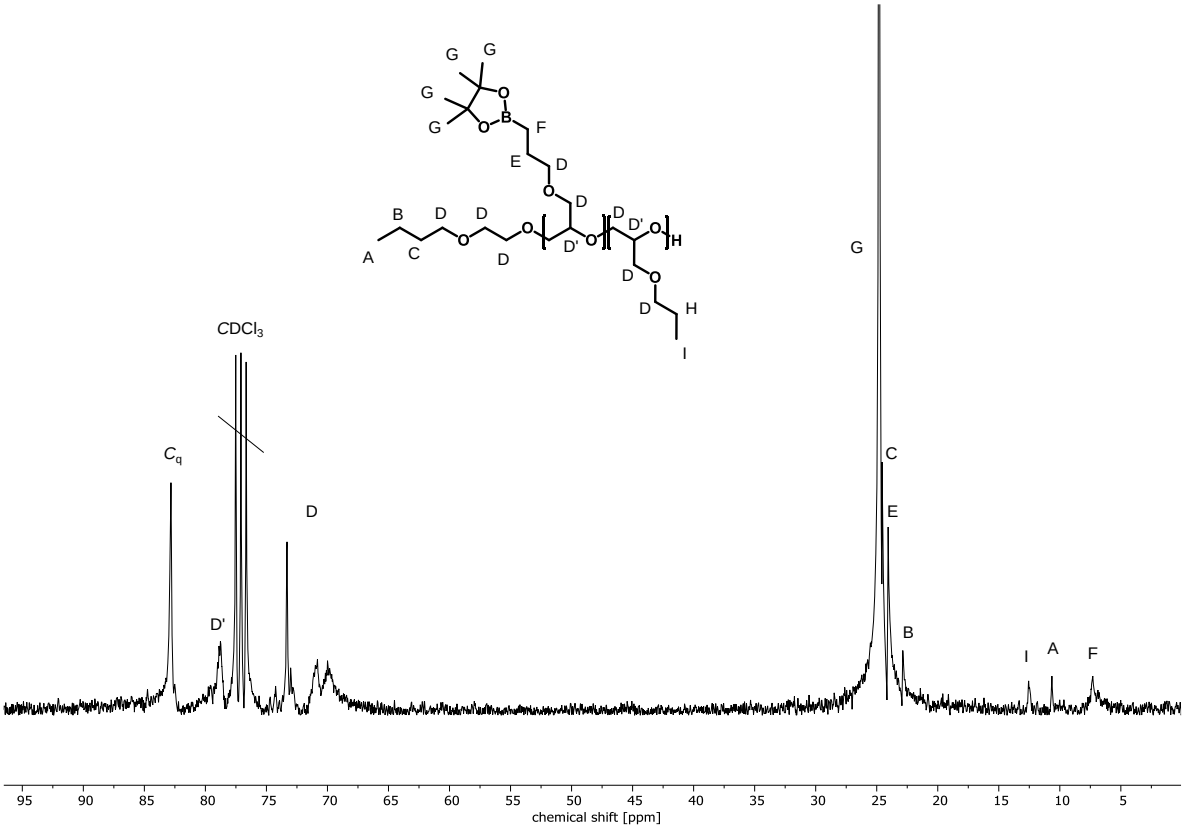

Figure S4: ^{13}C NMR spectrum ($CDCl_3$, 75 MHz) of EGBE-P(PGE$_7$-co-BpinAGE$_{25}$).

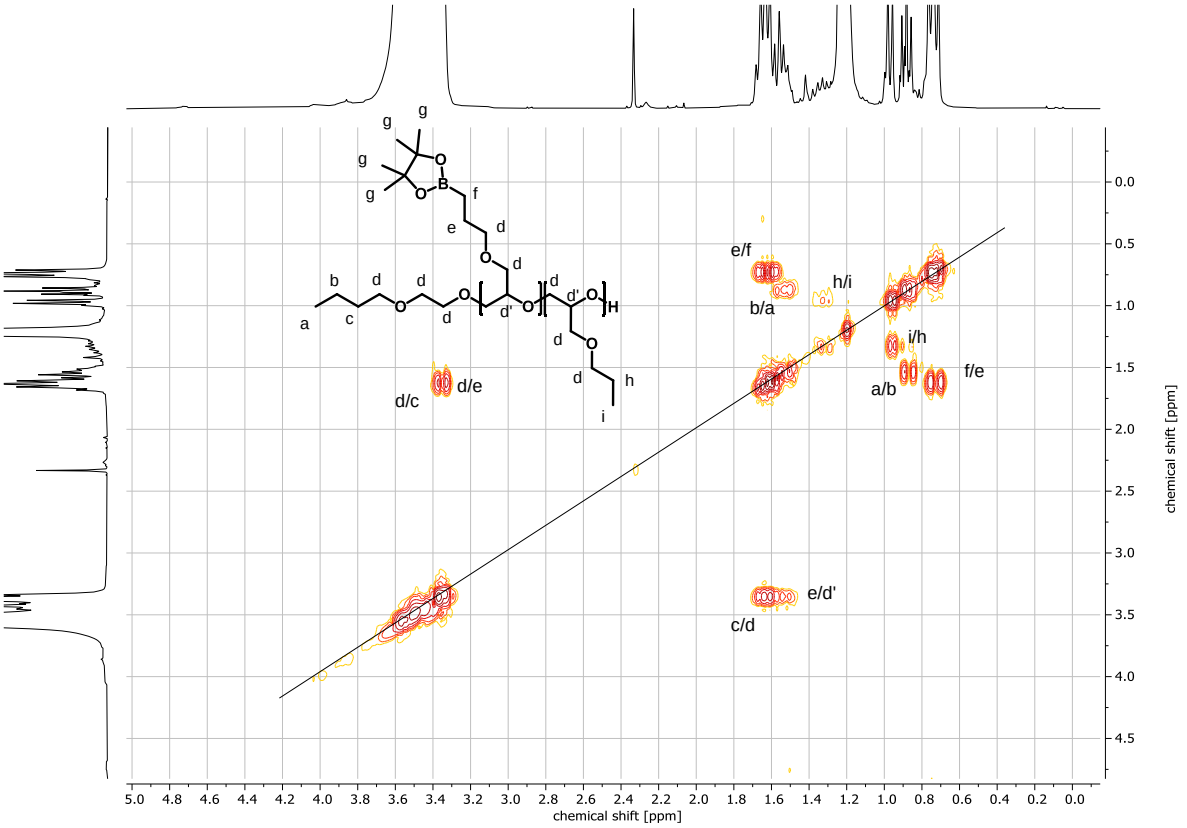

Figure S5: ^{1}H, ^{1}H COSY NMR spectrum ($CDCl_3$, 300 MHz) of EGBE-P(PGE_7-co-$BpinAGE_{25}$).

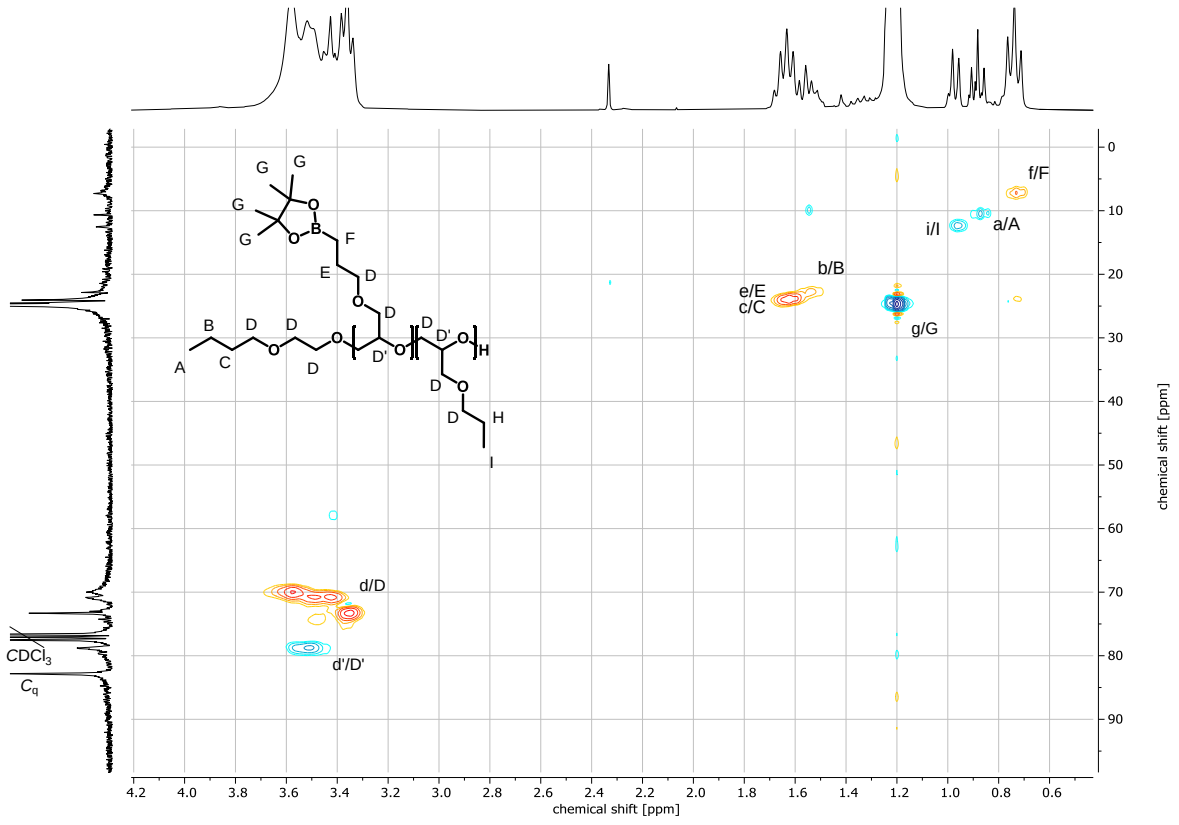

Figure S6: ^{1}H, ^{13}C HSQC NMR spectrum ($CDCl_3$) of EGBE-P(PGE_7-co-$BpinAGE_{25}$).

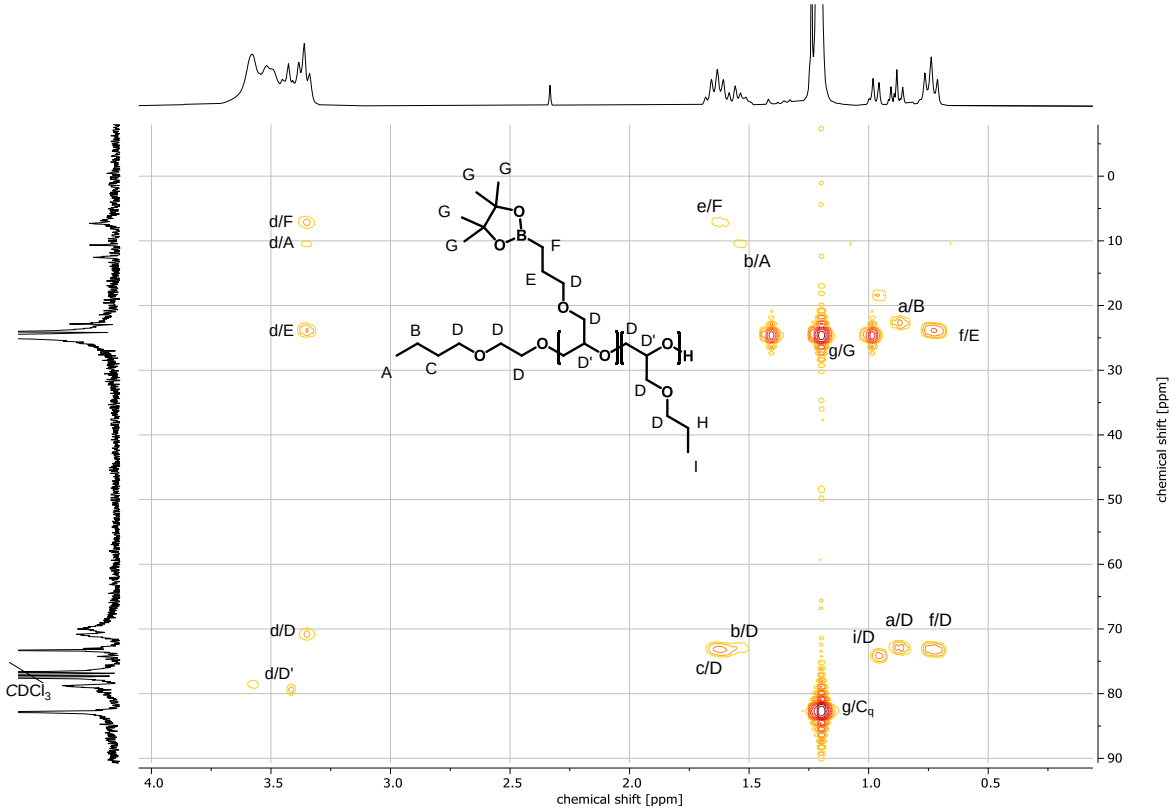

Figure S7: ^{1}H, ^{13}C HMBC NMR spectrum ($CDCl_3$) of EGBE-P(PGE$_7$-co-BpinAGE$_{25}$).

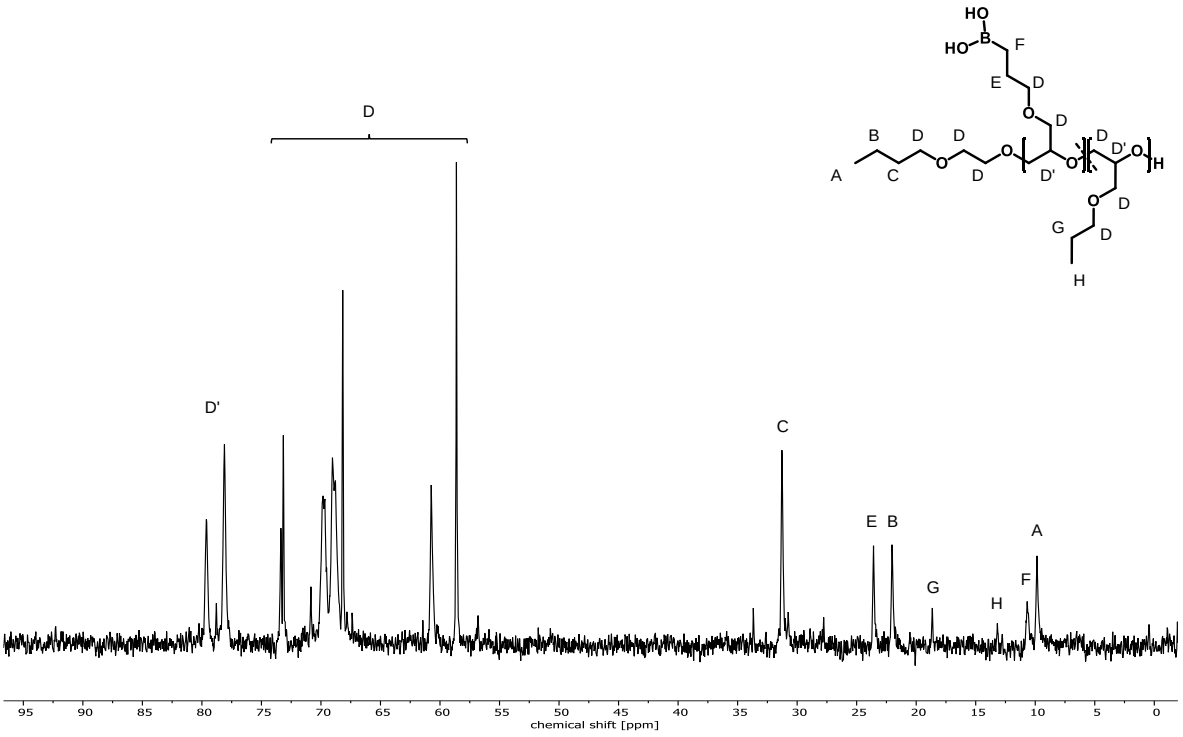

Figure S8: ^{13}C NMR spectrum (D_2O, 75 MHz) of EGBE-P(PGE$_7$-co-BpinAGE$_{25}$).

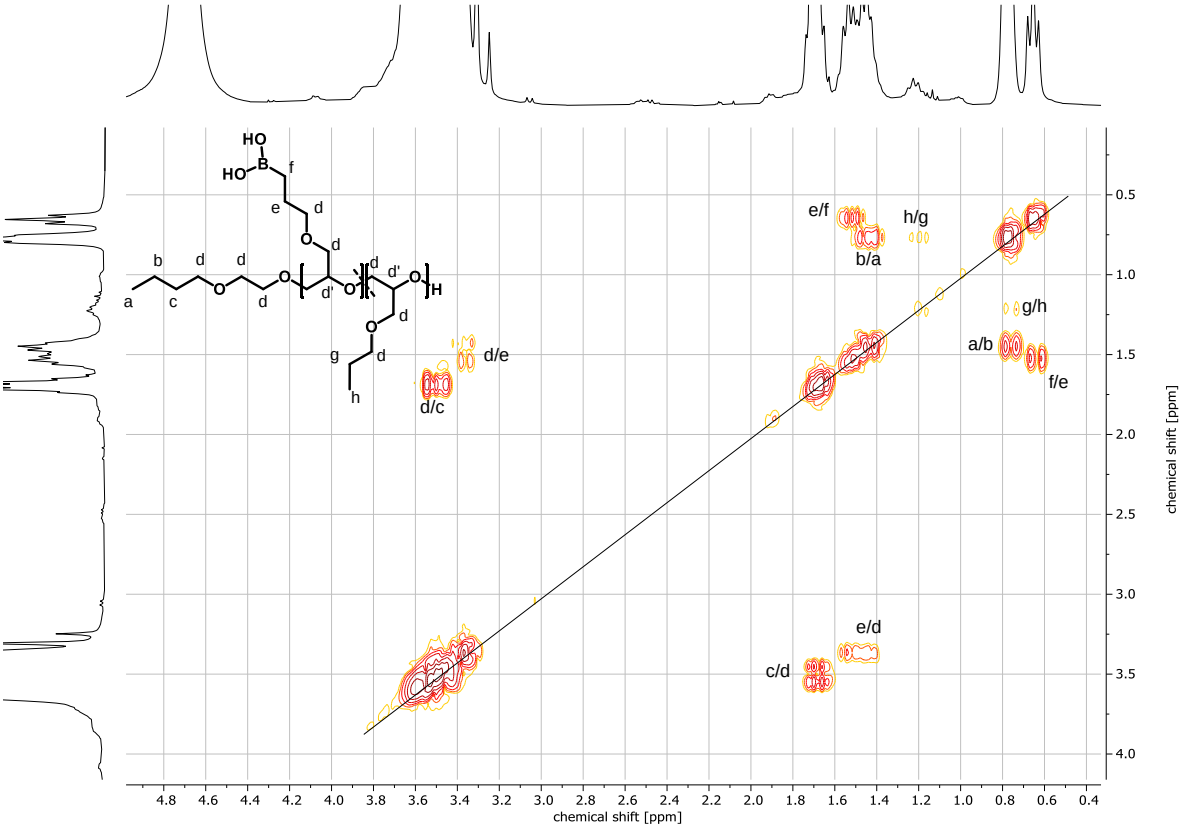

Figure S9: ^{1}H, ^{1}H COSY NMR spectrum (D_2O, 300 MHz) of EGBE-P(PGE$_7$-co-BpinAGE$_{25}$).

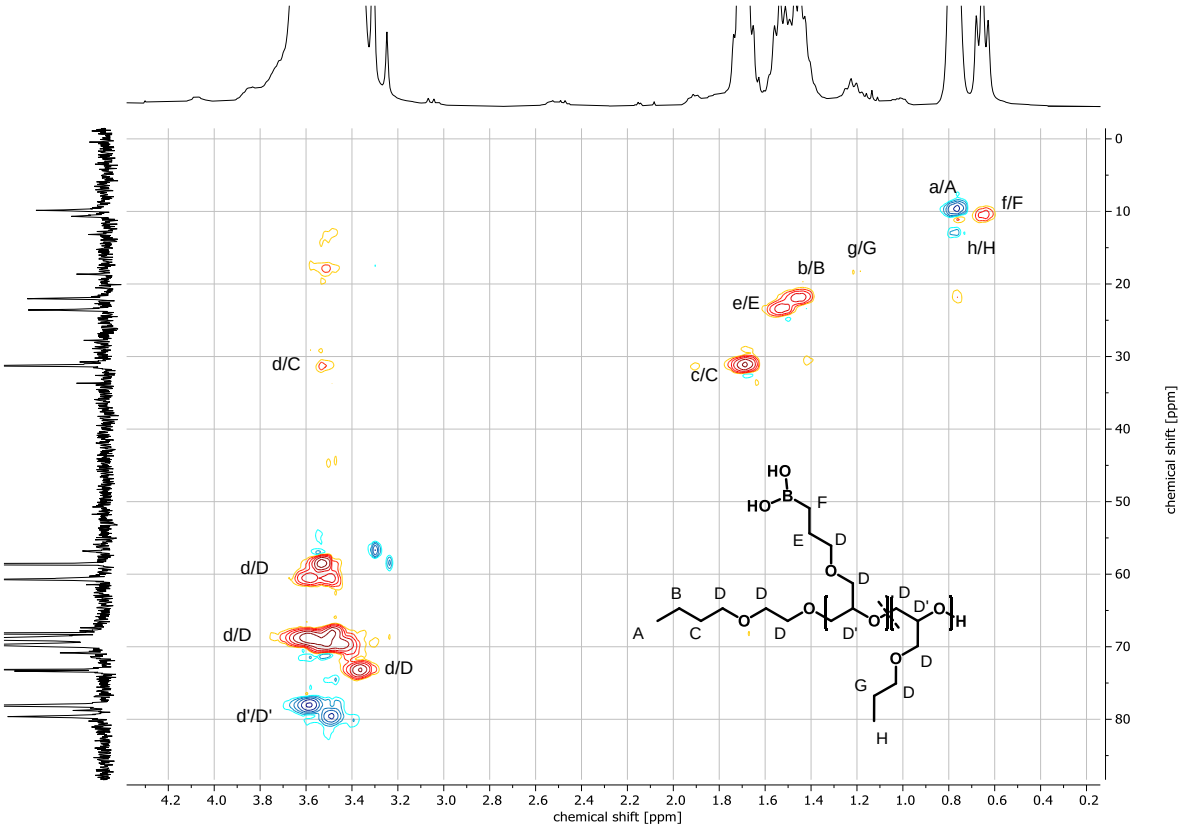

Figure S10: ^{1}H, ^{13}C HSQC NMR spectrum (D_2O) of EGBE-P(PGE$_7$-co-BpinAGE$_{25}$).

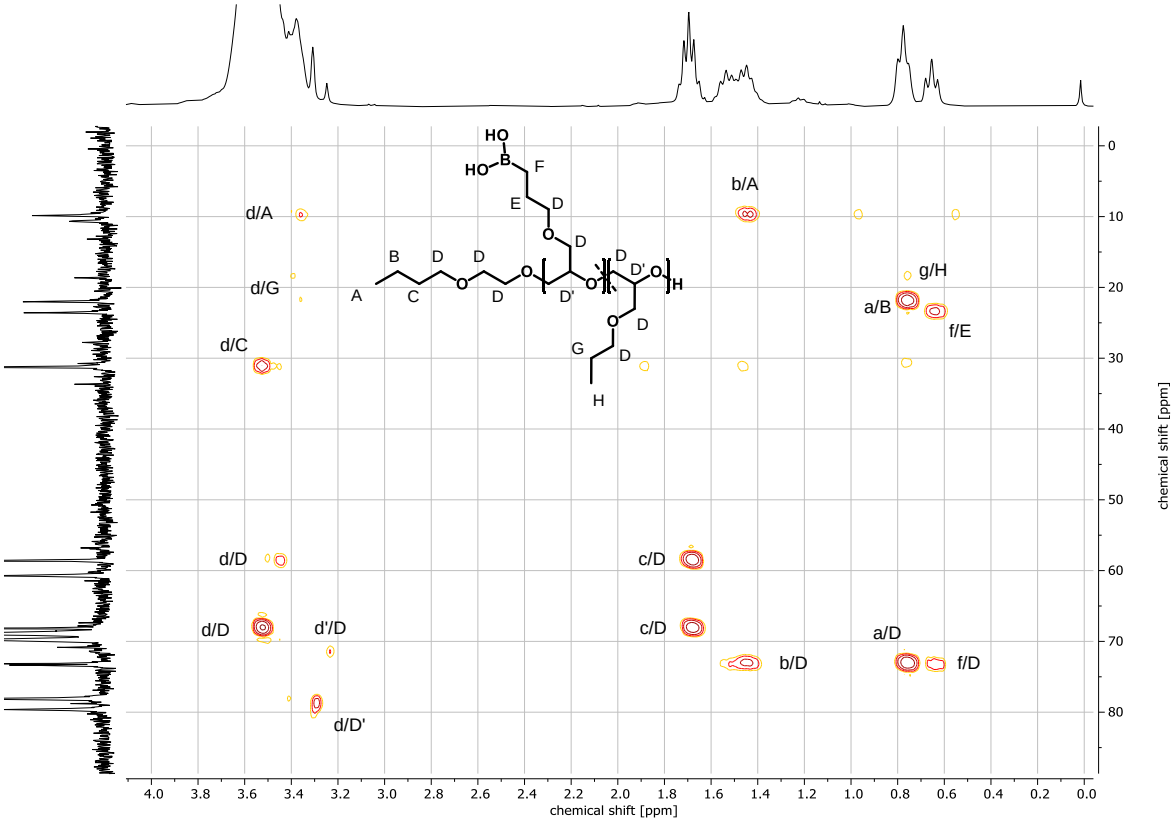

Figure S11: ^{1}H, ^{13}C HMBC NMR spectrum (D_2O) of EGBE-P(PGE$_7$-co-BpinAGE$_{25}$).

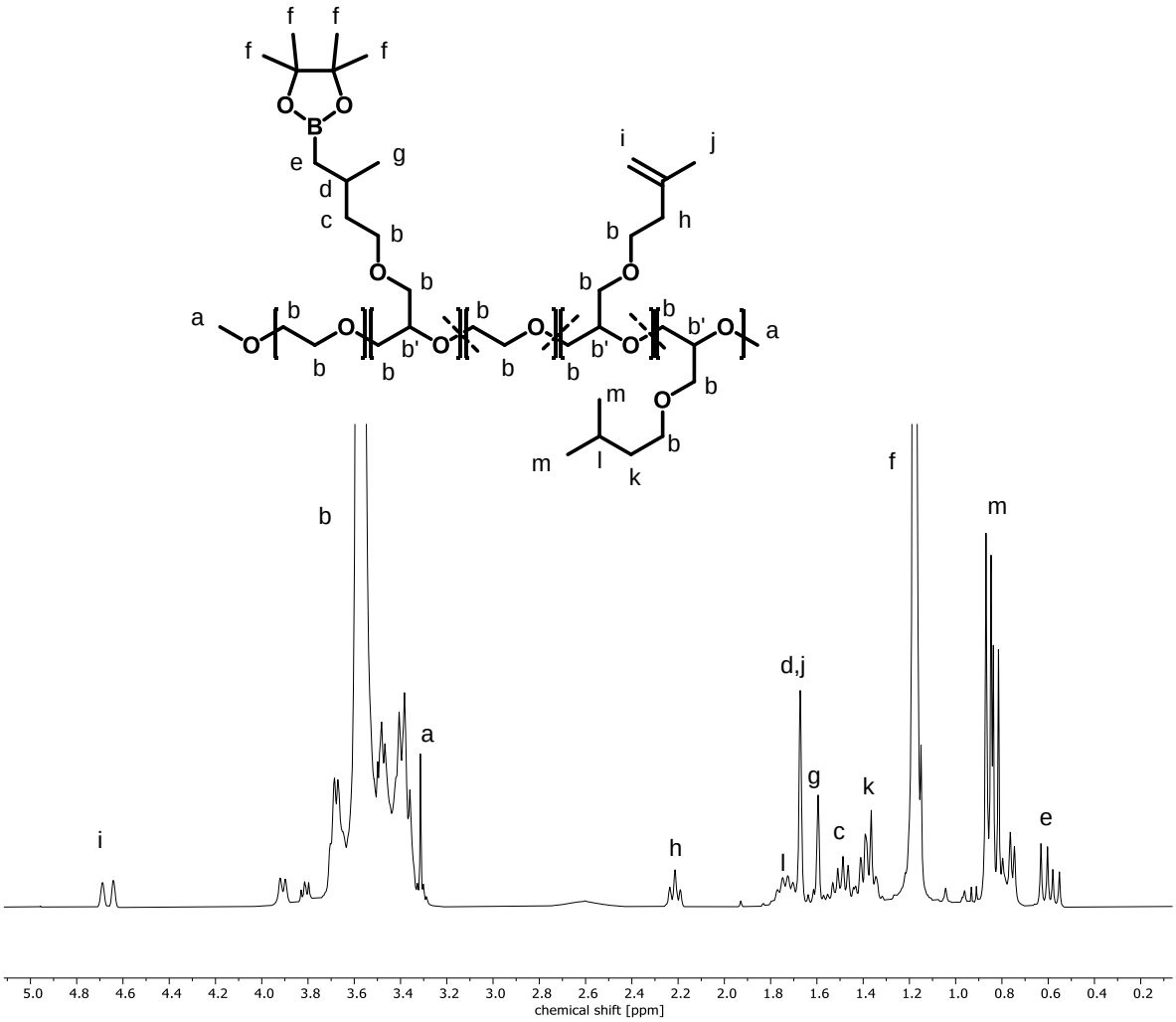

Figure S12: ^{1}H NMR spectrum ($CDCl_3$, 300 MHz) of $mPEG_{123}$-b-P(EG_{32}-co-IsoPreGE$_2$-co-HydPreGE$_8$-co-BpinIsoPreGE$_4$)Me.

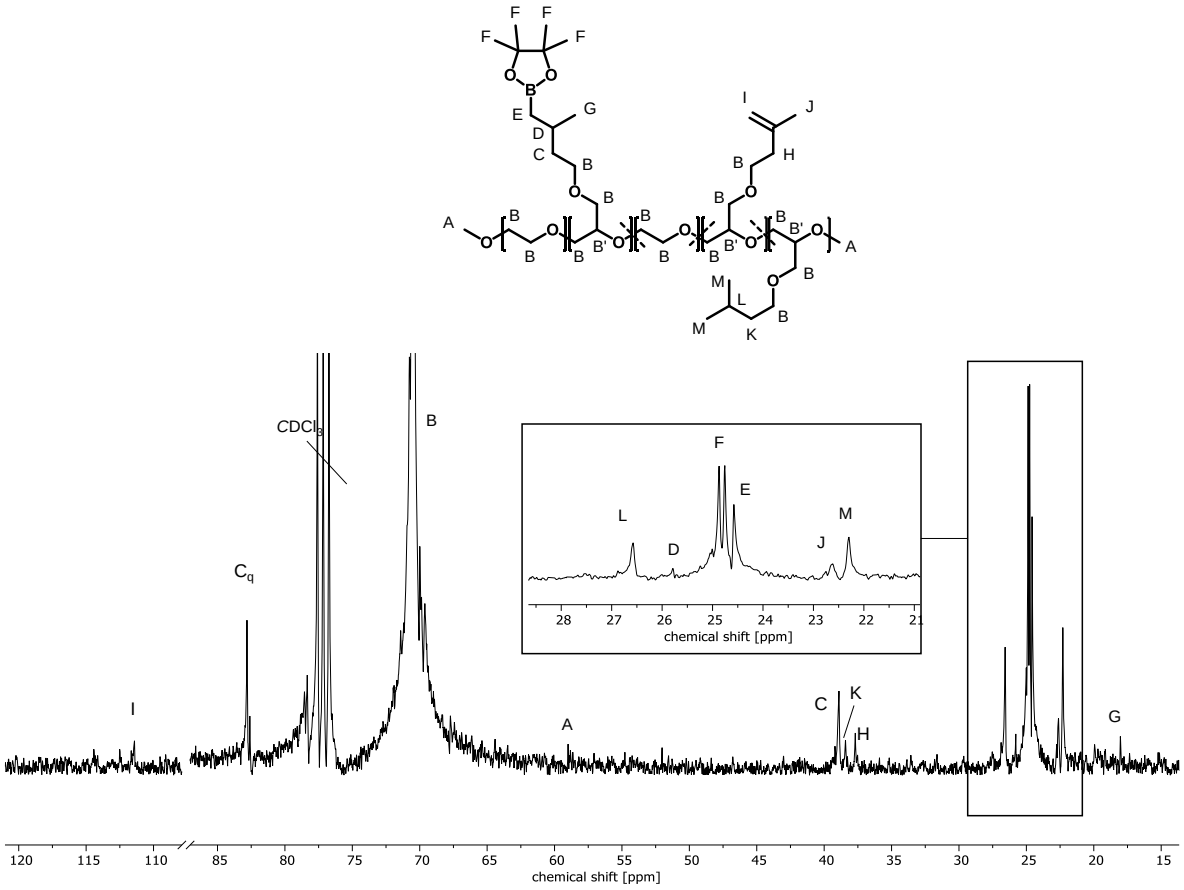

Figure S13: ^{13}C NMR spectrum ($CDCl_3$, 75 MHz) of $mPEG_{123}$-b-P(EG_{32}-co-$IsoPreGE_2$-co-$HydPreGE_8$-co-$BpinIsoPreGE_4$)Me.

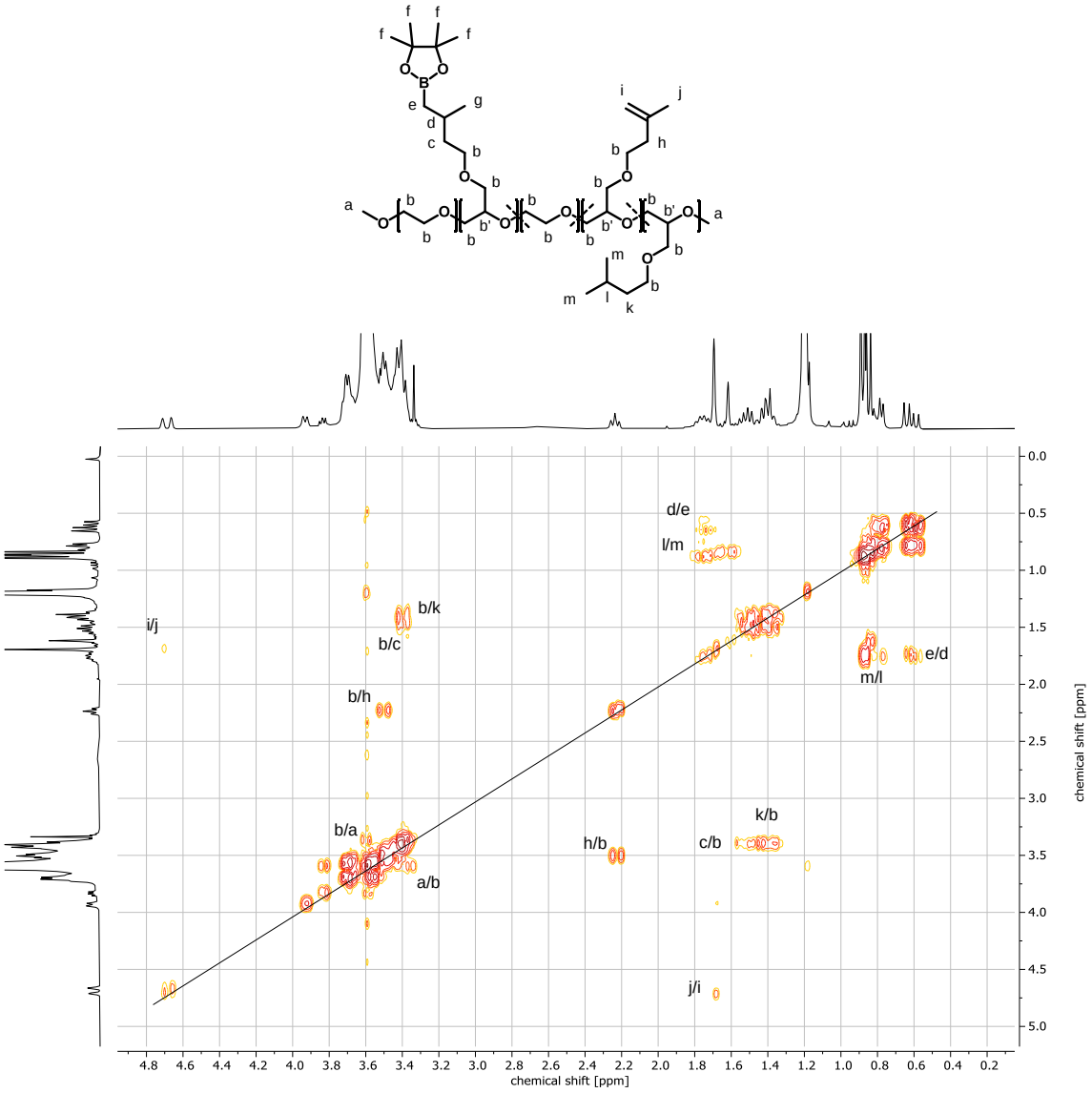

Figure S14 ^{1}H, ^{1}H COSY NMR spectrum ($CDCl_3$, 300 MHz) of $mPEG_{123}$-b-P(EG_{32}-co-IsoPreGE$_2$-co-HydPreGE$_8$-co-BpinIsoPreGE$_4$)Me.

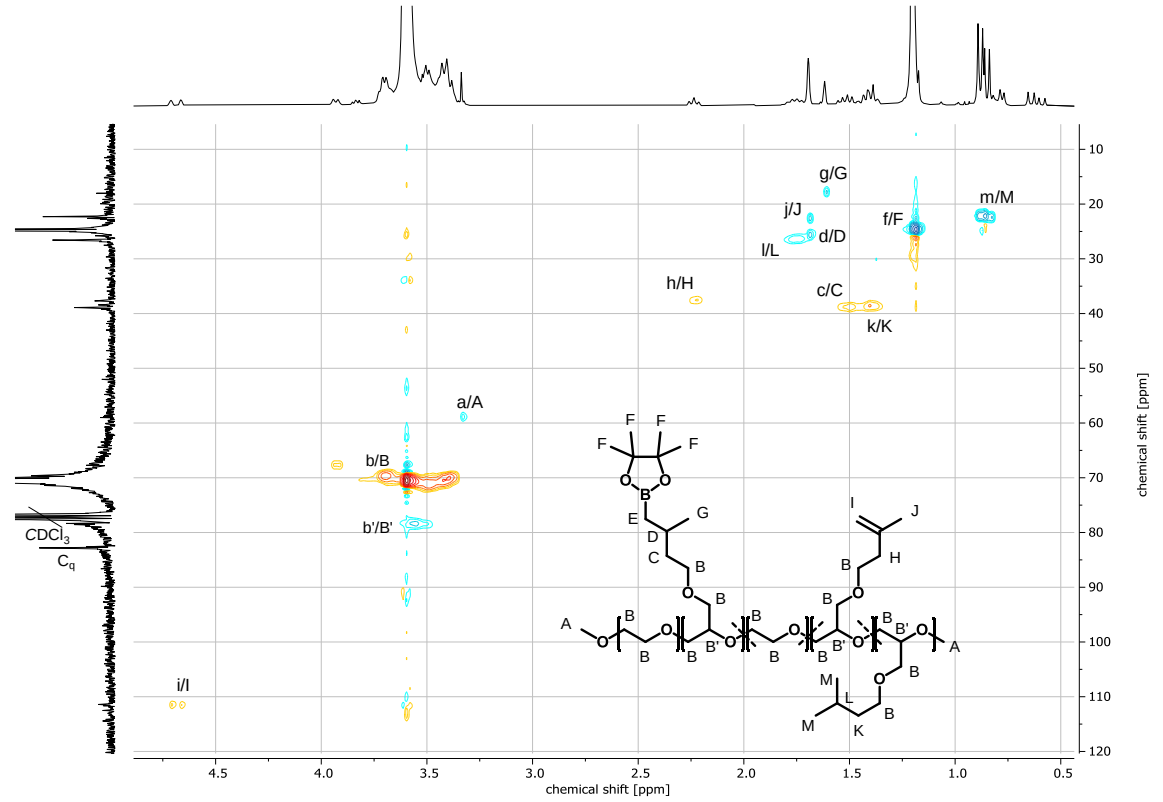

Figure S15: ^{1}H, ^{13}C HSQC NMR spectrum ($CDCl_3$) of $mPEG_{123}$-b-P(EG_{32}-co-$IsoPreGE_2$-co-$HydPreGE_8$-co-$BpinIsoPreGE_4$)Me.

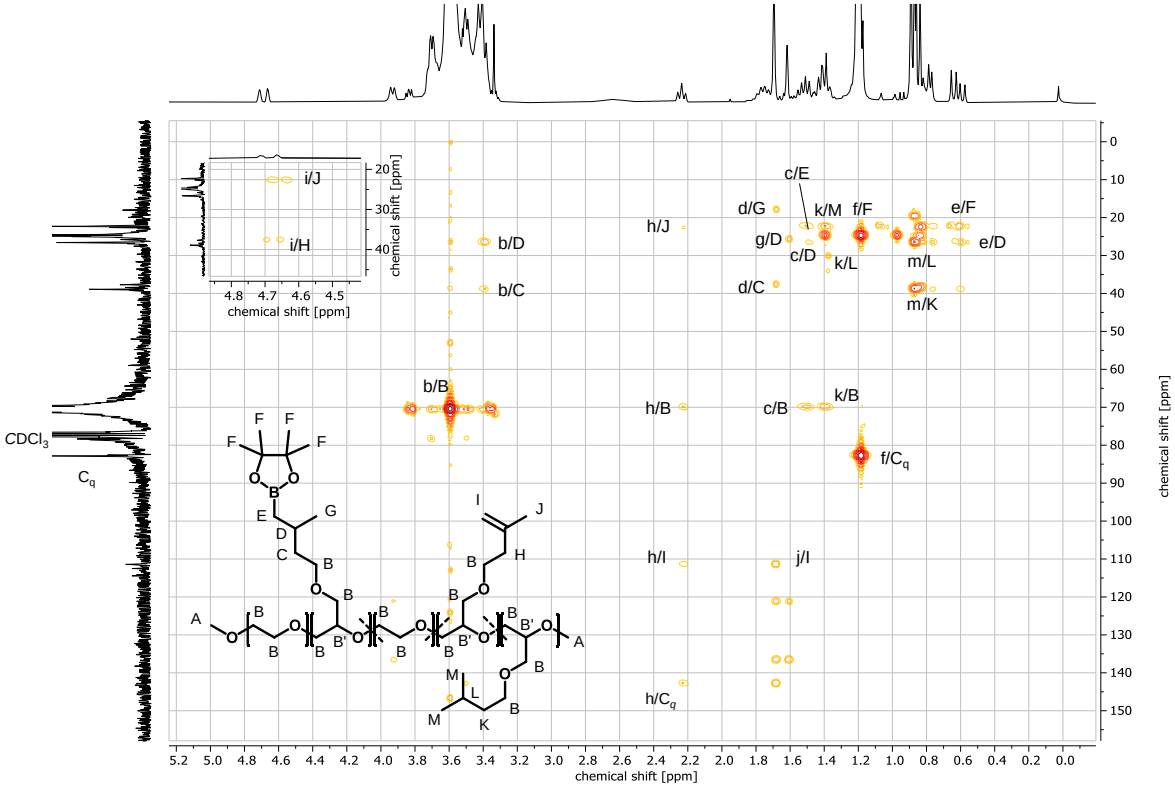

Figure S16: ^{1}H, ^{13}C HMBC NMR spectrum ($CDCl_3$) of $mPEG_{123}$-b-P(EG_{32}-co-$IsoPreGE_2$-co-$HydPreGE_8$-co-$BpinIsoPreGE_4$)Me.

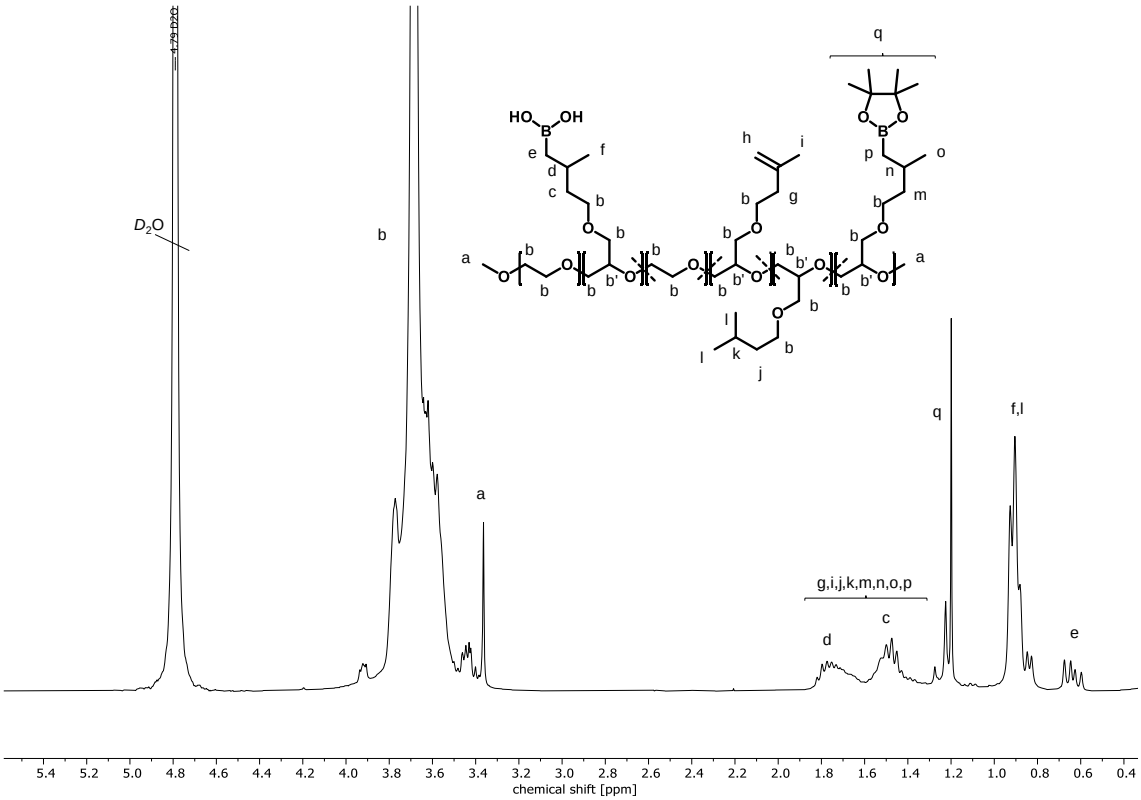

Figure S17: ^{1}H NMR spectrum (D_2O, 300 MHz) of $mPEG_{123}$-b-P(EG_{32}-co-$IsoPreGE_2$-co-$HydPreGE_8$-co-($HOBIsoPreGE_{0.94}$-co-$BpinIsoPreGE_{0.06}$)$_4$)Me.

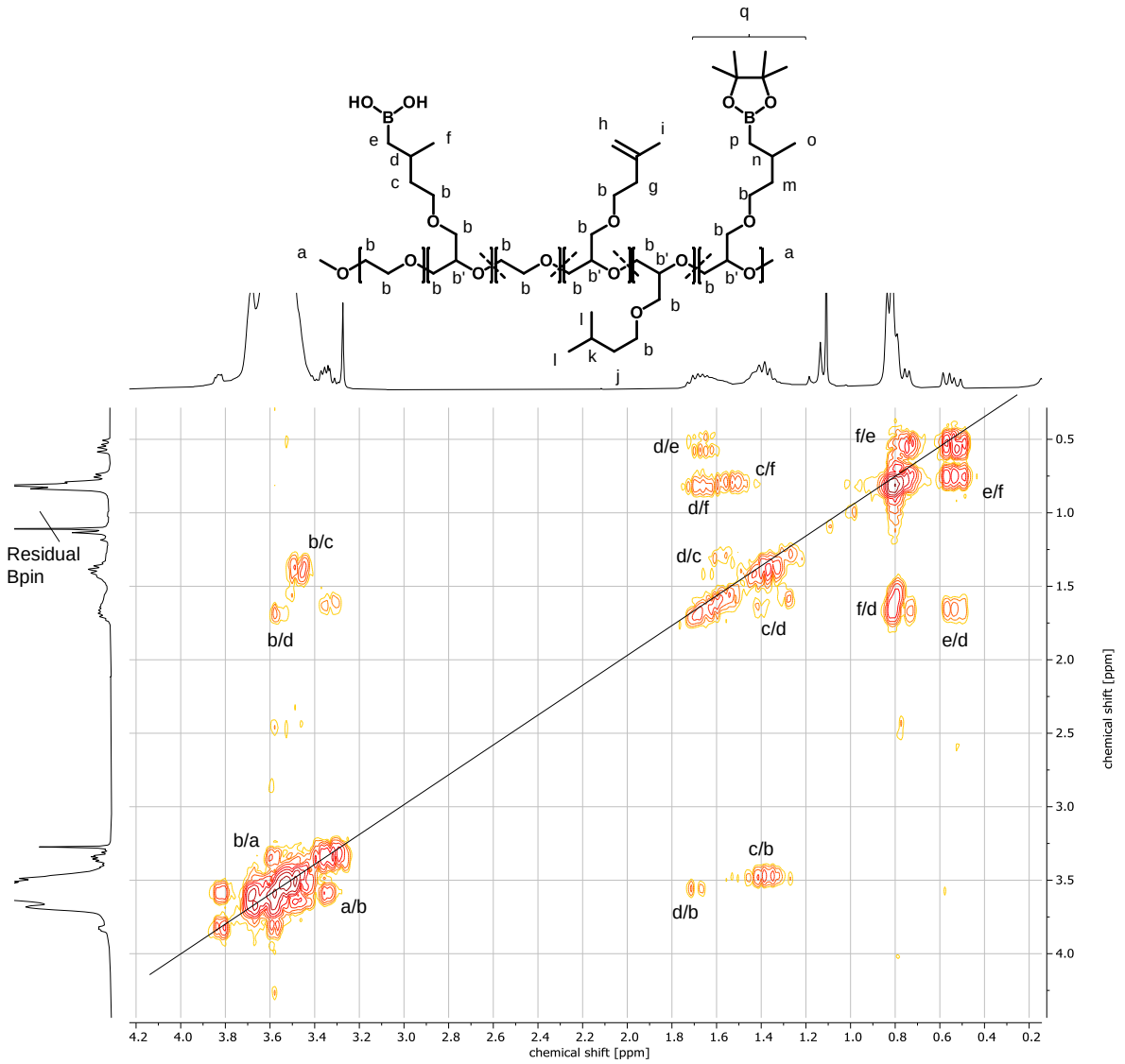

Figure S18: ^{1}H 1H COSY NMR spectrum (D_2O, 300 MHz) of mPEG$_{123}$-b-P(EG$_{32}$-co-IsoPreGE$_{2}$-co-HydPreGE$_{8}$-co-(HOBIsoPreGE$_{0.94}$-co-BpinIsoPreGE$_{0.06}$)$_{4}$)Me.

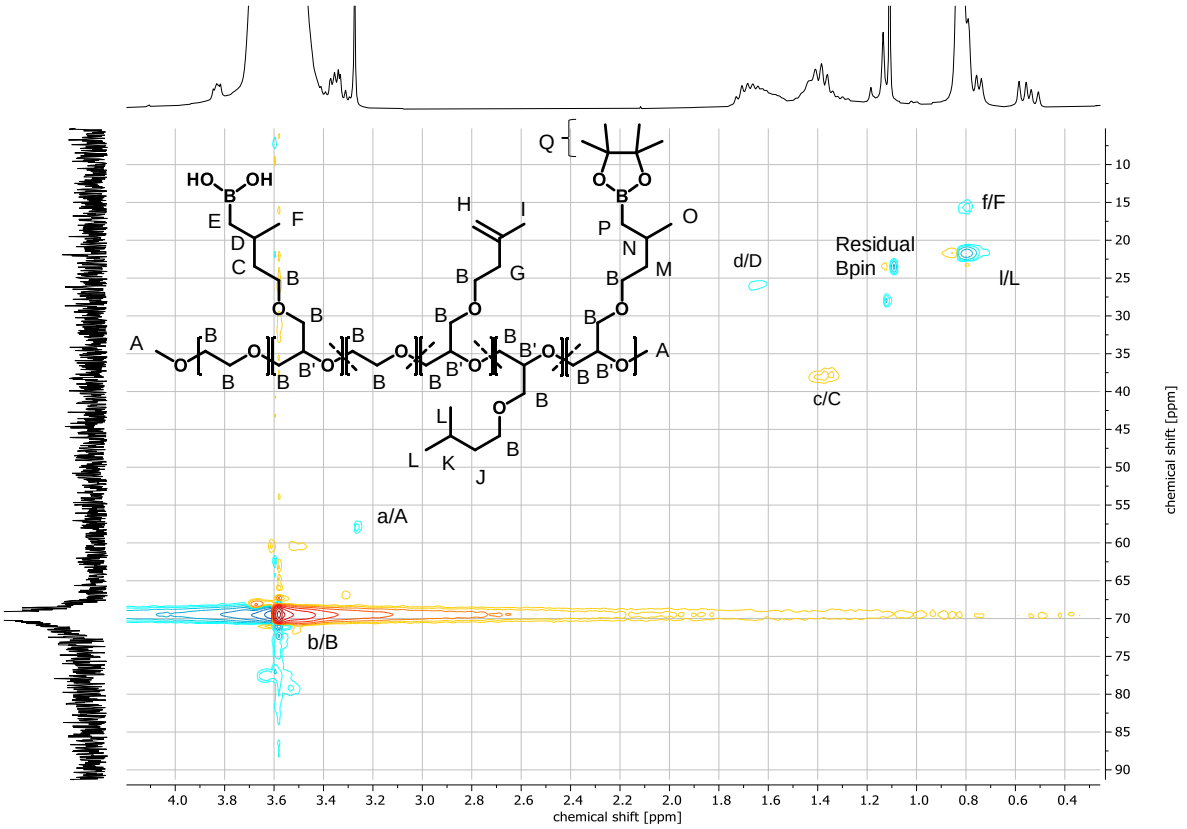

Figure S19: ^{1}H ^{13}C HSQC NMR spectrum (D_2O) of $mPEG_{123}$-b-P(EG_{32}-co-$IsoPreGE_2$-co-$HydPreGE_8$-co-($HOBIsoPreGE_{0.94}$-co-$BpinIsoPreGE_{0.06}$)$_4$)Me.

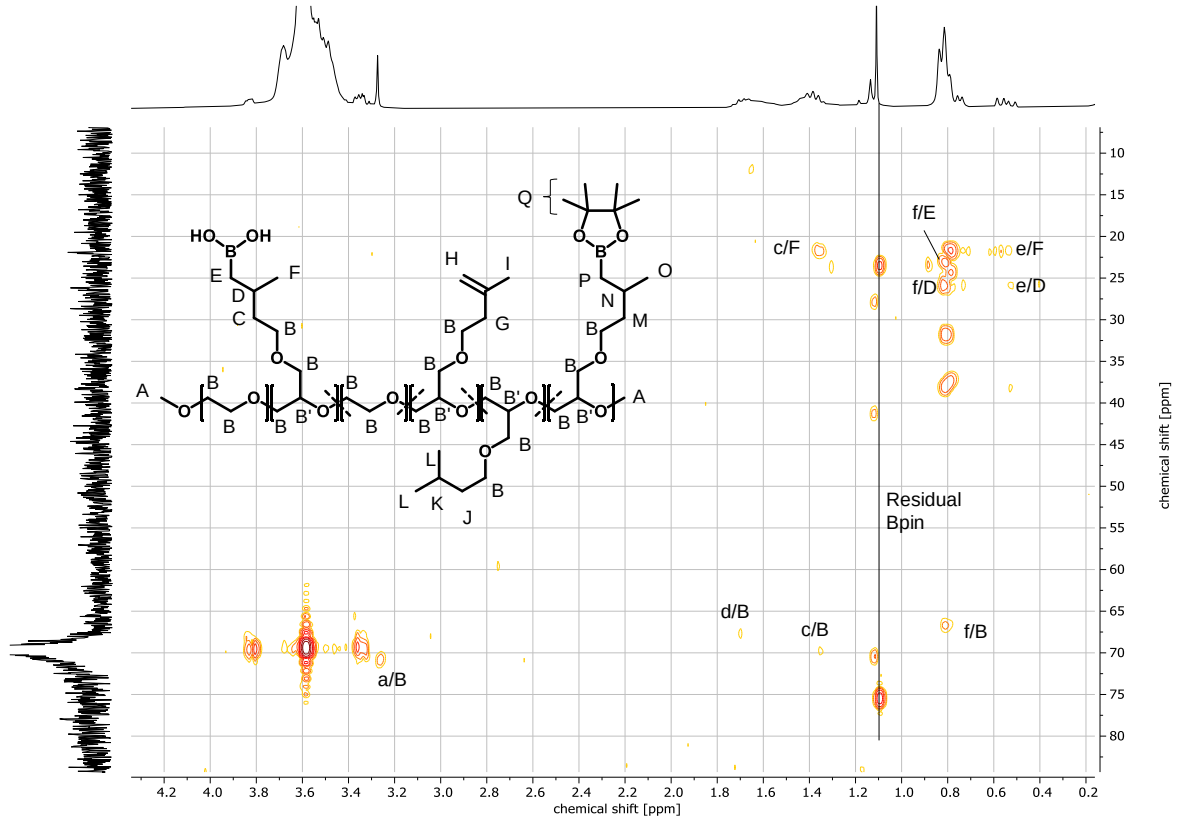

Figure S20: ^{1}H ^{13}C HMBC NMR spectrum (D_2O) of $mPEG_{123}$-b-P(EG_{32}-co-$IsoPreGE_2$-co-$HydPreGE_8$-co-($HOBIsoPreGE_{0.94}$-co-$BpinIsoPreGE_{0.06}$)$_4$)Me.

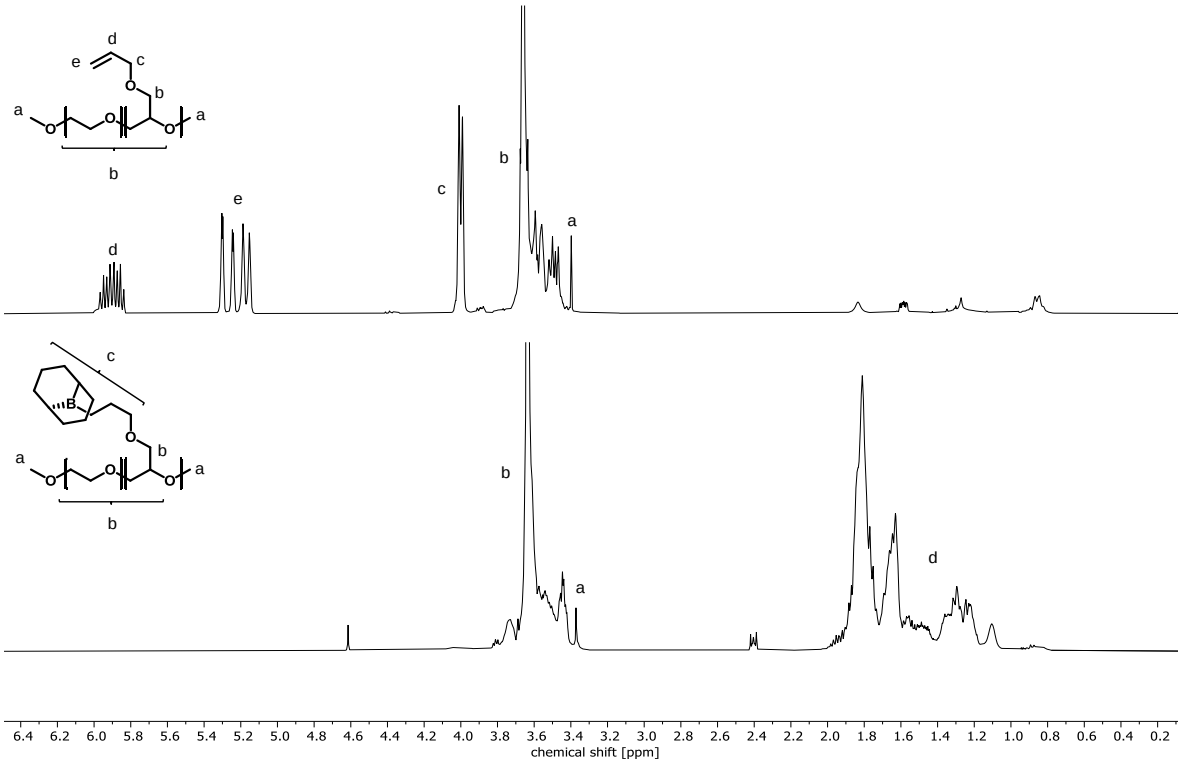

Figure S21: ^{1}H NMR spectrum ($CDCl_3$, 300 MHz) of $mPEG_{51}$-b-$PAGE_{28}Me$ (top) and $mPEG_{51}$-b-$PBBNAGE_{28}Me$ (bottom).

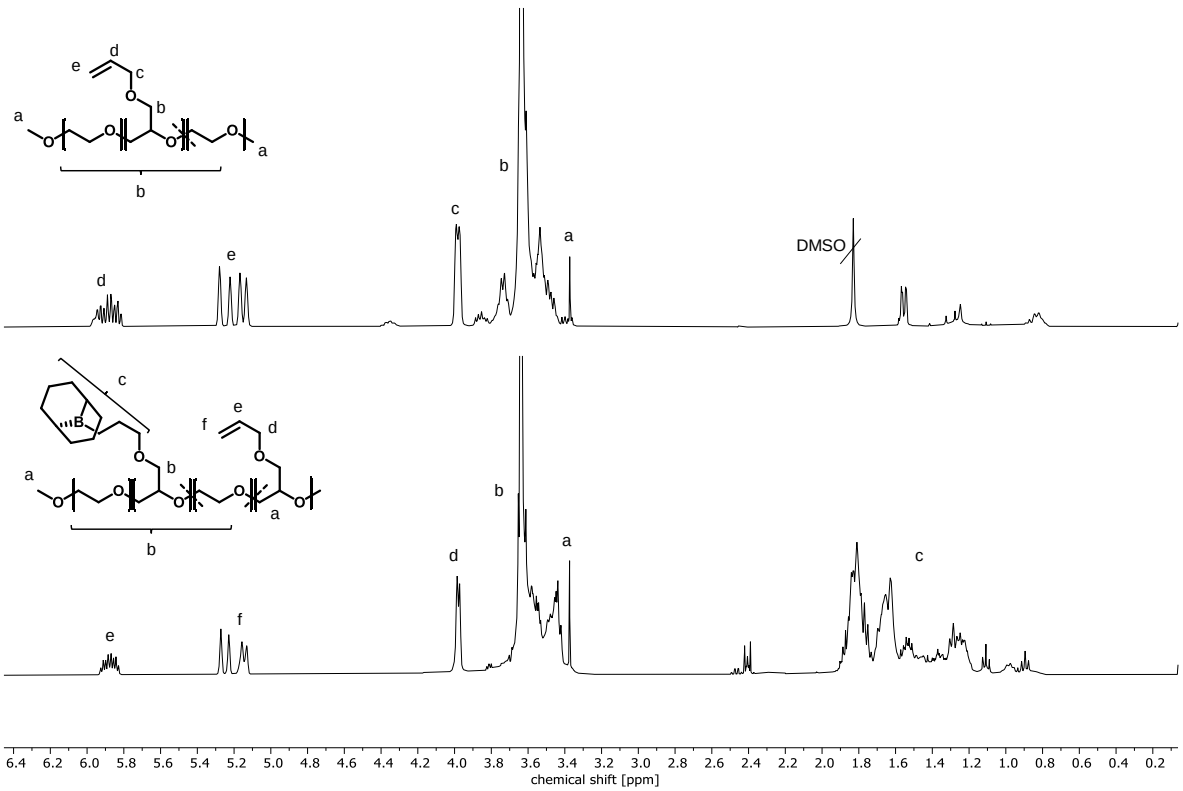

Figure S22: ^{1}H NMR spectrum ($CDCl_3$, 300 MHz) of $mPEG_{123}$-b-$P(EG_{25}$-co-$AGE_{24})Me$ (top) and $mPEG_{123}$-b-$P(EG_{25}$-co-$BBNAGE_{6}$-co-$BBNAGE_{18})Me$ (bottom).

Representative characterisation of synthesised PPOs

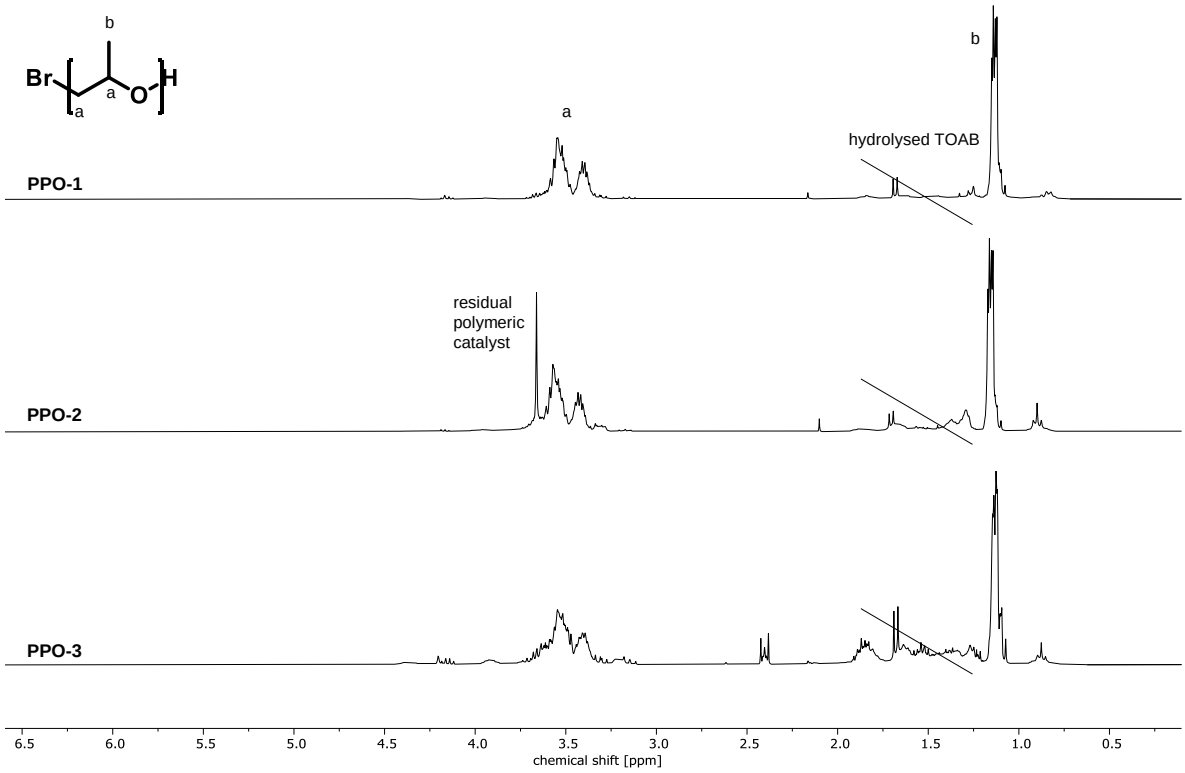

Figure S23: ^{1}H NMR spectrum ($CDCl_3$, 300 MHz) of PPO. Top: PPO-1 (EGBE-PBBNAGE$_{32}$Me catalyst); middle: PPO-2 (mPEG$_{51}$-b-P(AGE$_4$-co-BBNAGE$_{24}$)Me catalyst); bottom: PPO-3(mPEG$_{123}$-b-P(EG$_{25}$-co-AGE$_1$-co-BBNAGE$_{23}$)Me catalyst).

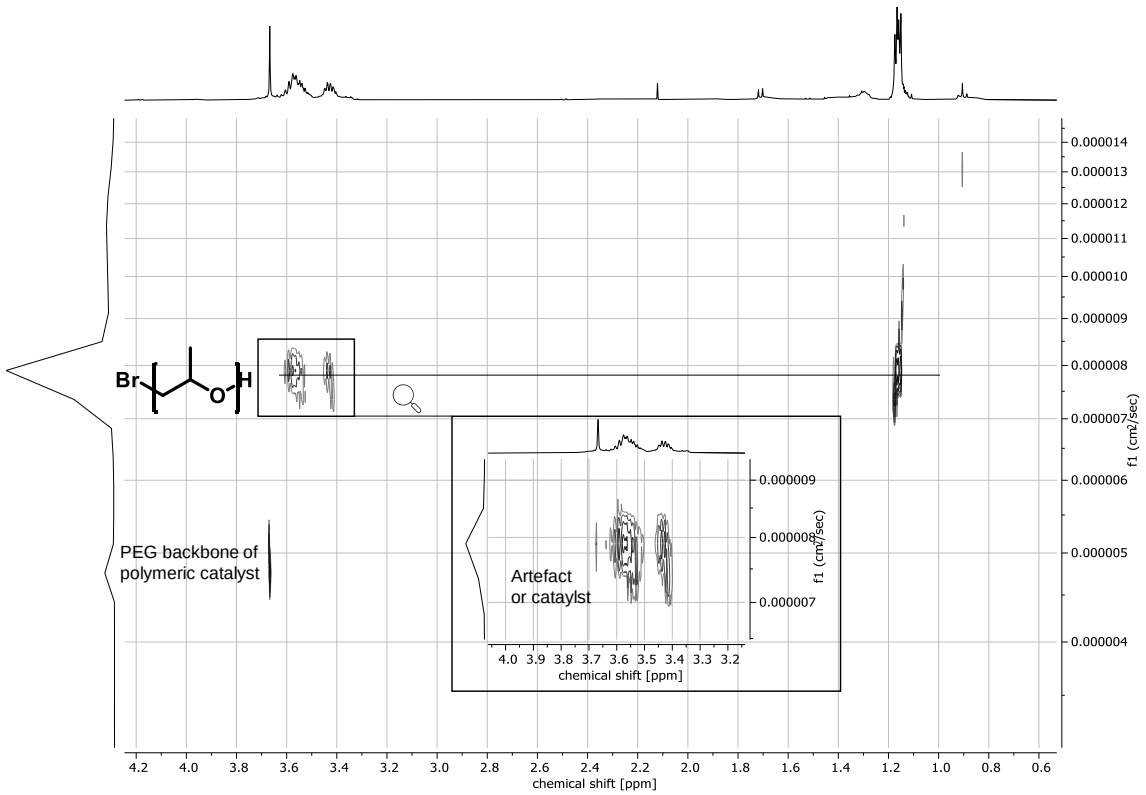

Figure S24: ^{1}H DOSY NMR spectrum ($CDCl_3$, 400 MHz) of PPO-2 synthesised using the $mPEG_{51}$-b-$P(AGE_4$-co-$BBNAGE_{24})Me$ catalyst.

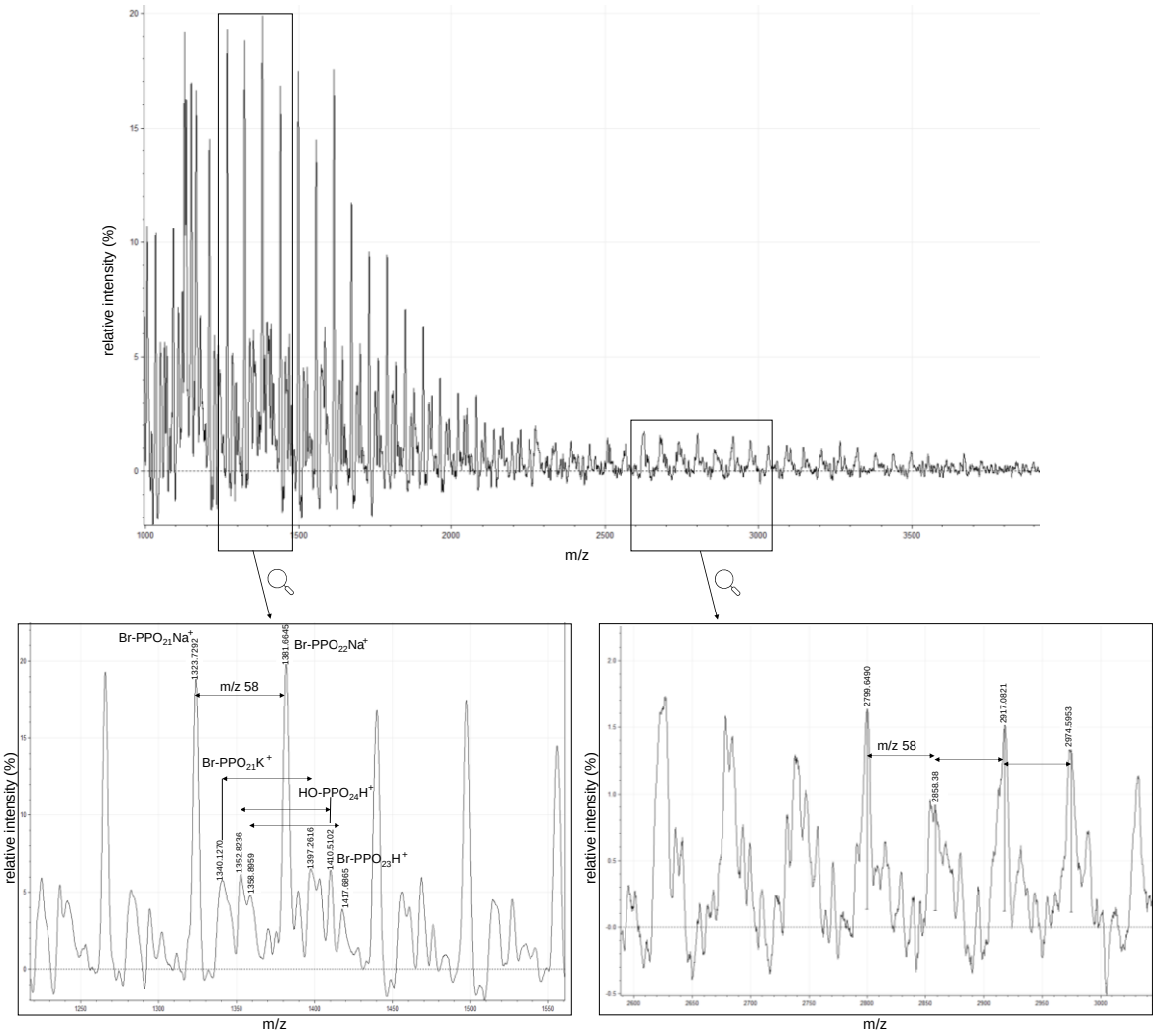

Figure S25: MALDI ToF spectrum and zoom in of PPO-3 synthesised via mPEG$_{123}$-b-P(EG$_{25}$-co-AGE$_{6}$-co-BBNAGE$_{18}$)Me catalyst.

Representative characterisation of synthesised long-chain poly alkylene oxides

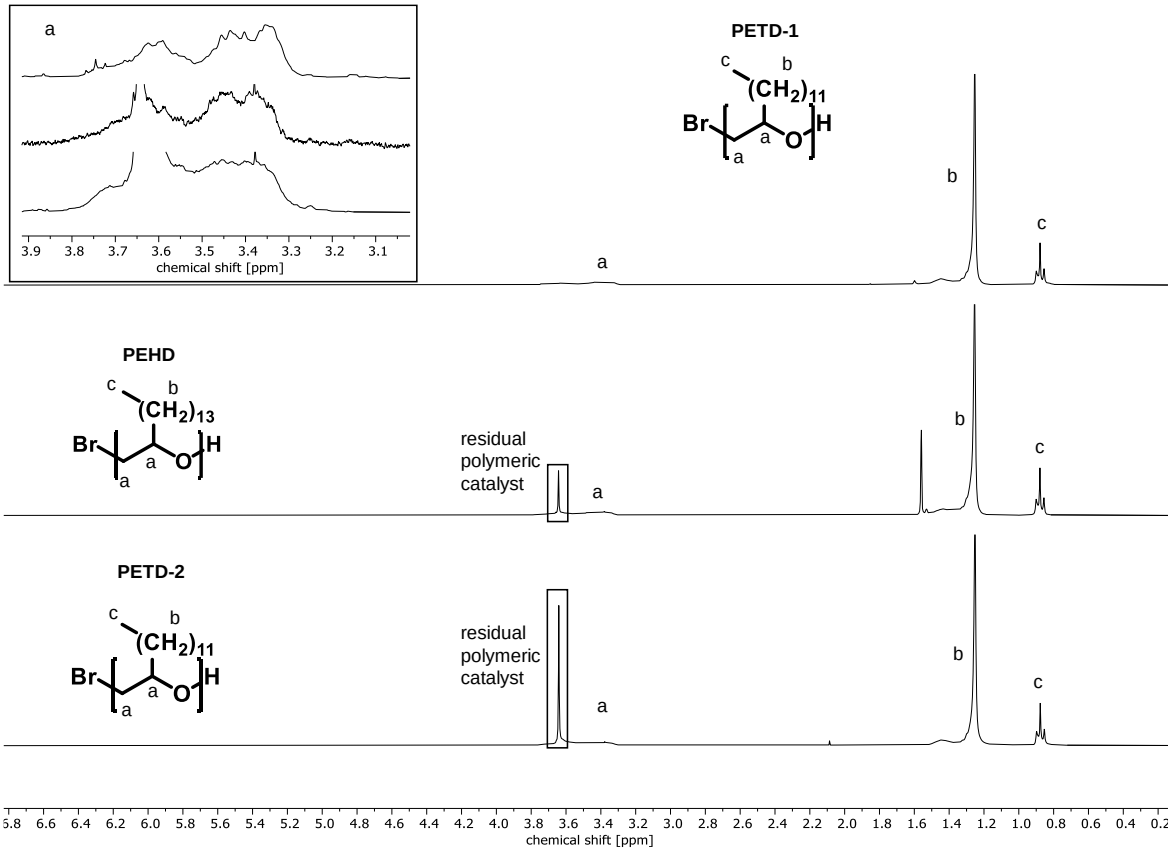

Figure S26: ^{1}H NMR spectrum ($CDCl_3$, 300 MHz) of poly (alkylene oxide)s. Top: PETD-1 (EGBE-$PBBNAGE_{32}$Me catalyst), middle: PEHD ($mPEG_{51}$-b-P(AGE_4-co-$BBNAGE_{24}$)Me catalyst); bottom: PETD-2 ($mPEG_{123}$-b-P(EG_{25}-co-AGE_6-co-$BBNAGE_{18}$)Me catalyst).

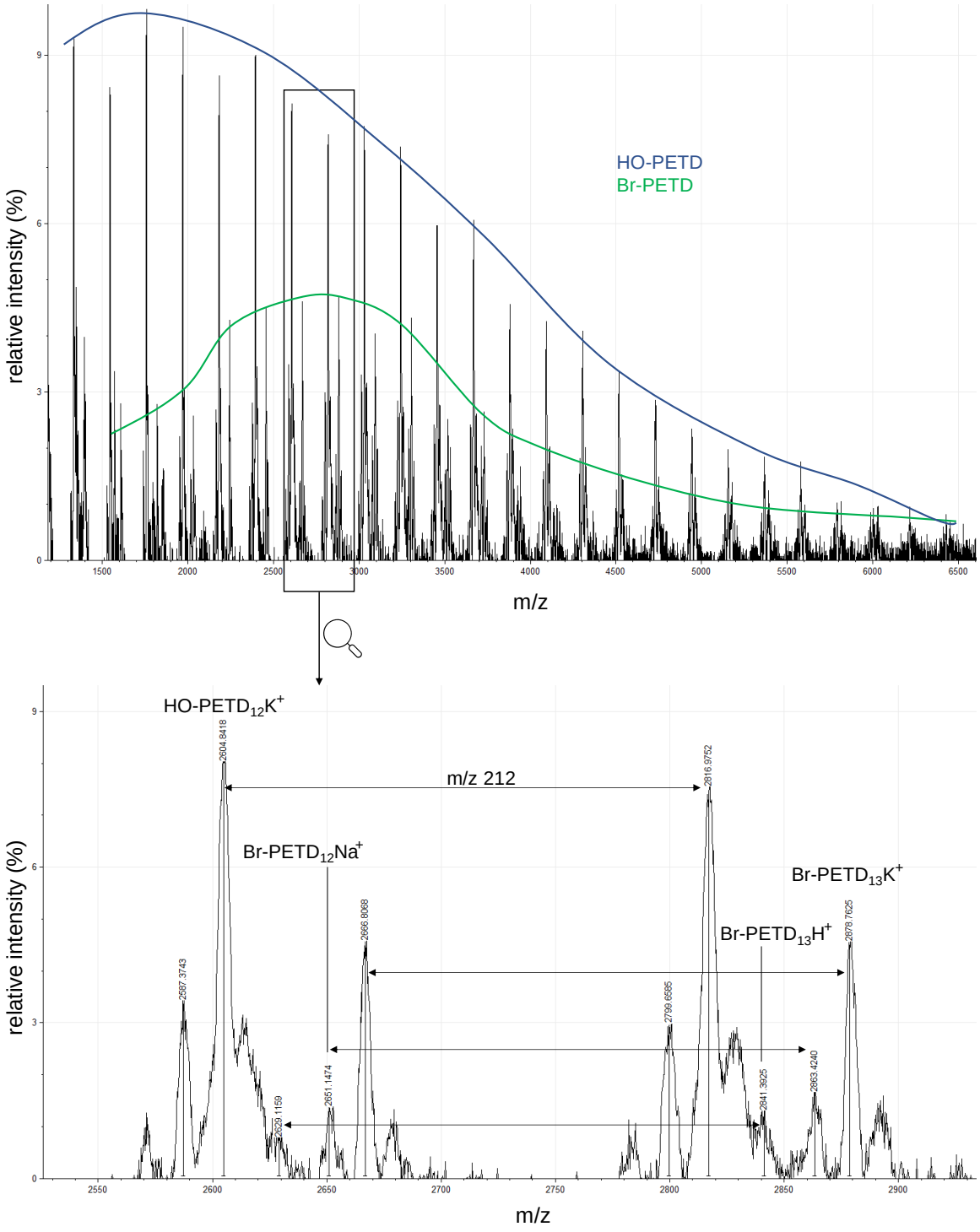

Figure S27: MALDI ToF spectrum and zoom in of PETD-1 synthesised via EGBE-PBBNAGE$_{32}$Me catalyst.

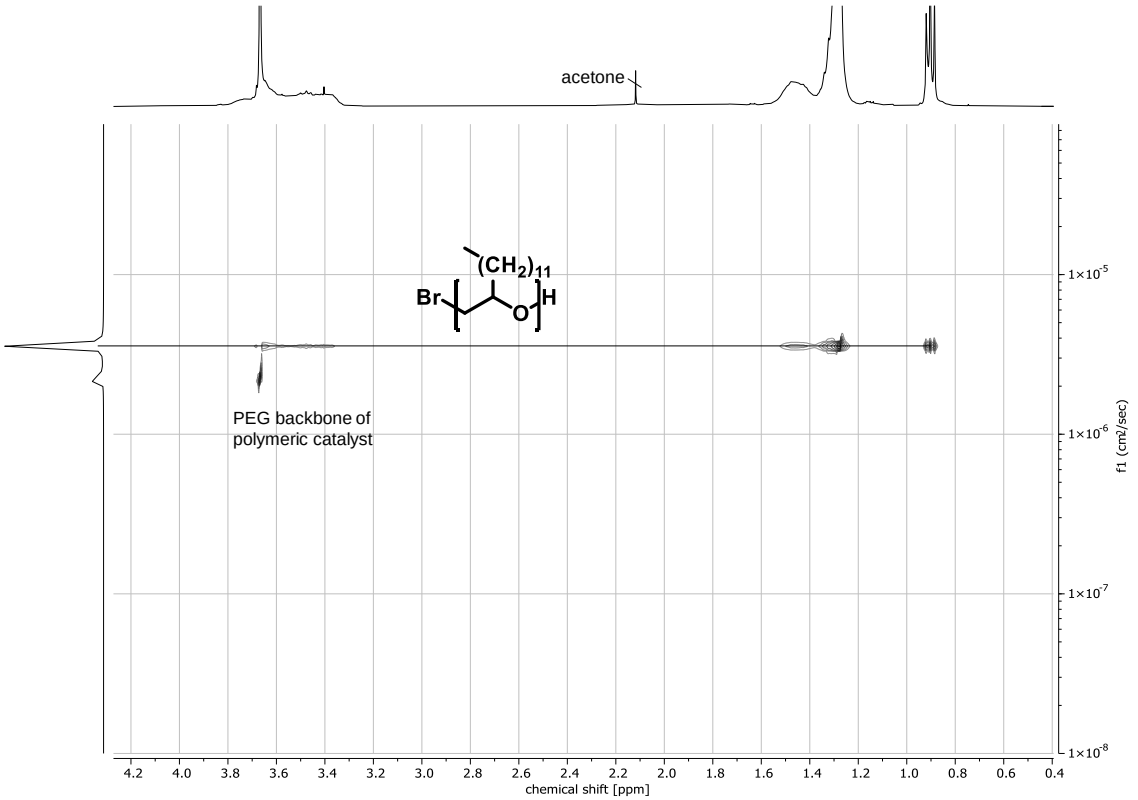

Figure S28: ^{1}H DOSY NMR spectrum ($CDCl_3$, 400 MHz) of PETD-2 synthesised using the $mPEG_{123}$-b-$P(EG_{25}$-co-AGE_6-co-$BBNAGE_{18})$Me catalyst.

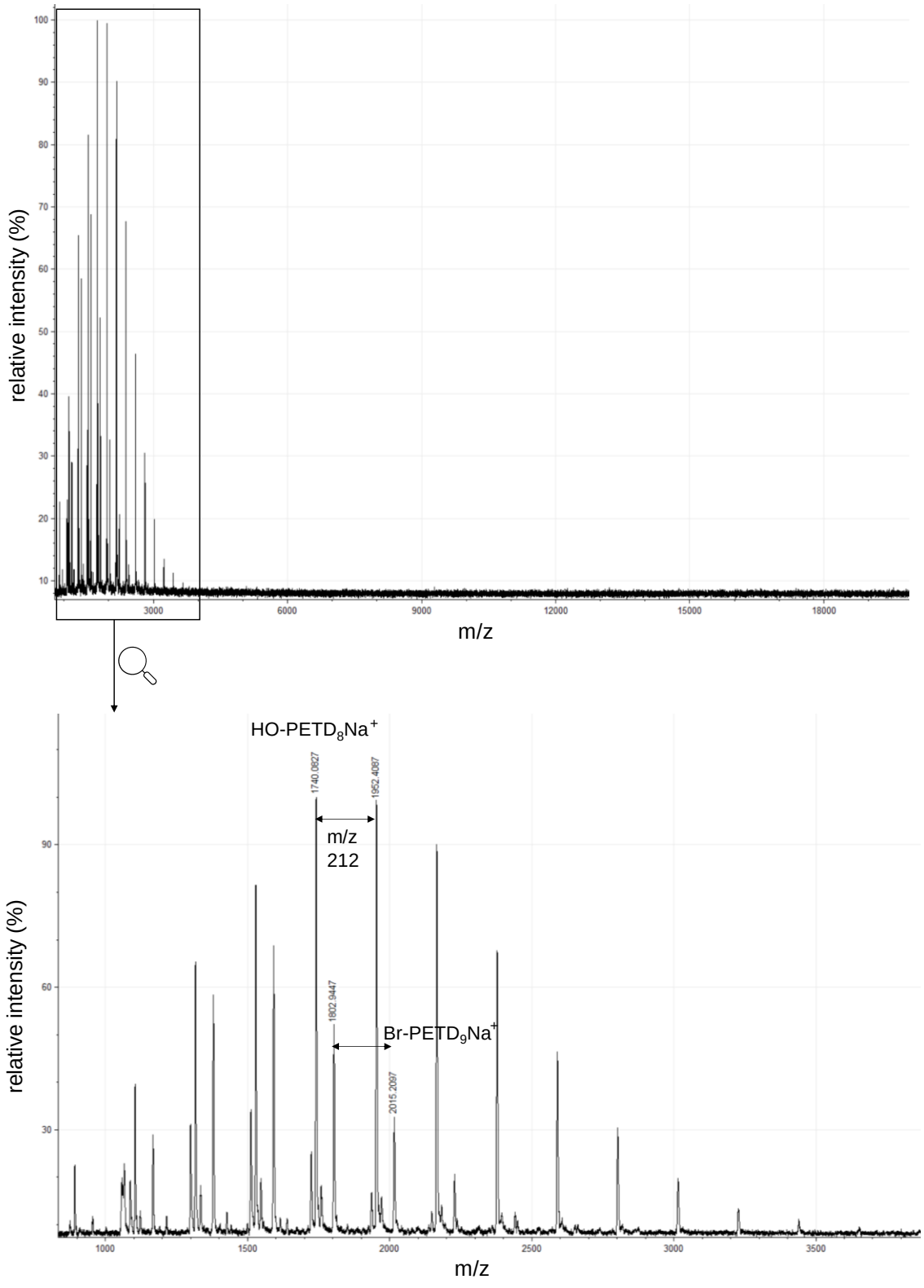

Figure S29: MALDI ToF spectrum and zoom in of PETD-2 synthesised via mPEG$_{123}$-b-P(EG$_{25}$-co-AGE$_{6}$-co-BBNAGE$_{18}$)Me catalyst. Sample preparation with DCTB and NaI.

^{1}H NMR spectra of the recyclability study

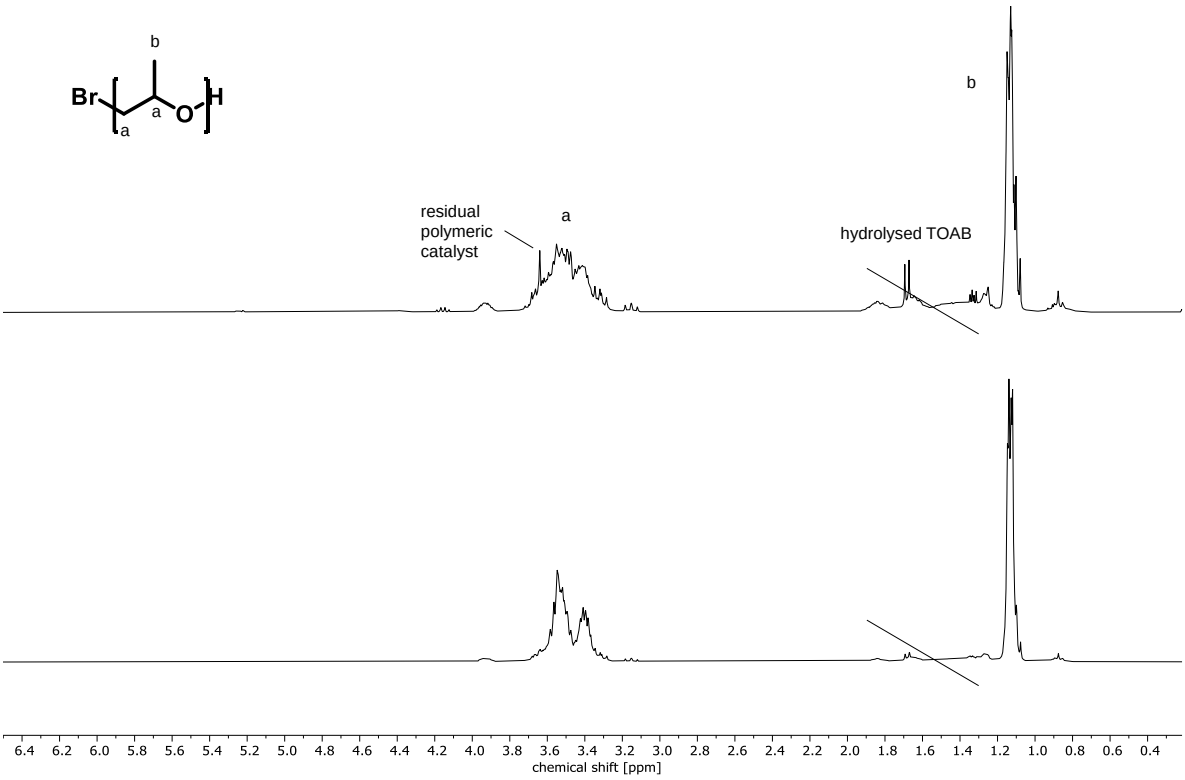

Figure S30: ^{1}H NMR spectrum ($CDCl_3$, 300 MHz) of synthesised PPO under $mPEG_{123}$-b-P(EG_{25}-co-$BBNAGE_6$-co-$BBNAGE_{18}$)Me) catalysis: run 1 (top) and 2 (bottom).

Representative characterisation of poly (cyclohexene carbonate)

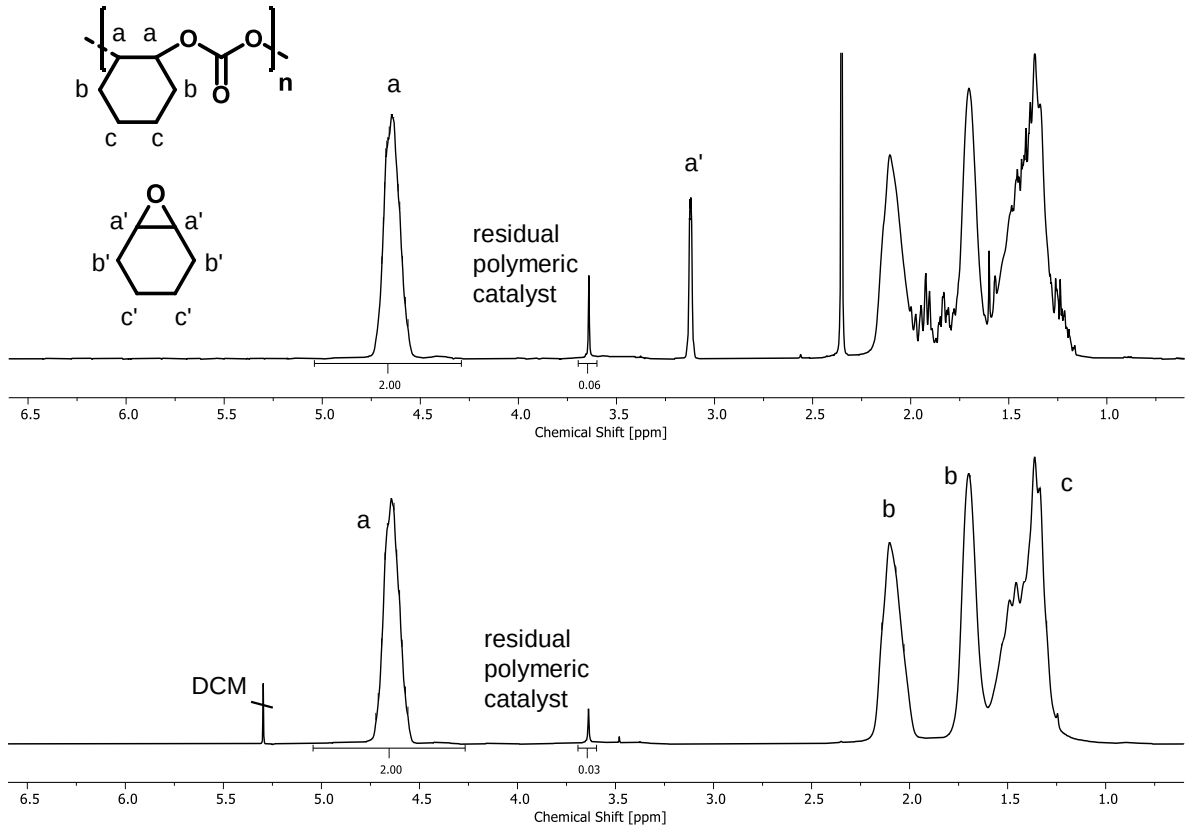

Figure S31: ^{1}H NMR spectrum ($CDCl_3$, 300 MHz) of synthesised poly (cyclohexene carbonate). Synthesis using the catalysts $mPEG_{51}$-b-P(AGE_6-co-$BBNAGE_{22}$)Me).

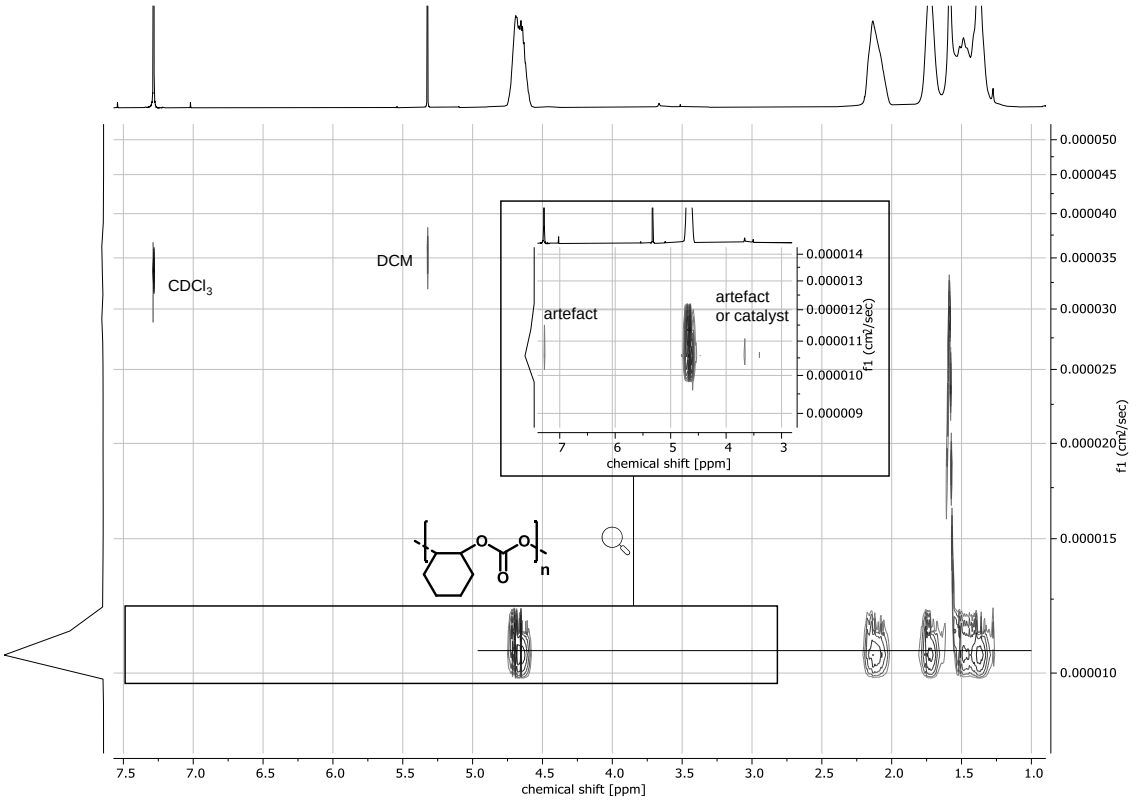

Figure S32: ^{1}H DOSY NMR spectrum ($CDCl_3$, 400 MHz) of poly (cyclohexene carbonate) synthesised using the $mPEG_{51}$-b-P(AGE_6-co-$BBNAGE_{22}$)Me) catalyst.

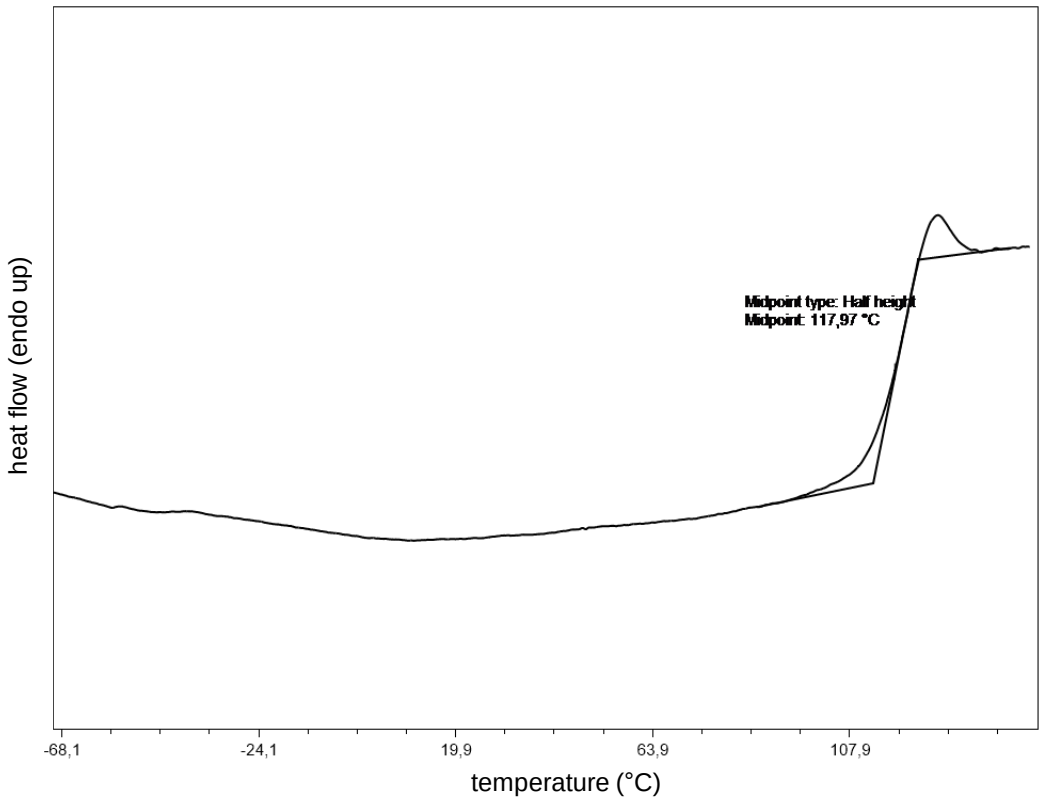

Figure S33: DSC measurement of poly (cyclohexene carbonate) (2nd heating curve, heating and cooling rate 20 °C min^{-1}).

Appendix

A1 – Verfahren zur Herstellung von fluorierten Polymeren

Larissa Limmer,[a] Tom Reimers,[a] Reiner Friedrich,[b] Holger Frey[a*]

[a] Johannes Gutenberg-Universität Mainz, Department of Chemistry, Duesbergweg 10 - 14, 55128 Mainz, Germany

[b] Merck KGaA, Frankfurter Straße 250, 64293 Darmstadt, Germany

This patent was filed on the research conducted in chapter 3 of this thesis. The text was written by [redacted] with support from Larissa Limmer and Prof. Holger Frey. In the following, the patent priority application EP22213760.6 (invention disclosure [redacted]) is attached. Data regarding [redacted] were supported by experiments conducted by Tom Reimers.

.

Curriculum Vitae

Larissa Limmer

Personal Information

Address [redacted]

E-Mail [redacted]

Date of birth [redacted]

Nationality [redacted]

Education

06/2019 – now — PhD candidate in chemistry

Johannes Gutenberg-University Mainz; Research group H. Frey

Design, synthesis, and analysis of functional polyethers for biomedical applications, textile coating, surfactants, and oil production

Industry collaboration with Merck KGaA

Internationale collaborations: Groups of M. A. Kelland (university of Stavanger, Norway) and M. K. Brown (university of Bloomington, USA)

05/2022 – 08/2022 — Research stay

University of Bloomington, USA; Research group M. K. Brown

Photocatalytic CH-functionalisation and hydroboration

10/2017 – 03/2019 — M. Sc. Biomedical chemistry

Johannes Gutenberg-University Mainz

Final grade 1,3

Focus on macromolecular chemistry

Thesis: “Synthesis and toxicity of amino functional polyethers”

10/2013 – 06/2017 — B. Sc. Biomedical chemistry

Johannes Gutenberg-University Mainz

Final grade 1,7

Focus on biochemistry and macromolecular chemistry

Thesis: “Study of ABC-transporters regarding their structure-effect relationship”

2005 – 2013 — Abitur

Immanuel Kant Gymnasium Rüsselsheim

Work Experience

06/2019 – now	Research fellow
	Johannes Gutenberg-University Mainz
	Supervision and teaching of students
	Coordination of collaboration between academia and industry
	Application oriented project development and management
	Writing and review of scientific documents and presentations
10/2018 – 03/2019	Group of H. Frey
	Monomer and polymer synthesis
	Teaching assistant for biopolymers
01/2018 – 02/2018	Group of D. Schneider
	Planning and execution of biotechnological polymer synthesis
09/2016 – 10/2016	Group of R. Zentel
	Organic synthesis

Skills

Languages	German (first language)
	English (fluent)
Leadership	Supervision of 5 lab courses with 20–50 students, 4 Tutorials, 1:1 supervision of 1 bachelor student, 2 master students and 1 visiting researcher
Courses *By GDCh*	Certified project manager in industrial chemistry (innovation and strategy management, competitor analysis, strategic marketing and project management in the chemical industry
	Leadership for future leaders
By Johannes Gutenberg-University	Intercultural communication
	Purposive communication and conflict management
	Good Scientific Practice
IT	Microsoft Office, MNova, WinGPC UniChrom, mmass, ChemDraw, Origin
Chemical analysis	NMR spectroscopy, GPC, MALDI-ToF MS-spektrometry, contact angle goniometry, Du Noüy ring method
Chemical synthesis	anionic and monomer-activated anionic ring-opening polymerisation, multistep synthesis

List of Publications

Contribution as equally

Zhang, Q.; Limmer, L.; Frey, H.; Kelland, M. A. *N*-Oxide Polyether as Kinetic Hydrate Inhibitors: Side Chain Ring Size Makes the Difference. Energy Fuels, 2021, 35, 5, 4067-4074, DOI: 10.1021/acs.energyfuels.0c04333.

To be submitted

Limmer, L.; Bros, M.; Frey, H. Copolymers of glycidyl amines and ethylene oxide as transfection agents with controllable charge density. To be submitted.

Limmer, L.; Holzmüller, P.; Schüttner, S.; Brown, K. M.; Frey, H. Versatile borane polyethers as recyclable catalysts for the synthesis of polyethers and CO_2 based polycarbonates. To be submitted.

Limmer, L.; Reimers, T.; Linden, G. M.; Liermann, J.; Friedrich, R.; Frey, H. Surface Active Polyethers with Degradable Fluorinated Side Chains. To be submitted.

Patents

Limmer, L.; Reimers, T.; Frey, H.; Friedrich, R. Verfahren zur Herstellung von fluorierten Polymeren. Patent pending; filed 2022; EP22213760.6.

Contribution as coauthor

Zhang, Q.; Kelland, M. A.; Frey, H.; Blankenburg, J.; Limmer, L. Amine *N*-Oxide Kinetic Hydrate Inhibitor Polymers for High-Salinity Applications. Energy Fuels 2020, 34, 5, 6298-6305, DOI: 10.1021/acs.energyfuels.0c00838.

Conferences

09/2021	Biennial Meeting of the GDCh Division of Macromolecular Chemistry, online Poster: “Polymeric Amine-N-oxides as Kinetic Gas Hydrate Inhibitors”
02/2023	Macromolecular Colloquium Freiburg Poster: “Synthesis and Kinetic Gas Hydrate Inhibition Activity of a Novel Polyether Class: Poly(glycidyl amine-N-oxide)s”